20000726063

328197

ADA017459

107600-10-T

An IRIA State-of-the-Art Report

ATMOSPHERIC TRANSMITTANCE AND RADIANCE: METHODS OF CALCULATION

ANTHONY J. LaROCCA and ROBERT E. TURNER
Infrared Information and Analysis Center
Infrared and Optics Division

JUNE 1975

~~Approved for public release; distribution unlimited.~~

Reproduced From
Best Available Copy

Office of Naval Research
Department of the Navy
Arlington, Virginia 22217
Contract Nos. N00014-73-A-0321-0002
and N00014-74-C-0285

ENVIRONMENTAL
RESEARCH INSTITUTE OF MICHIGAN
FORMERLY WILLOW RUN LABORATORIES, THE UNIVERSITY OF MICHIGAN
BOX 618 • ANN ARBOR • MICHIGAN 48107

REPRODUCED BY
NATIONAL TECHNICAL
INFORMATION SERVICE
U.S. DEPARTMENT OF COMMERCE
SPRINGFIELD, VA. 22151

NOTICES

Sponsorship. The work reported herein was conducted by the Environmental Research Institute of Michigan for Office of Naval Research, Contract Nos. N00014-73-A-0321-0002 and N00014-74-C-0285. Dr. William J. Condell was Technical Monitor. Contracts and grants to the Institute for the support of sponsored research are administered through the Office of Contracts Administration.

Final Disposition. After this document has served its purpose, it may be destroyed. Please do not return it to the Environmental Research Institute of Michigan.

lja

UNCLASSIFIED

SECURITY CLASSIFICATION OF THIS PAGE (When Data Entered)

REPORT DOCUMENTATION PAGE		READ INSTRUCTIONS BEFORE COMPLETING FORM
1. REPORT NUMBER 107600-10-T	2. GOVT ACCESSION NO.	3. RECIPIENT'S CATALOG NUMBER
4. TITLE (and Subtitle) ATMOSPHERIC TRANSMITTANCE AND RADIANCE: METHODS OF CALCULATION		5. TYPE OF REPORT & PERIOD COVERED IRIA State-of-the-Art Report 6. PERFORMING ORG. REPORT NUMBER 107600-10-T
7. AUTHOR(s) Anthony J. LaRocca and Robert E. Turner		8. CONTRACT OR GRANT NUMBER(s) N00014-74-C-0285 N00014-73-A-0321-0002
9. PERFORMING ORGANIZATION NAME AND ADDRESS Environmental Research Institute of Michigan Infrared and Optics Division, P. O. Box 618 Ann Arbor, Michigan 48107		10. PROGRAM ELEMENT, PROJECT, TASK AREA & WORK UNIT NUMBERS NR 315-001
11. CONTROLLING OFFICE NAME AND ADDRESS Office of Naval Research Department of the Navy Arlington, Virginia 22217		12. REPORT DATE June 1975 13. NUMBER OF PAGES 508
14. MONITORING AGENCY NAME AND ADDRESS (if different from Controlling Office)		15. SECURITY CLASS. (of this report) UNCLASSIFIED 15a. DECLASSIFICATION/DOWNGRADING SCHEDULE

16. DISTRIBUTION STATEMENT (of this Report)

Approved for public release; distribution unlimited.

17. DISTRIBUTION STATEMENT (of the abstract entered in Block 20, if different from Report)

18. SUPPLEMENTARY NOTES

For announcement only by EDC. All secondary distribution of this document by the IRIA Center.

19. KEY WORDS (Continue on reverse side if necessary and identify by block number)

Absorption	Line-by-line
Atmosphere	Radiance
Band Models	Scattering
Extinction	Transmittance

20. ABSTRACT (Continue on reverse side if necessary and identify by block number)

The effort represented by this report was a result of the need to bring a description of the state-of-the-art of methods of calculating atmospheric transmittance and radiance up-to-date. The report is broadly divided into the categories of scattering and absorption, with the greater stress laid on absorption. The essential material is presented in Sections 3, 6, 7, and 8, in which specific methods are described. Section 3 is devoted to scattering calculation techniques, while Sections 6, 7, and 8 cover methods of calculating transmittance. The (Continued)

DD FORM 1 JAN 73 1473 EDITION OF 1 NOV 65 IS OBSOLETE

UNCLASSIFIED

SECURITY CLASSIFICATION OF THIS PAGE (When Data Entered)

20. Continued

first of these is the so-called line-by-line direct integration method, which requires a detailed compilation of the characteristics of individual molecular lines. Some familiar numerical integration techniques are used to effect quadrature in the most convenient and economical way.

The second of the absorption methods of calculation presented is the band-model technique. In this method, the line spectrum is approximated by some mathematically manipulatable distribution function with undetermined band-model parameters. By comparison of calculated results with laboratory experimental data the parameters are defined, and the band-model is used for calculating transmittance under any required meteorological conditions.

The third general set of techniques is given the heading "Multi-Parameter Analytical Procedures." These techniques are derived from the band-model concept incorporating a larger number of parameters, with presumably greater accuracy in the resultant calculations.

The rest of the report is either tutorial or supportive, presenting details of information which is required as input to the calculation procedures. The major input is the meteorology required to describe absorber concentrations, pressures, temperatures, and other necessary physical entities.

An assessment is made of the various techniques of calculation in terms of accuracy, computer time needed to perform calculations, adaptability to specific problems, and practicality.

PREFACE

The IRIA (Infrared Information and Analysis) Center is a Department of Defense information and analysis center operated by the Environmental Research Institute of Michigan (ERIM) under contract to the Office of Naval Research. Its mission is to collect, analyze, and disseminate to authorized recipients information concerning infrared and electro-optical research and development. To this end, the IRIA Center publishes and distributes IRIA Annotated Bibliographies, the Infrared Newsletter, IRIA Data Compilations, the Proceedings of the Infrared Information Symposia (Proc IRIS), the proceedings and/or minutes of the meetings of the six Specialty Groups of IRIS, IRIA State-of-the-Art Reports, and proceedings of the DoD Conferences on Laser Technology. The center serves as a national reference library in military infrared technology, offering assistance and advice to visitors having the appropriate clearances and need-to-know. Special bibliographies and searches are prepared for IRIA-IRIS members upon request.

All IRIA-IRIS publications through 1 February 1971 are available from the Defense Documentation Center (DDC). Since that date, such publications are available only from the IRIA Center on a service charge basis. Membership in IRIA-IRIS is available by annual subscription, and includes receipt of documents as they are published.

Inquiries concerning the annual subscription plan should be directed to:

IRIA Center
Environmental Research Institute of Michigan
P. O. Box 618
Ann Arbor, Michigan 48107
Telephone (313) 483-0500 Ext. 281

Department of Defense Agencies desiring to join IRIA-IRIS should write:

Office of Naval Research
Boston Branch Office
495 Summer St.
Boston, MA 02210

Attn: Mr. T. B. Dowd

FOREWORD

Approximately eight years ago the Environmental Research Institute of Michigan's (ERIM) Infrared Information and Analysis (IRIA) Center supported, under contract to the Navy, an effort to produce a State-of-the-Art Report covering methods of calculating atmospheric transmittance using band-models. In the intervening years many investigators have been busy either in improving band-model methods or producing other techniques for calculating atmospheric transmittance. It was considered appropriate, therefore, to investigate the present state-of-the-art and publish a report describing it.

The result of this investigation is the subject matter contained in this volume. This effort was also supported through IRIA by the U. S. Navy under ONR Contracts N00014-73-A-0321-0002 and N00014-74-C-0285. Technical monitor for the project was Dr. William J. Condell, Director of the Physics Program, Office of Naval Research.

This report goes beyond simply demonstrating methods for calculating transmittance. Since the major work described in many of the efforts cited in the report has been directed toward determining the transfer of radiation in the atmosphere, it was recognized that the state-of-the-art encompasses the whole concept of radiative transfer. No one has yet solved the total problem of radiative transfer, nor do we propose to try to show how it is done here. We have been satisfied to separate the problem into two major categories, that of scattering, and that of absorption; and present an overview of how people are currently trying to achieve results incorporating the most accurate (or most convenient) approximations in the simplest or least costly ways possible.

This report differs, then, from the previous one in two important ways. It covers the entire problem of radiative transfer rather than just transmittance, and it covers techniques which go beyond mere calculation with more-or-less simple band models.

The cut-off period for the material contained in this report is approximately mid-1974.

Because of the assistance they rendered in the compilation of this report, we would like to acknowledge the efforts of Mrs. Grace Teng for attending to many of the details of computation and assembly, and Mrs. Rose Coleman for typing the rough manuscript. We very much appreciate the fact that the manuscript was

Preceding page blank

critically reviewed by Dr. George Zissis, Director of IRIA, and by other recognized experts in the field of radiative transfer outside of our laboratory. For their part in reviewing the manuscript, we wish to thank Dr. S. Roland Drayson of the University of Michigan's Department of Atmospheric and Oceanic Science; Dr. Aharon Goldman of the University of Denver's Department of Physics and Astronomy; and Dr. Benjamin M. Herman of the University of Arizona's Institute of Atmospheric Physics. The responsibility for any discrepancies that have eluded their scrutiny is naturally assumed by the authors.

TABLE OF CONTENTS

1. INTRODUCTION: DESIGN AND USE OF THE REPORT 19
1.1 Purpose and Scope 19
1.2 Overview of Report 19
1.3 Chapter-by-Chapter Reviews 21
1.3.1 Chapter 2. Radiative Transfer Theory 21
1.3.2 Chapter 3. Methods of Calculating Radiative Transfer for Scattering 21
1.3.3 Chapter 4. Theory of Atmospheric Absorption 22
1.3.4 Chapter 5. Generalization of Methods of Calculating Atmospheric Absorption 22
1.3.5 Chapter 6. Details of the Line-by-Line Method of Calculation 23
1.3.6 Chapter 7. Illustrations of Band-Model Methods 25
1.3.7 Chapter 8. Multi-Parameter Analytical Procedures 28
1.3.8 Chapter 9. Laboratory Measurements, Field Measurements and the Results of Calculation for Absorption 29
1.3.9 Chapter 10. Atmospheric Constituents 29
1.4 Some Topics Not Covered in this Report 30
1.5 Use of the Report 30

2. RADIATIVE-TRANSFER THEORY 34
2.1 Introduction 34
2.2 Equation of Radiative Transfer 34
2.3 The Formal Solution 40
2.4 Boundary Conditions 46
2.5 Radiation Components 49

3. METHODS OF CALCULATING RADIATIVE-TRANSFER FOR SCATTERING 54
3.1 Introduction 54
3.2 Exact Solutions 54
3.3 Adaptations to Exact Solutions 57
3.3.1 Iterative Method 57
3.3.2 Spherical Harmonics Method 58
3.3.3 Discrete Ordinates Method 64
3.3.4 Invariant Imbedding 65
3.3.5 Doubling Technique 69
3.3.6 Moment Methods 69
3.3.7 Monte Carlo 70
3.4 Approximate Methods 71
3.4.1 Schuster-Schwarzschild Method 71
3.4.2 Eddington Method 72
3.4.3 Romanova's Method 73
3.4.4 The Turner Method 74

4. THEORY OF ATMOSPHERIC ABSORPTION 85
4.1 Introduction 85
4.2 Radiative Transfer Equation for Molecular Absorption 85
4.3 Description of the Absorption Coefficient 88
4.4 Determination of Transmittance or Absorptance 95
4.5 Determination of Line Parameters 96

4.5.1 Techniques of Benedict and Collaborators 96
4.5.2 Low-Resolution Techniques 109
4.5.3 Laser Methods 110
4.6 Description of the Line Parameters of the Major Absorbers 111
4.6.1 Accumulation of Line Data 111
4.6.2 The AFCRL Compilation 114
4.6.3 Other Absorption Gases and Absorption Mechanisms 141

5. GENERALIZATION OF METHODS OF CALCULATING ATMOSPHERIC ABSORPTION 142
5.1 Line-by-Line Method of Atmospheric Transmittance Calculations 142
5.2 Band Model Methods of Atmospheric Transmittance Calculations 144
5.2.1 Introduction to the Band-Model Concept 144
5.2.2 A Single Lorentz Line 145
5.2.3 Elsasser Model 147
5.2.4 Statistical Band Model 153
5.2.5 Random-Elsasser Band Model 160
5.2.6 Quasi-Random Model 161
5.2.7 Temperature and Frequency Dependence of Band-Model Parameters 163
5.2.8 Determination of Band-Model Parameters 166
5.2.9 The Curtis-Godson Approximation 175

6. DETAILS OF THE LINE-BY-LINE METHOD OF CALCULATION 183
6.1 Justification of the Method: Band Model Limitations 183
6.2 Drayson's Method 184
6.2.1 Preliminary Setup 184
6.2.2 Transmittance Calculation 191
6.3 The Method of Kunde and Maguire 195
6.3.1 Application 195
6.3.2 Transmittance Calculation 196
6.3.3 Setup of the Program 197
6.3.4 Some Results 201
6.4 Kyle's Method 205
6.5 The Method of Scott in Direct Integration 209
6.5.1 Determination of Integration Intervals 211
6.5.2 Simplifications 212
6.5.3 Evaluation of Results 214
6.6 An Intermediate Method of Transmittance Computation 214
6.6.1 Determination of the Distribution Function 214

7. ILLUSTRATIONS OF BAND MODEL METHODS 218
7.1 Statistical Model (Ellingson; Rodgers and Walshaw; Goldman and Kyle) 218
7.1.1 Specification of the Models 219
7.1.2 Scaling the Path Quantities (Ellingson; Rodgers and Walshaw) 222
7.1.3 Model for CH_4 and N_2O (Ellingson) 226
7.1.4 Specialization to High Altitude (Ellingson) 229
7.1.5 Ellingson's 57- and 100-Interval Models 231
7.1.6 Transmittance in the Continuum Region 234
7.1.7 Calculations of Heating Rates (Ellingson; Rodgers and Walshaw) 234
7.2 Use of the Quasi-Random Model (Kunde; Haurwitz) 239
7.3 Other Published Single-Model Computations 271
7.3.1 Method of G. Daniels 271
7.3.2 Method of H. T. Jackson 278
7.4 Aggregate Method 284

7.4.1 Types of Models Used 294
7.4.2 Scattering 302
7.4.3 Recent Techniques in Band Parameter Calculation Suggested for the Aggregate Method 303
7.4.4 Comparisons of Calculated Values and the Values from Field Experimental Data 307
7.5 LOWTRAN 2 Method 308
7.5.1 Method of Development 321
7.5.2 Determination of Absorber Amount 327
7.5.3 Use of the LOWTRAN Method 333
7.5.4 Comparisons of Calculated Values and the Values from Field Experimental Data 339

8. MULTI-PARAMETER ANALYTICAL PROCEDURES 346
8.1 Zachor's Formulation 346
8.1.1 Derivations of Known Models 349
8.1.2 Generalization of Zachor's Formulation 349
8.1.3 Results of Zachor's Method 356
8.2 The Five-Parameter Formulation of Gibson and Pierluissi 356
8.3 Polynomial Representation of Smith 365

9. LABORATORY MEASUREMENTS, FIELD MEASUREMENTS AND THE RESULTS OF CALCULATION FOR ABSORPTION 379
9.1 Laboratory Measurements 379
9.2 Field Measurements 383
9.2.1 Some Examples of Field Measurements 385
9.3 Comparisons of the Calculations 388

10. ATMOSPHERIC CONSTITUENTS 421
10.1 Introductory Remarks 421
10.2 Principal Gases for Absorption 422
10.2.1 Carbon Dioxide (CO_2) 422
10.2.2 Nitrous Oxide (N_2O) 422
10.2.3 Carbon Monoxide (CO) 425
10.2.4 Methane (CH_4) 425
10.2.5 Nitric Acid (HNO_3) 425
10.2.6 Water Vapor (H_2O) 429
10.2.7 Ozone (O_3) 429
10.3 Scattering Constituents 437
10.3.1 Extraterrestrial Radiation 437
10.3.2 Aerosols 441
10.3.3 Scattering Parameters 443
10.3.4 Visibility 456
10.3.5 Particle Distribution to Supplement Band Model Calculations in the IR Spectrum 463

REFERENCES 468
BIBLIOGRAPHY 485
APPENDIX . . . . .
LIST OF SYMBOLS 489

FIGURES

1. Description of Radiance 36
2. Solar Scattering Configuration 42
3. Reflected versus Incident Energy 47
4. Components of the Radiation Field 50
5. Transmitted and Reflected Total Intensity, Percent Polarization 59
6. Measured and Theoretical Transmitted Intensities 59
7. Invariant Imbedding Configuration 67
8. Additive Slab Configuration for Invariant Imbedding 67
9. Normalized Downward Diffuse Irradiance vs Optical Thickness for Various Surface Reflectances 76
10. Planetary Albedo vs Optical Thickness for Various Surface Reflectances . . 78
11. Normalized Path Radiance at the Top of the Atmosphere vs Optical Thickness for Several Surface Reflectances 79
12. Normalized Path Radiance at the Top of the Atmosphere vs Optical Thickness for Various Solar Zenith Angles 81
13. Sky Radiance vs Solar Zenith Angle 82
14. Total Spectral Radiance in the Solar Plane at the Top of a Rayleigh Atmosphere Bounded by a Surface With Lambertian Reflectance ρ 83
15. Turner Radiative Transfer Model 84
16. Transmittance Path Configuration 87
17. Features of a Lorentz Line 90
18. Computational Regions Used for the Voigt Profile 94
19. Spectral Absorptance, $A(\nu)$, and Smoothed Absorptances as Functions of $(\nu - \nu_0)$, the Distance From Line Center 98
20. Spectral Absorptance, $A(\nu)$, and Smoothed Absorptances as Functions of $(\nu - \nu_0)$, the Distance From Line Center 99
21. Spectral Absorptance, $A(\nu)$, and Smoothed Absorptances as Functions of $(\nu - \nu_0)$, the Distance From Line Center 100
22. Examples of the Type of Absorption Spectra of HCl From Which Equivalent Width Measurements Were Made Illustrating Typical Signal-to-Noise Ratios and Resolution Employed 104
23. Plot of W^0 versus Pressure for Lines R(2) of HCl^{35} and HCl^{37} 106
24. Plot of the Ladenburg-Reich Function 106
25. Examples of Curves of Growth for the Lines $|m| = 1$ and ℓ 107
26. Experimental Values of Line Widths per atm (α_{L0}) versus m for the HCl 1-0 Band 108
27. "Infinitely" Resolved Transmittance as a Function of Frequency 143

28. Absorption vs Frequency for a Single Line 146
29. Absorption by a Single Elsasser Band 149
30. Absorption as a Function of $\beta\psi = Sw/d$ for the Elsasser Model 152
31. Absorption as a Function of $\beta\psi = 2\pi\alpha Sw/d^2$ for the Elsasser Model 152
32. Absorption Divided by β as a Function of $\psi = Sw/2\pi\alpha$ for the Elsasser Model 157
33. Absorption as a Function of $\beta\psi = Sw/d$ for the Statistical Model 157
34. Absorption as a Function of $\beta^2\psi = 2\pi\alpha Sw/d^2$ for the Statistical Model . . . 159
35. Absorption Divided by β as a Function of $\psi = Sw/2\pi\alpha$ for the Statistical Model 159
36. Weak-Line Approximation to the Elsasser Model 170
37. Strong-Line Approximation to the Elsasser Model 170
38. Nonoverlapping-Line Approximation to the Elsasser Model 170
39. Working Graph for Estimating S/d 171
40. Working Graph for Estimating $2\pi\alpha_{L0}S/d^2$ 71
41. Working Graph for Estimating $2\pi\alpha_{L0}/d$ and $S/2\pi\alpha_{L0}$ 171
42. Optical Depths for a Layer in a Mixed Atmosphere With $P_1 = 3P_2$ 178
43. The Error, $\delta_x = \tau_x$ (Exact) - τ_x (Approximate), in the Optical Depth for a Lorentz Line for Several Approximations to the Pressure Integral, as a Function of the Reduced Frequency $x - x_0$ Relative to the Line Center 182
44. Schematic of Variable Wave Number Mesh for 0.1 cm^{-1} Interval With Two Sub-Intervals in d_1 200
45. Homogeneous Path Comparison for 667 cm^{-1} CO_2 Band at Room Temperature 202
46. Homogeneous Path Comparison for 1595 cm^{-1} H_2O Band at Room Temperature 203
47. Homogeneous Path Comparison for 701 cm^{-1} O_3 Band at Room Temperature 204
48. Water Vapor Continuum Absorption Coefficient for the 600-1400 cm^{-1} Region 205
49. Illustration of Two Integration Nets, With $\Delta = 0$, and $\Delta \neq 0$ 208
50. Error of Integrated Absorptance of a Lorentz Line for the Step Sizes, D/α_L 208
51. Maximum Integrated Absorptance Error as a Function of Step Size 208
52. Error of Integrated Absorption of an Atmospheric Line for the Step Sizes, D/α_L 210
53. Error of Integrated Absorptance of a Doppler Line for the Step Sizes, D/α_L 210
54. Schematic Comparison of the Integration Step $\delta\nu$ and of the Representation Step $\Delta\nu(z)$ in Two Different Layers of the Atmosphere . . 213
55. Schematic for Determining the Distribution Function, h(K) 217

56. The k-Distribution Function for the Portion of the CO_2 15 μm Band From 675 to 715 cm^{-1} at a Temperature of 250 K and Pressures of 1, 0.1, and 0.01 atm 217

57. Comparison of Absorption Spectrum Obtained by Line-by-Line Calculation, Curve 1, and by Statistical Model Calculation, Curve 2, for the 9.6 μm Ozone Band for $\Delta\nu$ = 1.6 cm^{-1} 220

58. Comparison of Absorption Spectrum Obtained by Line-by-Line Calculation, Curves 1, and by the Statistical Model Calculation, Curves 2, for the 9.6 μm Ozone Band for $\Delta\nu$ = 2.5 cm^{-1} 221

59. Comparison of Transmittance Obtained by Statistical Model with Exponential Intensity Distribution, Curves 1, and with Exponential-Tailed S^{-1} Intensity Distribution, Curves 2. 221

60. Comparison of Transmittance Obtained by Line-by-Line Calculation, Curve 1, and by Statistical Model Calculation, Curve 2, for the 2.7 μm H_2O Band for $\Delta\nu$ = 8 cm^{-1} 223

61. The Temperature Dependence of ϕ and χ for Some Intervals in the 6.3 μm Water Vapor Band 225

62. The Temperature Dependence of ϕ and χ for Some Intervals in the 9.6 μm Ozone Band 227

63. The Temperature Dependence of ϕ and χ for Some Intervals in the 1.5 μm Carbon Dioxide Band 228

64. The IRIS Observed and 100-Interval Model Calculated Spectrally Averaged Specific Intensities 241

65. Absorptance of 2.7 μm H_2O Band. 260

66. Absorptance of 6.3 μm Band 261

67. Comparison of Theoretical Results with the Experimental Measurements of Burch, Gryvnak and Williams 262

68. Calculated and Experimental Transmissivities vs Frequency for Different Pressures and Optical Masses 267

69. Density Profiles of Atmospheric Constituents for Model Atmosphere Used in Calculations. 276

70. Approximation of Doppler Profile at High Altitudes by Lorentz Profile. . . 279

71. Methane Transmittance in 7.7 μm Band at a Pressure Where Doppler Broadening Dominates Line Shape 280

72. S/d versus Wave Number with Temperature as a Parameter 283

73. S/d versus Temperature with Wave Number as a Parameter 285

74. $S^{1/2}/d$ versus Wave Number with Temperature as a Parameter 286

75. $S^{1/2}/d$ versus Temperature with Wave Number as a Parameter 287

76. Schematic of Optical Path for Transmission and Radiance Calculations . . 293

77. Comparison of Spectra 305

78. Comparison Between Transmittances Calculated by the Aggregate Method and the Experimental Data of Yates and Taylor (1960) 309

79. Comparison Between Transmittances Calculated by the Aggregate Method and the Experimental Data of Taylor and Yates (1957) 310

80. Comparison Between Transmittances Calculated by the Aggregate Method and the Experimental Data of Taylor and Yates (1957) 313
81. Comparison Between Transmittances Calculated by the Aggregate Method and the Experimental Data of Streete (1968) 316
82. Comparison Between Transmittance Calculated by the Aggregate Method and the Experimental Data of Ashley (Private Communication) 318
83. Schematic of the Plot of Data for Calculating LOWTRAN Parameters, $\bar{\tau}_{\Delta\nu}(\nu)$ versus log w 324
84. Schematic Composite of Adjusted Data, $\bar{\tau}_{\Delta\nu}(\nu)$ versus log w P^n 324
85. Prediction Chart for Water Vapor Transmittance 325
86. Example Showing the Development of Transmittance Functions for Ozone and the Uniformly Mixed Gases 326
87. Equivalent Sea Level Path Length of Water Vapor as a Function of Altitude for Vertical Atmospheric Paths 328
88. Equivalent Sea Level Path Length of Uniformly Mixed Gases as a Function of Altitude for Vertical Atmospheric Paths 331
89. Transmission vs Wavelength for Water Vapor 334
90. Transmission vs Wavelength for Carbon Dioxide 336
91. Transmission vs Wavelength for Ozone and Nitrous Oxide 338
92. Comparison of LOWTRAN 2 Radiance Calculation with Nimbus Data . . . 340
93. Comparison of LOWTRAN 2 Predictions with Measurements 341
94. Atmospheric Transmittance for a 1.9 km Path at 5.2 km Altitude 342
95. Atmospheric Transmittance, 10,679 ft (3.25 km) Path at Sea Level 343
96. Atmospheric Transmittance, Calculated and Measured 345
97. A Plot of log (A) Against log (wP) for a Typical Laboratory Run or Absorption Band Model 348
98. A Comparison of τ (Solid Curves) and τ^* (Dots) 350
99. A Plot of the Strong-Line Transmission Function Proposed by King (1964) 354
100. Transmittance Spectra Computed From Table 50 (Crosses) and From Burch, Gryvnak and Patty (1964) (Solid Curves) 361
101. Measured (——) and Calculated (-0-) Transmittance for CO_2 Band 364
102. Comparison Between Experimental (Burch et al., 1962) and Calculated (Drayson and Young, 1966) Transmittance Spectra for CO_2 and Transmittance Spectra Derived From the Empirical Transmittance Coefficients Given in Table 54 375
103. Comparison Between Observed (via Balloon-Borne Interferometer) and Calculated (via Empirical Transmittance Coefficients) Upward Radiance Spectra Near Palestine, Texas 376
104. Comparison Between Transmittance Spectra for H_2O Calculated by Bolle and Transmittance Spectra Calculated From the Empirical Transmittance Coefficients Given in Table 53 377

105. Atmospheric Transmission 386
106. Atmospheric Transmission Spectra 387
107. Atmospheric Transmission Measurements From 57 to 1300 Meters in the 2-5 μm Region 389
108. Atmospheric Transmission Measurements From 57 to 1300 Meters in the 4-14 μm Region 390
109. Transmission Measurements of the Atmosphere at Desert and Sea Coast Locations 391
110. High Resolution Transmission Measurement of the Atmosphere for Path Lengths of 161 feet and 39,000 feet 392
111. Atmospheric Transmission 393
112. Transmittance for Aggregate Model Atmosphere in the 8-14 μm Region for a Vertical Path Looking Down From 100 km 394
113. Transmittance for a Vertical Path Looking Down From 100 km 395
114. Transmittance for a Vertical Path Looking Down From 100 km 397
115. Transmittance for a Vertical Path Looking Down From 100 km 399
116. Transmittance for a Vertical Path Looking Down From 100 km 401
117. Transmittance for a Vertical Path Looking Down From 100 km 403
118. LOWTRAN 2 Spectral Radiance for Six Model Atmospheres 406
119. Nimbus IV (IRIS) Satellite Data 407
120. Comparison Between Radiance for Calculation by the Aggregate Method and Observed Nimbus IV Satellite Data 413
121. Aggregate Model Atmosphere (Temperate Winter) for a Vertical Path Looking Down From 100 km 415
122. Aggregate Model Atmosphere (Tropic) for a Vertical Path Looking Down From 100 km 416
123. Aggregate Model Atmosphere (Arctic Summer) for a Vertical Path Looking Down From 100 km 417
124. Aggregate Model Atmosphere (Arctic Winter) for a Vertical Path Looking Down From 100 km 418
125. The 400 to 1000 cm^{-1} Portion of the Nimbus Spectrum 420
126. Model Atmospheres—Nitric Acid Mixing Ratio 427
127. Distribution of HNO_3 with Altitude as Determined From Atmospheric Emission Data 428
128. Model Atmospheres—Water Vapor Mixing Ratio 435
129. Mixing Ratio of Water Vapor as Derived From a 15-Layer and a 10-Layer Calculation Using the 25 μm Line Group for the 22 February 1971 Balloon Flight 436
130. Model Atmospheres—Ozone Mixing Ratio 438
131. Average and Extreme Range of Vertical Ozone Distribution Data 439
132. Spectral Solar Irradiance 440

133. The Refractive Index of Various Aerosols as a Function of Wavelength . . .444
134. Haze-Type Distribution Functions 449
135. Summary of Size Distribution Measurements Over the North Atlantic . . .450
136. Some of the Data From Figure 135, but Separated Into Days with and Without Sahara Dust to Demonstrate the Distribution of the Mineral Dust Component 451
137. Idealized Diagram of the Various Components of the Undisturbed Marine Aerosol 452
138. Angular Dependence of Single-Scattering Phase Functions in Any Azimuthal Plane 456
139. Comparison of Deirmendjian's Phase Functions at Different Wavelengths for Water Haze L 457
140. Henyey-Greenstein Phase Function for Different Values of the Anisotropy Parameter η 458
141. Comparison of Deirmendjian's Phase Function for Water Haze L at λ = 0.45 μm and the Henyey-Greenstein Phase Function with Anisotropy Parameter η = 0.9493 459
142. Variation of Visual Range with Extinction Coefficient 461
143. Optical Depth versus Visual Range and Altitude 462
144. Maritime Haze Water Droplet Distribution 464
145. Aerosol Number Density versus Altitude 464
146. Normalized Particle Size Distribution for Aerosol Models 465
A-1. Parameters Defining Geometry of Slant Path 492
A-2. Schematic Diagram of Atmospheric Refracted Path 493
A-3. Geometrical Path Configurations 495

TABLES

1. Radiative-Transfer-Atmospheric Model Rating (Scattering) 33
2. Atmospheric Absorption Method Rating 33
3. Net Fluxes for a Mie Atmosphere of One Optical Thickness 63
4. Storage Requirements for Double Precision 63
5. Examples to Indicate the Independence of Equivalent Width Upon Spectral Slit Width 101
6. Examples of Typical Wing Corrections in Equivalent Width Measurements 103
7. Isotopic Abundances 115
8. Vibrational Energy Levels and Molecular Constants for CO_2 118
9. Band Origins and Strengths for CO_2 120
10. Vibrational Energy Levels and Molecular Constants for N_2O 124
11. Summary of N_2O Band Systems 128
12. N_2O Band Strengths 130
13. Rotational Constants Used in the Calculation of CO Line Positions 133
14. Strengths of CO Bands 133
15. Summary of Principal Data Sources for Water-Vapor Energy Levels . . .136
16. Water Vapor Band Strength Data 138
17. Ozone Transitions Included in Data Compilation 139
18. Methane Bands Included in Data Compilation 140
19. Regions of Validity of Various Approximations for Band Absorption. . . .150
20. Summary of Closed-Form Expressions for Spectral Absorption 164
21. Polynomial Coefficients for the Approximation of $E_2(x)$ 187
22. Polynomial Coefficients for the Approximation of $E_3(x)$ 188
23. Polynomial Coefficients for the Approximation of $E_4(x)$ 189
24. Band Strengths Used in Calculating Rotational Line Intensities 190
25. Relative Abundance of Isotopic Molecules. 190
26. Summary of Parameters Necessary to Calculate Approximate Corrections of the Transmission Function for Doppler Effects 232
27. Approximate Correction Factors for the Random Exponential Band Model for Doppler Effects. 232
28. Widths of Spectral Intervals for the 57-Interval Model 232
29. Fine-Scale Division of the 15 μm Carbon Dioxide Bands From 600 to 800 cm^{-1} 233
30. Spectral Intervals Used for Water Vapor in the 600 to 800 cm^{-1} Region. 233

31. Fine-Scale Divisions of the Spectrum Between 1000 and 1180 cm^{-1} 235
32. A Comparison of the Spectral Characteristics of the Rodgers and Walshaw (1966) and 100-Interval Models 235
33. The Spacings of the Levels of Computation in the Radiative Transfer Model 240
34. Percent Differences Between Observed and Calculated Upward Intensities for the Five Comparisons 246
35. Some Statistics on the Observed and Calculated Upward Intensities 247
36. Average Transmittance at Center and Boundary of Subinterval δ 251
37. Homogeneous Paths for Which Transmission Data are Tabulated 253
38. Quasi-Random Transmittance for Lorentz Line Shape and for Mixed Line Shape 259
39. Comparison of Quasi-Random and Experimental Integrated Absorptances for the 6.3 μm H_2O Band 265
40. Comparison of Quasi-Random and Experimental Integrated Absorptances for the 15 μm CO_2 Band 266
41. Percentage Differences Between Theoretical and Experimental Total Absorptions for the 6.3 μm Water Vapor Band Relative to the Experimental Values 272
42. Percentage Differences Between Theoretical and Experimental Values of Fractional and Total Absorptions for the 15 μm Carbon Dioxide Band Relative to the Experimental Values 272
43. Percentage Contributions to the Overall Water Vapor Cooling Rates From Each of the Nine Subintervals 273
44. Mixing Ratio for "Wet" Stratosphere Model 274
45. Reference Half-Widths (223 K, 760 MM HG) and Line Shape Freezing Altitudes, z_1 281
46. The Spectral Band Parameter S/d as a Function of Temperature 288
47. The Spectral Band Parameter (S 1/2)/d as a Function of Temperature . . . 290
48. Summary of Band Models Used in Computer Program 295
49. Transmittance Parameters for CO_2 Between 4590.2 and 5346.0 cm^{-1} 357
50. Transmittance Parameters and Statistics for CO_2 at 298 K Averaged Over 5-cm^{-1} Intervals 363
51. Pressures, Temperatures, and Path Lengths of Tabulated Transmittance Data 368
52. Empirical Absorption Coefficients for Water Vapor 369
53. Empirical Absorption Coefficients for Carbon Dioxide 372
54. Comparison of Experimental and Empirical Transmittances 374
55. Summary of Laboratory Measurements of Homogeneous-Path Absorption Spectra 380
56. Summary of Laboratory Transmittance Measurements 381
57. Summary of Atmospheric Transmission Field Measurements 384

58. Concentrations of Carbon Dioxide 423
59. Concentrations of Uniformly Mixed Gases 423
60. Concentration of Nitrous Oxide 424
61. Concentration of Carbon Monoxide 426
62. Model Atmospheres Used as a Basis of the Computation of Atmospheric Optical Properties 430
63. Some Important Sources of Atmospheric Aerosols 442
64. Size Distribution of Aerosol Particles 446
65. Aerosol Models: Vertical Distribution for a "Clear" and "Hazy" Atmosphere 466

ATMOSPHERIC TRANSMITTANCE AND RADIANCE: METHODS OF CALCULATIONS

1 INTRODUCTION - DESIGN AND USE OF THE REPORT

1.1 PURPOSE AND SCOPE

This report has three major objectives: (1) to bring current awareness of the various techniques for calculating atmospheric transmittance and atmospheric radiance up to date; (2) to assist the designer of military systems in studies of systems effectiveness; and (3) by assembling a variety of calculation techniques and auxiliary information, to make a report generally useful in the comparison and assessment of such methods by anyone seeking atmospheric transmittance and radiance calculations.

It was not intended that the user be able to make calculations directly from the material in the report. Although to do so would be very useful, a far greater, and obviously infeasible, effort would have been required than was expended in the construction of this report. Most of the methods covered require the use of complicated programs, some of which are not universally available, and would, in addition, probably not be too useful without consultation or extensive documentation from the originator. On the other hand, we would hope that it is possible, on the basis of the material presented here, for the user to choose the technique best suited to his needs and resources, and make whatever arrangements are needed to perform a successful calculation. We do not presume, furthermore, to present complete information covering the complex field of radiative transfer. This would certainly take the report beyond its scope, which is to review the state-of-the-art of methods of calculating atmospheric transmittance and radiance.

1.2 OVERVIEW OF REPORT

Early in 1967, IRIA published its first state-of-the-art report covering atmospheric phenomena [1]. Since then the activity in this field has been considerable; sufficiently so that the early report no longer describes the state-of-the-art. It is considered timely, therefore, to update the old report which has served a very useful purpose over this span of eight years. Because of the scope of activity in this field, this requires, however, more than just a substitution of new data for old. For example, whereas the old report concentrated exclusively on the calculation of molecular absorption through the use of band models, we now also consider the radiative properties of the atmosphere. These are important to the

1. D. Anding, Band Model Methods for Computing Atmospheric Slant-Path Molecular Absorption, Rept. No. 7142-21-T, Willow Run Laboratories of the Institute of Science and Technology, University of Michigan, Ann Arbor, 1967.

field experimenter in the discrimination between signals from discrete radiators and the atmospheric background, and to the meteorologist in studies of radiative transfer. This report also includes the effect of particles in the atmosphere, both in their effect on simple extinction of radiation and in multiple scattering.

To distinguish further between this and the original report, the total dependence on band models for atmospheric absorption has been rendered needless because the old arguments for avoiding molecular line-by-line calculations now have less validity. One reason is that high-speed calculations can be done more cheaply than before since they can be performed more efficiently with modern hardware and software. Many investigators have developed elaborate programs for making such calculations. Another reason is that more and better data are available on line parameters, and more confidence, therefore, can be placed in their use. By no means, however, have band models been discarded, and they remain the best methods by which calculations can be made where cost and time are inportant and some accuracy can be compromised.

Persons with experience in the field of atmospheric phenomena will notice that we have virtually avoided the huge mass of European and other foreign literature in assembling this report. Unfortunately this represents a significant void, especially from the standpoint of the Russian and Japanese work in this area. Limitations on time and resources, however, prevented broadening the scope of the effort to include these valuable additions. The reader is referred to the various international conferences, such as the one recently held at the University of California [2].

Because of the traditional approaches to the study of these atmospheric radiation mechanisms, they have come to be more-or-less associated with different spectral regions; absorption is generally assigned to the infrared, and scattering to the visible, with some degree of overlap in the near-infrared region. This disassociation is retained in the report, and is manifest essentially in the separation of the report into two parts, one devoted to molecular absorption, the other to multiple scattering. However, those models which treat single scattering as just another extinction mechanism to supplement molecular absorption, retain their integrity.

This report follows the pattern of the previous state-of-the-art report. Each model is presented in as much detail as is needed to describe it amply without overburdening the report. It is impossible, in attempting to cover a field that is moving so rapidly and that cuts

2. J. G. Kuriyan (ed.), The UCLA International Conference on Radiation and Remote Probing of the Atmosphere, UCLA, Los Angeles, August 1973.

across so many disciplines, not to have omitted, in some cases, important information*. Rectifications for such omissions can be made in future up-dating of the state-of-knowledge.

1.3 SECTION-BY-SECTION REVIEWS

1.3.1 SECTION 2. RADIATIVE TRANSFER THEORY

This section is devoted to a treatment of the general equation of radiative transfer. The emphasis in describing the set-up of the equation is toward scattering, because the greatest complexity in the solution of the equation is in its scattering phase. Indeed, the foremost facet in the solution of the radiative transfer equation is its geometrical complexity, which tests the ingenuity of the investigator in attempting to derive cost-saving methods of computation which retain an acceptable degree of accuracy.

The tutorial approach to Section 2 was intended to help the uninitiated user to become sufficiently based in understanding of the essential theory and nomenclature to help him understand more thoroughly the relatively complex ideas to be presented in later sections.

1.3.2 SECTION 3. METHODS OF CALCULATING RADIATIVE TRANSFER FOR SCATTERING

Certainly many man-hours of effort have been spent in recent years on the development of various computational methods for the solution of radiative-transfer problems. In spite of all this work, however, there remain many "unsolved" problems. They are unsolved in the sense that: (1) an exact mathematical solution may not exist; (2) the computation time is so long that a reasonably accurate solution is not feasible; or (3) the mathematical formulation of the problem has not been sufficiently developed. Our interest here is not so much in the specification and analysis of theoretical models of radiative transfer per se, but rather in the description of reasonable computation methods which can be used in the development of or use of a comprehensive atmospheric radiative-transfer model.

*To get some idea of the scope of this subject one need only refer to the bibliography of Howard and Garing [3], with approximately 750 entries covering only about three years work, and that of Laulainen [4] with over 1300 entries covering a 30-year period [5].

3. J. N. Howard and J. Garing, "Atmospheric Optics and Radiative Transfer," EOS, Vol. 52, No. 6, IUGG 371, June 1971.

4. N. Laulainen, Project ASTRA, Astronomical and Space Techniques for Research on the Atmosphere, ASTRA Publication No. 18, University of Washington, Seattle, 1972.

5. N. Laulainen, "Bibliography of the Spectra of Atmospheric Minor Gases," Appl. Opt., Vol. 12, No. 3, 1973, p. 617.

The computation methods reviewed are as follows:

1. exact solutions
2. iterative method
3. spherical harmonics method
4. discrete ordinates method
5. invariant imbedding technique
6. doubling technique
7. moment methods
8. Monte Carlo method
9. Schuster-Schwarzchild method
10. Eddington's method
11. Romanova's method
12. Turner's method.

The format in presenting scattering methods is thus somewhat different from that for absorption, in that the goal in the absorption methods is actually to produce transmittance and radiance models, in addition to reviewing the mathematical techniques.

1.3.3 SECTION 4. THEORY OF ATMOSPHERIC ABSORPTION

After reviewing the radiative transfer equation, we discuss the formal solution, showing that the important part is integration over wavelength or frequency, inasmuch as the very large spectral variation in the absorption coefficient requires the use of numerical methods. This presents a different format than for scattering, for which the spectral variation is small. A description of the major absorbers is given along with some of the mechanisms for absorption. The Air Force Cambridge Research Laboratories (AFCRL) Compilation of line parameters is discussed in this section.

1.3.4 SECTION 5. GENERALIZATION OF METHODS OF CALCULATING ATMOSPHERIC ABSORPTION

The two general methods of numerically integrating within finite spectral intervals are the so-called line-by-line, direct integration method, and the category of what are generally known as band models. As stated earlier in this section, the aversion to the line-by-line method no longer exists except that computing costs can sometimes be excessive. As far as band-models are concerned, this section devotes attention mainly to the more-or-less "classical" models, or adaptations from them. Much of what has been available in the literature for some time is presented here. We show also some of the more recently reported methods for deriving band-model parameters, especially using line parameters as compiled, for example, by AFCRL.

Because the parameters derived for band-model calculations are usually pertinent to the homogeneous atmosphere, and because slant-path calculations involving inhomogeneous

atmospheres are more interesting than horizontal-path calculations, methods are derived to use homogeneous data in non-homogeneous cases. The Curtis-Godson approximation is discussed and certain critiques of it are given.

1.3.5 SECTION 6. DETAILS OF THE LINE-BY-LINE METHOD OF CALCULATION

Using a compilation of line parameters and the appropriate equations relating these parameters to the absorption coefficient, one could, with a simple trapezoidal-rule (or more accurately, Simpson-rule integration), reproduce the line structure of molecules and calculate the spectral transmittance for known atmospheric paths. The cost, however, would be large. Methods have been devised to take advantage of the peculiarities in the line structure and perform a direct integration at lower cost. Nevertheless, the cost of calculating by the direct method is still very high in comparison with the use of band-models methods.

Some of the methods, namely those of Kyle [6] and Scott [7], use a constant spacing of points on the abscissa for the integration interval, but achieve an efficient calculation by optimizing the size of the spacing. In this way, they are able to obtain a reasonable accuracy while limiting, to some extent, the computation time. In Kyle's method, the region near the line center can be accomodated with a relatively coarse mesh, but, as mentioned by Gille (in Kuriyan, 1973), the disadvantage is in requiring a relatively fine mesh for the line wings, where coarser meshes can be accommodated.

In Scott's method the mesh size for integration is determined by the half-width of the line. But since the half-width varies with altitude, the mesh size varies also with altitude. The smallest mesh size is determined by the half-width at the highest altitude used in the calculation.

Checking the accuracy of these different methods would require making independent calculations, deemed infeasible in this study, even if the programs were available. Availability can be ascertained only by contacting the authors, which was not done for this report in these cases. The major feature of these methods seems to be speed of computation, although in Kyle's case it is not obvious that this is always achieved. No assessment of Scott's technique has been made except that presented in Section 6 from Scott's paper.

---

6. T. G. Kyle, "Net Interval for Calculating Absorption Spectra," J. Opt. Soc. Am., Vol. 58, No. 2, 1968(c), pp. 192-195.

7. N. A. Scott, "A Direct Method of Computation of the Transmission Function of an Inhomogeneous Gaseous Medium, I: Description of the Method," J. Quant. Spec. Rad. Trans., Vol. 14, 1974, pp. 691-704.

The Drayson technique [8] and the Kunde and Maguire technique [9], which is patterned after Drayson's, do not shift the constant mesh, as does Kyle, but use a variable width of intervals. In this way, they can compute with high resolution at the line centers and coarser resolution away from the centers of lines. This technique optimizes quadrature, evaluating the absorption coefficient at the fewest number of wavenumbers by using Gaussian quadrature. Very high fidelity can be achieved if the quadrature intervals are spaced closely; however, ~1% can be achieved by making the intervals coarser. At the same time this allows the program to run faster.

The availability of the Drayson and Kunde-Maguire programs is not known, although they were made available to IPIA. We have not used the Kunde-Maguire program, nor have we discussed its use with the originators. We have used the Drayson program, but only with close consultation with Drayson. It is likely that anyone applying this program to an atmospheric problem would require the same, unless Drayson publishes it along with extensive documentation.

Drayson alleges (in a private communication) that an "independent check with Kunde shows a maximum error in transmittance of about 0.0001 using the most accurate options in the program. It may be made faster (but somewhat less accurate) by using lower order quadrature or larger intervals." We have used Drayson's program on an IBM 360 computer and found that, as a very rough rule of thumb, the cost of computing, in the calculations we made with a low-order quadrature, was perhaps in excess of $0.15 per spectral line. (Caution, however; this number could be considerably different,up or down.) We would expect that the computing time of the Kunde-Maguire program is at least comparable. One has the option in Drayson's program of ignoring weak lines, but it is obvious that, in the Q-branches of bands where the lines number in the thousands, the cost of a direct integration can be considerable. You pay a stiff price for accuracy, and in many cases there is no other choice, because band-models simply cannot reproduce actual conditions as well as line-by-line calculations.

None of the line-by-line methods are able to account adequately for absorption in the so-called continuum regions of the spectrum. Therefore, the effect of the continuum (especially H_2O) must be accounted for empirically, as with band models.

Arking and Grossman [10], following an earlier precedent, have described a technique for avoiding a direct line-by-line integration without resorting to the usual band-model

8. S. R. Drayson, The Calculation of Long-Wave Radiative Transfer in Planetary Atmospheres, Report No. 07584-1-T, University of Michigan, Ann Arbor, 1967.

9. V. G. Kunde and W. C. McGuire, "Direct Integration Transmittance Model," J. Quant. Spect. Rad. Transf., Vol. 14, 1974, p. 803.

10. A. Arking and K. Grossman, "The Influence of Line Shape and Band Structure on Temperatures in Planetary Atmosphere," J. Atmos. Sci., Vol. 29, 1972, pp. 937-949.

methods. The technique of substituting an absorption coefficient distribution (k-distribution) for the actual ordering of spectral lines is described in this section, giving some simple distributions related to relatively unrealistic-models, but also to some actual line data. A serious restriction of this method is that the atmosphere must be homogeneous. Gille (in Kuriyan, 1973) points out that in a given real band, the distribution forms a "histogram of absorption coefficients," and that the transmittance is calculated from

$$\tau(w) = \sum_{i=1}^{N} b_i e^{-k_i w}$$

where $\sum_{i=1}^{N} b_i = 1$, and b_i and k_i are functions of the conditions in the homogeneous layer.

1.3.6 SECTION 7. ILLUSTRATIONS OF BAND-MODEL METHODS

As band-model techniques were presented in the former state-of-the-art report [Anding, 1967], the methods of various investigators are described in Section 7. These methods all depend directly on the use of one of the original band models described in Section 5, or adaptations from them, in one way or another. The methods included are:

Statistical Model - Ellingson; Rodgers and Walshaw; Goldman and Kyle

Quasi-Random Model - Kunde; Haurwitz

Other published Single-Model Computations - Daniels; Jackson

Aggregate Method - Anding, Rose, Walker

LOWTRAN 2 Method - AFCRL/McClatchey, Selby, et al.

The statistical model calculation methods of Ellingson [11], Rodgers and Walshaw [12] (after whom Ellingson patterned his approach), and Goldman and Kyle, are straightforward applications of the "classical" models. The importance of their contributions to the state-of-the-art lies mainly in the explicitness with which the techniques are described, and the detail in which the line parameters were applied. We should expect that the results represent accuracies limited only by the basic limitations in band-model methods and the atmospheric data used in the calculation. All of the methods are adequately explained in the original papers, and with a reasonable thoroughness in this section. It would not be a simple matter to apply these methods directly to an individual's problem, because the computation techniques are generally unavailable in the publications, and, except for a few small spectral

11. R. G. Ellingson, A New Long-Wave Radiative Transfer Model: Calibration and Application to the Tropical Atmosphere, Report No. 72-4, Florida State University, Tallahassee, 1972.

12. C. D. Rodgers and C. D. Walshaw, "The Computation of Infrared Cooling Rate in Planetary Atmospheres," Qrtly. J. Royal Meteor. Soc., Vol. 92, 1966, pp. 67-92.

intervals, few band-model parameters are included. It is the absence of the latter, however, which is the more serious, since programming the equations should be no difficult matter, although perhaps tedious. Anyone seriously interested in performing atmospheric transmittance and radiance calculations should be familiar with these techniques, notwithstanding the absence of some peripheral material.

The quasi-random method of Kunde [13] and of Haurwitz [14] are direct applications of the methods advanced in the work of Wyatt, Stull and Plass [15] and Stull, Wyatt and Plass [16]. Kunde includes a program in his report for the computation of H_2O vapor transmittance. The program can be obtained by consulting the original work [13].

Quasi-random techniques have not received the serious consideration in the literature that they perhaps deserve. Given a set of line parameters from which to calculate band-model data, it seems that one has unlimited potential for performing calculations with reasonable accuracy and a range of spectral resolutions suited to his own taste. But since the cost vs accuracy tradeoff often resides at one of the two extremes, the quasi-random model is usually neglected.

The methods of Daniels and Jackson are presented because they also represent contributions to the state-of-the-art. The computer program generated by Daniels [17] has not been openly published although it may be available from the originator. Jackson's work has limited accessibility because it is described in a report with limited distribution. Daniel's method has been described, however, in one of the trade journals [18], and is accessible, therefore, in principle, at least through a description of the method used.

The last two methods presented in Section 7, the Aggregate method and the LOWTRAN 2 method are the two models, to our knowledge, which have complete, or nearly complete, availability and accessibility. The Aggregate method is described in an Aerospace Corporation

13. V. G. Kunde, Theoretical Computations of the Outgoing Infrared Radiance from a Planetary Atmosphere, NASA Report No. TN-D-4045, Goddard Space Flight Center, Greenbelt, Md., 1967(b).

14. F. D. Haurwitz, The Distribution of Tropospheric Infrared Radiative Fluxes and Associated Radiative Fluxes and Associated Heating and Cooling Rates in the Southern Hemisphere, University of Michigan, Ann Arbor, 1972.

15. P. J. Wyatt, V. R. Stull and G. N. Plass, Infrared Transmission Studies, Vol. 2: The Infrared Absorption of Water Vapor, Report No. SSD-TDR-62-127-Vol. 2., Ford Motor Company, 1962(a).

16. V. R. Stull, P. J. Wyatt and G. N. Plass, Infrared Transmission Studies, Vol. 3: The Infrared Absorption of Carbon Dioxide, Report No. SSD-TDR-62-127-Vol. 3, Ford Motor Company, 1963.

17. G. Daniels, AVCO Everett Research Laboratory private communication, 1973.

18. G. Daniels, "A Computer Program for Atmospheric Infrared Transmission and Background Calculations," Optical Engr., Vol. 13, No. 2, 1974, pp. 92-97.

report by Hamilton, Rowe and Anding [19], and a synopsis of the method is contained in this report in Section 7.4. The Aggregate method was so named because it is a compilation of the various models, or adaptations of them, which were explained in the IRIA 1967 state-of-the-art report. The compilation was later formulated in a computer program by Anding, Rose and Walker at the Environmental Research Institute of Michigan (ERIM).

There is sufficient coverage of various models in the Aggregate method to make it a reasonably accurate technique for calculation, certainly within 20% of reality except under severe conditions; but hardly better than a few, say 5%, under optimum conditions. These same statistics hold for LOWTRAN 2, which is perhaps no more than one should expect to achieve, considering the poor availability of reliable atmospheric environmental data which are essential inputs to either method. The Aggregate method suffers from a minor drawback, the fact that the spectral resolution inherent in the result is not consistent with what is achievable with even moderately good spectral instruments. Furthermore, the results vary from relatively good resolution, approximately 1 cm^{-1}, to values of the order of 100's of cm^{-1}. The cost of running a spectrum in transmittance and radiance is attractive, as is the case with LOWTRAN 2, being on the order of $5.00 to cover the range to 30 μm. The spectral resolution, for LOWTRAN 2 is a constant 20 cm^{-1}.

LOWTRAN 2 differs from the Aggregate method in a rather basic way. It is a completely empirical method, being derived from no particular formal model, but based on the fit of an empirical formula to experimental data and data calculated from the AFCRL compilation of line parameters. Since a single, empirically derived, function is expected to perform the work of the many different functions in the Aggregate method, LOWTRAN 2 is much neater and more easily manageable; but it seems not as adaptable to changes in atmospheric constituents, and is, therefore, more subject to error. However, in view of the usually poor knowledge we have of meteorological conditions for a given circumstance, we are not necessarily seriously hampered by a minor lack of accuracy in the band model. Thus, there seems from these considerations, to be a toss-up in choice between the Aggregate and the LOWTRAN 2 methods.

From the point of view of availability and accessibility, LOWTRAN 2 seems to edge out the Aggregate. LOWTRAN 2 is available in a card deck which can be obtained from Air Force Cambridge Laboratories. The report issued to explain the use of LOWTRAN 2 [20] has adequate documentation so that the use of the program on the cards is easy. Furthermore,

19. J. N. Hamilton, J. A. Rowe and D. Anding, Atmospheric Transmission and Emission Program, Report No. TOR-0073(3050-02)-3, Aerospace Corporation, 1973.

20. J. Selby and R. M. McClatchey, Atmospheric Transmittance from 0.25 to 2.85μm: Computer Code LOWTRAN 2, Report No. AFCRL-72-0745, Air Force Cambridge Research Laboratories, Bedford, Mass., 1972.

the method is graphically represented in another report [21] which makes it easy to perform spot-check spectral transmittances in a very short time.

The program for the Aggregate method is obtainable from ERIM, and elsewhere, but at present the documentation is not explicitly described as for LOWTRAN 2. Neither method is easily adaptable to atmospheric parameters aside from the ones provided in tne five atmospheric models given in Section 10.

1.3.7 SECTION 8. MULTI-PARAMETER ANALYTICAL PROCEDURES

The calculation methods presented in this section are based on functions which incorporate a larger number of parameters than the band models described in Section 7. We have found only a few documented methods which fit into this category, but it seems apparent that the large number of feasible variations is limitless, if perhaps needless. As is the case in the rest of the report, the methods presented in this section are representative, since it would be impossible to present every technique created, even if they could all be found. We did not attempt to include anything which pre-dates Zachor's work [22]. Those presented here represent the investigations of Zachor, Gibson and Pierluissi,and Smith.

Each method presented here would appear to be an attractive candidate as a calculation technique, from the viewpoint of both simplicity and accuracy; however, they have been created for singular purposes, and are not easily adaptable to outside use. Zachor presents parameters in his report [23] which would allow a user to perform calculations in a limited region for CO_2. Smith's data set [24] is also limited, although in a different region, and for H_2O and CO_2.

Gibson and Pierluissi [25] published a long list of coefficients which were derived from the data of Wyatt, Stull and Plass (1962a) and Stull, Wyatt and Plass (1963). These data have been found slightly deficient, particularly in certain Q-branches, and Pierluissi [26]

21. R. A. McClatchey, et al., Optical Properties of the Atmosphere, Third Edition, Report No. AFCRL-72-0497, Air Force Cambridge Research Laboratories, Bedford, Mass., 1972.

22. A. S. Zachor, "A General Approximation for Gaseous Absorption," J. Quant. Spect. Rad. Trans., Vol. 8, 1968(a), pp. 771-781.

23. A. S. Zachor, "Equations for the Transmittance of the 2μ CO_2 Bands," J. Quant. Spect. Rad. Trans., Vol. 8, 1968(b), pp. 1341-1349.

24. W. L. Smith, A Polynomial Representation of Carbon Dioxide and Water Vapor Transmission, Report No. NESC 47, National Environmental Satellite Center, Washington, D. C., 1969.

25. G. A. Gibson and J. H. Pierluissi, "Accurate Formula for Gaseous Transmittance in the Infrared," Appl. Opt., Vol. 10, No. 7, 1971, pp. 1509-1518.

26. J. H. Pierluissi, "Polynomial Representation of Transmittance Models," Appl. Opt., Vol. 12, No. 4, 1973, pp. 776-778.

published another paper with a partial listing of coefficients derived from experimental data.

Unless the user is prepared to perform a considerable effort in compiling parameters for his own use, it seems he will only be able to put the methods of Zachor, Gibson-Pierluissi, and Smith (and presumably others) to limited use. Still, the accuracy achieved by them is favorable, at least on the basis of comparisons made by the original investigators, and they appear straightforward to program and use.

1.3.8 SECTION 9. LABORATORY MEASUREMENTS, FIELD MEASUREMENTS AND THE RESULTS OF CALCULATION FOR ABSORPTION

The first part of this section is included to give the user a guide to the kinds of data that have been used for generating parameters for the various calculation methods. One should be able to obtain in part from this, in conjunction with the assessments of the formulations of the computation techniques, the range of conditions from which he can expect the best accuracies in calculation, and thus, at what points the extrapolated values are likely to seriously limit accuracies.

In the rest of this section, we have attempted to delineate some of the types of field measurements that have been reported, to give the user a guide to what comparisons can be made to judge the accuracy of calculated results. The reader will find, however, that these judgments are not so easy to make, even though the experimental results are probably reliable, and certain of the meteorological conditions are adequately documented. However, certain trends can be observed, and from this viewpoint, at least, inclusion of some of the experimental results is warranted.

In addition, comparisons are made between the calculated results obtained using the Aggregate and LOWTRAN 2 methods. The reader is referred to the body of the report for a more in-depth discussion of the comparisons that are made.

1.3.9 SECTION 10. ATMOSPHERIC CONSTITUENTS

This section surveys a small realm of meteorology with the intent of leading the user to some of the sources of this most important element in the calculation of atmospheric transmittance and radiance. To give some idea of the scope of a more complete effort, we should like to direct the reader to a study, the results of which are not yet openly available. This study is the result of a program in the Department of Transportation entitled Climatic Impact Assessment Program (CIAP), designed to determine regulatory constraints on flights in the stratosphere such that no adverse environmental effects result. Much of the program is documented in six supporting monographs, describing the atmosphere and things that impact on the atmosphere. We believe these will be an extremely useful set of documents.

The subject matter of this section is very important. We have laid a reasonable amount of stress in previous sections on techniques of calculation, and the fidelity with which they represent the actual physical process of absorption and scattering. We have found, however, that if one is willing to compromise on accuracy, the choice of a method can at times be made arbitrarily. For the most part, in previous sections, when we have stressed the variability of accuracy, we have, at the time, chosen to ignore the atmosphere. We can no longer do so, because the highest achievement in accuracy can be utterly destroyed by the choice of even a slightly devious set of atmospheric parameters.

We hope that the references, at least in part, make up for the huge mass of information which obviously could not be included in the report.

1.4 SOME TOPICS NOT COVERED IN THIS REPORT

The emphasis in this report has been on processes involving radiative equilibrium. We have essentially ignored non-equilibrium phenomena in atmospheric emitted radiation for at least two reasons. First, because drawing the dividing line between the incorporation of equilibrium (thermally induced) processes, and non-equilibrium phenomena in no way compromises the calculation of transmittance. Second, because not nearly as many non-equilibrium results have been found which can be used with the same finality and confidence as those produced in the numerous investigations on equilibrium phenomena.

A similar decision had to be made regarding the matter of turbulence in the atmosphere. It is recognized from the point of view, especially, of imaging systems that the subject of atmospheric turbulence is one of utmost importance. But it is difficult enough to model the atmosphere even in its stable mode.

1.5 USE OF THE REPORT

The primary objective of this report, as already stated, is to present the state-of-the-art of the subject matter. From a broader viewpoint, however, it is meant also to be more directly applicable to user needs.

One reader may wish to have an in-depth understanding of the subject. He will have to make more than a passing perusal of the various sections summarized above. For this type of reader, it is assumed that his interest goes beyond merely finding the right method for making a calculation, but encompasses also the making of judgments requiring a more-or-less full understanding of the techniques used. He will also have to consult the references cited, because the sections in this report were intended only to give sketches of the greater detail to be found in the original works.

On the other hand, there is likely to be also the reader with only a passing interest in the subject. He should be reasonably satisfied having read only the preceding synopsis. Also, one may wish to find quickly the method he needs to serve his immediate purpose. He will undoubtedly want to read through the material in this report, but without necessarily referring, except in specific instances, to the original works. For his purpose, we have included the sort of guide to selection that follows.

We assume that, from the user's point of view, a given model should possess the following criteria: (1) accuracy; (2) speed (low computation times); (3) adaptability; and (4) practicality. The model should not be so crude that results differ greatly from exact formulations. Speed of computation is also important especially if one is interested in varying a large number of model parameters. Adaptability is of importance since practical applications usually require the alteration of boundary conditions or the changing of physical and geometrical parameters in the problem to be solved. Finally, a useful model should be practical in the sense that it encompasses the majority of the necessary elements for computing its expected range of parameters. Further, the practicality of a model must be judged in accordance with its accessibility.

Although it is almost impossible to ascertain which models have been developed for all the various applications, we will present here a general chart of the overall acceptability of mathematical models of radiative transfer, from the point of view of scattering, based primarily upon the above mentioned criteria (Table 1). The model or descriptive names should be interpreted as referring to a particular technique rather than an individual specialized model or computer program. The methods are ranked as excellent (E), good (G), fair (F), or poor (P).

It is immediately evident that persons more intimately familiar with different techniques will surely rate the different methods differently. We have tried implicitly to integrate the four enumerated qualities into one entity, utility. We realize, however, as pointed out by one of our reviewers (Herman, private communication) that, in any calculations of radiative transfer, one must decide what features are important, and what features are not. The Turner method, for example, appears from Table 1 to have perhaps greater utility than other methods. However, if the state of polarization of the diffuse field is a requirement, the Turner and other methods fail to score with decent accuracy. On the other hand, the adaptability of the Turner method is high enough that polarization could feasibly be included in any modification to the technique. This may very well be true of other methods as well, although the lack of accessibility of specific information on computing techniques may conceal their real adaptability.

We have tended to score practicality heavily on the basis of accessibility. As pointed out in Section 1.1, the primary emphasis on the utilitarian aspect of this report is toward

assistance to the military systems designer who sometimes needs only moderately accurate answers, but quickly. On the other hand, a score of P on the basis of computer time used could easily be ignored by someone whose main interest is fidelity to the real world. One who has constant access to a facility-owned computer might readily ignore the computer time column altogether. Doing so would give greater attractiveness to methods which otherwise score poorly.

We must concede also that the accuracy column can only be used in some cases as a rough guide. Admittedly, all models have not been tested and some of these assessments have to be made on the basis of our judgments derived from consulting other sources. On the other hand, the indefinite nature of the entries in Table 1 (and Table 2 later) appear to reflect a certain awareness that accuracy is a quality which is better left to the ultimate judgment of the user.

As far as the Aggregate and LOWTRAN 2 methods are concerned, if we should rate them in the same way as the scattering models, they would probably come out about equal on the basis of "computer time," "adaptability," and "practicality." As far as "accuracy" is concerned, we believe that the Aggregate method is probably more accurate because it is more parameter-dependent. But again, we must remember that accuracy is usually more greatly affected by factors outside the calculation method than it is on the method itself (which, of course, is equally true of the scattering methods). From the point of view of availability, we believe the LOWTRAN 2 method rates higher.

The only absolute basis we have for judging accuracy is a direct comparison between calculated and measured data, several cases of which are given throughout the report. The best test is with controlled experiments in the field, but most of these are restricted to horizontal paths which do not provide a valid test of the effect of temperature, pressure and concentration changes. One reasonable guideline is that using the models outside of the ranges of variables provided by the laboratory experiments (see Section 9) can be expected to incur errors commensurate with the extent of the extrapolation.

If we lump the absorption methods into six broad categories and tabulate them as for the scattering methods, we are likely to come up with something similar to Table 2.

Note: Because of the large number of symbols and nomenclature used in this report, and because it was necessary to repeat some symbols to represent different quantities, it is essential that a list of symbols and nomenclature be included. For the convenience of the reader a list of symbols is placed at the very end of the report for easy reference.

TABLE 1. RADIATIVE-TRANSFER-ATMOSPHERIC MODEL RATING (SCATTERING)

Model	Accuracy	Computer Time	Adaptability	Practicality
Exact Solutions	E	F	P	P
Iterative Method	G	F-P	F	F
Spherical Harmonics Method	G	F-G	F-G	P
Discrete Ordinates Method	G	P	G	F-G
Invariant Imbedding Technique	G	P	G	F
Doubling Technique	G	E	P	F
Moment Methods	G	P	F	F
Monte Carlo	G	P	E	F-P
Schuster-Schwarzchild Method	P	E	G	F
Eddington Method	P	E	F	F
Romanova's Method	F	F	F	G
Turner's Method	G-F	E	G-F	G

TABLE 2. ATMOSPHERIC ABSORPTION METHOD RATING

Method	Accuracy	Computer Time	Adaptability	Practicality
General Statistical	G-F	G-E	F	G-F
Quasi-Random	G-E	P-F	F	F
Aggregate	G-F	E	F	G-F
LOWTRAN 2	G-F	E	F	G
Multi-Parameter	G	G	F	F
Line-by-Line	E	P	F	G

2
RADIATIVE-TRANSFER THEORY

2.1 INTRODUCTION

In this chapter we shall delineate some of the basic quantities in radiative-transfer analysis by describing the equation used to represent the transport of radiation through a scattering and absorbing medium.

The fundamental quantity used to define the amount of radiant energy at a point at some time is the spectral radiance for a given polarization state. We shall neglect polarization and define spectral radiance as the energy per unit time per unit area per unit solid angle per unit spectral interval which crosses a small surface oriented normal to the direction of propagation. The symbol for spectral radiance is L_λ or L_ν and the units generally used are watts per square centimeter per steradian per spectral interval. The spectral dependence is as readily given in terms of wavenumber (ν) as it is in terms of wavelength (λ). In the former case, the unit interval is cm^{-1} and in the latter, it is μm (i.e., reciprocal centimeters and micrometers respectively).

Another radiometric quantity of importance in the consideration of radiation transport is the spectral irradiance, or the spectral radiant energy per unit time per unit area incident on a surface. To obtain irradiance on a surface element (dA) one must integrate all of the incoming radiation over the hemisphere centered in dA, so,

$$E_\lambda = \int_{hemi} L_\lambda \cos\theta \, d\Omega \tag{1}$$

where θ is the angle between the direction of propagation and the normal to the surface, and $d\Omega$ is a differential solid angle whose apex is at dA. The functional dependence of L_λ (or L_ν) and E_λ (or E_ν) will be shown in the following discussion.

2.2 EQUATION OF RADIATIVE TRANSFER

Radiative transfer theory can be defined as the quantitative study of the transfer of radiant energy through a medium which can scatter, absorb, and emit radiation. Its origin can be traced to a paper by Schuster on "Radiation Through a Foggy Atmosphere" [27]. Later, important contributions were made by Schwarzschild, Milne, Eddington, and in more recent times by Chandrasekhar and Sekera. Much of the impetus was provided by astrophysics in the study of the transfer of radiation in stars and stellar envelopes. Today, the theory of the transport of energy encompasses neutron transport theory, radiative transport theory,

27. A. Schuster, "Radiation Through a Foggy Atmosphere," Astrophys. J., Vol. 21, 1905, p. 1.

cosmic-ray transport, and plasma theory. There are many analogies and in many cases the mathematical procedures used in the analyses are quite similar.

The axiomatic basis for the study of radiation transport is the Liouville equation in which one must consider the distribution function which characterizes all particles in phase space. By integrating over the coordinates of all particles except one we get the one-particle distribution function which is used to describe the properties of a "dilute" gas; that is, we are neglecting the simultaneous interactions of more than two particles. Thus, we are led to a Boltzmann type equation for a description of the transfer of radiation through a scattering, absorbing, and emitting medium.

The spectral radiance, defined by $\partial L/\partial\lambda$ (or $\partial L/\partial\nu$), should strictly retain the subscript, λ or ν, as L_λ or L_ν. We shall retain it in the ensuing discussion, and later, for the sake of simplicity, assume it implicit in the expression. We can consider a beam of monochromatic radiation with radiance $L_\lambda(\lambda, s, \theta, \phi, t)$ which travels along a path s in a direction θ, ϕ (the usual polar angles) as shown in Figure 1. We can denote the increased spectral radiance $L_\lambda(\lambda, s + ds, \theta, \phi, t)$ at $s + ds$ by $L_\lambda(\lambda, s, \theta, \phi, t) + dL_\lambda(\lambda, s, \theta, \phi, t)$. The change in radiance over the distance ds can be written in terms of the following components (neglecting changes with time):

$$\frac{dL_\lambda(\lambda, s, \theta, \phi)}{ds} = \epsilon(\text{spontaneous emission}) + \epsilon(\text{stimulated emission}) + \epsilon(\text{in-scattering}) + \epsilon(\text{intrinsic}) - \epsilon(\text{absorption}) - \epsilon(\text{out-scattering}) \quad (2)$$

where spontaneous emission is independent of the radiation field and stimulated emission depends on the radiation field, behaving as negative absorption. The term in-scattering refers to the radiation which is scattered from all directions into a specific direction θ, ϕ. This depends on the radiation field and is given by:

$$\epsilon(\text{in-scattering}) = \frac{k_s'(\lambda, s)}{4\pi}\int_{4\pi} p(\lambda, s, \theta, \phi, \theta', \phi')L(\lambda, s, \theta', \phi')\,d\Omega \quad (3)$$

where $k_s'(\lambda, s)$ is the volume scattering coefficient. This is the scattering cross section per unit volume, or the probability per unit length that an individual photon will be scattered. Its units are cm^{-1}. The quantity $p(\lambda, s, \theta, \phi, \theta', \phi')$ is the single-scattering phase function and is a measure of the probability of scattering from a direction θ', ϕ' into a direction θ, ϕ. It is normalized such that its integral over a complete sphere is unity, i.e.,

$$\frac{1}{4\pi}\int_{4\pi} p(\lambda, s, \theta, \phi, \theta', \phi')\,d\Omega' = 1 \quad (4)$$

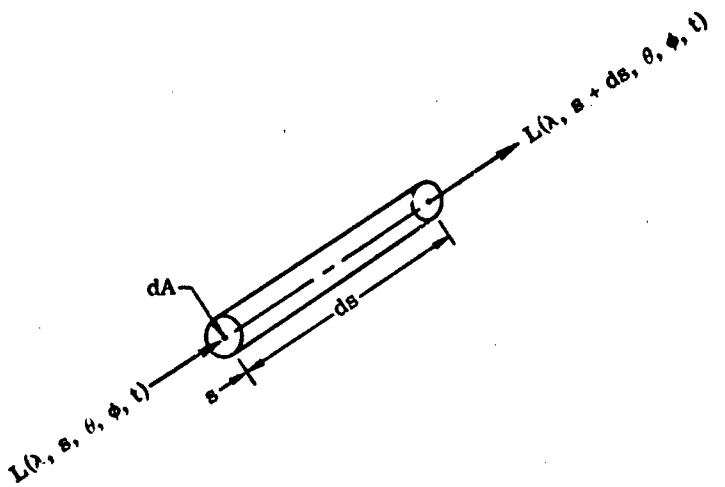

FIGURE 1. DESCRIPTION OF RADIANCE

The intrinsic term refers to a specific autonomous source placed in the medium. These four terms comprise the gain of radiant energy at wavelength λ at a point s in the medium for radiation traveling in direction θ, ϕ at time t. Loss of radiation occurs by means of absorption and the scattering of radiant energy out of the beam which are given by:

$$\epsilon(\text{absorption}) = -k'_a(\lambda, s)L_\lambda(\lambda, s, \theta, \phi) \tag{5}$$

and

$$\epsilon(\text{out-scattering}) = -k'_s(\lambda, s)L_\lambda(\lambda, s, \theta, \phi) \tag{6}$$

where $k'_a(\lambda, s)$ is the volume absorption coefficient, or the probability per unit length for the absorption of an individual photon. Its units are cm^{-1}. These quantities can be combined into an extinction coefficient $k'(\lambda, s)$:

$$k'(\lambda, s) = k'_a(\lambda, s) + k'_s(\lambda, s) \tag{7}$$

where $k'(\lambda, s)$ is the probability per unit length of an individual photon undergoing either absorption or scattering, given in units of cm^{-1}.

Combining all of these terms gives us the net gain in radiance per unit length:

$$\frac{dL_\lambda}{ds} = \gamma'(\lambda, s)J(\lambda, s, \theta, \phi) + \gamma''(\lambda, s)L_\lambda(\lambda, s, \theta, \phi)$$

$$+ \frac{k'_s(\lambda, s)}{4\pi}\int_{4\pi} p(\lambda, s, \theta, \phi, \theta', \phi')L_\lambda(\lambda, s, \theta', \phi')\,d\Omega'$$

$$+ q(\lambda, s, \theta, \phi) - k'(\lambda, s)L_\lambda(\lambda, s, \theta, \phi) \tag{8}$$

where $\gamma'(\lambda, s)$ is a coefficient for spontaneous emission and $J(\lambda, s, \theta, \phi)$ is the source function which is independent of the radiation field. Likewise, $\gamma''(\lambda, s)$ is the corresponding coefficient for stimulated emission and $q(\lambda, s, \theta, \phi)$ is the intrinsic emission term. The terms $\gamma'(\lambda, s)$ and $\gamma''(\lambda, s)$ are related to the familiar Einstein A and B coefficients. For a more detailed treatment of these coefficients consult Goody [28] and Stewart [29]. The complete (time-independent) three-dimensional radiative-transfer equation for an absorbing, scattering, and emitting isotropic* inhomogeneous atmospheric medium is therefore

*By isotropic it is meant that the scattering and absorption coefficients are independent of direction.

28. R. M. Goody, Atmospheric Radiation, Oxford University Press, 1964(a).

29. J. C. Stewart, Some Topics in Radiative Transfer in Developments in Transport Theory, E. Inonu and P. F. Zweifel (eds.), Academic Press, N. Y., 1967.

$$\frac{dL_\lambda}{ds} = -[k'(\lambda, s) - \gamma''(\lambda, s)]\, L_\lambda(\lambda, s, \theta, \phi)$$

$$+ \frac{k'_s(\lambda, s)}{4\pi}\int_{4\pi} p(\lambda, s, \theta, \phi, \theta', \phi')L_\lambda(\lambda, s, \theta', \phi')\, d\Omega'$$

$$+ \gamma'(\lambda, s)J(\lambda, s, \theta, \phi) + q(\lambda, s, \theta, \phi) \qquad (9)$$

If the medium is not in thermodynamic equilibrium, the term $\gamma''(\lambda, s)$ corresponding to stimulated emission may be greater than $k'(\lambda, s)$, the extinction term. In that case, the medium acts as a source of coherent radiation as in a laser. Under conditions of local thermodynamic equilibrium however, the population of states is such that $k'(\lambda, s) > \gamma''(\lambda, s)$ and the source term $J(\lambda, s, \theta, \phi)$ becomes the Planck function which is only dependent upon wavelength and temperature:

$$J(\lambda, s, \theta, \phi) \xrightarrow[LTE]{} L^*_\lambda(\lambda, T) = \frac{2hc^2}{\lambda^5[e^{hc/\lambda kT} - 1]} \quad \left[\text{or } L^*_\nu(\nu, T) = \frac{2c^2h\nu^3}{[e^{hc\nu/kT} - 1]}\right] \qquad (10)$$

where h is Planck's constant, k is Boltzmann's constant and T is temperature. For the purpose of this discussion, we shall neglect the effects of stimulated emission and assume that the condition of local thermodynamic equilibrium holds and that the source of radiation is described by the Planck function of Eq. (10). Thus, the basic radiative-transfer equation is given by:

$$\frac{dL_\lambda}{ds} = -k'(\lambda, s)L_\lambda(\lambda, s, \theta, \phi)$$

$$+ \frac{k'_s(\lambda, s)}{4\pi}\int_{4\pi} p(\lambda, s, \theta, \phi, \theta', \phi')L_\lambda(\lambda, s, \theta', \phi')\, d\Omega'$$

$$+ k'_a(\lambda, s)L^*_\lambda(\lambda, T) + q(\lambda, s, \theta, \phi) \qquad (11)$$

Now, defining the single scattering albedo $\omega_0(\lambda, s)$ as

$$\omega_0(\lambda, s) \equiv k'_s(\lambda, s)/k'(\lambda, s) \qquad (12)$$

and

$$Q(\lambda, s, \theta, \phi) = q(\lambda, s, \theta, \phi)/k'(\lambda, s) \qquad (13)$$

Eq. (11) becomes

$$\frac{dL_\lambda}{ds} = -k'(\lambda, s)\left\{L_\lambda(\lambda, s, \theta, \phi) - \frac{\omega_0(\lambda, s)}{4\pi}\int_{4\pi} p(\lambda, s, \theta, \phi, \theta', \phi')L_\lambda(\lambda, s, \theta', \phi')\,d\Omega'\right.$$

$$\left. - [1 - \omega_0(\lambda, s)]L_\lambda^*(\lambda, T) - C(\lambda, s, \theta, \phi)\right\} \tag{14}$$

We shall limit ourselves to the description of radiation in an atmosphere in which there are no intrinsic sources. Thus, we have

$$\frac{dL_\lambda}{ds} = -k'(\lambda, s)\left\{L_\lambda(\lambda, s, \theta, \phi) - \frac{\omega_0(\lambda, s)}{4\pi}\int_{4\pi} p(\lambda, s, \theta, \phi, \theta', \phi')L_\lambda(\lambda, s, \theta', \phi')\,d\Omega'\right.$$

$$\left. - [1 - \omega_0(\lambda, s)]L_\lambda^*(\lambda, T)\right\} \tag{15}$$

This concludes the simple derivation of the radiative transfer equation. A more detailed treatment of transport theory can be found in Kourganoff [30], Samuelson [31], and Turner [32].

We can now consider special cases of Eq. (15). First, suppose that there are no interactions, either scattering or absorption. Then $k'(\lambda, s) = 0$ and we have

$$\frac{dL_\lambda}{ds} = 0 \tag{16}$$

The radiance is constant everywhere in this nonparticipating medium. Second, suppose we have no scattering. This means that $\omega_0(\lambda, s) = 0$ and Eq. (15) becomes

$$\frac{dL_\lambda}{ds} = -k'(\lambda, s)\left\{L_\lambda(\lambda, s, \theta, \phi) - L_\lambda^*(\lambda, T)\right\} \tag{17}$$

Third, let us consider a purely scattering medium, i.e., one in which no absorption occurs. In this case there can be no emission and $\omega_0(\lambda, s) = 1$. Equation (15) then becomes

30. V. Kourganoff, Introduction to the General Theory of Particle Transfer, Gordon and Breach, N. Y., 1969.

31. R. E. Samuelson, Radiative Transfer in a Cloudy Atmosphere, NASA Report No. TR-R-215, Goddard Space Flight Center, Greenbelt, Md., Office of Technical Services, Dept. of Commerce, Washington, D. C., 1965.

32. R. E. Turner, Transport of High-Energy Cosmic Rays in the Interstellar Medium, Ph.D Thesis, Washington University, St. Louis, Mo., 1970.

$$\frac{dL_\lambda}{ds} = -k'(\lambda, s)\left\{L_\lambda(\lambda, s, \theta, \phi) - \frac{1}{4\pi}\int_{4\pi} p(\lambda, s, \theta, \phi, \theta', \phi')L_\lambda(\lambda, s, \theta', \phi')\,d\Omega'\right\} \tag{18}$$

Fourth, let us consider the case in which the scattering law is isotropic, i.e., $p(\lambda, s, \theta, \phi, \theta', \phi') = 1$. Equation (15) then becomes

$$\frac{dL_\lambda}{ds} = -k'(\lambda, s)\left\{L_\lambda(\lambda, s, \theta, \phi) - \frac{\omega_0(\lambda, s)}{4\pi}\int_{4\pi} L_\lambda(\lambda, s, \theta', \phi')\,d\Omega' - [1 - \omega_0(\lambda, s)]L_\lambda^*(\lambda, T)\right\} \tag{19}$$

2.3 THE FORMAL SOLUTION

In this section, we consider the formal solution of the time-independent integrodifferential equation of radiative-transfer Eq. (15). This can be written for some path s:

$$\frac{1}{k'(\lambda, s)}\frac{dL_\lambda}{ds} + L_\lambda(\lambda, s, \theta, \phi) = -\frac{\omega_0(\lambda, s)}{4\pi}\int_{4\pi} p(\lambda, s, \theta, \phi, \theta', \phi')L_\lambda(\lambda, s, \theta', \phi')\,d\Omega' - [1 - \omega_0(\lambda, s)]L_\lambda^*(\lambda, T) \tag{20}$$

for which the solution is:

$$L_\lambda(\lambda, s, \vartheta, \phi) = L_\lambda(\lambda, s_0, \theta, \phi)\exp\left[-\int_{s_0}^{s} k'(\lambda, s')\,ds'\right] + \frac{1}{4\pi}\int_{s_0}^{s}\omega_0(\lambda, s')k'(\lambda, s')\int_{4\pi} p(\lambda, s', \theta, \phi, \theta', \phi')L_\lambda(\lambda, s', \theta', \phi')\,d\Omega'$$
$$\exp\left[-\int_{s'}^{s} k'(\lambda, s'')ds''\right]ds' + \int_{s_0}^{s}[1 - \omega_0(\lambda, s')]L_\lambda^*(\lambda, T)$$
$$\exp\left[-\int_{s'}^{s} k'(\lambda, s'')\,ds''\right]k'(\lambda, s')\,ds' \tag{21}$$

where s is a general point along the path and s_0 is a boundary. Formally, then, Eq. (21) is the solution to the integrodifferential equation of radiative-transfer. The first term on the right side of Eq. (21) represents the attenuation of the boundary radiance $L_\lambda(\lambda, s_0, \theta, \phi)$. The

second term represents the contribution of all scattered radiation along the path and the last term represents the thermal radiance along the path.

For most practical applications of radiative-transfer theory, one can consider the earth's atmosphere to be a plane-parallel medium especially for multiple scattering in which complications multiply, otherwise. Problems in scattering in which the earth's curvature is taken into account are those for which the radiance is to be determined at extreme altitudes or for conditions of large solar zenith angles. For this discussion, however, we shall determine the formal solution for a plane-parallel atmosphere.

Consider solar radiation entering the atmosphere at zenith angle $\theta_0 \left(= \cos^{-1} \mu_0\right)$ and azimuthal angle ϕ_0 as indicated in Figure 2. Since all quantities have spectral dependence, we can drop the explicit dependence on wavelength and write Eq. (15) as

$$\xi \frac{\partial L}{\partial x} + \zeta \frac{\partial L}{\partial y} + \mu \frac{\partial L}{\partial z} = -k'(x, y, z)L(x, y, z, \mu, \phi) + \frac{k'_s(x, y, z)}{4\pi} \int_0^{2\pi} \int_{-1}^{1} p(x, y, z; \mu, \phi, \mu', \phi')L(x, y, z, \mu', \phi')\, d\mu'\, d\phi' + k'_a(x, y, z)L^*[T(x, y, z)] \tag{22}$$

where $\mu = \cos \theta$

$\mu' = \cos \theta'$

$\xi = \sin \theta \cos \phi$

$\zeta = \sin \theta \sin \phi$

To solve Eq. (22) is very difficult in general, especially if one considers horizontally inhomogeneous atmospheres with inhomogeneous boundaries. In this discussion, we shall consider one-dimensional atmospheres, i.e., those which possess horizontal homogeneity, and for which:

$$\frac{\partial L}{\partial x} = \frac{\partial L}{\partial y} = 0 \tag{23}$$

$$k'_a(s) = k'_a(z) = k'(z)[1 - \omega_0(z)] \tag{24}$$

$$k'_s(s) = k'_s(z) = k'(z)\omega_0(z) \tag{25}$$

$$k'(s) = k'(z) \tag{26}$$

Defining the dimensionless quantity optical depth as

$$dq = -k'(z)\, dz \text{ or } q = \int_h^{\infty} -k'(z)\, dz \tag{27}$$

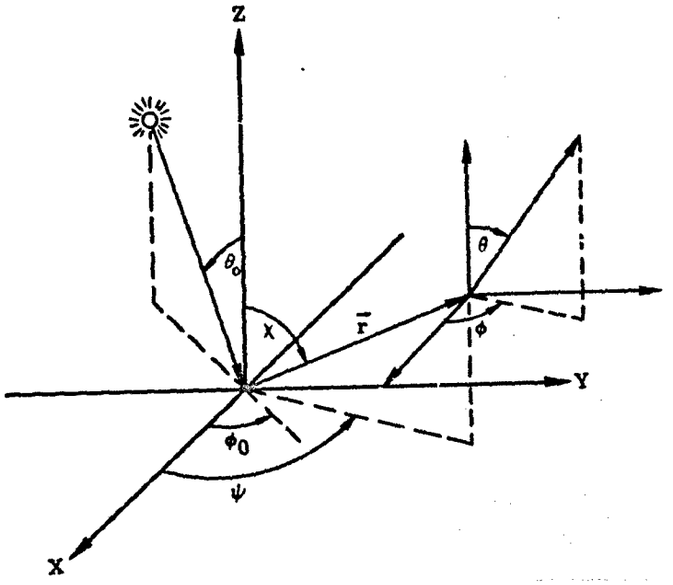

FIGURE 2. SOLAR SCATTERING CONFIGURATION

we get for an equivalent form of Eq. (15):

$$\mu \frac{dL}{dq} = L(q, \mu, \phi) - \frac{\omega_0(q)}{4\pi} \int_0^{2\pi} \int_{-1}^{1} p(q; \mu, \phi, \mu', \phi') L(q, \mu', \phi') \, d\mu' \, d\phi' - [1 - \omega_0(q)] L^*(q) \quad (28)$$

Thus, Eq. (28) is an integrodifferential equation which is used to describe the spectral radiance in a vertically inhomogeneous, multiply scattering, isotropic atmosphere in which conditions of local thermodynamic equilibrium are assumed to hold.

We now consider the solar radiation incident upon earth's atmosphere. The angular size of the sun is about 30 minutes of arc but for practical purposes we shall assume that the sun is a point source. Hence, we can write for the solar radiance at any point within the atmosphere

$$L_H(q, \mu, \phi) = E_H(q) \delta(\mu + \mu_0) \delta(\phi - \phi_0) \quad (29)$$

where $E_H(q)$ is the solar spectral irradiance on a flat surface normal to the direction of incidence. The extraterrestrial value of the solar spectral irradiance E_0 has been determined by a number of investigators [33]. Most of the work over the past half century has been in the form of ground-based measurements with extrapolations through the atmosphere to determine the extraterrestrial value. More recently, high-altitude balloons, aircraft, and spacecraft [34] have been used in order to eliminate the uncertainties due to the atmosphere. The NASA Standard Extraterrestrial Solar Spectrum is now available in punched card form from the Goddard Space Flight Center [35]. It should be noted that 99 percent of the solar energy is in the range 0.276 μm to 4.96 μm, and 99.9 percent of the solar energy is in the range 0.217 μm to 10.97 μm. The solar constant, which is the solar spectrum integrated over wavelength has a value of 135.30 mW/cm^2 at a distance of one astronomical unit. The total annual variation is about 6 percent, from a high of 139.9 mW/cm^2 at perihelion to a low of 130.9 mW/cm^2 at aphelion.

It is convenient to separate the direct solar radiation field from the diffuse radiation field in analytical studies. Thus, we can write the total spectral radiance as

$$L(q, \mu, \phi) = L_H(q, \mu, \phi) + L_D(q, \mu, \phi) \quad (30)$$

---

33. S. T. Henderson, Daylight and Its Spectrum, American Elsevier Publishing Company, New York, 1970, pp. 72-73.

34. J. C. Arvesen, R. N. Griffin, Jr. and B. D. Pearson, Jr., "Determination of Extraterrestrial Solar Spectral Irradiance from a Research Aircraft," Appl. Optics, Vol. 8, No. 11, 1969.

35. M. P. Thekackara, Proposed Standard Values of the Solar Constant and the Solar Spectrum, J. Environ. Sci., Vol. 13, No. 4, September-October 1970, pp. 6-9.

in which $L_H(q, \mu, \phi)$ represents the direct solar radiance as given by Eq. (29) and $L_D(q, \mu, \phi)$ is the diffuse radiance. After substituting Eq. (30) into Eq. (28) we get

$$\mu \frac{dL_D}{dq} = L_D(q, \mu, \phi) - \frac{\omega_0(q)}{4\pi}\int_0^{2}\int_{-1}^{1} p(q; \mu, \phi, \mu', \phi')L_D(q, \mu', \phi')\, d\mu'\, d\phi'$$

$$- \frac{\omega_0(q)}{4\pi} E_H(q)p(q; \mu, \phi, -\mu_0, \phi_0) - [1 - \omega_0(q)]\, L^*(q) \qquad (31)$$

where

$$E_H(q) = E_0\, e^{-q/\mu_0} \qquad (32)$$

No exact solution of Eq. (31) has been found for a general scattering law. We can, however, convert the integrodifferential equation of radiative-transfer into an integral equation. Thus, for the upwelling and downwelling radiances, respectively,

$$L_D(q, \mu, \phi) = L(q_0, \mu, \phi)\, e^{-(q_0-q)/\mu}$$

$$+ \frac{\omega_0(q)}{4\pi\mu}\int_0^{2\pi}\int_{-1}^{1}\int_q^{q_0} p(q'; \mu, \phi, \mu', \phi')\, e^{-(q'-q)/\mu}\, L_D(q', \mu', \phi')\, dq'\, d\mu'\, d\phi'$$

$$+ \frac{E_0\, e^{q/\mu}}{4\pi\mu}\int_q^{q_0} \omega_0(q')p(q'; \mu, \phi, -\mu_0, \phi_0)\, e^{-(1/\mu_0+1/\mu)q'}\, dq'$$

$$+ \frac{1}{\mu}\int_q^{q_0} [1 - \omega_0(q')]\, L^*(q')\, e^{(q'-q)/\mu}\, dq' \qquad 0 < \mu \le 1 \qquad (33)$$

and

$$L_D(q, -\mu, \phi) = L(0, -\mu, \phi)\, e^{-q/\mu}$$

$$+ \frac{\omega_0(q)}{4\pi\mu}\int_0^{2\pi}\int_{-1}^{1}\int_0^{q} p(q'; -\mu, \phi, \mu', \phi')\, e^{-(q-q')/\mu}\, L_D(q', \mu', \phi')\, dq'\, d\mu'\, d\phi'$$

$$+ \frac{E_0\, e^{-q/\mu}}{4\pi\mu}\int_0^{q} \omega_0(q')p(q'; -\mu, \phi, -\mu_0, \phi_0)\, e^{-(1/\mu_0-1/\mu)q'}\, dq'$$

$$+ \frac{1}{\mu}\int_0^{q} [1 - \omega_0(q')]\, L^*(q')\, e^{-(q-q')/\mu}\, dq' \qquad 0 < \mu \le 1 \qquad (34)$$

where $q_0 = \int_0^\infty -k'(z)\,dz$ is the optical thickness of the atmosphere. Equation (33) describes the upwelling diffuse spectral radiance at some optical depth q in an inhomogeneous atmosphere, whereas Eq. (34) describes the downwelling diffuse spectral radiance. For homogeneous atmospheres, the single-scattering albedo $\omega_0(q)$ and the single-scattering phase function are independent of the optical depth q. In this case, some of the integrals can be evaluated and we obtain

$$L_D(q, \mu, \phi) = L(q_0, \mu, \phi)\, e^{-(q_0-q)/\mu}$$
$$+ \frac{\omega_0}{4\pi\mu}\int_0^{2\pi}\int_{-1}^{1} p(\mu, \phi, \mu', \phi')\int_q^{q_0} e^{-(q'-q)/\mu}\; L_D(q', \mu', \phi')\,dq'\,d\mu'\,d\phi'$$
$$+ \frac{\omega_0\mu_0 E_0 p(\mu, \phi, -\mu_0, \phi_0)}{4\pi(\mu+\mu_0)}\left[e^{-q/\mu_0} - e^{-q_0/\mu_0}\, e^{-(q_0-q)/\mu}\right]$$
$$+ \frac{1-\omega_0}{\mu}\int_q^{q_0} e^{-(q'-q)/\mu}\; L^*(q')\,dq' \qquad 0 < \mu \le 1 \qquad (35)$$

and

$$L_D(q, -\mu, \phi) = L(0, -\mu, \phi)\, e^{-q/\mu}$$
$$+ \frac{\omega_0}{4\pi\mu}\int_0^{2\pi}\int_{-1}^{1} p(-\mu, \phi, \mu', \phi')\int_0^{q} e^{-(q-q')/\mu}\; L_D(q', \mu', \phi')\,dq'\,d\mu'\,d\phi'$$
$$+ \frac{\omega_0\mu_0 E_0 p(-\mu, \phi, -\mu_0, \phi_0)}{4\pi(\mu-\mu_0)}\left[e^{-q/\mu} - e^{-q/\mu_0}\right]$$
$$+ \frac{1-\omega_0}{\mu}\int_0^{q} e^{-(q-q')/\mu}\; L^*(q')\,dq' \qquad 0 < \mu \le 1;\ \mu \neq \mu_0 \qquad (36)$$

$$L_D(q, -\mu_0, \phi) = L(0, -\mu_0, \phi)\, e^{-q/\mu_0}$$
$$+ \frac{\omega_0}{4\pi\mu_0}\int_0^{2\pi}\int_{-1}^{1} p(\mu_0, \phi, \mu', \phi')\int_0^{q} e^{-(q-q')/\mu_0}\; L_D(q', \mu', \phi')\,dq'\,d\mu'\,d\phi'$$
$$+ \frac{\omega_0\mu_0 E_0 p(-\mu_0, \phi, -\mu_0, \phi_0)}{4\pi\mu_0}\,\frac{q}{\mu_0}\,e^{-q/\mu_0} + \frac{1-\omega_0}{\mu_0}\int_0^{q} e^{-(q-q')/\mu_0}\; L^*(q')\,dq'$$
$$\mu = \mu_0 \qquad (37)$$

2.4 BOUNDARY CONDITIONS

In principle one should be able to find a complete solution to the radiation-transfer equation provided the boundary conditions $L(q_0, \mu, \phi)$ at the bottom surface, and $L(0, -\mu, \phi)$, at the top of the atmosphere, are specified. If the sun is the only source of radiation external to the atmosphere then the diffuse radiation entering the atmosphere is zero (i.e., $L(0, -\mu, \phi) = 0$). The conditions involving the bottom surface, considered to be opaque, are more complicated. In order to deal with the surface one must consider the so-called bi-directional spectral reflectance and the directional spectral emittance. Let us consider a surface element dA with its normal in the z-direction as illustrated in Figure 3. The differential area dA is at point P(x, y, z), with z = 0. The incident radiance is denoted by $L(x, y, z = 0, \mu', \phi')$ and the elemental reflected radiance $dL(x, y, 0, \mu, \phi)$. The amount of radiant power incident on the surface element per unit area is $L(x, y, 0, -\mu', \phi')\mu' d\Omega'$. We then define a bi-directional reflectance function as

$$f(x, y, 0, \mu', \phi', \mu, \phi) \equiv \frac{dL(x, y, 0, \mu, \phi)}{L(x, y, 0, -\mu', \phi')\mu' d\Omega'} \tag{38}$$

Helmholtz [36] showed that certain reciprocity relations exist for the bi-directional reflectance function, i.e.,

$$f(x, y, 0, \mu', \phi', \mu, \phi) = f(x, y, 0, \mu, \phi, \mu', \phi') \tag{39}$$

The reflection properties of a surface are completely determined by specifying the bi-directional reflectance function for all angles in hemispherical space and for all points (x, y) on the surface for a given wavelength, or wavelength region, and polarization state. Most of the determinations must be done experimentally [37], [38], and for that reason the data to be collected are quite voluminous. Hence, it is convenient to deal with directional reflectances, i.e., those reflectances which depend upon only one solid angle instead of two as in the bi-directional reflectance. For a more complete treatment of reflectance definitions, one should consult McNicholas [39], Durkle [40], and Siegel and Howell [41].

---

36. H. L. Helmholtz, Physiological Optics, 3rd Ed., 1909.

37. Target Signature Analysis Center, Data Compilation, Eleventh Supplement: Vol. I, Bidirectional Reflectances; Definition, Discussion and Utilization, and Vol. II: Bidirectional Reflectance; Graphic Data, Report No. AFAL-TR-72-266, TSAC, Willow Run Laboratories of the Institute of Science and Technology, University of Michigan, Ann Arbor, 1972.

38. D. Carmer, Target Signature Analysis Center: Data Compilation, 7th Supplement, Infrared & Optical Sensor Laboratory, Willow Run Laboratories of the Institute of Science and Technology, University of Michigan, Ann Arbor, 1969.

39. H. J. McNicholas, "Absolute Methods of Reflectometry," J. Res. Natl. Bur. Std., Vol. 1, 1928, pp. 29-72.

(References Continued)

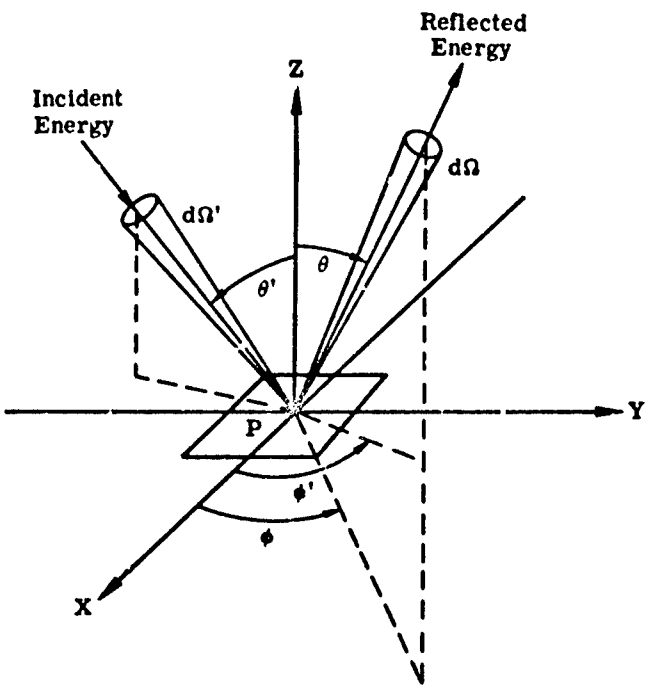

FIGURE 3. REFLECTED VERSUS INCIDENT ENERGY

In many studies of radiative-transfer one makes use of the concept of Lambertian surface, i.e., a surface which is perfectly diffuse. Consider the radiance reflected from a general surface. From Eq. (38) we get

$$L(x, y, 0, \mu, \phi) = \int_0^{2\pi}\int_0^1 f(x, y, 0, \mu, \phi, \mu', \phi')L(x, y, 0, -\mu', \phi')\,\mu'\,d\mu'\,d\phi' \tag{40}$$

If the bidirectional reflectance is independent of angles, then Eq. (40) becomes

$$L(x, y, 0, \mu, \phi) = f(x, y, 0)\int_0^{2\pi}\int_0^1 L(x, y, 0, -\mu', \phi')\,\mu'\,d\mu'\,d\phi' \tag{41}$$

But, by definition the integral is just the irradiance $E(x, y, 0)$ on the surface. Thus,

$$L(x, y, 0, \mu, \phi) = f(x, y, 0)E(x, y, 0) \tag{42}$$

If we now integrate this result over the hemisphere, we get a quantity called radiant exitance, caused by reflection from the surface:

$$M(x, y, 0) = \int_0^{2\pi}\int_0^1 L(x, y, 0, \mu, \phi)\,\mu\,d\mu\,d\phi$$

$$= \rho(x, y, 0)E(x, y, 0) \tag{44}$$

where $\rho(x, y, 0) = \int_0^{2\pi}\int_0^1 f(x, y, 0)\,\mu\,d\mu\,d\phi$

$$= \pi f(x, y, 0)$$

The albedo of the surface can be defined as the ratio of this exitance to the irradiance, i.e.,

$$\rho(x, y, 0) = M(x, y, 0)/E(x, y, 0) \tag{45}$$

Therefore, for a Lambertian surface, the reflected radiation is given by:

$$L(x, y, 0) = \frac{\rho(x, y, 0)}{\pi}E(x, y, 0) \tag{46}$$

The total radiance from the surface is the resultant of the reflected radiation as developed in the preceding equation, and the emitted radiation.

---

40. R. V. Dunkle, Spectral Reflectance Measurements, Surface Effects on Spacecraft Materials. J. Clauss (ed.), John Wiley & Sons, N. Y., 1960.

41. R. Siegel and J. R. Howell, Thermal Radiation Heat Transfer, New York, McGraw-Hill, N. Y., 1972.

Summarizing, we can now write down the general boundary conditions for the transfer of radiant energy through a plane-parallel, vertically inhomogeneous, isotropic, atmosphere illuminated by a point source infinitely far away.

$$L(0, -\mu, \phi) = 0 \tag{47}$$

$$L(q_0, \mu, \phi) = L_{GE}(q_0, \mu, \phi) + \int_0^{2\pi}\int_0^1 f(\mu, \phi, -\mu', \phi')L(q_0, -\mu', \phi')\,\mu'\,d\mu'\,d\phi' \tag{48}$$

where L_{GE} is the emitted radiation from the surface, f is explained above, and $L(q_0, -\mu', \phi')$ is the total (solar plus diffuse) radiance at the surface. Using the relation (Eq. 38) for the solar radiance we get

$$L(q_0, \mu, \phi) = L_{GE}(q_0, \mu, \phi) + \mu_0 E_0\, e^{-q_0/\mu_0} f(\mu, \phi, -\mu_0, \phi_0)$$
$$+ \int_0^{2\pi}\int_0^1 f(\mu, \phi, -\mu', \phi')L_D(q_0, -\mu', \phi')\,\mu'\,d\mu'\,d\phi' \tag{49}$$

Therefore, the radiances $L_D(q_0, \mu, \phi)$ and $L(q_0, -\mu, \phi)$ are related by the boundary condition. It should be noted that Eq. (49) represents the surface radiance, which, in turn depends upon the atmosphere. One can also define an intrinsic surface radiance which is independent of the atmosphere. If, in Eq. (49) we let the optical thickness q_0 be zero, then we have no atmosphere and the intrinsic radiance is

$$L_I(\mu, \phi) = L_{GE}(\mu, \phi) + \mu_0 E_0 f(\mu, \phi, \mu_0, \phi_0) \tag{50}$$

Denoting the quantity e^{-q_0/μ_0} by τ_0, the atmospheric transmittance, we have for the surface radiance $L(q_0, \mu, \phi)$

$$L(q_0, \mu, \phi) = L_I(\mu, \phi) - \mu_0 E_0(1 - \tau_0) f(\mu, \phi, \mu_0, \phi_0)$$
$$+ \int_0^{2\pi}\int_0^1 f(\mu, \phi, -\mu', \phi')L_D(q_0, -\mu', \phi')\,\mu'\,d\mu'\,d\phi' \tag{51}$$

2.5 RADIATION COMPONENTS

It is sometimes helpful to define the individual components of the radiation field. Consider a plane-parallel inhomogeneous atmosphere bounded by a flat, uniform non-Lambertian surface at temperature, T, a side view of which is shown in Figure 4. The (upwelling) radiances for a downward looking observer are denoted by the numbers 1-6 and the (downwelling) radiances for an upward looking observer are denoted by numbers 7-10. The first component is the surface radiance arising from the intrinsic emittance of the surface. It is given by

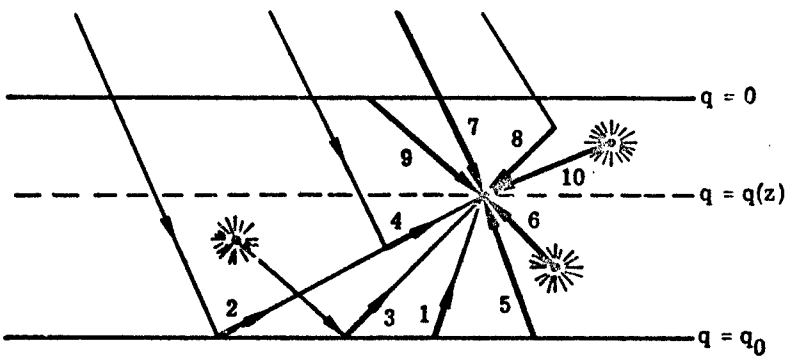

FIGURE 4. COMPONENTS OF THE RADIATION FIELD

$$L_{GE}(q_0, \mu, \phi) = \epsilon(\mu, \phi)L^*(T) \tag{52}$$

where $\epsilon(\mu, \phi)$ is the directional surface emissivity. The second component is that due to the solar attenuated beam having been reflected at the surface. It is

$$L_{GH}(q_0, \mu, \phi) = \mu_0 E_0 \, e^{-q_0/\mu_0} f(\mu, \phi, \mu_0, \phi_0) \tag{53}$$

The third component is the radiance at the surface due to diffusely scattered radiant energy having been reflected. It is

$$L_{GS}(q_0, \mu, \phi) = \int_0^{2\pi}\int_0^1 f(\mu, \phi, -\mu', \phi')L_D(q_0, -\mu', \phi')\,\mu', d\mu' d\phi' \tag{54}$$

The sum of these three components is called the surface or ground radiance, i.e.,

$$L_G(q_0, \mu, \phi) = L_{GE}(q_0, \mu, \phi) + L_{GH}(q_0, \mu, \phi) + L_{GS}(q_0, \mu, \phi) \tag{55}$$

A component not illustrated in the figure is the ground radiance after having been attenuated over a path from the ground to the point at some optical depth q. It is the beam radiance and is given by

$$L_B(q_0, \mu, \phi) = L_G(q_0, \mu, \phi)\, e^{-(q_0-q)/\mu} \tag{56}$$

where μ is the cosine of the nadir angle. Note that this is the same as the first term on the right hand side of Eq. (33). The fourth component is the singly scattered solar radiance and is

$$L_{HSS}(q', \mu, \phi) = \frac{\omega_0(q')}{4\pi\mu} E_H(q')p(q'; \mu, \phi, -\mu_0, \phi_0) \tag{57}$$

whereas its integrated value over the path is called the singly-scattered path radiance and is given by

$$L_{PSS}(q, \mu, \phi) = \frac{E_0 \, e^{q/\mu}}{4\pi\mu}\int_q^{q_0} \omega_0(q')p(q'; \mu, \phi, -\mu_0, \phi_0)\, e^{-(1/\mu_0+1/\mu)q'} dq' \tag{58}$$

which, for a homogeneous atmosphere becomes

$$L_{PSS}(q, \mu, \phi) = \frac{\omega_0\mu_0 E_0 p(\mu, \phi, -\mu_0, \phi_0)}{4\pi(\mu + \mu_0)}\left[e^{-q/\mu_0} - e^{-q_0'/\mu_0}\, e^{-(q_0-q)/\mu}\right] \tag{59}$$

The fifth component is the radiance along a path for which radiant energy is being emitted by the atmosphere in local thermodynamic equilibrium. It is

$$L_{PE}(q, \mu, \phi) = \frac{1}{\mu}\int_{q}^{q_0}[1 - \omega_0(q')]\, L^*(q')\, e^{-(q'-q)/\mu}\, dq' \tag{60}$$

which, for a homogeneous atmosphere becomes

$$L_{PE}(q, \mu, \phi) = \frac{1 - \omega_0}{\mu}\int_{q}^{q_0} e^{-(q'-q)/\mu} \quad L^*(q')\, dq' \tag{61}$$

The sixth component is the radiance along a path resulting from multiply scattered radiation. It is given by

$$L_{PMS}(q, \mu, \phi) = \frac{\omega_0(q)}{4\pi\mu}\int_0^{2\pi}\int_{-1}^{1}\int_{q}^{q_0} p(q'; \mu, \phi, \mu', \phi')\, e^{-(q'-q)/\mu} \quad L_D(q', \mu', \phi')\, dq'\, d\mu'\, d\phi' \tag{62}$$

which becomes

$$L_{PMS}(q, \mu, \phi) = \frac{\omega_0}{4\pi\mu}\int_0^{2\pi}\int_{-1}^{1} p(\mu, \phi, \mu', \phi')\int_{q}^{q_0} e^{-(q'-q)/\mu} \quad L_D(q', \mu', \phi')\, dq'\, d\mu'\, d\phi' \tag{63}$$

for a homogeneous atmosphere.

The sum of the last three components is called path radiance, i.e.,

$$L_P(q, \mu, \phi) = L_{PSS}(q, \mu, \phi) + L_{PE}(q, \mu, \phi) + L_{PMS}(q, \mu, \phi) \tag{64}$$

Therefore, we can write for the total upwelling radiance the general relation

$$L_{UP}(q, \mu, \phi) = L_G(q_0, \mu, \phi)\tau(q, q_0, \mu) + L_P(q, \mu, \phi) \tag{65}$$

where

$$\tau(q, q_0, \mu) = e^{(q_0-q)/\mu} \tag{66}$$

is the transmittance.

We can now consider the same relations for the radiation observed by an upward looking observer. The seventh component is the direct solar attenuated beam given by

$$L_H(q, -\mu, \phi) = E_H(q)\delta(\mu - \mu_0)\delta(\phi - \phi_0) \tag{67}$$

The eighth component is the singly-scattered solar radiance, i.e.,

$$L_{HSS}(q, -\mu, \phi) = \frac{E_0\, e^{-q/\mu}}{4\pi\mu}\int_0^{q}\omega_0(q')p(q'; -\mu, \phi, -\mu_0, \phi_0)\, e^{-(1/\mu_0 - 1/\mu)q'}\, dq' \tag{68}$$

which for homogeneous atmospheres becomes

$$L_{HSS}(q, -\mu, \phi) = \frac{\omega_0 \mu_0 E_0 p(\cdot \mu, \phi, -\mu_0, \phi_0)}{4\pi(\mu - \mu_0)} \left[e^{-q/\mu} - e^{-q/\mu_0} \right]; \qquad \mu \neq \mu_0 \tag{69}$$

The ninth component is the radiance along a path due to emission by the atmosphere. It is

$$L_{PE}(q, -\mu, \phi) = \frac{1}{\mu} \int_0^q [1 - \omega_0(q')] L^*(q') \, e^{-(q-q')/\mu} dq' \tag{70}$$

which, for homogeneous atmospheres is

$$L_{PE}(q, -\mu, \phi) = \frac{1 - \omega_0}{\mu} \int_0^q e^{-(q-q')/\mu} \quad L^*(q') \, dq' \tag{71}$$

Finally, the tenth component is the downward radiance due to multiply scattered radiation. It is

$$L_{PMS}(q, -\mu, \phi) = \frac{\omega_0(q)}{4\pi\mu} \int_0^{2\pi} \int_{-1}^{1} \int_0^q p(q'; -\mu, \phi, \mu', \phi') \, e^{-(q-q')/\mu} \quad L_D(q', \mu', \phi') \, dq' \, d\mu' \, d\phi' \tag{72}$$

which becomes

$$L_{PMS}(q, -\mu, \phi) = \frac{\omega_0}{4\pi\mu} \int_0^{2\pi} \int_{-1}^{1} p(-\mu, \phi, \mu', \phi') \int_0^q e^{-(q-q')/\mu} \quad L_D(q', \mu', \phi') \, dq' \, d\mu' \, d\phi' \tag{73}$$

for a homogeneous atmosphere. The sum of the last three components gives us the so-called sky, or downwelling, radiance.

$$L_{DN}(q, -\mu, \phi) = L_{HSS}(q, -\mu, \phi) + L_{PE}(q, -\mu, \phi) + L_{PMS}(q, -\mu, \phi) \tag{74}$$

3
METHODS OF CALCULATING RADIATIVE-TRANSFER FOR SCATTERING

3.1 INTRODUCTION

Scattering occurs from aerosols as well as from molecules in the atmosphere. Compared to aerosol scattering, molecular scattering is negligible outside of the visible part of the spectrum. Significantly, the sun's emission spectrum peaks in the center of the visible region. Thus, scattering by molecules can be considered confined mainly to the visible region, the sun being the chief emitter of radiation scattered from molecules, since the peak of the atmospheric radiation, emitted mainly by molecules, occurs beyond 10 μm. On the other hand, scattering by aerosols, depending on their sizes, is less strongly dependent on wavelength and, in cases of heavy haze, can be effective in both the visible and infrared regions. In this report, we shall be concerned mostly with aerosols of the sizes consistent with so-called clear-sky or near-clear-sky conditions, so that aerosol scattering in the long wavelength infrared region can usually be neglected. In the region of overlap between the visible and infrared parts of the spectrum, or in the long wavelength regions for cases when aerosol scattering is not insignificant, we shall consider the mathematical representations of scattering and molecular absorption to be completely separable.

In this section, we shall consider only the effects of scattering by gases, and scattering and absorption by aerosols, in the spectral region $0.3 \lesssim \lambda \lesssim 2$ μm. All methods described are not given equal space, especially if they have adequate exposure in the external literature. The Turner method, for example, is given large coverage because its description is found only in the reporting of contract work.

3.2 EXACT SOLUTIONS

The origins of modern radiative-transfer theory can be traced to the classic works of Chandrasekhar [42] and Ambartsumian [43] in which they developed the fundamental mathematics for the analysis of radiation in plane-parallel atmospheres. Although the original work related primarily to astrophysical problems, further advances in the theory during the last thirty years have led to computational methods which are employed to solve many problems in atmospheric physics and neutron transport theory.

The mathematical complexities of radiative-transfer theory present major difficulties to investigators who want to model the natural or artificial radiation field in a scattering medium. The problem in the determination of the radiation field is basically due to: (1) the

42. S. Chandrasekhar, Radiative Transfer, Oxford University Press, 1950.

43. V. A. Ambartsumian, "Diffuse Reflection of Light by a Foggy Medium," Compt. rend. (Doklady) Acad. Sci., USSR, Vol. 38, 1943, p. 229.

uncertainty in the knowledge of the physical state of the medium as a result of one's inability to measure enough state parameters, and (2) the complexity of the mathematical analysis or the length of computer time needed to obtain significant results. It is the latter of the two problems to which we will address ourselves in this section.

It is somewhat difficult to define an exact solution to radiative-transfer problems. One can have an exact mathematical solution to an equation or system of equations which in turn approximates the real physical medium. We shall mean by exact, those solutions for which there are no approximations in the basic mathematical formulations of the radiative-transfer equation for ideal atmospheres. Chandrasekhar was able to derive a set of nonlinear equations which could be solved to determine the radiation field for a homogeneous plane-parallel atmosphere which is illuminated by solar radiation. He also considered polarization. Results based on his analysis for the case of a pure Rayleigh atmosphere are given by Coulson, et al. [44]. The computations are very laborious and are limited to small optical thicknesses and to the radiant energy emerging from the top and bottom of the atmosphere. Later, an extended mathematical study by Busbridge [45, 46], Mullikin [47, 48, 49, 50], and Sekera [51] showed that one can also use the nonlinear equations to determine the radiation field within the atmosphere and for very large as well as small optical thicknesses. The solutions are exact for any optical thickness. For the case of inhomogeneous atmospheres as given by Eq. (31) the analysis is less well developed. Only in recent years have investigators made

44. K. L. Coulson, J. V. Dave and Z. Sekera, Tables Related to Radiation Emerging from a Planetary Atmosphere with Rayleigh Scattering, University of California Press, Berkeley, 1960.

45. I. W. Busbridge, Astrophys. J., Vol. 122, 1955, p. 327.

46. I. W. Busbridge, The Mathematics of Radiative Transfer, Cambridge University Press, 1960.

47. T. W. Mullikin, "Radiative Transfer in Finite Homogeneous Atmospheres with Anisotropic Scattering, II: The Uniqueness Problem for Chandrasekhar's ψ_ℓ and ϕ_ℓ Equations," Astrophys. J., Vol. 139, No. 4, 1964(a).

48. T. W. Mullikin, "Radiative Transfer in Finite Homogeneous Atmospheres with Anisotropic Scattering, I: Linear Singular Equations," Astrophys. J., Vol. 139, No. 1, 1964(b).

49. T. W. Mullikin, "Chandrasekhar's X and Y Equations," Trans. of the Amer. Math. Soc., Vol. 113, No. 2, 1964(c).

50. T. W. Mullikin, "The Complete Rayleigh-Scattered Field Within a Homogeneous Plane Parallel Atmosphere," Astrophys. J., Vol. 145, No. 3, 1966.

51. Z. Sekera, Reduction of Equations of Radiative Transfer in a Planetary Plane-Parallel Atmosphere, RM-4951-PR and RM-5056-PR, The RAND Corporation, Santa Monica, Calif., 1966.

progress on an exact solution for inhomogeneous atmospheres [52, 53, 54]. It should be pointed out, however, that this is a special form of inhomogeneity for which exact analytic solutions are possible; it does not necessarily correspond to realistic atmospheric inhomogeneities.

A powerful mathematical method which has been used in recent years to find a rigorous solution to the radiative-transfer equation is the Normal-Mode Expansion Technique developed by Case [55, 56]. It is basically an attempt to formulate a solution to the linear transport equation by using singular eigenfunctions, the unknown expansion coefficients of which are determined by constraining the solution to fit the boundary conditions. In this way, it is similar to the classical methods of solving partial differential equations in mathematical physics. Some of the advantages of this method are: (1) it allows one to understand the nature of the solutions, and (2) the method can easily be adapted to approximation procedures. This method, as well as others, allows one to consider the case when $\omega_0(\tau) > 1$, i.e., a multiplication of the particles. It is beyond the scope of this report to go into the mathematical details of this method but the essential ideas can be found in Refs. [57, 58, 59, 60, 61 and 62].

52. Z. Sekera, RAND Publication R-413-PR, RAND Corporation, Santa Monica, Calif., 1963.

53. J. W. Chamberlain and M. B. McElroy, Astrophys. J., Vol. 144, 1966, p. 1148.

54. A. L. Fymet and K. D. Abhyankar, "Theory of Radiative Transfer in Inhomogeneous Atmospheres, I. Perturbation Method," Astrophys. J., No. 158, 1969.

55. K. M. Case, "Elementary Solutions of the Transport Equation and Their Applications," Ann. Phys. (N.Y.), Vol. 9, 1960, pp. 1-23.

56. K. M. Case, Recent Developments in Neutron Transport Theory, Michigan Memorial Phoenix Project, Lectures Presented at the Neutron Physics Conference, University of Michigan, Ann Arbor, 1961.

57. K. M. Case and P. F. Zweifel, Linear Transport Theory, Addison-Wesley Publishing Company, Reading, Mass., 1967.

58. E. Inonu and P. F. Zweifel (eds.), Developments in Transport Theory, Academic Press, N. Y., 1967.

59. N. J. McCormick and I. Kuscer, "Half-Space Neutron Transport with Linearly Anisotropic Scattering," J. Math. Phys., Vol. 6, 1965, pp. 1939-1945.

60. K. M. Case, On the Boundary Value Problems of Linear Transport Theory, Transport Theory, Vol. I, R. Bellman, G. Birkhoft and I. Abu-Shumays (eds.), Proceedings of a Symposium in Applied Mathematics of the American Mathematical Society and the Society for Industrial and Applied Mathematics, Providence, R.I., 1969.

61. M. N. Ozisik, Radiative Transfer and Interactions with Conduction and Convection, John Wiley & Sons, N. Y., 1973.

62. B. W. Ro , Analytic Functions and Distributions in Physics and Engineering, John Wiley & Sons, N. Y., 1969.

Although the number of physical problems which can be solved by exact methods is quite limited, these techniques allow one to understand the physical principles and also serve as standards against which the approximate methods can be compared. We shall now consider the more practical computation models which are used to calculate the radiation field in Earth's atmosphere.

3.3 ADAPTATIONS TO EXACT SOLUTIONS

3.3.1 ITERATIVE METHOD

Let us write the equation for total radiance in a homogeneous atmosphere in short wavelength spectral regions for which thermal emission is considered negligible (or separable) Inasmuch as in this section we shall be interested only in diffuse radiation, we shall, for the sake of simplicity, ignore the subscript, D, and assert in what follows that $L \equiv L_D$.

$$L(q, \mu, \phi) = L(q_0, \mu, \phi)\, e^{-(q_0-q)/\mu} + \frac{\omega_0}{4\pi\mu}\int_0^{2\pi}\int_{-1}^{1}\int_q^{q_0} p(q', \mu, \phi, \mu', \phi')\, e^{-(q'-q)/\mu} \times L(q', \mu', \phi')\, dq'\, d\mu'\, d\phi' \tag{75}$$

or, in a more general form as

$$L(q) = L(q_0)\tau + \omega_0 HL(q) \tag{76}$$

where $\tau = e^{-(q_0-q)/\mu}$ and the operator H is defined by

$$HL(q) = \frac{1}{4\pi\mu}\int_0^{2\pi}\int_{-1}^{1}\int_q^{q_0} p(q', \mu, \phi, \mu', \phi')\, e^{-(q'-q)/\mu} L(q', \mu', \phi')\, dq'\, d\mu'\, d\phi' \tag{77}$$

Equation (76) can formally be written as

$$(I - \omega_0 H)L(q) = L(q_0)\tau \tag{78}$$

and the solution is

$$L(q) = (I - \omega_0 H)^{-1} L(q_0)\tau \tag{79}$$

where $(I - \omega_0 H)^{-1}$ denotes the inverse operator and I is a unit operator. Thus,

$$L(q) = \left(I + \omega_0 H + \omega_0^2 H^2 + \ldots + \omega_0^n H^n\right) L(q_0)\tau \tag{80}$$

$$= L(q_0)\tau + \omega_0 HL(q_0)\tau + \omega_0^2 H^2 L(q_0)\tau + \ldots + \omega_0^n H^n L(q_0)\tau \tag{81}$$

which will converge to the exact solution as $n \to \infty$ providing certain conditions hold true for ω_0 and the operator H. For this Neumann series to converge

$$|\omega_0| < 1/M(q_0 - q) \tag{82}$$

where M is the maximum value of the kernel in integral equation (75). Physically the first term in Eq. (81) is the directly attenuated radiance, the second term is the singly scattered radiance, and so on up to the n-th term which represents the scattering of a photon n times in the atmosphere. It can be seen from Eq. (81) that if the single-scattering albedo ω_0 is small, i.e., if there is little scattering or much absorption, the series can converge rapidly and only a few terms will provide a reasonable solution. Irvine [63, 64, 65] has applied the Neumann series method [66] to the solution of radiative transfer problems, and Herman and Browning [67] have used the Gauss-Seidel method of iteration [68]. Some results of Herman and Browning's method are illustrated in Figure 5, with polarization included. Here they calculated the radiance emerging from the top and bottom of a homogeneous, plane-parallel atmosphere with Rayleigh scattering and compared the results with those of Coulson, et al. [1960]. Herman et al. [69] extended this analysis to include aerosol scattering in more realistic atmospheres. Figure 6 illustrates typical results of their calculations for a fit to experimental data on optical thickness of the atmosphere in the Tucson, Arizona area. The normalized radiance is shown in the solar plane for a solar zenith angle of ~22.5°. The quantity q_m is the aerosol optical thickness and q_T is the total (aerosol plus Rayleigh).

It should be understood that the iteration technique can be quite time-consuming on a computer, especially if large optical thicknesses and vertical inhomogeneity is considered, although the computer time can be drastically cut if polarization is neglected.

3.3.2 SPHERICAL HARMONICS METHOD

The spherical harmonics method has been used for quite some time by investigators in neutron transport studies. Here we consider its use for the one-dimensional radiative-transfer problem. The basic equation for homogeneous atmosphere is:

---

63. W. M. Irvine, Astrophys. J., Vol. 152, 1968, p. 823.
64. W. M. Irvine, "Multiple Scattering by Large Particles, II: Optically Thick Layers," Astrophys. J., Vol. 152, June 1968.
65. W. M. Irvine, An Evaluation of Romanova's Method in the Theory of Radiative Transfer, in The Atmospheres of Venus and Mars, J. C. Brandt and M. B. McElroy (eds.), Gordon and Breach, N. Y., 1968.
66. F. B. Hildebrand, Methods of Applied Mathematics, Prentice-Hall, N. Y., 1952.
67. B. M. Herman and S. R. Browning, "A Numerical Solution to the Equation of Radiative Transfer," J. Atmos. Sci., Vol. 22, No. 5, 1965, pp. 559-566.
68. F. B. Hildebrand, Introduction to Numerical Analysis, McGraw-Hill, N. Y., 1956.
69. B. M. Herman, S. R. Browning and R. J. Curran, "The Effect of Atmospheric Aerosols on Scattered Sunlight," J. Atmos. Sci., Vol. 28, No. 3, 1971, pp. 419-428.

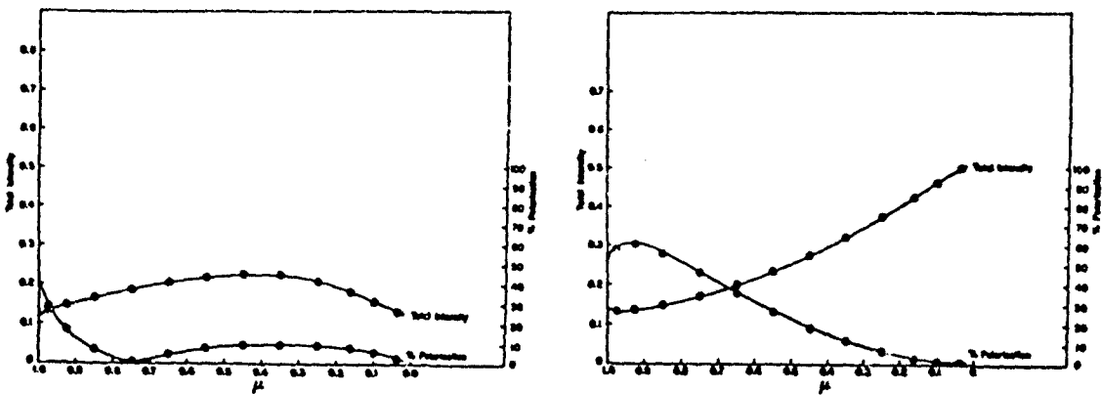

(a) Transmitted (b) Reflected

FIGURE 5. TRANSMITTED AND REFLECTED TOTAL INTENSITY, PERCENT POLARIZATION. The solid curves are from Coulson, et al. (1960) while the encircled points are from the calculations of Herman and Browning (1971). ($q = 1.0$; $\mu = 0.4$; $\phi = 0$).

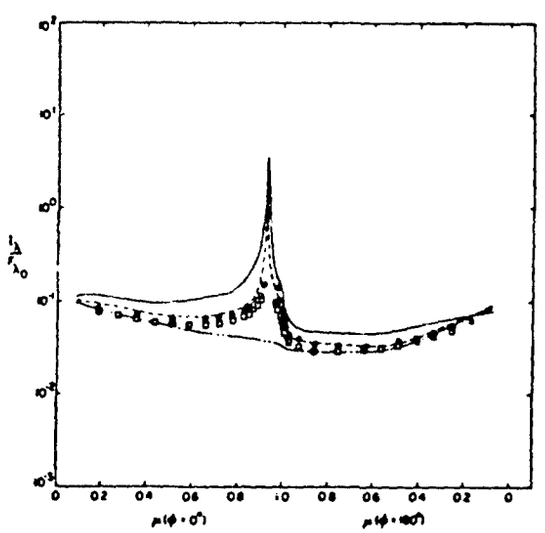

$\frac{I}{F_{\lambda_0}}$

$\mu(\phi = 0°)$ $\mu(\phi = 180°)$

$q_m = 0.23$, $q_T = 0.50$ ——

$q_m = 0.07$, $q_T = 0.34$ - - -

—·—· Pure Rayleigh ($q_R = 0.27$)

- 6/15/67 $q_T = 0.35$ Tucson $\mu_0 = 0.9397$
- 6/8/67 $q_T = 0.31$ Tucson $\mu_0 = 0.9272$

FIGURE 6. MEASURED AND THEORETICAL TRANSMITTED INTENSITIES. (Reproduced from Herman, Browning and Curran, 1965 [69].)

$$\mu\frac{dL}{dq} = L(q, \mu, \phi) - \frac{\omega_0}{4\pi}\int_0^{2\pi}\int_{-1}^{1} p(\mu, \phi, \mu', \phi')L(q', \mu', \phi')\,d\mu'\,d\phi'$$

$$- \frac{\omega_0}{4\pi}p(\mu, \phi, -\mu_0, \phi_0)E_0\, e^{-q/\mu_0} \tag{83}$$

The basic idea is quite simple; we merely represent the scattering phase function by an expansion in Legendre polynomials, P_ℓ, i.e.,

$$p(\xi) = \sum_{\ell=0}^{N} A_\ell P_\ell(\xi) \tag{84}$$

where one uses the orthogonality property of the polynomials to obtain the expansion coefficients A_ℓ, i.e.,

$$A_\ell = \frac{2\ell + 1}{2}\int_{-1}^{1} p(\xi)P_\ell(\xi)\,d\xi \tag{85}$$

In actual practice, the representation of a typical atmospheric haze type polydisperse phase function will require up to 200 terms. Using the additive properties of the spherical harmonics we get

$$p(\mu, \phi, \mu', \phi') = \sum_{\ell=0}^{N} A_\ell \left[P_\ell(\mu)P_\ell(\mu') + 2\sum_{m=1}^{\ell} \frac{(\ell - m)!}{(\ell + m)!} P_\ell^m(\mu)P_\ell^m(\mu') \cos m(\phi' - \phi) \right] \tag{86}$$

If we now expand the radiance in a set of spherical harmonics as

$$L(q, \mu, \phi) = \sum_{m=0}^{\infty} \sum_{\ell=m}^{N} A_{\ell m}(q)P_\ell^m(\mu) \cos m(\phi_0 - \phi) \tag{87}$$

and insert this expression into Eq. (83) we get a system of differential equations

$$\frac{(\ell - m)}{(2\ell - 1)}\frac{dA_{\ell-1,m}}{dq} + \frac{(\ell + m + 1)}{(2\ell + 3)}\frac{dA_{\ell+1,m}}{dq}$$

$$= \left(1 - \frac{\omega_0 A_\ell}{2\ell + 1}\right)A_{\ell m} - \frac{\omega_0 E_H(q)(2 - \delta_{0m})b_{\ell m}(-1)^{m+\ell}P_\ell^m(\mu_0)}{4\pi} \tag{88}$$

where

$$b_{\ell m} = A_\ell \frac{(\ell - m)!}{(\ell + m)!} \tag{89}$$

with the conditions

$$(\ell = m, \ldots, N; \quad 0 \le m \le N) \tag{90}$$

Assuming a solution of the form

$$A_{\ell m}(q) = g_{\ell m}(\xi)\, e^{\xi q} \tag{91}$$

we get an eigenvalue problem. Substituting Eq. (91) into Eq. (88) leads to the matrix equation

$$\tilde{\tilde{A}}\tilde{V}_m = \lambda \tilde{V}_m \tag{92}$$

where $\tilde{\tilde{A}}$ is a square matrix of order 2r, where r is the number of terms chosen, and $\lambda = 1/\xi$.

$$\tilde{\tilde{A}} = \begin{pmatrix} 0 & \beta_m & 0 & 0 & \cdots & 0 \\ \alpha_{m+1} & 0 & \beta_{m+1} & 0 & \cdots & 0 \\ \cdot & \cdot & \cdot & \cdot & \cdots & \cdot \\ \cdot & \cdot & \cdot & \cdot & \cdots & \cdot \\ \cdot & \cdot & \cdot & \cdot & \cdots & \beta_{2r-2+m} \\ 0 & 0 & \cdot & \cdot & \alpha_{2r-1+m} & 0 \end{pmatrix} \tag{93}$$

and the matrix elements are given by

$$\alpha_{m+1} = \frac{(\ell + m)(2\ell + 1)}{(2\ell - 1)(2\ell + 1 - \omega_0 A_\ell)} \tag{94}$$

$$\beta_{m+1} = \frac{(\ell + m + 1)(2\ell + 1)}{(2\ell + 3)(2\ell + 1 - \omega_0 A_\ell)} \tag{95}$$

The eigenvalues are found by taking the determinant of the matrix equation:

$$\det(\tilde{\tilde{A}} - \lambda \tilde{\tilde{I}}) = 0 \tag{96}$$

Knowing the eigenvalues $\lambda(=1/\xi)$ allows one to use Eqs. (91) and (87) along with the appropriate boundary conditions to determine the coefficients $A_{\ell m}(\tau)$.

This method has been used by neutron transport theorists [70, 71, 72, 73, 74] and by investigators of radiative-transfer problems (Chandrasekhar, 1950, and Refs. [75, 76, 77, 78]).

70. B. Davison, Neutron Transport Theory, Oxford University Press, 1957.

71. J. Yvon, "La Diffusion Macroscopique des Neutrons: Une Methode d' Approximation," J. Nucl. Energy I, Vol. 4, 1957, pp. 305-318.

(References Continued)

One of the problems encountered in using this method is the propagation of roundoff errors. The matrices are ill-conditioned in some instances and the system is numerically unstable. Canosa and Penefiel, however, were able to produce well conditioned matrices and eliminate most of numerical instability by using various transformations on matrices. Under certain conditions as for example, a Rayleigh-type atmosphere, the spherical harmonics method is much faster and more accurate than the iterative technique, but for realistic atmospheres with strongly anisotropic aerosol scattering the advantage over the iterative technique is not that great. This is because many coefficients (A_ℓ) are required in Eq. (84) to represent the scattering phase function, which increases the size of the matrix (Eq. 93), whereas the iterative method is independent of the degree of anisotropy. Because of recent advancements in matrix computer analysis [78], the spherical harmonics (P_ℓ) method can be made more efficient than the iterative technique for thick atmospheres. Typical computer times are given in Table 3 by Canosa and Penefiel for the calculation of fluxes in homogeneous atmospheres, i.e., integrals over the angles θ and ϕ. The work was done using FORTRAN IV with an H compiler on an IBM 360/195. Table 4 gives the storage requirements using double precision arithmetic.

There are other methods which have been used which are quite similar to the spherical harmonics or P_ℓ method. One is the Gauss quadrature method which approximates the scattering integral by polynomials (Kofink, 1967). Another variation, used especially in neutron transport studies is the double P_ℓ method in which the radiance is expanded into separate Legendre series, one for $\mu > 0$ and one for $\mu < 0$. This gives a better representation of the

---

72. E. M. Gelbard, Spherical Harmonics Methods: P_ℓ and Double-P_ℓ Approximations, in Computing Methods in Reactor Physics, H. Greenspan, C. N. Kelber and D. Okrent (eds.), Gordon and Breach, N. Y., 1968.

73. W. Kofink, Recent Developments in the Spherical Harmonics Method and New Integral Solutions of the Boltzmann Equation in Spherical Geometry, in Developments in Transport Theory, E. Inonu and P. F. Zweifel (eds.), Academic Press, N. Y., 1967.

74. M. M. R. Williams, Mathematical Methods in Particle Transport Theory, Wiley-Interscience, N. Y., 1971.

75. E. M. Feigelson, M. S. Malkevich, S. Ya. Kogan, T. D. Koronatova, K. S. Glazova and M. A. Kuznetsova, Calculation of the Brightness of Light in the Case of Anisotropic Scattering, Consultants Bureau Inc., N. Y., 1960.

76. J. Marengo, "Application Numerique de la Methode des Harmoniques Spheriques," Nouv. Rev. d'Optique Appliquie, Vol. 1, No. 3, 1970, pp. 181-190.

77. J. C. Guillemot, "Contribution a L' Etude du Transfert de Rayonnement dans les Nuages par la Methods des Harmoniques Spheriques," Revue d'Optique, Vol. 46, No. 6, 1967, pp. 281-308.

78. J. Canosa and H. R. Penafiel, "A Direct Solution of the Radiation Transfer Equation: Application to Rayleigh and Mie Atmospheres," J. Quant. Spect. Rad. Trans., Vol. 13, 1973, pp. 21-39.

TABLE 3. NET FLUXES FOR A MIE ATMOSPHERE OF ONE OPTICAL THICKNESS. All cases solved using 64 layers. (From Canosa and Penafiel, 1973 [78].)

Cosine of the sun's zenith angle (μ_0)	Haze*	Wavelength (μ)	Net Flux: Integral equation iteration method, Top	Net Flux: Integral equation iteration method, Bottom	Net Flux: Spherical harmonics (P_L) method**, Top	Net Flux: Spherical harmonics (P_L) method**, Bottom	L	No. of Conditioning Points	Computation time (sec) IBM 360/195, t_i	Computation time (sec) IBM 360/195, t_{sh}
1.0	L	2.45	2.7193	2.7193	2.7193	2.7193	9	0	18.41	
0.5	L	2.45	1.0612	1.0605	1.0599	1.0600	9	0	20.84	0.17†
1.0	L	0.595	2.8130	2.8176	2.8130	2.8130	21	2	21.17	
0.5	L	0.595	1.1402	1.1387	1.1394	1.1395	21	2	21.17	0.86†
1.0	L	0.3025			2.8078	2.8078	41	4		
0.5	L	0.3025	1.1511	1.1501	1.1506	1.1507	41	4	24.15	4.19†
0.5	M	0.3025	1.1825	1.1818	1.1821	1.1822	67	8	24.77	16.78‡
1.0	M	0.3025			2.8466	2.8466	67	8		
0.8	M	0.3025			2.1747	2.1748	67	8		
0.6	M	0.3025			1.5076	1.5077	67	8		
0.4	M	0.3025			0.8693	0.8694	67	8		
0.2	M	0.3025			0.3275	0.3278	67	8		19.28§

† This timing is for the two values of μ_0 shown for the given wavelength, which are solved in one pass.

‡ This timing is only for the value $\mu_0 = 0.5$.

§ This time is for the five values of μ_0 shown for Haze M, $\lambda = 0.3025\ \mu$, which are solved in one pass.

*L = terrestrial haze; M = marine haze

**L + 1 = No. of terms in expansion

TABLE 4. STORAGE REQUIREMENTS FOR DOUBLE PRECISION (From Canosa and Penafiel, 1973 [78].)

Approximation L	No. of layers	No. of cond. points	Storage
7	64	3	115K
7	128	3	120K
15	128	17	130K
21	64	3	250K
41	64	5	306.3K
67	64	9	585K
7	512	33	156K

radiance than twice as many terms in the single Legendre series. An outline of this is given by Case and Zweifel (1967) and Gelbard (1968). So far this method has not been tried for radiative transfer problems.

3.3.3 DISCRETE ORDINATES METHODS

There are many problems, especially in nuclear reactor analysis, which are extremely difficult to solve analytically by the usual methods. An approximate technique which has been used for some time is that of discrete ordinates. One can discretize the angular variables, the space variables, or both in order to arrive at a set of difference equations. This method is therefore more easily adapted to computer methods.

The first method using discrete ordinates was that of Wick [79] in which the angular integration is replaced by a weighted sum. For simplicity let us consider the radiative-transfer equation with azimuthal symmetry:

$$\mu \frac{dL(q, \mu)}{dq} = L(q, \mu) - \frac{\omega_0}{2} \int_{-1}^{1} p(\mu, \mu') L(q, \mu')\, d\mu' \tag{97}$$

The angular integral is replaced by a summation

$$\int_{-1}^{1} p(\mu, \mu') L(q, \mu')\, d\mu' \approx \sum_{i=1}^{N} p(\mu, \mu_i) L(q, \mu_i) w_i \tag{98}$$

where the μ_i are zeros of the Legendre polynomials $P_N(\mu)$ and the w_i are Christoffel numbers or relative weights. Recently, an efficient variation of this method has been developed by Whitney [80] based upon a special choice of discrete angles. According to Whitney, the computer program is much faster than previous programs and certainly faster than Monte Carlo programs. At the present time, some of the disadvantages are that it is difficult to use unless curvature is significant, and that fluxes are difficult to determine. Also, it is desirable that estimates be made of computer time and accuracy.

Another variation of the discrete ordinates method is the S_N method in which the angular interval $-1 \le \mu \le 1$ is divided into N subintervals $[\mu_{i-1}, \mu_i]$, $i = 1, 2, \ldots, N$ and the radiance is assumed to vary linearly with μ:

$$L(q, \mu) = \frac{\mu - \mu_{i-1}}{\mu_i - \mu_{i-1}} L(q, \mu_i) + \frac{\mu_i - \mu}{\mu_i - \mu_{i-1}} L(q, \mu_{i-1}) \tag{99}$$

79. G. C. Wick, Z. Phys., Vol. 121, 1943, p. 702.

80. C. Whitney, "Implications of a Quadratic Stream Definition in Radiative Transfer Theory," J. Atmos. Sci., Vol. 29, No. 8, November 1972, pp. 1520-1530.

When Eq. (99) is substituted into the radiative-transfer equation, a set of N equations results, known as the S_N set. This procedure has the advantage that it can be applied to a large number of geometric configurations both of boundaries and sources. Some of the disadvantages are that negative fluxes may result and a very fine mesh is needed for high accuracy. Because of its utility in nuclear reactor problems, many programs and options have been developed over the years. A summary of some of these programs is given by Lathrop [81] and Carlson and Lathrop [82], and the basic ideas of the S_N method are described by Lee [83]. For investigations in radiative-transfer, these programs are somewhat cumbersome to use. Nevertheless, an almost complete compilation is provided by the Radiation Shielding Information Center at the Oak Ridge National Laboratory.

The discrete ordinates approach to solving the radiative-transfer equation is regarded by some as a more fundamental method of solving the equation rather than being an approximation to an exact formulation. Thus, there has emerged a rigorous basis for the so-called discrete space theory by Preisendorfer [84]. These ideas have culminated in the practical application of discrete space theory to the solution of the radiative-transfer equation by Grant and Hunt [85, 86], and Hunt and Grant [87]. This method has been applied to a number of practical problems but limitations do exist. So far only a Lambertian surface has been considered and multidimensional problems have not been investigated in detail. Also the computer time can be significant especially for a large number of parameter values.

3.3.4 INVARIANT IMBEDDING

Another method which has been successfully used in the analysis of transport problems is that of invariant imbedding. Many of the ideas of the invariant imbedding approach were

81. K. D. Lathrop, "Discrete Ordinates Methods for the Numerical Solution of the Transport Equation," Reactor Technology, Vol. 15, No. 2, 1972, pp. 107-135.

82. B. G. Carlson and K. D. Lathrop, "Transport Theory, The Method of Discrete Ordinates," Computing Methods in Reactor Physics, H. Greenspan, C. N. Kelber and D. Okrent, (eds.), Gordon and Breach, New York, 1968.

83. C. E. Lee, The Discrete S_N Approximation for Transport Theory, Report No. LA-2595, Los Alamos Scientific Laboratory of the University of Calif., Los Alamos, N. M., 1962.

84. R. Preisendorfer, Radiative Transfer on Discrete Spaces, Pergamon Press, Oxford, 1965.

85. I. P. Grant and G. E. Hunt, "Discrete Space Theory of Radiative Transfer, I: Fundamentals," Proc. Roy. Soc. Lond. A., Vol. 313, 1969(a), pp. 183-197.

86. I. P. Grant and G. E. Hunt, "Discrete Space Theory of Radiative Transfer, II: Stability and Non-Negativity," Proc. Roy. Soc. Lond. A., Vol. 313, 1969(b), pp. 199-216.

87. C. E. Hunt and I. P. Grant, "Discrete Space Theory of Radiative Transfer and Its Application to Problems in Planetary Atmospheres," J. the Atmos. Sci., Vol. 26, September 1969, pp. 963-972.

formulated by Ambarzumian (1943) and Chandrasekhar (1950) based upon fundamental principles of invariance. However, the first application of invariant imbedding to the practical solution of radiative-transfer problems was by Bellman and Kalaba [88] with numerical results by Bellman, Kalaba, and Prestrud [89] and Bellman, Kagiwada, Kalaba, and Prestrud [90].

For the purposes of illustrating the invariant imbedding approach to the solution of radiative-transfer problems, let us consider radiation incident on a thin slab and at an angle θ_0 with respect to the outward normal to the surface. The reflected radiation will be at some angle θ as illustrated in Figure 7. The beam intensity will be reduced by an amount $e^{-k'x}$ through the infinitesimal slab of thickness x, or ~1-k'x. A fraction of the energy is reradiated. This fraction is the single-scattering albedo ω_0. For simplicity, we shall have azimuthal symmetry and assume that each scattering is isotropic. If we denote $I(\theta_0, \theta, x)$ as the specific intensity of reflected radiation (in using I, we retain the nomenclature of the original work), then for the specific intensity at $x + \Delta$ as illustrated in Figure 8 we get

$$I(\theta_0, \theta, x+\Delta) = \left(1 - \frac{k'(x)}{\mu_0}\Delta\right) I(\theta_0, \theta, x) \left(1 - \frac{k'(x)}{\mu}\Delta\right) + \frac{k'(x)\omega_0(x)\Delta}{4\pi\mu_0}$$

$$+ \frac{2\pi k'(x)\omega_0(x)\Delta}{4\pi\mu_0}\int_0^{\pi/2} I(\theta_0', \theta, x) \sin\theta_0' \, d\theta_0'$$

$$+ 2\pi\int_0^{\pi/2} \frac{k'(x)\omega_0(x)\Delta}{4\pi\mu'} I(\theta_0, \theta', x) \sin\theta' \, d\theta'$$

$$+ 4\pi^2\left[\int_0^{\pi/2} I(\theta_0, \theta', x) \frac{k'(x)\omega_0(x)\Delta}{4\pi\mu'} \sin\theta' \, d\theta'\right]\left[\int_0^{\pi/2} I(\theta_0', \theta, x) \sin\theta_0' \, d\theta_0'\right] \tag{100}$$

where $\mu = \cos\theta$ and $\mu_0 = \cos\theta_0$. The first term in Eq. (100) is due to losses (absorption) in passing through the layer of thickness Δ on the way in and on the way out. The second term is the contribution due to direct scattering from the layer of thickness Δ while the third term is due to radiation which is scattered in the layer of thickness Δ and then reflected from the slab of thickenss x. The fourth term represents radiation reflected from the slab of thickness x

88. R. Bellman and R. Kalaba, "On the Principle of Invariant Imbedding and Propagation Through Inhomogeneous Media," Proc. Nat. Acad. Sci., USA, Vol. 42, 1956, pp. 629-632.

89. R. Bellman, R. Kalaba and M. Prestrud, Invariant Imbedding and Radiative Transfer in Slabs of Finite Thickness, American Elsevier Publishing Company, New York, 1963.

90. R. Bellman, H. Kagiwada, R. Kalaba and M. Prestrud, Invariant Imbedding and Time Dependent Processes, American Elsevier Publishing Company, New York, 1964.

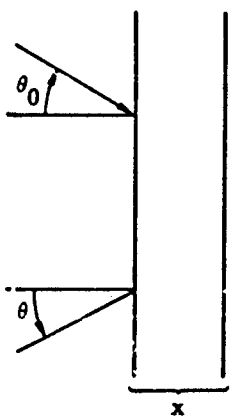

FIGURE 7. INVARIANT IMBEDDING CONFIGURATION

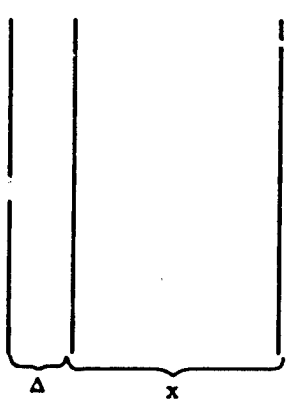

FIGURE 8. ADDITIVE SLAB CONFIGURATION FOR INVARIANT IMBEDDING

and then scattered in the layer of thickness Δ. The last term, which is nonlinear represents the contribution of radiation that is reflected from the slab of thickness x, scattered in the layer of thickness Δ, and then rereflected from the slab of thickness x. Additional terms of order Δ^2 are small and are ignored. Passing to the limit as $\Delta \to 0$ and defining

$$R(\mu, \mu_0, x) = I(\theta_0, \theta, x)\mu_0/4 \tag{101}$$

we get the following nonlinear integrodifferential equation:

$$\frac{1}{k'(x)\omega_0(x)}\left[\frac{\partial R}{\partial x} + k'(x)\left(\frac{1}{\mu_0} + \frac{1}{\mu}\right)R\right] = \left[1 + \frac{1}{2}\int_0^1 R(\mu, \mu', x)\frac{d\mu'}{\mu'}\right]\left[1 + \frac{1}{2}\int_0^1 R(\mu'', \mu_0, x)\frac{d\mu''}{\mu''}\right] \tag{102}$$

with the initial condition

$$R(\mu, \mu_0, 0) = 0 \tag{103}$$

Thus, we see that we have a non-linear integrodifferential equation subject to an initial value condition instead of the usual linear transport equation with a two-point boundary condition. The advantage of using this method is that an initial value problem can be solved easily by means of a simple iteration procedure on a computer whereas the classical approach using the two-point boundary condition usually involves the solving of a large system of linear equations. Also, there is the additional advantage that the radiation field is calculated as a function of the distance x into the slab and thus we are able to determine the internal radiation field. For computations, Eq. (102) can be converted into a system of ordinary differential equations using a quadrature integration method for the integrals.

In recent years, the invariant imbedding approach has been applied to a great number of problems, including anisotropic scattering [91], spherical shell atmospheres [92] and time dependence [93]. Comparisons have been made between Chandrasekhar's results and those based on invariant imbedding, and the agreement is good. Some of the disadvantages of this technique are the long computer time especially for optically thick media and the fact that each problem requires a whole new formulation of equations.

---

91. H. H. Kagiwada and R. E. Kalaba, "Estimation of Local Anisotropic Scattering Properties Using Measurements of Mulitply Scattered Radiation," J. Quant. Spect. Rad. Trans., Vol. 7, 1967, pp. 295-303.

92. S. Ueno, H. Kagiwada and R. Kalaba, "Radiative Transfer in Spherical Shell Atmospheres with Radial Symmetry," J. of Math. Physics, Vol. 12, No. 6, 1971, pp. 1279-1285.

93. R. E. Bellman, H. H. Kagiwada and R. E. Kalaba, Time-Dependent Diffuse Reflection From Slabs with Multiple Scattering, Memo RM-5070-PR, The RAND Corporation, July 1966.

3.3.5 DOUBLING TECHNIQUE

In the case of the iterative solution we found that convergence of the Neumann series was very slow, especially for thick atmospheres. Also, in the invariant imbedding method the addition of many thin layers to obtain a thick atmosphere is time consuming. It was van de Hulst [94] who first considered the simplification of adding layers of which each successive one was twice the optical thickness of the preceding layer. Thus, even though one starts the computational process with a very thin layer τ_0, after say 10 cycles, a thickness of $2^{10}\tau_0$ is reached. Hence, we have a very rapid computational procedure. Some of the disadvantages are that only homogeneous atmospheres can be dealt with efficiently and the overall accuracy is difficult to estimate. Nevertheless, some interesting results have been found using this method in the analysis of clouds by Hansen [95, 96].

3.3.6 MOMENT METHODS

Another mathematical method which has been devised to solve radiative-transfer problems is the moments method originally devised by Krook [97] and later developed by Sherman [98] and Liner [99]. Basically, the method is quite simple. One defines the quantities

$$M_n = \frac{1}{2}\int_{-1}^{1} \mu^n L(q, \mu)\, d\mu \tag{104}$$

with the corresponding positive and negative half moments,

$$M_n^+ = \frac{1}{2}\int_{0}^{1} \mu^n L(q, \mu)\, d\mu \tag{105}$$

$$M_n^- = \frac{1}{2}\int_{-1}^{0} \mu^n L(q, \mu)\, d\mu \tag{106}$$

---

94. H. C. Van de Hulst and K. Grossman, "Multiple Light Scattering in Planetary Atmospheres," The Atmospheres of Venus and Mars, J. C. Brandt and M. B. McElroy (eds.), Gordon and Breach, N. Y., 1968.

95. J. E. Hansen, "Exact and Approximate Solutions for Multiple Scattering by Cloudy and Hazy Planetary Atmospheres," J. Atmos. Sci., Vol. 29, No. 3, May 1969(a), pp. 478-487.

96. J. E. Hansen, "Radiative Transfer by Doubling Very Thin Layers," Astrophys. J., Vol. 155, February 1969(b).

97. M. Krook, Astrophys. J., Vol. 122, 1955, p. 488.

98. M. P. Sherman, "Moment Methods in Radiative Transfer Problems," J. Quant. Spect. Rad. Trans., Vol. 7, 1967, pp. 29-109.

99. R. T. Liner, Jr., Moment and Discrete Ordinate Methods in Radiative Transfer Problems, Vol. 9, 1969, pp. 721-732.

It should be noted that the zenith moment is the average radiance and the first moment is the irradiance or flux. Hence, one can use these expressions in the radiative-transfer equation to get a solution to any order n, i.e.,

$$L(q, \mu) = \sum_{n=0}^{n-1} A_n(q)\mu^n \qquad (107)$$

where the A_n are expansion coefficients. It turns out that this procedure is equivalent to the discrete ordinates method using a half range with similar degrees of accuracy.

3.3.7 MONTE CARLO

A statistical procedure called Monte Carlo has been used in particle transport analysis for the past thirty years. It consists basically of a particle counting method with probabilities associated with the physical processes involved. Much of the early work dealt with neutron transport in complicated geometrical systems whereas in recent years the method has been applied to a variety of problems including photon transport in the atmosphere.

The basic description of a Monte Carlo process is as follows: One devises a computer program in which the physics of the problem is described in a probabilistic manner. Along with a well-defined coordinate system and boundary conditions the particles are released from a source and then they are followed as they undergo scattering and absorption. The processing continues until reasonable statistical estimates have been obtained. In this general way, Collins and Wells [100], Collins [101], and Wells and Marshall [102] have calculated the visible radiation field within the atmosphere and Plass and Kattawar [103], and Kattawar and Plass [104] have done similar calculations for clouds.

The main advantage of the Monte Carlo procedure is that very complicated geometrics can be considered. The main disadvantage is the excessive amount of computer time which is

100. D. G. Collins and M. B. Wells, Monte Carlo Codes for Study of Light Transport in the Atmosphere, Vol. I. Description of Codes, Vol. II, Utilization, ECOM-00240-F I, ECOM-00240-F II, 1965.

101. D. G. Collins, Atmospheric Path Radiance Calculations for a Model Atmosphere, Report No. AFCRL-68-0124, Air Force Cambridge Research Laboratories, Bedford, Mass., 1968.

102. M. B. Wells and J. D. Marshall, Monochromatic Light Intensities Above the Atmosphere Resulting from Atmospheric Scattering and Terrestrial Reflection, Radiative Research Assoc., Inc., Ft. Worth, Tex., 1968.

103. G. N. Plass and G. W. Kattawar, "Influence of Single Scattering Albedo on Reflected and Transmitted Light from Clouds," Appl. Optics, Vol. 7, No. 2, February 1968, pp. 361-367.

104. G. W. Kattawar and G. N. Plass, "Infrared Cloud Radiance," Appl. Optics, Vol. 8, No. 6, June 1969, pp. 1169-1178.

expended to obtain reasonably accurate values. The accuracy is proportional to the square root of the number of particles counted. Except for unusually complicated geometries it is probably best that the user apply less computer-time consuming techniques.

3.4 APPROXIMATE METHODS

The methods discussed in the preceding sections all have one thing in common: they provide mathematically exact solutions to certain classes of radiative-transfer problems if one continues to increase the number of terms in a series or if the computer time is increased. High accuracy, however, is not always necessary, especially in many engineering applications, because usually one does not know the pertinent input parameter values well enough. Speed and overall efficiency of operations are often more important and for these reasons it is desirable to have mathematically approximate models which use very little computer time and which give reasonably accurate results.

3.4.1 SCHUSTER-SCHWARZSCHILD METHOD

Early in the twentieth century, Schuster (1905) and Schwarzschild [105] introduced a simple method of directional averaging. The radiation field is assumed to be nearly isotropic and averages are taken over the upward and downward hemispheres:

$$L_+(q) \equiv \int_0^{2\pi}\int_0^1 L(q, \mu, \phi)\, d\mu\, d\phi \tag{108}$$

$$L_-(q) \equiv \int_0^{2\pi}\int_{-1}^0 L(q, \mu, \phi)\, d\mu\, d\phi \tag{109}$$

and also a weighted average,

$$E_+(q) \equiv \int_0^{2\pi}\int_0^1 \mu L(q, \mu, \phi)\, d\mu\, d\phi \tag{110}$$

$$E_-(q) \equiv \int_0^{2\pi}\int_{-1}^0 \mu L(q, \mu, \phi)\, d\mu\, d\phi \tag{111}$$

Then, with the assumption of a nearly isotropic field we have

$$\begin{aligned} E_+(q) &\cong \tfrac{1}{2} L_+(q) \\ E_-(q) &\cong \tfrac{1}{2} L_-(q) \end{aligned} \tag{112}$$

105. K. Schwarzschild, "Uber das Gleichgewicht der Sonnenatmosphere," Gottinger Nachrichten, Vol. 41, 1906.

Using these formulas in the radiative-transfer equation with an isotropic scattering law,

$$\mu \frac{dL}{dq} = L(q, \mu, \phi) - \frac{\omega_0}{4\pi} \int_0^{2\pi} \int_{-1}^{1} L(q, \mu', \phi') \, d\mu' \, d\phi' \tag{113}$$

provides us with two differential equations instead of the integro-differential equation.

$$\frac{dE_+(q)}{dq} = (2 - \omega_0) E_+(q) - \omega_0 E_-(q) \tag{114}$$

$$\frac{dE_-(q)}{dq} = \omega_0 E_+(q) - (2 - \omega_0) E_-(q) \tag{115}$$

When these coupled equations are solved using the appropriate boundary conditions one obtains the irradiance (upward and downward) at any point in the medium. Because of the assumptions on the directionality of the field (Eq. 112) we expect a model based upon these assumptions to be especially valid deep within an atmosphere rather than near the boundaries.

3.4.2 EDDINGTON METHOD

In 1926, Eddington [106] introduced another averaging method. This time we average over all space rather than over hemispheres, i.e.,

$$\bar{L} = \frac{1}{4\pi} \int_0^{2\pi} \int_{-1}^{1} L(q, \mu, \phi) \, d\mu \, d\phi \tag{116}$$

Integrating Eq. (113) gives

$$\frac{d\Phi}{dq} = \bar{L}(q) - \omega_0 \bar{L}(q) \tag{117}$$

which shows that the flux $\Phi(q)$ is a constant if there is no absorption. Multiplying Eq. (113) by μ and integrating over all space gives

$$\frac{dK}{dq} = \Phi(q) \tag{118}$$

where

$$\Phi(q) = \frac{1}{4\pi} \int_0^{2\pi} \int_{-1}^{1} \mu L(q, \mu, \phi) \, d\mu \, d\phi \tag{119}$$

and

106. A. S. Eddington, The Interval Constitution of the Stars, Cambridge University Press, 1926.

$$K(q) = \frac{1}{4\pi}\int_0^{2\pi}\int_{-1}^{1}\mu^2 L(q, \mu, \phi)\, d\mu\, d\phi \tag{120}$$

The Eddington assumption is that the field is almost isotropic, i.e.,

$$K(q) \cong 1/3\,\bar{L} \tag{121}$$

or

$$\frac{d^2\bar{L}}{dq^2} = 3(1 - \omega_0)\bar{L}(q) \tag{122}$$

We expect this approximation to hold when we have very thick atmospheres.

Comparisons have been made between the Schuster-Schwarzschild (two-stream) model and the Eddington model (Irvine, 1968). The conclusion is that the two-stream model is better when low order scattering dominates. The Eddington method fails for conditions near the boundary (i.e., for large solar angles).

3.4.3 ROMANOVA'S METHOD

One of the major difficulties involved in the solution of the radiative-transfer equation is how to deal with the high degree of anisotrophy of the scattering phase function. Romanova [107, 108, 109] has developed a method based upon a small angle approximation similar to that used by Wang and Guth [110] in nuclear physics. If one were to expand the phase function in a series of Legendre polynomials many terms would be required and this leads to the rather difficult eigenvalue problem in the spherical harmonics method. Romanova's method consists of expressing the radiance as the sum of two terms, one for small angles, i.e., the highly anisotropic part of the phase function, and another for the remaining part of the phase function.

$$L(q, \mu, \phi) = L_{sa}(q, \mu, \phi) + \tilde{L}(q, \mu, \phi) \tag{123}$$

The $L_{sa}(q, \mu, \phi)$ solution is found by replacing μ by μ_0 in the radiative-transfer equation and new boundary conditions, i.e.,

---

107. L. M. Romanova, "The Solution of the Radiative-Transfer Equation for the Case When the Indicatrix of Scattering Greatly Differs from the Spherical One, I," Opt. Spek., Vol. 13, 1962(a), p. 429.

108. L. M. Romanova, "Solution of the Radiative-Transfer Equation for the Case of a Highly Nonspherical Scattering Index, II," Opt. Spek., Vol. 13, 1962(b), p. 819.

109. L. M. Romanova, "Radiation Field in Plane Layers of a Turbid Medium with Highly Anisotropic Scattering," Opt. Spek., Vol. 14, 1963, p. 262.

110. M. C. Wang and E. Guth, Phys. Rev., Vol. 84, 1951, p. 1092.

$$\tilde{L}(q, \mu, \phi) = 0, \quad \mu > 0$$
$$\tilde{L}(q, \mu, \phi) = -L_{sa}(q, \mu, \phi), \quad \mu < 0 \tag{124}$$

The radiance $\tilde{L}(q, \mu, \phi)$ can then be expanded in a series of Legendre polynomials and presumably it will require fewer terms since most of the anisotropy is accounted for by the $L_{sa}(q, \mu, \phi)$ term. Irvine (1968) has made comparisons between Romanova's method and the doubling method and found excellent agreement over a wide range of angles and optical thicknesses. No estimate is given for the amount of computer time but it is considerably reduced over the other more conventional techniques.

3.4.4 THE TURNER METHOD

The development of large-scale computer processing of multispectral remote sensing data has led to the requirement that atmospheric corrections be made on a point-by-point basis. Thus, it is necessary to know radiances and other radiometric quantities at many points throughout a scene. What is needed then, is an atmospheric radiative-transfer model which is fast, accurate, and adaptable to a range of environmental conditions. Turner [111, 112, 113, 114] has developed a modified two-stream iterative model especially designed for hazy atmospheres.

The one dimensional radiative-transfer equation to be solved is

$$\mu \frac{dL}{dq} = L(q, \mu, \phi) - \frac{\omega_0}{4\pi}\int_0^{2\pi}\int_{-1}^{1} p(\mu, \phi, \mu', \phi')L(q, \mu', \phi')\, d\mu'\, d\phi' - \frac{E_H(q)\omega_0}{4\pi}p(\mu, \phi, -\mu_0, \phi_0) \tag{125}$$

where the scattering phase function is approximated as

$$p(\mu, \phi, \mu', \phi') = 4\pi\eta\delta(\mu' - \mu)\delta(\phi' - \phi) + 4\pi(1 - \eta)\delta(\mu' + \mu)\delta(\phi' - \pi - \phi) \tag{126}$$

where η represents the fraction of the radiation scattered into a forward hemisphere, i.e.,

111. R. E. Turner, Remote Sensing in Hazy Atmospheres, Proceedings of ACSM/ASP, Meeting in Washington, D. C., March 1972.

112. R. E. Turner, "Atmospheric Effects in Remote Sensing," Remote Sensing of Earth Resources, Vol. II, F. Shahrokhi (ed.), University of Tennessee, 1973.

113. R. E. Turner, "Contaminated Atmospheres and Remote Sensing," Remote Sensing of Earth Resources, Vol. III, F. Shahrokhi (ed.), University of Tennessee, 1974.

114. R. E. Turner, Radiative Transfer on Real Atmospheres, Report No. 190100-24-T, Environmental Research Institute of Michigan, Ann Arbor, July 1974.

$$\eta = \frac{1}{4\pi}\int_0^{2\pi}\int_0^1 p(\xi)\,d\xi\,d\chi \tag{127}$$

$$= \frac{1}{2}\int_0^1 p(\xi)\,d\xi \tag{128}$$

For Rayleigh scattering $\eta = 0.5$ whereas for aerosol scattering in the visible region $\eta \sim 0.95$. Using Eq. (126) in Eq. (125) and a similar assumption regarding the radiation field, i.e.,

$$L(q, \mu, \phi) = \frac{1}{\mu_0}[E'_+(q)\delta(\mu - \mu_0)\delta(\phi - \pi - \phi_0) + E'_-(q)\delta(\mu + \mu_0)\delta(\phi - \phi_0)] \tag{129}$$

where $E'_+(q)$ and $E'_-(q)$ are irradiances in the upward and downward directions respectively, we get two complex linear differential equations for $E'_+(q)$ and $E'_-(q)$:

$$\frac{dE'_+(q)}{dq} = \frac{1 - \omega_0\eta}{\mu_0}E'_+(q) - \frac{\omega_0(1 - \eta)}{\mu_0}E'_-(q) - \omega_0(1 - \eta)E_s(q) \tag{130}$$

$$-\frac{dE'_-(q)}{dq} = \frac{1 - \omega_0\eta}{\mu_0}E'_-(q) - \frac{\omega_0(1 - \eta)}{\mu_0}E'_+(q) - \omega_0\eta E_s(q) \tag{131}$$

The $1/\mu_0$ dependence is included to normalize the diffuse irradiance field. The primed quantities indicate that we are calculating the field for a surface albedo of zero. The solution to these equations and similar ones for an isotropic radiation reflected from a Lambertian surface are too complicated to be presented here but their functional form is given by

$$E_+(q) = \mu_0 E_0 f_+(\mu, k, \omega_0, \mu_0, \rho, q, q_0) \tag{132}$$

$$E_-(q) = \mu_0 E_0 f_-(\eta, k, \omega_0, \mu_0, \rho, q, q_0) \tag{133}$$

$$\tilde{E}_-(q) = \mu_0 E_0\left[f_-(\eta, k, \omega_0, \mu_0, \rho, q, q_0) + e^{-q/\mu_0}\right] \tag{134}$$

where $E_+(q)$, $E_-(q)$, and $\tilde{E}_-(q)$ are the upward diffuse, downward diffuse, and total downward irradiances respectively, and

$$k = \sqrt{(1 - \omega_0)(1 + \omega_0 - 2\eta\omega_0)}/\mu_0 \tag{135}$$

A computer program was written which allows one to calculate these irradiance components as a function of wavelength, solar zenith angle, single-scattering albedo, surface albedo, altitude, visual range, and optical depth. Figure 9 illustrates the diffuse downward component for the Turner method where $\eta = 0.5$ and $\theta_0 = 0^o$, thus simulating a Rayleigh atmosphere.

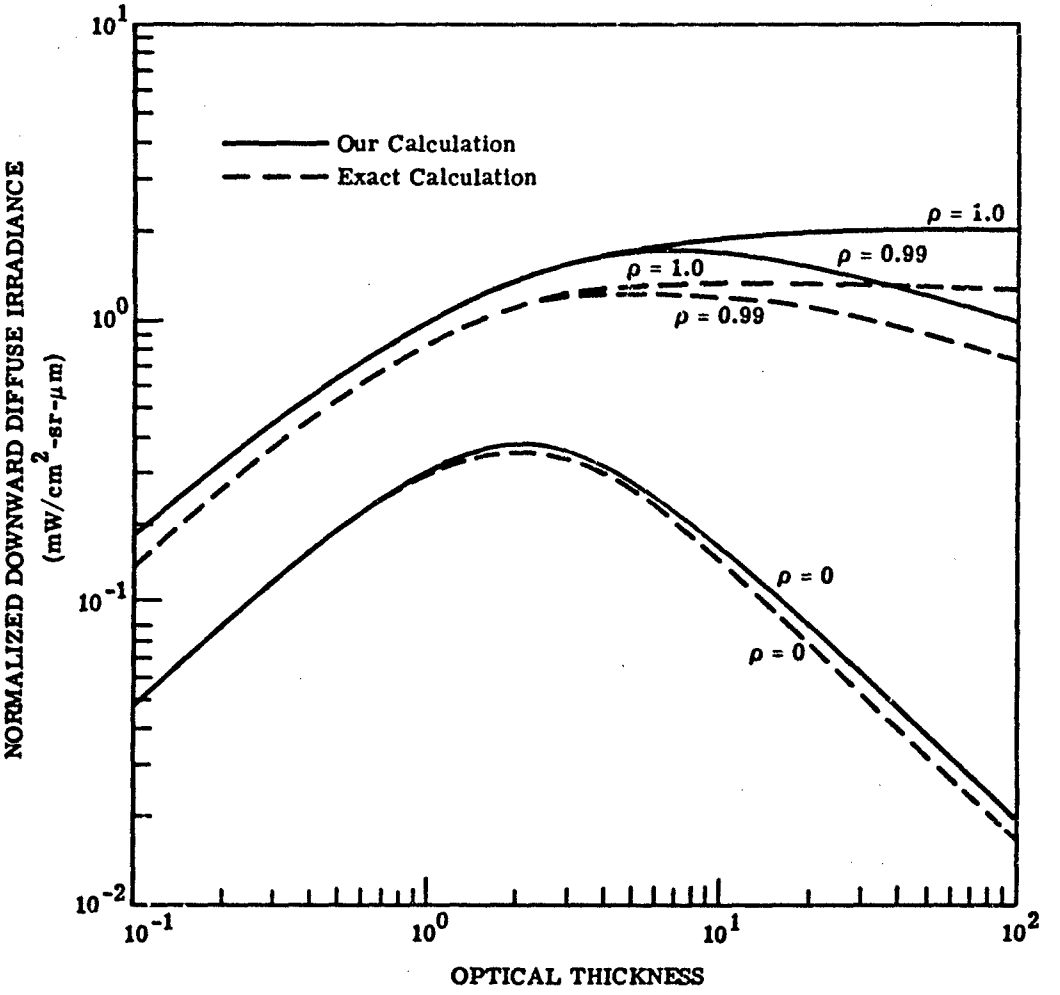

FIGURE 9. NORMALIZED DOWNWARD DIFFUSE IRRADIANCE VS OPTICAL THICKNESS FOR VARIOUS SURFACE REFLECTANCES. ρ = surface reflectance; solar zenith angle = 0°; no absorption; Rayleigh atmosphere.

Kahle [115] carried out a similar calculation using the results of Chandrasekhar's exact calculation for a Rayleigh atmosphere. Using the scattering functions calculated by Sekera and Kahle [116] we have also calculated the exact results and compared them with the approximate calculations as are illustrated in Figure 9. The agreement is good considering the approximations that are used. It should be noted, however, that a homogeneous atmosphere is assumed and polarization is not included in the present development. For the usual optical thicknesses for Earth's atmosphere and reasonable reflectances the agreement is quite good. A similar comparison, shown in Figure 10 was carried out for the diffuse radiation emitted by the atmosphere. One advantage of the approximate model, as with some other models as well, is that the irradiances can be determined at any interior point of the medium. Thus, it is possible to see how the radiation field changes as one goes from the bottom to the top of the atmosphere [117].

Using a relation similar to Eq. (129) and the irradiances as determined above one can then find the spectral radiances. These are given formally as

$$L_S = L_S(\eta, k, \omega_0, \mu_0, \mu, \phi, \bar{\rho}, q, q_0) \tag{136}$$

$$L_P = L_P(\eta, k, \omega_0, \mu_0, \mu, \phi, \bar{\rho}, q, q_0) \tag{137}$$

$$L_T = L_T(\eta, k, \omega_0, \mu_0, \mu, \phi, \rho, \bar{\rho}, q, q_0) \tag{138}$$

where L_S is the spectral sky radiance at any point in the medium (i.e., the radiance for an observer looking into the upper hemisphere) and L_P is the path radiance (i.e., the radiance for an observer looking into the lower hemisphere at a target with zero reflectance). L_T is the total spectral radiance for a downward looking observer. It should be noted that L_T is not only a function of the background albedo $\bar{\rho}$ but also of the target reflectance ρ. In general then,

$$L_T = L_G\tau + L_P \tag{139}$$

where L_G represents the radiance at the surface and τ is the transmittance from the surface to the observer.

The computational accuracy of this model was tested by comparing it with exact results. Figure 11 illustrates the comparison between the Turner method calculations and those of

115. A. B. Kahle, "Global Radiation Emerging from a Rayleigh-Scattering Atmosphere of Large Optical Thickness," Astrophys. J., Vol. 151, February 1968.

116. Z. Sekera and A. B. Kahle, Scattering Functions of Rayleigh Atmospheres of Arbitrary Thickness, R-4520PR, The RAND Corporation, Santa Monica, Calif., 1965.

117. W. A. Malila, R. B. Crane, A. Omarzu and R. E. Turner, Studies of Spectral Discrimination, Report No. 31650-22-T, Willow Run Laboratories of the Institute of Science and Technology, University of Michigan, Ann Arbor, 1971.

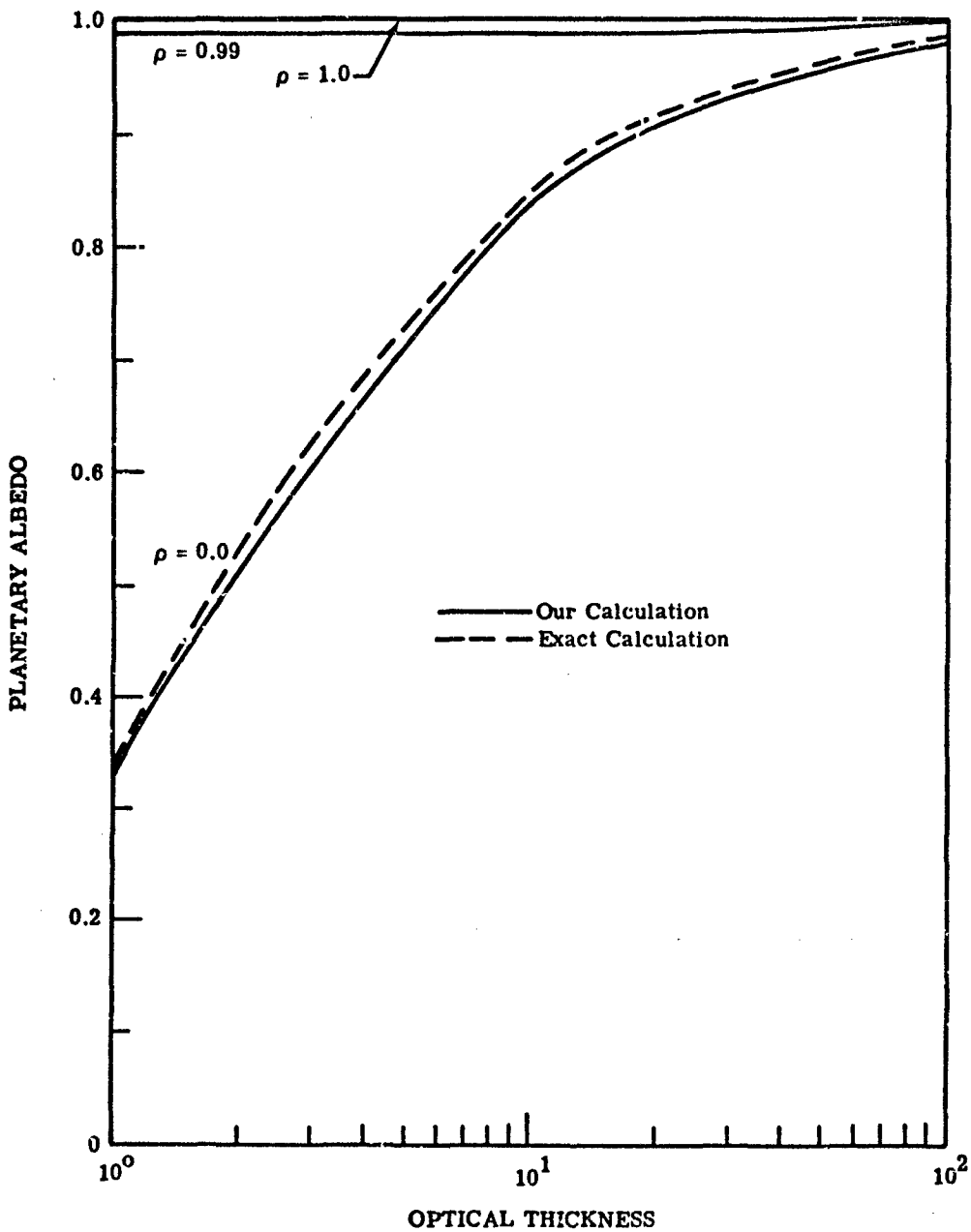

FIGURE 10. PLANETARY ALBEDO VS OPTICAL THICKNESS FOR VARIOUS SURFACE REFLECTANCES. Solar zenith angle = 0°; no absorption; scan angle = 0°; Rayleigh atmosphere.

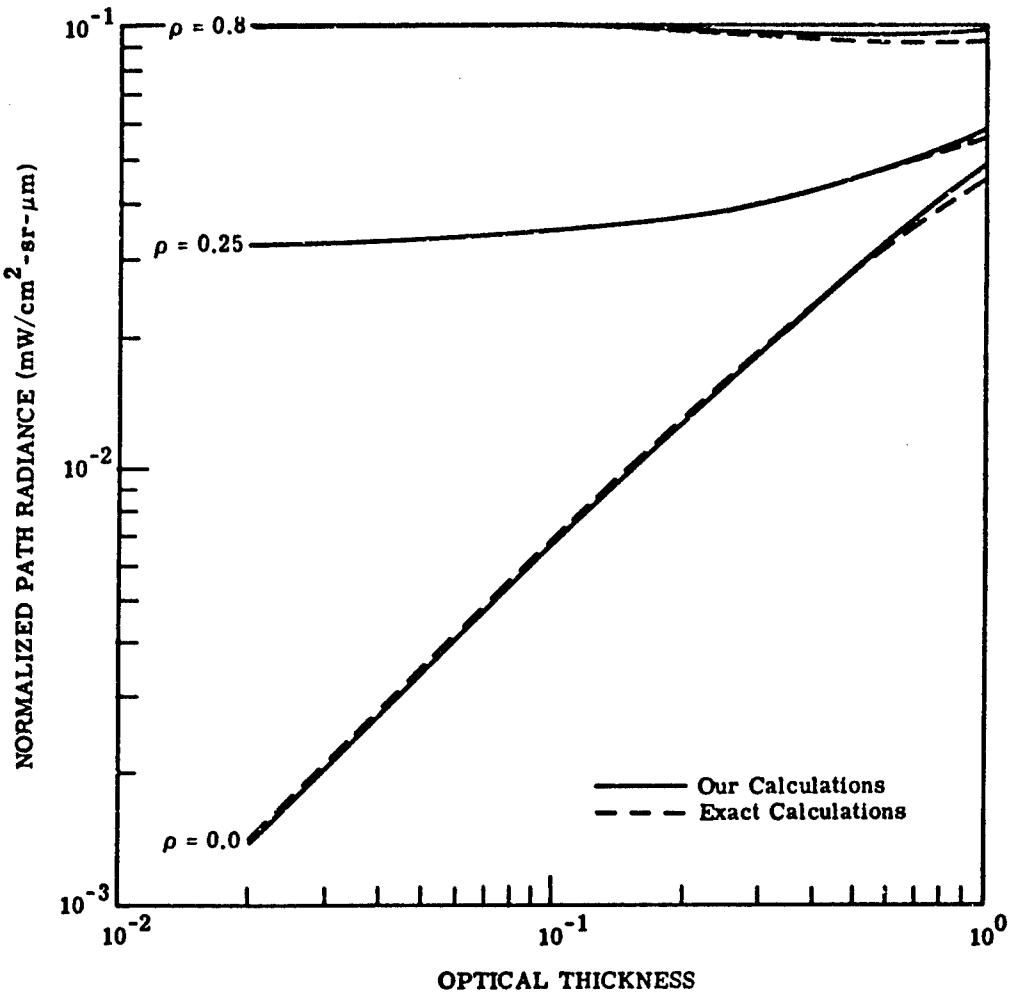

FIGURE 11. NORMALIZED PATH RADIANCE AT THE TOP OF THE ATMOSPHERE VS OPTICAL THICKNESS FOR SEVERAL SURFACE REFLECTANCES. ρ = surface reflectance; solar zenith angie = 0^{o}; no absorption; Rayleigh atmosphere.

Coulson et al. (1960). E_0 is the extra-terrestrial irradiance due to the sun. Figure 12 depicts the path radiance as a function of q_0 for those sun angles. For certain angles and for large optical thicknesses there is some discrepancy between the exact and approximate calculations. In figure 13, we see the variation of sky radiance with solar zenith angle for two different optical thicknesses. Both the magnitudes and the angular variations agree well except for the case of large solar angles ($\tilde{>}75^o$) and larger optical thicknesses. As a final illustration of the accuracy of the approximate model we present the total spectral radiance as a function of nadir angle in Figure 14. Other results have been reported in the literature [118].

The method is quite adaptable to a wide range of geometrical problems. For example, the influence of background albedo or target radiance vs multiple scattering is being explored (Turner, 1974) and various other multidimensional models are under investigation. Finally, we present in Figure 15 a diagram which illustrates the basic radiation-transfer multiple scattering model as developed at ERIM.

118. W. A. Malila, R. B. Crane and R. E. Turner, Information Extraction Techniques for Multispectral Scanner Data, Report No. 31650-74-T, Willow Run Laboratories of the Institute of Science and Technology, University of Michigan, Ann Arbor, 1972.

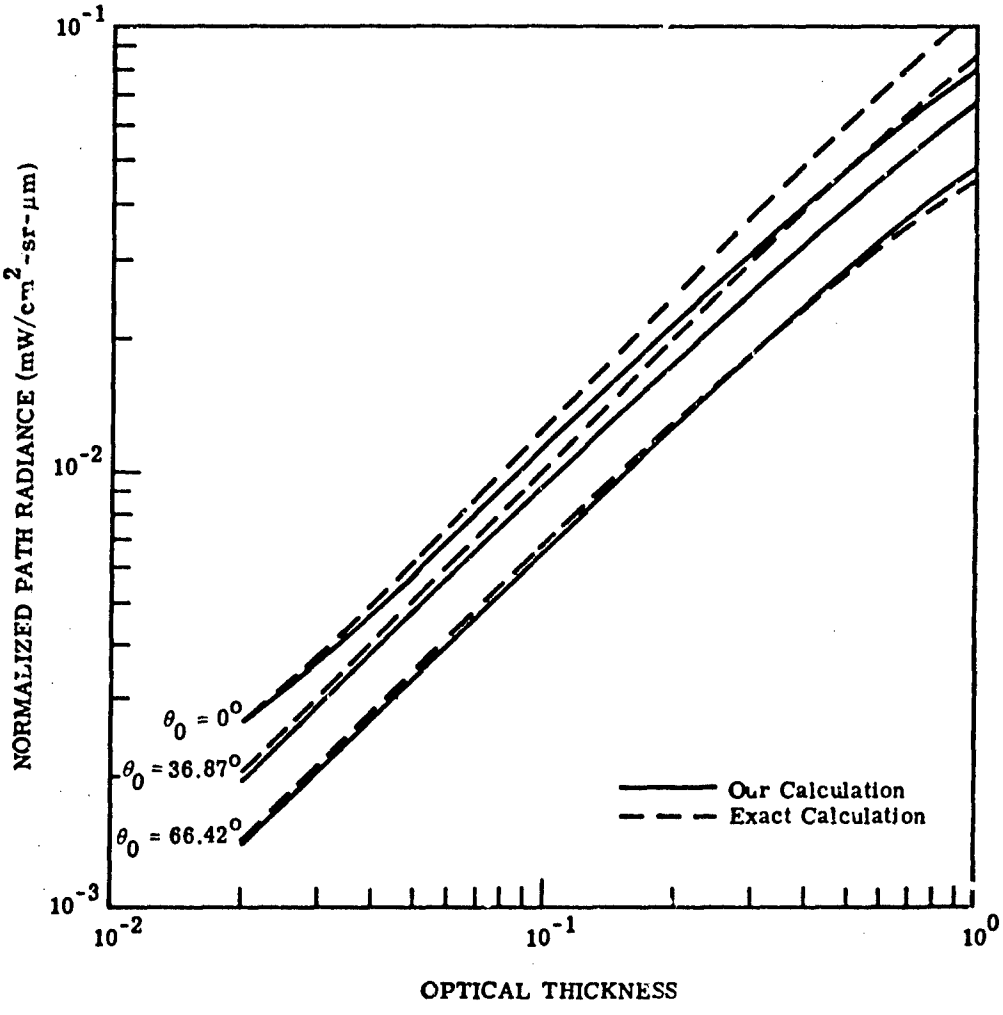

FIGURE 12. NORMALIZED PATH RADIANCE AT THE TOP OF THE ATMOSPHERE VS OPTICAL THICKNESS FOR VARIOUS SOLAR ZENITH ANGLES. Surface reflectance = 0.0; no absorption; scan angle = 0°; Rayleigh atmosphere.

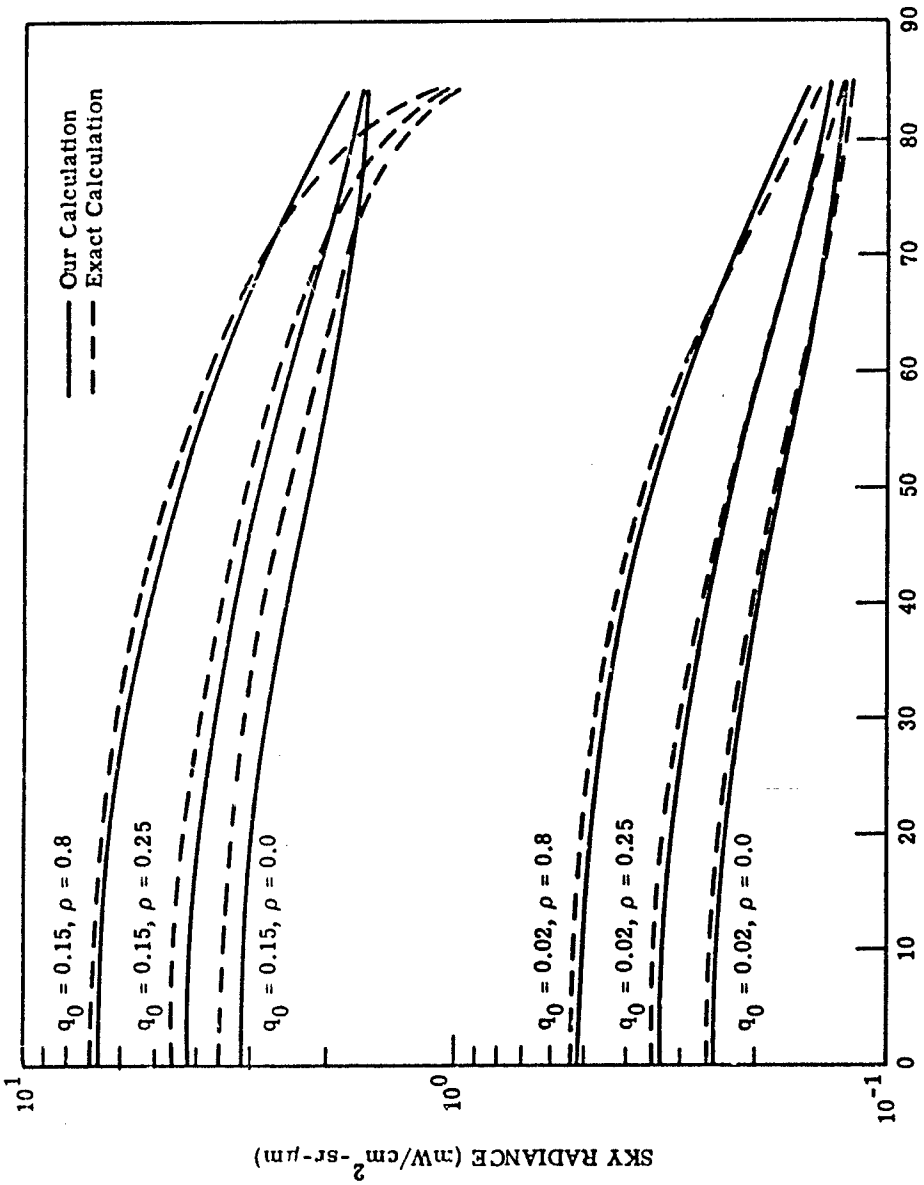

FIGURE 13. SKY RADIANCE VS SOLAR ZENITH ANGLE. q_0 = optical thickness; ρ = surface reflectance; scan angle = 0°; Rayleigh atmosphere.

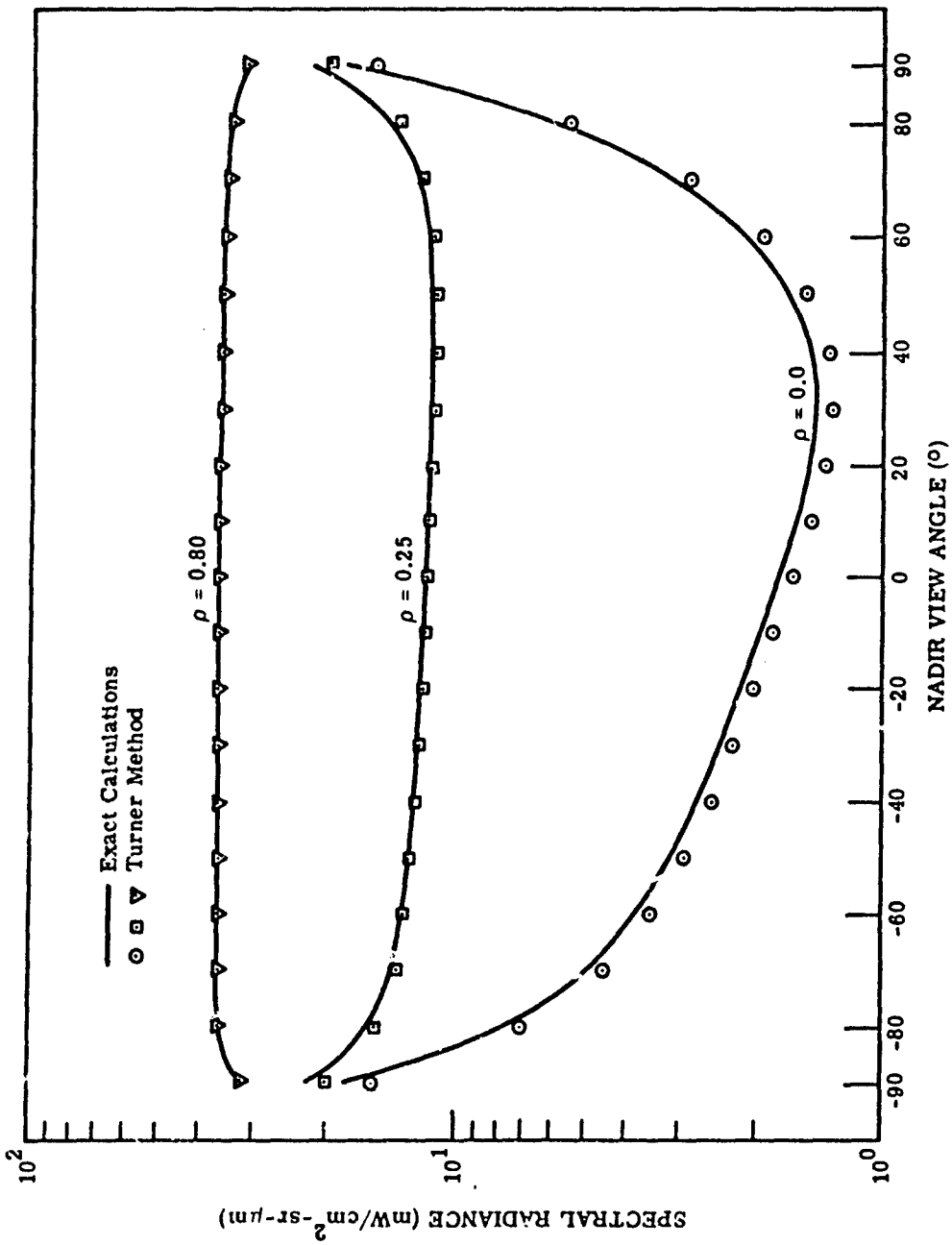

FIGURE 14. TOTAL SPECTRAL RADIANCE IN THE SOLAR PLANE AT THE TOP OF A RAYLEIGH ATMOSPHERE BOUNDED BY A SURFACE WITH LAMBERTIAN REFLECTANCE ρ. Wavelength = 0.546 μm; solar zenith angle = 36.87°; optical thickness = 0.1.

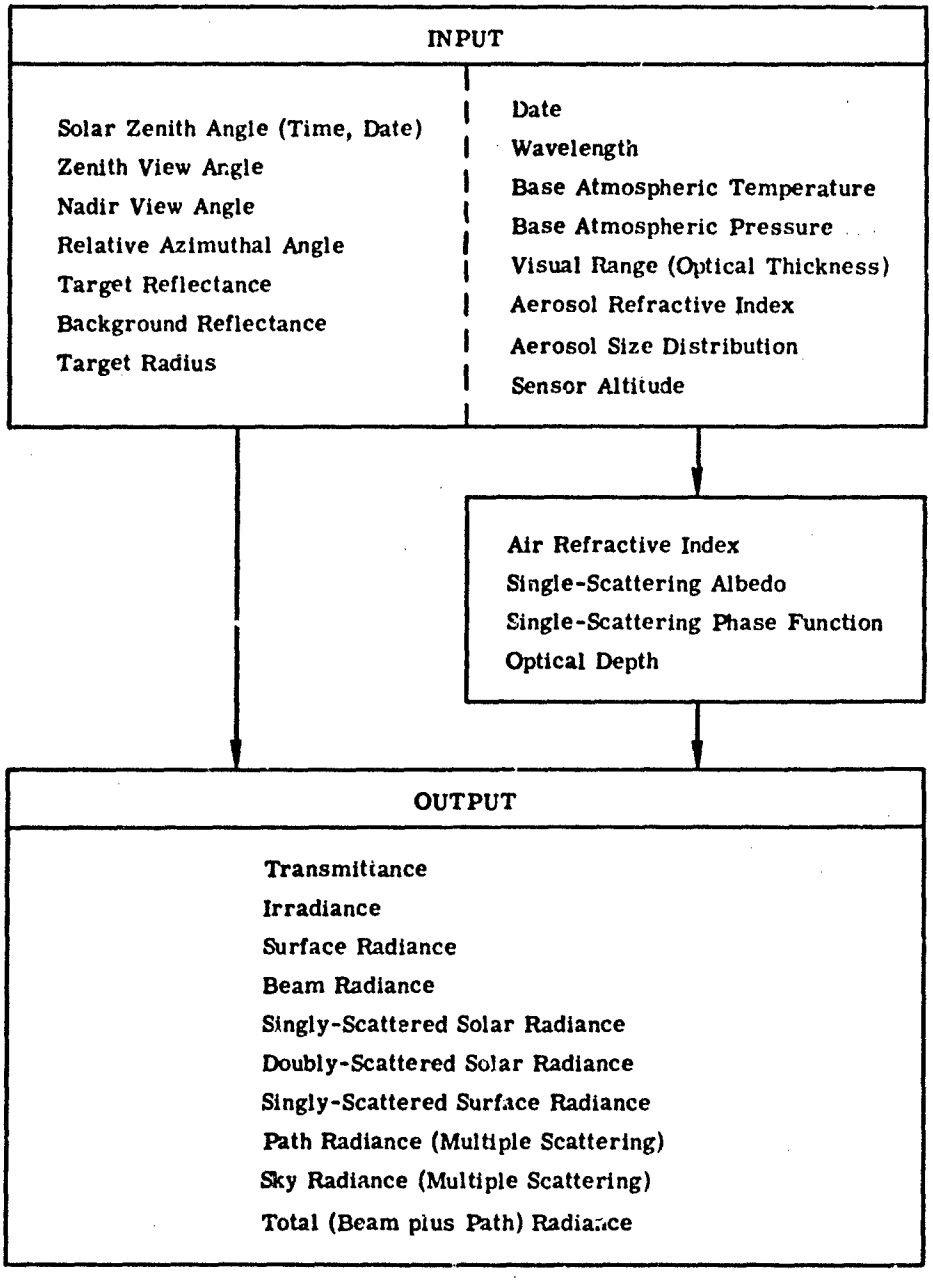

FIGURE 15. TURNER RADIATIVE TRANSFER MODEL

4
THEORY OF ATMOSPHERIC ABSORPTION

4.1 INTRODUCTION

In this chapter we continue to maintain the separability of the scattering and molecular absorbing parts of the radiative transfer equation. In this way we can discuss the process of absorption as if no radiation were scattered from the beam, so that only molecular absorption occurs. This is analogous to the manner in which we ignored molecular absorption in the discussion of scattering. Thus, the report can be separated into two essentially independent parts, one devoted to scattering and one to molecular absorption, the latter being discussed in this section.

4.2 RADIATIVE TRANSFER EQUATION FOR MOLECULAR ABSORPTION

It is seen from the general discussion of the radiative transfer equation that Eq. (21) in Section 2.3 simplifies to a non-scattering representation of the transfer of radiation by the elimination of the middle term by setting $\omega_0 = 0$. This will be true if the scattering coefficient $k'_s(\lambda, s) = 0$, leaving $k'(\lambda, s) = k'_a(\lambda, s)$. Thus, Eq. (21) for the spectral radiance at s becomes (the direction of s' is from s to R):

$$L_\lambda(\lambda, s) = L_\lambda(\lambda, R) \exp - \int_s^R k_a(\lambda, s')\rho(s')ds' + \int_s^R L^*_\lambda[\lambda, T(s')]$$

$$\exp - \left[\int_s^{s'} k_a(\lambda, s'')\rho(s'')ds''\right] k_a(\lambda, s')\rho(s')ds' \qquad (140)$$

where $k_a = k'_a/\rho$ is the mass absorption coefficient. To show explicitly the dependence of the spectral absorptance, $A(\lambda)$, on the mass of the substance through which the radiation travels and not merely the distance, the mass absorption coefficient is used, and the optical path or optical depth is given by:

$$q(\lambda) = \int k(\lambda, s)\rho(s)ds \qquad (141)$$

where $\rho(s)$ is the path-dependent mass density of the absorber in grams per cm^3, when s is the distance in cm. The units for k are, therefore, $(gm\text{-}cm^{-2})^{-1}$. Equation (140) is thus written:

$$L_\lambda(\lambda, s) = L(\lambda, R)\,\tau(\lambda, R) + \int_s^R L_\lambda^*[\lambda, T(s')]\,\rho(s')k(\lambda, s')\,x$$

$$\exp - \left[\int_s^{s'} \rho(s'')k(\lambda, s'')\,ds''\right] ds' \qquad (142)$$

It should be noted, however, that since the spectral transmittance, τ, is:

$$\tau(\lambda) = 1 - A(\lambda) = \exp\left[-\int_s^{s'} \rho(s'')k(\lambda, s'')\,ds''\right] \text{ in general (see Section 1)} \qquad (143)$$

the expression $\rho(s')k(\lambda, s') \exp - \left[\int_s^{s'} \rho(s'')k(\lambda, s'')\,ds''\right]$ in Eq. 142 is nothing more than $d\tau/ds'$, so that Eq. (142) can be written very simply

$$L_\lambda(\lambda, s) = L_\lambda, (\lambda, R)\tau(\lambda, R) + \int_s^R L_\lambda^*[\lambda, T(s')]\frac{d\tau(\lambda, s')}{ds'}\,ds' \qquad (144)$$

where, if $\tau(\lambda, s')$ is the transmittance between the point of observation (s), and some point (s') in the path, $d\tau(s')$ is defined as $\tau(\lambda, s' + ds') - \tau(\lambda, s')$. See Figure 16. The term $L_\lambda(\lambda, R)$ is the spectral radiance of a source at the point R, which is transmitted through the atmosphere between s and R, the transmittance being given by $\tau(\lambda, R)$. $L_\lambda^*[\lambda, T(s')]$ is the (Planckian) source function for a radiator at temperature, T(s'), defined at some point, s'.

Thus, the calculation of the radiance at some point, s, caused by emission from a source at some point, R, and the emission of the atmosphere between s and R (which is assumed to limit the path) amounts simply to calculating the transmittance between s and every point in the path out to R. Since the expressions in Eq. (144) cannot usually be obtained in closed form, the calculations are generally performed numerically, by subdividing the atmosphere into increments within which the atmospheric parameters are considered to be constant. These increments are formed by the shells which are demonstrated in Section 7.4. As explained in a report by Hamilton, et al. (1973), the contributions forming the shells which compose the boundaries of the layers containing the absorbing substance are summed up as follows:

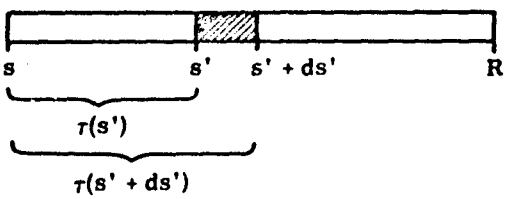

FIGURE 16. TRANSMITTANCE PATH CONFIGURATION

$$L_\lambda = \epsilon_s(\lambda)L^*(T_s)\tau_c(\lambda)\tau_n(\lambda) + \epsilon_c(\lambda)L^*_\lambda(T_c)\tau_j(\lambda) + \sum_{i=1}^{j} L^*_\lambda(T_i)[\tau_i(\lambda) - \tau_{i+1}(\lambda)/\tau_i'(\lambda)]$$

$$+ \tau_c(\lambda) \sum_{i=j+1}^{n} L^*_\lambda(T_i)[\tau_i(\lambda) - \tau_{i+1}(\lambda)/\tau_i(\lambda)] \qquad (145)$$

The details of this equation are explained in Section 7.4.

4.3 DESCRIPTION OF THE ABSORPTION COEFFICIENT

The factors of importance to this discussion are the terms $\tau(\lambda)$ and the parameters which define them. As noted above in Eq. (143):

$$\tau(\lambda) = 1 - A(\lambda) = \exp - \int k(\lambda, x)\rho(x)dx$$

Since the factor $k(\lambda, x)$ is a strongly varying function of wavelength (or frequency, ν)*, it is extremely important that its effect on atmospheric transmittance be examined in detail. It can be derived simply out of consideration of the effect only of the absorptive effect of the atmosphere on radiation traversing it. The change in the amount of radiation traversing an elemental distance, dx, containing $\rho(x)dx$ grams of absorbers per cm^2 is proportional to the number of absorbers and to the number of photons, representable by L_λ. With all appropriate constants implicit in it, the proportionality factor, a function of the frequency and of a particular place in the atmosphere, is designated as $k(\nu, x)$, so that

$$dL_\nu(\nu, x) = -k(\nu, x)\, L_\nu(\nu, x)\rho(x)dx$$

which very simply solves, for a path from 0 to x_0, as:

$$L_\nu(\nu, 0) = L_\nu(\nu, x_0) \exp \left[-\int_0^{x_0} k(\nu, x)\rho(x)dx \right]$$

giving, as above:

$$\tau(\nu, x_0) = \exp \left[-\int_0^{x_0} k(\nu, x)\rho(x)dx \right] \qquad (146)$$

The expression $\tau(\nu, x_0)$ is the monochromatic atmospheric transmittance for the conditions given; i.e., the value at one and only one frequency, ν.

*The reader should expect to encounter, during the course of this report, frequent changes in the description of the spectral character of parameter between the use of λ, the wavelength, usually in micrometers, μm; and ν, the frequency usually in reciprocal centimeters, cm^{-1}. It is to be noted in these cases that $\lambda = 1/\nu \times 10^4$.

There is usually little interest in the monochromatic transmittance, particularly for comparison between calculated and measured results, which are obtained by instruments whose spectral resolution is sufficiently poor to integrate over some reasonable width of the spectrum. The greater interest, thus, is in the average* transmittance over the spectral interval $\Delta\nu$ given by:

$$\bar{\tau}_{\Delta\nu}(\nu, x_0) = \frac{1}{\Delta\nu} \int_{\Delta\nu} \left\{ \exp \left[-\int_0^{x_0} k(\nu, x)\rho(x)\,dx \right] \right\} d\nu \tag{147}$$

One might consider this as the average transmittance over a spectral interval $\Delta\nu$ centered at ν, or the effective transmittance over a variable slit function whose effective width is that of a rectangle with the same area as that under the spectral slit function.

The greatest part of the problem of solving $\bar{\tau}_{\Delta\nu}$ is to find, if possible, an analytical solution for the integration over ν, which involves a knowledge of the actual character of $k(\nu)$ (dropping the path dependence for convenience). Using the results of classical kinetic theory, the nature of $k(\nu)$ is shown, according to Lorentz, to be:

$$k(\nu) = \frac{S}{\pi} \frac{\alpha_L}{(\nu - \nu_0)^2 + \alpha_L^2} \tag{148}$$

where S is the line strength in units $(gm^{-1}\text{-}cm)$ (since $k = (gm\text{-}cm^{-2})^{-1}$)

α_L is the Lorentz line half-width in cm^{-1} (see Figure 17)

ν_0 is the frequency, in cm^{-1}, at the center of the line

When the line representing a transition has this shape it is said to be collision, or pressure, broadened as a result of impacts of the molecule with neighboring molecules. Thus, the line half-width depends upon pressure and temperature, and is often approximated as follows:

$$\alpha_L = \alpha_{L0} \left(\frac{P}{P_0} \right) \left(\frac{T_0}{T} \right)^n \tag{149}$$

where α_{L0} is the half-width (in cm^{-1}) at standard conditions, P_0, T_0

P is the pressure of the gas

T is the temperature

n is an empirically determined exponent, with a theoretical value of 1/2

*Actually what is desired is a weighted average to take into effect the (variable) spectral "slit function" of the instrument which should be convolved with the monochromatic transmittance. This will be ignored in the discussion.

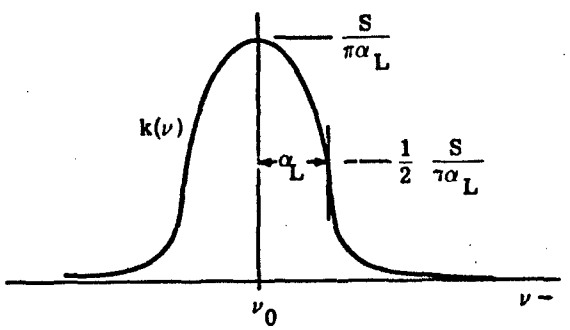

FIGURE 17. FEATURES OF A LORENTZ LINE

The line strength has a temperature dependence which gives it the form:

$$S = S_0(T_0/T)^m \exp\left(-\frac{E''}{k}\frac{T_0 - T}{T_0 T}\right) \tag{150}$$

where E'' is the vibration-rotation energy of the initial state giving rise to a particular absorption line; k is the Boltzmann constant, m is an exponent which depends on the type of absorbing gas.

The theory of molecular line absorption in the atmosphere is covered in many texts, of which the one by Goody (1964) is probably the most recent, comprehensive, and available. For the purpose of completeness, however, the theory will be reviewed briefly here, partially extracted from the earlier state-of-the-art report by Anding (1967).

A study by Winters, et al. [119] of an isolated CO_2 spectral line showed that the intensity in the wings of the line decreased more rapidly than predicted by the Lorentz expression. On the basis of this study, Benedict proposed the following empirical expression for the spectral line shape of CO_2:

$$k(\nu) = \frac{S}{\pi}\frac{\alpha_L}{(\nu - \nu_0)^2 + \alpha_L^2} \qquad |\nu - \nu_0| \leq d \tag{151a}$$

$$k(\nu) = \frac{S}{\pi}\frac{A\alpha_L \exp\left(-a|\nu - \nu_0|^b\right)}{(\nu - \nu_0)^2 + \alpha_L^2} \qquad |\nu - \nu_0| \geq d \tag{151b}$$

where d is the average spacing between spectral lines

$a = 0.0675$

$b = 0.7$

$d = 2.5\ cm^{-1}$

The value of A is chosen to make the two forms continuous at $|\nu - \nu_0| = d = 2.5\ cm^{-1}$.

There is a second cause of line broadening known as the Doppler effect which is related to the relative motions of the molecules. The pure Doppler broadened line is given by

$$k(\nu) = k_0 e^{-y^2} \tag{152}$$

119. B. H. Winters, et al., "Line Shape in the Wing Beyond the Band Head of the 4.3μ Band of CO_2," J. Quant. Spec. Rad. Trans., Vol. 4, 1964, pp. 527-537.

where

$$k_0 = \frac{S}{\alpha_D}\left(\frac{\ell n\, 2}{\pi}\right)^{1/2}$$

$$y = \frac{(\nu - \nu_0)}{\alpha_D}(\ell n\, 2)^{1/2}$$

and α_D, the Doppler half-width (in cm^{-1}) at half maximum, is given by

$$\alpha_D = \frac{\nu_0}{c}\left(2k\ell n 2\,\frac{T}{M}\right)^{1/2}$$

where M = molecular weight ($gm\text{-}mole^{-1}$), and k is the Boltzmann constant.

For lower altitudes where the atmospheric pressure is high, the Lorentz half-width, α_L, is dominant. As the atmospheric pressure decreases, the Lorentz half-width decreases and the influence of Doppler broadening becomes more marked. For the 15-μ CO_2 band, the Doppler and Lorentz half-widths are equal at about 10 mb [120] and at lower pressures the Doppler half-width is greater. Thus, over a wide range of atmospheric pressures, it is necessary to consider the mixed Doppler-Lorentz (Voigt) line shape to be completely accurate. The absorption coefficient for the mixed broadening is given by Young [121]:

$$k(\nu) = \frac{k_0 u}{\pi}\int_{-\infty}^{\infty}\frac{e^{-t^2}}{u^2 + (y - t)^2}\,dt \qquad (153)$$

where k_0, y are as before and

$$u = \frac{\alpha_L}{\alpha_D}(\ell n\, 2)^{1/2}$$

In the calculation of transmittance using direct integration over the absorption lines (Section 5) the greatest accuracy can be obtained only by using the Voigt profile to describe the line shape. A compromise in simplicity to the exclusive use of the Lorentz profile for all altitude regimes,as is usually done in calculation by band models (Section 8), results in an error which is often unacceptable. Calculation using the Voigt profile, however, imposes

120. S. R. Drayson, Atmospheric Slant-Path Transmission in the 15μ CO_2 Band, Report No. 05863-6-T, University of Michigan, Ann Arbor, 1964.

121. C. Young, "Calculation of the Absorption Coefficient for Lines with Combined Doppler-Lorentz Broadening," J. Quant. Spect. R. . Trans., Vol. 5, 1965, pp. 549-552.

hardships in terms of computer time; and methods have been described in the literature (e.g., see Refs. [121] and [122] for easing the complications in computation. Drayson, by private communication, has indicated a computer routine explained in a paper to be published soon. This routine is currently part of his method of performing a direct integration of individual absorption lines for calculating atmospheric transmittance, and uses what he considers to be the best of the Young and Armstrong techniques.

Drayson's aim in setting up a special computer routine is to achieve both rapid computation and an accuracy in transmittance good to approximately one digit in the fourth decimal place. In order to achieve this trade-off, he set up several regions in the u - y plane to define limiting values of these variables for which different calculational techniques were used. They were set up as follows (see Figure 18):

Region I. $y \leq 1.0, u \geq 5.0 - 0.8y$

Dawson's function, $F(x) = e^{-x^2}\int_0^x e^{t^2}\,dt$ is first evaluated:

(a) $0 \leq u \leq 2$ Series expansion [123]

(b) $2 < u < 4.5$ Chebyshev expansion [124]

(c) $4.5 \leq u$ Asymptotic expansion [123]

followed by Taylor series expansion [125].

Region II. $y > 1.0$ and $u < 1.85\,(3.6-u)$

Continued fraction [126].

Region III. All (u, y) not in I and II

(a) $y \geq 11.0 - 0.6875u$ 2-point Gauss-Hermite quadrature

(b) $y < 11.0-0.6875u$ 4-point Gauss-Hermite quadrature

122. B. H. Armstrong, "Spectrum Line Profiles: The Voigt Function," J. Quant. Spect. Rad. Trans., Vol. 7, 1967, pp. 61-88.

123. A. Erdelyi, et al., Higher Transcendental Functions, Vol. 2, McGraw-Hill, N. Y., 1953, p. 147.

124. D. Hummer, Maths. Comput., Vol. 18, 1964, p. 317.

125. V. Feddeyeva and N. Tarentev, Tables of the Probability Integral for Complex Argument, Pergamon Press, N. Y., 1961.

126. B. Fried and S. Conte, The Plasma Dispersion Function, Academic Press, N. Y., 1961.

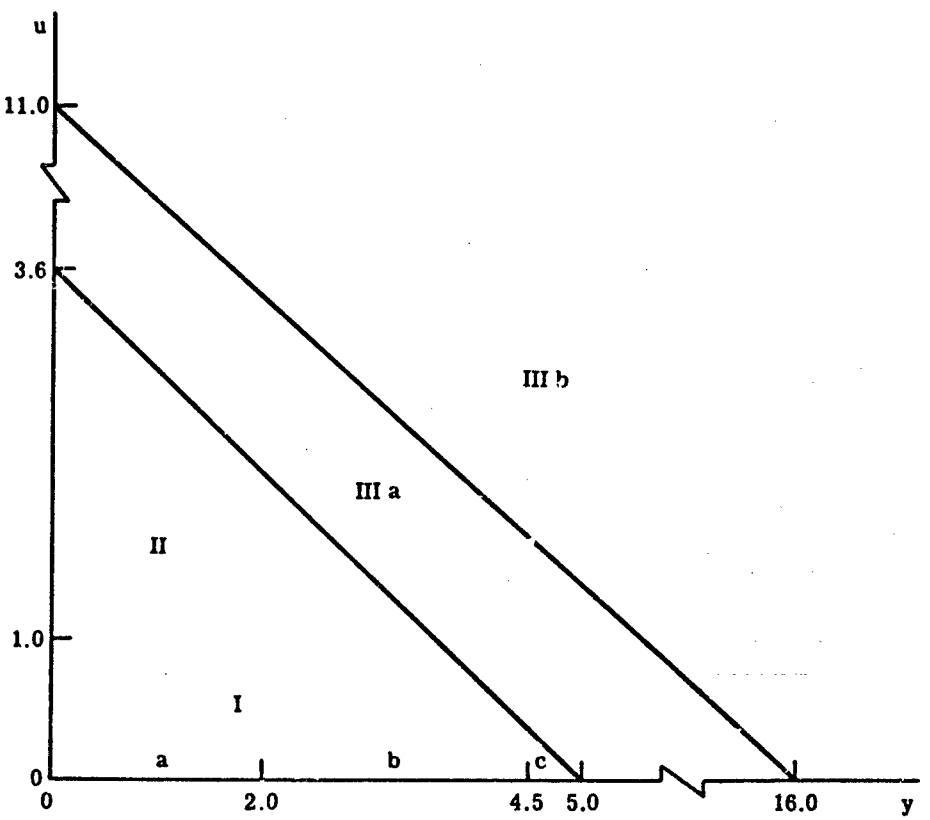

FIGURE 18. COMPUTATIONAL REGIONS USED FOR THE VOIGT PROFILE
(by Drayson)

4.4 DETERMINATION OF TRANSMITTANCE OR ABSORPTANCE

Four different forms for $k(\nu)$ have been stated, each form accurately representing the shape of a spectral line if the appropriate conditions are satisfied. Therefore, to completely specify the absorption from Eq. (147), it is necessary to substitute the appropriate form of $k(\nu)$.

Let us assume that the spectral interval over which Eq. (147) is defined contains many spectral lines. Then we have

$$A_{\Delta\nu} = 1 - \tau_{\Delta\nu} = \int_{\Delta\nu} \left\{ 1 - \exp\left[-\sum_{i=1}^{N} \int_{0}^{x_0} k_i(\nu)\, \rho(x)\, dx \right] \right\} d\nu \tag{154}$$

Equation (154) is the general equation for specifying the absorption of a given species over an atmospheric slant path, with the range of pressures encompassed by the path defining the specific form for the absorption coefficient $k(\nu)$.

To better understand the parameters that must be specified before Eq. (154) can be evaluated, let us assume that the slant path is such that the Lorentz line shape is valid. Then Equation (154) becomes

$$A\Delta\nu = \int_{\Delta\nu} \left\{ 1 - \exp\left[-\frac{1}{\pi} \sum_{i=1}^{N} \int_{0}^{X} \frac{S_i \alpha_i \rho(x)}{(\nu - \nu_{0_i})^2 + \alpha_i^2} dx \right] \right\} d\nu \tag{155}$$

The summation is over the total number of lines in the spectral interval and S_n is the strength of the n-th line, α_n is the half-width of the n-th line, and ν_{0_n} is the center frequency of the n-th line.

We shall see in Section 5 that Eq. (155) can be solved by a method known as the line-by-line, or direct integration method, used by a number of investigators. There are reasons, however, why this method is often shunned, the largest being the cost of performing a calculation of this sort. The logical step in lieu of this is to resort to calculation by the use of band models.

The problem of determining slant-path transmission spectra is then to evaluate Eq. (155) for each frequency within the spectral interval of interest. To perform this evaluation, the following four parameters must be specified:

(1) The shape of each spectral line
(2) The location of each spectral line
(3) The strength and half-width of each line and their variations with temperature and pressure
(4) The density of the absorber at each point in the path.

4.5 DETERMINATION OF LINE PARAMETERS

4.5.1 TECHNIQUES OF BENEDICT AND COLLABORATORS

The determination of line parameters is inseparably dependent on accurate, highly-resolved laboratory spectral data from the molecules of atmospheric constituents, and on practicable theories predicting the physical characteristics of molecules. As already indicated, there are a number of things which have to be known about an absorbing molecule before calculations can be made, among which are the strengths of the individual lines and knowledge of the shapes of the lines, as well as precise determinations of the spectral position of the centers of the lines. Presumably, all of these factors could be obtained exclusively from a well-designed experiment measuring the spectral absorptance of a collection of the molecules as a gas. In practice, however, certain physical limitations arise to thwart attempts to do so, and one must resort, in absorptance calculations, to the results of theoretical determinations of line parameters, using the best of both techniques in a complementary fashion to derive those values which can most realistically reproduce more general experimental results.

In outlining techniques for getting line parameters from laboratory experimental data, we have chosen to emphasize the method delineated by Benedict, et al. [127, 128] because the reader, in later checking details, will find their treatment to be probably more complete than that of other authors. But it should be understood that the approaches of other investigators, which do not differ greatly from those of Benedict, et al., or from each other, are equally valid. Actually, the refinements reported in later papers are required reading for the person whose interest goes beyond the rudiments. In fact, since the treatment here is more-or-less superficial, the reader will want to consult the original papers, and perhaps delve into other texts as well. To cite only a few, there are the texts of Penner [129] and Goody (1964), as well as the paper of Korb, Hunt and Plyler [130], and the report by Burch and Gryvnak [131]. Goody treats

---

127. W. S. Benedict, R. Herman, S. Moore and S. Silverman, "The Strengths, Widths and Shapes of Infrared Lines, I. General Considerations," Canadian J. of Physics, Vol. 34, 1956(a), pp. 830-849.

128. W. S. Benedict, R. Herman, S. Moore and S. Silverman, "The Strengths, Widths and Shapes of Infrared Lines, II. The HCl Fundamental," Canadian J. of Physics, Vol. 34, 1956(b), pp. 850-875.

129. S. Penner, Quantitative Molecular Spectroscopy and Gas Emissivities, Addison-Wesley, Reading, Mass., 1959.

130. C. L. Korb, R. Hunt and E. Plyler, "Measurement of Line Strengths at Low Pressures: Application to the 2-0 Band of CO," J. Chem. Phys., Vol. 48, No. 9, May 1968, p. 1452.

131. D. E. Burch and D. A. Gryvnak, Strengths, Widths and Shapes of the Lines of the 3ν CO Band, Report No. U-3972, Philco-Ford Corporation, 1967.

Doppler broadening of the Lorentz profile. Korb, Hunt and Plyler give base and wing corrections. Burch and Gryvnak and other authors have investigated the corrections described by Benedict, et al. to the Lorentz line in the far wings.

Usually the investigator responsible for calculating line parameters either gathers his own laboratory results, or works in collaboration with the experimentalist. He can then assure himself of the accuracy of the laboratory results, or accept full resporsibility for the erroneous results to follow. This means that gas-handling techniques must be impeccable, because minute quantities of foreign gases can at times introduce serious errors. In addition, the best techniques must be applied to measuring the physical properties of the gas samples, concentrations, pressures, temperatures, etc.; as well as to measuring the sometimes minute signals at the output of the spectrometer. With the precisely known wavelengths of certain standard emitters and absorbers, there is hardly any difficulty in establishing a standard from which all line centers can be read, once the position of the line center on the output chart is precisely located.

If one can measure the equivalent width (see Section 4.3) of a spectral line at different optical depths, he often has the essential experimental information needed for determining line parameters. In the infrared region, however, even those spectrometers with the highest practicably achievable resolution have spectral slit widths which are noticably larger than the half-width of a spectral line, though in the better cases they are on the order of the half-width. One cannot expect, therefore, to reproduce the exact spectral shape of the line, but only an approximation to it, resorting to calculation for yielding the true shape. However, Penner (1969) and others (e.g., Benedict, et al., 1956b) have shown that the equivalent width of a spectral line is independent of the slit function of the spectrometer, although the distortion of the line by the slit can be considerable as demonstrated in Figures 19, 20, and 21. In each of these figures, one sees the exact shape of a pressure-broadened line with a given shape factor, along with the distortions caused by a triangular slit function and by a rectangular slit function. Table 5 (reproduced from Benedict, et al., 1956b) shows that the equivalent width is unaffected on the basis of experimental evidence, even when the slit function changes in width by nearly an order of magnitude from 0.24 cm^{-1} to 1.78 cm^{-1} in the measurement of the spectrum, say, of HCl.

Although it is not always recommended in actual practice, in most calculations the Lorentz line shape is assumed as an approximation to the true shape, with corrections being made to account for discrepancies caused by deviations from the Lorentz shape. An expression is given in Section 4.3 for the Lorentz line shape as well as for the Doppler line shape, which becomes effective at low pressures. Even in those cases where the influence of pressure on the broadening overcomes the Doppler effect, the Lorentz shape, while quite accurate near the line center, is sometimes only a rough approximation in the wings. Because of the exceedingly

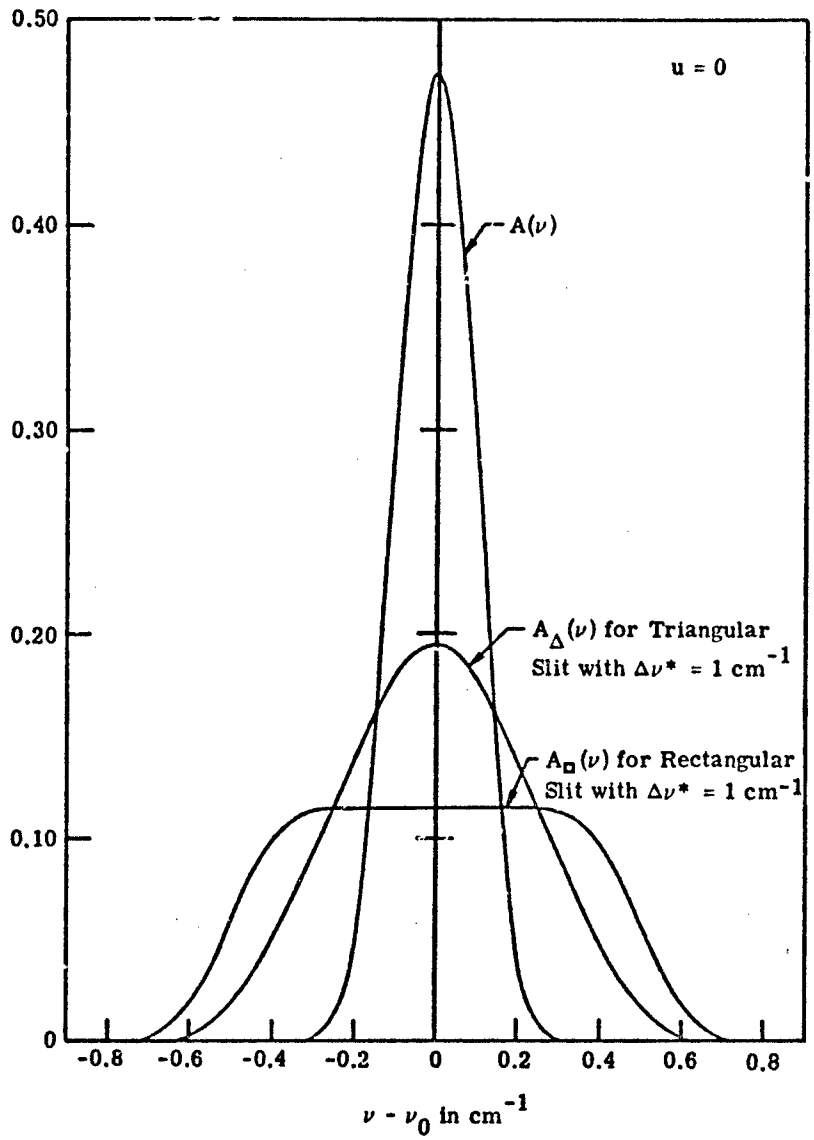

FIGURE 19. SPECTRAL ABSORPTANCE, $A(\nu)$, AND SMOOTHED ABSORPTANCES AS FUNCTIONS OF $(\nu - \nu_0)$, THE DISTANCE FROM LINE CENTER. $u = \alpha_L/\alpha_D(\ell n\ 2)^{1/2}$; α_L = Lorentz half-width; α_D = Doppler half-width = 0.10 cm^{-1}; $\Delta\nu^*$ = Slit function limiting width. (Adopted from Penner, 1959 [129].)

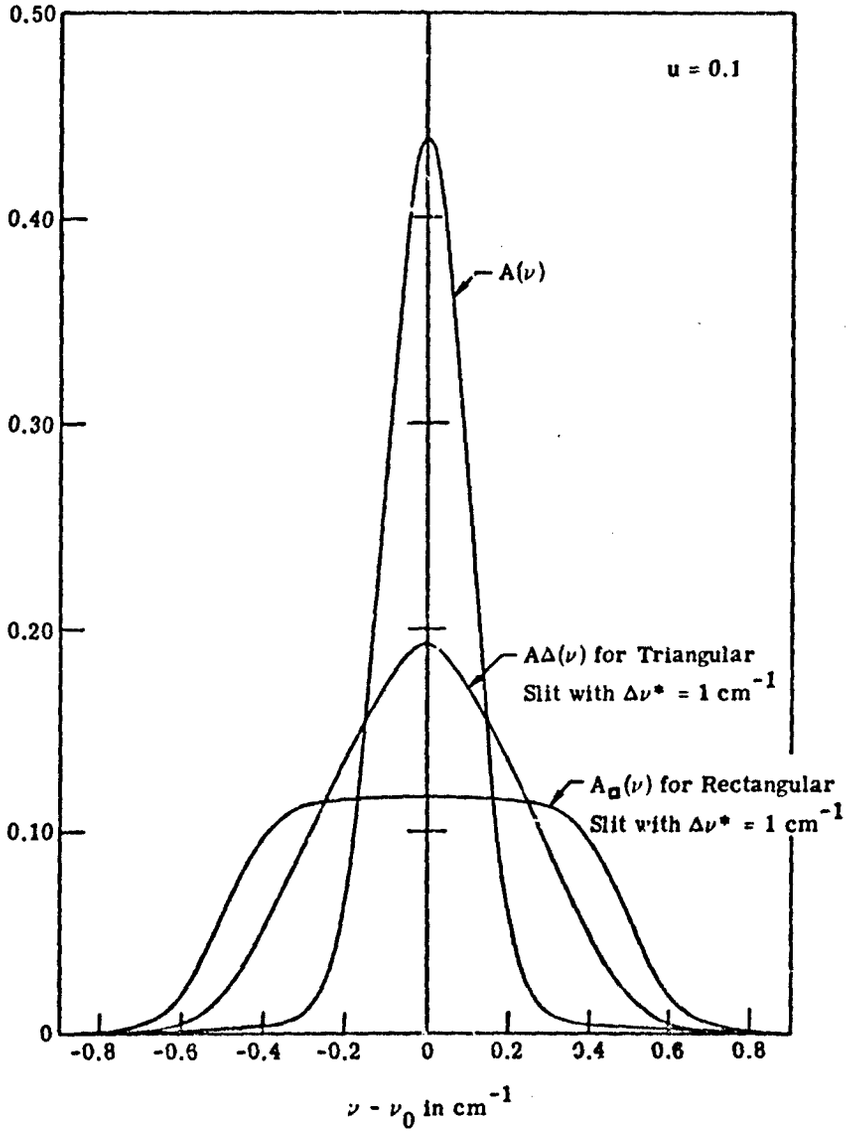

FIGURE 20. SPECTRAL ABSORPTANCE, $A(\nu)$, AND SMOOTHED ABSORPTANCES AS FUNCTIONS OF $(\nu - \nu_0)$, THE DISTANCE FROM LINE CENTER. $u = \alpha_L/\alpha_D(\ell n\ 2)^{1/2}$; α_L = Lorentz half-width; α_D = Doppler half-width = 0.10 cm^{-1}; $\Delta\nu^*$ = Slit function limiting width. (Adopted from Penner, 1959 [129].)

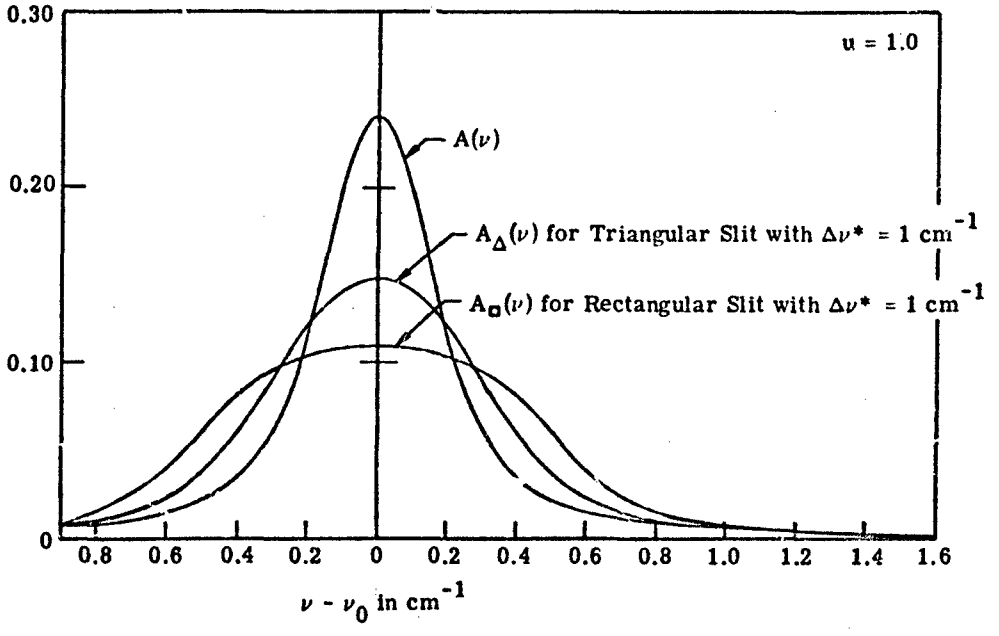

FIGURE 21. SPECTRAL ABSORPTANCE, $A(\nu)$, AND SMOOTHED ABSORPTANCES AS FUNCTIONS OF $(\nu - \nu_0)$, THE DISTANCE FROM LINE CENTER. $u = \alpha_L/\alpha_D(\ln 2)^{1/2}$; α_L = Lorentz half-width; α_D = Doppler half-width = 0.10 cm^{-1}; $\Delta\nu^*$ = Slit function limiting width. (Adopted from Penner, 1959 [129].)

TABLE 5. EXAMPLES TO INDICATE THE INDEPENDENCE OF EQUIVALENT WIDTH UPON SPECTRAL SLIT WIDTH (From Benedict, et al., 1956a [128].)

Slit (cm^{-1})	R(5)— HCl^{35} W (cm^{-1})	R(5)— HCl^{37} W (cm^{-1})
0.24	0.525	0.322
0.29	0.546	0.306
0.34	0.564	0.327
0.41	0.560	0.319
0.47	0.566	0.322
0.71	0.538	0.314
1.02	0.536	0.308
1.78	0.522*	0.297*

*These values were obtained by measuring the sum of the HCl^{35} and HCl^{37} lines and decomposing this area in the theoretically expected ratio for these lines, $HCl^{35}/HCl^{37} = (3.07)^{1/2}$.

small absorption in the wings, however, it is usually impossible to observe an effect greater than the noise of the measurement system. It becomes necessary to make a correction, therefore, to the equivalent width of the spectral line as obtained by integration. Corrections for the wings of a rotational line in the HCl spectrum (Benedict, et al., 1956b) are shown in Table 6.

To the extent that a spectral line can be isolated in an absorption experiment, the area under the line is exactly represented (provided a Lorentz shape can be assumed) by the Ladenburg-Reiche equation [132] (refer to Section 5.2.2):

$$W = 2\pi\alpha_L L(\psi)$$

where

$$L(\psi) = \psi e^{-\psi}[I_0(\psi) + I_1(\psi)]$$

and*

$$\psi = Sw/(2\pi\alpha_L)$$

If the experiment is run at different pressures and path lengths a typical pair of spectra as shown in Figure 22 (taken from Benedict, et al., 1956b) may be obtained. This particular example shows tracings of part of the R-branch of HCl with the two isotopes HCl^{35} and HCl^{37} being demonstrated for two different pressures in the absorption cell, and two different path lengths. Taking the area under each line, say at R(2), one obtains the equivalent width, W, which, when divided by the pressure (obtaining W^o) and plotted against pressure, yields a curve such as that shown in Figure 23 (taken from Benedict, et al., 1956b). One notes that for a large portion of the curve the value W^o is independent of pressure, as indeed it should be for a Lorentz shape. In order to reproduce the experimental points theoretically, Benedict, et al. had to include Doppler broadening in their calculations for low pressures and overlapping of the isotopic lines for high pressures. By making the appropriate adjustments for these deviations one can obtain a series of values, W^o, for a large range of path lengths. According to Section 5, W^o is proportional to the value of ψ for small quantities of the absorber, and proportional to $\psi^{1/2}$ for large quantities. Benedict, et al., evaluate W^o of HCl for a number of cell path lengths (note that $\psi \approx 1$) varying from 0.028 to 140 cm.

Having so obtained the values of W^o and w (the absorber amount) for any given experiment, one can plot log W^o versus log w, superimpose this on a plot of the Ladenburg-Reiche curve as

*Note that we have used w for the absorber amount instead of ℓ as used by Benedict, et al. in order to retain consistency with its common use in the report. Thus, w here corresponds to the path length.

132. R. Ladenburg and F. Reiche, "Uber Selektive Absorption," Ann. Phys., Vol. 42, 1913, p. 181.

TABLE 6. EXAMPLES OF TYPICAL WING CORRECTIONS IN EQUIVALENT WIDTH MEASUREMENTS. Lines R(0) of HCl, path length 0.109 cm; W^o values are in cm^{-1} atm^{-1}. (From Benedict, et al., 1956a [123].)

	W^o, HCl^{35}		W^o, HCl^{37}	
Run	Uncorrected	Corrected	Uncorrected	Corrected
1	0.3922	0.4205	0.1401	0.1574
2	0.4258	0.4473	0.1523	0.1694
3	0.3714	0.4056	0.1309	0.1502
4	0.4117	0.4415	0.1530	0.1676
5	0.4291	0.4536	0.1425	0.1670
Average	0.4060	0.4337 cm^{-1}	0.1438	0.1623 cm^{-1}
Std. dev.	0.0217	0.0180	0.0082	0.0072

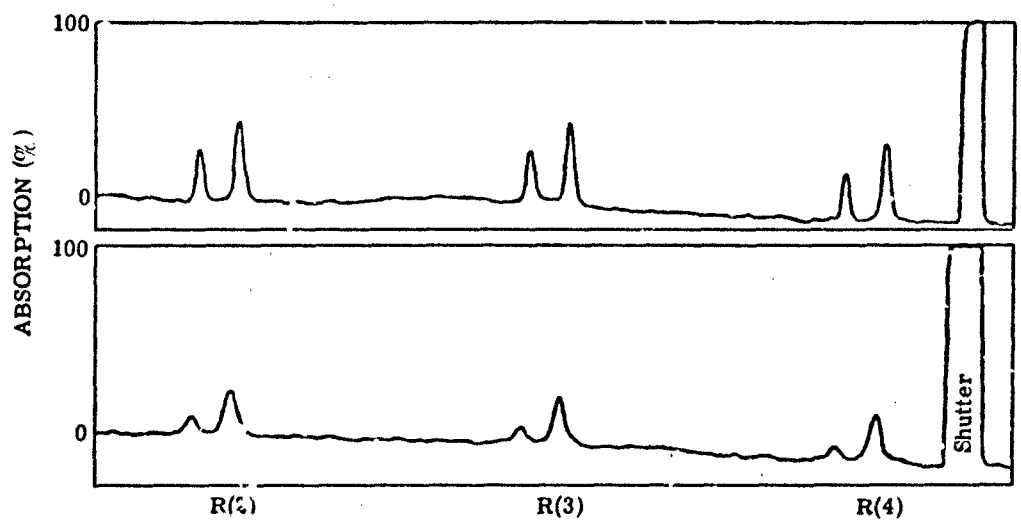

FIGURE 22. EXAMPLES OF THE TYPE OF ABSORPTION SPECTRA OF HCl FROM WHICH EQUIVALENT WIDTH MEASUREMENTS WERE MADE ILLUSTRATING TYPICAL SIGNAL-TO-NOISE RATIOS AND RESOLUTION EMPLOYED. The lower tracing taken at w = 0.028 cm and P = 1 atm shows R-branch lines in the linear region of the curve of growth. The upper tracing taken at w = 20 cm and P = ~0.01 atm shows the same lines in the square-root region. (Redrawn from Benedict, et al., 1956b [128].)

shown in Figure 24, and fit the experimental points to the theoretical curve. The intersection of the asymptote for the "linear" portion of the curve with the vertical line corresponding to log W = 0, yields the value log S^o ($S^o = S/P$). In addition, since the asymptote for the linear and square root portions of the curve must have slopes of 1 and 1/2, respectively, the intersection of these two straight lines defines the value $W^o = 4\alpha_L^o \left(\alpha_L^o = \alpha_L/P\right)$, since:

$$L(\psi) \cong \psi(1 - \psi/2 + \ldots)$$

with

$$W^o = W/P \cong S^o w\left[1 - W^o\Big/\left(4\pi\alpha_L^o\right) + \ldots\right];$$

and for ψ large

$$L(\psi) \cong (2\psi/\pi)^{1/2}[1 - 1/(8\psi) + \ldots]$$

with

$$W^o \cong 2\left(S^o\alpha_L^o w\right)^{1/2}\left[1 - \pi\left(\alpha_L^o/W^o\right)^2 + \ldots\right].$$

In the paper (Benedict, et al., 1956b) which accompanied the tutorial paper (Benedict, et al., 1956a) being discussed in this section, the same investigators applied, in addition to purely analytical techniques, the graphical method outlined above to the HCl^{35} and HCl^{37} molecules and the curve of growth reproduced in Figure 25 for a few of the lines. Using line strengths calculated on another basis they plotted the abscissa as $S^o w$ instead of just w so that the curves of growth of all lines would coincide in the linear region. In this way, they intended to investigate what differences existed in line widths in the square root region. The intersection of the asymptotes for lines with small J's yields a value $\alpha_L^o = 0.218$ cm^{-1} atm^{-1}. Note, however, that for the example shown for higher J values the asymptote drops below that for low J values. On an experimental basis, therefore, this means that the half-widths are narrower for lines with higher rotational quantum numbers. In fact, as Figure 26 shows, there is a considerable variation in α_L^o with the value of the rotational quantum number.

Another method described in the tutorial paper is that of determining the strength-width products and shapes from measurements of the breadths of strong lines. The breadth, b, is the actual width of the absorption measured at a given optical depth, q_ν where

$$q_\nu = \frac{S^o\alpha_L^o wP}{\pi\left[(\nu - \nu_0)^2 + \left(\alpha_L^o P\right)^2\right]} = \frac{2\psi\left(\alpha_L^o\right)^2 P^2}{(\nu - \nu_0)^2 + \left(\alpha_L^o P\right)^2}$$

and

$$b = 2(\nu - \nu_0)$$

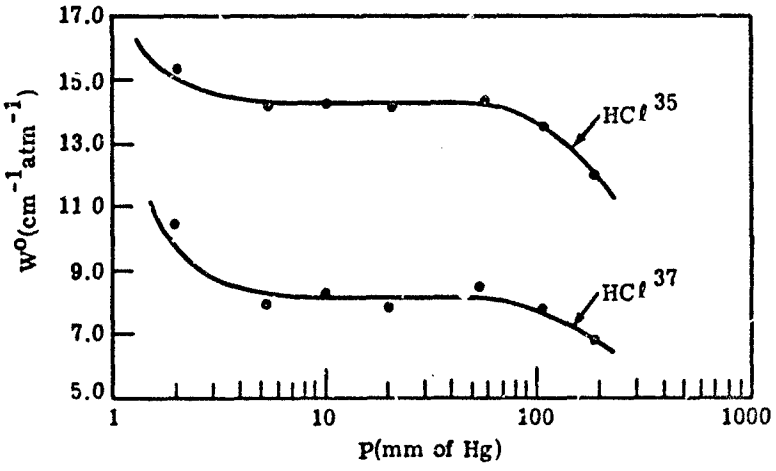

FIGURE 23. PLOT OF W^0 VERSUS PRESSURE FOR LINES R(2) OF HCl^{35} AND HCl^{37}. Showing experimental points and theoretical curves calculated for Lorentz collision broadening and including the effects of both Doppler broadening and overlapping of isotropic lines. (Redrawn from Benedict, et al., 1956b [128].)

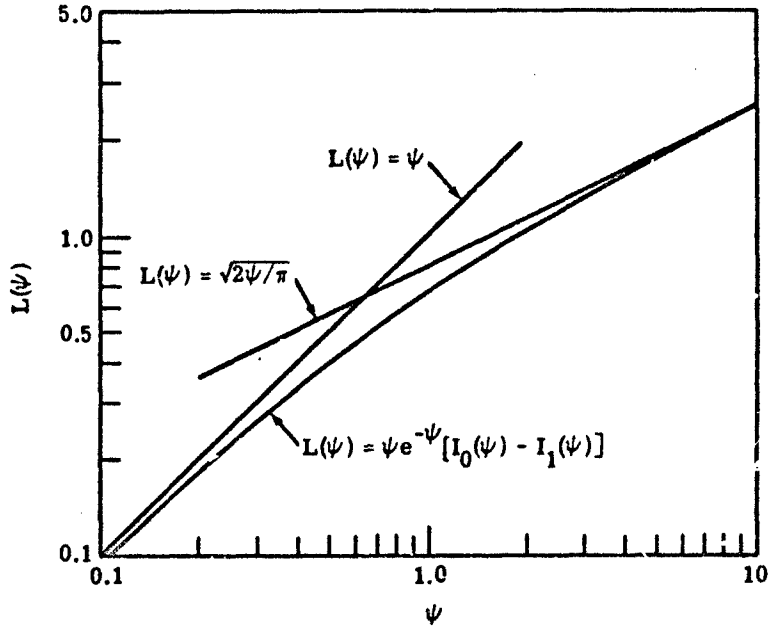

FIGURE 24. PLOT OF THE LADENBURG-REICH FUNCTION. Showing also the limiting small ψ ("linear") and large ψ ("square-root") asymptotes. (Redrawn from Benedict, et al., 1956b [128].)

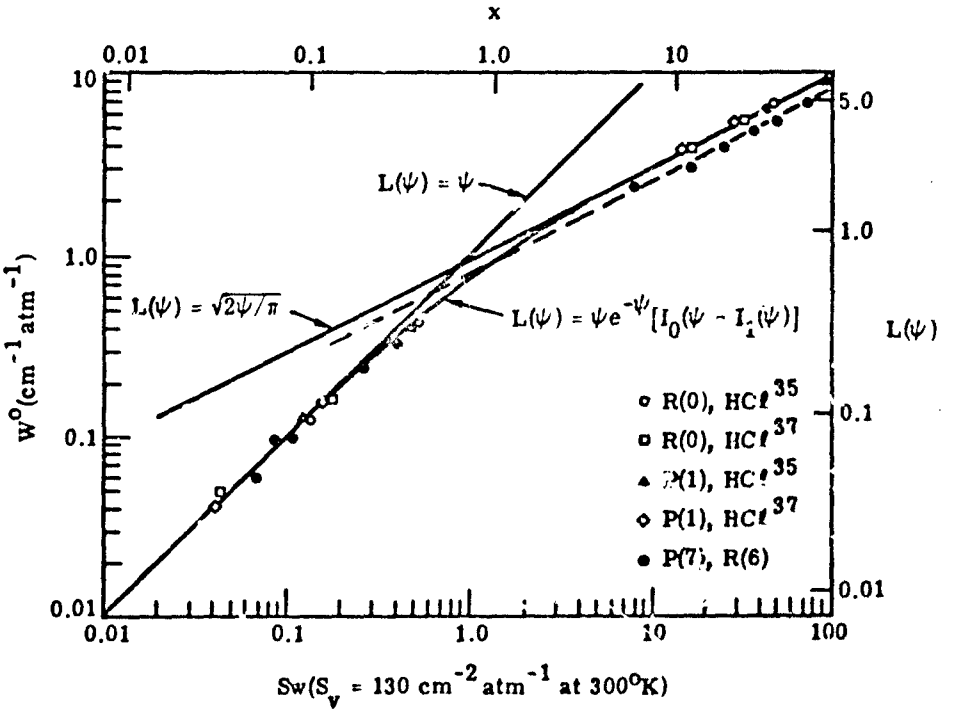

FIGURE 25. EXAMPLES OF CURVES OF GROWTH FOR THE LINES $|m| = 1$ AND 7. The solid curve and asymptotes for the case $|m| = 1$ are calculated from the Ladenburg-Reiche equation. (Redrawn from Benedict, et al., 1956b [126].)

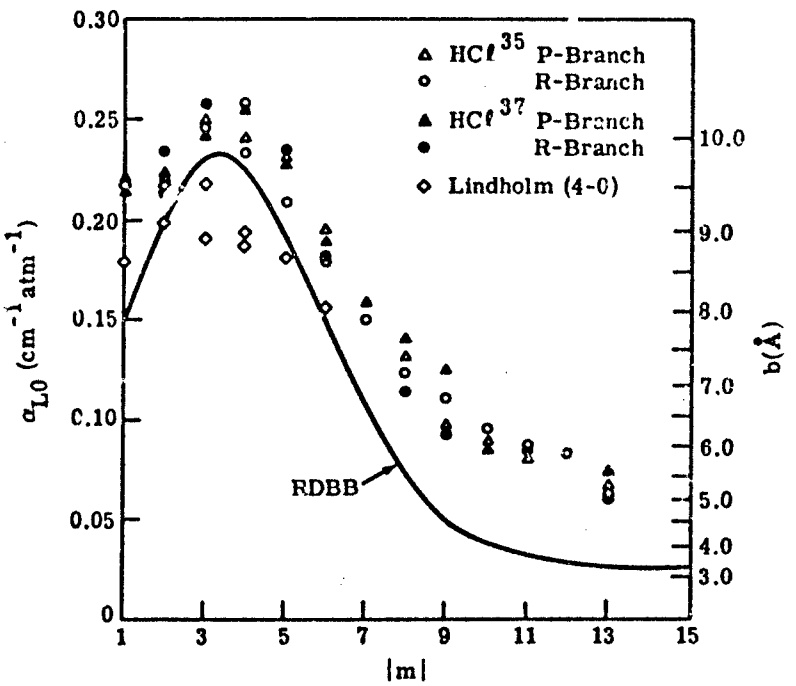

FIGURE 26. EXPERIMENTAL VALUES OF LINE WIDTHS PER ATM (α_{L0}) VERSUS |m| FOR THE HCl 1-0 BAND. The theoretical curve is that calculated for the resonant-dipole-billiard ball (RDBB) approximation. The corresponding collision diameters b are given. Line widths measured by Lindholm in the 4-0 band are shown for comparison. (Redrawn from Benedict, et al., 1956b [128].)

is related to the strength-width product by:

$$S^0\alpha_L^0 = \frac{\pi q b^2}{4Pw}\left[1 + \left(\frac{2\alpha_L^0 P}{b}\right)^2\right]$$

The value of α_L^0 in the correction term is an estimate. Since the breadth cannot be measured directly from experimental data, two corrections must be made, the first for the spectrometer slit function which, for a triangular slit of width a, is written:

$$\Delta b = \frac{2q - 3}{3}\frac{a^2}{b}$$

and the second for overlapping lines. Note than the slit width correction is zero for q = 3/2 and small for b large. The simplest and perhaps least accurate approach to overlapping correction is to assume an Elsasser distribution of lines from which the corrected value of the strength-width product (incorporating also the slit function correction) becomes:

$$S^0\alpha_L^0 = \frac{\pi q b^2}{4Pw}\left[1 + 4\left(\frac{\alpha_L^0 P}{b}\right)^2 + \frac{4q - b}{3}\left(\frac{a}{b}\right)^2 - 0.822\left(\frac{b}{d}\right)^2\right]$$

where d is the constant spacing of the Elsasser lines. When greater accuracy is required the Elsasser approximation must be dropped and the contribution of the overlapping lines to the absorptions at the line of interest calculated directly, if the frequency, strength and width of the interfering lines are known. Since the correction for overlap is relatively small, these values can probably be estimated from other methods of measurement.

A third method of determining line structure is derived by Benedict, et al., but will not be described here. The reader is referred to the original text of these investigators. As stated in the tutorial article, if the same α_L^0 is obtained from all methods, then the validity of the Lorentz shape is demonstrated over the frequency range spanned by the calculations. The authors consider the equivalent width measurement to be the best method for obtaining the Lorentz α_L^0 since it favors the regions near the line center which are probably determined by the impact theory.

4.5.2 LOW-RESOLUTION TECHNIQUES

The methods exemplified by the work of Benedict and his co-workers are not the only ones that can be used to determine line parameters. Aside from techniques used for determining band-model parameters, discussed in Section 5.2.8, there are others employing low resolution measurements, i.e., resolution not sufficient to resolve individual lines. The simplest (and least accurate) method is to extrapolate data to zero absorption. Assuming weak-line approximation valid under these conditions, the slope of the absorption (Sw) (see Section 5) plotted against

the amount of absorber, w, gives the band strength S. A good example of a molecule for which this method has been applied is that of ozone. References to this technique are Walshaw [133] and McCaa and Shaw [134].

More sophisticated techniques may be employed if one has a good idea of the positions of the lines in the absorption bands. By choosing different band strengths and half-width, one can perform a direct line-by-line calculation (see Section 5) to obtain the absorption for the same conditions used in the experimental measurement of absorption with moderate spectral resolution. The parameters are adjusted until one obtains satisfactory agreement between the theoretical and experimental values of absorption. This method was used by Drayson [135] in the determination of transmittance for use in the remote measurement of atmospheric profiles of temperature, and water vapor and ozone concentrations.

4.5.3 LASER METHODS

As opposed to the methods in the preceding section, we are able to obtain much higher resolutions with the use of lasers than with conventional spectroscopic techniques. Lasers with fixed frequency are useful for gases for which they have been constructed, such as CO_2. By changing the mode of the laser, the parameters of many different lines can be measured. By varying the pressure of the gas in the absorption cell, the shape of the line can vary from nearly purely Doppler-broadened to purely Lorentz-broadened. Ely and McCubbin [136], for example, have determined the temperature dependence of the self-broadened half-width of the P-20 line in the 001-100 band of CO_2 using a CO_2 - N_2 laser with a cavity 1.3 m long.

To get greater versatility, it is necessary to use a tunable laser. In the infrared region, the most useful types presently are diode lasers which can be tuned over a span of several wavenumbers, giving one the opportunity to scan individual lines with virtually "infinite"

---

133. C. Walshaw, "Integrated Absorption by the 9.6 μm Band of Ozone," Quant. J. Roy. Meteorol. Soc., Vol. 83, 1957 pp. 315-321.

134. D. J. McCaa and J. H. Shaw, "The Infrared Spectrum of Ozone," J. Mol. Spec., Vol. 25, pp. 374-397.

135. S. R. Drayson, "Transmittances for Use in Remote Soundings of the Atmosphere," Space Research XI, Akademie-Verlag, Berlin, 1971, p. 585.

136. R. Ely and T. McCubbin, "The Temperature Dependence of the Self-Broadened Half Width of the P-20 Line in the 001-100 Band of CO_2," Appl. Opt., Vol. 9, No. 5, May 1970, p. 1230.

resolution. The reader is referred to Hinkley, Nill and Blum [137] for a further elaboration of the subject matter. We should expect to see many further developments in this field of endeavor with the use of tunable lasers.

4.6 DESCRIPTION OF THE LINE PARAMETERS OF THE MAJOR ABSORBERS

The task of calculating atmospheric transmittance (or atmospheric radiance) from the infinitely resolved line structure of atmospheric molecules is straightforward, but is also lengthy, time-consuming, and can be costly. Not so straightforward, however, is the process of accumulating the enormous quantity of data required to make a line-by-line calculation. For each absorbing molecule in the atmosphere, a number of important parameters are needed, among which is the exact (to within the accuracy required or available) position of each line in the spectrum which is considered effective in contributing to the absorption of radiation. In accumulating line data, a decision to retain or reject a line is made based on its intensity relative to some predetermined criterion. The strength of each line is another essential parameter in the calculation of atmospheric radiance, along with the line width and the energy of the lower state in the transitions which produces the line.

These parameters, in addition to the quantity of absorber present, are the least of the totality needed for making an absorption calculation; and even then, only the standardized conditions for which the parameters were formulated are used. For more generalized calculations, allowing for changes in atmospheric conditions, other parameters such as temperature, pressure, and specific characteristics of the molecule must be explicitly entered into the calculation. These parameters are no more than are usually needed for any other calculation, but when they are coupled with the enormous quality of data involved in a line-by-line calculation of atmospheric absorption, the result is a relatively large expenditure of computer time. Methods for reducing the time involved in line-by-line calculations will be demonstrated in the ensuing section.

4.6.1 ACCUMULATION OF LINE DATA

A lot of work has been done for a number of years in studying the properties of molecules in relation to their radiative characteristics. In his bibliographic volume, Laulainen (1972) cites references dating back to 1940. For this report, it is sufficient to refer to some of the significant work started about 10 years ago, and which has continued by various investigators

137. E. D. Hinkley, K. Nill and S. Blum, "Laser Spectroscopy of Atoms and Molecules," Topics in Applied Physics, Vol. 2, H. Walther (ed.), Springer-Verlag, Berlin, 1974.

up to the present time. McClatchey, et al. [138] cite the work of Gates, et al. [139] as the initiation of continuing effort aimed at compiling spectroscopic data on the vibration-rotation structure, first of H_2O vapor in the 2.7 μm region, and later of CO_2 in the 2.05 and 2.7 μm bands [140]; and of H_2O vapor in the 1.9 and 6.3 μm bands [141].

The only existing complete compilation of line parameters (McClatchey, et al., [138]) appears to trace a lineage of government-supported work from which it evolved. Much of this work was originally directed less toward completeness than toward specificity. However, McClatchey, et al acknowledge the work of earlier investigators as establishing a solid base of information, in addition to that cited above. Among those cited are the work of Drayson and Young [142] for the 15 μm bands of CO_2; Clough and Kneizys [143] for the 9.6 μm bands of O_3; Kunde [144] for the CO fundamental bands near 5 μm; Kyle [145, 146] for the CH_4 bands near 3 and 7.5 μm; and the unpublished rotational structure of H_2O vapor from Benedict and Kaplan tabulated in Goody's (1964, p. 84) text.

---

138. R. A. McClatchey, et al., AFCRL Atmospheric Absorption Line Parameters Compilation, Report No. AFCRL-TR-73-0096, Air Force Systems Command, 1973.

139. D. M. Gates, R. F. Calfee and D. W. Hansen, et al., Line Parameters and Computed Spectra for Water Vapor Bands at 2.7μ, National Bureau of Standards, Monograph No. 71. 1964.

140. R. F. Calfee and W. S. Benedict, Carbon Dioxide Spectral Line Positions and Intensities Calculated for the 2.05 and 2.7 Micron Regions, Technical Note 332, National Bureau of Standards, 1966.

141. W. S. Benedict and R. F. Calfee, Line Parameters for the 1.9 and 6.3 micron Water Vapor Bands, ESSA Professional Paper 2, (June 1967) U. S. Government Printing Office, June 1967.

142. S. R. Drayson and C. Young, The Frequencies and Intensities of Carbon Dioxide Absorption Lines Between 12 to 18 Microns, Report No. 08183-1-T, University of Michigan, Ann Arbor, 1967.

143. S. A. Clough and F. X. Kneizys, Ozone Absorption in the 9.0 Micron Region, Report No. AFCRL-65-862, Air Force Cambridge Research Laboratories, Bedford, Mass., 1965.

144. V. G. Kunde, Tables of Theoretical Line Positions and Intensities for the $\Delta V = 1$, $\Delta V = 2$, and $\Delta V = 3$ Vibration-Rotation Bands of $C^{12}O^{16}$ and $C^{13}O^{16}$, NASA Report No. TMX-63183, Goddard Space Flight Center, Greenbelt, Md., 1967(a).

145. T. G. Kyle, "Absorption by Doppler-Lorentz Atmospheric Lines," J. Quant. Spect. Rad. Trans., Vol. 8, 1968(a), pp. 1455-1462.

146. T. G. Kyle, Line Parameters of the Infrared Methane Bands, Report No. AFCRL-68-0521, Air Force Cambridge Research Laboratories, Bedford, Mass., 1968(b).

The earlier work of Drayson and Young (1967) has been revised [147] to produce more accurate line parameters for CO_2 between 12 and 20 μm, derived mainly from the laboratory measurements of Chaney [148]. The revision has resulted in: changes in positions of most of the lines (but small ones, of less than 0.05 cm^{-1}); changes in strengths; and additional bands. The absolute strengths of the lines included were restricted to those greater than 1×10^{-6} cm^{-1} $(atm \cdot cm)^{-1}$ at 300 K, which corresponds to about 4×10^{-26} $cm^{-1}/(mol\ cm^{-2})$, the units recommended by McClatchey, et al. (1973). These values are approximately a factor of 2 higher than the lower limit set in the compilation. Note also that these units differ from the ones presented earlier in this section. All of them are equally valid and dependent on individual usage.

The interested reader is referred to the bibliography by Laulainen (1972) for an insight into the huge volume of spectral information available in the literature, some of which presumably influenced the derivation of the compilation of line parameters. Much of the latest Drayson [147] data were unavailable for inclusion. These data would not alter the line positions greatly, although a spot check of Drayson's data with the compilation showed differences in the intensities of the order of a few percent. There is a good account in the report by McClatchey et al. of those data which directly influenced the compilation, the product of an effort at Air Force Cambridge Research Laboratories (AFCRL) initiated around 1968.

Since the group at AFCRL exerted much controlling influence on the separate efforts by investigators to obtain experimental data on line parameters, they were able to elicit many of the results where they were most needed. Indeed some of the authors of the compilation report were the investigators responsible for generating the data. In general, however, the sources of data on line parameters are relatively widespread with a heavy dependence for their accuracy, indeed validity, on the numerous high-resolution measuremnts made in the laboratory and in the field. Further discussion is centered on the subjects of laboratory and field measurements in Section 9. Many of the data used in the AFCRL compilation are not cited in Laulainen's bibliography, and conversely many of the references cited in the latter work apparently were not used in compiling the line parameters. The reasons for the choice of data for the compilation are not evident; on the other hand, it would be ridiculous even to contemplate using the uncountable quantity of existing data, even if it were all equally good. Furthermore, much of the work cited in the compilation is derived from reports of government-sponsored work which do not necessarily get reported in the open literature. These references would not necessarily appear in the usual bibliography, since they are often unavailable to the general public.

147. S. R. Drayson, A Listing of Wave Numbers and Intensities of Carbon Dioxide Absorption Lines Between 12 and 20μm, Report No. 036350-4-T, University of Michigan, Ann Arbor, 1973.

148. L. W. Chaney, High Resolution Spectroscopic Measurements of Carbon Dioxide and Carbon Monoxide, Rept. No. 036350-3-T, University of Michigan, Ann Arbor, 1972.

Because the AFCRL compilation is one-of-a-kind, it is appropriate that a list of the subject matter used be singled out here for critique by anyone who questions its specificity or completeness. Many of the references cited in McClatchey, et al. (1973) are unavailable, either because the information was privately transmitted directly from the researcher to the authors, or because the works were as yet unpublished when the compilation was produced. The authors are quick to note that an opus of this magnitude is likely to contain errors, recognizing that its usefulness will be determined by its accuracy and completeness, which in turn are assured by the cooperation of the user in citing new laboratory data or theoretical work. The bibliography at the end of this report presents works related to the various absorbing atmospheric species.

4.6.2 THE AFCRL COMPILATION

The compilation generated by AFCRL contains data on over 100,000 lines, mainly in the infrared and microwave regions, from H_2O, CO_2, O_3, N_2O, CO, CH_4 and O_2 in the atmosphere, and is described in the report (McClatchey, et al., 1973) cited earlier. It is, presumably, the most nearly complete compilation of data of this type, derived from a number of sources. Whereas many investigators ignore the presence of oxygen in the absorption spectrum of the atmosphere, the AFCRL compilation includes it. On the other hand, HNO_3, considered to be important at high altitudes, is not included in the compilation. The effect of HNO_3 is, to be sure, secondary to that of the more common absorbing gases. And of course the more-or-less common atmospheric polluting gases have been excluded, probably for a number of reasons. Their importance is secondary; they would not fit into the scope of the general atmospheric problem since any interest in them would be provincial. And certainly, some have exceedingly complicated structures, with far less data collected on them than on the more common atmospheric constituents. The fact that HNO_3 actually falls, to a large extent, into this class of absorbers, may be the reason for its exclusion.

According to a statement of McClatchey, et al. (1973), the compilation is available to persons interested in obtaining it. It is contained on magnetic tape in 7-track, 8000 BPI characters. The format is described in the report and will not be reproduced here. It contains information on the positions of the more than 100,000 lines included, in addition to the line strengths and half-widths corresponding to a temperature of 296 K and a pressure of 760 mm Hg, i.e., one standard atmosphere. For ease of use in generalized atmospheric calculations, the compilation also includes the energy of the ground state for each line, as well as several sets of identification numbers. The strengths are derived on the basis of the number of molecules of the isotopes in their normal abundance. The isotopic abundances used are shown in Table 7. The nomenclature used is given in the following example: $H^1O^{16}H^1$–161. For usage of these numbers, see McClatchey, et al. (1973).

TABLE 7. ISOTOPIC ABUNDANCES. (From McClatchey, et al., 1973 [138].)

Molecule	Isotope	Abundance	Molecule	Isotope	Abundance
H_2O	161	0.99729	CH_4	211	0.98815
	162	0.000300		311	0.01110
	181	0.00204	CH_3D	212	0.00060
	171	0.000370			
CO_2	626	0.98414	O_2	66	0.99519
	636	0.01105		68	0.00407
	628	0.00402		67	0.00074
	627	0.000730			
	638	0.0000452			
	637	0.0000220			
	828	0.00000412			
O_3	666	0.99279			
	668	0.00406			
	686	0.00203			
N_2O	446	0.99022			
	456	0.00368			
	546	0.00368			
	448	0.00202			
	447	0.00037			
CO	26	0.98652			
	36	0.01107			
	28	0.00202			
	27	0.000369			

Determinations of the values compiled in the report by McClatchey, et al. are evidently an intricate combination of theoretical and experimental results, each being used as a check on the other. Included in the report is a set of nomenclature which form the basis for the calculation of the more than 100,000 lines, a printout of which stacks approximately one foot high. It is obviously beyond the scope of this report to reproduce these lines. One could perform many of the calculations from the set of data tabulated in the report, but this would be a rather costly and useless task, considering that the line parameters apparently are available to anyone who has a clean tape to send to AFCRL.

Basically, for linear molecules (CO_2 and N_2O), the compilation originates in the following equation for the unperturbed vibrational energy levels:

$$G_v^{unp} = \sum_i \omega_i v_i + \sum_i \sum_j x_{ij} v_i v_j + g_{22} \ell^2 + \sum_i \sum_{j \geq i} \sum_{k \geq j} y_{ijk} v_i v_j v_k \qquad (156)$$

where the v_i are the vibrational quantum numbers and ℓ is a quantum number (angular momentum associated with the degeneracy introduced by the quantized angular momenta. The ω_i, x_{ij}, y_{ijk} and g_{22} are coefficients. In this form, the vibrational energy level is referred to the lowest vibrational energy level. Perturbations of these energy levels to account for different effects results in a resolution of energy level degeneracies and a splitting of energy levels. Coupled with multiplicity of lines due to the different isotopes of any given molecule, this splitting and the resultant multiplicity of rotational lines, results in a large number of lines associated with any given vibrational band. The description in McClatchey, et al. (1973) of the energy levels for various molecules reflects this complexity, so that it is important to refer to the report for an understanding of the labels attached to the lines in the compilation.

4.6.2.1 Carbon Dioxide (CO_2)

For the linear molecules CO_2 and N_2O with only one degenerate vibration, the G_v^{unp} is:

$$G_v^{unp} = \sum_i \omega_i v_i + \sum_i \sum_{j>i} x_{ij} v_i v_j + g_{22} \ell^2 + \sum_i \sum_{j \geq i} \sum_{k \geq j} y_{ijk} v_i v_j v_k \qquad (157)$$

and the rotational energy corresponding to each quantum number, J, is:

$$E_{v,j} = G_v + B_v[J(J+1) - \ell^2] - D_v[J(J+1) - \ell^2]^2 + H_v[J(J+1) - \ell^2]^3 + \ldots\ldots \qquad (158)$$

where the G_v (vibrational energy level modified by reasonance perturbation), B_v, D_v and H_v are tabulated in the report. The H_v are quite small and thus omitted for most levels. The so-called ℓ-type doubling (see, e.g., Ref. [149]) causes a splitting of rotational levels into two levels close

149. G. Herzberg, Infrared and Raman Spectra of Polyatomic Molecules, Van Nostrand, N. Y., 1945.

together in energy. The rotational constants associated with these levels are designated in the tables with an addition of a c or d. If $\ell = 1$ the values B_v for the c and d components differ as do those for D_v and H_v. If $\ell = 2$ the B_v values are equal but the D_v and H_v values differ for c and d. If $\ell = 3$ only the H_v values for c and d differ. A further explanation of the use of these symbols in calculating energy levels is given in the report along with the general equation for calculating the wavenumber of an allowed transition:

$$J(m) = G_v + am + bm^2 + cm^3 + dm^4 + em^5 + fm^6 \qquad (159)$$

where $a = (B'_v + B''_v)$; $b = (B'_v - B''_v - D'_v + D''_v)$; $c = -2(D'_v + D''_v)$;

$d = -(D'_v - D''_v)$; $e = 3(H'_v + H''_v)$; $f = (H'_v - H''_v)$

and $m = J'' + 1$ for the R-branch $(J'' \rightarrow J'' + 1)$

$= -J''$ for the P-branch $(J'' \rightarrow J'' - 1)$

$= J''$ for the Q-branch $(J'' \rightarrow J'')$ (A slightly modified equation is used for the Q-branch; See Eq. (160)).

The primed values refer to the upper vibrational state and the double-primed values refer to the lower vibrational state. The selection rules governing the occurrence of a transition are as follows:

When $\Delta\ell = 0$, $\Delta J = \pm 1$, c—c, and d—d; when $\Delta\ell = 1$, $\Delta J = \pm 1$, c—c, and d—d; and when $\Delta J = 0$, c—d.

where, for example, c—c implies that the letter assigned to the rotational level does not change in the transition, etc.

Certain vibrational energy levels and molecular constants for the various isotopes of CO_2 reported in the compilation report are tabulated in Table 8. In Table 9 are tabulated the band centers corresponding to transitions between the vibrational energy levels, also shown in the table, as well as the unperturbed strength of each band. Techniques are explained in the compilation report for taking interaction effects into consideration. It should be noted, incidentally, that the values tabulated do not always correspond to those used in generating the magnetic tape.

4.6.2.2 Nitrous Oxide (N_2O)

For N_2O, data are reported which are similar to those given for CO_2, although the energy level designation is slightly different. Explanations are given for the manner in which the band data are used to take into account the effects of interactions. The vibrational energy levels and molecular constants are given in Table 10; these are inserted into Eq. (159) to obtain line positions for the P- and R-branches. For the Q-branch, use ($\Delta J = 0$, $m = J''$):

TABLE 8. VIBRATIONAL ENERGY LEVELS AND MOLECULAR CONSTANTS FOR CO_2. (From McClatchey, et al., 1973 [138].)

Energy Level	G (cm^{-1})	B (cm^{-1})	D Multiply by 10^{-7} (cm^{-1})
	Isotope 626		
00001	0.00	0.390218	1.331
01101 c	667.379	.390643	1.355
01101 d		.391253	1.355
10002	1285.412	.390481	1.563
02201 c	1335.129	.391682	1.389
02201 d			1.379
10001	1388.187	.390188	1.142
11102 c	1932.470	.390736	1.441
11102 d		.391680	1.501
03301 cd	2003.238	.392420	1.403
10101 c	2076.855	.390416	1.281
11101 d		.391344	1.195
00011	2349.146	.387140	1.325
30003	2548.380	.391183	1.76
12202 c	2585.006	.391843	1.45
12202 d			1.25
20002	2671.113	.389556	1.331
04403 cd	2671.690	.391162	1.42
12201 c	2760.735	.391535	1.44
12201 d			1.25
20001	2797.154	.390563	0.985
01111 c	3004.016	.387593	1.349
01111 d		.388190	1.349
21103 c	3081.850	.391028	1.63
21103 d		.392316	1.75
13302 cd	3340.564	.392696	1.51
21102 c	3379.340	.390035	1.37
21102 d		.391145	1.37
05501 cd	3340.475	.393908	1.44
13301 cd	3442.256	.392312	1.35
21101 c	3500.990	.390461	1.10
21101 d		.391700	1.01
10012	3612.844	.387496	1.57
03311 c	3659.277	.388647	1.383
02211 d			1.373
10011	3714.781	.387051	1.13
30004	3792.702	.391760	2.02
12203 c	3821.984	.392359	1.46
12203 d			1.48
14402 cd	3898.117	.393414	1.54
30003	3942.492	.389584	1.66
12202 c	4007.850	.391485	1.47
12202 d			1.40
30002	4063.908	.389606	0.935
14401	4142.347	.393036	1.36
12201 c	4197.613	.391719	1.63
12201 d			1.13
30001	4225.110	.391090	0.531
11112 c	4267.713	.387773	1.49
11112 d		.388690	1.56
03311 cd	4314.913	.389387	1.405
11111 c	4390.620	.387350	1.34
11111 d		.388230	1.17
00021	4673.327	.384083	1.319
31104 c	4414.150	.391357	1.63
31104 d		.393078	1.76
31103 c	4541.110	.389225	1.53
31103 d		.391348	1.48
31102 c	4753.454	.389700	1.20
31102 d		.391098	1.33
20013	4953.673	.388158	1.77
12212 c	4987.970	.389958	1.33
12212 d			1.43
31101 c	4930.410	.389358	0.995
31101 d		.391130	0.808
04401 cd	4970.909	.390148	1.42
20012	4977.830	.386529	1.35
12211 c	5061.776	.388508	1.28
12211 d			1.12
20011	5099.660	.387648	0.921
01121 c	5315.730	.384569	1.46
01121 d		.385148	1.46
40004	5197.249	0.390092	1.89
32203 c	5241.449	.391498	1.335
32203 d			1.535
21113 c	5475.071	.388153	1.61*
21113 d		.389123	1.705
40002	5478.565	.390093	0.895*
13312 cd	5531.279	.392732	1.52
05511 cd	5627.254	.390913	1.44
21112 c	5632.760	.387010	1.265
21112 d		.388128	1.385
13311 cd	5730.618	.389279	1.51
21111 c	5790.579	.387413	1.125
21111 d		.388613	1.025
10022	5915.209	.384228	1.57
02221 c	5950.539	.385417	1.35
02221 d			1.31
10021	6016.690	.383917	1.17
30014	6075.983	.389496	2.052
22213 c	6103.670	.389428	1.29
22213 d			1.67
14412 c	6176.623	.390485	1.54
31102 c	6179.010	.389642	1.33
30013	6227.924	.386697	2.643
22212 c	6288.492	.388472	1.38
22212 d			1.28
30012	6347.854	.386451	0.951
41101 c	6388.085	.390790	0.93
14411 cd	6398.047	.390017	1.37
22211 c	6474.530	.388662	1.53
22211 d			1.21
30011	6503.881	.387976	0.719
11122 c	6537.958	.384804	1.475
11122 d		.385722	1.606
11121 c	6679.709	.384310	1.318
11121 d		.385127	1.115
00031	6972.578	.380990	1.331
31114 c	6698.274	.388547	1.735
31114 d		.390746	1.425
31113 c	6863.553	.386930	1.401
31113 d		.388332	1.485
31112 c	7023.672	.385755	1.19
31112 d		.388127	1.165
20023	7133.819	.385288	1.75
12223 c	7168.049	.386917	1.15
12222 d			1.23
31111 c	7303.824	.387407	1.05
31111 d		.389117	0.85
12221 c	7338.149	.385487	1.33
12221 d			1.28
20021	7377.678	.384403	1.48
01131 c	7602.529	.381503	1.315
01131 d		.382069	1.355
40015	7283.981	.389550	2.31
32214 c	7307.651	.389942	1.03
32214 d			1.54
40014	7460.530	.387322	1.93
32213 c	7505.219	.388632	1.23
32213 d			1.34
40013	7593.687	.385567	1.06
32212 c	7684.616	.388252	1.18
32212 d			1.14
40012	7734.492	.386954	0.59
21123 c	7743.740	.385358	1.75
21123 d		.386408	1.73
32211 c	7897.573	.388965	1.33*
32211 d			0.939**
21122 c	7901.479	.384008	1.31*
21122 d		.385128	1.380**
40011	7920.940	.388558	0.60
21121 c	8056.824	.384408	1.11
21121 d		.385525	1.06
10032	8192.556	.381561	1.56
02231 c	8332.880	.382600	1.30
02231 d			1.28
10031	8293.097	.380805	1.13
41114 c	8081.179	0.387643	1.56
41114 d		.389753	1.66
41113 c	8250.644	.386233	1.355
41113 d		.387813	1.355
41112 c	8425.000	.386817	0.935
41112 d		.388517	0.965
11132 c	8803.265	.381858	1.49
11132 d		.382744	1.55
03331 cd	8863.648	.383420	1.40
11131 c	8944.146	.381264	1.22
11131 d		.381874	1.18
20033	9388.990	.38234	1.71
12232 c	9419.189	.38307	1.37
12232 d			1.25
20032	9516.970	.38048	1.39
12231 c	9589.929	.38247	1.43
12231 d			1.53
20031	9631.350	.38125	1.04
21133 c	9987.48	.38251	1.55
21133 d		.38351	1.61
21132 c	10145.43	.38058	1.25
21132 d		.38258	1.35
21131 c	10297.05	.38127	1.10
21131 d		.38237	1.00
	Isotope 636		
00091	0.00	.380235	1.330
01101 c	648.484	.390398	1.330
01101 d		.391236	1.330
10002	1265.820	.390020	1.58
02202 c	1297.265	.391603	1.274
02202 d			1.334
10001	1370.067	.389707	1.160
01102 c	1896.69	.391137	1.48
01102 d		.392086	1.13
03301 cd	1966.343	.390293	1.34
11101 c	2037.093	.390015	1.18
11101 d		.390979	1.13
00011	2283.490	.387300	1.325
20003	2507.50	.391815	1.76
12202 c	2531.63	.39220	1.22
12202 d			1.40
04401 cd	2595.614	.392987	1.34
20002	2545.086	.389826	1.46
12201 c	2700.25	.39126	1.30
12201 d			1.34
20001	2750.48	.389670	0.91
01111 c	2920.244	.387664	1.325
01111 d		.388286	1.325
31103 c	3127.28	.39155	1.70
31103 d		.39308	1.68
13302 cd	3169.21	.39272	1.45
31102 c	3289.71	.39001	1.25
31102 d		.39128	1.29
13301 cd	3361.57	.39109	1.25
31101 c	3433.70	.39092	1.04
31101 d			1.10
10013	3627.760	.388030	1.56
02211 c	3557.214	.386568	1.28
02211 d			1.33
10011	3632.917	.386726	1.21
30001	4145.95	.39010	1.22*
11113 c	4147.234	.38911	1.49*
11113 d		.38915	1.59
03311 cd	4194.704	.389348	1.33
11111 c	4287.695	.387654	1.27
11111 d		.387977	1.26
00021	4543.552	.384360	1.33
20013	4748.058	.388945	1.815
12212 c	4770.905	.38925	1.25
12212 d			1.27
04411 cd	4831.99	.39003	1.34

*,** J-dependent interactions

TABLE 8. VIBRATIONAL ENERGY LEVELS AND MOLECULAR CONSTANTS FOR CO_2. (From McClatchey, et al., 1973 [138].) (Concluded)

Energy Level	G (cm^{-1})	B (cm^{-1})	D Multiply by 10^{-7} (cm^{-1})
20012	4887.390	0.386847	1.47
12211 c	4938.80	.38831	1.44
12211 d			1.40
20011	4991.950	.386705	0.94
01121 c	5168.800	.384595	1.33
01121 d		.385309	1.33
21113 c	5397.004	.388616	1.30
21113 d		.390108	1.68
13312 cd	5397.09	.32978	1.30
21112 c	5519.944	.387038	1.16
21112 d		.388206	1.36
13311 cd	5569.17	.38907	1.64
21111 c	5662.269	.387737	1.10
21111 d		.387936	1.00
30014	5951.600	.389640	2.326
22213 c	5970.949	.389913	1.57
22213 d			1.93
30013	6119.618	.387540	1.786
22212 c	6155.37	.38853	1.36
22212 d			1.30
30012	6241.964	.385859	1.113
22211 c	6326.049	.386163	1.04
22211 d			1.35
30011	6362.616	.387033	0.906
11122 c	6374.[illegible]97	.39521	1.46
11122 d		.38507	1.56
00031	6780.219	.381353	1.33
31114 c	6552.954	.390958	1.63
31114 d		.390896	1.83
31113 c	6736.696	.387368	1.63
31113 d		.390908	1.58
31112 c	6892.054	.385372	1.23
31112 d		.387706	1.48
31111 c	7046.029	.386458	1.33
31111 d		.388236	0.83
01131 c	7293.599	.391803	1.23
01131 d		.382391	1.35
40013	7681.510	.385415	0.33
40012	7800.130	.385815	0.63
10032	7961.180	.382375	1.52
10031	8089.040	.380735	4.36
	Isotope 638		
00001	0.00	.368164	1.31
01101 c	662.308	.368588	1.13
01101 d		.369128	1.13
10002	1250.038	.368114	1.36
02201 c	1325.15	.369520	1.20
02201 d			1.16
10001	1388.045	.368502	0.982
12202 c	1901.749	.36845	1.23
12202 d		.36935	1.38
03301 cd	1980.328	.370182	1.30
12201 c	2049.366	.36060	1.06
12201 d		.36954	1.91
00011	2338.112	.361267	1.11
20003	2508.776	.368413	1.04
12202 c	2549.425	.36954	1.25
12202 d			1.27
20002	2614.215	.367807	1.04
04401 cd	2651.875	.37095	1.22
12201 c	2728.264	.36964	1.30
12201 d			1.07
20001	2757.229	.369039	0.77
01111 c	2982.136	.365707	1.13
21103 c	3127.31	.36955	1.34
21103 d		.36557	1.41
13302 cd	3200.15	.37023	1.38
21102 c	3261.87	.36817	1.14
21102 d	3281.07	0.36916	1.12
13301 cd	3404.93	.37077	1.30
21101 c	3453.99	.36881	0.98
21101 d		.37007	0.90
10012	3571.143	.365284	1.27
02211 c	3612.52	.366595	1.19
d			1.25
10011	3675.130	.365534	0.95
30003	3858.657	.367405	1.24
30002	3987.610	.368174	0.91
11112 c	4201.19	.365674	1.23
11112 d		.364423	1.20
03311 cd	4203.35	.36726	1.19
11111 c	4346.13	.365716	1.05
11111 d		.364368	1.00
00021	4639.502	.363372	1.11
20013	4791.260	.365734	1.50
12212 c	4836.63	.366707	1.25
d			1.37
20012	4904.850	.364844	1.11
12211 c	5012.55	.366735	1.26
d			1.06
20011	5063.570	.366124	0.95
01131 c	5277.147	.367548	1.06
d		.363356	1.06
21113 c	5406.068	.365833	1.41
d		.366904	1.31
21112 c	5550.853	.365318	1.10
d		.364240	1.10
21111 c	5727.048	.365940	1.11
d		.367138	0.81
10022	5858.022	.362490	1.357
02221 c	5915.23	.36376	1.18
d			1.15
10021	5959.594	.362605	0.896
30014	5983.581	.364337	1.78
30013	6127.782	.364495	1.31
30012	6254.592	.363276	0.80
30011	6429.179	.364614	0.60
00031	6832.210	.359479	1.10
10032	8130.104	.359484	1.25
10031	8230.363	.358836	0.95
	Isotope 637		
00001	0.00	.378641	1.305
01101 c	664.735	.379065	1.22
01101 d		.379639	1.22
10003	1271.875	.378738	1.48
02201 c	1329.87	.380061	1.34
02201 d			1.22
10004	1376.30	.378808	1.04
12202 c	1916.31	.37901	1.27
12202 d		.37989	1.32
03301 cd	1995.36	.37977	1.22
12201 c	2052.41	.37894	1.15
12201 d		.37787	1.10
00021	2340.01	.375659	1.20
20003	2522.50	.37934	1.60
12202 c	2566.33	.380125	1.35
12202 d			1.29
20002	2641.26	.37814	1.18
12201 c	2743.68	.38005	1.30
12201 d			1.23
20001	2776.00	.37927	0.88
01111 c	2992.310	.374103	1.22
01111 d		.376664	1.22
10012	3591.86	.3758.5	1.38
02211 c	3645.02	.377091	1.24
02211 d			1.22
10011	3693.64	.375754	1.06
11113 c	4229.33	0.37616	1.31
11112 d		.37700	1.34
11111 c	4367.08	.37600	1.18
11111 d		.37686	1.15
00021	4655.305	.373674	1.20
20013	4821.500	.376411	1.82
20012	4939.350	.375133	1.21
20011	5064.910	.376321	1.00
11112 c	5593.645	.375625	1.22
11112 d		.376759	1.22
00031	6945.610	.369691	1.20
	Isotope 636		
00001	0.00	.368180	1.11
01101 c	643.23	.36857	1.12
01101 d		.36915	1.12
10002	1244.93	.36830	1.[illegible]
02201 c	1286.86	.36951	1.14
02201 d			1.11
10001	1343.37	.36844	0.90
00011	2265.973	.365388	1.11
20002 c	2538.43	.36778	1.04
01111 c	2897.58	.36579	1.12
01111 d		.36633	1.12
10002	3490.39	.36588	1.26
02211 c	3529.99	.36671	1.10
02211 d			1.12
10011	3587.54	.36522	1.01
00021	4508.749	.36260	1.11
20012	4814.570	.364818	1.11
	Isotope 637		
00001	0.00	.378658	1.21
01101 c	645.72	.379036	1.22
01101 d		.378627	1.22
10003	1254.83	.37800	1.40
02201 c	1293.80	.38000	1.22
02201 d			1.22
10001	1355.52	.37848	1.06
00011	2274.33	.37579	1.21
01111 c	2918.38	.37617	1.22
01111 d		.37675	1.22
10002	3508.07	.37641	1.41
10001	3609.05	.37540	1.11
	Isotope 636		
00001	0.00	.368799	1.04
01101 c	657.33	.367224	1.04
01101 d		.367736	1.04
10003	1230.20	.36630	
02201 c	1315.08	.36812	1.10
02201 d			1.04
10001	1347.22	.36776	
00011	2313.97	.36412	1.04
01111 c	2959.08	.36455	1.04
01111 d		.36506	1.04
10002	3525.309	.363860	1.16
10001	3630.067	.363336	0.907
	Isotope 728		
00001	0.00	.35695	1.07
01101 c	659.78	.35737	1.08
01101 d		.35799	1.08
00011	2322.52	.35419	1.07

TABLE 9. BAND ORIGINS AND STRENGTHS FOR CO_2. (From McClatchey, et al., 1973 [138].)

Band Center ν_o (cm^{-1})	Upper Level	Lower Level	Isotope	S^0 at 296K (multiply by 10^{-22} cm^{-1} m^2 s^{-1})	
471.415	20003	11101	626	0.0087	
479.829	11302	12201	626	.0012	
494.537	12202	11101	636	.00079	g
508.141	12202	11101	626	.0516	
510.337	21101	20002	636	.0840	
526.423	11102	10001	636	.025	
535.963	11102	10001	628	.0611	g
543.186	21102	20001	636	.00711	
544.383	11102	10001	636	2.723	
548.275	11302	04401	628	0.00036	g
557.742	14402	05501	636	.00253	
561.097	12202	01301	628	.0058	
564.889	20001	11101	628	.0047	
568.874	11302	04401	636	.0716	
570.67	12202	01301	627	.00032	g
573.536	11302	04401	636	.00115	
576.508	11102	02201	628	.160	
578.605	21102	12201	636	.0376	
578.85	30002	11101	627	.00072	g
586.616	22202	13302	636	.0076	
591.746	13302	05501	636	1.934	
595.287	13302	05501	636	.834	
598.64	11102	02201	627	.0439	
599.43	21102	12201	636	.00085	g
604.348	20002	11101	636	.958	
606.66	21102	12202	636	.0830	
606.644	21102	12202	636	.397	
607.082	10002	01101	628	5.19	
607.341	11102	02201	636	52.88	
609.028	20002	11102	636	0.021	
609.221	11102	02201	636	.788	
661.70	10002	01101	638	.058	
667.14	10002	01101	637	1.17	
667.27	20002	11101	638	0.021	
667.993	20002	11101	636	.0811	
668.038	10012	01101	636	.0175	
668.11	10002	01101	637	.0106	
611.01	20002	11101	636	.182	
615.010	20002	11102	636	0.05	
617.336	10002	01101	636	20.9	
618.023	10002	01101	636	1456.	
619.78	21102	20002	636	0.0008	
633.170	21102	20002	636	.049	
636.754	01111	00011	636	.0121	
637.38	11302	12202	636	.063	
640.678	11102	10002	636	2.66	
642.110	11102	10002	628	0.78	
643.23	02201	00001	636	1.17	
644.038	11302	10002	627	0.15	
645.72	02201	00001	627	.042	
646.11	02201	00001	637	.008	
647.056	11102	10002	636	.222	
648.464	02201	00001	636	880.	
648.705	02201	00001	636	73.4	
649.074	02201	00001	636	4.69	
649.331	02401	01101	636	0.366	
649.360	05501	04401	636	.0142	
650.02	12202	11102	627	.0110	
652.536	12202	11102	636	36.52	
654.697	01111	00011	636	0.605	
655.560	11302	12202	636	0.990	
657.33	02201	00001	628	.365	
657.69	02202	00111	628	.0277	
657.339	10402	11202	636	.0442	
658.79	02201	00001	720	.0615	
661.32	11302	12201	636	.0958	
662.389	02201	00001	638	330.	
663.782	02201	00001	628	20.2	
663.157	12201	11101	636	0.106	
663.178	02202	00201	628	1.90	
663.547	04401	01101	628	0.078	
666.725	02201	00001	627	62.2	
668.135	02202	00101	627	0.88	
668.69	02202	00201	627	0.305	
667.526	11101	10001	636	1.98	
667.379	01101	00001	636	83500.	
667.750	02201	01101	636	6602.	
668.109	01201	00201	636	387.6	
668.227	21102	20002	636	0.312	
668.452	04402	01301	636	18.45	
669.748	05501	04401	636	0.976	
669.106	06401	05501	636	.077	
670.910	12201	11101	628	.068	
671.27	12201	11101	627	.0082	g
681.521	11301	12201	626	.460	
683.501	11101	10001	628	.77	
683.870	12201	11101	636	9.05	
684.13	11101	10001	627	0.13	
688.678	11101	10001	636	146.9	
696.823	22301	21101	636	0.0105	
697.14	10001	01101	638	.058	
703.477	10021	01101	628	0.30	
703.47	21101	20001	636	0.346	
707.083	20002	11101	637	.936	
709.68	10001	01101	637	.0094	
710.765	10011	01111	636	.0202	
711.455	10021	01101	627	1.75	
712.697	20002	11102	628	0.013	
713.367	20001	11101	636	.047	
713.59	20001	11101	627	.0038	
720.209	20001	11101	636	4.784	
720.808	10021	01101	636	1853.	
721.583	10002	01101	636	17.9	
724.198	11101	01201	638	0.315	
724.95	20002	11102	627	.0024	g
732.54	11101	01201	627	.0476	
733.45	21101	20001	636	.0021	g
738.643	20002	11102	636	3.021	
739.864	11101	02301	638	0.70	
739.936	12201	01301	638	.0157	
739.935	21101	12201	636	.176	
741.736	11101	02201	636	79.01	
747.22	12201	01301	627	0.0222	g
748.546	20002	11102	636	.4178	
753.025	13301	04401	638	.00338	g
754.134	21102	12202	636	.1607	
757.497	12201	03701	636	3.258	
765.996	13301	04401	636	0.02173	g
770.335	13301	04401	636	.1351	
771.273	11101	10002	636	.138	
781.872	14401	05501	636	.0051	
788.914	11101	10002	638	.0026	
790.516	11101	10002	637	.0010	g
791.060	21102	20002	636	.0048	
791.493	11101	10002	636	11.73	
803.76	12202	11102	636	0.6353	
832.816	12202	11102	638	.0069	g
838.263	12202	11102	636	.391	
839.667	21102	20002	636	.0048	
857.259	13301	12202	636	.0110	
864.504	20001	11101	636	.0433	
883.151	01111	11101	636	.00039	
886.543	02211	12201	636	.0132	
913.483	00011	10001	636	.0014	
915.596	21102	12202	638	.00198	g
917.637	10011	20001	636	.0087	
927.151	01111	11101	638	.1588	
932.748	01111	11101	618	.00178	
941.731	10012	20002	628	.01108	
952.310	21101	20002	638	.00054	g
960.950	00011	10001	638	6.910	
961.73	00011	10001	637	.0032	
966.267	00011	10001	628	.0108	
1017.670	00011	10002	636	.0728	
1023.744	01111	11102	636	.00572	
1063.734	00011	10002	626	0.334	
1069.135	00011	10001	627	.0067	
1071.846	01111	11101	636	.040	
1072.652	00011	10002	638	.0003	
1074.371	02211	12202	636	.0227	
1080.258	01111	11102	636	.00243	
1239.380	11102	02201	638	0.0251	
1244.95	10002	00001	638	.0000	
1259.436	10002	00001	638	.031	
1271.875	10002	00201	627	.0120	
1262.37	10001	00001	638	.0063	
1265.845	10001	00001	628	.041	
1274.20	10002	00001	637	.0123	
1286.978	11201	01101	636	.0816	
1846.321	21103	02201	636	.00033	-.15
1850.02	10003	01101	636	.00016	-.15
1860.232	20004	11102	636	.00004	-.12
1861.667	20003	11101	636	.00007	-.12
1880.901	20003	01101	636	.0156	-.20

TABLE 9. BAND ORIGINS AND STRENGTHS FOR CO_2. (From McClatchey, et al., 1973 [138].) (Continued)

Band Center ν_0 (cm^{-1})	Upper Level	Lower Level	Isotope	S^0 at 296K (multiply by 10^{-22} cm^{-1} / cm^{-2} cm^{-1})	%
1063.146	12202	01101	636	0.00149	-.06
1069.518	22203	11102	626	.00137	-.08
1096.490	21102	00001	636	.0149	-.06
1896.838	21103	10002	636	.01101	-.07
1901.746	11102	00001	628	.01376	-.06
1905.435	11302	02201	626	.1786	-.06
1917.627	12202	01101	626	.4226	-.055
1930.985	12202	11101	626	.00082	-.06
1932.478	11102	00001	626	4.092	-.062
1953.153	21103	10001	626	.00707	-.06
1997.602	30003	01101	636	.0015	-.06
2003.734	30002	01101	626	.00818	-.03
2004.211	21102	02201	626	.00118	-.04
2012.822	30003	11103	626	.00013	-.05
2037.093	11101	00001	636	.184	-.05
2049.346	11101	00001	626	.0372	-.03
2055.846	12201	01101	628	.0252	-.03
2062.41	11101	00001	627	.0052	-.035
2075.380	22202	11102	626	.0049	-.04
2076.865	11101	00001	626	22.32	-.641
2093.356	12201	01101	626	3.956	-.038
2094.861	20001	01101	628	0.0053	-.04
2101.996	20001	01101	636	.0149	-.03
2107.127	11301	02201	636	.253	-.035
2112.461	21101	10001	636	.112	-.08
2119.119	14401	03301	626	.0156	-.033
2120.548	22201	11101	626	.0119	-.04
2127.235	12212	12201	626	.00347	
2129.775	20001	01101	636	1.302	-.7
2148.245	30001	11101	636	.00595	-.18
2157.673	10012	10001	636	.0152	
2165.461	21101	02201	626	.0595	-.08
2170.848	11112	11101	636	.0507	
2180.676	20012	20001	636	.00082	
2182.507	20013	20002	626	.00172	
2205.298	10012	10001	628	.00558	
2224.647	10013	10001	626	1.272	
2225.05	05511	05500	636	0.00261	
2227.88	13.42	13302	636	.00401	
2229.726	21113	21103	636	.00488	
2230.334	21112	21102	636	.00217	
2236.698	04411	04401	636	.0632	
2238.55	12211	12201	636	.0184	
2239.355	12212	12202	636	.139	
2246.558	20013	20003	636	.0734	
2260.87	20011	20001	636	.0122	
2262.696	20012	20002	636	.0258	
2262.776	00021	00011	628	.00126	
2262.73	02211	02201	636	.149	
2265.17	10011	10001	636	.0555	
2265.56	10012	10002	638	.0816	
2268.356	01121	01111	636	.0280	
2268.361	03313	03301	636	1.52	
2250.602	11111	11101	636	0.96	
2250.744	11112	11102	636	1.91	
2251.01	02211	02201	637	0.0264	
2251.24	10012	10002	637	0.0146	
2254.53	10011	10001	637	.0098	
2254.75	03113	03101	638	3.48	
2260.045	02211	02201	636	34.5	
2260.062	00021	00011	636	0.308	
2261.920	10012	10002	636	20.3	
2262.66	03111	03101	637	0.635	
2262.850	10011	10001	636	12.3	
2265.977	00511	00501	628	30.8	
2271.967	03111	03101	[illegible]	[illegible]	
2274.33	00011	00001	[illegible]	7.15	
2274.85	06.2	06401	[illegible]	0.0068	
2281.688	12211	12201	[illegible]	.0789	
2282.69	04411	04401	[illegible]	.0.47	
2283.850	00011	00001	[illegible]	0.0119	
2284.206	12211	12201	636	0.0119	
2286.779	05511	05501	636	.1943	
2287.205	12212	12202	628	.0363	
2288.352	13311	13301	636	.1183	
2290.615	20012	20002	628	.0187	
2290.884	20013	20003	628	.0188	
2290.715	13312	13302	636	.3125	
2293.478	21112	21102	636	.1919	
2295.621	21113	21103	636	.3965	
2296.784	11111	11101	628	.325	
2296.022	03113	03301	636	.406	
2299.319	04411	04401	628	4.895	
2299.362	02211	02211	636	0.076	
2299.443	11112	11102	628	0.606	
2301.041	12211	12201	626	3.17	
2301.73	01111	01101	628	0.31	
2301.909	10021	10011	626	0.0289	
2302.365	10022	10012	626	0.047	
2305.140	20013	20003	626	4.352	
2306.717	20012	20002	626	2.396	
2307.02	11112	11102	627	0.116	
2307.37	02211	02201	625	10.5	
2307.39	00021	00011	628	0.0791	
2308.285	10011	10001	626	6.47	
2311.675	03111	03101	626	122.8	
2311.713	10512	10002	628	7.29	
2311.715	01121	01111	626	1.793	
2313.764	11111	11101	626	8.56	
2313.97	00011	00001	628	3.60	
2315.15	02212	02202	627	1.91	
2315.263	12112	12102	626	17.11	
2317.36	10011	.8001	627	0.805	
2318.985	10012	10002	627	1.29	
2319.738	01111	01101	628	258.	
2322.52	00011	00001	728	1.35	
2324.148	02211	02201	626	3080.	
2324.182	00021	00011	626	20.98	
2332.594	10011	10001	636	2183.	
2327.432	10002	10002	626	1914.	
2327.575	01111	01101	627	49.7	
2332.112	00011	00001	628	3330.	
2336.637	01111	01101	626	76400.	
2340.01	00011	00001	627	637.	
2349.146	00011	00001	626	959800.	
2367.097	10011	10002	636	0.0131	
2415.700	10011	10002	628	.0056	
2428.547	20013	20002	626	.00146	
2429.368	10011	10002	626	1.059	
2429.550	20012	20002	626	0.00256	
2458.158	11111	11102	626	.0402	
2464.962	21103	01101	638	.0058	
2500.776	20003	00001	628	.075	
2523.58	20013	00001	627	.0060	
2568.43	20103	00001	638	.0020	
2614.235	20003	01001	628	.106	
2618.792	[illegible]02	01101	628	.0146	
2641.26	20003	00001	627	.018	
2757.229	20001	00001	628	.022	
2776.00	20001	00001	627	.0023	
2791.622	21101	01101	628	.0015	
3135.323	30004	01101	626	.00034	.40
3154.605	22203	01101	626	.00074	.40
3181.45	21103	00001	626	.00487	.30
3275.113	30003	01101	626	.0102	.02
3281.97	21102	00001	628	.00017	.14
3289.71	21102	00001	636	.00042	.14
3339.348	21102	00001	626	.0417	.14
3340.13	22202	01101	626	.0463	.14
3396.529	30003	01101	626	.00185	.30
3398.206	21113	11101	626	.00413	
3450.75	13311	03301	636	.0174	
3460.514	21113	11102	636	.0409	
3465.633	20013	10001	636	.1796	
3473.716	13312	02301	636	.3422	
3482.238	20013	10002	636	.450	
3483.851	21112	11101	636	.9174	
3490.390	10012	00001	638	.463	
3497.464	30001	01101	636	.0 part	
3498.750	11112	01101	636	7.314	
3500.590	21101	00001	636	.1052	.14
3505.330	21103	11102	628	.0110	
3504.933	14412	04401	626	.0475	
3506.67	10012	00001	637	.0771	
3509.207	21102	11101	638	.00462	
3511.58	11113	01101	628	.181	
3517.323	20012	10001	636	.177	
3525.205	10012	00001	628	.0508	
3527.703	30014	20003	626	.1034	
3527.746	10013	00001	636	94.2	
3527.757	22213	12201	636	.0376	
3531.83	20013	10001	628	.181	
3533.942	11122	01111	626	.0353	
3536.823	11112	01101	628	6.449	
3539.005	20012	10001	628	.0761	
3543.601	21113	11102	626	3.167	
3543.696	40002	11102	626	.0 part	

Reproduced from best available copy.

TABLE 9. BAND ORIGINS AND STRENGTHS FOR CO_2. (From McClatchey, et al., 1973 [138].) (Continued)

Band Center ν_0 (cm^{-1})	Upper Level	Lower Level	Isotope	S^0 at 296K (multiply by 10^{-22} mol^{-1} cm^2 cm^{-1})	½
3949.615	20013	10002	627	0.1224	
3550.730	30012	20001	626	0.1195	
3552.861	13212	03301	636	31.15	
3555.895	21112	11101	636	1.101	
3556.749	30013	20002	626	0.0679	
3559.595	11112	01101	627	.668	
3561.670	30012	20001	627	.0135	
3566.063	10022	00011	626	.208	
3568.208	20013	10002	636	33.78	
3571.143	10012	00001	628	52.2	
3578.670	22213	12202	626	0.138	
3580.314	11113	01101	636	801.5	
3583.710	10011	00001	638	0.703	
3590.68	10012	00001	627	8.41	
3604.05	10011	00001	637	0.126	
3612.844	10013	00001	636	10350.	
3621.283	20011	10001	636	0.783	
3622.570	20012	10002	636	0.435	
3631.454	21112	11101	636	.6433	
3635.176	21111	11101	636	.0326	
3637.917	10011	00001	636	160.	
3638.067	10111	00201	828	0.0782	
3641.727	13311	03301	636	.0780	
3649.277	03111	00001	626	(1.7-06 a)	
3655.62	20012	10002	628	.187	
3656.805	21112	11102	628	.0149	
3663.475	20012	10001	627	.0313	
3[illegible] 7.544	10121	00211	828	.389	
3676.130	10011	00001	638	6[illegible].8	
3679.634	11121	01111	626	0.0331	
3696.725	20011	10001	628	.164	
3696.742	30012	20002	628	.3915	
3[illegible]9.653	30013	20003	636	.0236	
3[illegible]3.762	11111	01101	628	3.824	
3697.702	21111	03111	628	0.0134	
3697.60	12311	02301	627	.143	
3697.618	20012	10002	636	42.4	
3703.830	10011	00001	627	10.2	
3708.086	20011	10001	627	0.0279	
3706.990	21112	11102	636	3.549	
3709.343	11111	01101	627	0.771	
3709.498	22212	12202	626	.1503	
3709.927	30111	20001	626	.0531	
3711.473	20011	10001	626	98.01	
4[illegible]3.714	21111	11101	636	2.816	
7[illegible]1.795	22311	12201	636	0.1094	
3714.781	10011	00001	626	15000.	
3723.249	11111	01101	636	1138.	
3726.530	20011	10002	636	0.0078	
3744.351	14411	04401	626	.0499	
3746.047	12211	02201	626	48.5	
3727.252	13311	03301	636	2.09	
3[illegible].48	30.1	10001	628	0.0035	
3[illegible].8[illegible]	40012	20003	636	.0028	
3[illegible]6.268	20011	10002	636	.770	
3[illegible]1.978	30011	20002	636	.00092	
3[illegible]8.107	21111	11102	636	.0251	
3[illegible]5.697	30003	00001	628	.016	
3807.218	30002	00001	628	.0149	
4[illegible]5.958	00311	01101	636	.00318	.14
4[illegible]6.150	31106	00001	636	.00037	.15
4[illegible]8.749	00[illegible].1	01101	636	.00106	
4[illegible]9.870	4[illegible]04	01101	636	.00023	.12
4[illegible]0.000	32201	01101	636	.00012	.20
4[illegible]1.318	31101	00001	636	.00705	.18
4[illegible]6.779	01121	01101	636	.01042	
4[illegible]9.563	00021	00001	628	.1302	
4[illegible]5.254	00021	00001	627	.0127	
4[illegible]3.850	22213	02201	636	.00149	
4[illegible]5.730	30014	10002	636	.00106	
4[illegible]7.795	30014	10001	636	.00534	
4[illegible]2.180	30013	00001	638	.00260	
4[illegible]8.52	21111	01101	636	.0288	
4[illegible]3.50	23113	03301	636	.00670	
4743.70	21113	01101	628	.0335	
4746.858	20013	00001	636	.314	
4753.450	31102	00001	626	.00398	.10
4755.705	31114	11102	636	.0179	
4758.561	22213	02201	636	.3904	
4764.875	30023	00011	636	.00149	
4766.898	31113	11101	636	.0119	
4781.571	30014	10002	636	.1562	
4781.960	30013	00001	628	.469	
4807.092	21113	01101	636	6.695	
4809.188	40002	01101	636	0. part	
4814.576	30012	00001	638	.0134	
4871.508	20013	00001	627	.0744	
4839.737	30013	10001	636	.1376	
4853.630	20013	00001	636	80.7	
4871.46	21112	01101	636	.234	
4887.370	30012	00001	636	2.976	
4887.970	12213	00001	636	(8.1-08 a)	
4894.195	21112	01101	628	.0801	
4904.850	30012	00001	628	7.118	
4925.010	30011	00001	638	0.00446	
4928.910	21112	01101	627	.00744	
4931.093	3111	11102	636	.0307	
4939.350	30013	00001	627	.2306	
4942.512	30013	10002	828	1.414	
4946.807	31112	11101	636	0.0591	
4951.363	22213	02201	636	1.042	
4959.647	30012	10001	636	0.837	
4965.301	21112	01101	636	34.56	
4977.830	30012	00001	636	349.7	
4981.33	30001	00001	636	7.12	
5013.785	21101	01101	638	0.1711	
5028.78	32211	02101	636	.00298	
5042.57	20011	00001	638	.227	
5051.776	12211	00001	626	(9.2-08 a)	
5062.042	30012	10002	636	.238	
5064.680	21111	01101	638	.368	
5068.910	30011	00001	627	.0632	
5059.86	30011	00001	636	112.3	
5114.894	30011	10001	636	0.388	
5121.70	21111	01101	626	10.16	
5149.401	22211	02201	626	0.408	
5168.60	01121	00001	636	.00372	
521[illegible].649	30001	10002	628	.0234	
5247.030	10023	01101	636	.0191	
5277.07	01121	00001	638	.00148	
5291.16	02221	01101	636	.0275	
5315.73	01121	00001	636	.398	
5349.36	10021	01101	636	.00508	
5584.391	00031	10001	636	.00707	
5687.166	00031	10002	636	.00731	
5858.022	10022	00001	628	.0[illegible]372	
5951.600	30014	00001	636	.00179	
5959.994	10021	00001	638	.00335	
5972.52	32216	02201	636	.00253	
5993.581	30014	00001	638	.00337	
6030.795	31114	01101	636	.0485	
6072.343	40014	10001	636	.00106	
6075.981	30014	00001	636	.454	
6078.21	31113	01101	636	.00238	
6150.30	31113	01101	638	.00398	
6119.618	30013	00001	636	.0250	
6127.782	30013	00001	638	.6230	
6149.760	41114	11102	636	.00179	
6170.000	32213	02201	636	.01345	
6175.113	40014	10002	636	.03359	
6175.950	30013	00001	627	.00328	
6179.01	41102	00001	635	(1.5-06 w)	
6186.174	31113	01101	636	.368	
6205.303	40013	10001	636	.0127	
6227.924	30013	00001	636	6.27	
6241.964	30012	00001	636	.0461	
6243.37	31112	01101	636	.00409	
6254.592	30013	00001	638	.01414	
6265.170	31112	01101	636	.00119	
6269.110	30012	00001	627	.00275	
6308.278	40013	10002	636	.03455	
6318.17	41113	11102	636	<00179	
6346.285	40012	10001	636	.0119	
6347.894	30012	00001	626	6.27	
6356.293	31112	01101	636	0.327	
6359.297	23212	02201	636	.0116	
6363.613	30011	00001	636	.0127	
6388.015	41101	00001	636	(6.0-06 w)	
6397.549	31111	01101	636	.00119	
6429.172	30011	00001	638	.00119	
6456.460	30023	01101	636	.00104	
6499.87	12222	01101	636	.00119	
6503.081	30011	00001	628	.498	
6532.653	40011	10001	636	.00130	

TABLE 9. BAND ORIGINS AND STRENGTHS FOR CO_2. (From McClatchey, et al., 1973 [138].) (Concluded)

Band Center ν_0 (cm^{-1})	Upper Level	Lower Level	Isotope	S^0 at 296K (multiply by 10^{-22} cm^{-1}) cm^2 cm^{-1}	
6536.645	31111	01101	636	.0478	
6537.950	11122	00001	636	.0223	
6562.644	32211	02201	636	.00323	
6679.709	11121	00001	636	.0703	
6745.115	01131	01101	636	.01329	
6780.215	00031	00001	636	.163	
6860.410	03111	03301	636	.00201	
6867.200	11131	11101	636	.00113	
6870.796	11132	11102	636	.00241	
6895.150	01131	01101	636	.00403	
6897.751	02231	02201	636	.0424	
6905.770	10031	10001	636	.0171	
6907.164	10032	10002	636	.0750	
6922.210	00031	00001	636	.0521	
6935.150	01131	01101	636	1.131	
6945.610	00131	00001	637	0.0112	
6972.570	00031	00001	636	14.99	
7283.981	40011	00001	636	0.00186	
7460.530	40014	00001	636	.6238	
7481.51	40013	00001	636	.00113	
7583.365	41113	01101	636	.00833	
7583.660	40013	00001	636	.1064	
7616.630	51102	00001	626	(1.12-06 W)	
7734.452	40012	00001	626	.0279	
7757.621	41112	01101	636	.00398	
7901.479	21122	00001	636	.00149	.010
7920.860	40081	00001	638	.00186	
7981.180	10032	00001	636	.00823	
8084.060	12332	02701	636	.00193	
8089.84	10031	00001	636	.08707	
8103.578	20033	10002	636	.00305	
8120.104	10032	00001	638	.00301	
8120.781	20032	10001	636	.00871	
8139.886	11132	01101	636	.0002	
8192.536	10031	00001	636	.636	
8220.363	10031	00001	638	.00371	
8243.163	20031	10001	636	.00180	
8254.800	12231	02301	635	.00164	
8276.767	11131	01101	636	.0061	
8293.957	10031	00001	636	.614	
9388.990	20033	00001	636	.00415	
9478.051	21132	01101	636	.00180	
9516.970	20032	00001	636	.0233	
9631.350	20031	00001	636	.0065	

Notes to Table 9.

Bands deriving all their strength from J-dependent perturbation are designated o part, when one near band provides the strength; π, when the listed strength is multiplied by $m(m + 1)$; and Δ, when the listed strength is multiplied by $m^2(m + 1)^2$.

Q designates bands with strength below the criterion limit, whose Q-branches are significant.

ζ is an interaction parameter. See McClatchey, et al. (1973).

TABLE 10. VIBRATIONAL ENERGY LEVELS AND MOLECULAR CONSTANTS FOR N_2O. (From McClatchey, et al., 1973 [138].)

*Energy Level	G (cm^{-1})	B (cm^{-1})	D Multiply by 10^{-7} (cm^{-1})	H Multiply by 10^{-12} (cm^{-1})
		Isotope 446		
$00^0 0$	0	0.4190113	1.795	1.17
$01^1{}^c 0$	588.767	0.4191777	1.785	1.17
$01^1{}^d 0$	588.767	0.4189695	1.785	1.17
$02^0 0$	1168.134	0.4189193	2.445	1.17
$02^2{}^c 0$	1177.750	0.4201253	1.165	1.17
$02^2{}^d 0$	1177.750	0.4201253	1.795	1.17
$10^0 0$	1284.907	0.4172563	1.775	1.17
$03^1{}^c 0$	1749.058	0.4196063	2.195	1.17
$03^1{}^d 0$	1749.058	0.4210883	2.195	1.17
$03^3{}^d 0$	1766.958	0.420674	1.805	2.20
$03^3{}^c 0$	1766.958	0.420674	1.805	0.14
$11^1{}^c 0$	1880.268	0.4174673	1.765	1.17
$11^1{}^d 0$	1880.268	0.4183803	1.775	1.17
$04^0 0$	2322.570	0.4206113	4.095	16.17
$04^2{}^c 0$	(2331.15)	0.4210113	1.350	1.17
$04^2{}^d 0$	(2331.15)	0.4210113	2.50	1.17
$12^0 0$	2461.998	0.4181483	2.465	3.77
$12^2{}^c 0$	2474.785	0.4187143	1.210	1.17
$12^2{}^d 0$	2474.785	0.4187143	1.700	1.17
$20^0 0$	2563.341	0.4224193	1.645	1.17
$00^0 1$	2223.756	0.4155613	1.795	1.17
$05^1{}^c 0$	2897.876		2.085	1.17
$05^1{}^d 0$	2897.876		2.355	1.17
$13^1{}^c 0$	3046.213	0.4177633	2.145	1.17
$13^1{}^d 0$	3046.213	0.4193783	2.165	1.17
$13^3{}^c 0$	3067.749	0.419109	1.805	0.47
$13^3{}^d 0$	3067.749	0.419109	1.805	1.87

TABLE 10. VIBRATIONAL ENERGY LEVELS AND MOLECULAR CONSTANTS FOR N_2O. (From McClatchey, et al., 1973 [138].) (Continued)

*Energy Level	G (cm^{-1})	B (cm^{-1})	D Multiply by 10^{-7} (cm^{-1})	H Multiply by 10^{-12} (cm^{-1})
		Isotope 446 (Contd)		
$21^{1c}0$	3165.857	0.4158333	1.595	1.17
$21^{1d}0$	3165.857	0.4169163	1.595	1.17
$01^{1c}1$	2798.290	0.4157723	1.795	1.17
$01^{1d}1$	2798.290	0.4165473	1.795	1.17
$14^{0}0$	3620.941	0.4187873	3.885	14.17
$14^{2c}0$	3631.601	0.4190143	0.375	1.17
$14^{2d}0$	3631.601	0.4190143	2.045	1.17
$22^{0}0$	3748.252	0.4163273	2.395	2.77
$22^{2c}0$	3766.060	0.4172013	1.200	1.17
$22^{2d}0$	3766.060	0.4172013	1.560	1.17
$30^{0}0$	3836.373	0.4141473	1.385	1.17
$02^{0}1$	3363.974	0.4165443	2.445	1.17
$02^{2c}1$	3373.137	0.4167523	1.195	1.17
$02^{2d}1$	3373.137	0.4167523	1.795	1.17
$10^{0}1$	3480.821	0.4137843	1.745	1.17
$23^{1c}0$	4335.798	0.4159193	2.045	1.17
$23^{1d}0$	4335.798	0.4176813	2.115	1.17
$31^{1c}0$	4446.379	0.4143703	1.625	1.17
$31^{1d}0$	4446.379	0.4156713	1.365	1.17
$03^{1c}1$	3931.258	0.4162253	1.915	1.17
$03^{1d}1$	3931.258	0.4176843	1.925	1.17
$03^{3c}1$	3948.344	0.417327	1.815	0.14
$03^{3d}1$	3948.344	0.417327	1.815	2.20
$11^{1c}1$	4061.979	0.4140513	1.775	1.17
$11^{1d}1$	4061.979	0.4149343	1.735	1.17
$40^{0}0$	5105.65	0.4131913	1.795	1.17
$32^{0}0$	5026.34	0.4143113	1.795	1.17
$20^{0}1$	4730.828	0.4121163	1.625	1.17
$12^{0}1$	4630.164	0.4147633	2.475	4.17
$12^{2c}1$	4642.463	0.4151583	1.315	1.17
$12^{2d}1$	4642.463	0.4151583	1.315	1.17
002	4417.379	0.4120963	1.765	1.17

TABLE 10. VIBRATIONAL ENERGY LEVELS AND MOLECULAR CONSTANTS FOR N_2O. (From McClatchey, et al., 1973 [138].) (Continued)

*Energy Level	G (cm^{-1})	B (cm^{-1})	D Multiply by 10^{-7} (cm^{-1})	H Multiply by 10^{-12} (cm^{-1})
Isotope 446 (Contd)				
$21^{1c}1$	5319.175	0.4124313	1.675	1.17
$21^{1d}1$	5319.175	0.4134703	1.555	1.17
$01^{1c}2$	4977.695	0.4123583	1.785	1.17
$01^{1d}2$	4977.695	0.4131183	1.785	1.17
Isotope 456				
$00^{0}0$	0	0.4189821	1.75	
$01^{1c}0$	575.5	0.419095	1.75	
$01^{1d}0$	575.5	0.419891	1.75	
$10^{0}0$	1280.5	0.41719	1.72	
$11^{1c}0$	1861.9	0.41734	1.71	
$11^{1d}0$	1861.9	0.41820	1.70	
$20^{0}0$	2554.3	0.41545	1.67	
$00^{0}1$	2177.659	0.41568	1.75	
$01^{1c}1$	2739.63	0.415855	1.75	
$01^{1d}1$	2739.63	0.416605	1.75	
$10^{0}1$	3430.95	0.41387	1.72	
Isotope 546				
$00^{0}0$	0	0.4048564	1.64	
$01^{1c}0$	585.320	0.4050304	1.65	
$01^{1d}0$	585.320	0.4057724	1.65	
$10^{0}0$	1269.894	0.403269	1.60	
$11^{1c}0$	1863.080	0.4034614	1.59	
$11^{1d}0$	1863.080	0.4043814	1.57	
$20^{0}0$	2534.21	0.401870	1.45	
$00^{0}1$	2201.604	0.401495	1.65	
$01^{1c}1$	2745.709	0.4017054	1.65	
$01^{1d}1$	2745.709	0.4024104	1.65	
$10^{0}1$	3443.659	0.399873	1.60	

TABLE 10. VIBRATIONAL ENERGY LEVELS AND MOLECULAR CONSTANTS FOR N_2O. (From McClatchey, et al., 1973 [138].) (Concluded)

*Energy Level	G (cm^{-1})	B (cm^{-1})	D Multiply by 10^{-7} (cm^{-1})	H Multiply by 10^{-12} (cm^{-1})
Isotope 448				
$00^0 0$	0	0.395577	1.65	
$01^{1c} 0$	584.1	0.395749	1.65	
$01^{1d} 0$	584.1	0.396461	1.65	
$10^0 0$	1247.9	0.394057	1.35	
$11^{1c} 0$	1839.8	0.39430	1.56	
$11^{1d} 0$	1839.8	0.39513	1.50	
$20^0 0$	2491.3	0.39279	1.31	
$00^0 1$	2218.37	0.392317	1.65	
$01^{1c} 1$	2788.80	0.392549		
$01^{1d} 1$	2788.80	0.393209		
$10^0 1$	3439.1	0.39078	1.55	
Isotope 447				
$00^0 0$	0	0.406691	1.72	
$01^{1c} 0$	586.3	0.406860	1.72	
$01^{1d} 0$	586.3	0.407610	1.72	
$10^0 0$	1265.5	0.405961	1.67	
$00^0 1$	2221.3	0.40334		
$01^{1c} 1$	2793.55	0.40357		
$01^{1d} 1$	2793.55	0.40430		

*Superscripts designate splitting. See Section 4.6.2.

$$\nu(J'') = G_v + (B' - B'')m + [(B' - B'')-(D' - D'')]m^2 - [2(D' - D'')-(H' - H'')]m^3$$

$$- [(D' - D'') - 3(H' - H'')m^4 + 3(H' - H'')m^5 + (H' - H'')m^6 \qquad (160)$$

For a fuller explanation of the inclusiveness of the data, the reader should refer to the compilation report. Table 11 reproduces the data in the band systems for N_2O, giving the main band center and the levels from which transitions in these bands arise, along with the strength of the system. The strengths of the individual lines included are greater than 4×10^{-23} molecules^{-1} cm^2 cm^{-1}, with the Q-branch of the band centered at 1974.571 included even though the individual strengths fall below the restrictive limit, because they are close enough together to be included aggregately by most slit functions. The individual bands in the system are broken down in Table 12.

4.6.2.3 Carbon Monoxide (CO)

Turning to the simple molecule, CO, there is little fanfare in the compilation report regarding its structure. Apparently, much of the ground work for determining the parameters used in calculating its line positions came from a report by Young [150], out of which are reproduced Tables 13 and 14. The first of these tables gives the spectroscopic constants for CO, and the second gives the integrated strengths for the fundamental and first two overtones of the molecule.

4.6.2.4 Oxygen (O_2)

In the compilation by McClatchey, et al. the O_2 molecule is considered last because, as a special case, it produces spectroscopic data produced by mechanisms somewhat different from those of the "conventional" IR-radiating and absorbing molecules. The energy level structure of the O_2 molecule is complex, but O_2 is considered here because the physical structure of a diatomic molecule puts it in the realm of the simple molecule. Actually, the characteristics of O_2 are presumed to be of lesser importance in this report because, as an absorber, O_2 tends to be effectively mainly in the near-IR (and visible) and in the microwave region, where the self-emission of the atmosphere is well below that at the mid-IR regions. Another, and perhaps more pertinent, reason for this presumption is that most of the models described in this report ignore O_2 as an absorber A good reason for including O_2, of course, is that it is the second most prevalent gas in the atmosphere, constituting approximately 20% of it. N_2, the most prevalent gas

150. L. A. Young, "CO Infrared Spectra," J. Quant. Spect. Rad. Trans., Vol. 8, 1968, pp. 693-716.

TABLE 11. SUMMARY OF N_2O BAND SYSTEMS. (From McClatchey, et al., 1973 [138].)

Center of Main Band (cm^{-1})	Upper Level	Lower Level	Strength of System Multiply by 10^{-20} Molecules^{-1} cm^2 cm^{-1}
588.767	01^10	00^00	118 ± 9
696.140	10^00	01^10	0.354 ± 0.020
938.849	00^01	10^00	0.254 ± 0.010
1168.134	02^00	00^00	38.5 ± 1.5
1284.907	10^00	00^00	996 ± 40
1634.989	00^01	01^10	0.278 ± 0.02
1749.058	03^10	00^00	0.241 ± 0.02
1880.268	11^10	00^00	1.66 ± 0.08
1974.571	20^00	01^10	S_Q = 0.024 ± 0.002*
2223.756	00^01	00^00	5710 ± 250
2322.624	04^00	00^00	2.7 ± 0.3
2461.998	12^00	00^00	33.4 ± 1.5
2563.341	20^00	00^00	135 ± 7
2798.290	01^11	00^00	9.62 ± 0.96
3363.974	02^01	00^00	10.6 ± 0.5
3480.821	10^01	00^00	197 ± 10
3620.941	14^00	00^00	0.56 ± 0.02, - 0.05
3748.252	22^00	00^00	4.12 ± 0.2
3836.373	30^00	00^00	8.15 ± 0.4
4061.979	11^11	00^00	0.111 ± 0.006
4335.798	23^10	00^00	0.1 ± 0.1, - 0.07
4417.379	00^02	00^00	6.9 ± 0.7
4630.164	12^01	00^00	0.68 ± 0.07
4730.828	20^01	00^00	4.4 ± 0.4
4977.695	01^12	00^00	0.070 ± 0.008
5026.34	32^00	00^00	0.29 ± 0.04
5105.65	40^00	00^00	0.29 ± 0.03

*Only the Q-branch at 1974.571 is listed because the lines in the P- and R-branches are very weak.

TABLE 12. N_2O BAND STRENGTHS. (From McClatchey, et al., 1973 [138].)

Band Center ν_c (cm^{-1})	Upper Level	Lower Level	Isotope	S_v at 296K (Multiply by 10^{-20} $Molecules^{-1}$ cm^2 cm^{-1})
588.767	01^10	00^00	446	98.4
579.367	02^00	01^10	446	4.90
588.983	02^20	01^10	446	11.26
580.924	03^10	02^00	446	0.599
571.308	03^10	02^20	446	0.256
589.208	03^30	02^20	446	0.958
595.361	11^10	10^00	446	0.216
585.320	01^10	00^00	546	0.356
575.5	01^10	00^00	456	0.356
586.3	01^10	00^00	447	0.039
584.1	01^10	00^00	448	0.197
696.140	10^00	01^10	446	0.294
938.849	00^01	10^00	446	0.223
1168.134	02^00	00^00	446	31.7
1160.291	03^10	01^10	446	5.72
1154.436	04^00	02^00	446	0.201
1153.40	04^20	02^20	446	0.228
1177.750	02^20	00^00	446	*
1284.907	10^00	00^00	446	872.
1291.501	11^10	01^10	446	100.6
1293.864	12^00	02^00	446	3.16
1297.035	12^20	02^20	446	5.92
1278.434	20^00	10^00	446	3.73
1297.155	13^10	03^10	446	0.390
1300.791	13^30	03^30	446	0.364
1285.589	21^10	11^10	446	0.412
1280.5	10^00	00^00	456	3.15
1286.4	11^10	01^10	456	0.354
1269.894	10^00	00^00	546	3.15
1277.760	11^10	01^10	546	0.362
1247.9	10^00	00^00	448	1.75
1255.7	11^10	01^10	448	0.200
1265.5	10^00	00^00	447	0.350
1634.989	00^01	01^10	446	0.231
1749.058	03^10	00^00	446	0.200
1880.268	11^10	00^00	446	1.41
1886.018	12^20	01^10	446	0.156
1873.231	12^01	01^10	446	0.053
1974.571	20^00	01^10	446	S_Q = 0.024
2181.66	06^00	10^00	446	*

*No value given.

TABLE 12. N_2O BAND STRENGTHS. (From McClatchey, et al., 1973 [138].) (Continued)

Band Center ν_c (cm^{-1})	Upper Level	Lower Level	Isotope	S_v at 296K (Multiply by 10^{-20} Molecules^{-1} $cm^2 cm^{-1}$)
2223.755	$00^0_1 1$	$00^0 0$	446	5023.
2209.523	$01^1 1$	$01^1 0$	446	568.
2195.840	$02^0 1$	$02^0 0$	446	16.8
2195.387	$02^2 1$	$02^2 0$	446	31.8
2195.914	$10^0 1$	$10^0 0$	446	10.1
2182.200	$03^1 1$	$03^1 0$	446	1.958
2181.386	$03^3 1$	$03^3 0$	446	1.88
2181.711	$11^1 1$	$11^1 0$	446	1.10
2193.623	$00^0 2$	$00^0 1$	446	0.201
2177.659	$00^0 1$	$00^0 0$	456	18.1
2164.13	$01^1 1$	$01^1 0$	456	2.04
2201.604	$00^0 1$	$00^0 0$	546	18.1
2187.389	$01^1 1$	$01^1 0$	546	2.10
2218.97	$00^0_1 1$	$00^0 0$	448	10.1
2204.70	$01^1 1$	$01^1 0$	448	1.15
2221.3	$00^0_1 1$	$00^0 0$	447	2.01
2207.25	$01^1 1$	$01^1 0$	447	0.234
2322.624	$04^0 0$	$00^0 0$	446	2.11
2309.109	$05^1 0$	$01^1 0$	446	0.54
2461.998	$12^0 0$	$00^0 0$	446	27.6
2457.446	$13^1 0$	$01^1 0$	446	4.68
2452.807	$14^0 0$	$02^0 0$	446	0.239
2453.851	$14^2 0$	$02^2 0$	446	0.321
2463.345	$22^0 0$	$10^0 0$	446	0.192
2563.341	$20^0 0$	$00^0 0$	446	120.
2577.090	$21^1 0$	$01^1 0$	446	12.2
2580.118	$22^0 0$	$02^0 0$	446	0.343
2588.310	$22^2 0$	$02^2 0$	446	0.648
2551.466	$30^0 0$	$10^0 0$	446	0.696
2554.21	$20^0 0$	$00^0 0$	546	0.454
2554.3	$20^0 0$	$00^0 0$	456	0.384
2491.3	$20^0 0$	$00^0 0$	448	0.192
2474.785	$12^2 0$	$00^0 0$	446	*
2798.290	$01^1 1$	$00^0 0$	446	8.06
2775.207	$02^0_2 1$	$01^1 0$	446	0.401
2784.370	$02^2 1$	$01^1 0$	446	0.912
2763.124	$03^1 1$	$02^0 0$	446	0.025
2753.508	$03^1 1$	$02^2 0$	446	0.020
2770.594	$03^3 1$	$02^2 0$	446	0.078
3383.974	$02^0_1 1$	$00^0 0$	446	8.82
3342.491	$03^1 1$	$01^1 0$	446	1.57

*No value given.

TABLE 12. N_2O BAND STRENGTHS. (From McClatchey, et al., 1973 [138].) (Concluded)

Band Center ν_c (cm^{-1})	Upper Level	Lower Level	Isotope	S_v at 296K (Multiply by 10^{-20} $Molecules^{-1}$ $cm^2 cm^{-1}$)
3480.821	$10^0 1$	$00^0 0$	446	173.
3473.212	$11^1 1$	$01^1 0$	446	19.24
3462.030	$12^0 1$	$02^0 0$	446	0.563
3464.713	$12^2 1$	$02^2 0$	446	1.064
3445.921	$20^0 1$	$10^0 0$	446	0.652
3443.659	$10^0 1$	$00^0 0$	546	0.627
3430.95	$10^0 1$	$00^0 0$	456	0.627
3439.1	$10^0 1$	$00^0 0$	448	0.348
3466.54	$06^0_2 0$	$00^0 0$	446	*
3474.65	$06^0 0$	$00^0 0$	446	*
3748.252	$22^0_1 0$	$00^0 0$	446	3.52
3747.031	$23^1 0$	$01^1 0$	446	0.512
3620.941	$14^0 0$	$00^0 0$	446	0.492
3836.373	$30^0 0$	$00^0 0$	446	7.28
3857.612	$31^1 0$	$01^1 0$	446	0.698
4061.979	$11^1 1$	$00^0 0$	446	0.092
4335.798	$23^1 0$	$00^0 0$	446	0.083
4417.379	$00^0 2$	$00^0 0$	446	6.07
4388.928	$01^1 2$	$01^1 0$	446	0.686
4630.164	$12^0 1$	$00^0 0$	446	0.597
4730.828	$20^0 1$	$00^0 0$	446	3.90
4730.408	$21^1 1$	$01^1 0$	446	0.410
4977.695	$01^1 2$	$00^0 0$	446	0.058
5026.34	$32^0 0$	$00^0 0$	446	0.255
5105.65	$40^0 0$	$00^0 0$	446	0.255

*No value given.

TABLE 13. ROTATIONAL CONSTANTS USED IN THE CALCULATION OF CO LINE POSITIONS. (From McClatchey, et al., 1973 [138].)

Symbol	Value
ω_e	2169.836
$\omega_e X_e$	13.295
$\omega_e Y_e$	0.0115
B_e	1.931285
α_e	0.017535
γ_e	1.01×10^{-5}
D_e	6.12×10^{-6}
β_e	-1.0×10^{-9}

TABLE 14. STRENGTHS OF CO BANDS. (From McClatchey, et al., 1973 [138].)

	1-0	2-0	3-0
Strength, S(cm^{-1}/molecule-cm^{-2})	9.70×10^{-18}	6.99×10^{-20}	4.83×10^{-22}

at approximately 80% is not considered in the compilation, although it is responsible for some continuum absorption. But its effect is minor, and ignored in most of the models described in this report.

One should consult a text like Herzberg [151] for a complete discussion of the O_2 molecule, but a thumbnail sketch of its more important features is given in the compilation report by McClatchey, et al. Without a complete description of terms used in the equations cited for the determination of line parameters, however, one must consult the original references (cited in the Bibliography) for a more thorough understanding of the use of the equations.

4.6.2.5 Water Vapor (H_2O)

One of the two most important molecules effective in atmospheric transmittance and radiative transfer is H_2O in the gaseous (vapor) form. McClatchey, et al. have drawn on a large number of sources for the accumulation of data on line parameters for H_2O. Table 15, taken from the compilation report, demonstrates this dependence on a large number of sources, by summarizing the origins of data on H_2O for all the spectral regions covered in the compilation. Because of the complicated nature of the non-linear H_2O molecule, much dependence has been placed on experimental data. Much of the confidence one feels in the compilation can be attributed to the self-consistency of the experimental data, along with the care taken by the AFCRL group in assembling and comparing them with the results of acceptable theory. It is recognized, nevertheless, that the accuracy of the compilation is strongly dependent on the plausibility of the theory and the accuracy of experimental data, upon which the theory depends for extending the limits of the compilation beyond many of the measurable limits. Table 16 reproduces the salient features of its source in the compilation report on vibration-rotation band data. The coefficients included in the original are excluded from this table since they have no meaning outside of context.

4.6.2.6 Ozone (O_3)

Whereas H_2O is one example of a triatomic, non-linear molecule effective in the absorption of atmospheric radiation, O_3 is the second example of one of the more important absorbers representative of this class of molecule. Table 17 reproduces the tabulations in the AFCRL report which is a collection of the band centers and intensities used in the compilation for O_3. The most important region for O_3 absorption comprises the 9.6 μm (designated ν_1 and ν_3 fundamentals) and the weaker 14 μm (designated ν_2) bands. The ν_1 and ν_3 bands are centered respectively at 1103 cm^{-1} and 1042 cm^{-1}.

151. G. Herzberg, Spectra of Diatomic Molecules, Van Nostrand, N. Y., 1950.

4.6.2.7 Methane (CH_4)

The next and most complex of the molecules included in the AFCRL line parameter compilation is CH_4. Many of the data are strictly empirical, unpredicted by theory at this time. So the information on some of the CH_4 data should be considered tentative. In Table 18 is a tabulation of the CH_4 bands with the pertinent data taken from the sources listed at the bottom of the table. As indicated above, the information in the compilation on CH_4 relied heavily on experimental data. The quantum number designations for the bands are as follows:

$$v_1 v_2 \ell_2 v_3 \ell_3 v_4 \ell_4 \ell$$

as described in the compilation report by McClatchey, et al. (1973). Included in the report are listings of spectroscopic parameters for the ground state of $^{12}CH_4$, the ν_3 band of $^{12}CH_4$, the ν_4 band of $^{12}CH_4$, the ν_2 band of $^{12}CH_4$, the ν_3 band of $^{13}CH_4$, the ν_4 band of $^{13}CH_4$, the $\nu_2 + \nu_4$ band of $^{12}CH_4$ and the $2\nu_4$ band of $^{12}CH_4$. It would serve no purpose to reproduce these tables here since there is not sufficient information which could be used to perform line parameter calculations.

In summary, it is evident that a very large amount of work has been put into assembling a collection of information which promises to be of unparalleled use to many investigators. Many of these data have existed for many years in one form or another. It is to be hoped that the plea by the authors of the report by McClatchey, et al (1973) will be heard, and that users will help determine the value of the compilation. Because of the complexity of the task, to say nothing of the complexity of the entities on which the task is performed, there are sure to be deficiencies in the compilation. So it is to the benefit of all that those who use the data help to alleviate the deficiencies and continuously improve the data.

A good deal of caution must be exerted in the use of the line parameter compilation because, even in its great usefulness, it is incomplete and, in some cases, in error. For work of moderate to good accuracy, it seems they can be used without trepidation. But for work which requires the extremes in accuracy, certain bands can be used with less confidence than others. The originators have found examples of misplaced lines which are being corrected in later tapes, but which naturally are retained in the earlier ones. In addition, certain "hot bands" are missing. The difficulty in experimentally determining the characteristics of ozone means that thorough scrutinizing of the O_3 parameters in the compilation may be required. Some investigators are now commencing programs from which more data on O_3 are expected to be derived. All in all, the compilation, now a useful tool, will become more useful as the inaccuracies are eliminated.

TABLE 15. SUMMARY OF PRINCIPAL DATA SOURCES FOR WATER VAPOR ENERGY LEVELS. (From McClatchey, et al., 1973 [138].)

Region cm^{-1}	Type of Measurement	Range of Levels			Strength Limit (296 K)	Precision of ν cm^{-1}	Ref.
		Vibrational	Rotational J	Rotational K_a			
0-25	L,181,171	0,010	10	6	<-27	.00001	152, 153
0-25	L,162,182	0,010	13	7	<-27	.00001	154, 155
30-250	L	0	13	7	-23	.005	156
250-550	L	0	15	11	-24	.03	157
480-690	LH	0	15	12	-25	.02	158
430-650	F	0,010 etc.	30	15	<-27	.05	159
700-1100	LH	0,010	19	12	-26	.1	160
750-1400	A	0,010	18	12	-25	.05	161
860-1160	A	0,010	18	12	-25	.02	162
1270-1450	LH	010,020	16	9	-27	.05	163
1200-1700	L,162	010	14	7	-27	.02	164
1330-1970	L,181,171	010	13	6	-26	.01	165
1840-2500	LH	010,020,001+	18	10	-26	.03	166
1925-2182	A,U	010,020,001+	28	10	<-27	.01	167
2390-2970	A,U	100,001, etc.	32	10	<-27	.01	167
2490-3030	L,162	100,020	18	10	<-27	.005	168
2900-3500	A	020,100,001	16	11	-26	.02	169
2800-3500	F	001,011, etc.	33	13	<-27	.02	170
2900-3330	L,162	001,100, etc.	14	9	-25	.005	171
3340-4030	L,181,171	001,100, etc.	13	7	-26	.01	172
3940-4300	F	001,011, etc.	33	19	<-27	.02	170
4032-5090	A,U	001,011,020 +	33	17	<-27	.01	173
3950-5200	A	001,030,011,etc	18	13	-26	.01	174
4500-5915	L,162	011,030,110,etc	14	8	-25	.005	171
5090-5575	L	011,110	12	7	-24	.005	175
5540-7000	A	011,021,120 +	16	9	-26	.01	174
5550-6720	A,U	011,021,120 +	24	11	<-27	.01	173
7000-7500	L	101,200	13	8	-24	.05	176
7400-9000	A	101,002,111 +	16	9	-26	.01	174
7390-8800	A,U	101,001,111 +	16	9	-25	.01	173
8300-10000	A	111,012,041	16	8	-25	.03	177
9150-9350	A	012,111	10	7	-27	.005	178

The data sources are of five types: L, laboratory absorption measurements on water vapor or moist air at room temperature; LH, similar measurements in cells heated to 75-540°C; F, laboratory measurements of emission from oxy-hydrogen or oxy-acetylene flames, yielding ~10^{19} molecules/cm^2 H_2O at +2500-3500K; A, measurements of solar radiation through the atmosphere, containing 10^{22}-10^{23} molecules/cm^2; U, observations of the ratioed spectrum of sunspot/photosphere, also containing about 10^{19} mol/cm^2 at ~3600K. Isotopic symbols are appended when enriched samples were studied, underlined when a major component, dashed when moderately increased above natural abundance. The range of vibrational and rotational levels is a rough indication of the extent of levels observable down to the intensity limit of S^o (cm^{-1}/mol cm^{-2}), corrected to 296K, with the resolving power used. The ground state, (v=0) is implied in all regions.

In reference 171, the observed contamination of the sample by deuterium to give the HDO abundances varying from 10-200 times normal was not reported.

References to Table 15

152. F. C. De Lucia, P. Helminger, R. L. Cook and W. Gordy, Phys. Rev. A 3, Vol. 5, 1972, p. 487.

153. G. Steenbeckeliers and J. Bellet, Comptes Rendus Acad. Sci., B273:288, Paris, 1971.

154. F. C. De Lucia, P. Helminger, R. L. Cook and W. Cordy, J. Chem. Phys., Vol. 55, 1971, p. 5334.

155. W. S. Benedict, S. A. Clough, W. J. Lafferty, L. Frenkel, T. E. Sullivan, J. Bellet and G. Steenbeckeliers, (1973), to be published.

156. R. T Hall and J. M. Dowling, J. Chem. Phys., Vol. 47, 1967, p. 2454.

157. K. N. Rao, W. W. Brim, J. L. Sinnett and R. M. Wilson, J. Opt. Soc. Am., Vol. 52, 1962.

158. J. R. Izatt, H. Sakai and W. S. Benedict, J. Opt. Soc. Am., Vol. 59, 1969, p. 19.

159. R. P. Madden and W. S. Benedict, J. Chem. Phys., Vol. 25, 1956, p. 294 and unpublished data, 1956.

160. D. E. Burch and D. Gryvnak, Unpublished data, (1971).

161. J. Dionne, Atmospheric Spectra from 9.1 to 11.6μ, Thesis, Université de Paris, 1972.

162. M. Migeotte, L. Neven and J. Swensson, The Solar Spectrum from 2.8 to 23.7 Microns, Measures and Identifications, Mem. Soc. Roy. Sci. Liege, Special Volume 2, 1957.

163. Y. Ben-Aryeh, J. Quant. Spec. Rad. Trans., Vol. 7, 1970, p. 211.

164. J. G. Williamson, K. N. Rao and L. H. Jones, J. Mol. Spect., Vol. 40, 1971.

165. N. M. Gallar and F. P. Dickey, J. Mole. Spect., Vol. 4, 1960, p. 1.

166. D. E. Burch and D. Gryvnak, Unpublished data, (1973).

167. D. N. B. Hall, Unpublished data, 1972.

168. W. S. Benedict, H. Chang, S. A. Clough and W. J. Lafferty, (1973), to be published.

169. R. Beer, Private communication (1970) to McClatchey, et al., 1973.

170. W. S. Benedict and R. Sams, Twenty-Sixth Symposium on Molecular Spectroscopy, Ohio State University, Columbus, 1971.

171. L. A. Pugh, A Detailed Study of the Near Infrared Spectrum of Water Vapor, Thesis, Ohio State University, Columbus, 1972.

172. P. E. Fraley, K. N. Rao and L. H. Jones, J. Mol. Spect., Vol. 29, 1969, pp. 312, 348.

173. D. N. B. Hall, Observations of the Infrared Sunspot Spectrum Between 11340 A and 24778 A, Thesis, Harvard University, Cambridge, 1970.

174. J. Connes, P. Connes and J. P. Maillard, Near Infrared Spectra of Venus, Mars, Jupiter and Saturn and Atlas of Near Infrared Spectra of Venus, Mars, Jupiter and Saturn, Centre National de la Recherche Scientifique, Paris, 1969.

175. J. M. Flaud, C. Camy-Peyret and A. Valentin, J. Phys., 8-9: 741, 1972.

176. R. C. Nelson, Atlas and Wavelength Tables, Summary Report IV, Northwestern University, Evanston, Ill., 1949.

177. J. Swensson, W. S. Benedict, L. Delbouille and G. Roland, The Solar Spectrum from λ 7498 to λ 12016. A Table of Measures and Identifications, Mem. Soc. Roy. Sci. Liege, Special Volume 5, 1970.

178. J. R. Breckenridge and D. N. B. Hall, Solar Physics, to be published, (1973).

TABLE 16. WATER VAPOR STRENGTH DATA. (From McClatchey, et al., 1973 [138].)

ν_0 cm^{-1}	Iso	v' v"	Rot Type	S_ν^0(296K) $cm^{-1}/mol\,cm^{-2}$	R Debyes
1403.489	162	010 000	A	8.0 -022	.066
			B	1.92 -021	.105
1556.895	161	020 010	B	8.61 -021	.171
1588.279	181	010 000	B	2.12 -020	.121
1591.32	171	010 000	B	3.93 -021	.121
1594.736	161	010 000	B	1.061-017	.121
2062.318	161	100 010	B	8.9 -023	.0167
2161.188	161	001 010	A	4.9 -022	.0394
2709.35	162	100 000	A	1.31 -024	.0437
2723.687	162	100 000	A	6.53 -027	.0437
			B	2.0 -023	.0076
2787.014	162	020 000	A	8.1 -023	.0153
			B	9.0 -024	.0051
3072.058	161	030 010	B	7.99 -029	.0121
3139.02	181	020 000	B	1.32 -022	.0070
3144.96	171	020 000	B	4.92 -023	.0070
3151.631	161	020 000	B	6.58 -019	.0070
3640.245	161	110 010	B	1.50 -022	.0149
3649.690	181	100 000	B	7.24 -022	0149
3653.14	171	100 000	B	1.33 -022	.0149
3657.054	161	100 00	B	3.62 -019	.0149
3707.459	162	001 000	A	1.2 -021	.0509
			B	3.0 -022	.0255
3736.509	161	011 010	A	3.30 -021	.0708
3741.571	181	001 000	A	1.60 -020	.0708
3748.36	171	001 000	A	2.96 -021	.0708
3755.924	161	001 000	A	7.894-018	.0708
4099.954	162	110 000	A	2.0 -023	.0069
			B	1.5 -024	.0024
4145.483	162	030 000	A	2.0 -023	0
			B	1.5 -024	
4666.720	161	030 000	B	2.0 -022	.00032
5089.539	162	011 000	A	3.0 -023	.0069
			B	6.0 -024	.0031
5180.36	161	120 010	B	1.17 -023	.0040
5221.28	161	110 000	B	3.66 -023	.0028
5227.75	171	110 000	B	6.77 -024	.0028
5234.981	161	110 000	B	1.83 -020	.0028
5276.776	161	021 010	A	7.45 -022	.0286
5310.43	181	011 000	A	1.81 -021	.0203
5320.25	171	011 000	A	3.36 -022	.0203
5321.245	161	011 000	A	9.06 -019	.0203
5372.114	162	200 000	A	1.2 -023	.0042
6679.2?	161	130 010	B	4.32 -024	.00194
6755.40	181	120 000	B	7.05 -024	.00112
6773.10	161	120 000	B	3.53 -021	.00112
6779.08	161	031 010	A	6.94 -023	.0076
6844.59	181	021 000	A	1.13 -022	.0044
6857.32	171	021 000	A	2.09 -023	.0044
6871.512	161	021 000	A	5.64 -020	.0044
7186.68	181	200 000	B	1.06 -022	.0042
7201.48	161	200 000	B	5.29 -020	.0042
7213.26	161	111 010	A	3.98 -022	.0157
7222.68	181	101 000	A	1.49 -021	.0157
7235.57	171	101 000	A	2.76 -022	.0157
7249.93	161	101 000	A	7.47 -019	.0157
7371.79	161	012 010	B	2.17 -024	.00134
7417.54	181	002 000	B	1.06 -023	.00131
7430.54	171	002 000	B	1.96 -024	.00131
7745.04	161	002 000	B	5.29 -021	.00131
8238.84	161	041 010	A	5.88 -024	.00204
8273.95	161	130 000	B	2.1 -022	.00027
8341.32	181	031 000	A	7.1 -024	.00102
8356.70	171	031 000	A	1.33 -024	.00102
8373.82	161	031 000	A	3.6 -02?	.00102
8734.97	161	121 010	A	4.10 -02.	.0037
8761.57	161	210 000	B	3.6 -022	.00031
8779.75	181	111 000	A	9.96 -023	.0037
8792.63	171	111 000	A	1.85 -023	.0037
8807.00	161	111 000	A	4.98 -020	.0037
8966.53	181	012 000	B	2.4 -024	.00057
8980.13	161	012 000	B	1.2 -021	.00057
9833.59	161	003 000	A	4.8 -023	.00011

TABLE 17. OZONE TRANSITIONS INCLUDED IN DATA COMPILATION.
(From McClatchey, et al., 1973 [138].)

Band Center cm^{-1}	$\Sigma_i S_i$ $\frac{cm^{-1}}{mol/cm^2}$	Vibrational Transition		Isotope
		Upper State	Lower State	
0.	4.13×10^{-19}	000	000	666
700.930	6.70×10^{-19}	010	000	666
1007.692	9.49×10^{-21}	101	100	666
1037.996	2.49×10^{-20}	001	000	686
1021.096	4.23×10^{-19}	011	010	666
1027.096	1.62×10^{-19}	002	001	666
1028.096	5.16×10^{-20}	001	000	668
1042.096	1.29×10^{-17}	001	000	666
1103.157	3.47×10^{-19}	100	000	666
2110.790	1.33×10^{-18}	101	000	666
2785.241	2.32×10^{-20}	111	000	666
3041.200	1.10×10^{-19}	003	000	666

TABLE 18. METHANE BANDS INCLUDED IN DATA COMPILATION. (From McClatchey, et al., 1973 [138].)

Isotope	Band	Center (cm^{-1})	Upper State	Lower State	Strength (cm^{-1}/mole-cm^{-2})
311	ν_4	1297.88[179]	00000111	00000000	6.59×10^{-20}*
211	ν_4	1305.9138[180]	00000111	00000000	5.87×10^{-18}[186]
211	ν_2	1533.289[181]	01100001	00000000	8.91×10^{-20}[186]
311	ν_3	3009.53[182]	00011001	00000000	1.36×10^{-19}*
211	ν_3	3018.9205[183]	00011001	00000000	1.21×10^{-17}[186]
211	$2\nu_4$	2600[184]	00000222	00000000	1×10^{-19}**
211	$\nu_2 + \nu_4$	2818, 2838[185]	01100112	00000000	8×10^{-19}***

179. T. G. Kyle, R. D. Blatherwick and F. S. Bonomo, J. Chem. Phys., Vol. 53, 1970, p. 2800.

180. F. Michelot and K. Fox, (1973), to be published.

181. M. Dang-Nhu, Thesis, Université de Paris, 1968.

182. R. S. McDowell, J. Mol. Spec., Vol. 21, 1966, p. 280.

183. B. Bobin and K. Fox, J. Chem. Phys. and J. Phys. (Paris), 1973.

184. K. Fox, Bull. Am. Phys. Soc., Vol. 18, 1973, p. 232.

185. W. S. Benedict, Private communication (1973) to McClatchey, et al., 1973.

186. R. L. Armstrong and H. L. Walsh, Spectrochim Acta, Vol. 16, 1960, p. 840.

*1/89 times value for corresponding band of 211 isotope

**1/100 times value for ν_3 of 211 isotope

***1/15 times value for ν_3 of 211 isotope

4.6.3 OTHER ABSORPTION GASES AND ABSORPTION MECHANISMS

There are several places in the spectrum which are designated continuum regions, but the most important from the standpoint of thermal radiation is between 8 and 14 μm. Some of the attenuation effect in this region is from the presence of aerosols, in the form of scattering. But except under rather hazy conditions, the effect of scattering is secondary, the major effect being apparently from the presence of very weak lines of water vapor, or, more significantly, from the wings of H_2O and the relatively less important CO_2 lines whose centers are distant from the region. Some effects from the agglomeration of H_2O into dimers has been postulated.

Because the uncertainty in the line structure used in the calculation of atmospheric transmittance, either directly or in band models, is greater in the wings than it is near the center, it is evident that calculations will introduce relative errors in this low-absorptance region which could well be unacceptable. Therefore, the continuum region is usually considered empirically using some of the original work on the subject performed by Bignell, et al. [187], and later results from Burch, et al. [188]. Bignell [189] found that in addition to foreign broadening effects, the continuum absorption is strongly dependent on the partial pressure of water vapor. Most models for atmospheric transmittance allow for this effect by applying parameters established from experimental data.

In addition to the major gases to which great care is given in all of the models, there exist the so-called minor gases which are strong absorbers, but which, because of their concentrations or locations in the atmosphere or in the spectrum, play less of a role in the general calculation of atmospheric transmittance. Most models account for these gases, and indeed they should be considered very carefully in the cases for which the high spectral purity, say, of laser radiation is involved; or for very long paths at low pressure. Chief among these gases are CO, N_2O, CH_4, which are included in the compilation; and HNO_3 and SO_2, which constitute part of what is commonly known as pollutants.

---

187. K. Bignell, F. Saiedy and P. A. Sheppard, "On the Atmospheric Infrared Continuum," J. Opt. Soc. Am., Vol. 53, No. 4, 1963, pp. 466-479.

188. D. E. Burch, D. A. Gryvnak and J. D. Pembrook, Investigation of the Absorption of Infrared Radiation by Atmospheric Gases, Report No. U-4829, Philco-Ford Corporation, 1970.

189. D. E. Burch, Investigation of the Absorption of Infrared Radiation by Atmospheric Gases, Air Force Cambridge Research Labs., Philco Report No. U-4784, Philco-Ford Corporation, 1970.

5

GENERALIZATION OF METHODS OF CALCULATING ATMOSPHERIC ABSORPTION

There is no known way of exactly solving Eq. (147) for a real atmosphere because of the complex frequency variability of $k(\nu)$. Even with our current understanding of the nature of line parameters, just a casual glance at Figure 27, a graphical representation of part of the transmission spectrum, assures us that numerical techniques are required for the calculation of "infinitely" resolved spectra.

5.1 LINE-BY-LINE METHOD OF ATMOSPHERIC TRANSMITTANCE CALCULATIONS

One method used in determining spectral transmittance of moderate resolution is to perform what we call a "line-by-line" calculation. What this means is that, from the contributions of all pertinent lines, we sum the values of the absorption coefficients, $k(\nu)$ in Eq. (154) for example, at as many discrete values of ν as will faithfully reproduce the spectrum. The result within the integral over ν is a set of discrete transmittance values which, when plotted, resemble Figure 27. A numerical integration over frequency within the proper interval $\Delta\nu$ results in the final spectrum of moderate resolution. Conceptually this calculation yields, to within any desired accuracy, the exact representation of the value which would be obtained by an instrument whose resolution was $\Delta\nu$ and whose spectral response over that interval was constant.

Unfortunately, many things are implied by this last statement. Instruments do not usually have constant spectral responses so this factor must be taken into account, which, again conceptually, is not difficult to do, but which incorporates a factor of complexity into the calculation. Other implications are that the line parameters, and the atmospheric parameters governing the proper choice of the absorber amount, are well known. Even when they are known, they can only be incorporated approximately. Uncertainties brought about by these factors, however, are inherent in any calculative method, including, and indeed especially, in the band models to be discussed in the succeeding section.

The only way, therefore, to assure the highest accuracy in calculating atmospheric transmittance is to use the line-by-line method with a set of accurate line parameters with appropriate meteorological data. Unfortunately this method, is time consuming and expensive to run on a computer. Furthermore, there are still gaps of uncertainty in the only "complete" compilation currently in existence, i.e., the AFCRL compilation (McClatchey, et al., 1973).

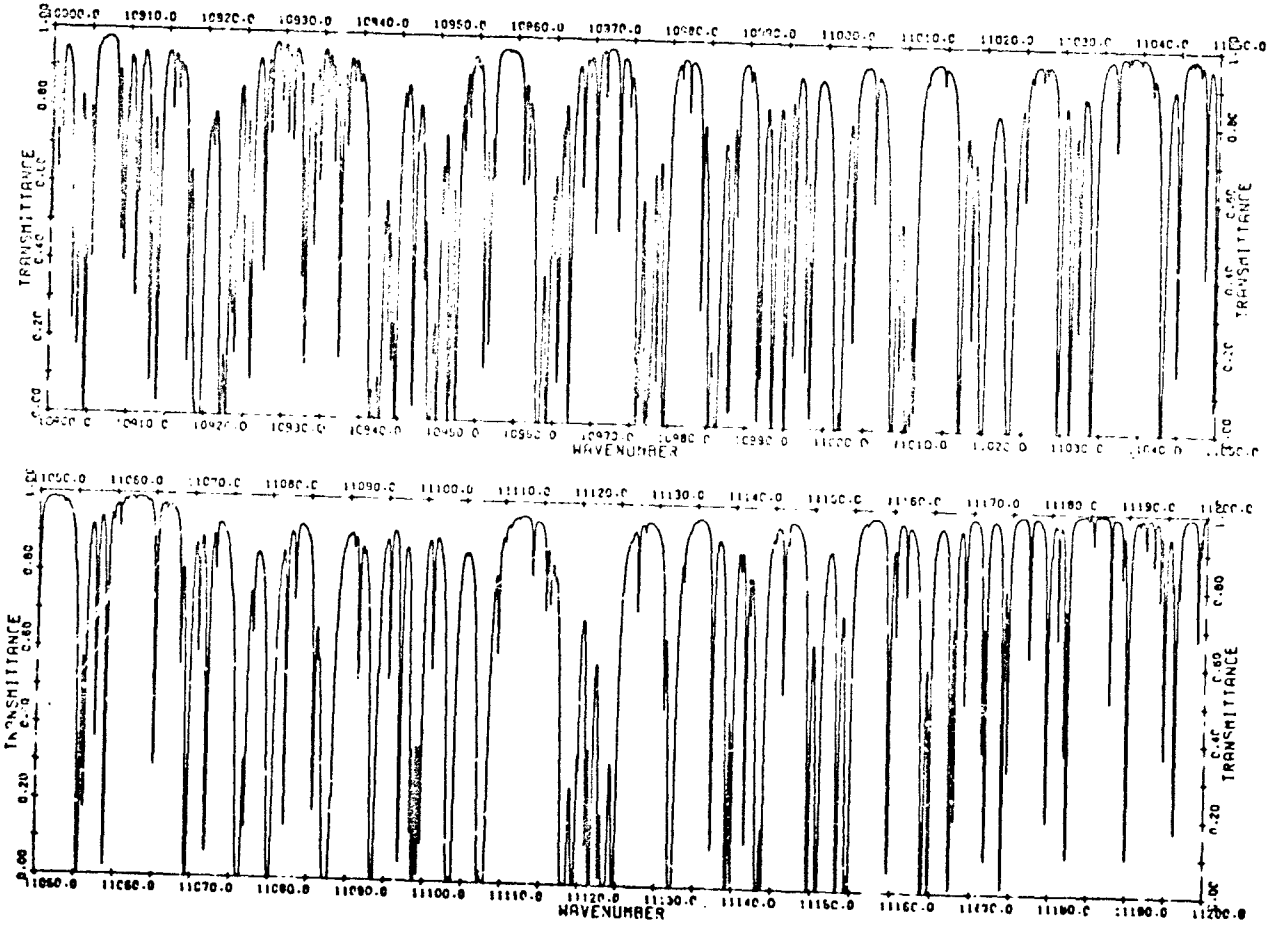

FIGURE 27. "INFINITELY" RESOLVED TRANSMITTANCE AS A FUNCTION OF FREQUENCY
(Reproduced from McClatchey and Selby, 1974 [190].)

190. R. A. McClatchey and J. E. A. Selby, Atmospheric Attenuation of Laser Radiation from 0.76 to 31.25 μm, Report No. TR-74-0003, Air Force Cambridge Research Laboratories, Bedford, Mass., January 1974.

FORMERLY WILLOW RUN LABORATORIES, THE UNIVERSITY OF MICHIGAN

5.2 BAND-MODEL METHODS OF ATMOSPHERIC TRANSMITTANCE CALCULATIONS

5.2.1 INTRODUCTION TO THE BAND-MODEL CONCEPT

Many applications do not require a highly accurate determination of the absorption spectra, but only a first-order approximation to the true spectra, and in many cases the spectra may have relatively low resolution. Therefore, almost all of the available methods for computing atmospheric absorption use approximations which reduce Eq. (154) to a form which expresses the transmission, averaged over some interval, in terms of elementary functions. The simplified equation is then used with laboratory homogeneous-path data to derive appropriate parameters and predict absorption for other homogeneous paths.

The classical approach used in performing the simplification of Eq. (154) is that of using a model of the band structure. That is, it is assumed that the line positions and strengths are distributed in a way that can be represented by a simple mathematical model. The most commonly used band models are listed here.*

(1) The Elsasser or regular model [191] assumes spectral lines of equal strength, equal spacing, and identical half-widths. The transmission function is averaged over an interval equal to the spacing between the line centers.

(2) The statistical or random model, originally developed for water vapor assumes that the positions and strengths of the lines are given by a probability function. The statistical model was suggested by Telles and worked out by Mayer [192] and (independently) Goody [193].

(3) The random-Elsasser model [194] is a generalization of the Elsasser model and the statistical model. It assumes a random superposition of any number of Elsasser bands of different strengths, spacings, and half-widths. Therefore, as the number of bands ranges from one to infinity, the band model extends, respectively, from the Elsasser model to the purely statistical model. This generalization, therefore, yields an infinite set of absorption curves between those of the Elsasser and statistical models.

*Other band models have been developed and are discussed in detail by R. M. Goody (1964).

191. W. M. Elsasser, Phys. Rev., Vol. 54, 1938, p. 126.

192. H. Mayer, Methods of Opacity Calculations, V. Effect of Lines on Opacity, Methods for Treating Line Contribution, Report No. AECD-1870, Los Alamos Scientific Laboratory, Los Alamos, Calif., 1947.

193. R. M. Goody, "A Statistical Model for Water-Vapour Absorption," Royal Meteor. Soc., Vol. 78, 1952, pp. 165-169.

194. G. N. Plass, "Models for Spectral Band Absorption," J. Opt. Soc. Am., Vol. 48, 1958, p. 690.

(4) The best available model is the quasi-random model [195]. It is capable of fairly accurate representation of the band, provided the averaging interval is made sufficiently small. However, of all the models, it requires the greatest amount of computation.

5.2.2 A SINGLE LORENTZ LINE

Let us consider the absorption caused by a single spectral line of a homogeneous path of a single absorbing gas. Let us assume that the shape of this line is represented by the Lorentz equation. For these conditions the absorption is given by

$$A\Delta\nu = \int_{\Delta\nu} \left\{ 1 - \exp \left[-\frac{1}{\pi} \int_0^x \frac{S\alpha_L \rho}{(\nu - \nu_0)^2 + \alpha_L^2} dx' \right] \right\} d\nu \tag{161}$$

For a homogeneous path S, α and ρ are constant; Equation (161) further reduces to

$$A\Delta\nu = \int_{\Delta\nu} \left\{ 1 - \exp - \left[\frac{S}{\pi} \frac{\alpha_L w}{(\nu - \nu_0)^2 + \alpha_L^2} \right] \right\} d\nu \tag{162}$$

where $w = \int_0^x \rho dx' = \rho x$ and is defined as the absorber amount.

A plot of absorption versus frequency is shown in Figure 28 for different path lengths, or for different values of w. The absorption caused by this line for an optical path of length x_1 would be considered a weak line since the absorption is small even at the line center. For a path of length x_3, the center of the line is completely absorbed and any further increase in path length would only change the absorption in the wings of the line. Absorption by paths of length equal to or greater than x_3 would, therefore, be considered strong-line absorption.

In Eq. (162), if it is assumed that the interval $\Delta\nu$ is such that the entire line is included, then the limits of integration can be taken from $-\infty$ to ∞ without introducing a significant error. When these limits are used, Eq. (162) can be solved exactly for the total absorption. Ladenburg and Reiche (1913) have solved the integral to obtain

$$A\Delta\nu = 2\pi\alpha_L \psi e^{-\psi} [I_0(\psi) + I_1(\psi)] \tag{163}$$

where $\psi = Sw/2\pi\alpha_L$ and I_0 and I_1 are Bessel functions of imaginary argument. Examining Eq. (163) under conditions of weak-line and strong-line absorption, we have for weak-line absorption $\psi << 1$; Eq. (163) reduces to

195. P. J. Wyatt, V. R. Stull and G. N. Plass, "Quasi-Random Model of Band Absorption," J. Opt. Soc. Am., Vol. 52, No. 11, 1932(b), p. 1209.

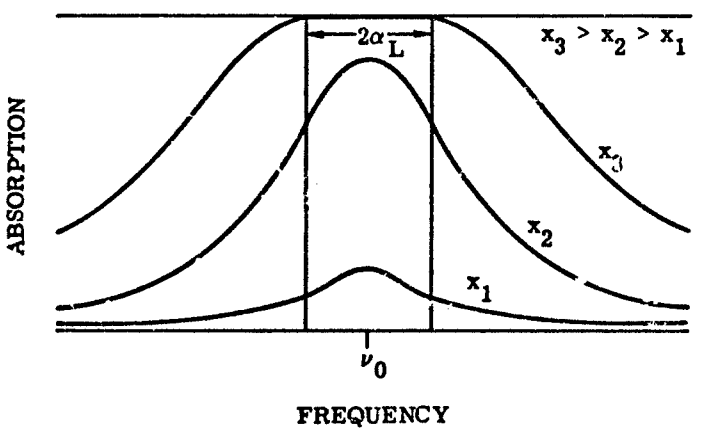

FIGURE 28. ABSORPTION VS FREQUENCY FOR A SINGLE LINE

$$A\Delta\nu = 2\pi\alpha_L\psi = Sw \tag{164}$$

and absorption is linear with the optical path length w. Under conditions of strong-line absorption ψ is large and Eq. (163) reduces to

$$A\Delta\nu = 2\sqrt{S\alpha_L w} \tag{165}$$

which is known as the square-root approximation. The above derivations are for a single spectral line but are also valid for absorption when many spectral lines are present but do not overlap. Therefore, for the nonoverlapping approximation the absorption is simply given by Eq. (163), (164) or (165), depending upon the value of ψ.

5.2.3 ELSASSER MODEL

The Elsasser model of an absorption band is formed by allowing a single Lorentz line to repeat itself periodically throughout the interval $\Delta\nu$. This gives rise to a series of lines that are equally spaced and that have a constant strength and half-width throughout the interval. This arrangement of spectral lines was first proposed by Elsasser (1938) and his derivation is presented here. The absorption coefficient for a periodic band is given by (for n integer):

$$k(\nu) = \sum_{n=-\infty}^{\infty} \frac{S}{\pi} \frac{\alpha_L}{(\nu - nd)^2 + \alpha_L^2} \tag{166}$$

It is possible to express Eq. (166) in terms of an analytical function owing to the fact that if such a function has only single poles, it is uniquely defined by these poles. Therefore, Eq. (166) is equivalent to

$$k(\nu) = \frac{S}{d} \frac{\sinh \beta}{\cosh \beta - \cos s} \tag{167}$$

where $\beta = 2\pi\alpha_L/d$

$s = 2\pi\nu/d$

If the averaging interval $\Delta\nu$ is taken as one period of the band ($\Delta\nu = 2\pi$), then the average absorption becomes:

$$A = \frac{1}{2\pi}\int_{-\pi}^{\pi} \{1 - \exp[-wk(\beta, s)]\}\, ds \tag{168}$$

This integral has been evaluated by Elsasser to give the general expression for absorption by an Elsasser band, namely

$$A = \sinh\beta \int_0^Y I_0(Y) \exp(-Y\cosh\beta)\, dY \tag{169}$$

where $\beta = 2\pi\alpha_L/d$

$Y = \beta\psi/\sinh\beta$

$\psi = Sw/2\pi\alpha_L$

d = mean spacing between spectral lines

I is a Bessel function of imaginary argument.

A plot of this function for various values of β is given in Figure 29. Because the function in its present form is difficult to evaluate, considerable effort has been expended comparing approximate formulae and evaluating the integral. Kaplan [196] has expanded the integral into a series which is convergent only for values of β less than 1.76. An algorithm for the Elsasser integral which is convergent for all values of β and ψ is written in a computer program used in the calculation of spectral transmittance with the Aggregate Method (see Section 7.4). However, it is frequently desirable to work with approximations to the function which are valid for certain conditions.

5.2.3.1 Weak-Line Approximation

In Figure 30, the absorption given by Eq. (169) is plotted as a function of the product $\beta\psi = Sw/d$ for four values of β. It is noted for $\beta \geq 1$ that the absorption curves become superimposed for all values of ψ. Since the parameter β measures the ratio of line width to the distance between neighboring lines, $\beta \geq 1$ implies that the spectral lines are strongly overlapping and spectral line structure is not observable. This condition corresponds to large pressures which would be realistic for atmospheric paths at low altitudes. For $\beta \geq 1$, Eq. (169) can be approximated by

$$A = 1 - e^{-\beta\psi} \tag{170}$$

Further, Eq. (170) is a good approximation to Eq. (169) whenever the absorption is small at the line centers (small ψ) regardless of the value of β. Therefore, this approximation is referred to as the weak-line approximation, and is independent of the position of the spectral lines within the band. Table 19 summarizes the regions of β and ψ for which the weak-line approximation is valid with an error of less than 10%. This approximation is particularly useful in extrapolating the absorption to small values of ψ and to large values of pressure. Note that the weak-line approximation reduces to the linear approximation when the absorption is small even if the lines overlap.

196. L. D. Kaplan, "Regions of Validity of Various Absorption-Coefficient Approximations," J. Meteorol., Vol. 10, 1953(a).

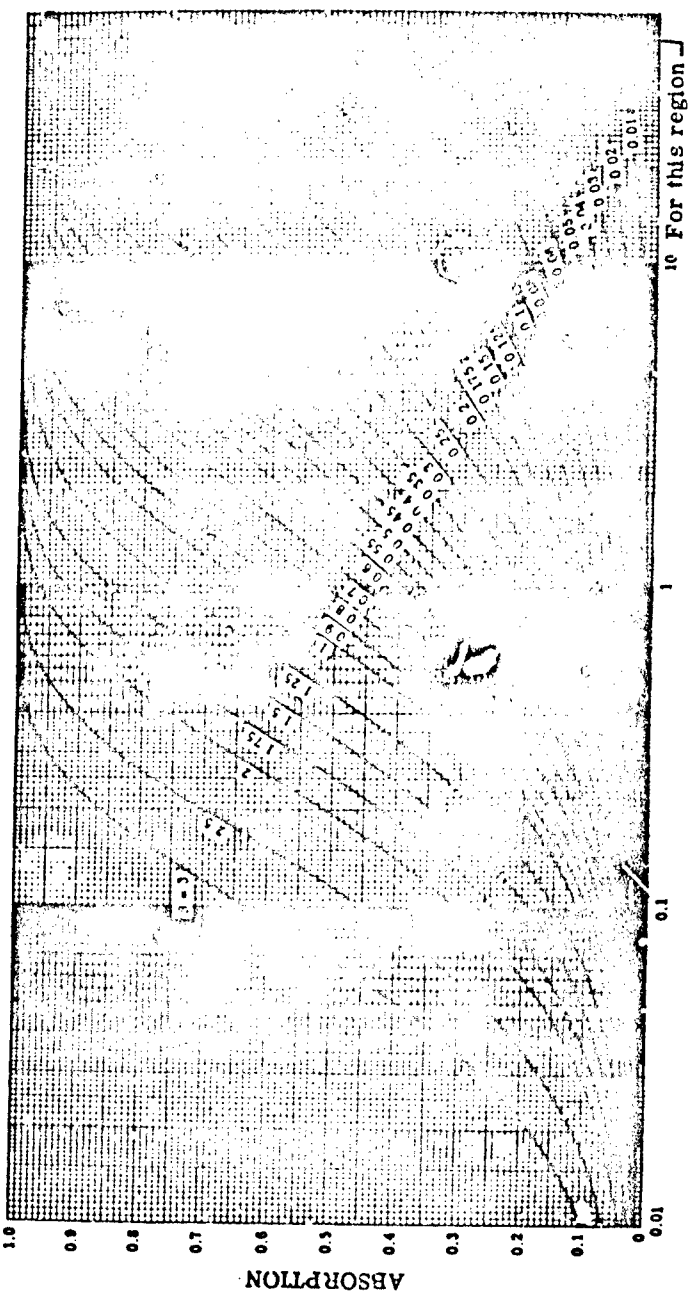

FIGURE 29. ABSORPTION BY A SINGLE ELSASSER BAND. For $\beta > 3$, $A \cong 1 - \exp\left(-\frac{S}{d}\frac{w}{}\right)$.

TABLE 19. REGIONS OF VALIDITY OF VARIOUS APPROXIMATIONS FOR BAND ABSORPTION*

Approximation	$\beta = 2\pi\alpha_L/d$	Elsasser Model	Statistical Model; All Lines Equally Intense	Statistical Model; Exponential Line Intensity Distribution
Strong-line approximation:	0.001	$\psi > 1.63$	$\psi > 1.63$	$\psi_0 > 2.4$
	0.01	$\psi > 1.63$	$\psi > 1.63$	$\psi_0 > 2.4$
	0.1	$\psi > 1.63$	$\psi > 1.63$	$\psi_0 > 2.3$
	1	$\psi > 1.35$	$\psi > 1.1$	$\psi_0 > 1.4$
	10	$\psi > 0.24$	$\psi > 0.24$	$\psi_0 > 0.27$
	100	$\psi > 0.024$	$\psi > 0.024$	$\psi_0 > 0.24$
Weak-line approximation:	0.001	$\psi < 0.20$	$\psi < 0.20$	$\psi_0 < 0.10$
	0.01	$\psi < 0.20$	$\psi < 0.20$	$\psi_0 < 0.10$
	0.1	$\psi < 0.20$	$\psi < 0.20$	$\psi_0 < 0.10$
	1	$\psi < \infty$	$\psi < 0.23$	$\psi_0 < 0.11$
	10	$\psi < \infty$	$\psi < \infty$	$\psi_0 < \infty$
	100	$\psi < \infty$	$\psi < \infty$	$\psi_0 < \infty$
Nonoverlapping-line approximation:	0.001	$\psi < 600{,}000$	$\psi < 63{,}000$	$\psi_0 < 80{,}000$
	0.01	$\psi < 6000$	$\psi < 630$	$\psi_0 < 800$
	0.1	$\psi < 60$	$\psi < 6.3$	$\psi_0 < 8$
	1	$\psi < 0.7$	$\psi < 0.22$	$\psi_0 < 0.23$
	10	$\psi < 0.02$	$\psi < 0.020$	$\psi_0 < 0.020$
	100	$\psi < 0.002$	$\psi < 0.0020$	$\psi_0 < 0.0020$

*When $\psi = Sw/2\pi\alpha_L$ satisfies the given inequalities, the indicated approximation for the absorption is valid with an error of less than 10%. For the exponential line intensity distribution, $\psi_0 = S_0 w/2\pi\alpha_L$, where $P(S) = S_0^{-1} \exp(-S/S_0)$.

5.2.3.2 Strong-Line Approximations

Of increasing interest are the long atmospheric paths at high altitudes which give rise to large values of w and small values of pressure. Under these conditions the absorption at the line centers is usually complete (large ψ), the half-widths are narrow, and the lines do not overlap strongly (small β). For large ψ and small β, Eq. (169) may be approximated by

$$A = \operatorname{erf}\left(\frac{1}{2}\beta^2\psi\right)^{1/2} \tag{171}$$

where

$$\operatorname{erf}(t) = \frac{2}{\sqrt{\pi}}\int_0^t e^{-t^2}\,dt$$

which is known as the strong-line approximation to the Elsasser band model. Figure 31 is a plot of Eq. (169) with absorption as a function of $\beta^2\psi$. For $\beta \leq 0.01$, Eqs. (169 and 171) are superimposed for $\beta^2\psi > 0.0003$. Clearly, given small β and large ψ, Eq. (171) is a particularly good approximation for representing the absorption when $\beta \leq 1$. If $\beta \leq 1$, then Eq. (171) is valid whenever $0.1 \leq A \leq 1$. This includes most values of absorption that are usually of interest. This case differs from the square-root approximation in that it is not necessary that the lines do not overlap. For overlapping spectral lines (larger β), the values of ψ for which the approximation is valid are simply restricted to large values of ψ. The specific regions of validity are given in Table 19.

5.2.3.3 Nonoverlapping Approximation

The third approximation to the Elsasser band model is known as the nonoverlapping approximation. The regions of validity for the strong-line and weak-line approximations depend only upon the value of absorption at the frequency of the line centers and do not depend upon the degree of overlapping of the spectral lines. On the other hand, the only requirement for the validity of the nonoverlapping-line approximation is that the spectral lines do not overlap appreciably. It is valid regardless of the value of the absorption at the line centers. This approximation is particularly useful for extrapolating the absorption to small values of w and small values of pressure which correspond to short paths at high altitudes. Under these conditions Eq. (169) reduces to

$$A = \beta\psi\, e^{-\psi}[I_0(\psi) + I_1(\psi)] \tag{172}$$

which is exactly the same expression as that obtained for the absorption by a single spectral line. This is an expected result, for if the lines do not overlap there will be only one line that contributes to the absorption at a given frequency.

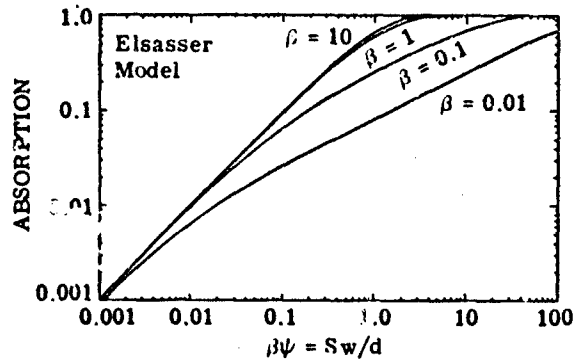

FIGURE 30. ABSORPTION AS A FUNCTION OF $\beta\psi$ = Sw/d FOR THE ELSASSER MODEL. The weak-line approximation is the uppermost curve.

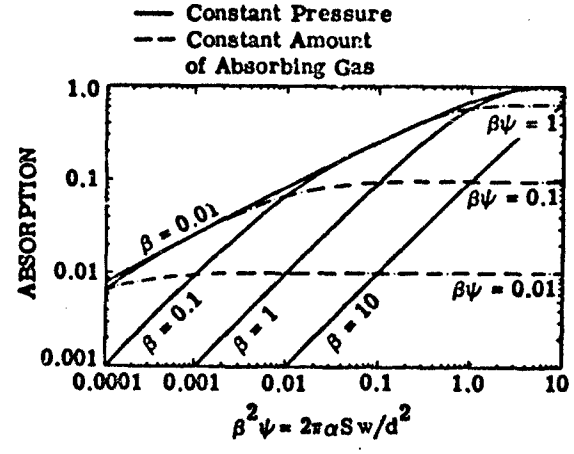

FIGURE 31. ABSORPTION AS A FUNCTION OF $\beta^2\psi = 2\pi\alpha\eta$, Sw/$d^2$ FOR THE ELSASSER MODEL. Curves are shown for constant pressure (β = constant) and for constant amount of the absorbing gas ($\beta\psi$ = constant). The strong-line approximation is the uppermost curve.

In Figure 32, A/β is given as a function of ψ. The uppermost curve is the nonoverlapping approximation. For $\psi << 1$, the curve has a slope of 1 (i.e., a region where the weak-line approximation is valid) and for $\psi >> 1$ the curve has a slope of one-half (i.e., a region where the strong-line approximation is valid). The region of validity for various values of β and ψ is given in Table 19.

The general expression for absorption by an Elsasser band given by Eq. (169) and the strong-line approximation Eq. (171) are useful for determining absorption by CO_2 since the bands consist of fairly regularly spaced lines. However, the bands of H_2O and O_3 have a highly irregular fine structure and cannot be well described by Eq. (169). To develop an analytical expression for the transmissivity function for H_2O and O_3, we must employ statistical methods.

Golden [197] has described an Elsasser regular model using the Doppler shape analog to the Lorentz line. The reader is referred to the original article for further elaboration.

5.2.4 STATISTICAL BAND MODEL

Let $\Delta\nu$ be a spectral interval in which there are n lines of mean distance d.

$$\Delta\nu = nd \tag{173}$$

Let $P(S_i)$ be the probability that the i-th line will have a strength S_i and let P be normalized; then

$$\int_0^\infty P(S)dS = 1 \tag{174}$$

We assume that any line has equal probability of being anywhere in the interval $\Delta\nu$. The mean absorption clearly does not depend upon ν provided we are far enough away from the edges of the interval. We shall, therefore, determine it for $\nu = 0$, the center of the interval. If we let the center of the i-th line be at $\nu_0 = \nu_i$, then the absorption coefficient becomes

$$k_i(S_i, \nu_i) = k(\nu = \nu_i - \nu_0 = 0)$$

The mean transmissivity is found by averaging over all positions and all strengths of the lines; thus

$$\tau = \frac{1}{(\Delta\nu)^n}\int_{\Delta\nu} d\nu_1 \cdots \int_{\Delta\nu} d\nu_n \int_0^\infty P(S_i)\, e^{-kw}\, dS_1 \cdots \int_0^\infty P(S_n)\, e^{-kw}\, dS_n$$

But since all integrals are alike,

197. S. A. Golden, "The Doppler Analog of the Elsasser Band Model," J. Quant. Spect. Rad. Trans., Vol. 7, 1967, pp. 483-494.

$$\tau = \left[\frac{1}{\Delta\nu}\int d\nu \int P(s)\, e^{-kw} dS\right]^n = \left[1 - \frac{1}{\Delta\nu}\int d\nu \int P(S)(1 - e^{-kw}) dS\right]^n$$

Since $\Delta\nu = nd$, when n becomes large the last expression approaches an exponential; therefore,

$$\tau = \exp\left[-\frac{1}{d}\int P(S)(A_1 \Delta\nu) dS\right] \tag{175}$$

where

$$[A_1 \Delta\nu] = \int_{\Delta\nu} (1 - e^{-kw})\, d\nu$$

A_1 is the absorptivity of a single line taken over the interval $\Delta\nu$.

5.2.4.1 Equal Intensity Lines

Equation (175) can be evaluated for two special cases. First, when all the lines have equal intensities Eq. (175) reduces to

$$\tau = e^{-A_1 \Delta\nu/d} = \exp\left\{-\beta\psi\, e^{-\psi}[I_0(\psi) + I_1(\psi)]\right\}$$

Rewriting in terms of absorption, we have

$$A = 1 - \exp\left\{-\beta\psi\, e^{-\psi}[I_0(\psi) + I_1(\psi)]\right\} \tag{176}$$

If each of the lines absorbs weakly so that ψ is small, then Eq. (170) reduces to

$$A = 1 - \exp(-\beta\psi) \tag{177}$$

This is the weak-line approximation to the statistical model with all lines equally intense. If the lines absorb strongly, then Eq. (176) reduces to

$$A = 1 - \exp\left(-2\sqrt{S\alpha_L w/d}\right) \tag{178}$$

In terms of β and ψ,

$$A = 1 - \exp\left[-\left(\frac{2}{\pi}\beta^2\psi\right)^{1/2}\right] \tag{179}$$

This is the strong-line approximation to the statistical model in which all lines are equally intense.

The nonoverlapping approximation to Eq. (176) is obtained from the first term in the expansion of the exponential, so that

$$A = \beta\psi\, e^{-\psi}[I_0(\psi) + I_1(\psi)] \tag{180}$$

This is the same expression as that obtained for the nonoverlapping approximation to the Elsasser model, Eq. (172).

5.2.4.2 Line Strength by Poisson Distribution

Next, let us consider the case where the lines are of different strength and the distribution for the probability of their strength is a simple Poisson distribution, namely,

$$P(S) = \frac{1}{S_0} e^{-S/S_0} \tag{181}$$

By letting $k = S_0 b(\nu)$ in Eq. (175), we obtain (where $b(\nu)$ is the shape factor):

$$\tau = \exp\left(\frac{1}{d}\int_{\Delta\nu} \frac{b(\nu) w S_0}{1 + b(\nu) w S_0} d\nu\right) \tag{182}$$

We now introduce the Lorentz line shape

$$b(\nu) = \frac{\alpha_L}{\pi\left(\nu^2 + \alpha_L^2\right)}$$

This vanishes fast enough for large $\Delta\nu$ that we can extend the integration in Eq. (182) from $-\infty$ to ∞, giving

$$\tau = \exp\left[-\frac{w S_0 \alpha_L}{d\sqrt{\alpha_L^2 + (w S_0 \alpha_L)/\pi}}\right] \tag{183}$$

Rewriting in terms of absorption and β and ψ, we have

$$A = 1 - \exp\left[-\beta\psi_0/(1 + 2\psi_0)^{1/2}\right] \tag{184}$$

where $\psi_0 = S_0 w/2\pi\alpha_L$. This is the formula developed by Goody and is therefore referred to as the Goody band model.

The weak-line approximation to Eq. (184) is obtained when $\psi_0 << 1$. Under these conditions Eq. (184) becomes

$$A = 1 - \exp(-\beta\psi_0) \tag{185}$$

The strong-line approximation to the statistical model with an exponential distribution of line strengths is obtained when $\psi_0 >> 1$. Under these conditions Eq. (184) becomes

$$A = 1 - \exp\left[-\left(\tfrac{1}{2}\beta^2\psi\right)^{1/2}\right] \tag{186}$$

The nonoverlapping approximation is obtained from Eq. (184) when the exponent is small and is therefore given by the first two terms of the expansion, or

$$A = \beta\psi_0 \Big/ (1 + 2\psi_0)^{1/2} \tag{187}$$

5.2.4.3 Strong-Line, Weak-Line, and Nonoverlapping Approximations

The three approximations to the two statistical models above will be discussed concurrently because they are so closely related. First, we shall consider the weak-line approximation. Recall for this case that absorption was given by $A = 1 - \exp(-\beta\psi)$, which is exactly the expression obtained for the weak-line approximation to the Elsasser band model. The same expression results when an exponential distribution of line strengths is assumed with ψ replaced by ψ_0. This confirms our earlier statement that under weak-line absorption, absorption is independent of the arrangement of the spectral lines within the band. Absorption versus $\beta\psi$ is plotted for Eq. (176) in Figure 33. The solid curves give the absorption for the statistical model for the case in which all lines are equally intense. The dashed curves give the absorption for the statistical model with an exponential distribution of line strengths. The uppermost solid and dashed curves represent the weak-line approximations for those intensity distributions. The regions of validity are given in Table 19. For the case in which all lines are equally intense, the weak-line approximation is always valid within 10% when $\psi < 0.2$. It is valid for the exponential intensity distribution when $\psi < 0.1$. If 1% accuracy is required, these values of ψ should be divided by 10.

The strong-line approximation to the statistical model for all lines of equal strength and for an exponential distribution of line strengths are given respectively by Eqs. (179 and 183). The absorption for these models as a function of $\beta^2\psi$ is shown in Figure 34. The strong-line approximation is the uppermost curve in the figure. The absorption can even become greater than the limiting values given by this curve. It is evident that the distribution of the line strengths in a band only slightly influences the shape of the absorption curve. As for the strong-line approximation to the Elsasser model, the strong-line approximation to the statistical model for either distribution of line strengths is always valid when $\beta \leq 1$ and $0.1 \leq A \leq 1$. The complete regions of validity are given in Table 19.

The last approximation to be discussed for the statistical model is the nonoverlapping approximation. For all lines of equal strength the absorption is given by the expression used for the nonoverlapping approximation to the Elsasser model, namely,

$$A = \beta\psi\, e^{-\psi}[I_0(\psi) + I_1(\psi)]$$

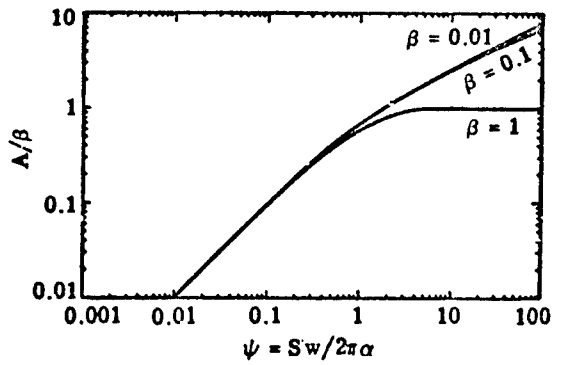

FIGURE 32. ABSORPTION DIVIDED BY β AS A FUNCTION OF $\psi = Sw/2\pi\alpha$ FOR THE ELSASSER MODEL. The nonoverlapping-line approximation is the uppermost curve.

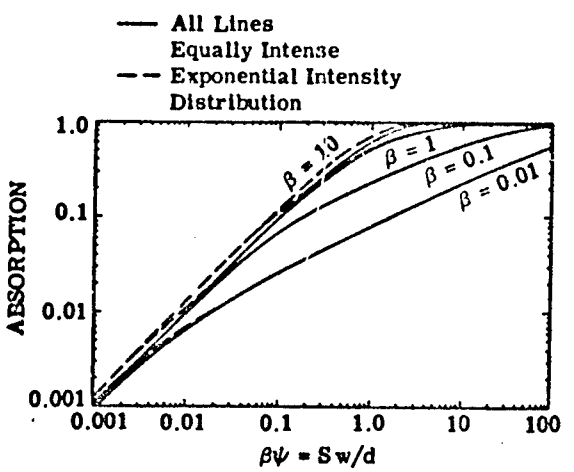

FIGURE 33. ABSORPTION AS A FUNCTION OF $\beta\psi = Sw/d$ FOR THE STATISTICAL MODEL. The absorption for a model in which the spectral lines are all of equal intensity is compared with that for a model in which the spectral lines have an exponential intensity-distribution function. The weak-line approximation is the uppermost curve.

For an exponential distribution of line strengths the absorption is given by Eq. (187). Therefore, the strength distribution, but not the regular or random spacing of the spectral lines, influences the absorption curve in this approximation. In Figure 35, A/β is plotted as a function of ψ for the statistical model. Note that if this figure is compared with the corresponding one for the Elsasser model the nonoverlapping approximation to the Elsasser model has a considerably larger region of validity. This is because the spectral lines begin to overlap at considerably larger path lengths for the Elsasser model than for the statistical model (cf. Table 19).

Three important approximations to the band models of Elsasser and Goody have been discussed above. These three approximations provide a reliable means for the extrapolation of laboratory absorption data to values of the pressure and path length that cannot easily be reproduced in the laboratory. For example, the absorption for large values of pressure can be obtained from the strong- and weak-line approximations, depending upon whether w is relatively large or small. For extrapolation to small values of pressure all three approximations may be used in their respective region of validity; however, the nonoverlapping-line approximation is valid over the largest range of values of w. For extrapolation to large values of w, either the strong- or weak-line approximation may be used, but the former approximation is valid over a much wider range of pressure than the latter. For extrapolation to small values of w, all three approximations may be used in their respective regions of validity; however, the nonoverlapping-line approximation is valid over a wider range of pressure. In general, atmospheric slant paths that are of interest to the systems engineer contain relatively large amounts of absorber and the range of pressures are such that the strong-line approximation to any of the models is applicable. As will be seen in Section 6, almost all researchers use the strong-line approximations to the various band models to develop equations for predicting absorption over a specified frequency band.

5.2.4.4 Exponential-Tailed S^{-1} Random Band Model

More recently, Malkmus [198] described a model comprising a line strength distribution which is defined by

$$P(S) \propto S^{-1} \exp\left[-\left(\frac{1}{\pi}\right)\frac{S}{S_E}\right]$$

where S_E is fixed in the expressions

$$\lim_{w \to 0} [(\overline{W}/d)/w] = S_E/d_E$$

198. W. Malkmus, "Random Lorentz Band Model with Exponential-Tailed S^{-1} Line-Intensity Distribution Function," J. Opt. Soc. Am., Vol. 57, No. 3, 1967, pp. 323-329.

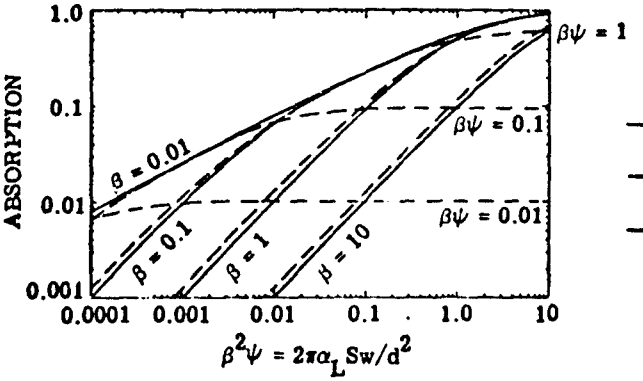

— All Lines Equally Intense, Constant Pressure
– – Exponential Intensity Distribution, Constant Pressure
– – All Lines Equally Intense, Constant Amount of Absorbing Gas

FIGURE 34. ABSORPTION AS A FUNCTION OF $\beta^2\psi = 2\pi\alpha_L Sw/d^2$ FOR THE STATISTICAL MODEL. Curves are shown for constant pressure (β = constant) and for constant amount of the absorbing gas ($\beta\psi$ = constant). The absorption is shown when all the spectral lines have equal intensity and when there is an exponential intensity-distribution function. The strong-line approximation is the uppermost curve.

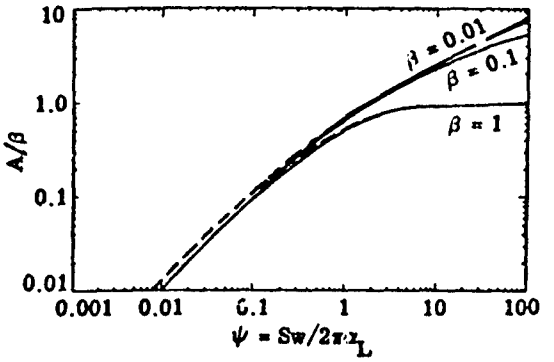

— All Lines Equally Intense
– – Exponential Intensity Distribution

FIGURE 35. ABSORPTION DIVIDED BY β AS A FUNCTION OF $\psi = Sw/2\pi\alpha_L$ FOR THE STATISTICAL MODEL. The absorption for a model in which the spectral lines are all of equal intensity is compared with that for a model in which the spectral lines have an exponential intensity-distribution function. The nonoverlapping-line approximation is the uppermost curve.

and

$$\lim_{w\to\infty} [(\overline{W}/d)w^{1/2}] = 2(S_E\alpha_L)^{1/2}/d_E$$

where

$$\overline{W}/d = -\ln \tau_{\Delta\nu}$$

The resultant transmittance is given by:

$$\tau_{\Delta\nu} = \exp\left\{-\frac{2\alpha_L}{d_E}\left[(1 + S_E w/\alpha_L)^{1/2} - 1\right]\right\} \tag{188}$$

$$= \exp\left\{-\frac{\beta_E}{\pi}\left[(1 + 2\pi\psi_E)^{1/2} - 1\right]\right\}$$

5.2.5 RANDOM ELSASSER BAND MODEL

At small values of ψ the same absorption is predicted by the statistical and Elsasser models, and is determined by the total strength of all the absorbing lines. However, as ψ increases the results calculated from these two models begin to diverge; the Elsasser theory always gives more absorption than does the statistical model for a given value of ψ. The reason for this is that there is always more overlapping of spectral lines with the statistical model than with the regular arrangement of lines in the Elsasser model; thus, for a given path length and pressure, the total line strength is not used as effectively for absorption in the statistical model.

An actual band has its spectral lines arranged neither completely at random nor at regular intervals. The actual pattern is formed by the superposition of many systems of lines. Therefore, for some gases and some spectral regions the absorption can be represented more accurately by the random Elsasser band model than by either the statistical or Elsasser model alone. The random Elsasser band model is a natural generalization of the original models which assumes that the absorption can be represented by the random superposition of Elsasser bands. The individual bands may have different line spacings, half-widths, and strengths. As the number of superposed Elsasser bands becomes large, the predicted absorption approaches that of the usual statistical model.

The absorption for N randomly superposed Elsasser bands with equal strengths, half-widths, and line spacings is given by

$$A = 1 - \left[1 - \text{erf}\left(\tfrac{1}{2}\beta^2\psi/N^2\right)^{1/2}\right]^N$$

The derivation of this equation and the more general equation for different strengths, half-widths, and the line spacings is discussed in detail by Plass (1958). The more general result is not presented here since the result given above is the only function which has received application.

5.2.6 QUASI-RANDOM MODEL

The fourth band model that has been developed, Ref. [199] and Wyatt, et al., (1962)—the quasi-random band model—reportedly presents a more realistic model of the absorption bands of water vapor and carbon dioxide. It does not require that the lines be uniformly nor randomly spaced, but can represent any type of spacing which may occur. It also accurately simulates the strength distribution of the spectral lines including as many of the weaker lines as actually contribute to the absorption. Furthermore, it provides a means of accurately calculating the effect of wing absorption from spectral lines whose centers are outside the given frequency interval. The quasi-random model allows for more accurate prediction of absorption than do the other three models but sacrifices simplicity in the process. When this model is used the general transmissivity function cannot be expressed in terms of elementary functions. Moreover, to determine accurate absorption spectra by this method, a priori knowledge of the band structure is required, as it is in the rigorous method.

The quasi-random model is characterized by the following features:

(1) The frequency interval $\Delta\nu$ for which the transmission is desired is divided into a set of subintervals of width δ. Within the small interval δ the lines are assumed to be arranged at random. The transmission over $\Delta\nu >> \delta$ is then calculated by averaging the results from the smaller intervals.

(2) The interval $\Delta\nu$ is divided into subintervals δ in an arbitrary manner. The transmission is first calculated for one mesh, which defines a certain set of frequency intervals. The calculation is repeated for another mesh which is shifted in frequency by $\delta/2$ relative to the first set. In principle, the mesh can be shifted n times by an amount δ/n. The final calculation is then the average of the results for each of these meshes.

(3) The transmission for each subinterval δ is calculated from expressions which are valid for a finite and possibly small number of spectral lines in the interval.

(4) The spectral lines in each frequency interval are divided into line-strength subgroups which are fine enough to simulate the actual strength distribution. In the calculation, the average strength of all the lines in each subgroup is used with the actual number of lines.

199. J. I. F. King, "Band Absorption Model for Arbitrary Line Variance," J. Quant. Spect. Rad. Trans., Vol 4, 1964, pp. 705-711.

(5) The contribution from the wings of the spectral lines whose centers are outside a given interval is included. The wing effect is treated in the same detailed manner used for evaluating the contribution from the lines within an interval.

Let us consider one interval δ_k of a given mesh. If there are n_k lines in the interval with their line centers at the frequencies $\nu_i (i = 1, 2, \ldots, n_k)$, then the transmission at the frequency ν is affected by these n_k lines so that

$$\tau_r(\nu) = \frac{1}{\delta_r^{n_r}} \prod_{i=1}^{n_r} \int_{\delta_r} \exp\left[-wk(\nu, \nu_i)\right] d\nu_i \tag{189}$$

where w is the amount of absorber and $k(\nu, \nu_i)$ may be expressed as $k(\nu, \nu_i) = S_i b(\nu, \nu_i)$. The quantity $b(\nu, \nu_i)$ is the line-shape factor (Lorentz, Doppler, etc.), and S_i is the strength of the i-th line. The transmission is calculated at some frequency ν which for convenience is usually taken at the center of the interval δ_r. Since this transmission corresponds to the average of all permutations of the positions of the spectral lines within the interval, it is also assumed to represent the most probable transmission for the interval.

To be completely rigorous the transmission of each spectral line should be calculated from its intensity and position and then substituted into Eq. (189). This procedure would require a computation time analogous to that required for the rigorous method and hence would defeat the purpose of employing a band model. Thus, a method is used which simulates the actual strength distribution.

The procedure adopted for line-strength simulation is to divide the lines in each frequency interval into subgroups by intensity decades. When the line strengths are calculated, the results are grouped according to these strength decades. The average strength $\bar{S}_i$ of the lines in each decade is then calculated.

Wyatt, Stull, and Plass (1962a) have found that only the first five strength decades for each frequency interval influence the value of transmission. Thus only the data for the five strongest strength decades need be retained for each frequency interval. It should be emphasized that the numerical range of the line-strength decades retained is quite different for a frequency interval which contains strong lines than for one which has weak lines. The criterion is applied separately to each frequency interval.

Thus, the transmission can be calculated by the following equation from the average value of the strength $\bar{S}_i$ together with the number of lines n in each line-strength decade:

$$\tau_r(\nu) = \prod_{i=1}^{5} \left(\frac{1}{\delta} \int_{\delta_r} e^{-\bar{S}_i w b(\nu, \nu_i)} d\nu_i \right)^{n_i} \tag{190}$$

The number of lines n_k in the frequency interval is given by

$$n_r = \sum_{i=1}^{5} n_i \tag{191}$$

Equation (190) represents the transmission at a frequency ν for the interval δ_r as affected by n_r spectral lines whose centers are within the interval δ_r. The integral in Eq. (190) represents the transmission over the finite interval δ_r of a single line representative of the average strength of the decade.

The transmission at a frequency ν is also influenced by the wings of the spectral lines whose centers lie in intervals outside the interval δ_k, denoted by δ_i. The wing transmission, τ_i, from each of these intervals δ_i is calculated by assuming a random distribution of the lines within the interval δ_i. Thus, by the random hypothesis, the transmission at the frequency ν is the product of all transmissions calculated for the lines with centers in intervals, outside δ_k, taken with the transmission for the interval δ_k. Therefore

$$\tau(\nu) = \prod_{i=1}^{\infty} \tau_i(\nu) \tag{192}$$

where the subscript i indicates that there are n_i lines in the frequency interval δ_i. The transmission for the lines whose centers are in the interval δ_i are given by Eq. (190). The lines in distant intervals from the particular frequency ν have a negligible effect on the transmission, so that in practice the product (Eq. 192) usually needs to be evaluated over only a few terms.

It is clear that the quasi-random model can reproduce the actual line structure fairly accurately if the chosen interval δ_k is small enough. However, the smaller the interval the greater the amount of computation required. The tradeoff between the two has not been discussed by the authors, but such an investigation would indeed be of interest since any particular application has a tolerable error which might be used to establish the frequency interval and hence the degree of computation.

5.2.7 TEMPERATURE AND FREQUENCY DEPENDENCE OF BAND-MODEL PARAMETERS

A summary of the band models that yield closed-form expressions for spectral-band absorption is presented in Table 20. All of these expressions are functions of two parameters, β and ψ, which are functions of temperature, pressure, absorber concentration, and frequency. Recall that

TABLE 20. SUMMARY OF CLOSED-FORM EXPRESSIONS FOR SPECTRAL ABSORPTION

Band Model	Approximation	Equation*
1. Single Lorentz Line	None	$A = \frac{1}{\Delta\nu}\ 2\pi\alpha_L\psi\ e^{-\psi}[I_0(\psi) + I_1(\psi)]$
2. Single Lorentz Line	Linear	$A = Sw/\Delta\nu$
3. Single Lorentz Line	Square Root	$A = 2\sqrt{S\alpha_L w/\Delta\nu}$
4. Elsasser Band	None	$A = \sinh\beta \int_0^Y I_0(Y)\exp(-Y\cosh\beta)\,dY$
5. Elsasser Band	Weak	$A = 1 - e^{-\beta\psi}$
6. Elsasser Band	Strong	$A = \mathrm{erf}\left(\frac{1}{2}\beta^2\psi\right)^{1/2}$
7. Statistical Band (Poisson)	None	$A = 1 - \exp\left[-\beta\psi_0/(1 + 2\psi_0)^{1/2}\right]$
8. Statistical Band	None	$A = 1 - \exp -\left\{\beta\psi\ e^{-\psi}[I_0(\psi) + I_1(\psi)]\right\}$
9. Statistical Band (Poisson)	Weak	$A = 1 - e^{-\beta\psi}$
10. Statistical Band (Poisson and equal)	Strong	$A = 1 - \exp\left[-\left(\frac{1}{2}\beta^2\psi_0\right)^{1/2}\right]$
11. Statistical Band (equal)	Strong	$A = 1 - \exp\left[-\left(\frac{2}{\pi}\beta^2\psi\right)^{1/2}\right]$
12. Exponential Tailed S^{-1} Statistical Band	Strong	$A = 1 - \exp\left\{-\frac{\beta_E}{\pi}\left[(1 + 2\pi\psi_E)^{1/2} - 1\right]\right\}$
13. Random Elsasser Band	Strong	$A = 1 - \left[1 - \mathrm{erf}\left(\frac{1}{2}\beta^2\psi/N^2\right)^{1/2}\right]^N$

* With appropriate subscripts: $\beta = \frac{2\pi\alpha_L}{d}$; $\psi = \frac{Sw}{2\pi\alpha_L}$; $\psi_0 = \frac{S0^w}{2\pi\alpha_L}$ where (see text)

S = line strength
α_L = Lorentz-line half-width
d = (mean) line spacing
w = absorber amount

(For ψ_E, β_E, see Section 5.2.4.4.)

$$\beta = \frac{2\pi\alpha_L}{d} = \frac{2\pi\alpha_{L0}}{d}\frac{P}{P_0}\left(\frac{T_0}{T}\right)^n$$

and

$$\psi = \frac{Sw}{2\pi\alpha_L} = \frac{Sw}{2\pi\alpha_{L0}}\frac{P_0}{P}\left(\frac{T}{T_0}\right)^n$$

including the dependence of line half-width on pressure and temperature. Also, the line strength is a function of temperature and frequency and is given in Section 4 as:

$$S = S_0\left(\frac{T_0}{T}\right)^m \exp\left[-\frac{E(\nu)''}{k}\left(\frac{T_0 - T}{TT_0}\right)\right]$$

where S_0 is the line strength at standard temperature and E" is the ground-level energy of a given spectral line. Because E" varies from line to line, the variation of line strength with temperature is different for each spectral line. As the temperature decreases, the line strengths near the center of the band increase and the line strengths in the wings of the band decreases; the area under the curve decreases slightly. If two homogeneous paths having different temperature were compared, the integrated absorption for the lower temperature path would be less than the integrated absorption for the higher temperature path. Drayson (1964) has shown that for two identical slant paths having temperature profiles that differ by a constant amount of 10 K the transmission varies as much as 10% in the wing of the band and somewhat less nearer the center of the band. He also concluded that the effect of temperature on line half-width has a secondary effect on transmission.

Since the variation of line strength with temperature is different for each spectral line, it would be impossible to include the effect of temperature on line strength and still retain the band-model expressions in closed form. For this reason, the band-model expressions in their present form can be used only to predict absorption for homogeneous paths that are at standard temperature. Further, since Drayson (1964) has shown that the effect of temperature on line half-width has a secondary effect on absorption, this dependence is neglected also. Therefore, if we let $T = T_0$, the expressions for β and ψ become

$$\beta = \frac{2\pi\alpha_{L0}}{d}\frac{P}{P_0} = \frac{2\pi\alpha^o_{L0}}{d}P \tag{193}$$

and

$$\psi = \frac{S_0 w}{2\pi\alpha_{L0}}\frac{P_0}{P} = \frac{S}{2\pi\alpha^o_{L0}}\frac{w}{P} \tag{194}$$

where α^o_{L0} is the half-width at standard temperature, per unit pressure.

The expressions listed in Table 20 are of the following general form:

(1) $A = A(\beta, \psi)$ when no approximation to the model is assumed

(2) $A = A(\beta^2\psi)$ for the strong-line approximation

(3) $A = A(\beta\psi)$ for the weak-line approximation.

Substituting Eqs. (193) and (194) into 1, 2 and 3, we have the first expression as a function of two frequency-dependent parameters, $2\pi\alpha^o_{L0}/d$ and $S/2\pi\alpha^o_{L0}$, and two path parameters, w and P. The second expression gives absorption as a function of one frequency-dependent parameter, $2\pi\alpha^o_{L0}S/d^2$ and two path parameters, w and P. The last is a function of S/d and w, being independent of pressure.

The next problem in completely specifying the absorption expressions is that of evaluating the frequency-dependent parameters by empirically fitting the respective equations to laboratory homogeneous absorption spectra. The empirical procedure is the most involved when no approximations to the model are assumed, since in this case two parameters must be evaluated, rather than only one for both the strong- and weak-line approximations. After the frequency-dependent parameters have been specified and the values of w and P have been determined for a given slant path, it becomes a simple matter to generate absorption spectra.

5.2.8 DETERMINATION OF BAND-MODEL PARAMETERS

Band models are used to avoid the explicit use of line parameters in the calculation of atmospheric transmittance. But since all band models are formulated in terms of certain parameters, these parameters must be obtained by eventually using the real line characteristics of the absorbing molecules, either by the use of the results of laboratory experiments, or through an examination of a set of compiled line parameters.

5.2.8.1 Empirical

In the purely empirical approach to the determination of band parameters, one does not usually have access to the two important line characteristics, $\bar{S}$ and α_L, to be used in band model calculations. Instead we must obtain implicit representations of them graphically in terms of experimentally produced data, i.e., the absorptance over a predetermined spectral region, $\Delta\lambda$ or $\Delta\nu$; the absorber amount; and the appropriate thermodynamic parameters. An excellent account of an empirical method of the determination of band parameters is given in the original state-of-the-art report by Anding (1967), derived from the work of various authors. Since the method is as valid now as it was then, and because of its importance to this subject, the steps shown by Anding are reproduced here.

The theory of band models is reasonably well defined and the resulting functions should be capable of specifying spectral absorption to a good approximation if, first, the conditions

inherent in the band-model development are satisfied, and second, rigorous empirical procedures are applied to high-quality laboratory homogeneous-path data to specify the absorption constants.

The first conditional restrictions are satisfied by most atmospheric slant paths of interest. Therefore, it seems hopeful that usable transmissivity functions could be developed if the second procedural restrictions are satisfied.

Oppel (see Anding, 1967) has postulated and employed certain rules for selecting laboratory data and performing an empirical fit. His approach is sound and is analogous to that suggested by Plass [200]. Hence, the methods of Oppel are those which are recommended for the determination of the spectral absorption constants and are stated below.

It has been found by most researchers that the quality and the reduction of the laboratory data have constituted the most critical step in determining the absorption constants. In order to insure satisfactory results from an empirical fitting procedure the following rules should be observed.

(1) The data should be consistent from one run to another; that is, all runs for a particular spectral interval should have the same resolution and spectral calibration. The absolute spectral calibration is not nearly as important as the relative spectral position from run to run, because the absorption constants can be determined for relative frequency units. Also, the spectrum can later be shifted if necessary.

(2) Only data with absorption between 5% and 95% should be used. Usually the data for very high or very low absorption values are questionable because of the uncertainty of the 0% and 100% levels, and relatively small differences may have an inordinately great effect on the determination of the unknown parameters.

(3) It is desirable to have spectra obtained over a range of paths and pressures which is wide enough that the function can be properly fitted to the data. Ideally, for each frequency, one would like to have data which would give absorptions between 5% and 95% and which include the following conditions:

(a) Pressure and absorption path are sufficiently small that there is negligible overlapping of the spectral lines.

(b) Pressure is high and absorption path is small so that there is heavy overlapping of the spectral lines.

200. G. N. Plass, "Useful Representations for Measurements of Spectral Band Absorption," J. Opt. Soc. Am., Vol. 50, 1960, pp. 868-875.

(c) Pressure is low and absorption path is large so that the spectral lines are opaque at their centers and the transmission is achieved only in the wings of the lines.

(4) Measurements for which pressure self-broadening is predominant, that is, where the absorbing-gas pressure is an appreciable part of the total pressure, should be discarded. This is necessary since self-broadened spectral lines need not be evaluated under real atmospheric conditions.

(5) In general, better results are obtained if spectral frequencies are selected at which absorption achieves a local maximum, minimum, or inflection point. Thus, the absorption constants should not necessarily be selected at uniform intervals but for spectral positions that are more easily measured. It has been frequently observed that published spectra are hand-plotted and that their author will tend to be more exact on the maxima, minima, and inflection points than he will be on any other part of the curve.

Atmospheric paths that are of greatest interest to the infrared researcher are long paths through an atmosphere of relatively low pressure. Such paths give rise to large values of w and small values of equivalent pressure $\tilde{P}$. The dominant spectral lines, those which account for 95% of the absorption, are opaque at their centers but do not display a significant amount of overlapping. Therefore, for such paths β is small ($\beta < 1$) and ψ is large ($\psi \gg 1$), and the strong-line conditions are valid. It is noted that strong-line absorption must be present for an atmospheric path to be reduced to an equivalent homogeneous path. For these reasons most researchers assume that absorption is represented by the strong-line approximation, $A = A(\beta\psi)$, and empirically fit this function to laboratory data. If the data used do not satisfy strong-line absorption conditions when such a procedure is used, erroneous constants will be determined.

After selecting the laboratory homogeneous-path spectra according to the above rules, and the appropriate model for representing absorption for a given absorption band, one has the proper foundation for performing an empirical fit which will yield a valid closed-form expression for predicting absorption for other homogeneous paths.

Basically, the absorption coefficients are determined by minimizing the sums of the squares of the errors between measured and calculated values of absorption. Before the least-squares iteration can begin, an initial estimate of the two parameters $2\pi\alpha^{o}_{L0}/d$ and $S/2\pi\alpha^{o}_{L0}$ must be made. The method of determination and the accuracy of these initial parameters does not affect the final accuracy except that poorly chosen estimates will considerably increase the iteration time. The method suggested is based on the fact that the three approximations to the Elsasser integral described in Section 5.2.3 always show greater absorption

than that given by the complete Elsasser integral and approach the complete expression in the limit. This method can be described as follows:

(1) Three master graphs are drawn on log-log paper. The first graph (Figure 36), is a plot of Beers' law, given by

$$A = 1 - \exp(-\beta\psi);\ \beta\psi = \frac{Sw}{d}$$

The second master graph (Figure 37) gives the strong-line approximation to the Elsasser integral:

$$A = \operatorname{erf}\left[\left(\frac{1}{2}\beta^2\psi\right)^{1/2}\right];\ \beta^2\psi = \frac{2\pi\alpha^{o}_{L0}S}{d^2}wP$$

where $\alpha^{o}_{L0} = \alpha_{L0}/P_0$, and P_0 is standard sea-level pressure. The third master graph (Figure 38) gives the nonoverlapping-line approximation:

$$A = \beta\psi[I_0(\psi) + I_1(\psi)]\ \exp(-\psi)$$

$$\beta = \frac{2\pi\alpha^{o}_{L0}}{d}P,\ \psi = \frac{S}{2\pi\alpha^{o}_{L0}}\frac{w}{P}$$

(2) Three working graphs are plotted for each spectral frequency for which absorption constants are to be determined.

(a) In the first working graph (Figure 39) fractional absorption A is plotted as a function of the absorption path w (atm cm).

(b) The second graph (Figure 40) gives fractional absorption versus absorption path times effective broadening pressure wP_e(atm cm × mm Hg). Note: $P_e = P + (B - 1)p$, where p_e is the total pressure of the gas mixture and p is the partial pressure of the absorbing gas.

(c) The third working graph (Figure 41) is a plot of the ratio of fractional absorption to effective broadening pressure, A/P_e (mm Hg^{-1}) versus absorption path/effective broadening pressure w/P_e (atm cm/mm Hg).

(3) The six graphs are now paired off in the following order: Figure 36 is superposed over Figure 39, Figure 37 over Figure 40, and Figure 38 over Figure 41. With a good spread of data, it now becomes apparent that the several approximations are limiting functions and all points on the graphs will fall below the limiting curve. Figure 36 is adjusted in the w direction, until all plotted points of Figure 39 fall below and to the right of the curve down on Figure 36. Thus, the curve of Figure 36 forms the limiting continuum for the points of Figure 39. The relative positions yield the approximate value

$$(S/d) = (\beta\psi/w)$$

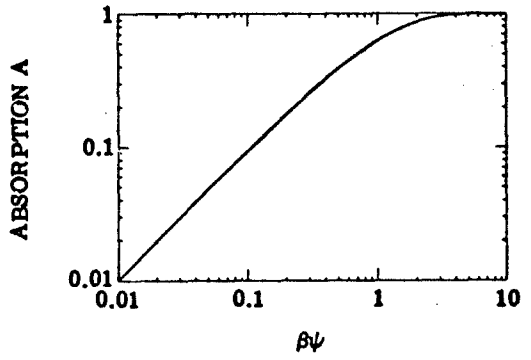

FIGURE 36. WEAK-LINE APPROXIMATION TO THE ELSASSER MODEL. $A = 1 - \exp(-\beta\psi)$; $\beta\psi = Sw/d$.

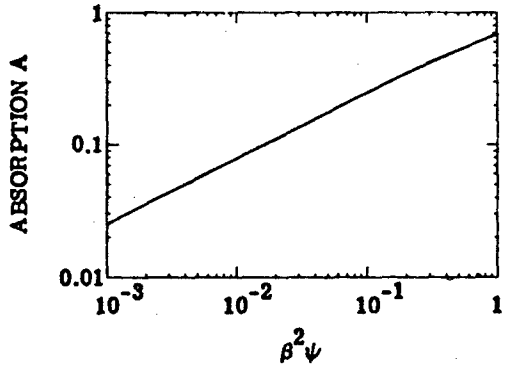

FIGURE 37. STRONG-LINE APPROXIMATION TO THE ELSASSER MODEL. $A = \text{erf}\,[(1/2\beta^2\psi)^{1/2}]$; $\beta^2\psi = (2\pi\alpha^{o}_{L0}S/d^2)wP$.

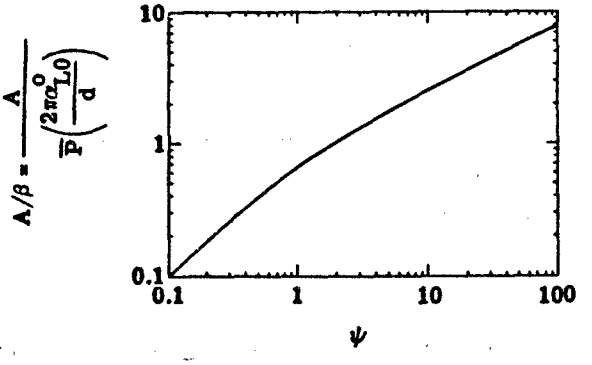

FIGURE 38. NONOVERLAPPING-LINE APPROXIMATION TO THE ELSASSER MODEL. $A/\beta = \psi[I_0(\psi) + I_1(\psi)]\exp -\psi$; $\psi = \left(S/2\pi\alpha^{o}_{L0}\right)(w/P)$.

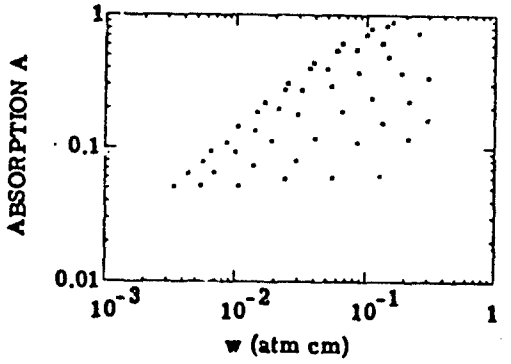

FIGURE 39. WORKING GRAPH FOR ESTIMATING S/d. For these data S/d ≈ 15.

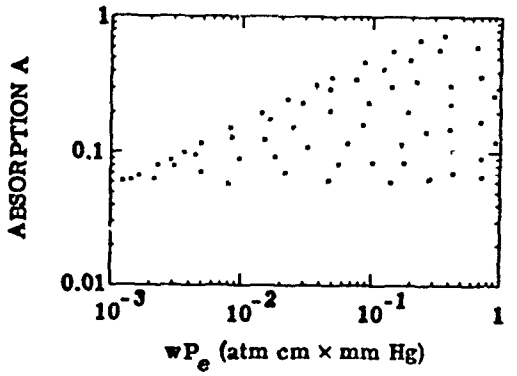

FIGURE 40. WORKING GRAPH FOR ESTIMATING $2\pi\alpha^o_{L0}S/d^2$. For these data $2\pi\alpha^o_{L0}S/d^2 \approx 4.5$.

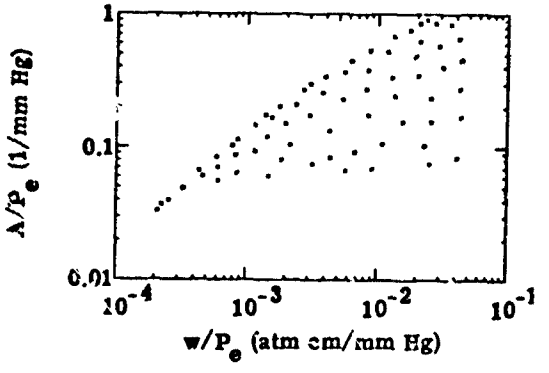

FIGURE 41. WORKING GRAPH FOR ESTIMATING $2\pi\alpha^o_{L0}/d$ and $S/2\pi\alpha^o_{L0}$. For these data $2\pi\alpha^o_{L0}/d \approx 0.3$ and $S/2\pi\alpha^o_{L0} \approx 500$.

Similarly, Figure 37 is superposed over Figure 40 and adjusted along the axis until the limiting continuum is found, yielding the approximate value

$$\left(\frac{2\pi\alpha_{L0}^{o}S}{d^2}\right) = \frac{(\beta^2\psi)}{(wP_e)}$$

The third pair (Figs. 38 and 41) can be adjusted in both directions to give approximations to two parameters:

$$\left(\frac{2\pi\alpha_0^o}{d}\right) = \frac{A/P_e}{(A/\beta)}$$

and

$$\left(\frac{S}{2\pi\alpha_{L0}^{o}}\right) = \frac{\psi}{(w/P_e)}$$

The three plots indicated above are not all necessary if sufficient data are available, since only two constants, α_{L0}^{o}/d and S/d (Note: $S/\alpha_{L0}^{o} = (S/d)/(\alpha_{L0}^{o}/d)$), are necessary to evaluate the Elsasser integral; however, experience has shown that sufficient spread of data is usually not available to adequately construct all of the graphs. For this reason, the best graphs should be chosen. In the event that the nonoverlapping approximation gives a good continuum, then it may be used alone for both approximations to the unknown parameters.

At this point it is assumed that the initial estimates of the parameters have been made and the laboratory data have been properly chosen. Beginning with the first estimates, the absorption is calculated for each value of absorber concentration and each value of equivalent pressure and compared with the measured value. The parameters are adjusted until the sums of the squared residuals between computed and measured absorption values are minimized.

A computer program has been written by Baumeister and Marquardt and distributed as a SHARE program [201]. This program, when coupled with the Elsasser-model algorithm, will optimize the parameters for the Elsasser function.

The procedure described above is that which can be used when fitting the complete Elsasser integral to laboratory data. It is emphasized that if the strong-line or weak-line approximation to the Elsasser model is used to represent atmospheric absorption, then the laboratory data must be such that these conditions are satisfied. This can be determined by using the initial estimates of $2\pi\alpha_{L0}^{o}/d$ and $S/2\pi\alpha_{L0}^{o}$ and the values of w and P to calculate β and ψ. These results can then be compared with the values in Table 20.

201. Baumeister and Marquardt, Least-Squares Estimation of Non-Linear Parameters, SHARE Program No. 1423, FORTRAN Program, IBM.

A completely analogous procedure can be used when fitting the Goody model to a set of laboratory data. That is, all three equations should be fitted to the data to obtain a set of frequency-dependent parameters. Parameters obtained in this manner will give valid results whether the absorption is strong, weak, or of some intermediate value.

Empirically fitting a band-model expression to homogeneous data generates coefficients that represent the best value for all available data. The absorption constants then do not actually represent the strengths, widths, and spacings of the spectral lines but can be interpreted as a set of lines giving equivalent absorption. It can be expected that calculations should be satisfactory for conditions bounded by the laboratory data. However, for extreme cases the results may be rather poor. It is difficult to theoretically analyze the accuracy with which a band model can be used to predict absorption, so the approach to be used here is simply to compare the results with field measurements.

It is important to emphasize here that the results of empirical fitting are only good for the temperature at which the data were taken. Problems arise, for example, when one attempts to apply room-temperature data to the cold atmosphere without making appropriate corrections.

5.8.2.2 Use of Line Data

Since the line parameter data (see Section 4) are now available, it is useful to take the approach suggested by Goody (1964, Section 4) and sum the lines in the spectral region of interest in the following special procedure. Goody shows that with the incorporation of line parameter data, the band-model parameters ψ and β can be obtained for different models using Lorentz lines. For the statistical model with an exponential distribution of line strengths, the following equations hold:

$$\frac{\psi}{w} = \frac{1}{8}\left(\frac{\sum_{i=1}^{N} S_i}{\sum_{i=1}^{N}\sqrt{\left[S_i \alpha_{L_i}\right]}}\right)^2 \tag{195}$$

and

$$\beta = \frac{8}{\Delta\nu}\frac{\left[\sum_{i=1}^{N}\sqrt{\left[S_i \alpha_{L_i}\right]}\right]^2}{\sum_{i=1}^{N} S_i} \tag{196}$$

where the spectral region of coverage $\Delta\nu$, containing N lines with strengths S_i and half-widths α_{L_i}. These line strengths and half-widths can be obtained, for example, from the AFCRL compilation of line parameters [McClatchey et al., 1972]. See Section 4.

If the distribution of strengths falls off less rapidly than exponentially, but instead, inversely as S, then according to Goody the equations take the form:

$$\frac{\psi}{w} = \frac{2}{\pi}\left(\frac{\sum_{i=1}^{N} S_i}{\sum_{i=1}^{N}\sqrt{\left\{S_i\alpha_{L_i}\right\}}}\right)^2 \tag{197}$$

and

$$\beta = \frac{\pi}{2\Delta\nu}\frac{\left[\sum_{i=1}^{N}\sqrt{\left\{S_i\alpha_{L_i}\right\}}\right]^2}{\sum_{i=1}^{N} S_i} \tag{198}$$

Goldman and Kyle [202] have calculated band model parameters for calculating transmittance in the 9.6 μm ozone band and the 2.7 μm water vapor band using an exponential tailed S^{-1} line strength distribution in the statistical model in the form:*

$$\bar{\tau}_{\Delta\nu} = \exp -\left(\frac{2\pi\alpha_L^0\omega}{d}P_e\frac{1}{\pi}\left\{\left[1 + 2\pi\left(\frac{\psi}{w}\right)w\right]^{1/2} - 1\right\}\right), \tag{199}$$

$$w = \frac{pL}{P_e} = \exp -\left(\beta_0 P_e/\pi\left\{\left[1 + 2\pi\psi\right]^{1/2} - 1\right\}\right)$$

L is the path length in cm

p is the partial pressure of the absorber

P_e is the equivalent total pressure given by $P_e = P + (B - 1)p$ where P is the total pressure of the gas mixture and B is a self-broadening coefficient for the absorber.

For this model Goldman and Kyle calculate the band model parameters for the exponential tailed S^{-1} statistical model from:

*Note that this corresponds to $\tau = \exp\left\{-\beta_E/\pi[(1 + 2\pi\psi_E)^{1/2} - 1]\right\}$ as formulated by Malkmus (1963). See Expression 12 in Table 20.

202. A. Goldman and T. G. Kyle, "A Comparison Between Statistical Model and Line-by-Line Calculation with Application to the 9.6μ Ozone and the 2.7μ Water Vapor Bands," Appl. Opt., Vol. 7, No. 6, 1968, pp. 1167-1177.

$$\frac{\psi}{w} = \frac{1}{2\pi}\left(\frac{\sum_{i=1}^{N} S_i}{\sum_{i=1}^{N}\sqrt{\{S_i \alpha_{L_i}\}}}\right)^2 \tag{200}$$

$$\beta = \frac{2\pi}{\Delta\nu}\,\frac{\left[\sum_{i=1}^{N}\sqrt{\{S_i \alpha_{L_i}\}}\right]^2}{\sum_{i=1}^{N} S_i} \tag{201}$$

Following from this, the average value of S/d (the average absorption coefficient) in $\Delta\nu$ is:

$$\frac{S}{d} = \sum_{i=1}^{N} S_i / \Delta\nu \tag{202}$$

No other formulations of this type have been found in the literature, although it would be straightforward to apply the Goody technique to other models, as long as the weak- and strong-line approximations can be determined. The expressions related to the Elsasser model are trivial, inasmuch as the lines are regular and of constant strength.

5.2.9 THE CURTIS-GODSON APPROXIMATION

In all band-model calculations, the transmittance is calculated for a path containing a fixed concentration of absorber at a fixed temperature and pressure, so that the path is homogeneous. These values are usually standardized to sea-level conditions under standard temperature and pressure. Since the dependence of the band parameters and absorber concentrations are known (or can be obtained), the adjustment of conditions to meet standard criteria can be made, so that calculations of transmittance can be made for any altitude in the atmosphere as long as the path remains homogeneous. When the path traverses the vertical, the atmospheric parameters change with altitude, causing line-parameter changes, and thus creating problems which usually must be attacked by the use of approximate methods of calculation. In this case, to keep calculations within reasonable limits, it is necessary to attempt to find equivalent, or effective, values for the atmospheric parameters which affect the passage of radiation under these pseudo-homogeneous conditions in the same way as if it were traversing a real, slant path. The method used to find these effective parameters is called the Curtis-Godson (CG) approximation.

5.2.9.1 Calculation of the Two-Parameter Approximation

Goody (1964) calls this the two-parameter approximation in contrast with the one-parameter or scaling approximation in which only w, the amount of absorber, in gm/cm^2 (or equivalent), is scaled in the form:

$$\tilde{w} = \frac{S(T)P^n}{S(\tilde{T})\tilde{P}^n}\,dw \tag{203}$$

where n, $\tilde{T}$, and $\tilde{P}$ are assigned fixed standard (average) values, and $\tilde{w}$, the effective absorber amount, is the sole adjusted parameter.

The two-parameter approximation requires that there be two conditions under which the transmittance may be calculated, these being the strong-line and weak-line limits of the band-model calculations. The calculation of the average transmittance over $\Delta\nu$ is:

$$\bar{\tau} = \frac{1}{\Delta\nu}\int_{\Delta\nu} d\nu \exp\left(-\int dw \sum_i \frac{\alpha_{L_i} S_i}{\pi\left\{(\nu-\nu_i)^2 + \alpha_{L_i}^2\right\}}\right) \tag{204}$$

The summation is taken over all lines in the interval, $\Delta\nu$. In the strong-line limit $\alpha_{L_i}^2$ in the denominator may actually be neglected since, for this case, the absorption all takes place in the wings of the lines for which $\nu - \nu_i >> \alpha_i$. Instead, however, the (more accurate) approach is taken in which $\tilde{\alpha}_i$ is substituted for α_{L_i} in the denominator, the value $\tilde{\alpha}_i$ being an effective width (see Eq. (210)), so that

$$\bar{\tau} \cong \frac{1}{\Delta\nu}\int_{\Delta\nu} d\nu \exp\left(-\int_{\text{path}} dw \sum_i \frac{\alpha_{L_i} S_i}{\pi\left\{(\nu-\nu_i)^2 + \tilde{\alpha}_i^2\right\}}\right) \tag{205}$$

The weak-line approximation to $\bar{\tau}$ truncates the infinite series representation of the exponential so that:

$$\bar{\tau} \cong \frac{1}{\Delta\nu}\int_{\Delta\nu} d\nu\left(1 - \int dw \sum_i \frac{\alpha_{L_i} S_i}{\pi\left\{(\nu-\nu_i)^2 + \tilde{\alpha}_i^2\right\}}\right) \tag{206}$$

which, because $\Delta\nu >> \tilde{\alpha}_i$, is approximated by:

$$\bar{\tau} \cong 1 - \frac{1}{\Delta\nu}\int dw \sum_i \int_{-\infty}^{\infty} \frac{\alpha_{L_i} S_i\, d\nu}{\pi\left\{(\nu-\nu_i)^2 + \tilde{\alpha}_i^2\right\}} = 1 - \frac{1}{\Delta\nu}\int dw \sum_i \frac{\alpha_{L_i}}{\tilde{\alpha}_i} S_i \tag{207}$$

This straightforward treatment is taken directly from the book by Goody in which he next equates Eq. (207) to the weak-line approximation of Eq. (204), given by:

$$\bar{\tau} = 1 - \frac{1}{\Delta\nu}\int dw \sum_i S_i \tag{208}$$

so that, since $\alpha_{L_i}/\tilde{\alpha}_i = P/\tilde{P}$,

$$\tilde{P} = \frac{\int dw\, P \sum_i S_i}{\int dw \sum_i S_i} \tag{209}$$

$$\left(\text{Note also that: } \tilde{\alpha} = \frac{\int dw\, \alpha_{L_i} \sum_i S_i}{\int dw \sum_i S_i}. \right) \tag{210}$$

where $\tilde{P}$ is the Curtis-Godson (CG) equivalent pressure. This pressure along with a scaled strength $\tilde{S}_i$ and scaled absorber amount $\tilde{w}$ can then be used in a homogeneous-path calculation of $\bar{\tau}$ to give:

$$\bar{\tau} \cong \frac{1}{\Delta\nu}\int_{\Delta\nu} d\nu \exp\left(-\tilde{w} \sum_i \frac{\tilde{\alpha}_i \tilde{S}_i}{\pi\left\{(\nu - \nu_i)^2 + \tilde{\alpha}_i^2\right\}} \right) \tag{211}$$

from which, by comparison with Eq. (205), Goody shows that the scaled absorber amount is determined by:

$$\tilde{w} = \frac{\int dw \sum_i S_i}{\sum_i \tilde{S}_i} \tag{212}$$

where $\tilde{S}_i$ is evaluated at some average temperature, $\tilde{T}_i$.

Goody argues that, although the derivation was made using a Lorentz shape, the approximation is good for a variety of shapes, and furthermore, for any model, regular or random. A comparison of the approximate optical depth for an atmospheric layer in which the pressure varies from P to 3P, with that from an exact calculation is given in Figure 42.

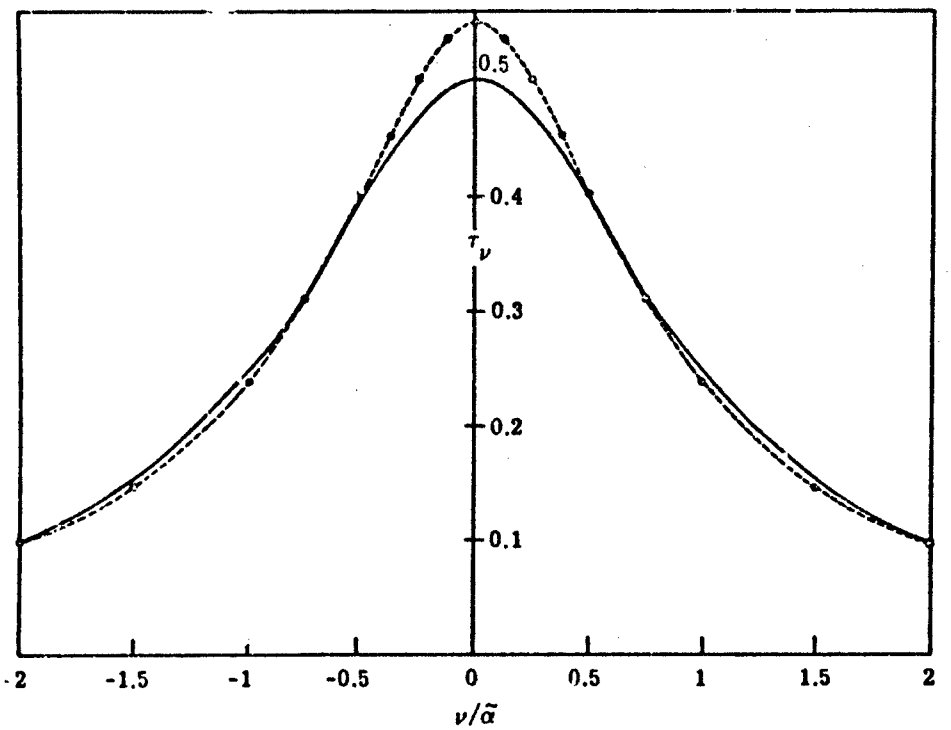

FIGURE 42. OPTICAL DEPTHS FOR A LAYER IN A MIXED ATMOSPHERE WITH $P_1 = 3P_2$. The broken line is an exact computation of the optical depth and the full line uses the Curtis-Godson approximation.

5.2.9.2 Critique of the CG Approximation

Other approximations have been presented for specific investigations, e.g., Yamamoto and Aida [203], Yamamoto, et al. [204], Ellingson (1972) (see Section 7.1, this report), Rodgers and Walshaw (1966), and others. It is beyond the scope of this report to pursue any further detail in the nature of these calculations. The reader is referred to the original documentation on these studies as well as to the original work of the authors of the CG approximation [205], [206].

Several critiques of the methods of approximation, in addition to that by Goody (1964), have been reported, among which are Ludwig, et al. [207], Kyle (1968a), Drayson (1967), Kaplan [208], Weinreb and Neuendorffer [209], and Goody [210], who cites the original approximations of Van de Hulst [211] which predates the work of Curtis and Godson.

A particularly interesting and pertinent discussion of the CG approximation is to be found in a paper by Armstrong [212], in which he expands the expression for the optical depth around a point in the region between two pressure levels, P_1 and P_2, and between which the transmittance is to be calculated. We note that if the hydrostatic approximation can be assumed in the region of the calculation, then:

$$-g\rho_{air}\,dz = dP \tag{213}$$

203. G. Yamamoto and M. Aida, "Transmission in a Non-Homogeneous Atmosphere with an Absorbing Gas of Constant Mixing Ratio," J. Quant. Spec. Rad. Trans., Vol. 10, 1970, pp. 593-608.

204. G. Yamamoto, et al., "Improved Curtis-Godson Approximation in a Non-Homogeneous Atmosphere," J. Atmos. Sci., Vol. 29, 1972, pp. 1150-1155.

205. A. R. Curtis, "Discussion of Goody's 'A Statistical Model for Water-Vapour Absorption'," Quart. J. Roy. Met. Soc., Vol. 58, 1952, p. 638.

206. W. L. Godson, "Spectral Models and the Properties of Transmission Functions," Proc. Toronto Meteor. Conf., 1953, pp. 35-42.

207. C. B. Ludwig, W. Malkmus, J. E. Reardon and J. A. L. Thomson, Handbook of Infrared Radiation from Combustion Gases, NASA Report No. SP-3080, Marshall Space Flight Center, 1973.

208. L. D. Kaplan, "A Method for Calculation of Infrared Flux for Use in Numerical Models of Atmospheric Motion," The Atmosphere and the Sea in Motion, The Rockefeller Institute Press, N. Y., 1959, pp. 170-177.

209. M. P. Weinreb and A. C. Neuendorffer, "Method to Apply Homogeneous-Path Transmittance Models to Inhomogeneous Atmospheres," J. Atmos. Sci., Vol. 30, 1973, pp. 662-666.

210. R. M. Goody, "The Transmission of Radiation Through an Inhomogeneous Atmosphere," J. Atmos. Sci., Vol. 21, No. 6, 1964(b), pp. 575-581.

211. H. C. Van de Hulst, "Theory of Absorption Lines in the Atmosphere of the Earth," Annales d'Astrophys., Vol. 8, 1945, pp. 21-34.

212. B. H. Armstrong, "Analysis of the Curtis-Godson Approximation and Radiation Transmission Through Inhomogeneous Atmospheres," J. Atmos. Sci., Vol. 25, 1968, pp. 312-322.

where g is the acceleration of gravity, ρ_{air} is the air density, and P is the total pressure of the atmosphere at z. Since the incremental path, ds, which a beam traverses can be written as dz/μ (where $\mu = \cos\theta$), the optical depth in terms of the mass absorption coefficient $k(\nu, s)$ is (between points s_1 and s_2).

$$q(\nu) = \int k(\nu, s)\,dw = \int_{s_1}^{s_2} k(\nu, s)\rho\,ds = \frac{1}{\mu}\int_{z_1}^{z_2} k(\nu, z)\frac{\rho}{\rho_{air}}\rho_{air}\,dz$$

$$= \frac{1}{\mu}\int_{z_1}^{z_2} k(\nu, z)M(z)\rho_{air}\,dz$$

where ρ = gas density and M(z) = mixing ratio and using Eq. (213),

$$-q(\nu) = \frac{1}{g\mu}\int_{P_1}^{P_2} k(\nu, P)M(P)\,dP \tag{214}$$

Writing $k(\nu, P)M(P) = S(P)b(\nu, P)$, where b is a line shape factor, we have:

$$-q(\nu) = \frac{1}{g\mu}\int_{P_1}^{P_2} b(\nu, P)S(P)\,dP \tag{215}$$

Expanding $b(\nu, P)$ in a Taylor series around a pressure P', between P_1 and P_2, there results from Eq. (215):

$$-q(\nu) = \frac{1}{g\mu}\left[b(\nu, P')\int_{P_1}^{P_2} S(P)\,dP + \left.\frac{db}{dP}\right|_{P'}\int_{P_1}^{P_2}(P - P')S(P)\,dP\right.$$

$$\left. + \frac{1}{2!}\left.\frac{d^2b}{dP^2}\right|_{P'}\int_{P_1}^{P_2}(P - P')^2 S(P)\,dP + \ldots\ldots\right] \tag{216}$$

Considering the 2nd and higher derivatives as small with respect to the first terms, the value of P' to be used in the first term as the equivalent homogeneous-path pressure is determined by choosing P' so that the second term is zero. This leads to:

$$P' = \frac{\int_{P_1}^{P_2} S(P)P\,dP}{\int_{P_1}^{P_2} S(P)\,dP} \tag{217}$$

which, one should note, is equivalent to Eq. (209) for a single line, the CG pressure. The form of Eq. (216) leads one to speculate what corrections one can make to the CG approximation by not ignoring the higher order terms. The approach is taken by Armstrong in a rather complete assessment of this and other approximations, including integration by Gaussian quadrature. The reader is referred to the paper by Armstrong (1968) for a complete discussion of this subject.

Except for directly integrating Eq. (214) through the path, which is usually not done because of the complexity of the computation, the CG approximation, or adaptations of it, is essentially the chief one used in the models which have had greatest exposure to the user. As stated above, there have been many examinations of the confidence with which one may use the CG approximation (see, for example, Fig. 42). Armstrong has plotted the percent difference between the exact calculation and the CG approximation evident in the curves of Figure 42. This result is reproduced in Figure 43, along with the corrected CG approximation obtained by taking into consideration a correction term in the Taylor expansion of the absorptance. Included also is the result obtained by applying Gaussian quadrature to the integral representing the optical depth.

5.2.9.3 Summary

The Curtis-Godson (CG) approximation seems to have withstood the test of hundreds of applications, which has made it the basis of nearly all calculations of atmospheric transmittance in slant paths. It is obviously not exact, and the accuracy of any results obtained by using it are open to question depending on the degree of derivation from the conditions upon which it was derived. The strong-line and weak-line conditions were invoked in its derivation, so that under intermediate conditions, the results should be expected to deviate from those obtained from an exact calculation.

Similarly, in the Taylor series approximation, the CG approximation resulted from a neglect of higher order terms, which should be consistent with an adherence to the weak- and strong-line criteria. Even with its shortcomings, however, the use of the CG approximation, or any counterpart to it, is essential for the calculation of transmittance in the atmosphere when band models are used.

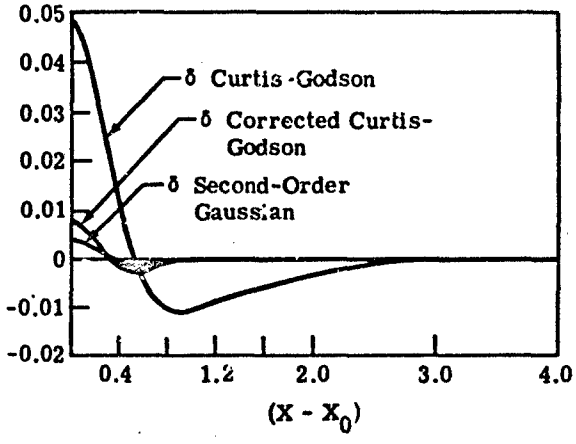

FIGURE 43. THE ERROR, $\delta_X = \tau_X$ (EXACT) - τ_X (APPROXIMATE), IN THE OPTICAL DEPTH FOR A LORENTZ LINE FOR SEVERAL APPROXIMATIONS TO THE PRESSURE INTEGRAL, AS A FUNCTION OF THE REDUCED FREQUENCY $x - x_0$ RELATIVE TO THE LINE CENTER. The base pressure P_1 of the atmospheric slab has the value 3.0, and the pressure P_2 at the top equals 1.0 (after Goody, 1964 [28], Fig. 6.1).

6

DETAILS OF THE LINE-BY-LINE METHOD OF CALCULATION

6.1 JUSTIFICATION OF THE METHOD - BAND MODEL LIMITATIONS

In setting the stage for the calculations that he reported for his doctoral dissertation, Drayson (1967), while asserting the importance of band models for certain atmospheric transmittance calculations, observed that they have limitations which need not necessarily be accepted today in view of the relative practicability of the method of direct integration. His list of limitations on band models include the following:

"(i) The spectral resolution of the transmittances is finite: for the Elsasser model it is a multiple of the line spacings, while the statistical model must use an averaging interval sufficiently large to ensure that the true distribution of the lines is adequately simulated by the statistical distribution. The finite resolution introduces further complications for atmospheric slant paths.

"(ii) Many band models do not allow for accurate contributions of the wings of lines lying outside the spectral region under consideration.

"(iii) The actual distribution of lines can only be approximated by the band models. In some regions, e.g., near Q-branches, it is extremely difficult, if not impossible, to accurately account for the complex distribution of lines. The development of the Quasi-Statistical or Quasi-Random model by Kaplan [213] and Wyatt, et al. (1962) has done much to overcome these objections. The resolution of the transmittances (for the quasi-random model) can be made arbitrarily small, the wings are accurately allowed for and the actual distribution of lines can be approached for sufficiently small averaging interval. It shares one problem with the other models:

"(iv) When the models permit accurate calculation of the absorption due to a real absorption band, the complexity and length of calculation is considerable, even for the Lorentz line shape. For other line shapes including the mixed Doppler-Lorentz line shape, the complexities are even greater."

According to Drayson, the method of integrating directly over the actual lines in a band was first used for part of the 9.6 μm ozone band by Hitchfield and Houghton [214], and later by other investigators. He (Drayson) cites the advantages as follows:

---

213. L. D. Kaplan, "A Quasi-Statistical Approach to the Calculation of Atmospheric Transmission," Proc. Toronto Meteor. Conf., 1953(b), pp. 43-48.

214. W. Hitschfield and J. T. Houghton, "Radiation-Transfer in the Lower Stratosphere Due to the 9.6 Micron Band of Ozone," Quart. J. Roy. Meteor. Soc., Vol. 87, 1961, pp. 562-577.

"(i) The resolution is not limited; the transmissivities may be weighted by an instrumental response function and compared with high resolution experimental spectra.

"(ii) There is considerably more flexibility in the calculations, especially when extended to non-homogeneous paths.

"(iii) The actual distribution of line positions and intensities is used and all contributions from the wings of distant lines are accurately included."

Drayson does not point out, however, that when the size of the band is large, the cost of performing a direct integration is considerably larger than calculation by band models, a factor which usually enters into any decision regarding the method to take in calculation. In addition, relevant and reliable line parameters are sometimes unavailable.

6.2 DRAYSON'S METHOD

6.2.1 PRELIMINARY SETUP

Drayson's model was designed expressly to calculate long-wave radiative transfer in a plane parallel atmosphere. His ultimate purpose was to calculate cooling rates in given atmospheres, so it was necessary to take the radiative transfer equation (see Section 2) beyond the stage for calculating simply path (or sky) radiance, and integrate the flux across horizontal surfaces. He considered only molecular absorption and obtained for the radiant exitance, M, the value (assuming no azimuthal variation):

$$M(P) = 2\pi \int_{\nu} \int_{\mu=-1}^{+1} L(\nu, q, \mu)\, \mu\, d\mu\, d\nu \tag{218}$$

with:

$$L(\nu, q, \mu) = L^*(\nu, T_g) e^{-(q_g - q)/\mu} + \int_{q}^{q_g} J(\nu, q) e^{-(t-q)/\mu} \frac{dt}{\mu} \qquad \text{for } (\mu > 0) \tag{219}$$

$$L(\nu, q, \mu) = \int_{0}^{q} J(\nu, t) e^{-(t-q)/\mu} \frac{dt}{\mu} \qquad \text{for } (\mu < 0) \tag{220}$$

where P is the pressure at some horizontal surface, the subscript, g, denotes ground level, and the other terms are as defined in Section 2.

The loss of flux per unit area over a layer is then determined by taking the difference between M(P) at the top and bottom of the layer, where, by substitution:

$$M(P) = 2\pi \int_{\nu} \left\{ \int_{0}^{1} \left[L^*(\nu, T_g) e^{-(q_g - q)/\mu} + \int_{q}^{q_g} J(\nu, t) \mu e^{-(t-q)/\mu} \frac{dt}{\mu} \right] d\mu \right.$$
$$\left. + \int_{-1}^{0} \left[\int_{0}^{q} J(\nu, t) e^{-(t-q)/\mu} \frac{dt}{\mu} \right] d\mu \right\} d\nu \qquad (221)$$

In order to set up equation (221) for closed-form integration, Drayson specified each of the μ-dependent integrals in terms of the exponential integral which has the form [215]:

$$E_n(x) = \int_{0}^{1} e^{-x/\mu} \mu^{n-1} \frac{d\mu}{\mu} \qquad \begin{matrix} n = 0, 1, 2, \ldots \\ x \geq 0 \end{matrix} \qquad (222)$$

and then devised a means of expanding the E_n in a series of polynomial approximations [216]. Comparison of Eq. (222) with (221) yields the expression for M(P) in terms of the exponential integral. Then, applying the expression,

$$\frac{dE_n(x)}{dx} = -E_{n-1}(x)$$

after integrating by parts the resultant of the combination of Eqs.(221) and (222), Drayson obtains:

$$M(P) = 2\pi \int_{\nu} \left\{ \left[L^*(\nu, T_g) - J(\nu, q_g) \right] E_3(q_g - q) + E_3(q) J(\nu, 0) + \int_{0}^{q_g} \frac{dJ}{dt} E_3(|t - q|)\, dt \right\} d\nu \qquad (223)$$

Using other recurrence relations (see Abramowitz and Stegun, 1964) on the derivative of M, one gets for the divergence of flux at a given layer, for which P is the pressure:

$$\frac{dM}{dP} = 2\pi \frac{d\mu}{dP} \int_{\nu} k_{\nu} \left\{ \int_{q}^{q_g} E_2(t - q) \frac{dJ}{dt}\, dt - \int_{0}^{q} E_2(q - t) \frac{dJ}{dt}\, dt - E_2(q) J(\nu, 0) \right\} d\nu \qquad (224)$$

Drayson used the polynomial approximation to the exponential integral for the zenith angle integration to avoid as many approximations as possible, and, incidentally, to enjoy a

215. M. Abramowitz and I. A. Stegun, Handbook of Mathematical Functions, National Bureau of Standards, Applied Math. Series No. 55, Washington, D. C., 1964.

216. S. R. Drayson, "Polynomial Approximations of Exponential Integrals," J. Quant. Spect. Rad. Trans., Vol. 8, 1968, pp. 1733-1738.

saving in computer time (average about 0.24 ms on the IBM 7090) over the computer system subroutine for the exponential function. The polynomial approximation is given by (for $q \equiv X$):

$$P_M(q) = \sum_{i=0}^{N} A_i q^i$$

for the interval q_1 to q_2, where the q's are the optical depths. Tables of polynomial coefficients for $E_2(X)$ $E_3(X)$ and $E_4(X)$ for given intervals X_1, X_2 are reproduced respectively in Tables 21, 22 and 23 from Drayson (1968). Armstrong [217] acknowledges that Drayson's method provides a very fast means of calculating the exponential integrals, but cautions that in some applications in radiative transfer, the accuracy (which, incidentally, is within about 1×10^{-7}) may not be sufficient. As alternatives, he cites approximations by Cody and Thatcher [218]; and Gaussian quadrature as applied in privately published work (Dave, [219] and Armstrong and Dave [220]). These alternative methods, however, are slower than Drayson's and the accuracy is not needed in the light of other special calculation techniques.

Because of Drayson's interest in cooling in the mesosphere, mesopause, and lower thermosphere due to absorption by the 15 μm band of CO_2, his coverage of the spectrum is somewhat limited; and furthermore, because of the atmospheric regime covered, depends heavily on non-equilibrium processes. The method of calculation is general, however, and is not applications-oriented. The only bands used for calculating rotational line parameters were those tabulated in Table 24 with isotopic relative abundances as given in Table 25. The value used for the Lorentz half-width was 0.08 cm^{-1} at 1 atm and 300 K. For specific details of the theoretical approaches used to formulate methods of calculation of cooling rates and for the results of calculations, the reader is referred to the thesis by Drayson [1967], published as a University of Michigan report for the National Science Foundation.

The significant factor in Drayson's calculation, as far as this section of this report is concerned, is the method of calculating the effect of molecular absorption. In order to perform the calculation in the line-by-line, direct integration method, he used line parameters previously compiled at The University of Michigan (Drayson and Young, 1967). Flux divergence was determined by taking finite differences of the flux equation which was written for numerical evaluation in the form:

217. B. H. Armstrong, "Exponential Integral Approximations," J. Quant. Spect. Rad. Trans., Vol. 9, 1969, pp. 1039-1040.

218. W. Cody and H. Thatcher, Jr., Math. Comp., Vol. 22, 1968, p. 641.

219. J. Dave, A Subroutine for Evaluation of the Exponential Integral with Fifteen Significant Figure Accuracy, Rept. No. 320-3251, IBM Palo Alto Science Center, Palo Alto, Calif., 1968.

220. B. H. Armstrong and J. Dave, Gaussian Quadratures of the Exponential Integral, Rept. No. 320-3250, IBM Palo Alto Sci. Center, Palo Alto, Calif., 1969.

TABLE 21. POLYNOMIAL COEFFICIENTS FOR THE APPROXIMATION OF $E_2(X)$. (From Drayson, 1968 [216].)

X1	X2	M	A(0)	A(1)	A(2)	A(3)	A(4)	A(5)	A(6)
.005	.01	5	.998638546E+00	-.649649842E+01	.286999844E+03	-.70230211E+05	.929872275E+06	-.18864517E+08	
.01	.02	5	.997198845E+00	-.57667626E+01	.14015630E+03	-.48733795E+04	.11095948E+06	-.11211459E+07	
.02	.03	5	.995170477E+00	-.52178244E+01	.81215706E+02	-.16637561E+04	.22506892E+05	-.13650376E+06	
.03	.05	5	.992274778E+00	-.47562499E+01	.50897054E+02	-.65548040E+03	.55339225E+04	-.20871535E+05	
.05	.08	5	.987434395E+00	-.42707709E+01	.31161615E+02	-.24919867E+03	.13013803E+04	-.30413637E+04	
.08	.14	5	.978908239E+00	-.37515615E+01	.18314077E+02	-.8771[illegible]E+02	.27097516E+03	-.37351801E+03	
.14	.25	6	.966177789E+00	-.32935617E+01	.11633582E+02	-.38542[illegible]E+02	.90594735E+02	-.12506067E+03	.75047664E+02
.25	.40	6	.942329031E+00	-.27602169E+01	.66185589E+01	-.13265705F+02	.18236745E+02	-.14695374E+02	.31126970E+01
.40	.70	6	.910025407E+00	-.23189262F+01	.40972991E+01	-.55123669E+01	.9C594481E+01	-.2737773RE+01	.65312935E+00
.70	1.00	5	.832571516E+00	-.18824257E+01	.18822436E+01	-.13316793F+01	.56534096E+00	-.97555565E-01	
1.00	1.50	6	.799444199E+00	-.14714204E+01	.14733368E+01	-.95177859E+00	.39167846F+00	-.93110982E-01	.97039862E-02
1.50	2.50	6	.676807997E+00	-.10419146F+01	.78456730E+00	-.35571203F+00	.98812997E-01	-.15521811E-01	.10573[illegible]E-02
2.50	4.00	6	.482616395E+00	-.57616476E+00	.31201474E+00	-.96201227E-01	.17[illegible]86F-01	-.17639563E-02	.7598887[illegible]E-04
4.00	6.00	6	.253148620E+00	-.22816343F+00	.89305074E-01	-.19262687F-01	.23975807F-02	-.16236047E-03	.4[illegible]299556E-05
6.00	8.00	5	.615207229E-01	-.36981421E-01	.90654130E-02	-.11287050F-02	.71170588F-04	-.18139326E-05	
8.00	10.00	4	.762280025E-02	-.30017878E-02	.44776459E-03	-.29916337E-04	.7558R8086E-06		
10.00	12.00	3	.509636095E-03	-.12675641E-03	.10549960E-04	-.29525857E-06			
12.00	14.00	2	.18470210E-04	-.26366002E-05	.94418581E-07				

Reproduced from best available copy.

FORMERLY WILLOW RUN LABORATORIES, THE UNIVERSITY OF MICHIGAN

TABLE 22. POLYNOMIAL COEFFICIENTS FOR THE APPROXIMATION OF $E_3(X)$. (From Drayson, 1968 [216].)

X1	X2	M	A(0)	A(1)	A(2)	A(3)	A(4)	A(5)	A(6)
.00	.01	5	.5000000[illegible]F+00	-.[illegible]F+00	.[illegible]F+01	-.[illegible]F+03	.[illegible]F+04	-.[illegible]F+05	
.01	.05	5	.4998[illegible]E+00	-.[illegible]F+00	.[illegible]E+01	-.[illegible]F+02	.[illegible]F+03	-.[illegible]E+03	
.05	.10	5	.4987[illegible]E+00	-.[illegible]F+00	.[illegible]E+01	-.[illegible]F+01	.[illegible]E+02	-.[illegible]E+02	
.10	.20	5	.4975[illegible]E+00	-.[illegible]F+00	.[illegible]E+01	-.[illegible]E+01	.[illegible]E+01	-.[illegible]E+01	
.20	.40	5	.4937[illegible]E+00	-.[illegible]E+00	.[illegible]E+01	-.[illegible]E+01	.[illegible]E+01	-.[illegible]E+00	
.40	.70	5	.4829[illegible]E+00	-.[illegible]E+00	.[illegible]E+00	-.[illegible]E+00	.[illegible]E+00	-.[illegible]E+00	
.70	1.00	5	.4670[illegible]E+00	-.[illegible]E+00	.[illegible]E+00	-.[illegible]E+00	.[illegible]E+00	-.[illegible]E-01	
1.00	1.50	5	.4422[illegible]E+00	-.[illegible]E+00	.[illegible]E+00	-.[illegible]E+00	.[illegible]E-01	-.[illegible]E-02	
1.50	2.00	4	.4368[illegible]E+00	-.[illegible]E+00	.[illegible]E+00	-.[illegible]E+00	.[illegible]E-01	-.[illegible]E-02	.[illegible]E-03
2.00	4.00	4	.4[illegible]E+00	-.[illegible]E+00	.[illegible]E+00	-.[illegible]E-01	.[illegible]E-01	-.[illegible]E-02	.[illegible]E-04
4.00	6.00	4	.2[illegible]E+00	-.[illegible]E+00	.[illegible]E-01	-.[illegible]E-01	.[illegible]E-02	-.[illegible]E-03	.[illegible]E-05
6.00	8.00	4	.[illegible]E-01	-.[illegible]E-01	.[illegible]E-02	-.[illegible]E-03	.[illegible]E-04	-.[illegible]E-05	
8.00	10.00	4	.6813[illegible]E-02	-.[illegible]E-02	.[illegible]E-03	-.[illegible]E-04	.[illegible]E-05		
10.00	12.00	3	.4474[illegible]E-03	-.[illegible]E-03	.[illegible]E-04	-.[illegible]E-06			
12.00	14.00	3	.1729[illegible]E-04	-.[illegible]E-04	.[illegible]E-07				

Reproduced from best available copy.

FORMERLY WILLOW RUN LABORATORIES, THE UNIVERSITY OF MICHIGAN

TABLE 23. POLYNOMIAL COEFFICIENTS FOR THE APPROXIMATION OF $E_4(X)$. (From Drayson, 1968 [216].)

X1	X2	M	A(0)	A(1)	A(2)	A(3)	A(4)	A(5)	A(6)
.00	.02	3	.33333321E+00	-.49991786E+00	.48723621E+00	-.48065675E+00			
.02	.10	4	.33333145E+00	-.49976349E+00	.48623636E+00	-.54877654E+00	.74277701E+00		
.10	.20	4	.33329039E+00	-.49810931E+00	.46314345E+00	-.28876234E+00	.73942719E+00		
.20	.40	4	.33306695E+00	-.49366872E+00	.42746140E+00	-.27717782E+00	.10435406E+00		
.40	.70	5	.33293226E+00	-.48847193E+00	.41709314E+00	-.26007767E+00	.11597315E+00	-.23091905E-01	
.70	1.00	4	.33261509E+00	-.44764367E+00	.30548652E+00	-.11924892E+00	.21083163E-01		
1.00	1.50	5	.33369356E+00	-.44028710E+00	.30183790E+00	-.12713362E+00	.31436526E-01	-.34847976E-02	
1.50	2.50	6	.33416286E+00	-.40980441E+00	.26366584E+00	-.10465057E+00	.26191493E-01	-.38026567E-02	.24618347E-03
2.50	4.00	6	.26476057E+00	-.29454781E+00	.14995841E+00	-.43917471E-01	.76716891E-02	-.74718008E-03	.31347324E-04
4.00	6.00	6	.16347763E+00	-.14351490E+00	.44817252E-01	-.11618356E-01	.14224296E-02	-.94471422E-04	.26884469E-05
6.00	8.00	5	.45803090E-01	-.27338178E-01	.66409363E-02	-.82506626E-03	.51796873E-04	-.13152097E-05	
8.00	10.00	4	.61685433E-02	-.26149872E-02	.35942825E-03	-.23983799E-04	.60455421E-06		
10.00	12.00	3	.43135188E-03	-.10716388E-03	.89272471E-05	-.24915099E-06			
12.00	14.00	2	.16129848E-04	-.23012068E-05	.82365827E-07				

FORMERLY WILLOW RUN LABORATORIES, THE UNIVERSITY OF MICHIGAN

TABLE 24. BAND STRENGTHS USED IN CALCULATING ROTATIONAL LINE INTENSITIES. (From Drayson, 1967 [8].)

	Level		Band Center	Strength
	Lower	Upper	($^{12}C\ ^{16}O_2$)	($cm^{-1}(atm\ cm)^{-1}$ at 300°K)
1	000:0	010:1	667.379	194
2	010:1	020:0	618.033	4.27
3	010:1	100:0	720.808	6.2
4	010:1	020:2	667.750	15.0
5	020:0	030:1	647.054	1.0
6	020:0	110:1	791.447	0.022
7	020:2	030:1	597.337	0.14
8	020:2	110:1	741.730	0.14
9	020:2	030:3	668.151	0.85
10	100:0	110:1	688.672	0.3
11	100:0	030:1	544.279	0.004
12	030:3	040:2	581.62	0.0042
13	030:3	120:2	757.47	0.0059
14	030:1	120:2	828.284	0.00049
15	030:1	120:0	738.364	0.014

TABLE 25. RELATIVE ABUNDANCE OF ISOTOPIC MOLECULES.(From Drayson, 1967 [8].)

	Molecule	Abundance Relative to $^{12}C\ ^{16}O_2$	Band Center Of Fundamental
0	$^{12}C\ ^{16}O_2$	1.00	667.4
1	$^{13}C\ ^{16}O_2$	1.12×10^{-2}	648.5
2	$^{12}C\ ^{18}O\ ^{18}O$	4.0×10^{-3}	662.3
3	$^{12}C\ ^{16}O\ ^{17}O$	8.0×10^{-4}	664.7
4	$^{13}C\ ^{16}O\ ^{18}O$	4.5×10^{-5}	643.6

$$M_m = 2\pi\left\{J(\nu, 0)\left[\int_\nu E_3(|q_m)\,d\nu\right] + \sum_{i=1}^{N}\Delta J_i\left[\int_\nu \frac{1}{\Delta q_i}\,|E_4(|q_m - q_i|)\right.\right.$$

$$\left.\left. - E_4(|q_m - q_{i-1}|)\,d\nu\right]\right\} \qquad (225)$$

for which the atmosphere is considered as divided into homogeneous layers, in which the source function is approximated by a polynomial in some vertical varying parameter, e.g., pressure. For details see the full report of this work. The factor of significance to this state-of-the-art report is the method of integrating the function over frequency, in which the line parameters are implicit in Eq. (225).

6.2.2 TRANSMITTANCE CALCULATION

For carrying out the integration in frequency of, say, Eq. (225), which is essentially a calculation of transmittance or absorption, another work by the same author is cited [221], in which the integration was exemplified in finding the average value of transmittance $\bar{\tau}$ in the frequency interval ν_1 to ν_2. As has already been seen there are a number of lines $k_i(\nu) = S_i b_i(\nu_1, \nu)$ in the interval ν_1 to ν_2 which contributed to the absorption, all characterized, among other things, by their centers, ν_i. The basis for the direct integration technique is to find an efficient way of numerically integrating the monochromatic transmittances in the band between ν_1 and ν_2. The setup of equations is given in the text of the U of M report (Drayson, 1967), but the specific details of the integration over frequency, which are of importance to the current state-of-knowledge, are referred to in the earlier work by Drayson and Young (1966). Therefore, it is pertinent to investigate the technique in terms of this earlier work.

A typical application of the integration technique is the weighting of $\tau(\nu)$ over the slit of a spectrometer, namely:

$$\bar{\tau}(\nu^*) = \int_{\nu_1}^{\nu_2} f(|\nu - \nu^*|, a)\tau(\nu)\,d\nu$$

where $f(|\nu - \nu^*|, a)$ is the normalized slit function, and (a) is the slit width at half intensity. Drayson and Young (1966) have applied the technique to the integration of variously broadened lines, although the form of the integrand is not of utmost importance. Shown below is the

221. S. R. Drayson and C. Young, Theoretical Investigations of Carbon Dioxide Radiative Transfer, Report No. 07347-1-F, University of Michigan, Ann Arbor, 1966.

complexity of the expressions for which the integrations over frequency were carried out, and in which the integration $\int_{P_1}^{P_2} k_i(\nu)\,dw$ is performed over the pressure range P_1 to P_2 to yield (for constant absorber-to-air mixing ratio and constant temperature):

$$\tau_i(\nu) = \int k_i(\nu)\,dw = \frac{cS_i}{2\pi\alpha_{L0}} \ln\left[\frac{\alpha_{L0}^2 P_2^2 + (\nu - \nu_i)^2}{\alpha_{L0}^2 P_1^2 + (\nu - \nu_i)^2}\right] \tag{226}$$

for Lorentz broadening,

where P_1 and P_2 are the pressures at the upper and lower boundaries of the layer

$c = dw/dP$

S_i is the mean line strength

α_{L0} is the line half-width per unit pressure at standard conditions

For the mixed Doppler-Lorentz broadening, a similar integration over pressure yields (for the conditions stated above):

$$\tau_i(\nu) = \frac{k_0 c}{2\pi u_0} \int_{-\infty}^{\infty} e^{-t^2} \ln\left[\frac{u_0^2 P_2^2 + (y - t)^2}{u_0^2 P_1^2 + (y - t)^2}\right] dt \tag{227}$$

where $y = \dfrac{(\nu - \nu_i)}{\alpha_D}\sqrt{\ell n 2}$ (α_D = Doppler half-width)

$u = \dfrac{\alpha_{Li}}{\alpha_D}\sqrt{\ell n 2}$ (α_L = Lorentz half-width = $\alpha_{L0}P$)

$u = u_0 P$

$k_0 = \dfrac{S_i}{\alpha_D}\sqrt{\dfrac{\ell n 2}{\pi}}$

The optical depth is obtained by summing up over all lines and over the path between the points in the atmosphere for which the transmittance is to be determined. Or, the atmosphere can be subdivided into homogeneous layers and a Curtis-Godson approximation (see Section 5) is used over each layer.

The evaluation of the frequency integral can be done numerically by using an appropriate quadrature formula, either a high-order one over the whole interval of integration, or a low-order one over successive portions of the interval. Drayson and Young (1966) have chosen the

latter because of the rapid fluctuation of $k(\nu)$. They found by a process of trial and error that 4-point Gaussian quadrature could be applied successfully to Lorentz or Voigt profiled lines near the centers over the intervals bounded by points 0.0, 0.001, 0.002, 0.003, 0.005 and 0.01 cm^{-1} on either side of the line center. The narrowness (0.001 cm^{-1}) of interval is required at low pressures but could be made wider for application in the troposphere. Four-point quadrature yielded accuracy of four decimal places in transmittance, whereas lower order quadrature introduced considerable error because of the rapid decrease in the absorption coefficient away from the line center. In the region between lines, away from line centers the variation of $k(\nu)$ is not as great, so that a coarser interval of integration may be used, specifically, 0.01 cm^{-1} subintervals for a distance of from 0.04 to 0.05 cm^{-1} from line centers, and 0.1 cm^{-1} subintervals elsewhere. In order to avoid round-off errors in the computer, the line frequencies were read in the computer to two decimal places, multiplied by 100, and converted from floating point to integer mode. To calculate the absorption in any 1 cm^{-1} interval, the frequencies were converted back to floating point, relative to the center of the interval. By calculating all frequencies relative to this point, the difference between neighboring frequencies could be accurately found.

It is important to note, and often overlooked, that Gaussian quadrature is used because the highest order approximation can be achieved for the smallest number of points.

Drayson and Young do not specify Eq. (227) for the calculation of transmittance using the Doppler-Lorentz broadening, but refer instead, for slant-path calculation, to the expression prior to pressure integration, namely:

$$\tau_i(\nu) = \int_{P_1}^{P_2} dP \frac{k_0 uc}{\pi} \int_{-\infty}^{\infty} \frac{\exp[-t^2]}{u^2 + (y - t)^2} dt \qquad (228)$$

They refer to a paper by Young (1965) for a description of the method for solving

$$k_i(\nu) = \frac{k_0 u}{\pi} \int_{-\infty}^{\infty} \frac{\exp[-t^2]}{u^2 + (y - t)^2} dt$$

A newer, much faster method (Drayson, [222]) is currently being used. In the earlier work, four-point Gauss-Hermit quadrature was used with $y \geq 7.0$ and u positive. For the other regimes: $u \leq 1.0$, $y < 7.0$ and $u > 1.0$, $y < 7.0$, the reader is referred to the paper by Young (1965). See also Section 5 of this report.

222. S. R. Drayson, Private communication, 1974.

Because there are so many lines over which the calculation must be made (see, for example, Fig. 27), approximations and other short-cuts must be performed to keep down the computer costs. A straightforward numerical integration over the AFCRL lines, for which a computer program is given in the AFCRL report (McClatchey, et al., 1973), requires a very large expenditure of computer time, with an average cost without short-cuts of a little under $1.00 per wavenumber, a cost which can escalate rapidly if the spectral region required is of any reasonable size. It must be realized, of course, that this cost depends on a number of factors, not the least important of which is the number of lines in a particular band.

Drayson and Young (1966) simplify their calculation by assuming the Lorentz half-width for the 15 μm band of air-broadening CO_2 to have the constant value of 0.08 cm^{-1} at 1 atm and 300 K, as the result of comparisons between the suggested values of different investigators In later work on radiative transfer, a variable half-width has been used. They used the pure Lorentz shape for pressures greater than 0.1 atm, and the mixed Doppler-Lorentz (Voigt) profile for pressures less than 0.1 atm. The Lorentz shape was used for $|\nu - \nu_1| > 0.2$ cm^{-1}. The Doppler half-width, which varies with frequency, changes sufficiently little to be effectively constant over a 1 cm^{-1} interval, the value being that calculated for the center of the interval. In the case of a constant-pressure path the quadrature calculation is applied to the line with these parameters in the vicinity of the line center as outlined above for whatever pressure is desired. For the layered atmosphere, the Curtis-Godson pressure for each layer is determined and the calculation performed for these pressures. This procedure yields more accurate results than obtaining the Curtis-Godson approximation over the entire path.

For lines whose centers are further than 3.5 cm^{-1} from the center of the 1 cm^{-1} interval considered above, an interpolation is preformed to determine their contributions to the interval from the wing contributions of the line evaluated at the midpoint and the two end points of the 1 cm^{-1} interval. The reason is that the variation of this part of a line over a 1 cm^{-1} interval is small, and much time is saved. These contributions will vary with temperature, so the calculations are made for six temperatures: 300, 275, 250, 225, 200 and 175 K. The interpolation is made over wavenumber and temperature to determine the wing contributions. In this way, the wing contribution can be included accurately (i.e., there is no need for an arbitrary cut-off); and non-Lorentz shapes can be used if desired. Thus, much CPU and storage time is saved without a compromise on accuracy.

Two further interpolation procedures are used for the absorption coefficient:

(a) Over 0.1 cm^{-1} intervals some lines closer than 3.5 cm^{-1} do not vary much in their contributions. So a computation is made for the sum of the absorption coefficients of these lines at the center of the interval and the two end points. The interpolation is made over wavenumber as required. Currently, the bounding value is 0.8 cm^{-1}, but this can be adjusted.

(b) Near the line center ($\nu_0 \pm 0.01$ cm^{-1}) using the small subintervals described earlier, an interpolation can be made for lines more distant than 0.1 cm^{-1} from the line center. These interpolations save much computer time without loss of accuracy.

6.3 THE METHOD OF KUNDE AND MAGUIRE

6.3.1 APPLICATION

The most recent calculation of Kunde and Maguire (1974) for a direct integration of the transmittance parameters is similar in procedure to that proposed by Drayson (1967). The application of the results was somewhat different, however, and many of the particulars in the use of approximations are peculiar to the use of the results. For example, Kunde and Maguire's expression of the radiative transfer equation, shown here as:

$$L_\nu(0) = L_\nu(R)\tau(\nu, R) + \int_0^R L_\nu^*(s)\, d\tau(\nu, s) \tag{229}$$

implies its eventual use in comparing theoretically predicted with experimentally observed radiances in the atmosphere. Their expression for the transmittance through a uniform slab (at pressure, P and temperature, T) is the usual exponential diminution at a specified frequency, in a form suitable for incorporation into their radiative transfer equation:

$$\tau(\nu, s) = \exp\left[-\sum_i k_i(\nu, P, T) w_i\right] \tag{230}$$

where $w = \rho R$ is the absorber amount in distance R. Density of the i-th gas is ρ_i and $k_i(\nu)$ is its absorption coefficient at frequency, ν. The average spectral transmittance over the interval, $\Delta\nu$, is written, as usual:

$$\bar{\tau}_{\Delta\nu} = \frac{\int \tau_\nu \, d\nu}{\Delta\nu} \tag{231}$$

and, with $\Delta\nu$ divided into a variable number of subintervals, k = 1, 2, . . . K, a four-point Legendre-Gauss quadrature (see, for example, Abramowitz and Stegun, 1964) is employed in each subinterval, such that:

$$\bar{\tau}_{\Delta\nu}(s) = \frac{\sum_{k=1}^{K} \frac{\nu_{B_k} - \nu_{A_k}}{2} \sum_{\ell=1}^{4} W_\ell \tau_{k\ell}(\nu, s)}{\Delta\nu} \tag{232}$$

where

$$\nu_{k\ell} = \frac{\nu_{B_k} - \nu_{A_k}}{2} y_\ell + \frac{\nu_{B_k} + \nu_{A_k}}{2}$$

and ν_{B_k} and ν_{A_k} are the upper and lower limits respectively of any subinterval. The W_ℓ and y_ℓ are respectively the weights and abscissae used in Gaussian quadrature.

6.3.2 TRANSMITTANCE CALCULATION

The object of the work reported by Kunde and Maguire was to calculate upwelling spectral radiance, neglecting any scattering effects. In Eq. (229) the lower limit of the path through which the radiance originates is designated as s = 0, and the upper limit (usually the top of the atmosphere) is designated as s = R. The expression for $\tau(\nu)$ to any point s from above the atmosphere is, of course, different from that in Eq. (230) because the path through the atmosphere is variable. Instead, there results:

$$\tau(\nu, s) = \exp\left[-\int_0^s \sum_i k_i(\nu, P, T)\rho_i \, ds'\right] \tag{233}$$

where, for the i-th gas, $w_i = \int \rho_i \, ds'$. The approximation of the integral in a summation leads to:

$$\tau(\nu, s) = \exp\left[-\sum_j \sum_i k_{ij}(\nu, \bar{P}_j, \bar{T}_j)\Delta w_j\right] \tag{234}$$

in which the atmosphere is divided into layers of constant T and constant P (j = 1, 2, . . , J) equal respectively to the average temperature and pressure over each layer. The four-point Legendre-Gaussian quadrature applied to τ over $\Delta\nu$, which is divided into K subintervals (k = 1, 2, . . , K), then yields:

$$\bar{\tau}_{\Delta\nu}(s) = \frac{\sum_{k=1}^{K} \frac{\nu_{B_k} - \nu_{A_k}}{2} \sum_{\ell=1}^{4} W_\ell \tau_{k\ell}(\nu, s)}{\Delta\nu} \tag{235}$$

The numerical approximation to Eq. (229) is:

$$L_\nu(\nu, 0) \cong L_{\Delta\nu}(0)/\Delta\nu = L^*_\nu(\nu, R)\bar{\tau}_{\Delta\nu}(R) + \sum_j \left[L^*_\nu\left(\nu, T(s)\right)\Delta\bar{\tau}_{\Delta\nu}(s)\right] \tag{236}$$

The value is taken at the midpoint of the increment. Thus, the average spectral radiance over the interval, $\Delta\nu$, is obtained from a knowledge of the Planck function at the center of a layer and the calculated transmittances originating at a prescribed set of atmospheric levels, approximately 30 in all, selected to yield nearly equal increments of $\Delta\bar{\tau}$. This results in a succession of levels which vary in incremental distances from 0.5 km at the lower surface to 4 km at the upper limit. The values of $\Delta\bar{\tau}$ are computed (in $\Delta\nu$ intervals of 0.1 cm^{-1}) for increments of 0.1 km by interpolation from the values of $\bar{\tau}_{\Delta\nu}$ computed from the 30 levels.

For comparison with satellite data, Kunde and Maguire averaged the spectral radiance over the presumed slit function of a spectrometer so that:

$$\bar{L}_{\Delta\nu}(\nu^*) = \int_{\nu_1}^{\nu_2} f(|\nu - \nu^*|, a) L_\nu(\nu)\, d\nu$$

where f is the normalized slit function

a is the full width of the slit at half of maximum intensity

ν^* is the center of the slit width,

ν_1, ν_2 are the zero points of the slit function.

In the approximation this integral is evaluated numerically as:

$$\bar{L}_{\Delta\nu}(\nu^*) = \sum_i \bar{f}\left(|\nu_i - \nu^*|, a\right) \bar{L}_{\Delta\nu}(\nu_i)\Delta\nu_i \qquad (237)$$

where $\bar{f}\left(|\nu_i - \nu^*|, a\right)$ is the average value of f over the interval $\Delta\nu_i$, and ν_i is the center of the i-th interval $\Delta\nu_i$. By performing a fast Fourier transform of $\bar{f}$ and $\bar{L}$ the convolution in Eq. (237) can be obtained by the product:

$$\bar{\mathscr{L}}(t) = \bar{F}(t)\cdot\bar{\mathscr{J}}_{\Delta\nu}(t)$$

where t is time, and $\bar{\mathscr{L}}$, $\bar{F}$ and $\mathscr{J}$ and the Fourier transforms of their respective functions.

6.3.3 SETUP OF THE PROGRAM

The outline of the numerical algorithm for determining $\bar{L}$ is taken directly from a preprint of Kunde and Maguire's paper on the direct integration of transmittance [223] as follows:

"1. Specify atmospheric model, vertical temperature profile, vertical gas concentration, and surface pressure.

"2. Specify molecular absorbing gases and appropriate line parameters.

223. V. G. Kunde and W. C. McGuire, Direct Integration Transmittance Model, NASA Report No. X-622-73-258, Goddard Space Flight Center, Greenbelt, Md., 1973.

"3. Set up vertical matrix of atmospheric temperatures, atmospheric effective pressures, and optical path lengths for each absorbing gas for each atmospheric layer.

"4. Determine the average transmittance for a 0.1 cm^{-1} interval for J atmospheric levels from Eq. (234) and (235).

"5. Determine the emergent radiance for each 0.1 cm^{-1} interval from Eq. (236) across the spectral region of interest.

"6. Determine the emergent radiance averaged over the instrument function as specified in Eq. (237) for comparison to the observed spectrum.

This algorithm has been programmed entirely in Fortran IV for an IBM 360 operating system."

In a manner similar to that by Drayson, Kunde and Maguire perform an integration over all the lines of the atmospheric molecules by considering two regimes over each line, namely (1) that region containing $\Delta\nu < \delta$, and (2) that containing $\Delta\nu \geq \delta$, where δ is a prescribed distance from the line center Specifically, for $\Delta\nu < \delta$ the quadrature points are closely spaced; for $\Delta\nu \geq \delta$ the quadrature points are spaced farther apart. The details in the Kunde and Maguire report are explicit and should be sought by the reader who has more than a passing interest. The expression for the absorption coefficient at a given frequency resulting from the accumulation of the effects of m lines of the i-th gas in the j-th layer with appropriate intensity is (see Eq. (234)):

$$k_{ij}(\nu_{k\ell}, \overline{P}_{ej}, \overline{T}_j) = \sum_m S_{im}(\overline{T}_j) b_{im}(\overline{P}_{ej}, \overline{T}_j) + k_i^o(\nu_{k\ell}, \overline{T}_j)\overline{P}_{ej}/P_r \qquad (238)$$

(Recall that k and ℓ refer respectively to the subdivision $\Delta\nu$, and the order of quadrature.) $\overline{P}_{ej}$ is the average effective pressure in the j-th layer, where $P_e = P + (B - 1)p_a$, such that P is the total pressure, p_a is the partial pressure of the absorbing gas and B is the self-broadening coefficient. The subscript r refers to reference conditions, i.e., conditions under which the line parameters were initially determined. The first term in Eq. (238) refers to that portion of all the line shapes at ν for which the distance, $\Delta\nu$, from a line center is less than δ(=3.5 cm^{-1}) The line shape $b_m(\overline{P}_e, \overline{T})$ is the mixed Lorentz-Doppler shape given as:

$$b(u, y) = \sqrt{\frac{\ell n 2}{\pi}} \frac{1}{\alpha_D} H(u, y)$$

$\left(u = \frac{\alpha_L}{\alpha_D}\sqrt{\ell n 2}$ and $y = \left[\frac{\nu - \nu_0}{\alpha_D}\right]\sqrt{\ell n 2}\right)$ when the distance from the line center is less than 0.2 cm^{-1}, and the pressure is less than 100 mb. The Lorentz line shape was used otherwise. The function H(u, y) was evaluated according to a numerical procedure given by Young (1965).

The second term in Eq. (238) corresponds to that portion of the lines effective at ν for which $\Delta\nu > \delta$. Since in this region the modified Lorentz shape is sufficiently accurate, the $k^o(\nu)$ is given by:

$$k^o(\nu) = \sum_{in} \frac{S_m(T)\alpha_{Lm}(P_r, T_r)}{\pi\left(\nu - \nu_{0_m}\right)^2}\left(\frac{T_r}{T}\right)^{\gamma} \tag{239}$$

γ is given here as 0.5.

As in the integration performed by Drayson and Young (1966), each quadrature calculation was made in intervals prescribed to keep the computer time to a minimum, while keeping the accuracy as high as possible. So instead of retaining a coarse quadrature interval and compromising accuracy, or a fine interval and sky-rocketing computer costs, the variable interval was tailored to the exact shape of the line. An excellent description of the frequency mesh used to perform the numerical integration on the spectral transmittance over $\Delta\nu$, taken from Kunde and Maguire (1973), is shown in Figure 44, in which the schematic representation of the central part of the line shape is severely distorted.

The interval chosen for $\Delta\nu$ is 0.1 cm^{-1}, which, therefore, limits the ultimate resolution. This is considered, however, to be always much smaller than the instrumental spectral resolution. This interval is subdivided for quadrature into smaller intervals, the fineness of the subinterval being determined by its closeness to the center of a line; namely, that which yields a mesh of about 0.001 cm^{-1} in the immediate vicinity of the center and 0.1 cm^{-1} interval in the wings. The scheme for dividing up the 0.1 cm^{-1} interval is shown in Figure 44. When there are no lines falling closer to the interval than δ, the four-point quadrature is performed over the entire 0.1 cm^{-1} interval as shown in Figure 44(a). The quadrature points are shown normally as short vertical marks at the bottom of the scale. If one line appears in the interval, it is divided up as shown into two intervals, d_1, on either side of the line center, and into d_2 and d_3 on either side of d_1. (See Fig. 44(b).) Each interval, d_1, is further subdivided into two parts and four-point Legendre-Gaussian quadrature performed on these parts. The accuracy in the transmittance is alleged to be good to two or three significant figures. Four-point Legendre-Gaussian quadrature is also performed on the intervals designated d_2 and d_3.

When there are two or more lines in the 0.1 cm^{-1} interval, the integration is performed as shown schematically in Figure 44(c). The major difference between this and the case with one line is the interval, circle 6, between lines. This interval is designated as d_4. Thus, in summary, when there are no lines in the 0.1 cm^{-1} interval, it is divided up into a total of four quadrature points. With one line in the interval, the total number of mesh points is 24; and with two lines in the interval the number of points is 44. There are correspondingly more points as the number of lines in the interval increases.

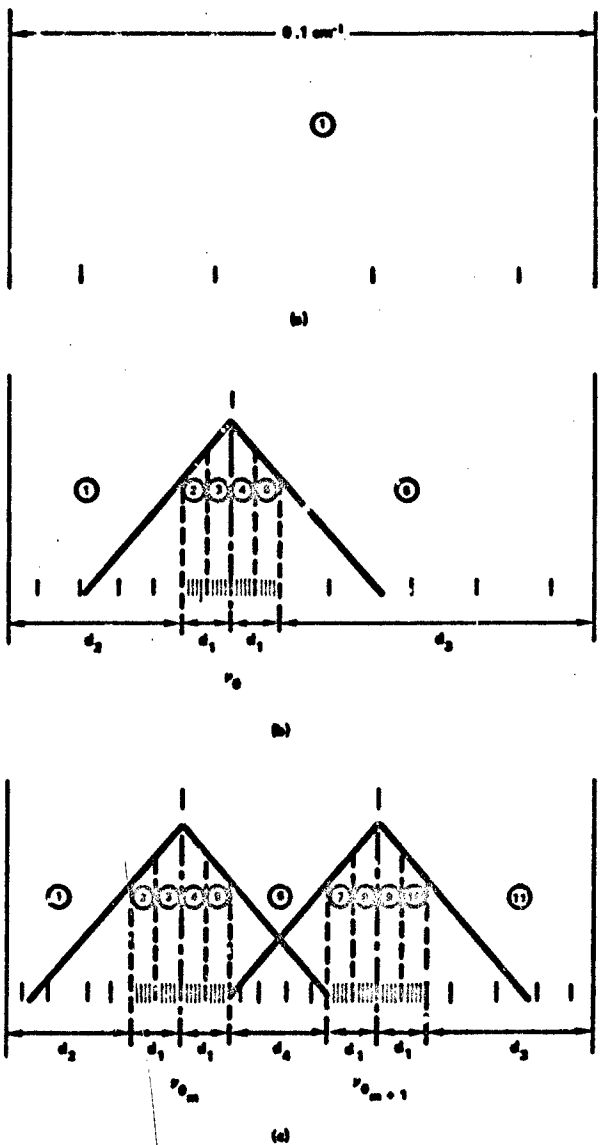

FIGURE 44. SCHEMATIC OF VARIABLE WAVE NUMBER MESH FOR 0.1 cm^{-1} INTERVAL WITH TWO SUB-INTERVALS IN d_1. (a) No molecular lines, 4 mesh points; (b) one molecular line, 6 sub-intervals; (c) two molecular lines, 11 sub-intervals, 44 mesh points. (Reproduced from Kunde and McGuire, 1974 [9].)

6.3.4 SOME RESULTS

Kunde and Maguire specify in their paper the number and types of line parameters used in their program. The AFCRL line compilation, however, can be readily adapted. Some comparisons where made with experimental data, of which three examples are shown in Figures 45, 46, and 47, taken from the report by Kunde and Maguire (1974). These figures depict, respectively, the homogeneous-path transmittance for CO_2, H_2O and O_3. In accordance with experimental evidence, modifications to the line shape were made to account for the reduced absorption by CO_2 in the continuum region within the 780-900 cm^{-1} range, but not shown in Figure 45. Thus for all CO_2 lines in the 500 to 800 cm^{-1} region, the line shape took the form:

$$\begin{aligned} b &= b_{Lorentz} && \text{for } |\nu - \nu_0| \le \nu_{min} \\ b &= b_{Lorentz} \exp\left[-a(|\nu - \nu_0| - \nu_{min})^b\right] && \text{for } |\nu - \nu_0| > \nu_{min} \end{aligned} \tag{240}$$

with $\nu_{min} = 3.5$ cm^{-1} from the line center. Best fit to the data was obtained with a = 1.4 and b = 0.25. Kunde and Maguire claim an agreement of better than 10% and suggest that the discrepancy in the Q-branch regions is more indicative of an incomplete knowledge of the instrument slit function than of a true difference in transmittance as determined theoretically and experimentally.

Much greater care, based on the results of several years of experimental and theoretical investigations, was exercised in generating the proper parameters for the continuum in H_2O. Shown in Figure 48 are the values adapted for the foreign- and self-broadening coefficients used in

$$\chi\left(P, p_{H_2O}, T\right) = k_1(T)P + k_2(T)p_{H_2O}$$

(P_{H_2O} is the partial pressure of H_2O vapor) to obtain the transmittance in the H_2O continuum regions between 400 and 1500 cm^{-1}. Comparison of results, however are shown between the values obtained by calculation and by experiment in the 1595 cm^{-1} H_2O band. The difference in apparent structure on either side of the center of the band is the result of a change in resolution from 5 cm^{-1} at 1200 cm^{-1} to 20 cm^{-1} at 2000 cm^{-1}. The agreement is better than 5%.

Comparison of earlier results (Conrath, et al., Ref. [224]) with Nimbus 3 data (see also Section 9) showed a deficiency in the O_3 part of the spectrum as a result of the neglect of certain upper-state bands. The recent data have been improved by the inclusion of the ν_2 band at

224. B. J. Conrath, R. Hanel, V. Kunde and C. Prabhahara, "The Infrared Interferometer Experiment on Nimbus 3," J. Geophys. Res., Vol. 75, No. 30, 1970, pp. 5831-5857.

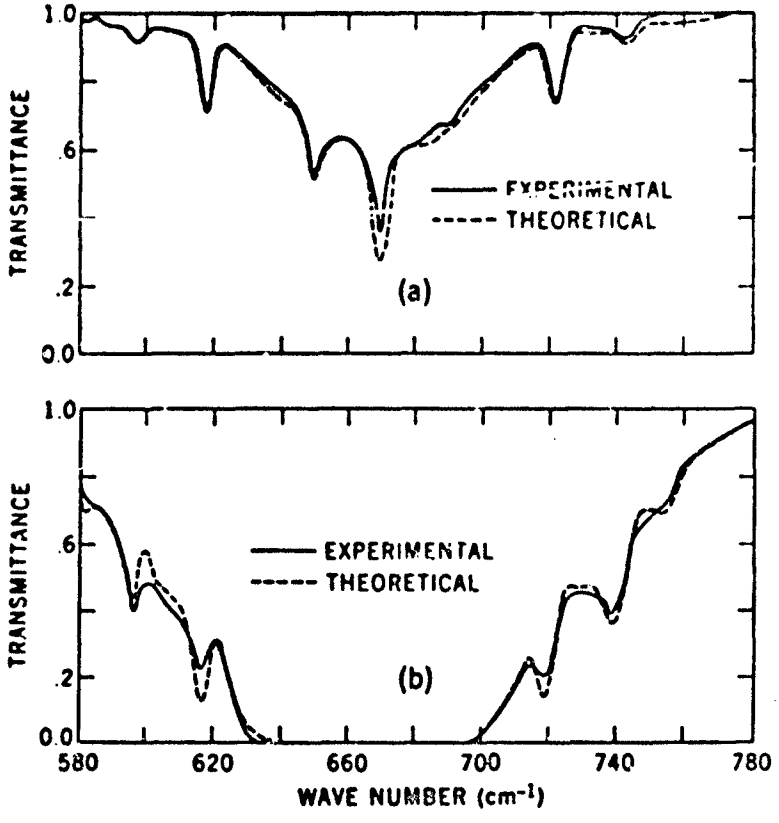

FIGURE 45. HOMOGENEOUS PATH COMPARISON FOR 667 cm^{-1} CO_2 BAND AT ROOM TEMPERATURE. (a) P_e = 0.2053 atm, w = 6.30 cm atm; (b) P_e = 0.0857 atm, w = 212.1 cm atm. (Reproduced from Kunde and McGuire, 1974 [9].)

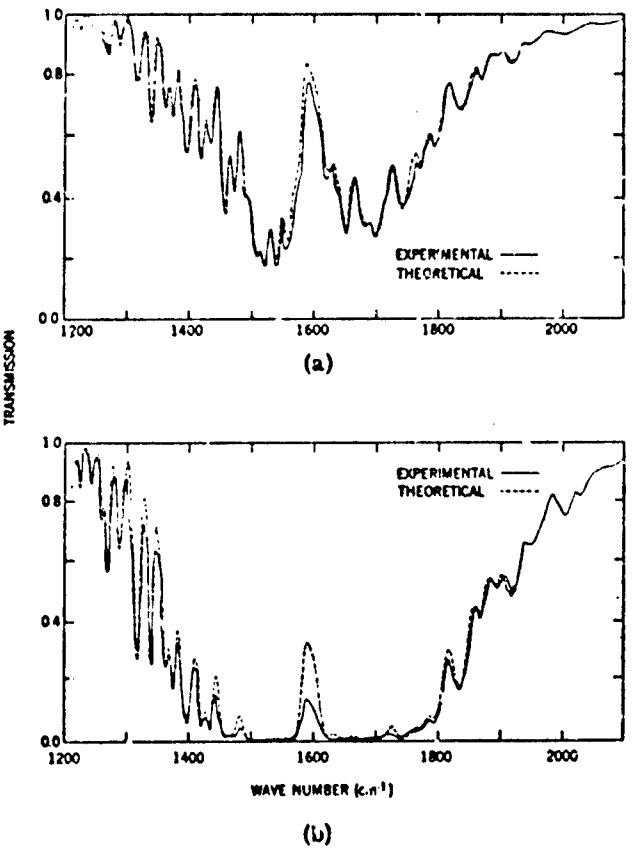

FIGURE 46. HOMOGENEOUS PATH COMPARISON FOR 1595 cm^{-1} H_2O BAND AT ROOM TEMPERATURE. (a) P_e = 140 mb, P = 100 mb, p_{H_2O} = 10 mb, w_{H_2O} = 0.0352 pr cm; (b) P_e = 1073 mb, P = 985 mb, p_{H_2O} = 22 mb, w_{H_2O} = 0.077 pr cm. (Reproduced from Kunde and McGuire, 1974 [9].)

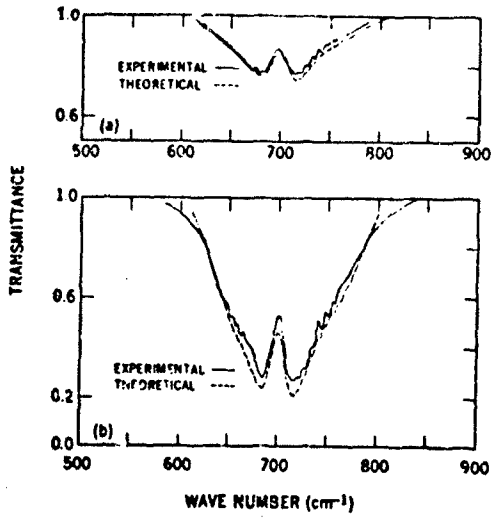

FIGURE 47. HOMOGENEOUS PATH COMPARISON FOR 701 cm^{-1} O_3 BAND AT ROOM TEMPERATURE. (a) P = 6.66 mb, w = 2 cm atm; (b) P = 533 mb, w = 9.4 cm·atm. (Reproduced from Kunde and McGuire, 1974 [9].)

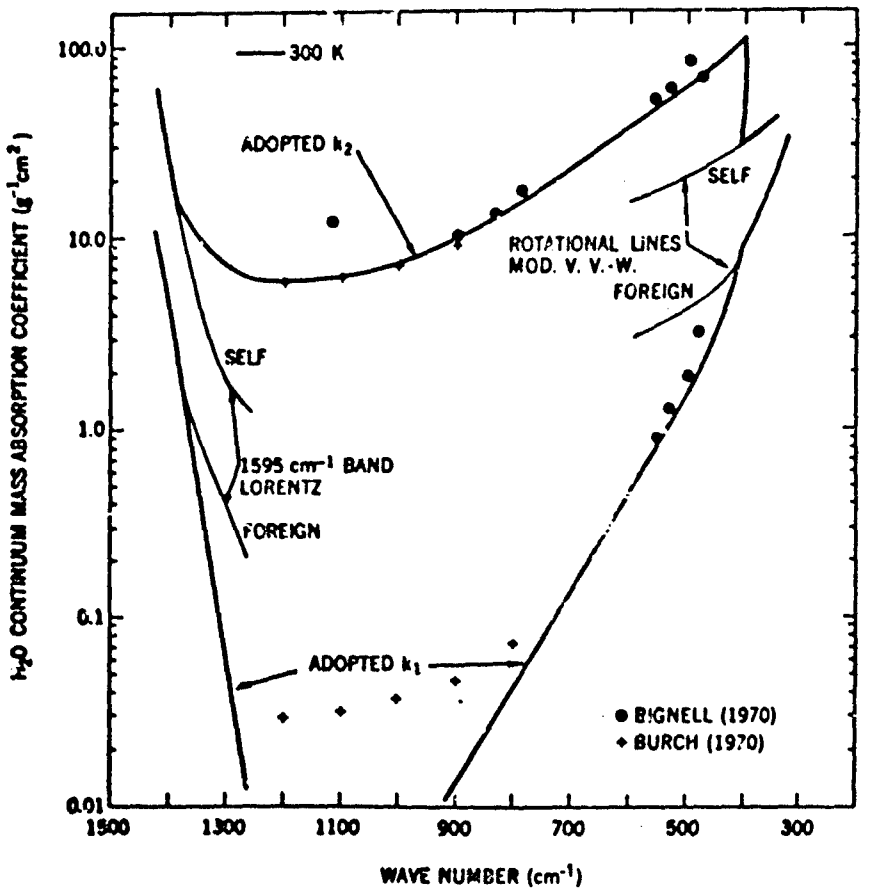

FIGURE 48. WATER VAPOR CONTINUUM ABSORPTION COEFFICIENT FOR THE 400-1400 cm^{-1} REGION. The k_2 component is normalized to the self-broadened modified Van Vleck-Weisskopf line shape for the rotational H_2O lines at 400 cm^{-1} and the self-broadened Lorentz line shape for the lines of the 1595 cm^{-1} H_2O band at 1400 cm^{-1}. The k_1 component is normalized in a similar manner to the foreign broadened water vapor components at 400 and at 1400 cm^{-1}. Only the k_1 and k_2 contributions are included in the 400-1400 cm^{-1} region. (Reproduced from Kunde and McGuire, 1974 [9].)

701.4 cm^{-1}, adequate representation of which is given by McClatchey, et al. (1973). Comparison of Kunde and Maguire's theoretical results for this band with the laboratory results of McCaa and Shaw (1967) is shown in Figure 47. The number of lines used in the calculation was 2158. The foreign-broadened half-width (self-broadening was assumed to be negligible) used was 0.07 cm^{-1} at 296 K for a Lorentz shape.

6.4 KYLE'S METHOD

Another, somewhat different, method of performing a line-by-line, calculation was developed by Kyle (1968c). His integration over the spectral lines is performed with a simple trapezoidal formulation, using a uniformly spaced integration net, optimized for a particular line shape. This would ordinarily be considered a brute-force attempt at integration, which would be most uneconomical in terms of computer time and costs. But Kyle has devised a scheme for broadening the net or integration interval, so that the number of computations is minimized. He writes for the generalized absorption coefficient the expression $k(\nu - \nu_0, \alpha)$, which, numerically integrated with a step size D, yields:

$$\sum_{n=-\infty}^{\infty} k(nD + \Delta, \alpha)D = 1. \tag{241a}$$

The value of Δ is calculated so that normalization over the interval remains unity. The physical representation of this type of numerical integration is shown in Figure 49.

With D taken outside of the summation, the summation resembles the expression for an Elsasser band, so that the result can be written directly for any line shape for which there is a known solution. In the case of the Lorentz line shape, the solution to Eq. (241a) is:

$$\frac{1}{\pi}\sum_{n=-\infty}^{\infty} \frac{D/\alpha_L}{(nD/\alpha_L + \Delta/\alpha_L)^2 + 1} = 1 \tag{241b}$$

or

$$\frac{\sinh (2\pi\alpha_L/D)}{\cosh (2\pi\alpha_L/D) - \cos (2\pi\Delta/D)} = 1 \tag{241c}$$

which when solved for Δ, yields:

$$\Delta = (D/2\pi) \cos^{-1} [\exp (-2\pi\alpha_L/D)] \tag{242}$$

Thus, with a chosen value D, the step size in the numerical integration, the choice of Δ is made according to Eq. (242). The error in the integrated absorptance of a line is dependent on

the choice of D/α_L. This error is shown plotted in Figure 50 as a function of $Sw/2\pi\alpha_L$, which specifies that reasonably large net sizes may be used before significant error occurs. Figure 51 shows how the peaks of the family of curves in (Fig. 50) vary as a function of the step size. In the same figure are plotted similar values for a Lorentz line for which the value of Δ is forced to zero; and for a so-called atmospheric line. The latter values are derived from the calculation of absorptance in a vertical path through the atmosphere, for a Lorentz line whose shape changes as the half-width, α_L, changes with pressure.

A Δ-value can be calculated for the atmospheric line by considering the shape derived by Goody (1964) for the optical depth calculated for a path vertically through the atmosphere. Thus, with the integrated value of the line shape normalized to unity as before, we have:

$$\sum_{n=-\infty}^{\infty} \frac{D}{2\pi\alpha_L} \ln \left[\frac{(nD + \Delta)^2 + \alpha_L^2}{(nD + \Delta)^2} \right] = 1 \tag{243}$$

According to Kyle, this leads to:

$$\Delta = \frac{D}{2\pi} \cos^{-1} \frac{1 + \exp(-2\pi\alpha_L/D)}{2} \tag{244}$$

A plot of the percent error as a function of $Sw/2\pi\alpha_L$ for various step sizes is shown in Figure 52. We note, incidentally, that as D approaches zero the ratio of Δ/D approaches 1/4 for the pure Lorentz line, whereas it approaches 1/6 for the pressure-reduced line in the atmospheric case.

For the Doppler line, the expression for the integrated line shape is given as:

$$\sum_{n=-\infty}^{\infty} D/\pi\alpha_D' \exp\left[-\left(\frac{nD + \Delta}{\alpha_D'} \right)^2 \right] = 1 \tag{245a}$$

where α_D' is half of the width of the line at an amplitude of e^{-1} of maximum. Since no simple solution exists for Δ, it is obtained by numerical solution of the equivalent of Eq. (245a), given by Kyle as:

$$\theta_3[\pi\Delta/D, \exp(-\pi\alpha'/D)^2] = 1 \tag{245b}$$

where θ_3 is the theta function given by:

$$\theta_3(z, q) = 1 + 2\sum_{n=1}^{\infty} q^{n2} \cos 2nz \tag{246}$$

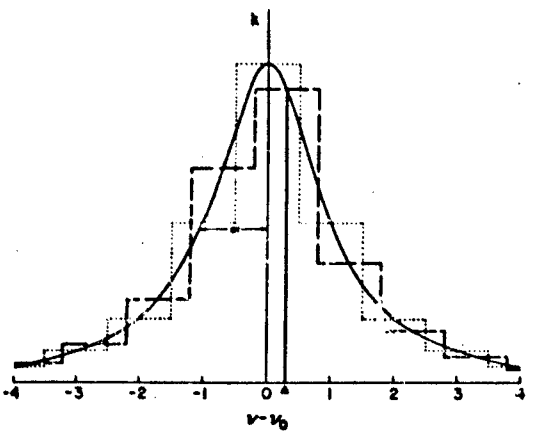

FIGURE 49. ILLUSTRATION OF TWO INTEGRATION NETS, WITH $\Delta = 0$, AND $\Delta \neq 0$. (Reproduced from Kyle, 1968c.)

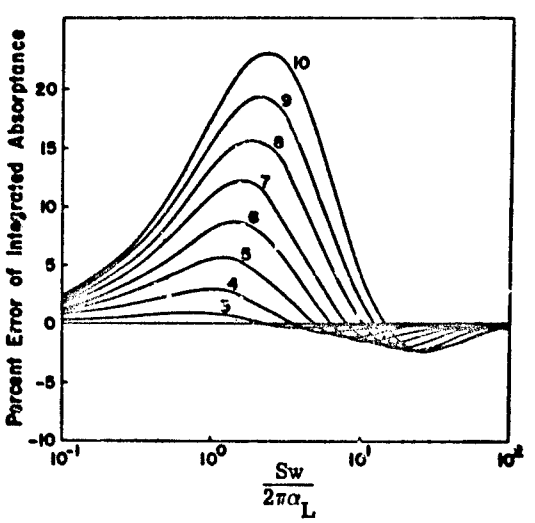

FIGURE 50. ERROR OF INTEGRATED ABSORPTANCE OF A LORENTZ LINE FOR THE STEP SIZES, D/α_L, SHOWN ABOVE THE CURVES. Δ is determined by Eq. (242). (Reproduced from Kyle, 1968c [6].)

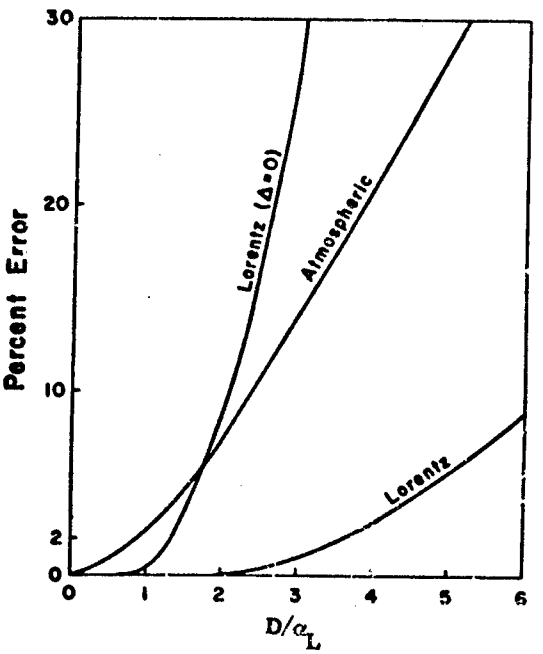

FIGURE 51. MAXIMUM INTEGRATED ABSORPTANCE ERROR AS A FUNCTION OF STEP SIZE. $\Delta \neq 0$ is determined by Eqs. (242) and (244) for the Lorentz and atmospheric cases, respectively. (Reproduced from Kyle, 1968c [6].)

The error in integration for the Doppler shape is given as a function of $Sw/2\pi\alpha'_D$ in Figure 53, for different values of the ratio D/α'_D. The unusual nature of the curves is a function of the rapid drop-off of the Doppler line, and is controlled to some extent in a real case for which the Lorentz broadening becomes dominant in the wings.

Kyle notes that a step size equal to the half-width should give adequate results for the Lorentz or Doppler shape, with a smaller size needed for the so-called atmospheric line. The fact that we are nearly always considering atmospheric cases seems to impose an upper limit of roughly 1/4 to 1/2 the half-width for a step size, if reasonable accuracy is to be achieved. Kyle argues that often the positions of lines are not well enough known to justify accuracies which require very small step sizes. He notes that if the line positions are known only within 0.01 cm^{-1}, with half-widths greater than 0.01 cm^{-1}, then a value of Δ as large as 0.005 cm^{-1} can be used and a step size of 0.01 cm^{-1} would be adequate.

6.5 THE METHOD OF SCOTT IN DIRECT INTEGRATION

Another technique, which its author claims is a computer-time-saving technique, is described by N. A. Scott (1974). The method is based on a direct numerical integration in frequency using the line structural properties to derive an economical spacing of the frequency mesh. As designated by Scott, the vertical transmittance is written as:

$$\tau(z_G, z_U) = \frac{1}{\nu_a - \nu_b} \sum_{i=1}^{N} W_i \exp\left\{ -\sum_{k=1}^{r} w_k \sum_{j=1}^{\ell} K_j(\nu_i, z_k) \right\} \tag{247}$$

where:

z_G, z_U = respectively, the lower and upper limits of integration in altitude
ν_a, ν_b = respectively, the lower and upper frequency limits of the spectral interval
W_i, w_k = respectively, the weights for integration over frequency and altitude
N, r = respectively, the number of integration points over frequency and altitude
ℓ = number of lines in the integration interval and
$K_j(\nu, z) = S_j(z) b_j(\nu, z) w(z)$

where:

$S_j(z)$ = strength of the j-th line at altitude, z;
$w(z)$ = concentration of the absorber at z; and
$b_j(\nu, z)$ = shape of the j-th line at z.

Recall that b_j is given by:

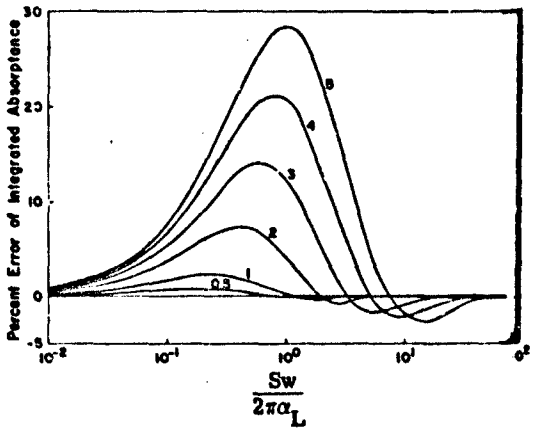

FIGURE 52. ERROR OF INTEGRATED ABSORPTION OF AN ATMOSPHERIC LINE FOR THE STEP SIZES, D/α_L, SHOWN ABOVE THE CURVES. Δ is determined by Eq. (244).

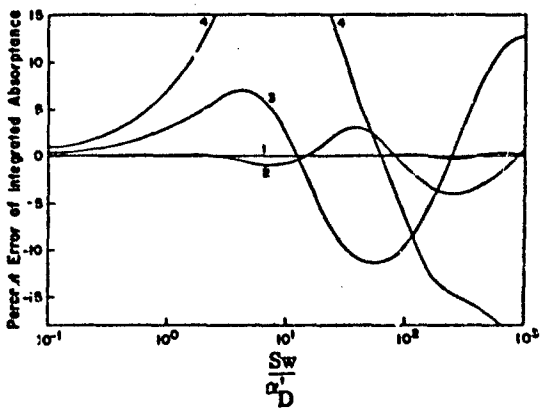

FIGURE 53. ERROR OF INTEGRATED ABSORPTANCE OF A DOPPLER LINE FOR THE STEP SIZES, D/α'_D, SHOWN ABOVE THE CURVES. Δ is determined by numerical solution of Eq. (245b).

$$\text{Lorentz: } \frac{1}{\pi}\frac{\alpha_L}{(\nu-\nu_j)^2+\alpha_L^2} \tag{248}$$

$$\text{Doppler: } \frac{1}{\alpha_D}\sqrt{\frac{\ell n\,2}{\pi}}\exp(-y^2); \tag{249}$$

$$\text{Voigt: } \frac{1}{\alpha_D}\sqrt{\frac{\ell n\,2}{\pi}}\,u\int_{-\infty}^{+\omega}\frac{e^{-t^2}}{u^2+(y-\alpha_L)^2}dt \tag{250}$$

$$\text{with: } y=\frac{\nu-\nu_j}{\alpha_D}\sqrt{\ell n\,2} \text{ and } u=\frac{\alpha_L}{\alpha_D}\sqrt{\ell n\,2}$$

6.5.1 DETERMINATION OF INTEGRATION INTERVALS

The altitude is divided into r layers, each with a mean pressure and a mean temperature, which are used for the computation of S, α and w. The frequency axis is divided into N equal segments, or steps, according to Weddle's integration formula (see, e.g., Ref [225]) The size of the interval, $\delta\nu = 1/N(\nu_a - \nu_b)$, is chosen to conserve computation time, yet preserve accuracy. Since the line half-width varies as a function of altitude, the integration step is chosen as a prescribed fraction of the half-width prevailing at the highest layer (given as z_r), in the vertical path through the atmosphere. Depending on where z_r occurs, the shape of the line could be determined by Eqs. (248), (249) or (250) in which cases:

$$\text{for Lorentz: } \delta\nu=\frac{\alpha_L(z_r)}{M} \tag{251}$$

$$\text{for Doppler: } \delta\nu=\frac{\alpha_0(z_r)}{M} \tag{252}$$

$$\text{for Voigt: } \delta\nu=\frac{\alpha_L(z_r)}{M} \text{ if } y\geq 1 \tag{253}$$

$$\text{or } \delta\nu=\frac{\alpha_D(z_r)}{M} \text{ if } y<1$$

where $M > 1$.

---

225. G. A. Korn and T. Korn, Mathematical Handbook for Scientists and Engineers, McGraw-Hill, N. Y., 1961.

To take account of the fact that the line half-width increases at the lower altitudes, and the integration can accommodate a larger integration step, Scott defines a "representation step," $\Delta\nu(z_k)$ shown in Figure 54, for the k-th layer, such that the frequency interval is divided into the steps:

$$\nu_a, \nu_a + \Delta\nu(z_k), \ldots, \nu_a + P\Delta\nu(z_k), \ldots, \nu_b$$

where $P = 0, \ldots, n(z_k)$ and $n(z_k)$ is the number of "representation points," in the frequency interval for the k-th layer. Note that there is no offset as recommended by Kyle. The total number of integration points, $N = \delta\nu\cdot(\nu_a - \nu_b)$, is the same, but the values between the "representation points" are obtained by interpolation. Scott claims that the interpolation represents a saving in computer time over a direct calculation of each of the N values for each layer.

6.5.2 SIMPLIFICATIONS

Ordinarily, it would be necessary to compute the value of the line shape $b_j(\nu, z) = b_j(\nu(P), z)$ for j lines, at r layers for each value of P, which would involve a large amount of computing. Scott proposes a simplification, the details of which can be found in the original article (Scott, 1974). The simplification entails allowing $(\nu_a - \nu_j)$, the difference between ν_a, the initial value of the integration interval, and ν_j, the center of the j-th line, to be an integral multiple, P', of $\Delta\nu(z_k)$. This amounts to computing:

$$\text{for Lorentz: } \frac{1}{\pi\alpha_L(z_k)}(1 + U^2)^{-1} \text{ and} \tag{254}$$

$$\text{for Doppler: } \frac{1}{\pi\alpha_D(z_k)}\sqrt{\frac{\ln 2}{\pi}}\exp(-U^2) \tag{255}$$

where in Eq. (254), $U = (P + P')/M$ and in Eq. (255), $U = (P + P')\sqrt{\ln 2}/M$, thus requiring only one computation for each U, satisfying all lines having a given half-width α_L or α_D. This requires, however, a sacrifice in accuracy, since those lines which are not an integral multiple of $\Delta\nu$ from ν_a must be shifted by the value $|\nu_j - \nu_j| \leq \Delta\nu(z_k)/2$, to ν_j'. The loss in accuracy on the other hand, of the order of 0.01 cm^{-1}, may not be much greater than the uncertainty in the positions of the lines. And furthermore, we may expect compensating offsets between the positive and negative shifts. The value of P + P' incidentally ranges from 0 to a value beyond which the computation of b_j can be halted, being a negligible contribution to the absorption coefficient.

When several gases are involved in the computation, the value $\delta\nu$ is chosen on the basis of the gas with the smallest half-width. Calculations of the contributions of the other gases are made in relation to the ratios of the half-width of the various gases. The reader is referred to Scott (1974) for details.

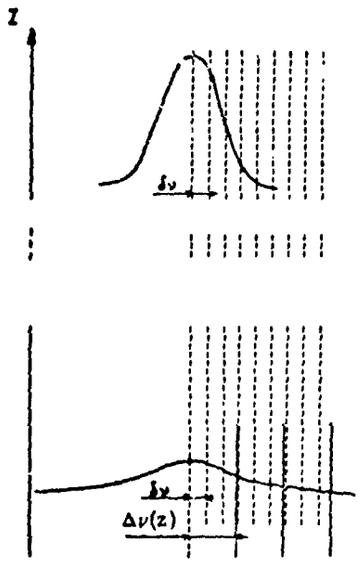

FIGURE 54. SCHEMATIC COMPARISON OF THE INTEGRATION STEP $\delta\nu$ AND OF THE REPRESENTATION STEP $\Delta\nu(z)$ IN TWO DIFFERENT LAYERS OF THE ATMOSPHERE. (Adopted from Scott, 1974 [7].)

6.5.3 EVALUATION OF RESULTS

A very significant contribution in Scott's article to an understanding of the usefulness of a computation technique - one not often found in similar descriptions - is an assessment of the sensitivity of the transmittance to changes in various parameters used in the computation. The sensitivities included in the articles are for changes in r, the number of atmospheric layers; A, the number of points in the wing included in the computation; M, the ratio of the half-width to the size of the mesh; and α_L, different values of the Lorentz half-width. Also, plotted are the arbitrary computation times as functions of r, ℓ (the number of lines), and N (the number of integration points). The alleged time required for computation of τ and $d\tau/dz$ is 20 seconds on a CDC 6600 computer, for N = 5500, r = 50 and ℓ = 200.

As is true with all techniques, the true value cannot be determined without a comparison with real results from experimental measurements. To perform this evaluation is no small feat because of the variety of parameters and the difficulty of achieving reliable physical data. On the other hand, it is valid to compare different techniques by applying identical, if artificial, data. This is not likely to happen, however, because, except in certain undocumented cases, the exchange of programs is presently impractical.

6.6 AN INTERMEDIATE METHOD OF TRANSMITTANCE COMPUTATION

The technique described in this section is one which avoids the use of direct integration over the lines for the computation of atmospheric transmittance; yet does not resort to the coarser techniques in the use of band models. It is included, thus, in this chapter as a sort of transition between the direct method and the band-model method. The technique is described by Arking and Grossman (1972), after an idea treated in a 1939 Russian paper by A. I. Lebedinsky, which is referenced by Kondratyev [226]. The basis of the technique is that the ordering of the absorption coefficient, k, with respect to ν is unimportant in the computation of the average τ over a finite spectral interval, but depends only on distribution of k-values within the spectral interval. (Compare the quasi-random model, Section 7.2.)

Use of the so-called k-distribution function avoids the need for direct integration, but retains a limitation in that it requires the atmosphere to be homogeneous, wherein the absorption coefficient is independent of pressure and temperature. The inhomogeneous atmosphere can apparently be accommodated but with an increase in the complexity of the technique.

6.6.1 DETERMINATION OF THE DISTRIBUTION FUNCTION

Arking and Grossman (1972) write the average transmittance for the i-th spectral interval, in the following form:

226. K. Ya. Kondratyev, Radiation in the Atmosphere, Academic Press, N. Y., 1969.

$$\bar{\tau}_i(w_1, w_2) = \frac{1}{\nu_i - \nu_{i-1}} \int_{\nu_{i-1}}^{\nu_i} \exp\left[-\int_{w_1}^{w_2} k(\nu, w)\, dw\right] d\nu \tag{256}$$

$w_1 \leq w_2$, are the amounts of absorber (mass per unit area), respectively, above altitude levels 1 and 2. If the distribution function for k is given by $h_i(k)$ in the i-th spectral interval, then Eq. (247) is rewritten as:

$$\bar{\tau}_i(w_1 w_2) = \int_0^{\infty} \exp\left[-k(w_2 - w_1)h_i(k)\, dk\right] \tag{257}$$

The determination of the distribution function, h(k), can be obtained in the following manner. Imagine a cut across the spectrum (See Figure 55) from ν_1 to ν_2 at k, of height dk. The accompanying value of $d\nu$ at each cut is given by $d\nu_j$, where j varies from 1 to J, the total number of cuts. The total frequency interval covered by the cuts is $\sum_{j=1}^{J} d\nu_j$, and this value divided by |dk| is the frequency interval per unit k interval. Dividing this quotient by $\nu_2 - \nu_1$ gives the fractional interval per unit k, which is the k-distribution function. Thus,

$$h(k) = \frac{1}{\nu_2 - \nu_1} \sum_{j=1}^{J} \left|\frac{d\nu_j}{dk}\right| \tag{258}$$

When this value is used in Eq. (248), the value $\bar{\tau}_i(w_1, w_2)$ in Eq. (247) is determined without resorting to direct integration. Arking and Grossman have obtained the k-distribution for several cases of line structure. These include realistic and some not-so-realistic line structures. Among the set are representations of square and triangular lines, and Lorentz- and Doppler-shaped lines in a regular band structure. The reader is referred to the original article (Arking and Grossman, 1972) for the descriptions. As an example, a regular pattern of non-overlapping Lorentz lines is chosen. A characteristic half-width, α_{LC}, defined by $\alpha_{LC} = \alpha_L/d$ $(=\beta/2\pi)$, is used in the Lorentz formula, in which the line spacing is d and the center frequency of a characteristic line is taken as zero. Thus:

$$h(\nu) = \frac{k_2}{1 + [\nu/(\alpha_{LC} d)]^2}, \text{ for } 0 \leq \nu \leq d/2 \tag{259}$$

with k_2 as the peak value of $k(\nu)$, given by $S/\pi\alpha_{LC} d$. Thus, inverting Eq. (259) we have:

$$h(k) = \frac{1}{\pi d} \sum_{j=1}^{n} \left|\frac{d\nu_j}{dk}\right| = \frac{k_2 \alpha}{k^{3/2}(k_2 - k)^{1/2}}, \text{ for } k_1 \leq \kappa \leq k_2 \tag{260}$$

with k_1 as the minimum value of k given as:

$$k_1 = \frac{k_2}{1 + [1/(2\alpha_{LC})]^2} \tag{261}$$

An example of the distribution function in an actual gas for a portion of the 15 μm CO_2 band between 675 and 715 cm^{-1} at 250 K and three different pressures is shown in Figure 56. The distribution function for each curve in (Fig. 56) has the form $h(k) \alpha k^{-n}$ where n is 0.75 for small k and 1.5 for large k. The minimum k is proportional to P_1, and the maximum k inversely proportional to p.

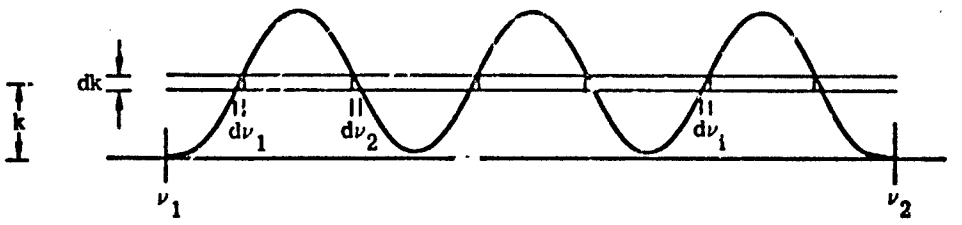

FIGURE 55. SCHEMATIC FOR DETERMINING THE DISTRIBUTION FUNCTION, h(k).

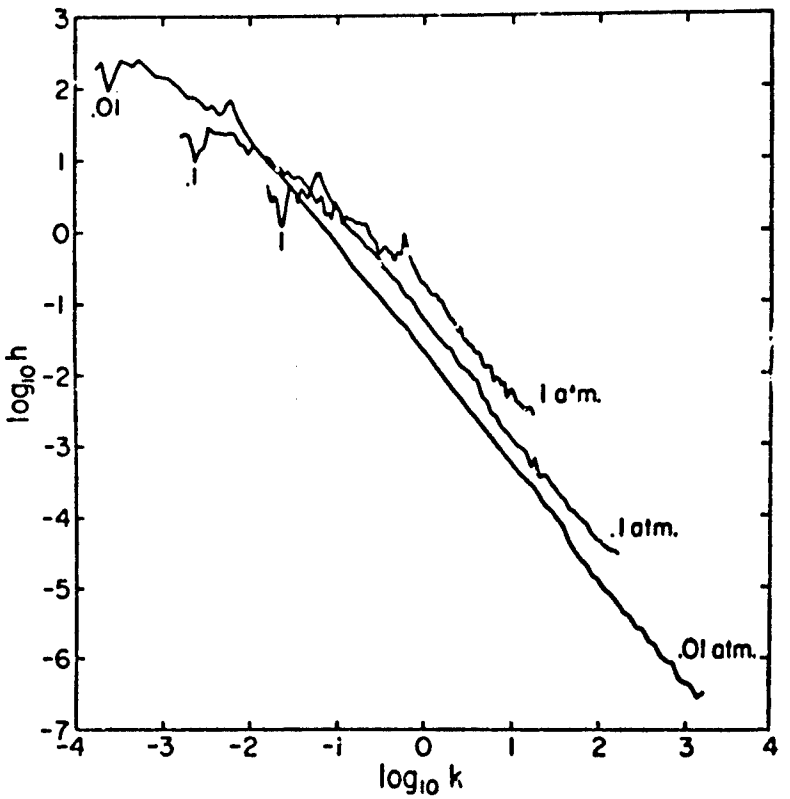

FIGURE 56. THE k-DISTRIBUTION FUNCTION FOR THE PORTION OF THE CO_2 15 μm BAND FROM 675 TO 715 cm^{-1} AT A TEMPERATURE OF 250 K AND PRESSURES OF 1, 0.1, AND 0.01 atm. It is based upon Lorentz profiles with a constant half-width of 0.08 cm^{-1} times the pressure. The line parameters were taken from Drayson and Young, 1967. (Reproduced from Arking and Grossman, 1972 [10].)

7
ILLUSTRATIONS OF BAND MODEL METHODS

7.1 STATISTICAL MODEL (ELLINGSON; RODGERS AND WALSHAW; GOLDMAN AND KYLE)

7.1.1 SPECIFICATION OF THE MODELS

The model used by Ellingson (1972) for the calculation of radiative transfer is the Goody random model (see Section 5) with an exponential probability distribution of line intensities, which gives, retaining some of Ellingson's notation:

$$\bar{\tau}_{\Delta\nu} = \exp\left[-C_1 w\left(1 + C_2 \frac{w}{P}\right)^{-1/2}\right] \tag{262}$$

where (see Section 5)

$$C_1 = \frac{1}{\Delta\nu}\sum_{i=1}^{n} S_i(T_0) \tag{263}$$

$$C_2 = \frac{1}{4}\left[\frac{\sum_{i=1}^{n} S_i(T_0)}{\sum_{i=1}^{n}\left\{S_i(T_0)\alpha_{L0_i}(T_0)\right\}^{1/2}}\right]^2 \tag{264}$$

and the Lorentz line shape is implied. These expressions are similar to the expressions in the earlier work of Rodgers and Walshaw (1966) and C_2 obtained from the work by Goody (1964). The definitions of terms are as follows:

w = absorber amount

P = Pressure (atmospheres)

T_0 = standard temperature

α_{L0_i} = half width for the i-th line at one atmosphere pressure

n = number of lines in the interval, $\Delta\nu$

Ellingson's justification for the use of the statistical model is the success achieved by other investigators, among the latest being the models of Rodgers and Walshaw (1966), and Goldman and Kyle (1968).

Goldman and Kyle, using the line parameter data of Clough and Kneizys (1965), compare the results of calculations using band models and line-by-line integrations of the 9.6 μm band of O_3 and the 2.7 μm band of H_2O vapor. The calculations of Goldman and Kyle employed the random model, with an exponential probability distribution at 9.6 μm, and with an S^{-1} line strength distribution at 2.7 μm. The comparative accuracy of the exponential and exponential-tailed S^{-1} band models are shown in a series of figures which are taken from the report by Goldman and Kyle (1968). The band parameters were calculated as shown in Section 5. In Figure 57, the line-by-line and model calculations are compared for the 9.6 μm O_3 band with a spectral resolution of 1.6 cm^{-1} which corresponds in the line-by-line calculation to a square slit function, and to which is attributed the jagged nature of the curves. The other line parameters pertinent to Figure 57 are as follows: the line half width is (at one atm) 0.08 cm^{-1}, temperature is 233 K, pressure is 0.0197 atm, and path length is 24.47 cm. The line-by-line calculation is displaced upward by 20% from the model calculation. Similar comparisons are made for O_3 with a resolution of 2.5 cm^{-1} and for two different absorber conditions, namely (1) pressure = 0.0197 atm with path = 24.47 cm and (2) pressure = 0.197 atm and path = 2.447 cm. These comparisons are shown in Figure 58. In Figure 59, the intent is to show the similarities between the band models using the exponential and the exponential-tailed S^{-1} distributions under physical conditions which are the same as those for Figure 58.

Goldman and Kyle ascertain that both the point-by-point accuracy of the curves and the accuracy integrated over the O_3 band are good (see below), especially when the line-by-line calculation is compared with the band model calculation using an exponential distribution. For the upper curve of Figure 59, the integrated absorption for the two different types of distribution compares as follows:

$$\int_{995.9}^{1068.7} A(\nu)\,d\nu = \begin{cases} 27.63\ cm^{-1}, & \text{exponential distribution} \\ 26.32\ cm^{-1}, & \text{exponential-tailed } S^{-1} \text{ distribution;} \end{cases}$$

for the lower curves it is

$$\int_{995.9}^{1068.7} A(\nu)\,d\nu = \begin{cases} 49.99\ cm^{-1}, & \text{exponential distribution} \\ 47.30\ cm^{-1}, & \text{exponential-tailed } S^{-1} \text{ distribution.} \end{cases}$$

Specifically, they claim a disagreement of about 5% in each of these cases, whereas the band model calculation of the integrated intensity with an exponential distribution agrees to within 1% of that obtained in the line-by-line method. In fact, the agreement remains good for all of the resolutions used. Goldman and Kyle attribute the agreement, at least partially, to the high density of lines in the spectral region. Tables by Clough and Kneizys (1965) show that in a 1.6 cm^{-1} interval, anywhere in the band, there are from about twenty to fifty lines.

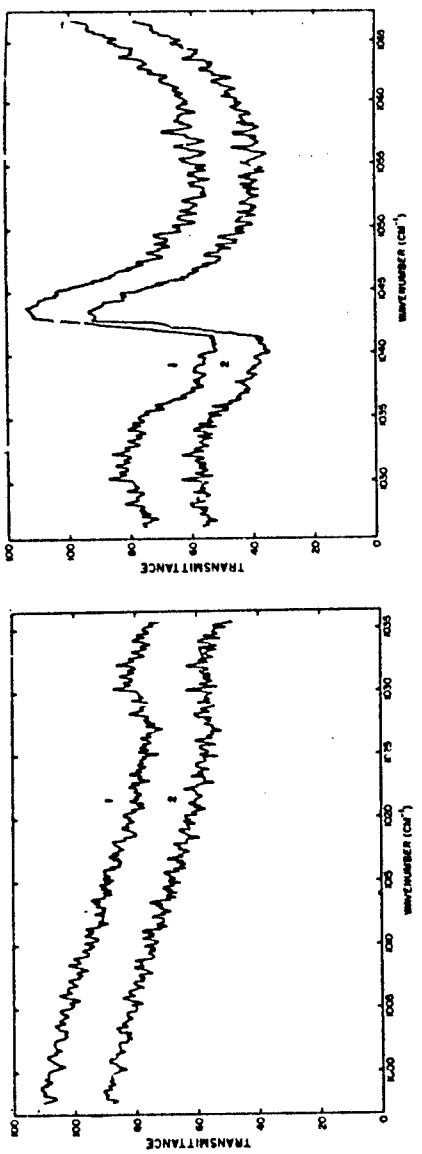

FIGURE 57. COMPARISON OF ABSORPTION SPECTRUM OBTAINED BY LINE-BY-LINE CALCULATION, CURVE 1, AND BY STATISTICAL MODEL CALCULATION, CURVE 2, FOR THE 9.6 μm OZONE BAND FOR $\Delta\nu$ = 1.6 cm^{-1}. Here α_{L0}^{0} = 0.08 cm^{-1} atm^{-1}, T = 233 K, P = 0.0197 atm, and w = 24.47 cm. The line-by-line calculation is displaced by 20%. (Reproduced from Goldman and Kyle, 1968.)

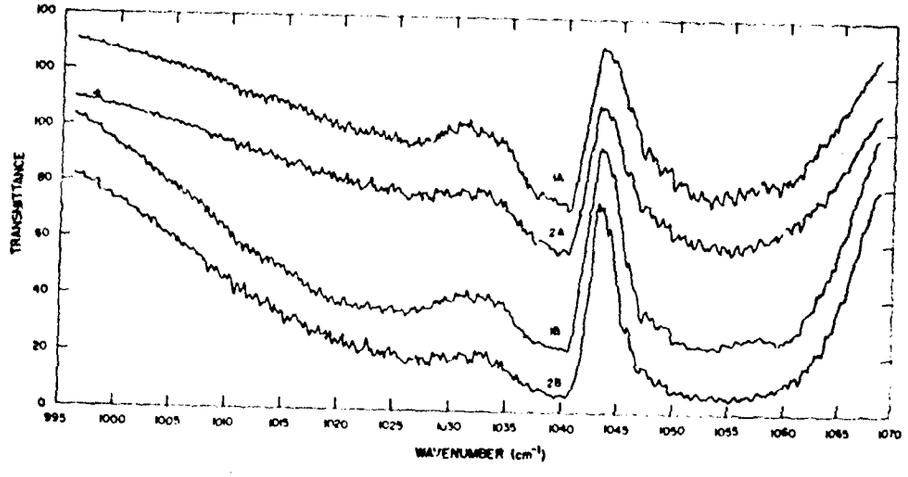

FIGURE 58. COMPARISON OF ABSORPTION SPECTRUM OBTAINED BY LINE-BY-LINE CALCULATION, CURVES 1, AND BY THE STATISTICAL MODEL CALCULATION, CURVES 2, FOR THE 9.6 μm OZONE BAND FOR $\Delta\nu$ = 2.5 cm^{-1}. α^{o}_{L0} = 0.08 cm^{-1} atm^{-1}, and T = 233 K; P = 0.0197 atm and w = 24.47 cm for the upper two curves while P = 0.197 atm and w = 2.447 cm for the lower two curves. The line-by-line calculations are displaced by 20%. (Reproduced from Goldman and Kyle, 1968 [202].)

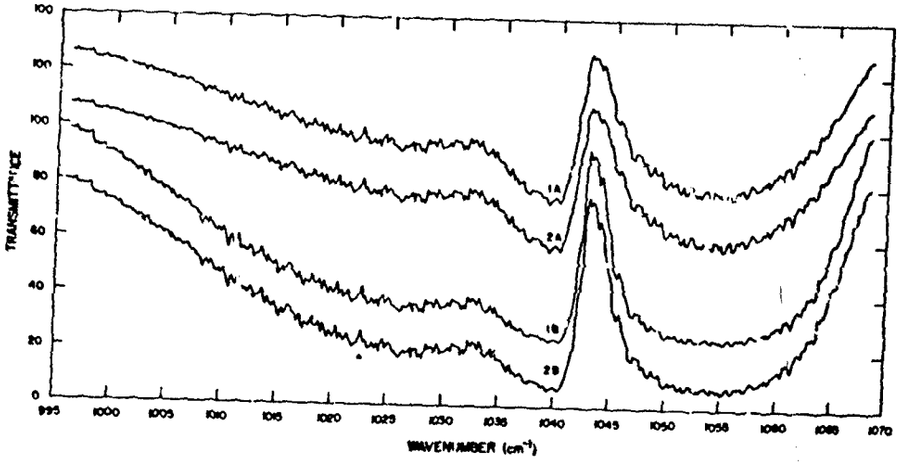

FIGURE 59. COMPARISON OF TRANSMITTANCE OBTAINED BY STATISTICAL MODEL WITH EXPONENTIAL INTENSITY DISTRIBUTION, CURVES 1, AND WITH EXPONENTIAL-TAILED S^{-1} INTENSITY DISTRIBUTION, CURVES 2. Here $\Delta\nu$ = 2.5 cm^{-1}, T = 233 K, and α^{o}_{L0} = 0.08 cm^{-1} atm^{-1}; P = 0.0197 atm, w = 24.47 cm for the upper two curves and P = 0.197 atm, w = 2.447 cm for the lower two curves. Curves 1 are each displaced by 20%. (Reproduced from Goldman and Kyle, 1968 [202].)

A similar treatment of the 2.7 μm band of H_2O vapor by Goldman and Kyle yields the curves of Figure 60. The temperature of the H_2O vapor was taken to be 1200 K for comparison with the results of experimental measurements [227]. The comparison in the curves of Figure 60, however, is between the results obtained from the line-by-line and the band model calculations. The distribution in this case was the exponential-tailed S^{-1}, which the authors claim gave better agreement than the exponential. The line parameters used were those of Gates, et al. (1964). The conditions for which the calculations were made were: temperature 1200 K, pressure 0.995 atm, path length 7.75 cm. The resolution was 8 cm^{-1}. The expression for the half-width used in the calculations is α_{L_i} (1200 K, 1 atm) = 1.275 α_{L_i} (300 K, 1 atm). Calculation of the integrated band strengths gave:

$$\int_{3153.8}^{4103.4} A(\nu)d\nu = \begin{cases} 181.3\ cm^{-1}, & \text{statistical model} \\ 180.8\ cm^{-1}, & \text{line-by-line,} \end{cases}$$

showing agreement to within 1%. Comparison with the laboratory results of Burch and Gryvnak (1962), however, showed a greater disparity, as large as 10%, in a point-to-point comparison. New values for the $2\nu_2$ (3150-3400 cm^{-1}) strength of Gates, et al. have been suggested by Burch, et al. [228], indicating an increase from 2.2×10^3 to 3.5×10^3 $cm^{-1}/g\ cm^{-2}$.

Ellingson cautiously adopts the random model for the 15 μm band of CO_2 on the basis that the many overtone, hot and isotopic bands combine to "randomize" the otherwise regular nature of the region which contains the fundamental band.

7.1.2 SCALING THE PATH QUANTITIES (ELLINGSON; RODGERS AND WALSHAW)

In allowing for the non-homogeneous nature of the slant path through which the radiance must be calculated, he uses the Curtis-Godson approximation according to the method applied by other investigators (e.g., Rodgers and Walshaw, 1966) using a quantity of absorber, $\overline{w}$, scaled in temperature, and a mean pressure $\overline{P}$, defined respectively by:

$$\overline{w}(z, z') = \int_z^{z'} \Phi(T)\, dw \qquad (265)$$

and

227. D. E. Burch and D. A. Gryvnak, Infrared Radiation Emitted by Hot Gases and Its Transmission Through Synthetic Atmospheres, Report No. U-1929, Philco-Ford Corporation, 1962.

228. D. E. Burch, D. A. Gryvnak and R. R. Patty, Absorption by H_2O Between 2800 and 4500 cm^{-1} (2.7 Micron Region), Report No. U-3202, Philco-Ford Corporation, 1965.

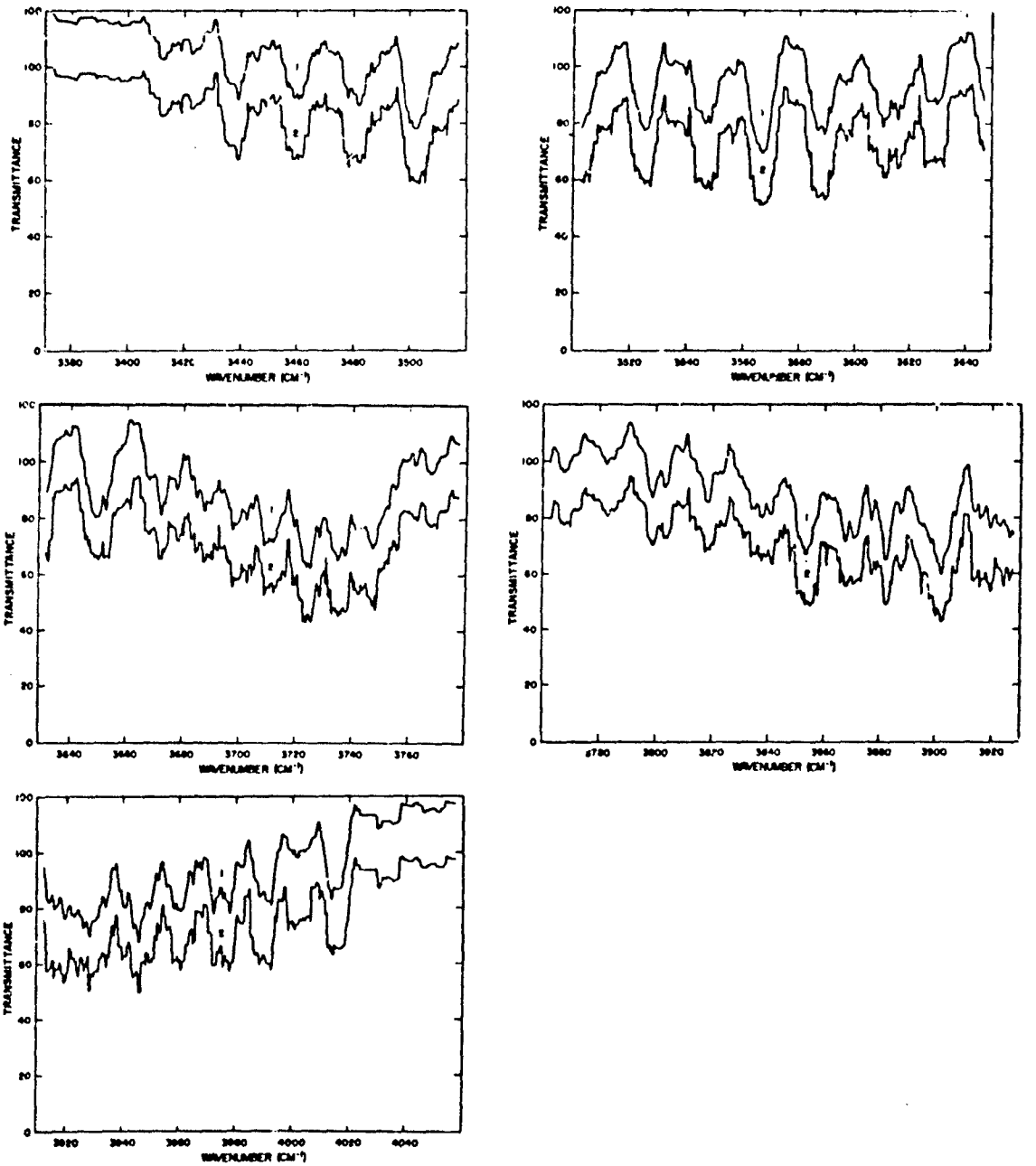

FIGURE 60. COMPARISON OF TRANSMITTANCE OBTAINED BY LINE-BY-LINE CALCULATION, CURVE 1, AND BY STATISTICAL MODEL CALCULATION, CURVE 2, FOR THE 2.7 μm H_2O BAND FOR $\Delta\nu$ = 8 cm^{-1}. Here $\alpha^{o}_{L0} = 1.275\ \alpha^{o}_{L0}$ at 300 K, 1 atm, T = 1200 K, P = 0.995 atm, and w = 7.75 cm. The line-by-line calculation is displaced by 20%. (Reproduced from Goldman and Kyle, 1968 [202].)

$$\overline{P}(z, z') = \frac{1}{w}\int_z^{z'} \chi(T) P \, dw \tag{266}$$

where

$$dw = \rho_g dz/\mu, \text{ and (P is in atmospheres)} \tag{267}$$

$$\Phi(T) = \frac{\sum_{i=1}^{n} S_i(T)}{\sum_{i=1}^{n} S_i(T_0)} \tag{268}$$

and

$$\chi(T) = \left[\frac{\sum_{i=1}^{n} \left\{ S_i(T) \alpha_{L0_i}(T) \right\}^{1/2}}{\sum_{i=1}^{n} \left\{ S_i(T_0) \alpha_{L0_i}(T_0) \right\}^{1/2}} \right]^2 \tag{269}$$

As did Rodgers and Walshaw (1966), Ellingson used an interpolative function for determining $\Phi(T)$ and $\chi(T)$, namely:

$$\Phi(T) = \exp\left\{ a(T - T_0) + b(T - T_0)^2 \right\} \tag{270}$$

and

$$\chi(T) = \exp\left\{ a'(T - T_0) + b'(T - T_0)^2 \right\} \tag{271}$$

The values of a, b, a' and b' were determined from a fit of discrete values as obtained by Eqs. (268) and (269). A check of this interpolation procedure showed it to give sufficiently representative values of the variables, within 5% of the results of exact calculations.

The compilation of Benedict and Calfee (1967) in the region between 1000 and 2014 cm^{-1} was used to calculate the average band strengths which were applied to Eqs. (270) and (271) for these vibration-rotation H_2O vapor lines. The line strengths and widths were calculated for the temperatures 220, 260, and 300 K and the summations performed for use in Eqs. (268) and (269). The value of $T_0 = 260$ was used in the calculation of the constants a, b, a' and b' in Eqs. (270) and (271). Figure 61 depicts the functions Φ and χ for 6 different intervals in the region between 1000 and 2014 cm^{-1}, the 6.3 μm band of H_2O vapor. Where isothermal conditions would be assumed the values of Φ and χ would be fixed at unity. For the rotational H_2O

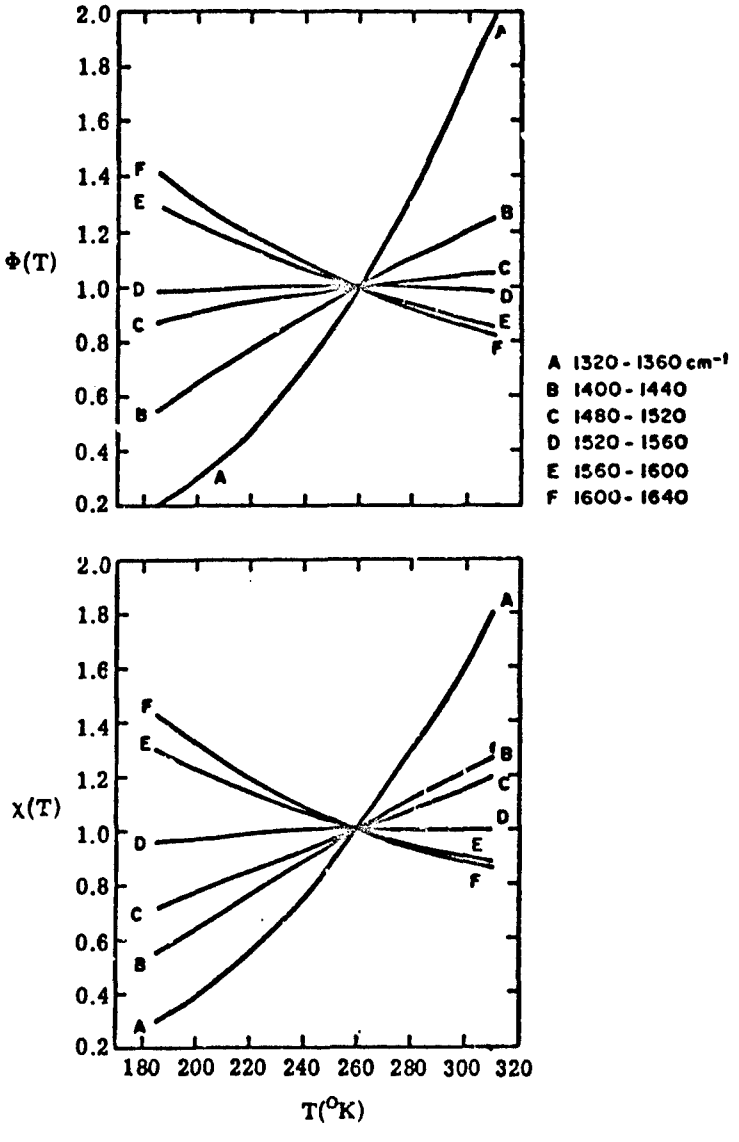

FIGURE 61. THE TEMPERATURE DEPENDENCE OF Φ AND χ FOR SOME INTERVALS IN THE 6.3 μm WATER VAPOR BAND. (Reproduced from Ellingson, 1972 [11].)

vapor band the unpublished data of Benedict and Kaplan (tabulated by Goody, 1954) were used in the model formulated by Ellingson on the lines out to 640 cm^{-1}. From this point to the region where the 6.3 μm band absorbs exclusively, the rotational band and the vibration-rotation band of 6.3 μm were combined and the lines submitted to Eqs. (270) and (271). Alternatively, spectral data supplied by AFCRL were used in the 600-800 cm^{-1} region where greater resolution of parameters was required.

For ozone, the data of Clough and Kneizys (1965) were used in the spectral region 960 to 1180 cm^{-1} (9.6 μm band). Unpublished data were used for the 14 μm band. The temperature range for the calculation of Φ and χ was 195 to 275 K to correspond to the temperature range important in the stratosphere to ozone. The value of T_0 was taken to be 235 K. Calculated values of Φ and χ for the 9.6 μm band of ozone are shown in Figure 62. The constant value 0.07 was used for the ozone half-width, as it was by Goldman and Kyle (1968).

The positions and strengths of lines tabulated by Drayson and Young (1967) for CO_2 in the region between 503 and 860 cm^{-1} were used to calculate the necessary parameters at temperatures of 175, 200, 225, 250, 275 and 300 K. The weak lines in these tables below 520 cm^{-1} and above 840 cm^{-1} were neglected. It is to be noted here, incidentally, that these parameters have been upgraded in a more recent publication, Drayson (1973). The increase in reliability, however, is not sufficient to result in any significant changes in the results computed by Ellingson. A constant half-width value of 0.102 cm^{-1} was used for the calculation of Φ and χ. The six temperatures listed above were used to obtain a best fit to the data, with T_0 = 250 K. Values corresponding to the indicated band of CO_2 for Φ and χ are shown in Figure 63.

7.1.3 MODEL FOR CH_4 AND N_2O (ELLINGSON)

Ellingson apparently had no data available at the time of his investigation on the 7.7 μm band of methane and the 7.8 μm band of N_2O. He resorted to the use of an earlier popular empirical model [229] given in the form:

$$\tau = \exp - (C_3 \overline{w}\, \overline{P})^{\eta} \qquad (272)$$

with η = 0.46 for CH_4 and η = 0.48 for N_2O, as determined by Green, et al. for the 7.8 μm band. Compare the expression in Eq. (272) with that given by Green, et al., to wit:

$$\tau = \exp - (w'/w_e)^{\eta}$$

where, for a fixed temperature,

229. A. E. S. Green, C. Lindenmeyer and M. Griggs, "Molecular Absorption in Planetary Atmosphere," J. Geophys. Res., Vol. 69, No. 3, 1964, pp. 493-504.

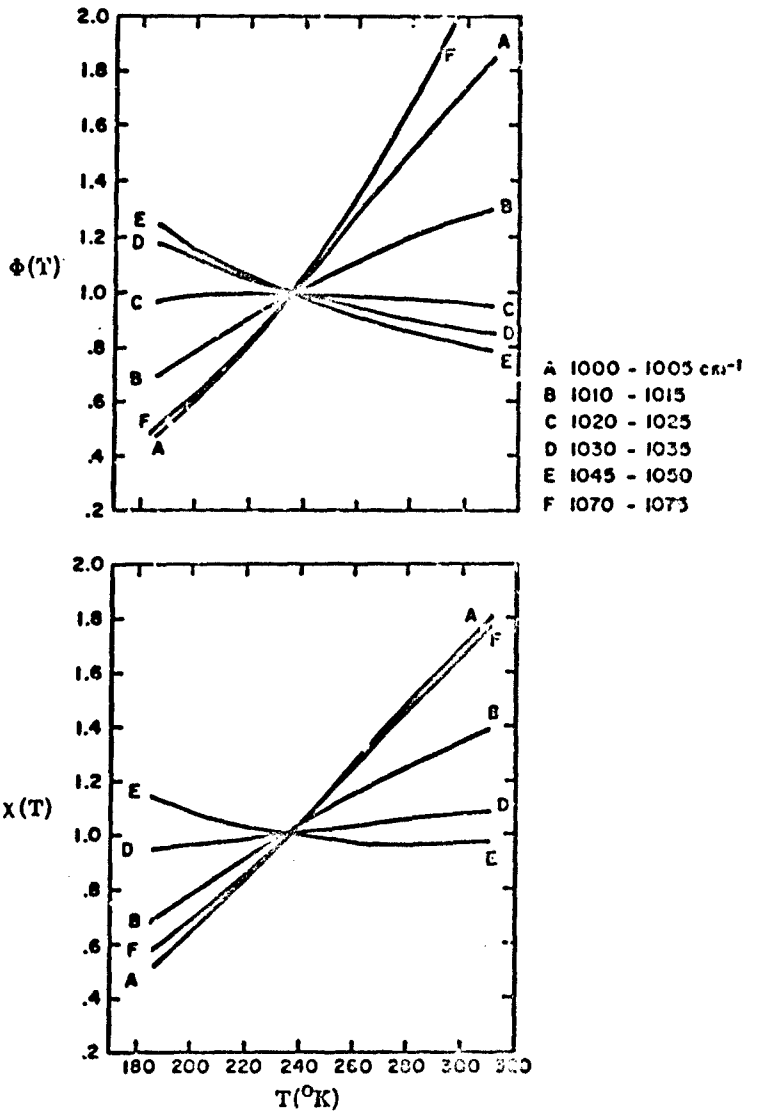

FIGURE 62. THE TEMPERATURE DEPENDENCE OF Φ AND χ FOR SOME INTERVALS IN THE 9.6 μm OZONE BAND
(Reproduced from Ellingson, 1972 [11].)

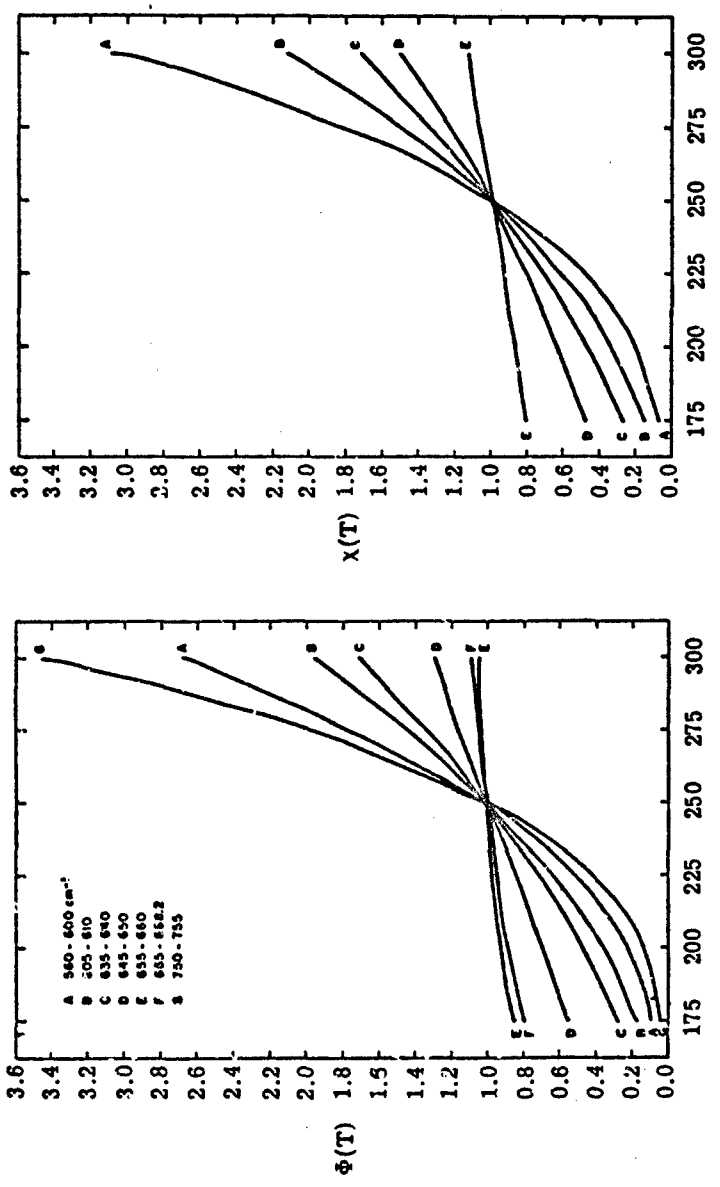

FIGURE 63. THE TEMPERATURE DEPENDENCE OF Φ AND χ FOR SOME INTERVALS IN THE 15 μm CARBON DIOXIDE BAND. (Reproduced from Ellingson, 1972[11].)

$$w' = w(P_e/P_s)$$

with

$$P_e = P + (B - 1)p_a$$

in the usual way. Ellingson effects consistency with this formula by calculating $\overline{w}$ and $\overline{P}$ (Eqs. (265) and (266)) with Φ and χ equal to unity. The graphical results of Green, et al. were used to compute C_3 for the particular model and resolution set by Ellingson.

7.1.4 SPECIALIZATION TO HIGH ALTITUDE (ELLINGSON)

It has been emphasized that the Lorentz profile inadequately represents the proper conditions above those altitudes for which the Doppler profile dominates. Ellingson's model is accurate for upwelling radiation only to 30 km, since he assumes the validity of the Lorentz line shape, stating, however, that this does not seriously limit the accuracy of the calculation of the down-welling radiation; and suggesting a method (Gille and Ellingson, [230]) for correcting the atmospheric transmittance by making a correction to that calculation using the Lorentz line shape. Thus, for the mixed Doppler-Lorentz, or Voigt, profile equivalent to the transmittance using only Lorentz, the expression is:

$$\tau_V = \tau_L^C \tag{273}$$

where τ_L = transmittance using the Lorentz shape

τ_V = transmittance using the Voigt shape

$C = \overline{A}_V/\overline{A}_L$

where $\overline{A}_V$ = mean absorption of a line with Voigt shape

$\overline{A}_L$ = mean absorption of a line with Lorentz shape

By defining:

$$h = 2\alpha_L/\alpha_D \tag{274}$$

and

$$H = \frac{C_2 wh\sqrt{\pi}}{2P} \tag{275}$$

230. J. C. Gille and R. G. Ellingson, "Correction of Random Exponential Band Transmissions for Doppler Effects," Appl. Opt., Vol. 7, No. 3, 1968, pp. 471–474.

and using these expressions, Gille and Ellingson obtain an expression (see Gille and Ellingson, 1968):

$$C = C(H, h) = \left[I(H, h)(2\psi_0 + 1)^{1/2}\right] \Big/ \pi\psi_0 h \tag{276}$$

in which $\psi_0 = S_0 w / 2\pi\alpha_L$ (see Eq. (281), Section 5), and I(H, h) is deduced from the line properties.

Thus, for the downwelling radiation from space in which the Doppler effect predominates, by neglecting variations in temperature, the non-homogeneous parameters $\overline{w}$ and $\overline{P}$, Eqs. (265) and (266) can be calculated for a variation in height from some arbitrary level to space, setting $\Phi(T)$ and $\chi(T)$ equal to unity. Using the hydrostatic equation:

$$dP = -g\rho_a\, dz$$

the values of $\overline{w}$ and $\overline{P}$ are obtained as follows:

$$\overline{w} = \int_z^\infty dw = \int_z^\infty \rho_g\, dz' = \int_z^\infty M(z')\rho_a\, dz' = -\int_P^0 M(P')\frac{dP'}{g}$$

where ρ_g = density of the absorbing gas

ρ_a = density of air

$M(z)$ = mixing ratio, assumed to be constant

g = acceleration of gravity

Thus:

$$\overline{w} = \frac{P_s M(z) P(z)}{g} \tag{277}$$

where P(z) = is in atmospheres

P_s = pressure at one atmosphere

Also:

$$\overline{P} = \frac{1}{w}\int_z^\infty P(z)\, dw = \frac{1}{w}\int_z^\infty P(z)\rho_g\, dz' = -\frac{1}{w}\int_P^0 M(z)P(z)\cdot\frac{dP}{g}$$

So:

$$\overline{P} = \frac{P(z)}{2} \tag{278}$$

The parameters h and H for the non-homogeneous case then become:

$$\bar{h} = \frac{\alpha_{L0}}{\alpha_D} P(z) \tag{279}$$

and

$$\bar{H} = \sqrt{\pi}\, C_2 \left(\frac{\alpha_{L0}}{\alpha_D}\right) \frac{P_s}{g} M(z) P(z) \tag{280}$$

All of the quantities in these equations are easily obtained except for the value C_2 which must be calculated from Eq. (264). Having obtained the values $\bar{h}$ and $\bar{H}$, the value C is obtained from the values tabulated by Gille and Ellingson (1968). Table 26 shows the values used to provide corrections tabulated in Table 27.

7.1.5 ELLINGSON'S 57- AND 100-INTERVAL MODELS

Ellingson (1972) presents two models, one derived from the specification of 57 different spectral intervals over which calculations are made in the spectral region from 0 - 2814 cm^{-1} (see Table 28); and the other derived from the specification of 100 spectral intervals to make up for deficiencies caused by the coarseness of the 57-interval model. The 100-interval model resulted from a need to reproduce the effect of the detailed structure of the band centers at 9.6 μm for O_3 and 15 μm for CO_2. The early data of Drayson and Young (1967) for CO_2 are delineated in 15 regions as shown in Table 24. The region between 600 and 800 cm^{-1} was divided into 33 intervals as demonstrated in Table 29. Thus, the Q-branches of the most intense bands (numbers 1-4 in Table 24) are concentrated in intervals numbered 19, 29, and 39. The widths of these intervals are small, whereas the widths of other intervals not containing strong Q-branch lines are larger and, as Ellingson points out, could be larger still without greatly affecting the average transmittance at those frequencies. The same intervals given in Table 29 are used for O_3, but for H_2O, which has fewer lines in the 600-800 cm^{-1} region, coarser intervals were used as shown in Table 30. When using the transmittance calculated from values in these intervals, the values for CO_2 and O_3 were summed to yield an average value over the larger interval.

Finally, the O_3 spectrum 9.6 μm was divided more finely than the H_2O spectrum in the region between 1000 and 1180 cm^{-1} as shown in Table 31. No attempt was made, however, to concentrate the Q-branch in a small interval as was done for CO_2. Taking the sum of all the intervals, it is noted that the 100-interval model is made up of the following:

$\Delta\lambda$ = 0-600 cm^{-1}	in 15 intervals	from Table 28
$\Delta\lambda$ = 600-800 cm^{-1}	in 33 intervals	from Table 29
$\Delta\lambda$ = 800-1000 cm^{-1}	in 5 intervals	from Table 28

TABLE 26. SUMMARY OF PARAMETERS NECESSARY TO CALCULATE APPROXIMATE CORRECTIONS OF THE TRANSMISSION FUNCTION FOR DOPPLER EFFECTS. (From Ellingson, 1972 [11].)

Gas	ν_0 cm^{-1}	α_{L0} cm^{-1}	α_{D0} cm^{-1}	M(z) gm/gm	C_2 cm^2/gm	$\bar{H}$	$\bar{h}$
Water vapor	400	0.1	6.89×10^{-4}	2.0×10^{-6}	10^3	3.65×10^5	145.4
Ozone	1040	0.07	1.09×10^{-3}	10^{-5}	10^5	1.17×10^3	63.9
Carbon dioxide	667	0.102	7.33×10^{-4}	4.84×10^{-4}	7.6×10^3	9.38×10^5	139.0

TABLE 27. APPROXIMATE CORRECTION FACTORS FOR THE RANDOM EXPONENTIAL BAND MODEL FOR DOPPLER EFFECTS. (From Ellingson, 1972 [11].)

Altitude (km)	Pressure (mb)	P	Correction Factor H_2O	O_3	CO_2
30	12.0	0.011800	1.0004	1.002	1.0000
35	5.8	0.005700	1.0010	1.014	1.0004
40	2.9	0.002800	1.0090	1.044	1.0030
45	1.5	0.001480	1.0220	1.136	1.0130
50	0.8	0.000789	1.0940	1.500	1.0480
60	0.2	0.000197	1.8000	4.000	1.4300

TABLE 28. WIDTHS OF SPECTRAL INTERVALS FOR THE 57 INTERVAL MODEL. (From Ellingson, 1972 [11].)

Interval No.	Range (cm^{-1})	Width (cm^{-1})
1 - 29	0 - 1160	40
30 - 31	1160 - 1200	20
32 - 56	1200 - 2200	40
57	2200 - 2814	614

TABLE 29. FINE SCALE DIVISIONS OF THE 15 μm CARBON DIOXIDE BANDS FROM 600 TO 800 cm^{-1}. (From Ellingson, 1972 [11].)

Interval No.	Range (cm^{-1})	Width (cm^{-1})
16 - 17	600.0 - 610.0	5.0
18	610.0 - 615.5	5.5
19	615.5 - 618.1	2.6
20	618.1 - 625.0	6.9
21 - 27	625.0 - 660.0	5.0
28	660.0 - 665.5	5.5
29	665.5 - 668.2	2.7
30	668.2 - 675.0	6.8
31 - 37	675.0 - 710.0	5.0
38	710.0 - 718.0	8.0
39	718.0 - 721.0	3.0
40	721.0 - 730.0	9.0
41 - 46	730.0 - 760.0	5.0
47 - 48	760.0 - 800.0	20.0

TABLE 30. SPECTRAL INTERVALS USED FOR WATER VAPOR IN THE 600 TO 800 cm^{-1}. (From Ellingson, 1972 [11].)

Interval No.	Range (cm^{-1})
17	600.0 - 610.0
20	610.0 - 625.0
23	625.0 - 640.0
25	640.0 - 650.0
27	650.0 - 660.0
29	660.0 - 668.2
31	668.2 - 680.0
35	680.0 - 700.0
37	700.0 - 710.0
39	710.0 - 721.0
42	721.0 - 740.0
46	740.0 - 760.0
47	760.0 - 780.0
48	780.0 - 800.0

$\Delta\lambda$ = 1000-1180 cm^{-1} in 20 intervals from Table 31
$\Delta\lambda$ = 1180-2814 cm^{-1} in 27 intervals from Table 28

7.1.6 TRANSMITTANCE IN THE CONTINUUM REGION

The local H_2O vapor lines are accounted for in the model, as shown in Table 32, which also shows the spectral regions of pertinence to the other gases, as well as a comparison with the analogous constituents in the work of Rodgers and Walshaw (1966). For the continuum region, in which the absorptance is caused by the wings of distant lines, Ellingson uses the empirical formula:

$$\tau_w = \exp\left(-k_c \overline{w}\,\overline{P} + k_e \overline{w}\,\overline{p}\right) \tag{281}$$

where k_c and k_e are mean values of the foreign- and self-broadening coefficient. The value $\overline{p}$ is the weighted partial pressure of H_2O vapor, analogous to $\overline{P}$, so that:

$$\overline{p} = \frac{1}{\overline{w}} \int p\, dw$$

7.1.7 CALCULATIONS OF HEATING RATES (ELLINGSON; RODGERS AND WALSHAW)

Ellingson applies the mathematical model, formulated through the above considerations, to the calculation of the radiative heating rate as a function of height in the atmosphere. The approach he takes, both in the formulation of a transmittance model and in the application to the calculation of heating rates is quite similar in many respects to the investigation by Rodgers and Walshaw (1966); so much so that, excluding results and the finer details, the work by Ellingson will be considered essentially representative in a first approximation to that of Rodgers and Walshaw. The fine details of the latter investigation, therefore, are cited only by reference. Calculation of the heating rate requires a knowledge of the upwelling and downwelling flux density at any point, and is given as the derivative of the net flux:

$$M'(z) = -\frac{dM_n(z)}{dz} \tag{282}$$

where:

$$M_n(z) = M^{\uparrow}(z) - M^{\downarrow}(z) \tag{283}$$

is the net flux density at z. The radiative transfer equation is set up in such a way as to simplify the computation involving derivatives of the transmittance function as much as possible. Retaining some of Ellingson's nomenclature, the more-or-less orthodox method of representing the radiance at z in a direction μ is given by:

TABLE 31. FINE SCALE DIVISIONS OF THE SPECTRUM BETWEEN 1000 TO 1180 cm^{-1}. (From Ellingson, 1972 [11].)

Interval No.	Width (cm^{-1}) O_3	Width (cm^{-1}) H_2O	Range
54 - 57	5	20	1000 - 1020
58 - 61	5	20	1020 - 1040
62 - 65	5	20	1040 - 1060
66 - 69	5	20	1060 - 1080
70	20	20	1080 - 1100
71	20	20	1100 - 1120
72	40	40	1120 - 1160
[illegible]	20	20	1160 - 1180

TABLE 32. A COMPARISON OF THE SPECTRAL CHARACTERISTICS OF THE RODGERS AND WALSHAW (1966) AND 100-INTERVAL MODELS. The Rodgers and Walshaw and 100-interval models are denoted RW and 100, respectively. (From Ellingson, 1972 [11].)

Active gas	Frequency range	Number of spectral intervals	Type of spectral data	Model
Water vapor	0 - 1000	10	Theoretical	RW
		34	Theoretical	100
	1000 - 1200	1	Empirical	RW
		9	Theoretical and laboratory	100
	1200 - 2200	9	Laboratory	RW
		25	Theoretical	100
	2200 - 2814	1	Theoretical	100
Carbon dioxide	582 - 752	1	Theoretical	RW
	520 - 840	36	Theoretical	100
Ozone	610 - 800	31	Theoretical	100
	960 - 1180	21	Theoretical	100
Methane	1200 - 1400	5	Laboratory	100
Nitrous oxide	1280 - 1400	3	Laboratory	100

$$L_\nu(\nu, z, +\mu) = L^*_\nu(\nu, 0)\tau(\nu, 0, +\mu) + \int_0^z L^*_\nu(\nu, z')\frac{d\tau(\nu, z', +\mu)}{dz'}dz' \tag{284}$$

for the upwelling radiance (see Section 2), where $L^*_\nu(\nu, 0)$ is the Planck function representing the surface, and the emissivity of the surface is assumed to be unity. The downwelling radiance is given by:

$$L_\nu(\nu, z, -\mu) = -\int_\tau^\infty L^*_\nu(\nu, z')\frac{d\tau(\nu, z', -\mu)}{dz'}dz' \tag{285}$$

By integrating over the spectral interval, $\Delta\nu$, Eq. (284) becomes:

$$\bar{L}_{\Delta\nu}(\nu, z, +\mu) = \frac{1}{\pi\Delta\nu}\left\{M^*_\nu(\nu, 0)\tau(\nu, 0, +\mu) + \int_0^z M^*_\nu(\nu, z')\frac{d\bar{\tau}_{\Delta\nu}(\nu, z', +\mu)}{dz'}dz'\right\} \tag{286}$$

and similarly for the downwelling radiance. Implicit in Eq. (286) are the statements:

$$M^* = \pi L^* \tag{287}$$

$$\bar{\tau}_{\Delta\nu}(\nu, z', \mu) = \frac{1}{\Delta\nu}\int_{\Delta\nu}\tau(\nu, z', \mu)\,d\nu \tag{288}$$

with $\bar{\tau}_{\Delta\nu}$ the band model calculations of transmittance in the different spectral regions, for the different gases. It is to be noted in all of the above equations that $\tau(\nu, \text{arg}, \ldots)$ denotes transmittance between the level z and that shown in the argument (arg). The derivative of the transmittance in Eqs. (284) and (285) can be removed in an integration by parts, and the upwelling and downwelling flux densities evolve respectively as:

$$M^{\uparrow}_\nu(z) = M^*(z) - \int_0^z \bar{\tau}_{\Delta\nu}(\nu, z')\frac{dM^*(z')}{dz'}dz' - \bar{\tau}_{\Delta\nu}(\nu, 0)[M^*(0) - M(0)] \tag{289}$$

and

$$M^{\downarrow}_\nu(z) = M^*(z) + \int_z^{z_T}\bar{\tau}_{\Delta\nu}(\nu, z')\frac{dM^*(z')}{dz'}dz' - \bar{\tau}_{\Delta\nu}(\nu, z_T)M(z_T) \tag{290}$$

where z_T is the top of the atmosphere. Note that an allowance is made, as it is by Rodgers and Walshaw (1966), for a discontinuity at the surface, as indicated by the term $[M^*(0) - M(0)]$, between the surface and the atmosphere above the surface. A similar term could have been included for radiation coming in from above the atmosphere, as it is by Rodgers and Walshaw. In Eqs. (289) and (290) the value of τ integrated over zenith angles is given by:

$$\bar{\tau}_{\Delta\nu}(\nu, z') = 2\pi\int_0^1 \bar{\tau}_{\Delta\nu}(\nu, z'; \mu)\mu\,d\mu \tag{291}$$

The heating rate is thus given by:

$$\frac{-dM(z)}{dz} = -[M^*(0) - M(0)]\frac{d\bar{\tau}_{\Delta\nu}(\nu, 0)}{dz} - M(z_T)\frac{d\bar{\tau}_{\Delta\nu}(\nu, z_T)}{dz}$$

$$+ \int_0^z \frac{d\bar{\tau}_{\Delta\nu}(\nu, z')}{dz}\frac{dM(z')}{dz'}dz' + \int_z^{z_T}\frac{d\bar{\tau}_{\Delta\nu}(\nu, z')}{dz}\frac{dM(z')}{dz'}dz' \qquad (292)$$

All that is needed, therefore, to calculate spectral radiance are the inputs to Eqs. (284) and (285) (or their equivalent as represented by Eq. (286)), which requires a knowledge of the Planck function or its derivative, and the transmittance function or its derivative. Similarly, from Eq. (282), the heating rate is calculated using the same function. As was shown previously, the transmittance is analytically expressed in terms of the Goody model (Eq. (262)), the Bignell model for H_2O continuum (Eq. (281)), or the Green, et al. model for CH_4 and N_2O (Eq. (272)). The derivatives of these expressions are fairly straightforward, yielding from the expression:

$$\frac{d\bar{\tau}_{\Delta\nu}(\nu, z'; \mu)}{dz} = \frac{d\bar{\tau}_{\Delta\nu}(\nu, z'; \mu)}{dw}\frac{dw}{dz} \qquad (293)$$

where $dw/dz = \rho_g/\mu$ for the slant path. Since $\bar{\tau}_{\Delta\nu}$ is implicitly a function of $\bar{w}$ and $\bar{P}$, the derivative of $\bar{\tau}_{\Delta\nu}$ can be expressed as:

$$\frac{d\bar{\tau}_{\Delta\nu}(\nu, z'; -\mu)}{dw} = \frac{\partial\bar{\tau}_{\Delta\nu}(\nu, z'; \mu)}{\partial\bar{w}}\frac{d\bar{w}}{dw} + \frac{\partial\bar{\tau}_{\Delta\nu}(\nu, z'; \mu)}{\partial\bar{P}}\frac{d\bar{P}}{dw} \qquad (294)$$

with

$$\frac{d\bar{w}}{dw} = \Phi(z) \qquad (295)$$

and

$$\frac{d\bar{P}}{dw} = \frac{1}{w}(\chi(z)P(z) - \Phi(z)\bar{P}) \qquad (296)$$

Differentiation of the expressions for $\bar{\tau}_{\Delta\nu}$ from the three models then yields:

1. Goody Model

$$\frac{d\bar{\tau}_{\Delta\nu}(\nu, z'; \mu)}{dw} = -C_1\Phi(z)\bar{\tau}_{\Delta\nu}(\nu, z'; \mu)\left(1 + C_2\frac{\bar{w}}{\bar{P}}\right)^{-3/2}\left(1 + \frac{C_2\bar{w}\chi(z)P(z)}{2\bar{P}^2\Phi(z)}\right) \qquad (297)$$

2. H_2O Continuum

$$\frac{d\bar{\tau}_{\Delta\nu}(\nu, z'; \mu)}{dw} = -P(z)\chi(z)\bar{\tau}_{\Delta\nu}(\nu, z'; \mu)\left(k_c + k_e \frac{p(z)}{P(z)}\right)$$

$$= -P(z)\bar{\tau}_{\Delta\nu}(\nu, z'; \mu)\left(k_c - k_e \frac{p(z)}{P(z)}\right) \text{ for } \chi(z) \equiv 1, \text{ i.e., } T = \text{const.} \quad (298)$$

3. CH_4 and N_2O

$$\frac{d\bar{\tau}_{\Delta\nu}(\nu, z'; \mu)}{dw} = -C_3 \eta P(z)\chi(z)\bar{\tau}_{\Delta\nu}(\nu, z'; \mu)(C_3 \bar{w} \bar{P})^{\eta - 1}$$

$$= -C_3 \eta P(z)\bar{\tau}_{\Delta\nu}(\nu, z'; \mu)(C_3 \bar{w} \bar{P})^{\eta - 1} \text{ for } \chi(T) \equiv 1 \quad (299)$$

In order to perform the calculation, Ellingson derives an expression for the spectral Planck function integrated over 5 cm^{-1} intervals for 14 temperatures spaced apart by 10 K from 180 K to 310 K. A fifth order polynomial was fitted to the resultant values and the final expression is:

$$M(T) = \sum_{i=0}^{5} g_{ri}(T - 260)^i \quad (300)$$

Integration over the variable μ is avoided by using the well-known diffusivity factor of Elsasser [231], given as r = 1.667.

Ellingson's physical model was a plane-parallel atmosphere made up of 100 levels for computation. The calculation of radiance, and hence fluxes and cooling rates, then amounts to the integration over a series of layers, represented in general by:

$$\int_{z_j}^{z_{j+1}} M(z_k, z') \frac{dM(z')}{dz'} dz'$$

where the integration is made to some prescribed level z_k, and is carried out in Gaussian quadrature for N(=2) as:

$$\frac{z_{j+1} - z_j}{2} \sum_{i=1}^{2N} W_i M(z_k, h_i)\left(\frac{dM(T)}{dT}\right)_{h_i}\left(\frac{dT}{dz'}\right)_{h_i} \quad (301)$$

The W's are the Gaussian weights and the h_i's are the values in the Gaussian formula corresponding to specified altitudes, calculated from:

231. W. M. Elsasser, Heat Transfer by Infrared Radiation in the Atmosphere, Report No. 6, Harvard University, Cambridge, 1942.

$$h_i = \frac{z_j + z_{j+1}}{2} + \frac{z_{j+1} - z_j}{2} Z_i \qquad (302)$$

where the Z_i are the Gaussian nodes. The values of the atmospheric parameters used as input to the calculations are obtained from radiosonde measurements of temperature, pressure and humidity. In Ellingson's work the z_j's are actually calculated as scale heights, H_j, given as $H \equiv -\ell nP$. His method of the specification of atmospheric parameters is not treated in this section. Integrations were made over a series of 99 layers in the atmosphere from the surface to 60 km. Details of the structure are shown in Table 33. The limit of 60 km was imposed for the purpose of making comparisons with satellite data.

In comparing his results with measured data, Ellingson averaged spectral radiance values from Nimbus 3 data over an interval of 20 cm^{-1} or less. His calculated values were averaged by a square slit function. The comparisons are shown as histograms in Figure 64. Tables 34 and 35 tabulate comparative values and show some of the statistics related to these comparisons.

7.2 USE OF THE QUASI-RANDOM MODEL (KUNDE, HAURWITZ)

Kunde (1967b) has applied the quasi-random model to the radiative transfer equation for thermal radiation superceded later by the direct integration method (Kunde and Maguire, 1973) as described in Section 6. The method is described in detail by Wyatt, Stull and Plass (1962a) for the H_2O molecule, and by Stull, Wyatt and Plass (1963) for the CO_2 molecule, which references must be consulted for an in-depth understanding of the procedure. For the reader who wants only peripheral information, a short description is given here, as applied by Kunde to H_2O and CO_2.

In accordance with Goody's (1964) development, the average value of transmittance in the range -1/2Nd to +1/2Nd for the random model is:

$$\bar{\tau} = \frac{\sum_{i=1}^{N} \int_{-1/2N}^{+1/2N} (d\nu_i/d) \exp(-w \cdot k_{\nu i})}{\sum_{i=1}^{N} \int_{-1/2N}^{+1/2N} (d\nu_i/d)}$$

One objection to the use of the random model is that the distribution of lines over the width considered for $\Delta\nu$ = Nd is not actually random, nor is the interval of integration infinitely wide, an approximation which had to be assumed as a necessary manipulation of the expression. Thus, for any chosen interval, the effect of lines outside the interval is not accounted for. The non-randomness of the lines, furthermore, causes different effects depending on how the lines actually became arranged. If they were actually more regular than randomness

TABLE 33. THE SPACINGS OF THE LEVELS OF COMPUTATION IN THE RADIATIVE TRANSFER MODEL. (From Ellingson, 1972 [11].)

Altitude range (km)	Thickness of layers (km)
0 - 12	0.3
12 - 30	0.5
30 - 48	1.0
48 - 60	2.0

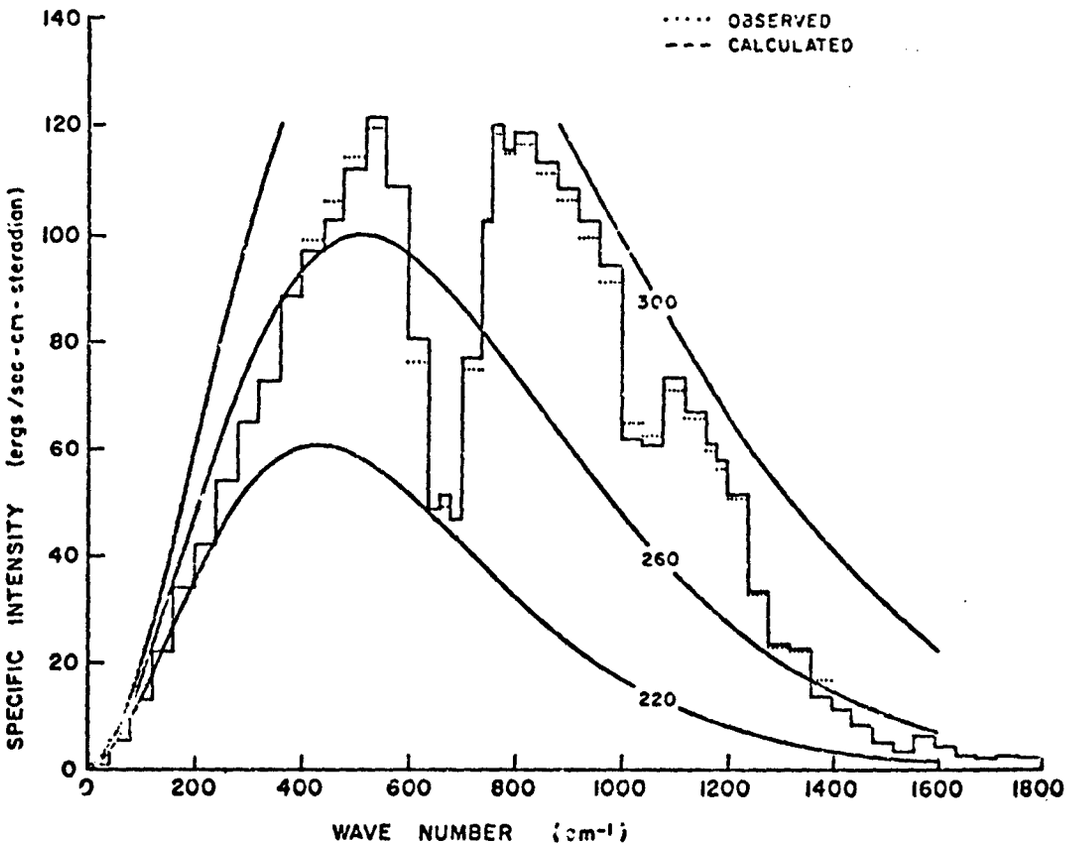

(a) June 1, 1969

FIGURE 64. THE IRIS OBSERVED AND 100-INTERVAL MODEL CALCULATED SPECTRALLY AVERAGED SPECIFIC INTENSITIES. The smooth curves give values of the Planck function for the indicated temperatures. (Reproduced from Ellingson, 1972 [11].)

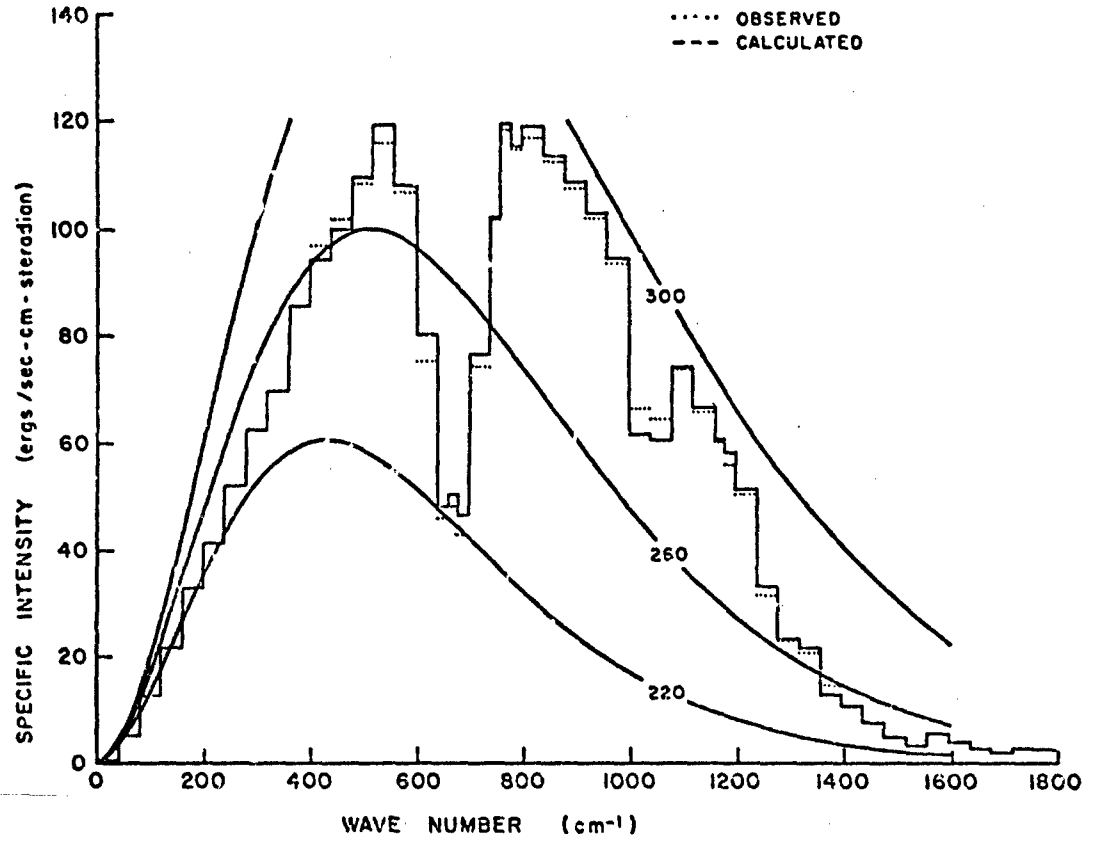

(b) June 3, 1969

FIGURE 64. THE IRIS OBSERVED AND 100-INTERVAL MODEL CALCULATED SPECTRALLY AVERAGED SPECIFIC INTENSITIES. The smooth curves give values of the Planck function for the indicated temperatures. (Reproduced from Ellingson, 1972 [11].) (Continued)

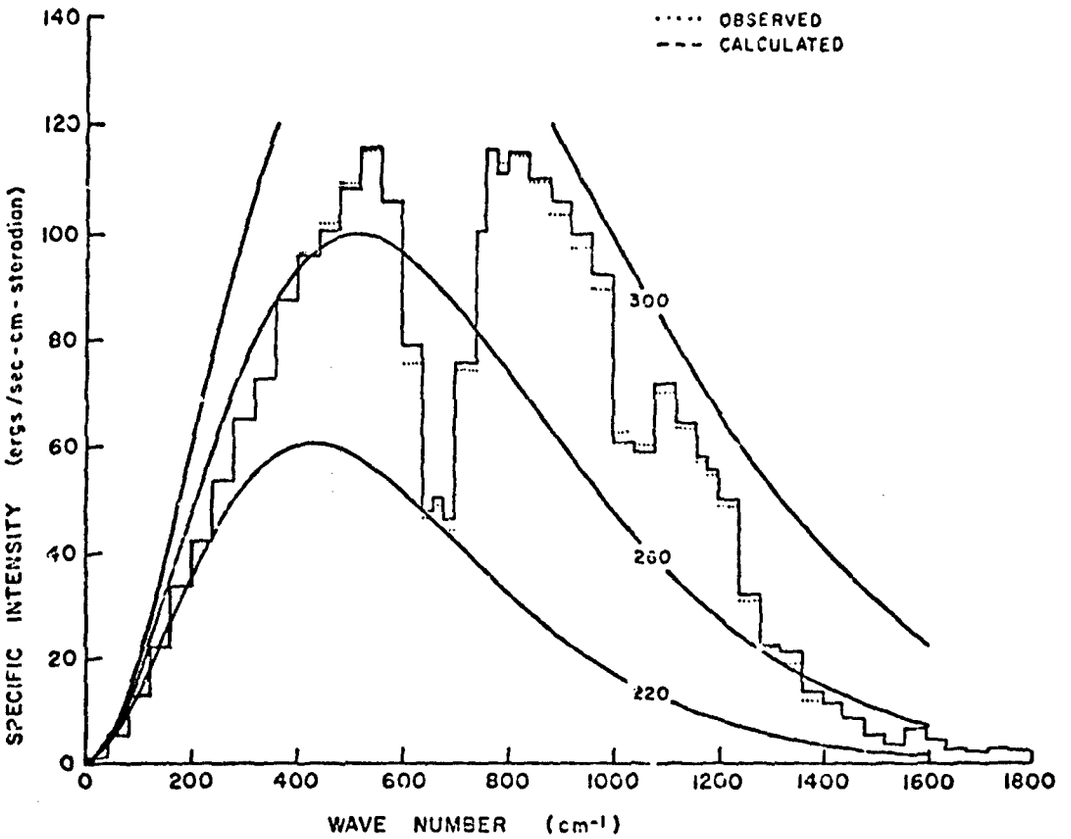

(c) June 4, 1969

FIGURE 64. THE IRIS OBSERVED AND 100-INTERVAL MODEL CALCULATED SPECTRALLY AVERAGED SPECIFIC INTENSITIES. The smooth curves give values of the Planck function for the indicated temperatures. (Reproduced from Ellingson, 1972 [11].) (Continued)

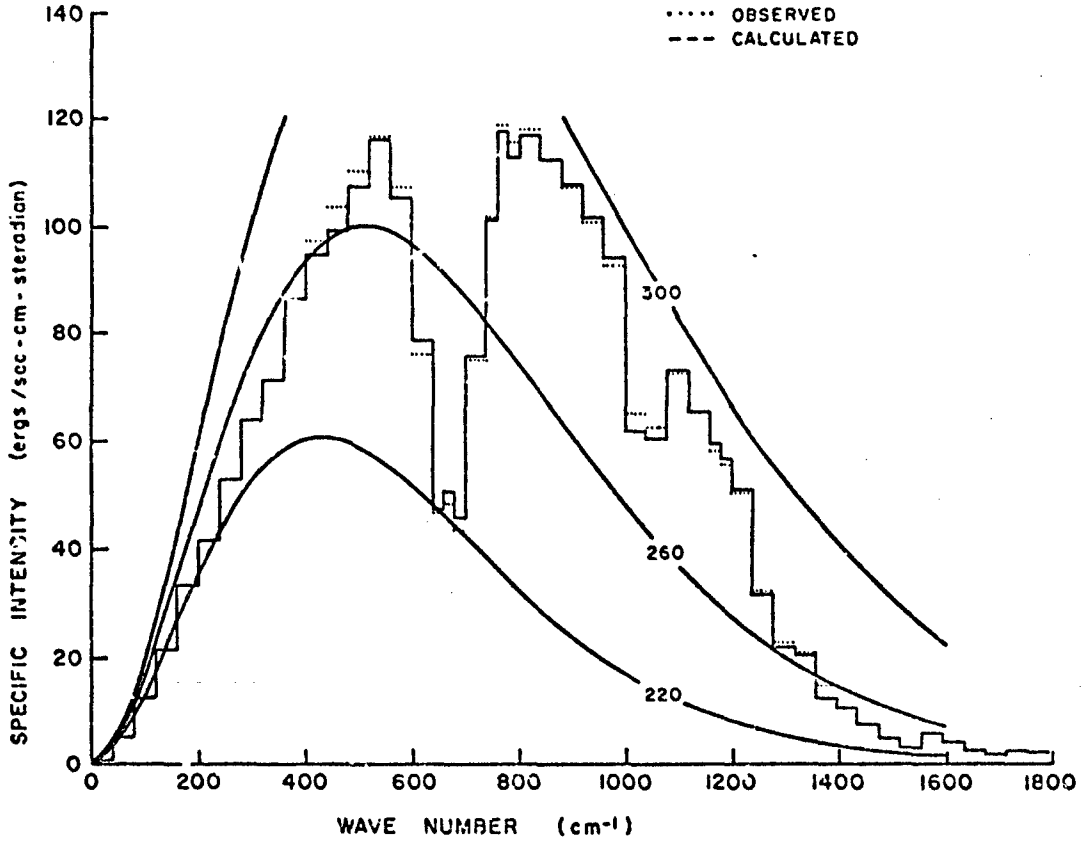

(d) June 8, 1969

FIGURE 64. THE IRIS OBSERVED AND 100-INTERVAL MODEL CALCULATED SPECTRALLY AVERAGED SPECIFIC INTENSITIES. The smooth curves give values of the Planck function for the indicated temperatures. (Reproduced from Ellingson, 1972 [11].) (Continued)

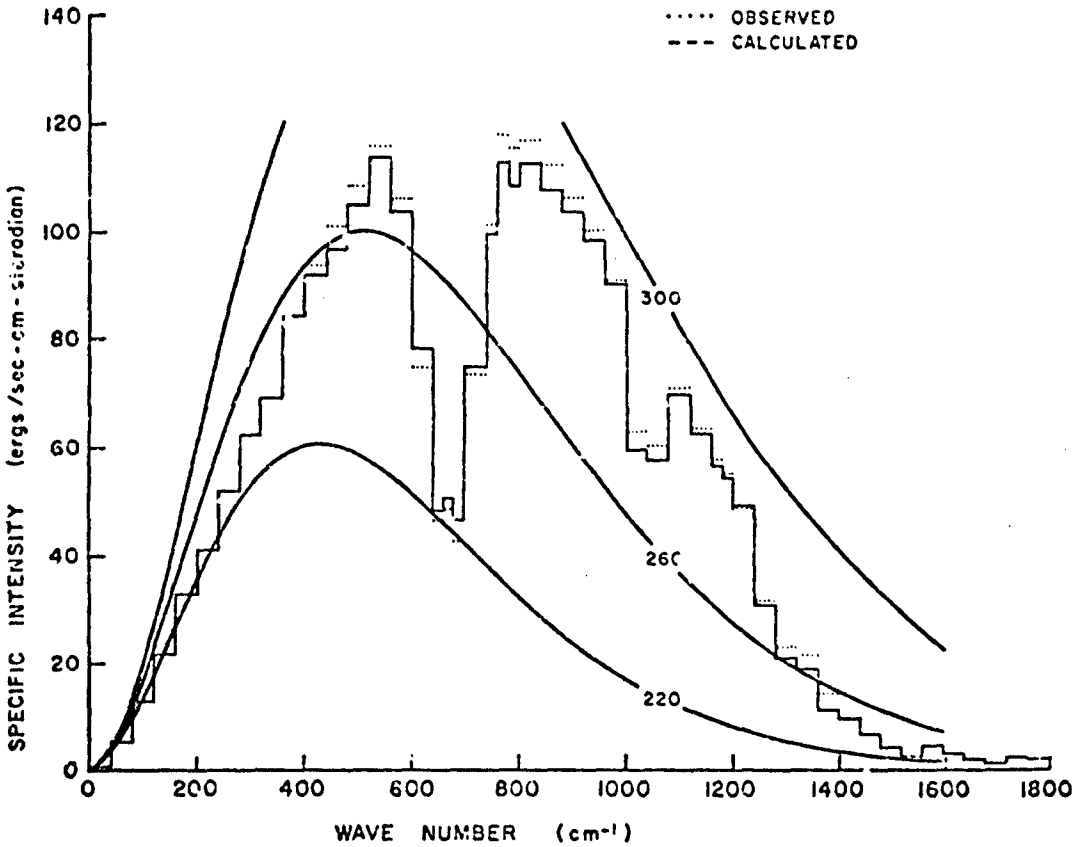

(e) July 1, 1969

FIGURE 64. THE IRIS OBSERVED AND 100-INTERVAL MODEL CALCULATED SPECTRALLY AVERAGED SPECIFIC INTENSITIES. The smooth curves give values of the Planck function for the indicated temperatures. (Reproduced from Ellingson, 1972 [11].) (Concluded)

TABLE 34. PERCENT DIFFERENCES BETWEEN OBSERVED AND CALCULATED UPWARD INTENSITIES FOR THE FIVE COMPARISONS. (From Ellingson, 1972 [11].)

Frequency range (cm^{-1})	Percent difference from observed Comparison number 1	2	3	4	5
400-440	-2.38	-2.68	- .33	-3.10	-2.19
440-480	-1.89	-1.89	-1.44	-4.16	-4.42
480-520	- .90	.77	- .92	-2.33	-3.12
520-560	1.53	2.90	.53	- .64	-1.85
560-600	.33	1.38	- .20	-1.46	-2.04
600-640	5.52	5.98	4.40	3.51	4.36
640-660	3.60	4.37	3.15	1.69	4.00
660-680	3.39	4.86	3.45	2.81	4.98
680-700	6.65	8.23	4.74	4.55	8.23
700-740	2.69	3.58	2.06	.78	2.21
740-760	- .58	.33	- .10	- .96	-1.80
760-780	1.33	1.25	.11	-1.44	-4.28
780-800	.47	.29	-1.39	-2.58	-6.11
800-840	1.72	1.87	.61	- .82	-4.11
840-880	1.69	1.24	.82	- .51	-3.83
880-920	2.32	1.53	2.25	.49	-2.45
920-960	2.64	.91	2.78	.97	-2.05
960-1000	3.22	1.40	3.20	1.39	- .65
1000-1040	-4.66	-6.99	-3.46	-5.25	-5.70
1040-1080	-3.30	-6.36	-2.34	-3.93	-4.10
1080-1120	3.38	.53	2.51	.78	-1.57
1120-1160	.80	1.45	1.51	.12	-1.19
1160-1180	1.82	.60	1.72	1.92	-2.52
1180-1200	3.25	3.59	1.88	1.69	-2.55
1200-1240	2.37	2.28	3.40	.91	1.87
1240-1280	1.36	5.34	3.82	-1.81	-3.16
1280-1320	1.81	1.03	1.59	-4.38	-7.47
1320-1360	.63	4.92	10.06	-1.48	-10.23
1360-1400	-19.02	-10.32	16.81	-15.23	-18.20
Totals					
400-1400	.81	.90	1.12	- .85	-2.26

TABLE 35. SOME STATISTICS ON THE OBSERVED AND CALCULATED UPWARD INTENSITIES. (From Ellingson, 1972 [11].)

Frequency range (cm^{-1})	Mean intensity (ergs $cm^{-1} sec^{-1}$ $steradian^{-1}$)		Percent difference	Standard deviation (ergs cm^{-1} sec^{-1} $steradian^{-1}$)	
	Observed	Calculated		Observed	Calculated
400-440	97.03	94.96	-2.14	2.08	2.01
440-480	103.15	100.02	-3.04	1.96	2.13
480-520	110.20	108.77	-1.30	1.75	2.42
520-560	116.91	117.49	.49	1.62	2.96
560-600	107.17	106.75	- .39	1.23	2.14
600-640	75.73	79.33	4.76	.40	.87
640-660	46.42	47.98	3.36	.19	.35
660-680	48.59	50.49	3.89	.28	.29
680-700	43.59	46.40	6.47	.53	.39
700-740	74.49	76.17	2.26	.50	.72
740-760	101.79	101.16	- .62	.75	1.01
760-780	117.94	117.29	- .55	1.21	2.84
780-800	115.02	112.87	-1.87	1.12	2.88
800-840	116.75	116.56	- .16	1.34	2.62
840-880	111.67	111.53	- .13	1.32	2.41
880-920	106.30	107.18	.82	1.50	2.11
920-960	100.06	101.10	1.04	1.68	1.93
960-1000	91.72	93.28	1.70	1.54	1.71
1000-1040	64.34	60.98	-5.23	1.57	1.02
1040-1080	61.83	59.38	-4.03	1.78	1.11
1080-1120	71.68	72.48	1.12	1.44	1.66
1120-1160	64.80	65.15	.54	1.28	1.66
1160-1180	58.52	58.94	.71	1.19	1.73
1180-1200	55.57	56.44	1.58	.57	1.68
1200-1240	49.59	50.66	2.16	1.00	.93
1240-1280	31.89	32.23	1.07	.88	1.05
1280-1320	22.82	22.47	-1.51	.51	.95
1320-1360	20.81	20.92	.50	1.24	1.05
1360-1400	14.59	13.03	-10.64	2.03	.82
Totals					
400-1400	76.29	76.25	- .05	.93	1.48

would imply, then the assumption of randomness would incorrectly accentuate overlap. On the other hand, there are cases where the clumping of lines occurs, for which absorption is complete only in the region of the clump. An assumed random distribution of these same strong lines often causes the calculation to yield erroneously high absorption.

The quasi-random model obviates these discrepancies to a large extent (Wyatt, Stull and Plass, 1962). By making the interval $Nd(=\Delta\nu)$ considerably smaller, say δ, the randomness of the distribution of lines within δ is more likely to be a reality. The interval can, of course, no longer be considered infinitely wide, nor can the number of lines be counted as infinitely great. Thus, no simple approximation to the integral can be made. The sub-intervals, δ_r, are all part of the larger interval, $\Delta\nu$, and each of the sub-intervals, δ_r, contains n_r lines with centers at $\nu_i (i = 1, 2, \ldots, n_r)$. In analogy with the random model, therefore, the average transmittance at the frequency (taken for convenience at the center of the interval) is:

$$\tau_r(\nu) = \frac{1}{\delta^{n_r}} \prod_{i=1}^{n_r} \int_{\delta_r} \exp\left[-k(\nu, \nu_i)w\right] d\nu_i \tag{303}$$

as shown in Section 5. Wyatt, et al. (1962) ascertain that Eq. (303) corresponds to the average transmittance over the interval, δ_r, inasmuch as it represents the average of the permutations of n_r positions of the spectral lines in the interval.

In accordance with Eq. (190) in Section 5,

$$\bar{\tau}_r(\nu) = \prod_{j=1}^{\infty} \left[\prod_{i=1}^{5} \left\{ \frac{1}{\delta} \int_{\delta_j} \exp\left[-\bar{S}_i wb(\nu, \nu_i)\right] d\nu_i \right\}^{n_i} \right] \tag{304}$$

Thus, in the calculation for $\bar{\tau}_r$, the direct contribution, i.e., the contribution from those lines in the interval containing ν, occurs for $j = r$. The wing contributions occur for all of the remaining intervals in which $j \neq r$.

Essentially, except for the complexity of the calculation, Eq. (304) represents the average transmittance at ν due to a chosen molecule for which the line parameters are known. Wyatt, Stull and Plass showed schematically, however, that the arbitrary choice of a boundary between two intervals can cause unnatural differences in the average transmittance between the two intervals. They proceeded to offset this error by merely calculating the transmittance for the given interval, and for the interval shifted to either side of the given interval. The shift was equal to one-half the size of the interval. The transmittance was weighted accordingly. Thus the calculations involved a set of unshifted intervals, δ_j^u and a set of shifted intervals, δ_j^s, yielding:

$$\bar{\tau}_r(\nu) = \frac{1}{3}\left[\bar{\tau}_{rs}(\nu - \delta/2) + \bar{\tau}_{ru}(\nu) + \bar{\tau}_{rs}(\nu + \delta/2)\right] \tag{305}$$

where the superscripts u and s refer respectively to the unshifted and shifted set of intervals, or meshes.

The basis for the calculation is the integral in Eq. (304), which is the average transmittance due to the line simulated in the i-th decade for the j-th interval. If the Lorentz shape is assumed, the expression:

$$\frac{1}{\delta}\int_{\delta} \exp\left[-\bar{S}_i wb(\nu, \nu_i)\right] d\nu_i$$

yields

$$\bar{\tau}_i(\nu) = \frac{1}{2}\int_{-1}^{1} \exp\left[\frac{-\rho^2 \xi_i}{(\epsilon - \eta)^2 + \rho^2}\right] d\eta \tag{306}$$

where $\xi_i = \bar{S}_i w/\pi\alpha_L$

$\rho = 2\alpha_L/\delta$

$\eta = 2y/\delta$

$\epsilon = 2z/\delta$

$y = \nu_i - \nu_0 - \delta/2$

$z = \nu - \nu_0 - \delta/2$

and the interval over which the integration is performed has the bounds $(\nu_0, \nu_0 + \delta)$. The reader is referred to the report by Wyatt, Stull and Plass (1962) for a delineation of the analytical solution to Eq. (306). Young [232] has demonstrated an expression analogous to Eq. (306) for the Doppler line shape:

$$\bar{\tau}_i(\nu) = \frac{1}{\delta}\int_{\delta_i} \exp\left[-\frac{\bar{S}_i w(\ell n\, 2)^{1/2}}{\alpha_D \pi^{1/2}} \exp\left(-\frac{(\nu - \nu_i)^2\, \ell n\, 2}{\alpha_D^2}\right)\right] d\nu_r$$

which is given by:

$$\bar{\tau}_i(\nu) = \frac{1}{2}\int_{-1}^{+1} \exp\left[-\xi_i' \exp\left(-\frac{\eta^2}{\beta'^2}\right)\right] d\eta \tag{307}$$

where:

232. C. Young, A Study of the Influence of Carbon Dioxide on Infrared Radiative Transfer in the Stratosphere and Mesosphere, Report No. 04682-1-T, University of Michigan, Ann Arbor, 1964.

$$\xi_i' = \frac{S_i w}{\alpha_D}\left(\frac{\ell n\, 2}{\pi}\right)^{1/2}$$

$$\beta' = \frac{2\alpha_D(\ell n\, 2)^{1/2}}{\delta}$$

Considering the complexity of the analytical form of the expression for the Lorentz shape, and the lack of an expression in analytical form for the Doppler and mixed shapes, Young designed a numerical technique using Legendre-Gauss quadrature for evaluating Eqs. (306) and (307). He did so by dividing the integration interval into seven sub-intervals comprising:

y = 0.0, 0.001, 0.005, 0.01, 0.05, 0.1, 0.5, 1.0

and applying the seven-point quadrature formula. Young claims to have obtained the same values for Eq. (306) as Wyatt, et al. obtained using the analytical technique. Kunde (1967b) used Young's technique in his theoretical computations of outgoing infrared radiance, except that he applied the eight-point instead of the seven-point quadrature formula. He claims to have obtained agreement with the values derived from the analytical form to within six significant figures. He also showed (see Table 36) that the assumption by Wyatt, et al. (1962), in which they evaluate the average transmittance at the center of the interval in the direct case as representative of the average value in the interval, is invalid when the average transmittance at the center is compared with that at the lower boundary of the interval. He suggests, however, that the averaging by shifted meshes helps validate the assumption.

The evaluation of the contributions of the wings of lines outside the interval is simpler than that of the direct contribution, but is still complicated, especially by the fact that, as suggested in other work [233], the simple Lorentz line shape must be modified (see Section 4). Since, for the wing contribution, the approximation $\alpha^2 << (\nu - \nu_0)^2$ can be made, the expression for the wing effect becomes (for the unmodified line):

$$\bar{\tau}_i(\nu) = \frac{1}{2}\int_{-1}^{+1} \exp\left[\frac{-\rho^2 \xi_i}{(\epsilon - \eta)^2}\right] d\eta \qquad (308)$$

and (for the Benedict-modified line):

$$\bar{\tau}_i(\nu) = \frac{1}{2}\int_{-1}^{+1} \exp - \left[\frac{A\,\xi_i \rho^2 \exp - \{a(\delta/2)^b |\epsilon - \eta|^b\}}{(\epsilon - \eta)^2}\right] d\eta \qquad (309)$$

233. W. S. Benedict, et al., "The Strengths, Widths, and Shapes of Lines in the Vibration-Rotation Bands of CO," Astrophys. J., Vol. 135, No. 1, pp. 277-297.

TABLE 36. AVERAGE TRANSMITTANCE AT CENTER AND BOUNDARY OF SUBINTERVAL δ. (From Wyatt, et al., 1962b [195].)

$\rho^2 \xi_1$	ρ	$\bar{\tau}(\nu_c)$	$\bar{\tau}(\nu_0)$
0.001	0.05	0.3724	0.9860
0.01	0.05	0.8454	0.9202
0.1	0.05	0.5413	0.7464
1.0	0.05	0.0897	0.3544
10.0	0.05	0.0	0.1108

where a = 0.0675

b = 0.7

A is a constant which makes the unmodified and modified forms continuous at $|\nu - \nu_i| = \delta$. The above are the values of the constants suggested by Wyatt, et al. The values suggested by Winters, et al. (1964) are: a = 0.08 and b = 0.8. Unlike Wyatt, et al., who assume an average transmittance in the interval equal to the transmittance at the center of the interval (obtaining $\tau(\nu) = \tau_{n_j}(\nu) \prod_{i=j} \tau_{n_i}(\nu)$, with the first and second terms respectively the direct and the wing contributions), Kunde applied 8-point Legendre-Gauss quadrature over the interval $\eta = -1$ to $\eta = +1$ in Eqs. (308) and (309). Differences are evident between the values calculated by the two different methods, especially for the interval adjacent to the one in which the transmittance is obtained.

Contributions to a given frequency from the wings extend infinitely far on both sides, so that some criterion is used to determine the points in the wings beyond which the calculations are terminated. These points coincide with the values $+\epsilon_M$ and $-\epsilon_M$ for which the transmittance $\bar{\tau}(\nu) = 0.999$. Using only the strongest intensity decade, the transmittance at ν can be written

$$\bar{\tau}(\nu) = \left\{ \exp\left(\frac{-\rho^2 \xi}{|\epsilon|^2} \right) \right\}^n$$

where ξ and n correspond to the strongest decade. Setting $\bar{\tau}(\nu)$ equal to 0.999 and calculating for ϵ_M^2 (see Kunde, 1967), the result is

$$\epsilon_M^2 = \text{const} \cdot P \cdot w$$

This expression is valid for the unmodified Lorentz line. An analogous expression can be obtained for the modified line.

Values for $\xi_0 (= \bar{S} P_0 / \pi \sigma_{L0})$ and for n have been tabulated for 5 cm^{-1}* unshifted and shifted meshes for H_2O vapor at 300, 250 and 200 K between 1000 and 10,000 cm^{-1} (Wyatt, et al., 1962). In the same report, the values of transmittance were calculated for different conditions. A list of these conditions is given in Table 37. Similar expressions have been calculated for CO_2 between 500 and 10,000 cm^{-1} (Stull, Wyatt and Plass, 1963). Table 37 also lists the transmission calculations that were made for CO_2 by the same authors. The reader is referred to the original reports for the mammoth sets of tables from which the determinations

*Note that 5 cm^{-1} is too large for some regions, e.g., near Q-branches. Hence, the calculated absorption is too large.

TABLE 37. HOMOGENEOUS PATHS FOR WHICH TRANSMISSION DATA ARE TABULATED

Line Shape	Gas	Wavelength Range (cm^{-1})	w Range (pr cm)	Pressure Range (atm)	Temperature ($^{\circ}K$)	Entries (cm^{-1})	Resolution (cm^{-1})
Lorentz	H_2O	1000-3400	0.001-50	0.01-1.0	200-300	2.5	5.0
Lorentz		1000-10,000	0.001-50	0.01-1.0	200-300	10	20
Lorentz		1000-10,000	0.001-50	0.01-1.0	200-300	25	50
Lorentz		1000-10,000	0.001-50	0.01-1.0	200-300	50	100
Benedict	CO_2	507.5-9250.	0.2-10,000	0.01-1.0	200-300	2.5	5
Lorentz		507.5-9255.	0.2-10,000	1.0	300	2.5	5
Benedict		520.0-9999.	0.2-10,000	0.01-1.0	200-300	10	20
Benedict		550.0-9975.	0.2-10,000	0.01-1.0	200-300	25	50
Benedict		600.0-9950.	0.2-10,000	0.01-1.0	200-300	50	100

ERIM
FORMERLY WILLOW RUN LABORATORIES THE UNIVERSITY OF MICHIGAN

of atmospheric transmittance can be made. In consideration of the recent set of line parameters available (McClatchey, et al., 1973), it may be more accurate for one to compile his own set of data, which would be a lengthy but relatively uncomplicated task using the procedure which is well detailed by Wyatt et al. (1962). The tables of transmittance compiled by Wyatt, Stull and Plass, and categorized in Table 37 has been available, apparently, from the authors on tape, as stated in their report, and indeed was made available to Kunde for his calculations. Whether it is still available some 7 years after Kunde's published results, has not been ascertained.

Using the recent AFCRL data one may generate a set of ξ_0 and n values similiar to those by Wyatt, et al. using the procedure delineated in their report, namely:

(1) [This step pertains to the determination of the line parameters]

"(2) On the basis of (1), the integrated intensities of all contributing vibration-rotation lines were calculated systematically.

"(3) As the intensity and frequency of each line was generated, the line was assigned to the frequency interval spanning it.

"(4) Once assigned to an interval, a given line was then grouped according to the intensity decade into which it fell. Within a particular decade a running count was made of the number of lines placed therein. Also retained was a net sum of the intensities of all those lines placed in each decade. If a line was generated with an intensity more than eight orders of magnitude below the strongest line already placed in the given frequency interval, it was ignored. On the other hand, ' stronger lines were subsequently generated, the data for weaker lines was dropped when they occurred in intensity groups which were more than four groups below the most intense. In short, either the top five strongest groups were retained, or only enough groups to span eight orders of magnitude. The latter choice resulted in less than five groups when the lines in that portion of the spectrum were very weak.

"(5) The coefficients ξ_{0_k} were then calculated for each frequency interval by dividing the intensity sums by the number of contributing lines and thence dividing the resulting average strengths by $\pi\alpha_{L0}$. For H_2O, the value $\alpha_{L0} = 0.10\ cm^{-1}$ was used.

"Once the coefficients ξ_{0_k} and n_k were generated, the effective transmissions were calculated at frequencies corresponding to the centers of the chosen frequency intervals of width $5\ cm^{-1}$. Sequentially, the coefficients ξ_k for various combination of the pressure* and amounts

*It should be mentioned that the term pressure is used here in the sense of Howard, Burch and Williams, viz for water vapor the effective broadening pressure is equal to the sum of the total pressure plus 5.3 times the partial water vapor pressure.

of absorbing gas were calculated ($\xi_k = \xi_{0_k}$ w/P). From each of these sets the effective transmissions were calculated as follows:

"(1) All the transmissions were set equal to unity.

"(2) Starting with the lowest frequency interval, the direct contributions to the transmissions were calculated at the center of the interval for each intensity group contained therein. These were then multiplied together and thence by the factor 1 initially set. Hence, the resulting transmission represented the direct contributions from the five intensity groups which represent all lines having an intensity within 10^{-6} of the strongest line in the frequency interval.

"(3) Subsequent to the calculation of the direct contributions, the coefficients were used to calculate the wing contributions to the transmissions at the center of the interval of interest. The wing contributions from lines at both lower and higher frequencies were considered. The calculation was made for the Lorentz line shape and, in the case of CO_2, for the Benedict modification. Thus, as any contribution to the transmission at a given frequency was generated (be their origin direct or wing), its value was multiplied into those previously calculated at that frequency.

"(4) The wing calculations were carried out at frequencies farther and farther from the chosen interval until their contributions to the transmissions exceeded 0.999."

As was done in the original work, one must calculate transmittances for special cases (see Table 37) and interpolate for those other cases pertinent to his own problem. Of course, the Curtis-Godson approximation can be used for the calculation of slant-path conditions, as it can in the calculations performed by other techniques. The interpolation technique formulated by Wyatt, et al. (1962) is reproduced as follows:

"The simplest analytical procedure is that consisting of logarithmic interpolation between non-zero values of the absorption A. Express the absorption in the form

$$A = 1 - \tau = e^{-f(P,T,w)}$$

where f is usually a complicated function of pressure (P), temperature (T), and absorber amount (w). At points where one or both of the tabular values of τ are identically equal to unity, linear interpolation on τ provides more than sufficient accuracy. Otherwise, it is far more accurate to interpolate f(P, T, w). This is true because the main part of the functional dependence of the absorption on P, T, and w is usually represented by the exponential factor. As only three significant figures are given in the tables, a first order interpolation generally provides sufficient accuracy. It should be noted that the entries for varying pressure and path length are given in terms of values that are nearly equidistant when plotted on a logarithmic scale (e.g., 1.0, 0.5, 0.2, 0.1, 0.05, . . .).

"From the above equation one has

$f(P, T, w) = -\ln A$

When the absorptance at constant P is plotted against w on a log-log graph, the resulting curve has only a small curvature and displays long linear sections. Similar remarks apply to an absorptance curve at constant w plotted against P. For these reasons, the most accurate interpolation is obtained by taking equal logarithmic intervals for P and w so that

$$\Delta f = \frac{\partial f}{\partial x}\Delta x + \frac{\partial f}{\partial T}\Delta T + \frac{\partial f}{\partial y}\Delta y$$

where $x = \ln P$ and $y = \ln w$. Thus,

$f(P + \Delta P, T + \Delta T, w + \Delta w) = f(P, T, w) + \Delta f$

and

$\tau(P + \Delta P, T + \Delta T, w + \Delta w) = 1 - A(P + \Delta P, T + \Delta T, w + \Delta w) = 1 - \exp - (f + \Delta f)$

"The following examples illustrate the method described above.

a) Given: P = 1 atm, T = 300 K
at w = 0.1, τ = 0.583, A = 0.417
at w = 0.2, τ = 0.439, A = 0.561

Find: at w = 0.17 for P = 1 atm, T = 300 K

Procedure: A(0.1) = 0.417; f(0.1) = 0.3747
A(0.2) = 0.561; f(0.2) = 0.5780
$\ell n(0.1) = -2.3026$
$\ell n(0.17) = 1.7720$
$\ell n(0.2) = -1.6094$

Hence: $\Delta f = \frac{\partial f}{\partial(\ell n\, w)}\Delta(\ell n\, w) = \frac{0.5780 - 0.8747}{-1.6094 + 2.3026}(-1.7720 + 2.3026)$

$= \frac{-0.2967}{0.6932}0.5306 = -0.2271$

Therefore: $f = f(0.1) + \Delta f = 0.8747 - 0.2271 = 0.6476$

$\tau(0.17) = 1 - e^{-0.6476} = 0.477$

b) Given: P = 1 atm, T = 300 K
at w = 2.0, τ = 0.648, A = 0.352
at w = 5.0, τ = 0.425, A = 0.575
P = 0.5 atm, T = 300 K
at w = 2.0, τ = 0.715, A = 0.285
at w = 5.0, τ = 0.545, A = 0.455

Find: $\tau(P, w)$ at w = 3.2, P = 0.75, T = 300 K

Procedure: A(1, 2.0) = 0.352; f = 1.0441
A(1, 5.0) = 0.575; f = 0.5534
A(0.5, 2.0) = 0.285; f = 1.2553
A(0.5, 5.0) = 0.455; f = 0.7875
$\ell n(2.0) = 0.6931$; $\ell n(1.0) = 0.0000$

$$\ell n(3.2) = 1.1631;\ \ell n(0.75) = -0.2877$$
$$\ell n(5.0) = 1.6094;\ \ell n(0.5) = -0.6931$$

Hence: $$\Delta f = \frac{\partial f}{\partial(\ell n\, w)}\Delta(\ell n\, w) + \frac{\partial f}{\partial(\ell n\, P)}\Delta(\ell n\, P)$$

$$= \frac{0.5534 - 1.0441}{1.6094 - 0.6931}(1.1631 - 0.6931)$$

$$+ \frac{1.2553 - 1.0441}{-0.6931 + 0.0000}(-0.2877)$$

$$= -0.2517 + 0.0877 = -0.1640$$

Therefore: $f(0.75, 3.2) = f(1, 2.0) + \Delta f = 1.0441 - 0.1640 = 0.8801$

$$\tau(0.75, 3.2) = 1 - e^{-0.8801} = 0.585."$$

It is pertinent to include here a description of Kunde's method for the calculation of atmospheric transmittance using the quasi-random model. He broke the spectral range into intervals of 5 cm^{-1} and used this as the value of δ, which then determined the limit of resolution of his calculated values. This allowed him to consult directly the values in the reports (Wyatt, Stull and Plass, 1962; Stull, Wyatt and Plass, 1963), for which the intervals chosen were 5 cm^{-1}. Quoting from Kunde (1967b), the following explanation is given.

"The transmittances are evaluated, considering the integrated absorption coefficients to be at an isothermal temperature along the atmospheric slant path. The isothermal temperature which best represents the temperature variation along the slant path must be chosen from 200 and 300 K for CO_2 and from 200, 250 and 300 K for H_2O. With the optical path length, the isothermal temperature and the average effective pressure known, the quasi-random transmittance can then be evaluated.

"The quasi-random transmittances for a given temperature, pressure, and optical path length are calculated as follows. To insure that the contributions of all lines are taken into account, all intervals from $\nu_I - \nu_M$ to $\nu_F + \nu_M$ must be considered. (ν_I is the center of the starting interval, δ; ν_F is the center of the final interval, δ.) For the above intervals, the coefficients ξ_{0_i} and η_i, corresponding to temperature T_I for both the unshifted and shifted meshes, are read from magnetic tape and put in core storage. The direct contribution is then computed for each 5 cm^{-1} interval from ν_I to ν_F using the numerical quadrature of Eq. (306). Next, the wing contribution is computed starting with the interval at $\nu_I - \nu_M$ and subsequently considering all intervals until the interval $\nu_F + \nu_M$ is reached. For a given interval, the associated coefficients were used to calculate the wing contribution to the transmittances at the center of all the other intervals from ν_I to ν_F. The wing contribution was computed for higher and lower wave numbers until the contribution exceeded 0.999. In each interval of interest, the wing contribution was multiplied into the values previously calculated. When the computation of the wing contribution was completed, the direct and wing contribution for each

interval of interest were multiplied together. The same procedure was then used for the shifted mesh. The quasi-random transmittance is then obtained by averaging the transmittances of the unshifted and shifted meshes according to Eq. (305). The transmittances are computed for each wave number range of interest starting with the level in the matrix representing the ground, and subsequently evaluating the transmittances for each level in the matrix until the top of the atmosphere is reached. The output of the calculation consists of a height vs transmittance matrix for each 5 cm^{-1} interval. This data is put on magnetic tape to serve as input data for one third section of the program."

Kunde calculated $\bar{\tau}_i(\nu)$ using the quasi-random model on the mixed line shape (see Section 4) applying 8-point Legendre-Gauss quadrature to the seven sub-intervals introduced earlier in this section, for pressures less than 100 mb and distances from the line center of less than 2.5 cm^{-1}. A comparison of the average transmittance as obtained with the Lorentz line with that obtained for a mixed line is shown in Table 38.

Comparisons are made of the results of the quasi-random model with experimental results and with the results of other methods by a number of investigators. Figures 65 and 66 make such a comparison in the 2.7 and 6.3 μm bands of H_2O vapor with the experimental results of Burch, et al. [234] for transmittance averaged over 20 cm^{-1}. Figure 67 shows CO_2 comparisons with the experimental results of Burch, Gryvnak and Williams [235] in three spectral regions. Although there tends to be an overestimate of CO_2 absorption in the Q-branches, the comparison on CO_2 is fairly good; on H_2O vapor it is relatively poor in certain regions. Kunde compared his calculated results with those of Burch, et al. (1962) for the 6.3 μm band of H_2O vapor. The results are shown in Table 39 for an integration between 1250 and 1590 cm^{-1} and between 1590 and 2100 cm^{-1}. When the disparity between calculated and experimental values was observed to be large, the calculation was repeated, and the half-width changed, by trial and error, from 0.10 to 0.16 (for 1250-1590 cm^{-1}) and 0.115 cm^{-1} (for 1590-2100 cm^{-1}). The integrated absorptances in the 15 μm band of CO_2 were also compared and the results are shown in Table 40. Here the values are compared with those of Young (1964) as well as with experiment.

Young made comparisons of his own from the quasi-random model, but using his line parameter data. Some examples of the spectral differences are shown for the 15 μm band of CO_2 in Figure 68. The calculated values are presented as histograms, representing values of transmittance averaged over 5 cm^{-1}. Young asserts that the quasi-random model tends to

234. D. E. Burch, D. A. Gryvnak and E. B. Singleton, et al., Absorption by Carbon Dioxide, Water Vapor, and Minor Atmospheric Constituents, Report No. AFCRL 62-298, Ohio State University, Columbus, 1962.

235. D. E. Burch, D. A. Gryvnak and D. Williams, Science Report No. 2, AF 19(604)-2633, Ohio State University, Columbus, January 1961.

TABLE 38. QUASI-RANDOM TRANSMITTANCE FOR LORENTZ LINE SHAPE AND FOR MIXED LINE SHAPE. T = 300 K. (From Kunde, 1967 [13].)

ν (cm^{-1})	Pressure	Optical Path Length	Transmittance	
			Lorentz	Mixed
585	100 mb	100 cm-atm	.7722	.7722
640	100 mb	100 cm-atm	.0605	.0605
665	100 mb	100 cm-atm	.0005	.0005
585	10 mb	10 cm-atm	.9745	.9738
640	10 mb	10 cm-atm	.7702	.7681
665	10 mb	10 cm-atm	.3528	.3501
585	10 mb	100 cm-atm	.9073	.9059
640	10 mb	100 cm-atm	.4169	.4146
665	10 mb	100 cm-atm	.0709	.0706
585	1 mb	10 cm-atm	.9902	.9864
640	1 mb	10 cm-atm	.9175	.9043
665	1 mb	10 cm-atm	.6791	.6578
585	.001 mb	10,000 cm-atm	.9894	.9142
640	.001 mb	10,000 cm-atm	.9172	.8522
665	.001 mb	10,000 cm-atm	.6789	.6197

ERIM
FORMERLY WILLOW RUN LABORATORIES, THE UNIVERSITY OF MICHIGAN

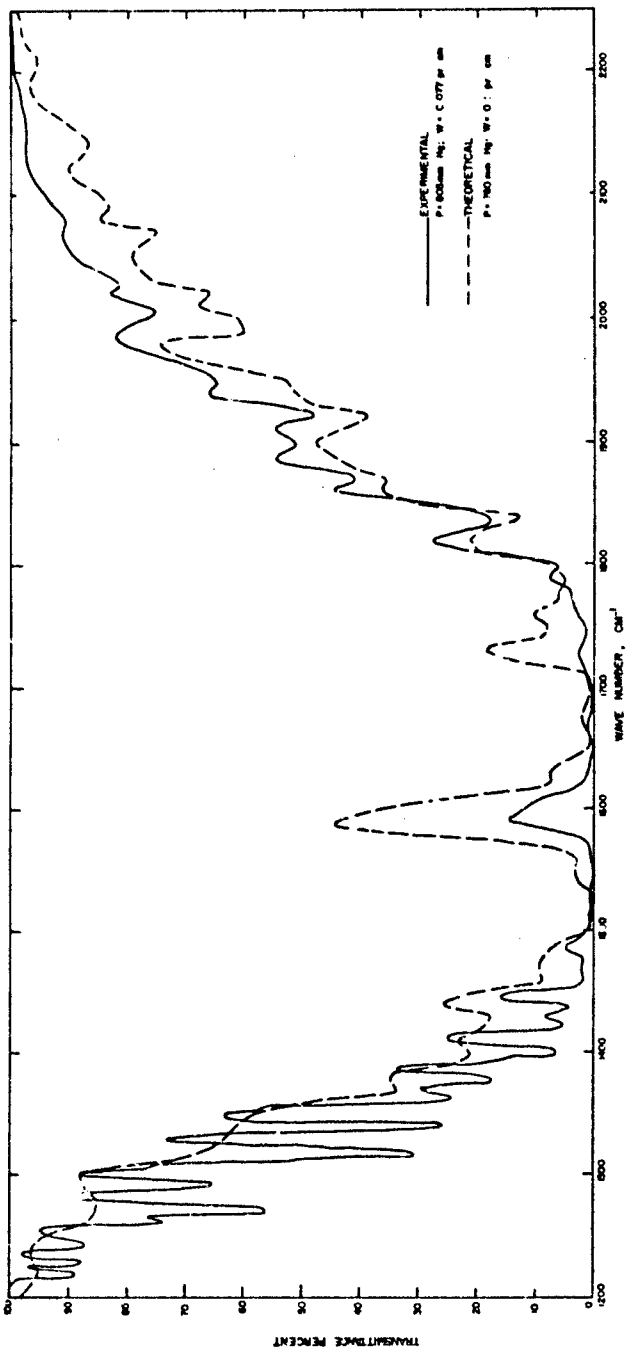

FIGURE 65. ABSORPTANCE OF 2.7 μm H_2O BAND. (Reproduced from Wyatt, et al., 1962a [15].)

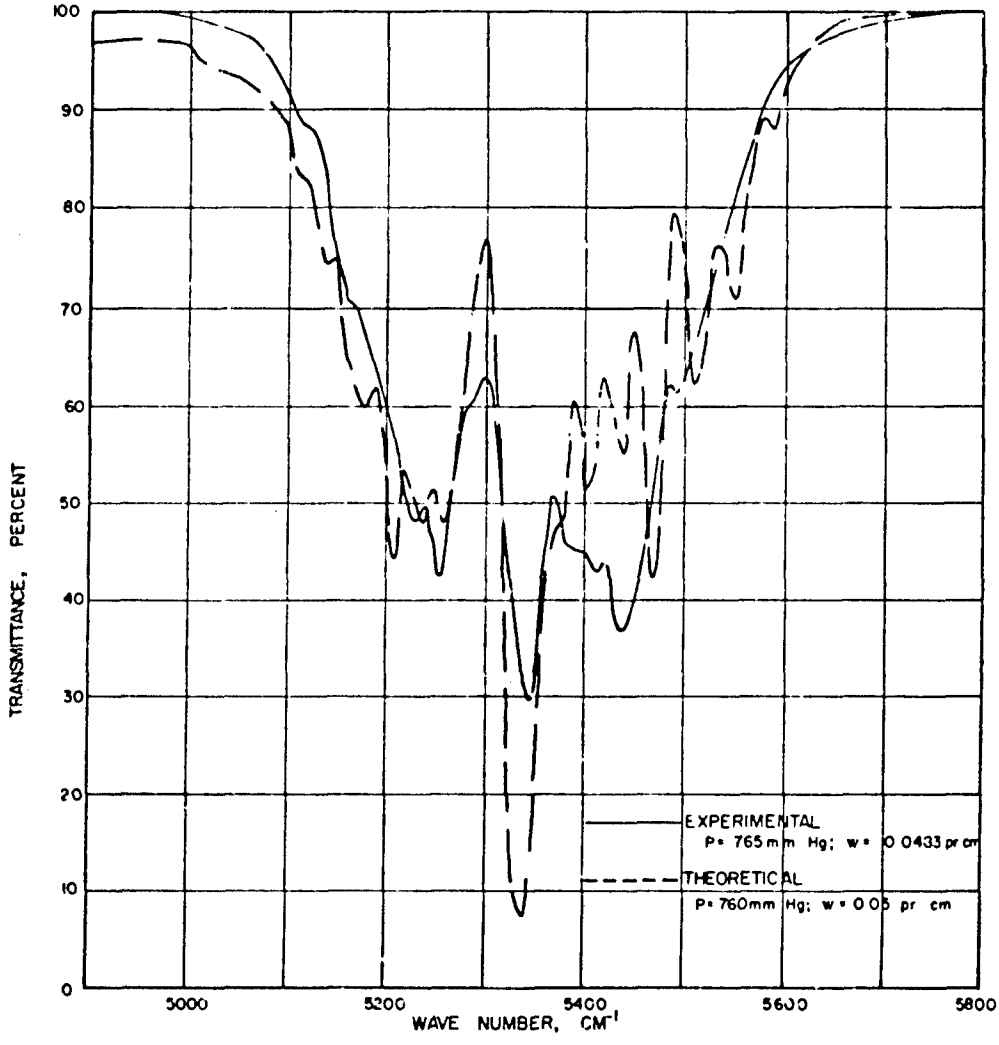

FIGURE 66. ABSORPTANCE OF 3.3 μm BAND. (Reproduced from Wyatt, et al., 1962a [15].)

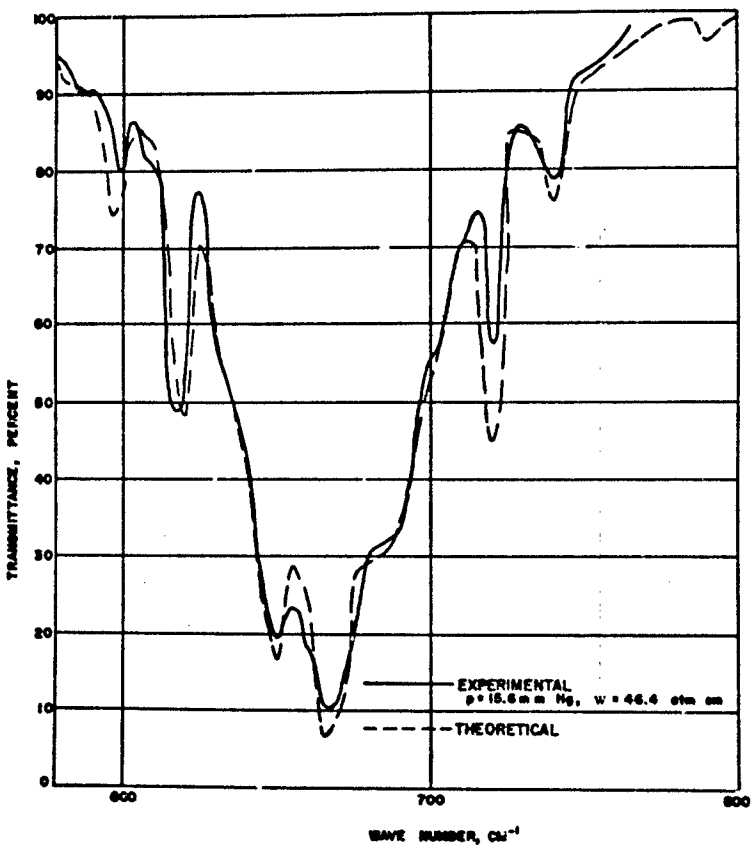

(a) 15 μm Band

FIGURE 67. COMPARISON OF THEORETICAL RESULTS WITH THE EXPERIMENTAL MEASUREMENTS OF BURCH, GRYVNAK AND WILLIAMS. (Reproduced from Stull, et al., 1963 [16].)

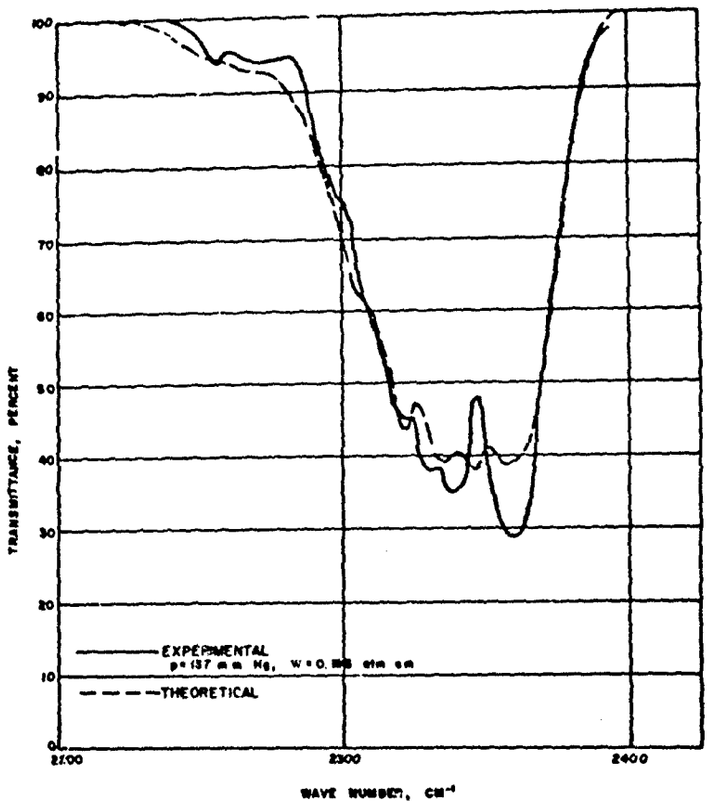

(b) 4.3 μm Band

FIGURE 67. COMPARISON OF THEORETICAL RESULTS WITH THE EXPERIMENTAL MEASUREMENTS OF BURCH, GRYVNAK AND WILLIAMS. (Reproduced from Stull, et al., 1963 [16].) (Continued)

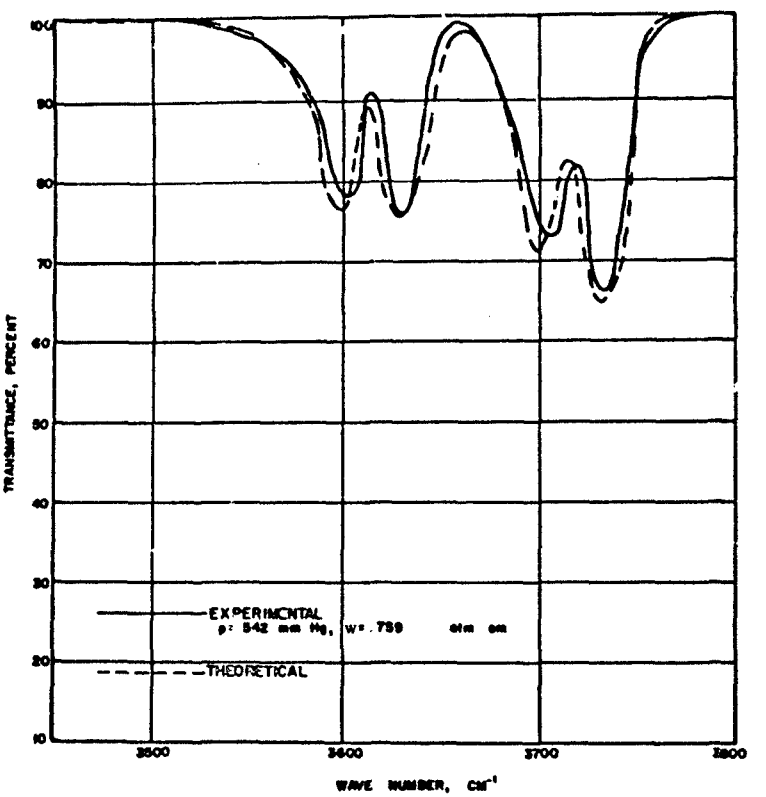

(c) 2.7 μm Band

FIGURE 67. COMPARISON OF THEORETICAL RESULTS WITH THE EXPERIMENTAL MEASUREMENTS OF BURCH, GRYVNAK AND WILLIAMS. (Reproduced from Stull, et al., 1963 [16].) (Concluded)

TABLE 39. COMPARISON OF QUASI-RANDOM AND EXPERIMENTAL INTEGRATED ABSORPTANCES FOR THE 6.3 μm H_2O BAND. (From Kunde, 1967 [13].)

			$\int A d\nu$ 1250-1590 cm^{-1}			$\int A d\nu$ 1590-2100 cm^{-1}		
Sample	P_e	w	Experimental	Calculated		Experimental	Calculated	
				α_L = 0.10	α_L = 0.16		α_L = 0.100	α_L = 0.115
	atm	pr cm						
1	.0194	.0017	12.3	9.6	15.0	12.7	13.4	15.4
2	.0232	.0018	14.9	10.9	17.1	14.4	15.4	17.6
3	.0345	.0019	17.0	13.4	20.9	16.4	18.9	21.6
4	.0530	.0019	21.1	16.2	25.0	22.4	22.9	26.1
5	.1167	.0017	30.0	21.3	32.6	30.3	30.3	34.5
6	.3540	.0019	50.9	35.1	51.8	50.9	50.3	56.7
7	1.0171	.0018	79.4	48.9	69.0	79.4	71.2	79.1
8	.0184	.0034	18.2	13.7	21.4	13.6	19.1	21.9
9	1.0171	.0036	102	70.1	94.8	114.	101	112
10	.0447	.0041	30.6	22.3	34.2	31.3	31.4	35.7
11	.0580	.0047	38.0	26.8	40.6	39.2	37.7	42.7
12	.0755	.0048	45.5	30.3	45.6	48.8	42.7	48.3
13	.1382	.0045	56.7	37.6	55.7	59.5	53.4	60.2
14	.0447	.0081	47.3	31.5	47.4	53.1	43.9	49.7
15	.0580	.0092	54.0	37.4	55.6	59.8	52.2	59.0
16	.0755	.0095	63.9	42.3	62.3	69.9	59.4	66.9
17	.1382	.0089	76.6	52.3	75.3	80.7	74.0	82.8
18	.0447	.0161	63.7	43.9	64.6	70.5	60.8	68.4
19	.0580	.0183	72.1	51.9	75.2	80.2	72.0	80.7
20	.0755	.0190	86.6	58.7	83.9	96.5	81.7	91.3
21	.1382	.0176	100	71.5	99.4	117.	101.	112.
22	.0447	.0322	78.9	60.5	86.4	99.5	83.1	92.8
23	.0580	.0364	90.4	70.8	99.2	108.	97.6	108
24	.0755	.0378	110.	79.5	110	125.	110.	122
25	.1382	.0352	131.	96.0	128	153.	135	148
26	.0487	.0045	33.8	24.3	37.1	38.1	34.1	38.8
27	.0491	.0089	48.1	34.3	51.4	55.3	47.8	54.1
28	.0496	.0179	69.7	48.2	70.4	79.2	66.7	74.9
29	.0500	.0359	93.0	66.4	93.8	109.	91.3	102
30	1.0658	.0102	153	113	141	181	164.	176
31	1.0632	.0198	190	144	172	226.	211	224
32	1.0605	.0389	220	178	204	273	263	275
33	1.0592	.0770	256	212	234	319	315	325

TABLE 40. COMPARISON OF QUASI-RANDOM AND EXPERIMENTAL INTEGRATED ABSORPTANCES FOR THE 15 μm CO_2 BAND. (From Kunde, 1967 [13].)

P_e (atm)	w (cm-atm)	$\int A d\nu$ (cm^{-1})		
		Experimental	Theoretical (Young)	Theoretical (Kunde Calculation)
0.00051	0.58	3.37	5.8	2.4
0.00137	1.53	8.86	10.1	6.3
0.00496	5.56	21.7	26.7	20.1
0.00827	9.20	32.6	39.3	30.4
0.0205	5.73	34.6	43.3	34.4
0.0397	5.73	43.8	54.0	42.8
0.0837	5.73	54.7	67.3	53.6
0.2052	5.73	69.5	83.6	68.1
0.3999	5.73	81.9	94.0	79.2
1.0089		95.3	103.9	93.2

ERIM
FORMERLY WILLOW RUN LABORATORIES, THE UNIVERSITY OF MICHIGAN

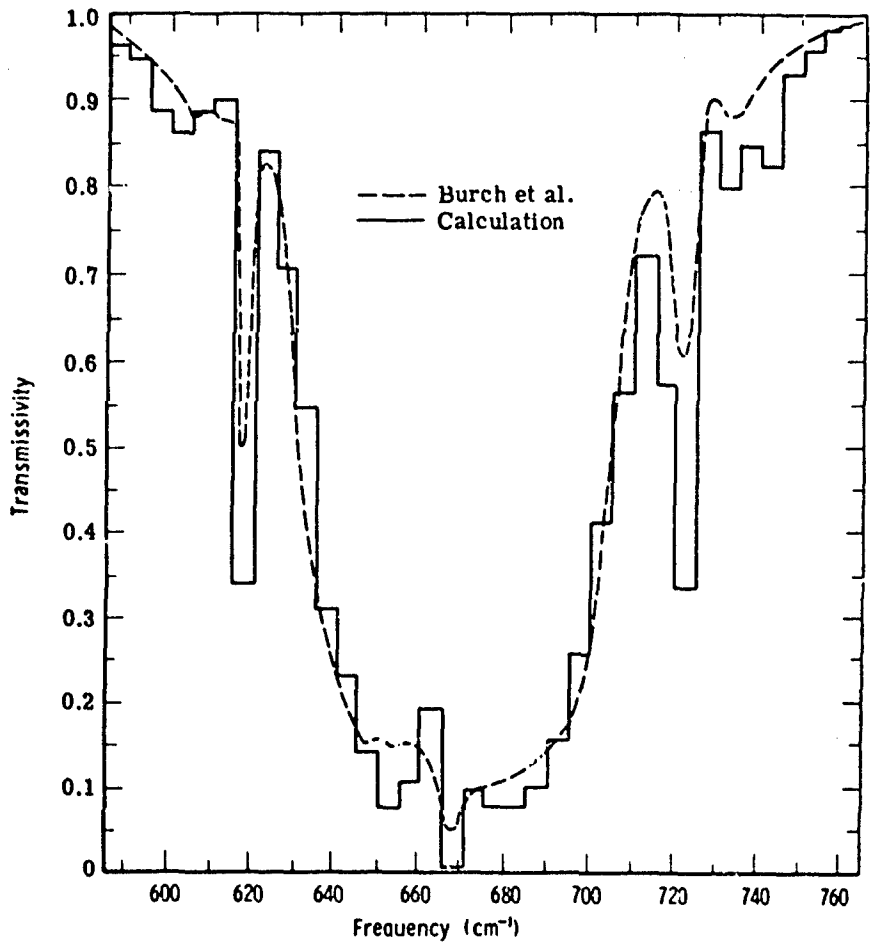

FIGURE 68. CALCULATED AND EXPERIMENTAL TRANSMISSIVITIES VS FREQUENCY FOR DIFFERENT PRESSURES AND OPTICAL MASSES. (Reproduced from Young, 1964 [232].)

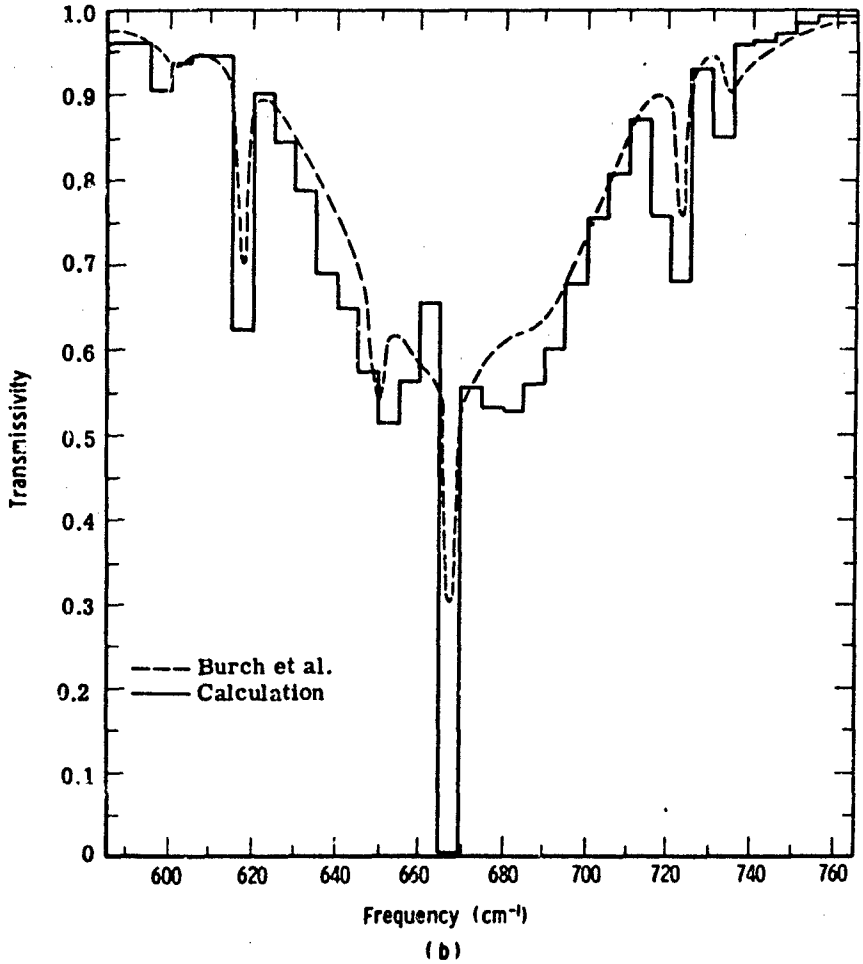

(b)

Pressure = 20.79 mb
Tmp = 300°K
w = 5.73 atm cm

FIGURE 68. CALCULATED AND EXPERIMENTAL TRANSMISSIVITIES VS FREQUENCY FOR DIFFERENT PRESSURES AND OPTICAL MASSES. (Reproduced from Young, 1964 [232].) (Continued)

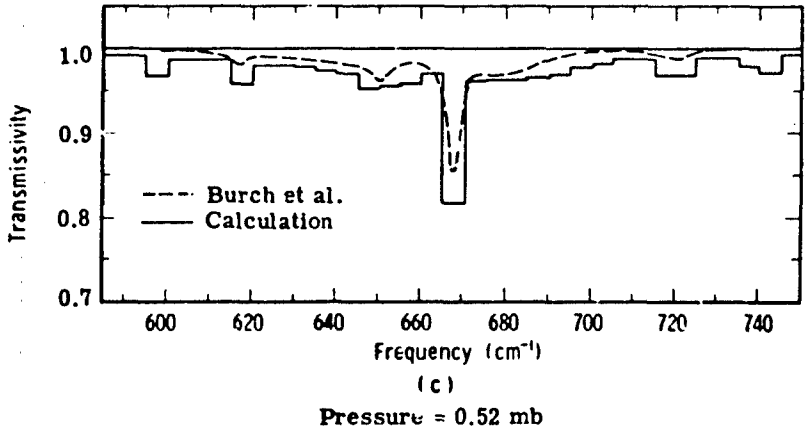

FIGURE 68. CALCULATED AND EXPERIMENTAL TRANSMISSIVITIES VS FREQUENCY FOR DIFFERENT PRESSURES AND OPTICAL MASSES. (Reproduced from Young, 1964 [232].) (Concluded)

underestimate the transmittance of the Q-branches because the lines are grouped closely and are neither uniformly nor randomly distributed over the averaging interval. Also, the lines are more-or-less evenly spaced, a fact which tends to underestimate the transmittance from the contribution due to the wings of the lines outside of the averaging interval. The latter effect, being dependent on pressure, tends to diminish with decreasing pressure.

Haurwitz (1972) calculated transmittances and infrared radiative fluxes in the following spectral regions using the quasi-random model:

H_2O (pure rotation band and 6.3 μm band) - using line-parameter data from Benedict and Calfee (1967) and Benedict and Kaplan [see, e.g., Goody (1964), p. 184]. The calculations were made for 200 and 300 K. The subintervals, chosen for the calculation were: 0-220, 220-440, 440-800, 800-1250, 1250-1420, 1420-1590, 1590-1845, 1845-2100, and 2100-2450 cm^{-1}.

CO_2 (15 μm band) - using the line parameter data of Drayson (see, e.g., Drayson, 1967). The band was divided into 6 subintervals. Because of its density of lines, the Q-branch was isolated and treated separately.

Haurwitz has evaluated each half of the integral

$$\int_0^1 \exp\left[-\frac{\rho^2\xi^2}{\eta^2+\rho^2}\right]d\eta = \int_0^{1/2} \exp\left[-\frac{\rho^2\xi^2}{\eta^2+\rho^2}\right]d\eta + \int_{1/2}^1 \exp\left[\frac{-\rho^2\xi^2}{\eta^2+\rho^2}\right]d\eta$$

using Simpson's rule,

$$\int_a^b f(x)\,dx = \frac{b-a}{2}\left\{\frac{1}{3}f(a) + 4f\left(\frac{b+a}{2}\right) + f(b)\right\}$$

[Note that he considers the transmittance at the center of the interval to represent the average value over the interval.]

Each half is again divided and the resulting integrals evaluated as before. This procedure is repeated until the sum of the two new integrals differs by less than 10^{-6} from the value of the preceding integral. Haurwitz claims that the procedure assures him an accuracy of four significant figures. Since this a time consuming process, he evaluates the integral for a fixed number of values of ξ_i and ρ within the range of his calculation. He calculates intermediate values, corresponding to parameters expected in a real situation, using the interpolation procedure of Wyatt, et al. (1962) described above. Incidentally, a check of the interpolation procedure with values calculated by quadrature allegedly demonstrated the realization of a possible accuracy of four figures using the interpolation technique.

A comparison of Haurwitz's results with the results of Burch, et al. (1962) for the 6.3 μm band of H_2O vapor is shown in Table 41. In the table are shown the percentage differences between theoretical and experimental results for a variety of (Curtis-Godson) pressures and

absorber amounts. For the 15 μm CO_2 band, using line parameter data obtained from Drayson and Young, a comparison was made with the experimental data of Burch, et al. (1962). Table 42 shows the percentage differences for the total absorption in the band, and for the fractional absorption in three bands, respectively: 545-617 cm^{-1}, 617-667 cm^{-1}, and 667-720 cm^{-1}.

An interesting result from Haurwitz's research, in which he calculates atmospheric cooling rates from H_2O, CO_2, and O_3, is shown in Table 43. The purpose of this table is to show the contributions from various subintervals to the H_2O cooling rate, from Haurwitz's calculation using the quasi-random model.

Plass [236] used the method of interpolation to calculate the spectral transmission over the slant paths from initial altitudes of 15, 25, 30, and 50 km to the outer limit of the atmosphere. Results are presented in the form of tables for paths from the vertical to the horizontal in 5° steps. Values are given for CO_2 from 500 to 10,000 cm^{-1} and for H_2O from 1000 to 10,000 cm^{-1} for both a "dry" stratosphere and a "wet" stratosphere.

Plass assumed that CO_2 was uniformly mixed throughout the atmosphere at 0.033% by volume. H_2O distributions were based on the work of Gutnick [237], [238]. For the "dry" stratosphere H_2O was assumed to be constant at 0.045 gm/kg air. For the "wet" stratosphere the values used are given in Table 44.

7.3 OTHER PUBLISHED SINGLE-MODEL COMPUTATIONS

7.3.1 METHOD OF G. DANIELS

Daniels (1974) makes straightforward use of the statistical model in a quasi-random format with a uniform distribution of strengths for which the transmittance can be written:

$$\tau(w, P, T) = \exp\left\{\frac{2\pi\alpha_L(P)}{d}\cdot L\left(\frac{S(T)w}{2\pi\alpha_L(P)}\right)\right\} \qquad (310)$$

where α_L = Lorentz line half-width in cm^{-1}

d = average line spacing within $\Delta\nu$ in cm^{-1}

$S(T)$ = line strength in $(atm\text{-}cm^2)^{-1}$

w = absorber amount

$L(x)$ = Ladenberg-Reiche function (see Section 5)

236. G. N. Plass, Infrared Transmission Studies, Vol. V - Transmittance Tables for Slant Path in the Stratosphere, Report No. SSD-TDR-62-127, Ford Motor Company, 1963.

237. M. Gutnick, "How Dry is the Sky?," J. Geophys. Res., Vol. 66, 1961, pp. 286-287.

238. M. Gutnick, "Mean Atmospheric Moisture Profiles to 31 km for Middle Latitudes," Appl. Opt., Vol. 1, 1962, p. 670.

TABLE 41. PERCENTAGE DIFFERENCES BETWEEN THEORETICAL AND EXPERIMENTAL TOTAL ABSORPTIONS FOR THE 6.3 μm WATER VAPOR BAND RELATIVE TO THE EXPERIMENTAL VALUES. (A negative value indicates that the theoretical value is larger.) (From Haurwitz, 1972 [14].)

Mass Path (gm/cm^2)	Curtis-Godson Pressure (mb)		
	133	330	1013
0.002	-30.8	-11.3	-1.8
0.004	-5.8	-1.3	7.2
0.010	9.4	6.5	4.8
0.020	8.2	7.3	0.0
0.040	9.0	5.3	-2.6
0.100	1.1	-6.6	-6.5
0.200	-3.7	-7.8	-10.5
0.400	-6.0	-9.3	-7.5
0.800	-4.0	-5.7	-8.4
0.999	-4.2	-2.8	-5.3

TABLE 42. PERCENTAGE DIFFERENCES BETWEEN THEORETICAL AND EXPERIMENTAL VALUES OF FRACTIONAL AND TOTAL ABSORPTIONS FOR THE 15 μm CARBON DIOXIDE BAND RELATIVE TO EXPERIMENTAL VALUES. (A negative values indicates that the theoretical value is larger.) (From Haurwitz, 1972 [14].)

Mass Path gm/cm^2	Pressure mb	Total Absorption-Percentage Differences	Fractional Absorption Percentage Differences		
			545-617 cm^{-1}	617-667 cm^{-1}	667-720 cm^{-1}
0.046	1016	-7.1	13.9	1.0	-4.5
0.091	405	-8.5	1.0	1.6	-3.9
0.091	1019	-6.4	12.9	-2.5	-4.0
0.190	411	-5.5	3.2	-1.0	-1.3
0.190	1024	-4.7	0.7	-1.1	-0.1
0.234	439	-5.8	3.0	-2.4	-1.2
0.379	292	-2.7	0.3	0.0	-0.9
0.379	3	-2.9	-1.1	-0.6	-1.0
0.379	1007	-2.3	-2.4	0.0	0.0
0.383	700	-3.3	4.3	-0.3	0.0

TABLE 43. PERCENTAGE CONTRIBUTIONS TO THE OVERALL WATER VAPOR COOLING RATES FROM EACH OF THE NINE SUBINTERVALS. (From Yaurwitz, 1972 [14].)

Pressure (mb) \ Subinterval (cm^{-1})	0-220	220-440	440-800	800-1250	1250-1420	1420-1590	1520-1845	1845-2100	2100-2450
950	0.0	0.0	77.0	15.1	4.9	0.2	0.2	2.5	0.2
884	0.0	0.0	74.7	19.0	4.6	0.0	0.1	1.5	0.1
817	0.0	0.2	82.5	8.5	6.8	0.1	0.2	1.6	0.1
750	0.0	0.2	79.4	10.3	8.2	0.1	0.3	1.5	0.1
684	0.0	1.5	74.4	11.4	9.5	0.8	1.1	1.3	0.5
617	0.0	12.1	71.0	4.0	8.9	1.7	1.6	0.8	0.0
550	0.3	23.8	55.0	6.0	8.1	3.2	2.8	0.6	0.0
484	2.7	44.7	37.2	4.5	4.3	3.5	2.5	0.3	0.0
417	7.2	56.1	29.3	0.7	2.5	3.3	2.1	0.0	0.0
350	13.2	66.0	15.9	2.9	0.4	1 5	0.1	0.1	0.0
284	22.6	62.3	9.9	1.8	1.1	1.4	0.6	0.0	0.0

TABLE 44. MIXING RATIO FOR "WET" STRATOSPHERE MODEL

Altitude (km)	Mixing Ratio (gm H_2O per kg air)
15	0.0090
16	0.0095
17	0.0105
18	0.012
19	0.015
20	0.018
21	0.022
22	0.027
23	0.033
24	0.040
25	0.048
26	0.058
27	0.069
28	0.087
29	0.11
30	0.13
31	0.16
32	0.18
33 and above	0.20

The computation is formalized in a computer program called AIRCAP which unfortunately is not available in the literature. The calculations involve the use of the AFCRL line-parameter compilation and a set of gas profiles which are demonstrated in Figure 69.

Daniels increments his interval in $\Delta\lambda$ according to line strength value, and his spherically symmetric atmosphere into layers (see Section 7.4) without regard to refractive index changes. The increments were defined according to the formula $\lambda/\Delta\lambda \equiv 100$, which gives a wavelength resolution of 0.1 μm at 10 μm. Calculations were made for the range 8 to 25 μm. The groupings of line strengths were made in such a way that, starting with the strongest line, the intensities in any group were within a factor of 3. Thus, if S_0 is the strength of the strongest line, the subsets of each increment contained lines such that $S_0/3^n < S \leq S_0/3^{n-1}$, where N(=1, 2, 3, . . .) is the number of the subset. In a quasi-random fashion the strength in each subset can be averaged, the result being used as the constant line strength applied in the statistical model with uniform distribution of line strength (Eq. 310). The resultant transmittance is multiplied with the values obtained using Eq. (310) with the other subsets, to obtain the total transmittance.

First, however, the Curtis-Godson approximation (see Section 5) must be applied to the absorber amount and the line half-width. After this is done, these quantities can be appropriately applied in the model (Eq. 310) for a homogeneous path. For this purpose, the average line strength in the subset, k, is obtained from:

$$\overline{S_{ij}(T_0)} = \frac{\sum_k S_{ijk}(\nu, T_0)}{m} \qquad (311)$$

where i pertains to the i-th gas constituent, and the summation is over the m lines in the subset. Since the line strengths are compiled for a single convenient temperature, T_0, the values $\overline{S_{ij}(T)}$ must be determined from the calculation of line strength averages at T_0 so that:

$$\overline{S_{ij}(T)} = \overline{S_{ij}(T_0)}\left(\frac{T_0}{T}\right)^n \exp\left\{\frac{hc\overline{E_{ij}}}{kT_0T}(T - T_0)\right\} \qquad (312)$$

where n = 1 for CO_2 and N_2O, and n = 3/2 for O_3, H_2O and CH_4. Daniels did not account for the temperature dependence of HNO_3 because data were not available. He estimated the average value $\overline{E_{ij}(T_0)}$, the average ground state energy, from:

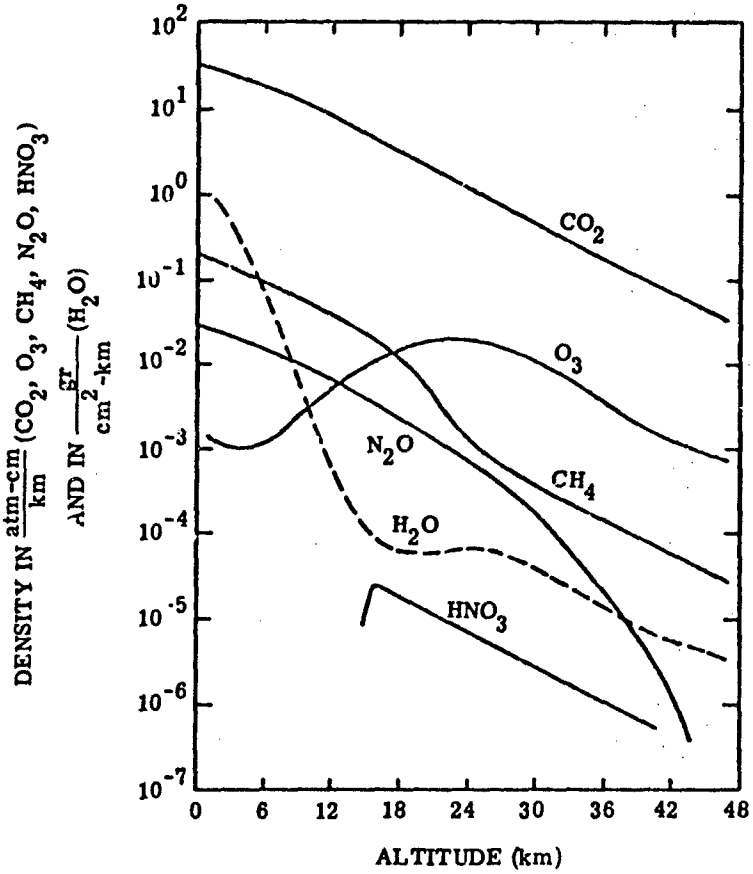

FIGURE 69. DENSITY PROFILES OF ATMOSPHERIC CONSTITUENTS FOR MODEL ATMOSPHERE USED IN CALCULATIONS. Note scale difference for H_2O. (Adapted from Daniels, 1974 [18].)

$$\overline{E_{ij}(T_0)} = \frac{\sum_k S_{ijk}(T_0)E_{ijk}}{\sum_k S_{ij}(T_0)} \tag{313}$$

where again the summation is over the m values of the lines in the subset. The Curtis-Godson effective absorber amount was then obtained from:

$$w_{ij}(CG) = \int_{z_0}^{R} \frac{\overline{S_{ij}(T_z)}}{\overline{S_{ij}(T_0)}} \rho_i(z) \frac{ds}{dz} dz \tag{314}$$

where T_i is taken as a mean, representative temperature for the path; in this case, 223 K or -50°C. The integration is, as usual, performed numerically by dividing the atmosphere in 1 km distant shells. The path is taken from some z_0 to R, which is a height above which atmospheric densities are negligible for the calculations, taken as 47 km by Daniels (1970).

The Curtis-Godson half-width, in the format designed from the averages calculated above, then has the special form (note that this and all previous calculations are for a particular frequency, centered in the spectral region over which the averages are taken):

$$\alpha_{ij}(CG) = \frac{\int_{z_0}^{z_1} \frac{\overline{S_{ij}(T_z)}}{\overline{S_{ij}(T_0)}} \left[\alpha_{L_i}(P_0, T_0) \left(\frac{P_z}{P_0}\right) \left(\frac{T_0}{T_z}\right)^{1/2} \rho(z) \frac{ds}{dz} dz \right]}{w_{ij}(CG)}$$

$$+ \int_{z_1}^{R} \frac{\overline{S_{ij}(T_z)}}{\overline{S_{ij}(T_0)}} \alpha_{D'}(z) \rho(z) \frac{ds}{dz} dz \tag{315}$$

The integration is split into two paths, z_0 to z_1, and z_1 to R (the upper limit), the first being the region in which pressure broadening dominates, the second where Doppler broadening (see Eq. (316) below) is the chief broadening mechanism. Daniel's approximation to the Doppler shape is to freeze the Lorentz profile at z_1 with respect to pressure and then from z_1 to R allow the half-width to vary at $T^{1/2}$ similar to the Doppler line. Thus, in Eq. (315) we have:

$$\alpha_{D'}(z) \equiv \alpha_{L_i}(z_\ell) = \alpha_{L_i}(z_1) \left(\frac{T_\ell}{T_1}\right)^{1/2} \tag{316}$$

where the subscript ℓ is a count of the atmospheric layer used in the summation which approximates the actual integration in Eq. (316).

The altitude at which this transition was chosen was obtained by letting (for a given gas constituent):

$$\alpha_L(z_1) = \frac{1}{\sqrt{\pi}}\alpha_D\left(T_{z_1}\right) \tag{317}$$

The relative shapes of the true Doppler and the approximate profile using Eq. (317) are shown in Figure 70. Daniels made a comparison of the transmittances obtained in the Doppler region for CH_4 with experimental results, using the true Lorentz shape, the frozen Lorentz shape with $\alpha_L = \alpha_{L0}$ and the frozen Lorentz shape using $\alpha_L = \alpha_{L0}/\sqrt{\pi}$. The results are shown in Figure 71. An empirical match of the parameters for the various constituents in the spectral region between 8 and 25 μm results in the tabulation of Table 45, giving the initial freezing altitudes.

7.3.2 METHOD OF H. T. JACKSON (see also Section 5, and Goldman and Kyle (1968))

In an attempt to calculate the emissivity of hot CO_2 in the 4.3 μm region, covering the frequency band from 2050 to 2400 cm^{-1}, Jackson [239] has applied the exponential-tailed S^{-1} (Malkmus, 1967) line intensity distribution to the statistical model to satisfy a range of gas temperatures from 300 to 2100 K. (Note that the attempt here is not to present results on models of high-temperature radiation; Jackson's method is one representation of a specific model.) A mathematical representation of the transmittance calculated with the exponential-tailed S^{-1} distribution is given as:*

$$\tau = \exp -\left(\beta_0 P_e/\pi\left\{\left[1 + 2\pi\psi\right]^{1/2} - 1\right\}\right) \tag{318}$$

where, as usual, $P_e = P + (B - 1)p$

$$\beta_0 = \frac{2\pi\alpha^o_{L0}}{d}$$

$$\psi = \frac{Sw}{2\pi\alpha_L}$$

$$w = \frac{P}{P_e}L$$

L = path length in cm

p = partial pressure of the absorber

Since Jackson wishes to compute $\epsilon = 1 - \tau$, the appropriate subtraction must be made. In addition, he makes the approximation $P_e = P$, the total pressure, disregarding the small

*Compare with Expression 12, Table 20.

239. H. T. Jackson Jr., A Model for the Spectral Emissivity of Carbon Dioxide in the 4.3-Micron Band, Rept. No. RE-TR-69-6, U.S. Army Missile Command, 1969.

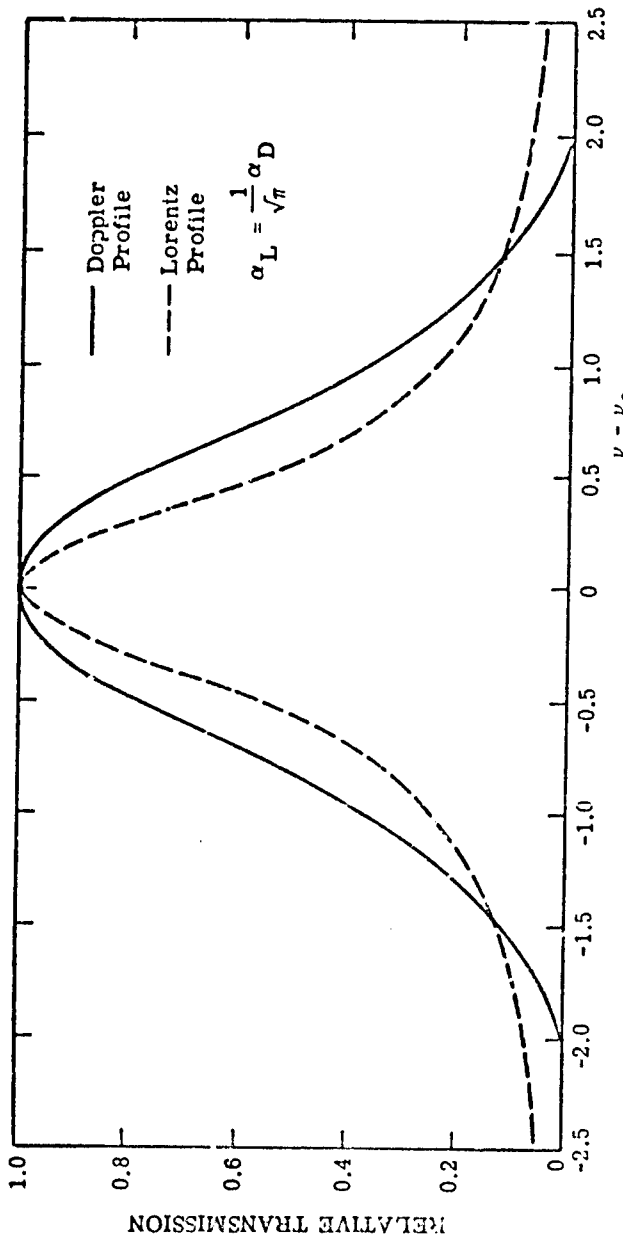

FIGURE 70. APPROXIMATION OF DOPPLER PROFILE AT HIGH ALTITUDES BY LORENTZ PROFILE. (Adapted from Daniels, 1974 [18].)

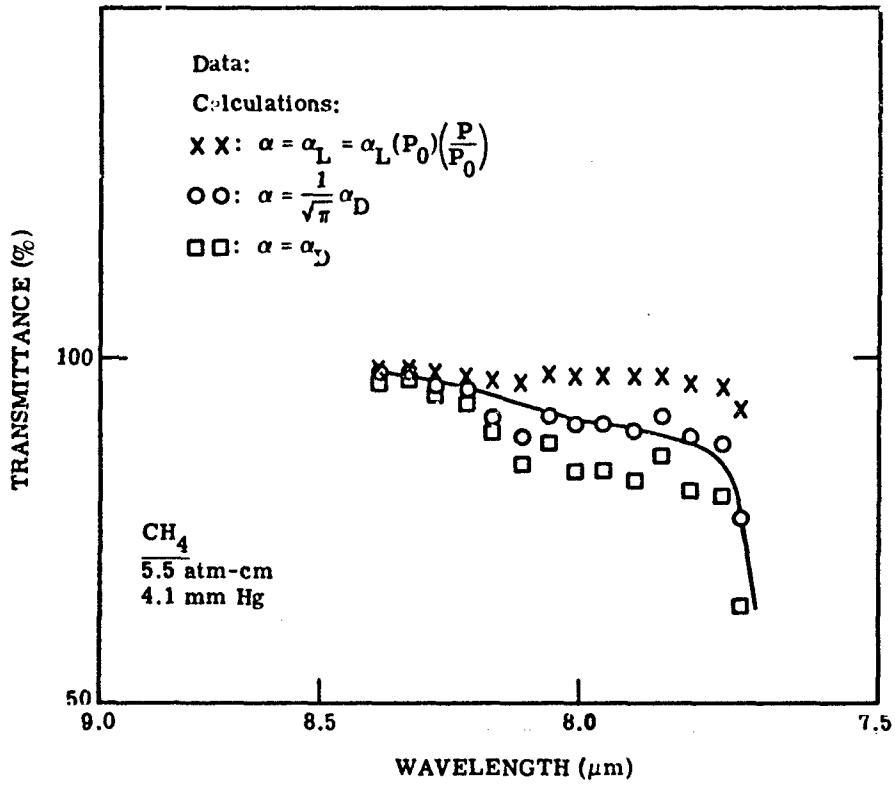

FIGURE 71. METHANE TRANSMITTANCE IN 7.7 μm BAND AT A PRESSURE WHERE DOPPLER BROADENING DOMINATES LINE SHAPE. (Adapted from Daniels, 1974 [18].)

TABLE 45. REFERENCE HALF-WIDTHS (223 K, 760 MM HG) AND LINE SHAPE FREEZING ALTITUDES, z_1. (From Daniels, 1973 [17].)

Constituent	Wavelength of Band Center	Band Number	Reference Half-widths	z_1
H_2O	6.3 μm	1	0.08 cm^{-1}	26 km
	10 μm	2†	0.08 cm^{-1}	31 km
	20 μm	3†	0.08 cm^{-1}	35 km
CO_2	10 μm	1	0.07 cm^{-1}	35 km
	15 μm	2	0.07 cm^{-1}	35 km
O_3	9.6 μm	1	0.11 cm^{-1}	36 km
	14 μm	2	0.98 cm^{-1}	38 km
N_2O	8 μm	1	0.1 cm^{-1}	35 km
	17 μm	2	0.1 cm^{-1}	38 km
CH_4	7.7 μm	1	0.06 cm^{-1}	29 km
HNO_3	Not needed or available*			

*Laboratory and atmospheric transmission data indicate that the atmospheric transmission of HNO_3 is always in the "weak-line" region where the transmission is independent of pressure and so the half-width is not of concern.

† The water vapor rotation lines are distributed from 10 μm to the microwave region. For these calculations artifical band centers were taken at 10 and 20 μm.

self-broadening correction. He then derives a procedure for the linearization of Eq. (318) for fitting to the line parameter data of Stull, et al. (1963), derived from the data in the quasi-random model (see Section 5) that were averaged over intervals 20 cm^{-1} wide. Thus, by taking the natural logarithms of both sides of Eq. (318) and rearranging, there results:

$$\frac{1}{4\alpha_L (S^{1/2}/d)^2} \ln(1/\tau) + \frac{1}{S/d} = \frac{w}{\ln(1/\tau)} \tag{319}$$

(for a pressure of 1 atm), which can be fitted to a plot of $\ln(1/\tau)$ versus $w/\ln(1/\tau)$, where the intercept of the straight line is $(S/d)^{-1}$ and the slope is $(S^{1/2}/d)^{-2}/4\alpha_L$. Mathematically the solution results from a least squares fit of empirical data, in this case the data of Stull, et al. (1963), from which:

$$\sum_{i=1}^{n} \frac{(w)_i}{\ln \tau_i} = -\frac{n}{(S/d)} + \frac{1}{4\alpha_L (S^{1/2}/d)^2} \ln\left\{\prod_{i=1}^{n} \tau_i\right\} \tag{320}$$

and

$$\sum_{i=1}^{n} (w)_i = -\frac{1}{(S/d)} \ln\left\{\prod_{i=1}^{n} \tau_i\right\} + \frac{1}{4\alpha_L (S^{1/2}/d)^2} \sum_{i=1}^{n} (\ln \tau_i)^2 \tag{321}$$

[Note: for n values of the variables, x_i and y_i, the differences at any point x_i between the chosen line and the point y_i is $y_i - (ax_i + b)$. Minimization of the sums of the squares of these differences yields

$$\sum_{i}^{n} [y_i - (ax_i + b)] = 0$$

and

$$\sum_{i}^{n} x_i [y_i - (ax_i + b)] = 0. \text{ End of Note.}]$$

The solution of these simultaneous equations yields the parameters S/d and $S^{1/2}/d$, which are sought for incorporation into the band model represented by Eq. (318).

Although Jackson's derivation pertains to the transmittance (actually emissivity) of CO_2 at 4.3 μm for a variety of gas temperatures, the only temperature of importance to this report is the lower one at 300 K. However, to show the effect of temperature on the various parameters used in the statistical model to calculate transmittance (emissivity), the values obtained by Jackson are reproduced here. Figure 72 shows the variation of the parameter

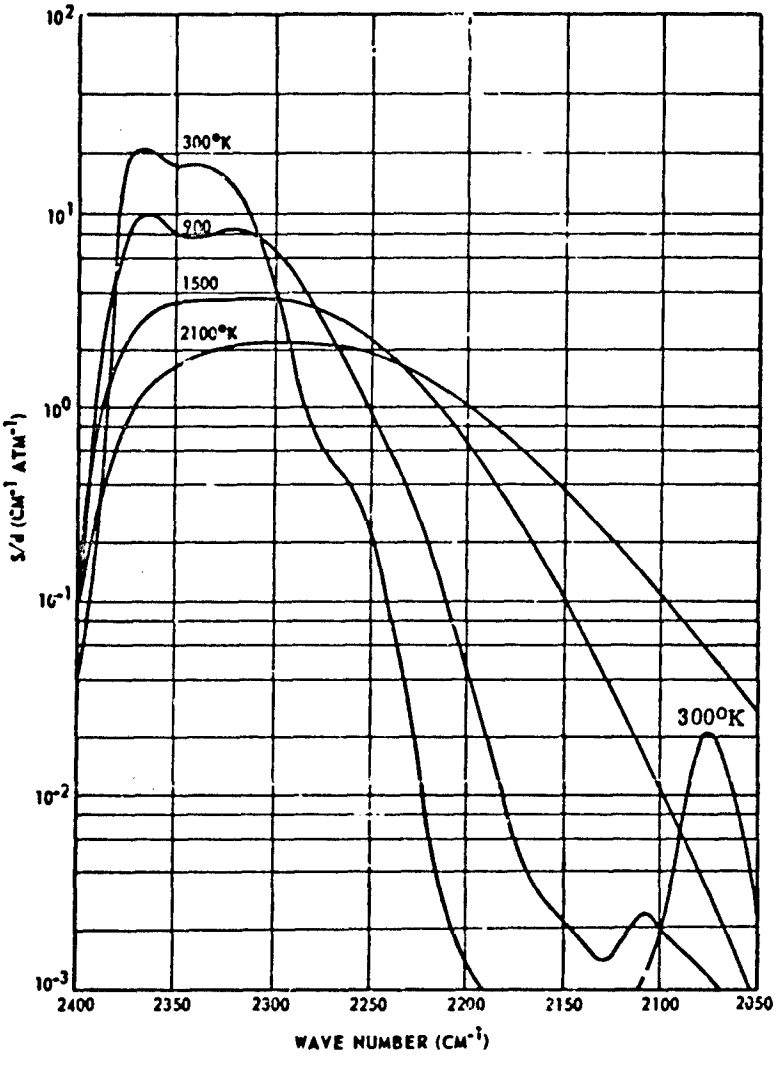

FIGURE 72. S/d VERSUS WAVE NUMBER WITH TEMPERATURE AS A PARAMETER. (Feproduced from Jackson, 1969 [239].)

S/d as a function of frequency for different values of temperature. Figure 73 is a plot of the same parameter as a function of temperature for different values of frequency. Recall that S/d and $S^{1/2}/d$ were obtained at 300 K from a fit of the data of Stull, et al. (1963). The reader is referred to the original report (Jackson, 1969) for the source of data at higher temperatures.

The parameter $S^{1/2}/d$ is shown plotted in Figure 74 as a function of frequency for different values of temperature, while the same parameter is plotted in Figure 75 as a function of temperature for different values of frequency. Tables 46 and 47 give the same parameters in tabular form.

7.4 AGGREGATE METHOD

The Aggregate Method was formulated and extensively used at the Environmental Research Institute of Michigan (ERIM) and published through support of the Aerospace Corporation by one of the authors of the model. It was originally assembled by D. Anding, who recently cooperated in publishing the program (Hamilton, Rowe and Anding, 1973), and by H. Rose and J. Walker. It was formulated as the result of a compilation of models which were reviewed in the original State-of-the-Art report (Anding, 1967) on the calculation of atmospheric effects. This method, and the LOWTRAN 2 method (Selby and McClatchey, 1972; see following section) are perhaps the most widely disseminated of all the programs for calculating absorptive atmospheric effects from band models. After the original State-of-the-Art was completed, the Aggregate atmospheric transmittance calculation method was formulated to organize into a single program the best traits of the numerous models that were in existence at that time. It has been gradually up-graded as new data appears and modified to calculate atmospheric radiance as well as transmittance, and to include scattering.

Calculations by the Aggregate method can be made from 1.05 to 30 μm at irregular spectral resolution from 0.01 μm at the short wavelengths to 0.44 μm at the long wavelengths, suited to the resolution of the experimental data used to calculate the line parameters. In the computer code for calculating transmittance and radiance, the atmosphere is divided into a (variable) number of spherical shells through which the path is taken unrefracted. See the Appendix for a consideration of refraction. The transmittance in the path is considered as the product of the transmittances due to the effects in the following list (from Hamilton, Rowe and Anding, 1973).

Transmittance through the gaseous constituents of the atmosphere, with

τ_{H_2O} = transmittance of water vapor in which the molecular line structure is adaptable to a band model

$\tau_{H_2O\ \text{continuum}}$ = transmittance of water vapor in the continuum region

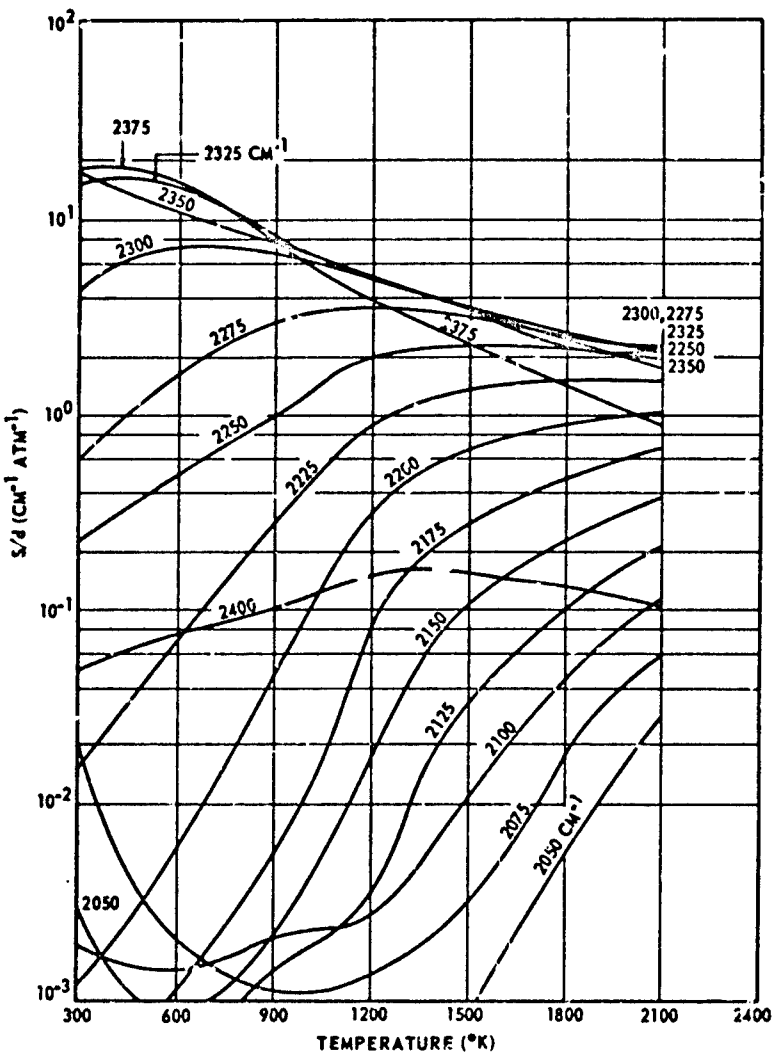

FIGURE 73. S/d VERSUS TEMPERATURE WITH WAVE NUMBER AS A PARAMETER. (Reproduced from Jackson, 1969 [239].)

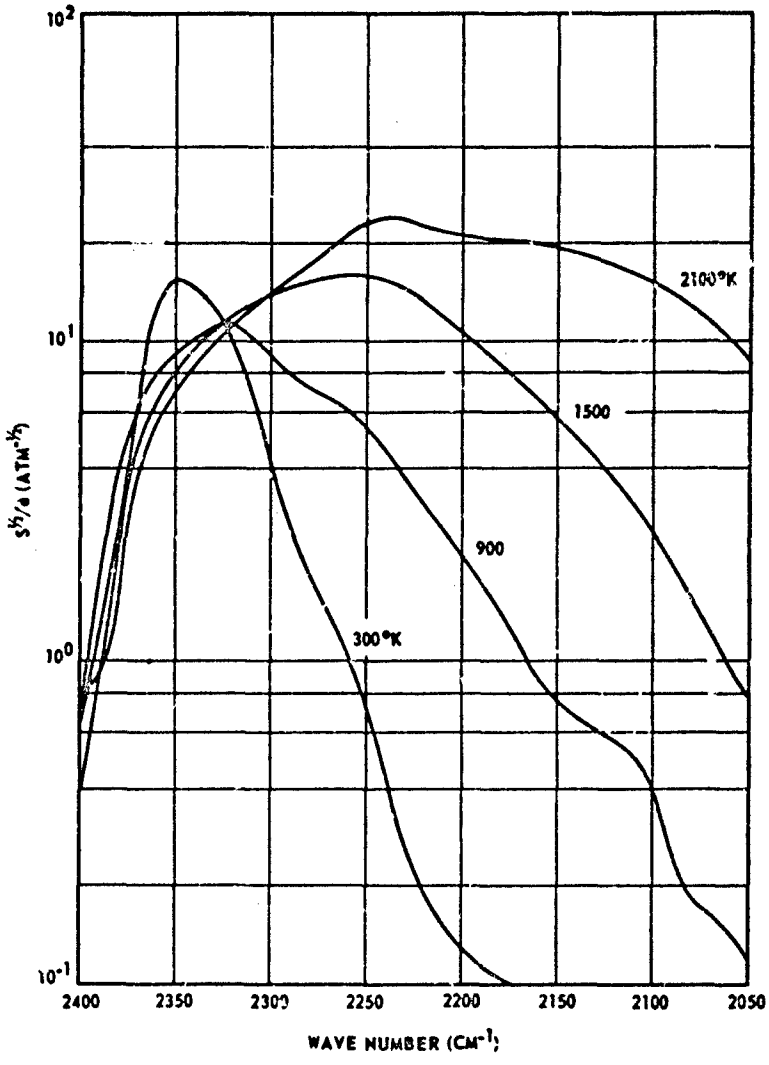

FIGURE 74. $S^{1/2}/d$ VERSUS WAVE NUMBER WITH TEMPERATURE AS A PARAMETER. (Reproduced from Jackson, 1969 [239].)

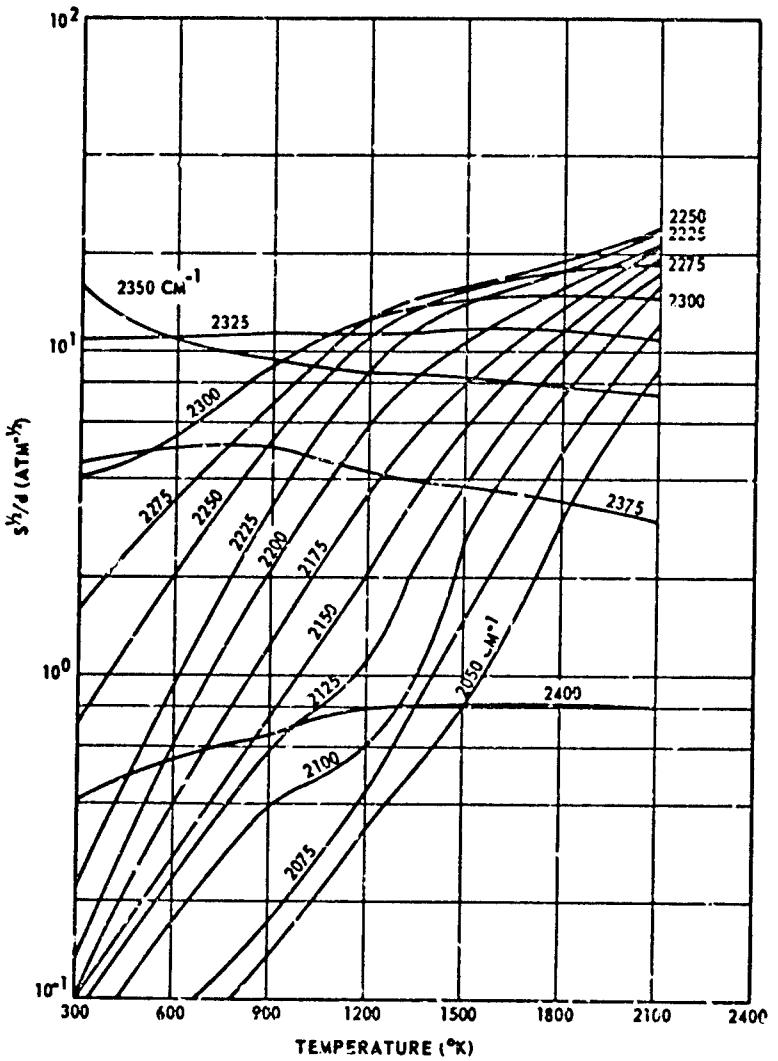

FIGURE 75. $S^{1/2}/d$ VERSUS TEMPERATURE WITH WAVE NUMBER AS A PARAMETER. (Reproduced from Jackson, 1969 [239].)

TABLE 46. THE SPECTRAL BAND PARAMETER S/d AS A FUNCTION OF TEMPERATURE. (From Jackson, 1969 [239].)

WAVE NUMBER (1/CM)	TEMPERATURE (DEGREES KELVIN) 300.	600.	900.	1200.	1500.	1800.	2100.
2050.	2.60E-03	4.80E-04	3.40E-04	4.10E-04	8.20E-04	5.70E-03	2.60E-02
2055.	4.80E-03	7.00E-04	4.50E-04	5.20E-04	1.08E-03	7.20E-03	3.00E-02
2060.	8.01E-03	1.03E-03	5.72E-04	6.37E-04	1.37E-03	9.08E-03	3.56E-02
2065.	1.40E-02	1.51E-03	7.53E-04	8.23E-04	1.77E-03	1.14E-02	4.12E-02
2070.	1.87E-02	1.89E-03	9.57E-04	1.06E-03	2.28E-03	1.42E-02	4.76E-02
2075.	2.02E-02	2.08E-03	1.15E-03	1.34E-03	2.95E-03	1.75E-02	5.47E-02
2080.	1.65E-02	1.99E-03	1.30E-03	1.66E-03	3.81E-03	2.13E-02	6.28E-02
2085.	1.08E-02	1.79E-03	1.44E-03	2.04E-03	4.96E-03	2.58E-02	7.21E-02
2090.	6.31E-03	1.63E-03	1.57E-03	2.54E-03	6.41E-03	3.08E-02	8.30E-02
2095.	3.21E-03	1.52E-03	1.77E-03	2.81E-03	8.23E-03	3.65E-02	9.51E-02
2100.	1.81E-03	1.47E-03	2.10E-03	2.65E-03	1.06E-02	4.28E-02	1.08E-01
2105.	1.33E-03	1.41E-03	2.35E-03	2.30E-03	1.36E-02	5.01E-02	1.24E-01
2110.	9.55E-04	1.26E-03	2.32E-03	1.89E-03	1.73E-02	5.86E-02	1.41E-01
2115.	6.95E-04	1.07E-03	2.08E-03	1.86E-03	2.21E-02	6.86E-02	1.60E-01
2120.	5.65E-04	8.82E-04	1.70E-03	2.46E-03	2.80E-02	8.05E-02	1.81E-01
2125.	5.13E-04	7.36E-04	1.40E-03	3.52E-03	3.51E-02	9.61E-02	2.05E-01
2130.	4.88E-04	6.96E-04	1.38E-03	4.98E-03	4.38E-02	1.15E-01	2.31E-01
2135.	4.80E-04	7.11E-04	1.53E-03	6.91E-03	5.46E-02	1.37E-01	2.61E-01
2140.	4.78E-04	7.30E-04	1.73E-03	9.55E-03	6.73E-02	1.63E-01	2.95E-01
2145.	4.82E-04	7.52E-04	1.95E-03	1.31E-02	8.27E-02	1.92E-01	3.32E-01
2150.	4.91E-04	7.81E-04	2.20E-03	1.82E-02	1.01E-01	2.25E-01	3.73E-01
2155.	5.05E-04	8.16E-04	2.47E-03	2.52E-02	1.24E-01	2.62E-01	4.18E-01
2160.	5.22E-04	8.56E-04	2.78E-03	3.43E-02	1.53E-01	3.06E-01	4.68E-01
2165.	5.47E-04	9.16E-04	3.25E-03	4.63E-02	1.88E-01	3.55E-01	5.22E-01
2170.	5.81E-04	1.01E-03	4.03E-03	6.16E-02	2.28E-01	4.07E-01	5.80E-01
2175.	6.28E-04	1.18E-03	5.68E-03	8.20E-02	2.76E-01	4.67E-01	6.42E-01
2180.	6.95E-04	1.46E-03	8.82E-03	1.09E-01	3.32E-01	5.36E-01	7.10E-01
2185.	7.83E-04	1.91E-03	1.40E-02	1.43E-01	3.95E-01	6.13E-01	7.82E-01
2190.	9.01E-04	2.60E-03	2.18E-02	1.88E-01	4.70E-01	7.00E-01	8.57E-01
2195.	1.06E-03	3.91E-03	3.34E-02	2.46E-01	5.58E-01	7.93E-01	9.32E-01
2200.	1.28E-03	6.27E-03	5.00E-02	3.15E-01	6.56E-01	8.93E-01	1.00E-00
2205.	1.69E-03	1.02E-02	7.20E-02	3.97E-01	7.67E-01	1.00E-00	1.08E-00
2210.	2.45E-03	1.65E-02	1.00E-01	4.92E-01	8.88E-01	1.11E-00	1.17E-00
2215.	4.28E-03	2.74E-02	1.41E-01	6.01E-01	1.01E-00	1.23E-00	1.26E-00
2220.	7.95E-03	4.54E-02	2.02E-01	7.28E-01	1.16E-00	1.35E-00	1.36E-00

TABLE 46. THE SPECTRAL BAND PARAMETER S/d AS A FUNCTION OF TEMPERATURE
(From Jackson, 1969 [239].) (Concluded)

WAVE NUMBER (1/CM)	TEMPERATURE (DEGREES KELVIN) 300.	600.	900.	1200.	1500.	1800.	2100.
2225.	1.60E-02	7.54E-02	2.79E-01	8.76E-01	1.31E-00	1.48E-00	1.45E-00
2230.	3.10E-02	1.22E-01	3.67E-01	1.04E-00	1.48E-00	1.61E-00	1.55E-00
2235.	5.71E-02	1.85E-01	4.73E-01	1.24E-00	1.65E-00	1.74E-00	1.64E-00
2240.	9.84E-02	2.66E-01	6.05E-01	1.46E-00	1.84E-00	1.86E-00	1.72E-00
2245.	1.56E-01	3.65E-01	7.70E-01	1.71E-00	2.03E-00	1.99E-00	1.80E-00
2250.	2.32E-01	4.86E-01	9.75E-01	1.98E-00	2.22E-00	2.11E-00	1.87E-00
2255.	3.15E-01	6.30E-01	1.22E-00	2.28E-00	2.42E-00	2.22E-00	1.93E-00
2260.	3.93E-01	7.98E-01	1.53E-00	2.60E-00	2.61E-00	2.32E-00	1.98E-00
2265.	4.63E-01	1.00E-00	1.90E-00	2.93E-00	2.79E-00	2.41E-00	2.03E-00
2270.	5.21E-01	1.26E-00	2.36E-00	3.27E-00	2.96E-00	2.49E-00	2.06E-00
2275.	6.17E-01	1.63E-00	2.89E-00	3.61E-00	3.12E-00	2.55E-00	2.08E-00
2280.	7.99E-01	2.20E-00	3.52E-00	3.94E-00	3.26E-00	2.61E-00	2.10E-00
2285.	1.17E-00	3.05E-00	4.25E-00	4.25E-00	3.38E-00	2.65E-00	2.11E-00
2290.	1.84E-00	4.32E-00	5.10E-00	4.53E-00	3.48E-00	2.69E-00	2.12E-00
2295.	2.89E-00	5.83E-00	5.96E-00	4.76E-00	3.55E-00	2.70E-00	2.12E-00
2300.	4.40E-00	7.42E-00	6.77E-00	4.95E-00	3.60E-00	2.71E-00	2.11E-00
2305.	6.36E-00	9.18E-00	7.44E-00	5.07E-00	3.62E-00	2.70E-00	2.10E-00
2310.	8.72E-00	1.12E+01	7.90E-00	5.14E-00	3.63E-00	2.69E-00	2.07E-00
2315.	1.11E+01	1.31E+01	8.16E-00	5.16E-00	3.62E-00	2.67E-00	2.05E-00
2320.	1.34E+01	1.46E+01	8.25E-00	5.14E-00	3.60E-00	2.65E-00	2.01E-00
2325.	1.53E+01	1.51E+01	8.18E-00	5.12E-00	3.59E-00	2.64E-00	1.99E-00
2330.	1.67E+01	1.42E+01	7.97E-00	5.08E-00	3.57E-00	2.61E-00	1.95E-00
2335.	1.75E+01	1.27E+01	7.70E-00	5.08E-00	3.56E-00	2.57E-00	1.90E-00
2340.	1.76E+01	1.11E+01	7.45E-00	5.10E-00	3.55E-00	2.53E-00	1.85E-00
2345.	1.74E+01	1.03E+01	7.43E-00	5.15E-00	3.52E-00	2.46E-00	1.76E-00
2350.	1.73E+01	1.11E+01	7.87E-00	5.27E-00	3.50E-00	2.40E-00	1.69E-00
2355.	1.81E+01	1.32E+01	8.85E-00	5.35E-00	3.43E-00	2.29E-00	1.59E-00
2360.	1.95E+01	1.56E+01	1.00E+01	5.33E-00	3.28E-00	2.12E-00	1.43E-00
2365.	2.09E+01	1.71E+01	1.01E+01	5.11E-00	3.05E-00	1.94E-00	1.29E-00
2370.	2.11E+01	1.80E+01	9.50E-00	4.90E-00	2.69E-00	1.67E-00	1.09E-00
2375.	1.82E+01	1.60E+01	7.83E-00	3.91E-00	2.28E-00	1.41E-00	8.50E-01
2380.	1.01E+01	7.20E-00	6.00E-00	3.07E-00	1.77E-00	1.05E-00	6.50E-01
2385.	1.19E-00	2.54E-00	3.45E-00	2.19E-00	1.35E-00	8.02E-01	4.50E-01
2390.	2.97E-01	9.97E-01	1.70E-00	1.20E-00	7.80E-01	4.80E-01	3.00E-01
2395.	9.75E-02	2.61E-01	3.62E-01	4.95E-01	3.81E-01	3.21E-01	1.75E-01
2400.	5.01E-02	7.50E-02	1.00E-01	1.50E-01	1.50E-01	1.30E-01	1.00E-01

TABLE 47. THE SPECTRAL BAND PARAMETER S(1/2)/d AS A FUNCTION OF TEMPERATURE. (From Jackson, 1969 [239].)

WAVE NUMBER (1/CM)	TEMPERATURE (DEGREES KELVIN) 300.	600.	900.	1200.	1500.	1800.	2100.
2050.	4.60E-02	6.60E-02	1.33E-01	3.35E-01	7.90E-01	2.90E-00	8.90E-00
2055.	4.90E-02	7.00E-02	1.37E-01	3.52E-01	8.85E-01	3.20E-00	9.39E-00
2060.	5.25E-02	7.50E-02	1.49E-01	3.76E-01	1.00E-00	3.60E-00	1.00E+01
2065.	5.68E-02	8.00E-02	1.59E-01	3.92E-01	1.13E-00	4.00E-00	1.07E+01
2070.	6.00E-02	3.42E-02	1.68E-01	4.10E-01	1.28E-00	4.40E-00	1.13E+01
2075.	6.31E-02	8.81E-02	1.76E-01	4.31E-01	1.45E-00	4.81E-00	1.19E+01
2080.	6.67E-02	9.25E-02	1.84E-01	4.56E-01	1.63E-00	5.23E-00	1.25E+01
2085.	7.06E-02	1.01E-01	2.06E-01	4.81E-01	1.84E-00	5.66E-00	1.31E+01
2090.	7.42E-02	1.19E-01	2.56E-01	5.09E-01	2.06E-00	6.10E-00	1.37E+01
2095.	7.71E-02	1.42E-01	3.23E-01	5.47E-01	2.30E-00	6.55E-00	1.42E+01
2100.	7.89E-02	1.67E-01	3.95E-01	6.00E-01	2.54E-00	7.00E-00	1.47E+01
2105.	8.01E-02	1.87E-01	4.58E-01	6.71E-01	2.78E-00	7.45E-00	1.52E+01
2110.	8.13E-02	2.01E-01	5.00E-01	7.60E-01	3.04E-00	7.90E-00	1.57E+01
2115.	8.25E-02	2.10E-01	5.29E-01	8.62E-01	3.30E-00	8.33E-00	1.62E+01
2120.	8.40E-02	2.19E-01	5.58E-01	9.73E-01	3.59E-00	8.76E-00	1.66E+01
2125.	8.54E-02	2.27E-01	5.86E-01	1.09E-00	3.89E-00	9.18E-00	1.70E+01
2130.	8.68E-02	2.35E-01	6.12E-01	1.24E-00	4.19E-00	9.60E-00	1.75E+01
2135.	8.82E-02	2.43E-01	6.38E-01	1.41E-00	4.50E-00	1.00E+01	1.78E+01
2140.	8.97E-02	2.50E-01	6.66E-01	1.60E-00	4.85E-00	1.04E+01	1.82E+01
2145.	9.12E-02	2.58E-01	6.99E-01	1.80E-00	5.22E-00	1.08E+01	1.86E+01
2150.	9.28E-02	2.66E-01	7.40E-01	2.01E-00	5.63E-00	1.12E+01	1.90E+01
2155.	9.44E-02	2.77E-01	7.96E-01	2.25E-00	6.06E-00	1.16E+01	1.94E+01
2160.	9.60E-02	2.95E-01	8.77E-01	2.51E-00	6.48E-00	1.20E+01	1.98E+01
2165.	9.74E-02	3.21E-01	9.81E-01	2.81E-00	6.91E-00	1.25E+01	2.01E+01
2170.	9.87E-02	3.55E-01	1.11E-00	3.15E-00	7.35E-00	1.30E+01	2.03E+01
2175.	1.00E-01	3.90E-01	1.25E-00	3.51E-00	7.80E-00	1.34E+01	2.04E+01
2180.	1.02E-01	4.22E-01	1.40E-00	3.91E-00	8.26E-00	1.39E+01	2.05E+01
2185.	1.06E-01	4.54E-01	1.55E-00	4.35E-00	8.75E-00	1.43E+01	2.05E+01
2190.	1.12E-01	4.90E-01	1.72E-00	4.81E-00	9.27E-00	1.47E+01	2.06E+01
2195.	1.20E-01	5.31E-01	1.90E-00	5.30E-00	9.86E-00	1.51E+01	2.08E+01
2200.	1.29E-01	5.81E-01	2.10E-00	5.81E-00	1.05E+01	1.56E+01	2.10E+01
2205.	1.40E-01	6.37E-01	2.31E-00	6.35E-00	1.12E+01	1.60E+01	2.13E+01
2210.	1.52E-01	6.97E-01	2.54E-00	6.90E-00	1.19E+01	1.64E+01	2.17E+01
2215.	1.67E-01	7.64E-01	2.77E-00	7.46E-00	1.26E+01	1.68E+01	2.21E+01
2220.	1.87E-01	8.40E-01	3.02E-00	8.02E-00	1.33E+01	1.72E+01	2.25E+01

TABLE 47. THE SPECTRAL BAND PARAMETER S(1/2)/d AS A FUNCTION OF TEMPERATURE. (From Jackson, 1969 [239].) (Concluded)

WAVE NUMBER (1/CM)	TEMPERATURE (DEGREES KELVIN) 300.	600.	900.	1200.	1500.	1600.	2100.
2225.	2.17E-01	9.40E-01	3.31E-00	8.57E-00	1.40E+01	1.77E+01	2.30E+01
2230.	2.65E-01	1.08E-00	3.65E-00	9.12E-00	1.45E+01	1.81E+01	2.35E+01
2235.	3.34E-01	1.26E-00	4.03E-00	9.66E-00	1.50E+01	1.86E+01	2.39E+01
2240.	4.31E-01	1.48E-00	4.43E-00	1.01E+01	1.55E+01	1.89E+01	2.41E+01
2245.	5.51E-01	1.75E-00	4.84E-00	1.06E+01	1.58E+01	1.90E+01	2.38E+01
2250.	6.93E-01	2.04E-00	5.25E-00	1.11E+01	1.59E+01	1.89E+01	2.33E+01
2255.	8.50E-01	2.34E-00	5.63E-00	1.15E+01	1.60E+01	1.87E+01	2.26E+01
2260.	1.01E-00	2.65E-00	5.99E-00	1.18E+01	1.59E+01	1.85E+01	2.17E+01
2265.	1.19E-00	2.93E-00	6.29E-00	1.21E+01	1.58E+01	1.82E+01	2.07E+01
2270.	1.38E-00	3.20E-00	6.55E-00	1.24E+01	1.57E+01	1.78E+01	1.96E+01
2275.	1.58E-00	3.46E-00	6.79E-00	1.26E+01	1.54E+01	1.72E+01	1.83E+01
2280.	1.81E-00	3.75E-00	7.06E-00	1.27E+01	1.52E+01	1.67E+01	1.74E+01
2285.	2.12E-00	4.05E-00	7.39E-00	1.28E+01	1.50E+01	1.62E+01	1.65E+01
2290.	2.57E-00	4.37E-00	7.80E-00	1.28E+01	1.48E+01	1.58E+01	1.59E+01
2295.	3.18E-00	4.78E-00	8.30E-00	1.28E+01	1.45E+01	1.53E+01	1.53E+01
2300.	4.01E-00	5.38E-00	8.90E-00	1.27E+01	1.42E+01	1.47E+01	1.45E+01
2305.	5.04E-00	6.22E-00	9.55E-00	1.25E+01	1.37E+01	1.42E+01	1.38E+01
2310.	6.26E-00	7.39E-00	1.02E+01	1.23E+01	1.32E+01	1.34E+01	1.30E+01
2315.	7.67E-00	8.71E-00	1.07E+01	1.20E+01	1.27E+01	1.28E+01	1.24E+01
2320.	9.31E-00	1.00E+01	1.12E+01	1.16E+01	1.22E+01	1.21E+01	1.15E+01
2325.	1.09E+01	1.10E+01	1.14E+01	1.13E+01	1.16E+01	1.14E+01	1.08E+01
2330.	1.22E+01	1.14E+01	1.12E+01	1.08E+01	1.10E+01	1.07E+01	1.00E+01
2335.	1.34E+01	1.13E+01	1.08E+01	1.03E+01	1.03E+01	9.86E-00	9.13E-00
2340.	1.44E+01	1.10E+01	1.04E+01	9.85E-00	9.70E-00	9.22E-00	8.52E-00
2345.	1.53E+01	1.06E+01	9.90E-00	9.16E-00	8.88E-00	8.36E-00	7.81E-00
2350.	1.59E+01	1.06E+01	9.50E-00	8.51E-00	8.15E-00	7.61E-00	7.22E-00
2355.	1.52E+01	9.45E-00	8.65E-00	7.77E-00	7.36E-00	6.85E-00	6.50E-00
2360.	1.30E+01	8.01E+00	7.60E-00	6.87E-00	6.33E-00	5.77E-00	5.45E-00
2365.	1.03E+01	7.27E-00	7.61E-00	6.15E-00	5.56E-00	5.05E-00	4.66E-00
2370.	6.97E-00	6.43E-00	5.90E-00	5.50E-00	4.58E-00	4.12E-00	3.67E-00
2375.	4.45E-00	4.95E-00	5.01E-00	4.10E-00	3.76E-00	3.36E-00	2.97E-00
2380.	2.65E-00	3.50E-00	4.10E-00	2.80E-00	2.30E-00	1.90E-00	1.60E-00
2385.	1.51E-00	2.28E-00	3.00E-00	2.05E-00	1.70E-00	1.27E-00	1.15E-00
2390.	9.98E-01	1.40E+00	1.90E-00	1.40E-00	1.20E-00	1.00E-00	9.00E-01
2395.	6.25E-01	7.59E-01	1.20E-00	1.09E-00	9.00E-01	8.65E-01	8.40E-01
2400.	4.03E-01	5.51E-01	6.63E-01	8.00E-01	8.00E-01	8.10E-01	8.00E-01

τ_{CO_2} = transmittance of carbon dioxide (CO_2)

τ_{O_3} = transmittance of ozone (O_3)

τ_{CH_4} = transmittance of methane (CH_4)

τ_{N_2O} = transmittance of nitrous oxide (N_2O)

τ_{HNO_3} = transmittance of nitric acid (HNO_3)

τ_{N_2} = transmittance of nitrogen continuum

Transmittance through aerosols, with:

τ_a = transmittance through haze with absorption as the attenuating mechanism

τ_b = transmittance through haze with scattering as the attenuating mechanism.

The radiation transfer equation is set up in the following way in relation to the geometrical configuration of the atmosphere as shown in Figure 76, with the observer, in this case, at the earth's surface, the target (or source) at the n-th layer, and a cloud deck at the j-th layer; with the spectral radiance given by:

$$L_\lambda = \epsilon_s(\lambda)L_\lambda^*(T_s)\tau_c(\lambda)\tau_n(\lambda) + \epsilon_c(\lambda)L_\lambda^*(T_c)\tau_j(\lambda)$$

$$+ \sum_{i=1}^{j} L_\lambda^*(T_i)[\tau_i(\lambda) - \tau_{i+1}(\lambda)/\tau_i'(\lambda)]$$

$$+ \tau_c(\lambda) \sum_{i=j+1}^{n} L_\lambda^*(T_i)[\tau_i(\lambda) - \tau_{i+1}(\lambda)/\tau_i'(\lambda)] \qquad (322)$$

where (with the subscripts s and c referring respectively to source and cloud):

$L_\lambda^*(T)$ = Planck radiance at temperature, T

$\epsilon(\lambda)$ = spectral emissivity

T_i = temperature of the i-th shell,

$\tau_i(\lambda)$ = spectral transmittance of the atmosphere from the observer to the i-th shell,

$\tau_i'(\lambda)$ = spectral transmittance of the i-th shell as affected by scattering.

The scattering considered in Eq. (322) is only a single scattering of radiation out of the line-of-sight between target and observer.

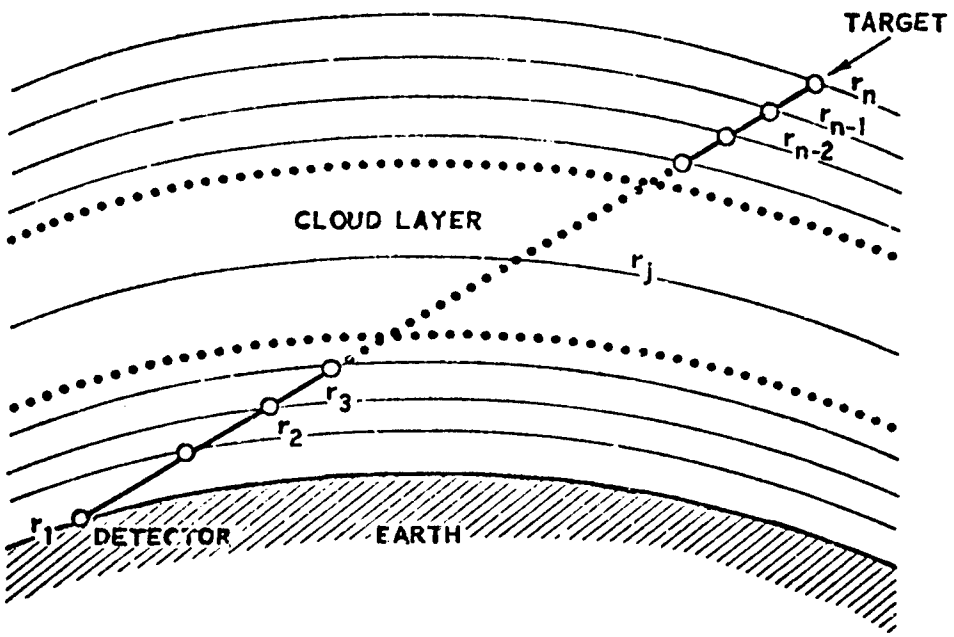

FIGURE 76. SCHEMATIC OF OPTICAL PATH FOR TRANSMISSION AND RADIANCE CALCULATIONS

7.4.1 TYPES OF MODELS USED

Because the Aggregate-method extends its spectral coverage from approximately 1 to 30 μm, and since it has been found (Anding, 1967) that different models are best suited for different spectral regions, the Aggregate method consists of a variety of models, with line parameters derived mainly empirically from a number of laboratory measurements. The models used, their regions of validity, and the approximate spectral resolution of the line parameter data are given in Table 48. Temperature dependence is usually ignored except in special cases (see, e.g., Section 7.4.1.2c). The exact forms of the equations describing the various models used in the Aggregate method are given as follows.

7.4.1.1 H_2O Vapor

(a) Strong-Line Goody Model (1 to 2 μm and 4.3 to 15 μm)

$$\tau(\lambda) = \exp\left[w^* K(\lambda)\right]^{1/2} \tag{323}$$

where
$$w^* = \rho_0 \int_0^R M(s) \left(\frac{P(s)}{P_0}\right)^2 \left(\frac{T_0}{T(s)}\right) \left(\frac{T_0'}{T(s)}\right)^{0.5} ds \quad \text{in pr cm} \tag{324}$$

$K(\lambda)$ = spectral coefficient, given in a set of tables, or stored in some storage device

ρ_0 = density of air at standard temperature and pressure

$M(s)$ = H_2O vapor mixing ratio in gm H_2O per gm dry air at s

P_0 = standard pressure = 760 mm Hg

T_0 = standard temperature = 288.15 K

T_0' = temperature at which band model parameters are defined usually $\neq T_0$

R = total path length in cm

(b) Goody Model (2 to 4.3 μm and 15 to 30 μm)

$$\tau(\lambda) = \exp\left\{-wK_1(\lambda)/\left[1 + 2wK_2(\lambda)/\overline{P}'\right]^{1/2}\right\} \tag{325}$$

where
$$w = \rho_0 \int_0^R M(s) \frac{P(s)}{P_0} \frac{T_0}{T(s)} ds \quad \text{in pr cm} \tag{326}$$

$$\overline{P}' = \frac{P_0}{w} \cdot w_2 \tag{327}$$

$$w_2 = \rho_0 \int_0^R M(s) \left(\frac{P(s)}{P_0}\right)^2 \left(\frac{T_0}{T(s)}\right) ds \tag{328}$$

TABLE 48. SUMMARY OF BAND MODELS USED IN COMPUTER PROGRAM.
(From Hamilton, et al., 1973 [19].)

Gas	Spectral Region (μm)	Approximate Resolution (μm)	Model	Coefficient Acquisition Procedure	Source of Data	Ref.
H_2O	1 to 2	0.1	Strong-Line Goody	Empirical Fit to Lab Data	Howard, et al., (1955)	[240]
	2 to 4.3	0.05	Goody	Empirical Fit to Lab Data	Burch, et al., (1962)	[234]
	4.3 to 15	0.5	Strong-Line Goody	Empirical Fit to Lab Data	Howard, et al., (1955)	[240]
	6.68 to 14.95	0.5	H_2O Continuum	Empirical Fit to Lab Data	Burch (1970) and Bignell (1970)	[189], [241]
	15 to 30	1.0	Goody	Direct from Line Parameters	McClatchey, et al. (1973)	[138]
CO_2	1.37 to 2.64	0.2	Tabular Data from Strong-Line Elsasser	Empirical Fit to Lab Data	Howard, et al., (1955)	[249]
	2.64 to 2.88	0.01	Classical Elsasser	Empirical Fit to Lab Data	Burch, et al., (1962)	[234]
	4.184 to 4.454	0.02	Classical Elsasser	Empirical Fit to Lab Data	Bradford, et al., (1963)	[242]
	4.465 to 5.355 9.13 to 11.67	0.5	Tabular Data from Strong-Line Elsasser	Empirical Fit to Lab Data	Howard, et al., (1955)	[240]
	11.67 to 19.92	0.10	Temperature Dependent Classical Elsasser	Empirical Fit to Line by Line Spectra	Drayson and Young (1967)	[142]
N_2O	4.228 to 4.73	0.5	Strong-Line Elsasser	Empirical Fit to Lab Data	Plyler and Barker (1931)	[243]
	7.53 to 8.91	0.5	Classical Elsasser	Empirical Fit to Lab Data	Burch, et al., (1962)	[234]
	15.4 to 19.3	0.5	Goody	Empirical Fit to Lab Data	Burch, et al., (1962)	[234]
N_2	3.76 to 4.83	0.5	N_2 Continuum	Empirical Fit to Lab Data	Burch, et al., (1970)	[188]
O_3	9.393 to 10.29	0.1	Modified Classical Elsasser	Empirical Fit to Lab Data	Walshaw (1957)	[133]
	11.7 to 15.4	0.5	Goody	Empirical Fit to Lab Data	McCaa and Shaw (1968)	[134]
CH_4	5.91 to 9.1	0.1	Classical Elsasser	Empirical Fit to Lab Data	Burch, et al., (1962)	[234]
HNO_3	5.8 to 5.944 7.45 to 7.80 10.9 to 11.67	0.5	Goody	Empirical Fit to Lab Data	Goldman, et al., (1971)	[244]

240. J. N. Howard, D. Burch and D. Williams, Near-Infrared Transmission Through Synthetic Atmospheres, Geophysics Research Paper No. 40, Report No. AFCRL-TR-55-213, Ohio State University, Columbus, 1955.

241. K. Bignell, "The Water Vapor Infrared Continuum," Quart. J. Roy. Met. Soc., Vol. 96, 1970, pp. 390-403.

242. W. R. Bradford, T. M. McCormick and J. A. Selby, Laboratory Representation of Atmospheric Paths for Infrared Absorption, Report No. DMP 1431, EMI Electronics, Hayes, Middlesex, England, 1963.

243. E. Plyler and E. Barker, "Infrared Spectrum and Molecular Configuration of N_2O," Phys. Rev., Vol. 38, 1931, p. 1827.

244. A. Goldman, T. G. Kyle and F. S. Bonomo, "Statistical Band Model Parameters and Integrated Intensities for the 5.9μ, 7.5μ, and 11.3μ Bands of HNO_3 Vapor," Appl. Opt., Vol. 10, No. 1, 1971, pp. 65-73.

$K_1(\lambda)$ = spectral coefficient (=S/d)

$K_2(\lambda)$ = spectral coefficient (=$S/2\pi\alpha^o_{L0}$)

α^o_{L0} = Lorentz line half-width per unit pressure

(c) H_2O Continuum (6.68 to 14.95 μm)

$$\tau(\lambda) = \exp -\left[\left(P\left\{C_1(\lambda)[C_2(\lambda)/C_1(\lambda)]^{(T-175)/125}\right\}\right.\right.$$
$$\left.\left. + p\left\{C_3(\lambda)[C_4(\lambda)/C_3(\lambda)]^{(T-175)/125}\right\}\right)w\right] \quad (329)$$

where P = pressure of the non-absorbing gas in atmospheres

p = pressure of the absorbing gas

T = absolute temperature

$C_1(\lambda)$ = spectral coefficient for foreign broadening at T = 175 K

$C_2(\lambda)$ = spectral coefficient for foreign broadening at T = 300 K

$C_3(\lambda)$ = spectral coefficient for self broadening at T = 175 K

$C_4(\lambda)$ = spectral coefficient for self broadening at T = 300 K

w = (see above, Eq. 328)

The water vapor continuum equation was derived from the work of Bignell (1970), in which two temperature-dependent coefficients are used, one corresponding to foreign-gas broadening, and one corresponding to self-broadening. In accordance with the work of Burch, et al. (1970), Anding (private communication) devised an exponential interpolative scheme for varying the coefficients with temperature in accordance with the two fixed, known values at 300 and 175 K. Hence, the equation (329). The value 175 K was chosen as representative of the lower expected values of the tropopause.

7.4.1.2 CO_2

(a) Classical Elsasser Model (2.64 - 2.88 μm and 4.184 - 4.454 μm)

$$\tau(\lambda) = 1 - \sinh\beta\int_0^Y I_0(y)\exp(-y\cosh\beta)\,dy \quad (330)$$

where $\beta = K_1'(\lambda)\overline{F}$

$\overline{P} = \frac{P_0}{w}\cdot w_1$, Curtis-Godson equivalent broadening pressure (in mm Hg)

$$w = \int_0^R M'(s) \frac{P(s)}{P_0} \left(\frac{T_0}{T(s)}\right) ds$$

$$w_1 = \int_0^R M'(s) \left(\frac{P(s)}{P_0}\right)^2 \left(\frac{T_0}{T(s)}\right) ds \qquad (331)$$

with $M'(s)$ = ratio of partial pressure of absorber to total pressure

$K_1'(\lambda)$ = spectral coefficient $(=2\pi\alpha_{L0}^o/d)$

α_{L0}^o = Lorentz line half-width per unit pressure

$y = \beta\chi/\sinh$

$\psi = K_2(\lambda)w/\overline{P}$ [compare: $\psi = Sw/2\pi\alpha_L$]

$K_2(\lambda)$ = spectral coefficient $(=S/2\pi\alpha_{L0}^o)$

$I_0(y)$ = associated Bessel function of zero order, $J_0(iy)$

Y = value of y at end of path

(b) Strong-Line Elsasser Model (2.64 - 2.88 μm and 4.184 - 4.454 μm)

Since this exact solution converges slowly for large values of χ, the strong-line approximation is used for $\psi > 20$:

$$\tau(\lambda) = 1 - \text{erf}\,[0.5\beta^2\psi)^{1/2}] \qquad (332)$$

where

$$\text{erf}\,(\xi) = \frac{2}{\sqrt{\pi}} \int_0^\xi \exp(-t^2)\,dt$$

(c) Temperature-Dependent Classical Elsasser Model (11.67 - 19.92 μm)

The Aggregate method uses the classical Elsasser model for the 15 μm band of CO_2, i.e., the spectral region extending from 11.79 to 19.92 μm. Transitions in this band, however, are highly temperature sensitive; therefore, in determining the equivalent-path parameters for the original version of the method, Anding and Rose developed a procedure for calculating the equivalent temperature of a variable-temperature path for this spectral region. The temperature determined by this method is calculated in the program from which transmittances and radiances are calculated with the Aggregate method.

The transmittance in a small spectral region, $\Delta\nu$, can be written for the slant path as:

$$\tau(\Delta\nu)_{\text{slant}} = \frac{1}{\Delta\nu} \int_{\Delta\nu} \exp\left[-\frac{1}{\pi}\sum_{i=1}^{N} \int_0^R \frac{S_i\alpha_{Li}\rho(s)\,ds}{(\nu - \nu_{0i})^2 + \alpha_{Li}^2}\right] d\nu \qquad (333)$$

For the equivalent homogeneous path:

$$\tau(\Delta\nu)_{homo} = \frac{1}{\Delta\nu}\int_{\Delta\nu} \exp\left[-\frac{1}{\pi}\sum_{i=1}^{N}\frac{S_{hi}\alpha_{Lhi}w_h}{(\nu-\nu_{0i})^2+\alpha_{Lhi}^2}\right] d\nu \tag{334}$$

where the subscript h signifies that the path is homogeneous. The density of the gas is

$$\rho(s) = \rho_0 \frac{P(s)}{P_0}\frac{T_0}{T(s)}$$

and the approximate line strength and width are respectively:

$$S(T) = S(T_0)(T_0/T)^{3/2} \exp\left\{-\frac{E''(\lambda)}{k}\left(\frac{1}{T}-\frac{1}{T_0}\right)\right\} \tag{335}$$

and

$$\alpha_L = \alpha_{L0}(T_0/T)^{1/2}(P/P_0) \tag{336}$$

where E'' = energy of the lower state

k = Boltzmann constant.

If the strong-line conditions are to be considered, then the line centers are completely absorbed, and only the wings $\left(\text{i.e., } (\nu-\nu_{0i})^2 >> \alpha_i^2\right)$ contribute to changes in transmittance. So, if the exponents of Eqs. (333) and (334) are equated, making the proper substitutions, the result is:

$$\sum_{i=1}^{N}\int_0^R \rho_0\left(\frac{T_0}{T(s)}\right)^3\left(\frac{P(s)}{P_0}\right)^2 \exp -\left(\frac{E''(\lambda)}{k}\frac{T_0-T(s)}{T_0T(s)}\right) ds$$

$$= \sum_{i=1}^{N}\left(\frac{T_0}{T_h}\right)^2\left(\frac{P_h}{P_0}\right)w_h \exp -\left(\frac{E''(\lambda)}{k}\frac{T_0-T_h}{T_0T_h}\right) \tag{337}$$

Maintaining the ratios of the strengths for the homogeneous and non-homogeneous paths either constant or monotonically changing, the two sides of Eq. (337) can be equated line for line so that the summation signs can be dropped. The result is solved for T_h by an iterative process.

It is evident from Eq. (337) that T_h is a function of wavelength and that it would be necessary to compute a homogeneous path for each wavelength of the band under consideration. For many atmospheric applications, however, it is possible to eliminate this spectral

dependence. Referring to Eq. (335) and recalling that E'' increases with spectral distance from its fundamental transition frequency, it can be deduced that, near the band center where E'' is small, the T_0/T term dominates the expression for S. In the wings, E'' is large and the exponential term becomes the primary factor. But the variability of S in these regions is such that by computation, spectral equivalent temperatures, T_h, vary by only a 3 or 4 K for a path looking straight up through the atmosphere. For practical purposes, errors of this magnitude do not seriously limit the accuracy of the band model and therefore a weighted mean is used as a constant for the value of E''.

Absorption calculations are made therefore using band model parameters derived at the temperature of the single homogeneous path. A complete capability would then consist of an a priori knowledge of the absorption coefficients as functions of wavelength and temperature. For the Aggregate method, in order to minimize the time and cost of carrying out the fitting procedure for many temperatures, two extremes in temperature were chosen (300 K and 220 K) to perform the fit; and a temperature interpolation scheme was devised to yield the absorption coefficients for all intermediate temperatures.

The values of the coefficients were calculated from:

$$\frac{S}{d} = \frac{A_1 \exp -(A_2/T_h)}{T_h^2} \tag{338}$$

and

$$\frac{2\alpha_{L0}S}{d^2} = \frac{A_3 \exp -(A_4 - T_h)}{T_h} \tag{339}$$

where A_1, A_2, A_3 and A_4 are the spectral parameters to be used for Eq. (330)

(d) Empirical Model (Using Tabular Data) (1.37 - 2.64 μm, 4.465 to 5.355 μm and 9.13 to 11.67 μm)

A simple empirical model is used in the Aggregate method for the spectral region between 4.465 and 5.355 μm. Altshuler [245] related the transmittance in his model to the argument $w^*K(\lambda)$ so that

$$\tau = \tau(w^*K(\lambda)) \tag{340}$$

245. T. L. Altshuler, Infrared Transmission and Background Radiation by Clear Atmospheres, No. 61SD109, General Electric Co., 1961, 140 pp.

where $w^* = \int_0^R M'(s)\left(\frac{P(s)}{P_0}\right)^2\left(\frac{T_0}{T(s)}\right)\left(\frac{T_0'}{T(s)}\right)^{0.5} ds$ (341)

$K(\lambda)$ = spectral coefficient

$M'(s)$ = (see Eq. (331)).

The Altshuler model was adopted for the spectral region mentioned and the values of $K(\lambda)$ and $w^*K(\lambda)$ are tabulated. The transmittance for any given condition is obtained by interpolation between tabulated values.

7.4.1.3 O_3

(a) Goody Model (11.7 to 15.4 μm)

In calculating the transmittance in the spectral region from 11.7 to 15.36 μm, the Aggregate method uses the Goody model as specified by:

$$\tau(\lambda) = \exp\left\{-wK_1(\lambda)/[1 + K_1(\lambda)w/4\bar{P}K_2(\lambda)]^{1/2}\right\} \quad (342)$$

where $K_1(\lambda)$, $K_2(\lambda)$ are spectral parameters. The values w and $\bar{P}$ are calculated as previously shown.

(b) Modified Elsasser (9.398 to 10.19 μm)

For the spectral region from 9.398 to 10.19 μm, the classical Elsasser model is used with the parameter β modified to:

$$\beta = \left(\frac{2\pi\alpha_{L0}}{d}\right)\left(\frac{\bar{P}}{P_0}\right)c(\lambda) \quad (343)$$

where $c(\lambda)$ = spectral parameter.

7.4.1.4 HNO_3

Goody Model (5.8 to 5.944 μm, 7.45 to 7.80 μm and 10.9 to 11.67 μm)

As shown in Table 48, the Goody model is used for nitric acid in all spectral regions and the equation defining its transmittance is given in Eq. (342), with the spectral parameters specific to HNO_3. It will be noted that the form of Eq. (342) is slightly different from that given for H_2O vapor in Eq. (325).

7.4.1.5 CH_4

Elsasser Model (5.91 to 9.1 μm)

As shown in Table 48, the classical Elsasser model, represented by Eqs. (330) and (331), is used to calculate the transmittance of methane.

7.4.1.6 N_2

Continuum (3.76 to 4.83 μm)

The Aggregate method for transmittance in the N_2 continuum region is adopted directly from the work of Burch, et al. (1970) covering the spectrum from 3.76 to 4.83 μm, and is given by:

$$\tau(\lambda) = \exp -[K_s(\lambda)w_s + K_f(\lambda)w_f] \tag{344}$$

where $K_s(\lambda)$ and $K_f(\lambda)$ are, respectively, the spectral coefficients for self-broadening and foreign broadening; and w_s and w_f are described as:

$$w_s = 2.69\int_0^R \left[\frac{P_s^*(r)}{P_0}\right]^2 \left[\frac{T_0}{T(r)}\right] dr \tag{345}$$

and

$$w_f = 2.69\int_0^R \frac{P_s^*(r)P_f^*(r)}{P_0^2} \left[\frac{T_0}{T(r)}\right] dr \tag{346}$$

given in the units (10^{-21}·molecules·atm/cm^2). The P_s^* and P_f^* are, respectively, the effective pressures for self-broadening and foreign gas broadening, and are given by:

$$P_s^* = P_{N_2}\left(1 + 0.001P_{N_2}/P_0\right) \tag{347}$$

and

$$P_f^* = P_{O_2}\left(1 + 0.001P_{O_2}/P_0\right) \tag{348a}$$

with P_{N_2} and P_{O_2}, respectively, the partial pressures of nitrogen and oxygen.

7.4.1.7 N_2O

(a) Strong-Line Elsasser Model (4.228 to 4.73 μm)

In the spectral region from 4.228 to 4.73 μm the strong-line approximation to the Elsasser model is used in the form shown in the following equation:

$$\tau(\lambda) = 1 - \text{erf}\,[w^*K(\lambda)]^{1/2} \tag{348b}$$

where $K(\lambda)$ = spectral coefficient

$$w^* = \int_0^R M(s)\left(\frac{P(s)}{P_0}\right)^2\left(\frac{T_0}{T(s)}\right)^{0.5} ds \tag{348c}$$

(b) Classical Elsasser (7.53 to 8.91 μm)

In the spectral region from 7.533 to 8.909 μm, the classical Elsasser model is used, as demonstrated in Eq. (330) and by the equation below Eq. (330) defining the equivalent amount of absorber.

(c) Goody Model (15.4 to 19.3 μm)

For the spectral region from 15.408 to 19.231 μm, the form of the Goody model represented by Eq. (342) is used and the optical depth is defined as in the case of O_3 where this equation is used.

7.4.2 SCATTERING

In addition to gaseous absorption by atmospheric molecules, the Aggregate method (see Hamilton, et al., 1973) accounts also for the single scattering of radiation from the observed target out of the line-of-sight, caused by particles in the atmosphere. The model uses a maritime haze distribution (see Section 10) in the equation:

$$\tau_{ext}(\lambda) = e^{-b_{ext}(\lambda)\cdot\ell} \tag{349}$$

representing extinction by particles, where $b_{ext}(\lambda)$ is the wavelength dependent extinction coefficient and ℓ is the path length. The two parts of the extinction coefficient, $b_a(\lambda)$ and $b_s(\lambda)$, for the absorption and scattering, respectively, are accounted for in the following equations in terms of the particle radius, r, and size distribution per cm^3, N(r):

$$b_{ext}(\lambda) = \int_0^\infty Q_{ext}(\lambda, r)\pi r^2 N(r)\, dr \tag{350}$$

and

$$b_s(\lambda) = \int_0^\infty Q_s(\lambda, r)\pi r^2 N(r)\, dr \tag{351}$$

where the efficiency factors Q_{ext} and Q_s are obtained from:

$$Q_{ext}(\lambda, r) = \frac{2}{x^2}\sum_{n=1}^{\infty}(2n+1)\,\text{Real}\,\{A_n[x, m(\lambda)] + B_n[x, m(\lambda)]\} \tag{352}$$

and

$$Q_s(\lambda, r) = \frac{2}{x^2}\sum_{n=1}^{\infty}(2n+1)\left\{|A_n[x, m(\lambda)]|^2 + |B_n[x, m(\lambda)]|^2\right\} \quad (353)$$

where: $x = 2\pi r/\lambda$

$m(\lambda)$ = complex index of refraction of the scatterers

A_n, B_n = scattering parameters.

For a more detailed discussion of the scattering phenomenon, the reader is referred to Section 2.

In the Aggregate method the total scattering in the path is accounted for by accumulating the effect in the non-homogeneous atmosphere over the various layers so that

$$\tau(\lambda) = \exp\{-[b_{ext}(\lambda)]_1 \ell_1\} \times \exp\{-[b_{ext}(\lambda)]_2 \ell_2\} \times \ldots$$

$$\ldots \times \exp\{-[b_{ext}(\lambda)]_n \ell_n\} \quad (354)$$

The Aggregate methods allows the particle distribution to remain constant with altitude with only the particle density varying. Since the extinction coefficient is normalized to the effect by 1 particle/cm^3, the transmittance is given by:

$$\tau_{ext}(\lambda) = \exp\left\{-[b_{ext}(\lambda)]_i \sum_{i=1}^{n} D_i \ell_i\right\}$$

where $D_i = \int_0^{\infty} N(r)\,dr$ is the particle density in the i-th layer.

7.4.3 RECENT TECHNIQUES IN BAND PARAMETER CALCULATION SUGGESTED FOR THE AGGREGATE METHOD

7.4.3.1 Description of the Technique

Rose [246] has suggested in an unpublished paper that, in an attempt to retain the simplicity and the low-cost advantage of the band model for spectral regions where few good laboratory data existed, and at the same time to make use of high resolution information resulting from a line-by-line approach, an up-to-date concept in band modeling be evolved. Indeed, Anding (1974) has begun to revise lines in the middle-to-long IR region by this technique in his newer version of the Aggregate method. The calculation approach differs from the original in that the band model utilizes absorption coefficients derived from some of the basic data generated in a line-by-line method.

246. H. Rose, Private communication - Line Parameter Determination of Band Model Parameters, 1974.

Rose presented the details pertinent to the derivation of the model for the 15 μm band of CO_2 using the Elsasser model. This spectral region was chosen for the initial work because of the "conspicuous lack of good modeling procedures," and also because of the added emphasis of newer technology in the long wavelength infrared. The analysis indicates the model's worth and a discussion regarding its application to atmospheric slant paths.

In choosing the approach, Rose adopted Drayson's (1967) development of rigorous line-by-line computational capability in the 15 μm band. The spectra he obtained (see Figure 77) resulting from Drayson's technique compare very well to both laboratory homogeneous data and to field measurement spectra obtained at high resolution (up to 0.1 cm^{-1}). It was concluded, therefore, that a band-model calculation of the parameters $2\pi\alpha_{L0}(\lambda)/d$ and $S(\lambda)/d$, based upon spectra produced by the Drayson technique, could be developed to produce more reliable spectra than from previous models.

The details involving the complete specification of the band model parameters, the so-called "fitting" procedure, are documented elsewhere (see Section 5). Otherwise, Rose presented the following pertinent insights. First, it is considered essential that application of the model be extended to absorber concentrations and pressures that are encompassed by the data used to perform the fit. This precaution insures that extrapolation of the original data need not be made. Also, since it is desired to apply the model later to slant path calculations, (w, P) pairs were chosen for the initial synthesis of spectra to represent a wide variety of atmospheric paths and at the same time yield a full range of absorptance values for each $\Delta\nu$.

These requirements point out an important advantage in using "synthetic" rather than laboratory data to perform the fit. Certain extreme path conditions are difficult if not impossible to achieve in the laboratory, whereas the rigorous method is not limited to as great an extent by these practical considerations. Thus, the line-by-line method can presumably supply spectra for the full extent of optical depth and pressure values. This advantage is most important at low values of pressure. For this condition, a second type of line broadening becomes important, the purely temperature broadened Doppler line. The Drayson program applies a mixed Doppler-Lorentz line shape for pressures below 100 mb while retaining the pure Lorentz shape for higher pressures. Using line-by-line synthetic data in the fitting procedure yields a band model technique which, at small pressures, compensates for the model's inherent inability to handle the Doppler broadened line. At the same time, it can be seen that band model methods derived directly from line parameters could not handle the Doppler-Lorentz line shape without destroying the band model's cost time advantage over a line-by-line approach.

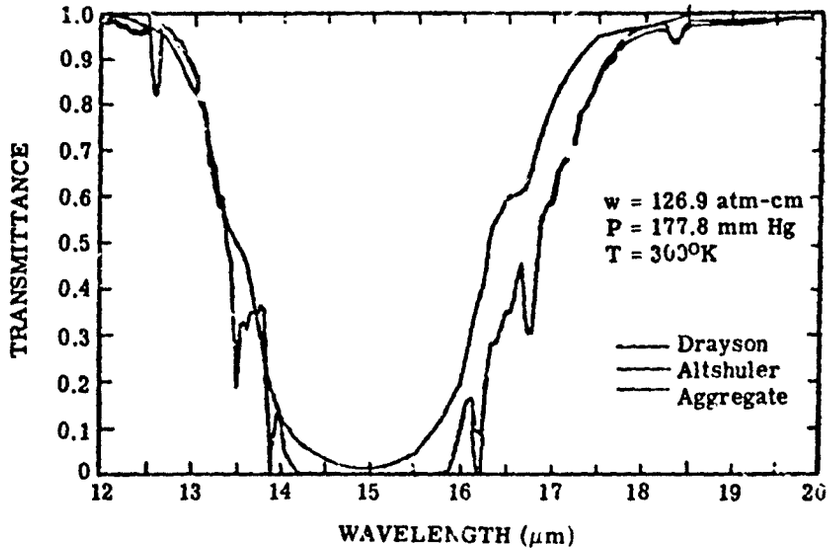

(a)

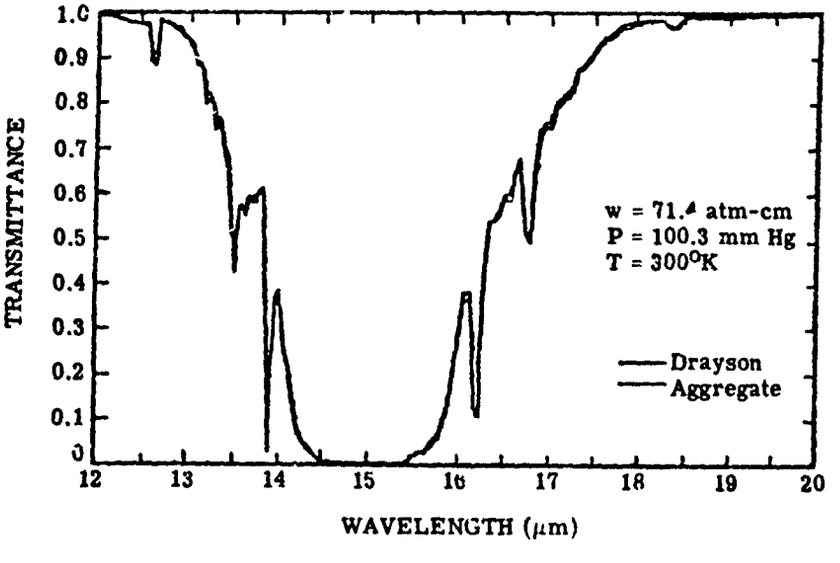

(b)

FIGURE 77. COMPARISON OF SPECTRA

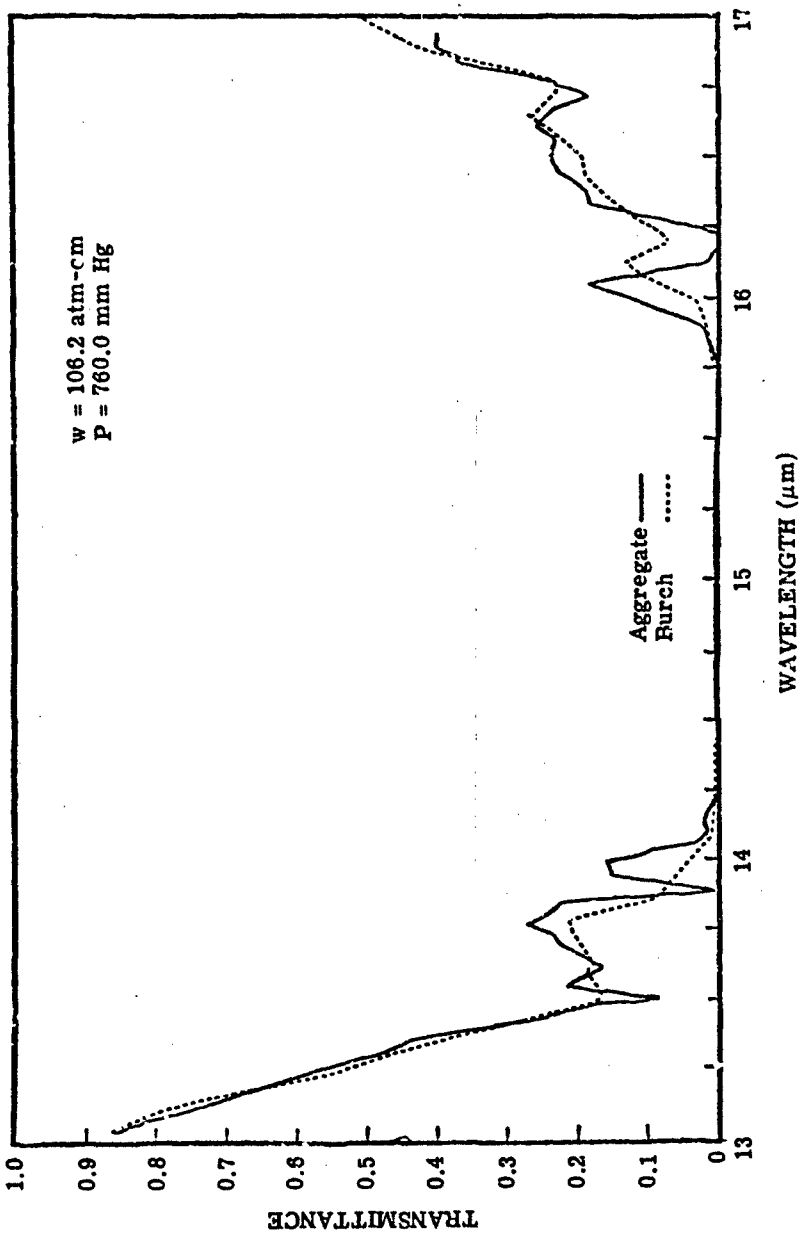

FIGURE 77. COMPARISON OF SPECTRA (Concluded)

The Drayson program was used to calculate spectra at 300 K for each path chosen and the data were smoothed to 5 cm^{-1} resolution with points every 2 cm^{-1}. The mechanics of determining the best parameters or absorption coefficients at each $\Delta\nu$ were handled by a least-squares minimization technique programmed by Baumeister and Marquardt. This method minimizes the sums of the squares of the differences between the absorption calculated by Drayson and that calculated by the Elsasser model for all the paths in question. The band model parameters were thus obtained throughout the 500-850 cm^{-1} interval consistent with the resolution of the line-by-line smoothed data.

7.4.3.2 Evaluation of the Technique

To evaluate the band model, comparisons were obtained among spectra produced by the model and two other sources of homogeneous data. It is expected, however, that for non-homogeneous paths, with temperature variations, the limitation in accuracy will be the same as with the models incorporating parameters derived from laboratory data. The first set of spectra (Fig. 77), exhibits the ability of the model to reproduce the spectra of Drayson from which the parameters were determined. In addition to the band model results and Drayson's data, Figure 77(a) also presents a curve obtained by the method of Altshuler (1961). The latter, having in the past been considered as state-of-the-art, is presented for comparison.

It appears, in comparing the result of the new technique with the "exact" calculation, that the major areas of large discrepancies are the very intensely absorbing Q-branches, in which results were not expected to be the quality of other spectral intervals. One general problem experienced with the Elsasser model in these regions is the tendency to overpredict absorption for large values of absorptivity and under-predict for small values. In an attempt to improve accuracies in the intense regions, "synthetic" data were also fitted to the Goody model. The standard errors,

$$\frac{1}{N}\sqrt{\sum_{I=1}^{N}[A(I)_{Drayson} - A(I)_{Model}]^2}$$

where N is the number of data points or paths, were, however, consistently greater for the statistical model than the Elsasser model.

7.4.4 COMPARISONS OF CALCULATED VALUES AND THE VALUES FROM FIELD EXPERIMENTAL DATA

The following figures portray comparisons between spectra calculated by the Aggregate method and others obtained experimentally in field measurements.

Figure 78, obtained from Anding [247] compares the calculated values with the measured values of Yates and Taylor [248] for relatively small quantities of absorber.

Figure 79, calculated for this report, compares the calculation with measured values of Taylor and Yates [249] for a larger path and larger quantities of absorber.

Figure 80, also calculated for this report, compares the calculation with measured values of Taylor and Yates (1957) for a still larger path and larger quantities of absorber.

Figure 81, calculated for this report, compares the calculation with the measured values of Streete [250] for a 25 km path and relatively large quantities of absorber.

Figure 82, calculated for this report, compares the calculation with the measured values of Ashley [251] for a 12 km path and absorber amounts intermediate to the values of Taylor and Yates and of Streete. No scattering is calculated.

A lack of perfect agreement can be attributed to a number of things in addition to the naturally limited accuracy of band models. In the first place we have used the generalized scattering calculation in the Aggregate program which may not account for actual conditions and by virtue of which, at shorter wavelengths, the difference might be sizable. Also some of the quantities of H_2O vapor are quite large creating a situation to which it becomes difficult to extrapolate. For reasonable quantities of H_2O vapor and with a reasonable understanding of atmospheric conditions, the agreement is expected to be better.

Even with good agreement we still have only limited comparisons because there are no conditions reproduced experimentally for which calculated and measured values have been compared for slant paths, particularly in a controlled environment. See, however, the conditional comparisons with Nimbus data shown in Section 9.

7.5 LOWTRAN 2 METHOD

The LOWTRAN code covers the spectral range from 0.25 to 28.5 μm (350 to 40,000 cm^{-1}) with line parameters defined to a resolution of 20 cm^{-1}, spaced apart in steps of 5 cm^{-1}. The calculation is made on an atmosphere represented by a 33-layer model of altitudes, pressures,

247. D. Anding, Private Communication, New Technique in Parameter Calculation, 1974.

248. H. W. Yates and J. H. Taylor, Infrared Transmission of the Atmosphere, NRL Report 5453, Naval Research Laboratory, Washington, D. C., 1960.

249. J. H. Taylor and H. W. Yates, "Atmospheric Transmission in Infrared," J. Opt. Soc. Am., Vol. 47, No. 3. 1957, pp. 223-226.

250. J. L. Streete, "Infrared Measurements of Atmospheric Transmission at Sea Level," Appl. Opt., Vol. 7, No. 8, 1968, pp. 1545-1549.

251. G. Ashley, Private communication, 1974.

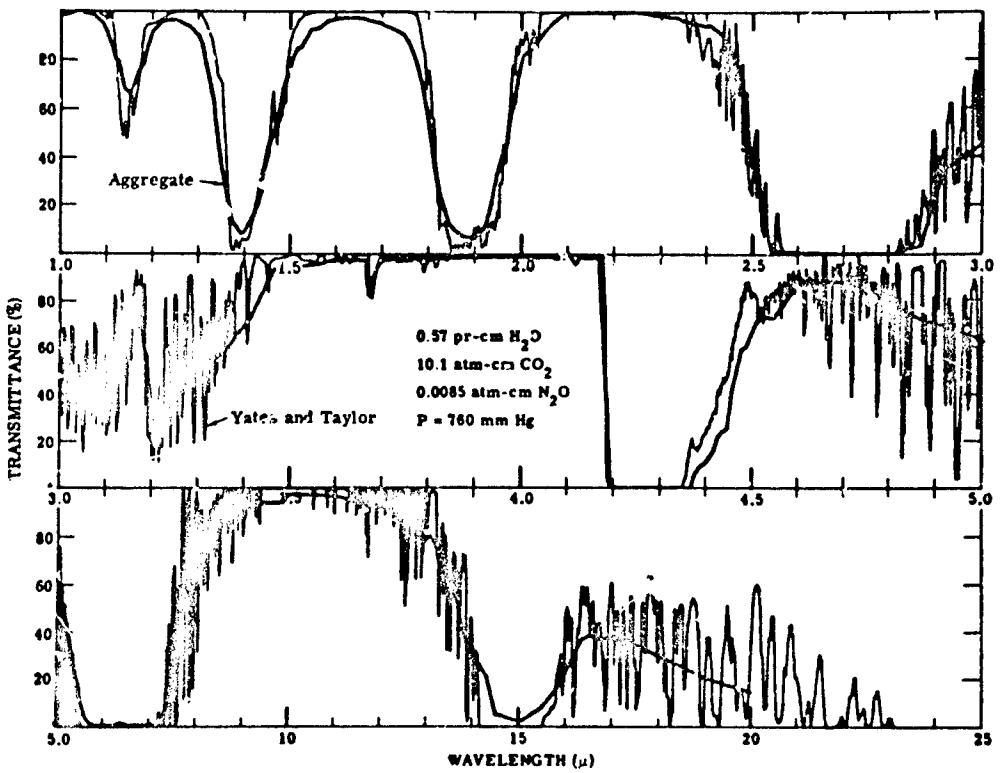

FIGURE 78. COMPARISON BETWEEN TRANSMITTANCES CALCULATED BY THE AGGREGATE METHOD AND THE EXPERIMENTAL DATA OF YATES AND TAYLOR (1960 [248].)

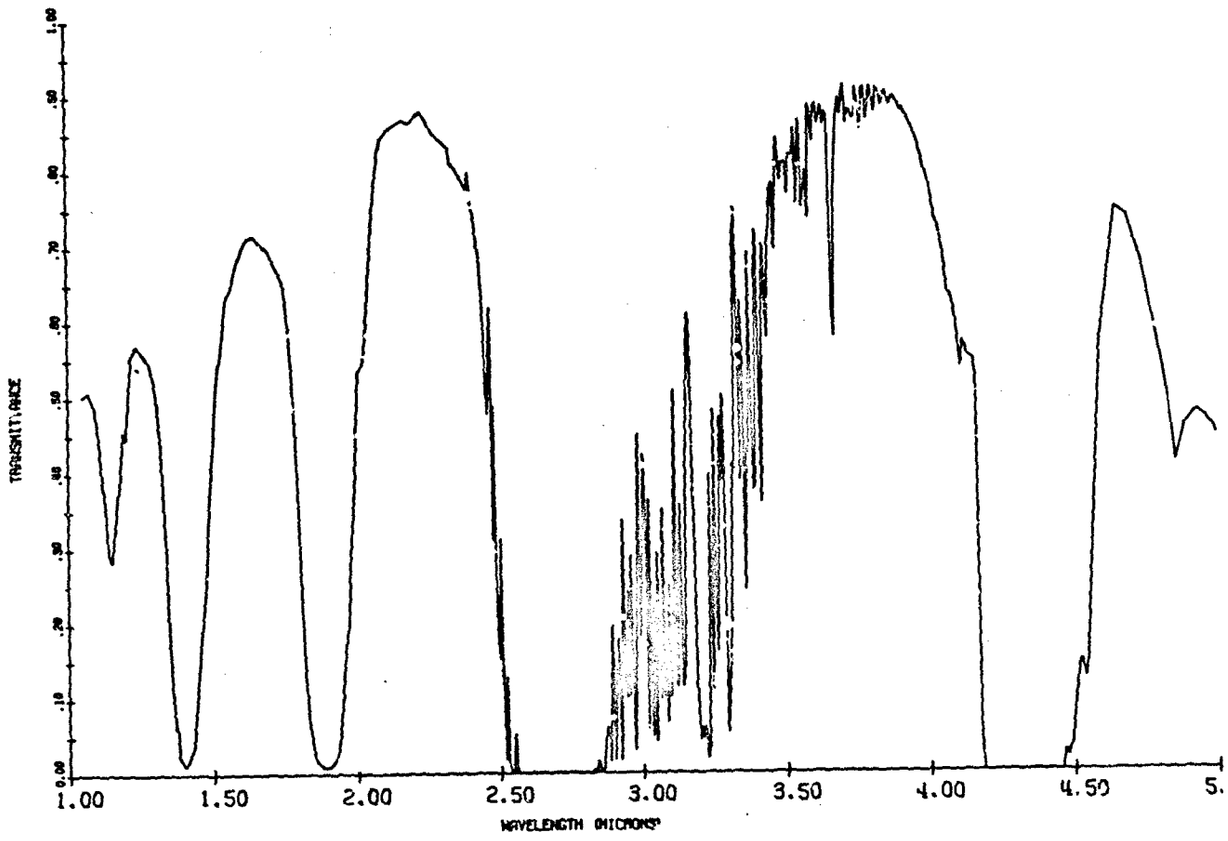

(a) Calculated

FIGURE 79. COMPARISON BETWEEN TRANSMITTANCES CALCULATED BY THE AGGREGATE METHOD AND THE EXPERIMENTAL DATA OF TAYLOR AND YATES (1957 [249]). H_2O = 13.7 pr mm.

ERIM
FORMERLY WILLOW RUN LABORATORIES, THE UNIVERSITY OF MICHIGAN

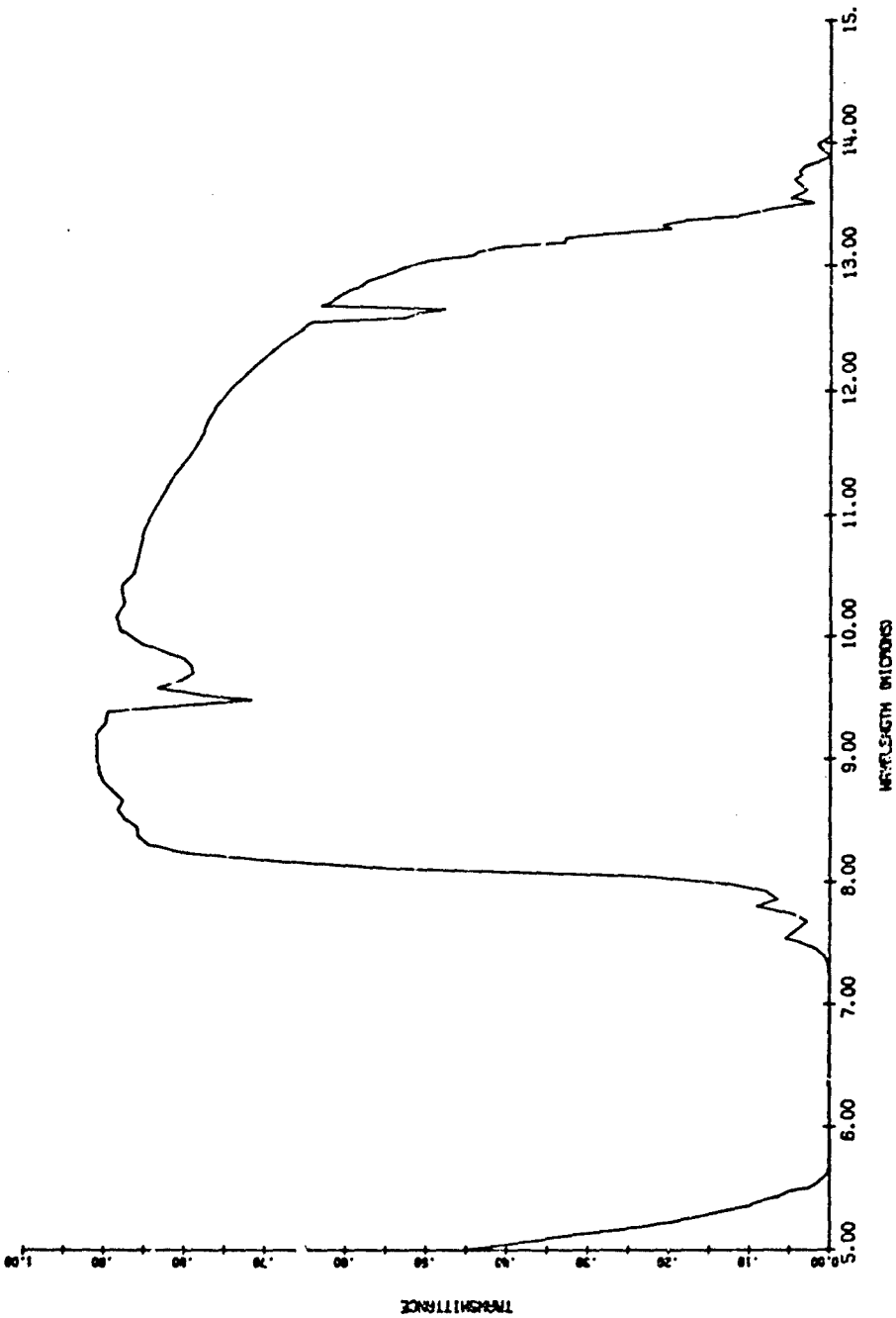

(a) Calculated (Concluded)

FIGURE 79. COMPARISON BETWEEN TRANSMITTANCES CALCULATED BY THE AGGREGATE METHOD AND THE EXPERIMENTAL DATA OF TAYLOR AND YATES (1957 [249]). H_2O = 13.7 pr mm. (Continued)

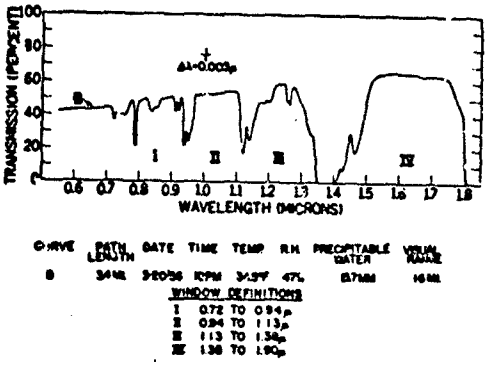

CURVE	PATH LENGTH	DATE	TIME	TEMP	R.H.	PRECIPITABLE WATER	VISUAL RANGE
B	34MI	3-20-56	10PM	34.5°F	47%	0.37MM	16 MI

WINDOW DEFINITIONS
I 0.72 TO 0.94μ
II 0.94 TO 1.13μ
III 1.13 TO 1.38μ
IV 1.38 TO 1.90μ

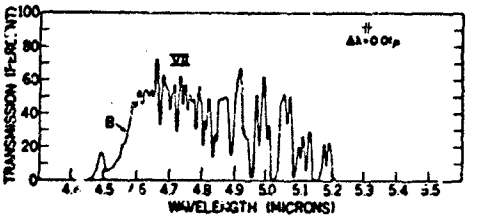

CURVE	PATH LENGTH	DATE	TIME	TEMP	R.H.	PRECIPITABLE WATER	VISUAL RANGE
B	34MI	3-20-56	10PM	34.5°F	47%	0.37MM	16 MI

WINDOW DEFINITION
VII 4.30 TO 6.0μ

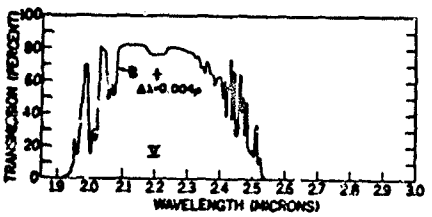

CURVE	PATH LENGTH	DATE	TIME	TEMP	R.H.	PRECIPITABLE WATER	VISUAL RANGE
B	34MI	3-20-56	10PM	34.5°F	47%	0.37MM	16 MI

WINDOW DEFINITION
V 1.90 TO 2.70μ

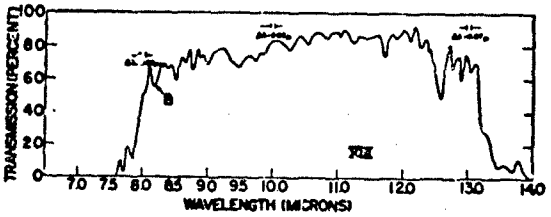

CURVE	PATH LENGTH	DATE	TIME	TEMP	R.H.	PRECIPITABLE WATER	VISUAL RANGE
B	34MI	3-20-56	10PM	34.5°F	47%	0.37MM	16 MI

WINDOW DEFINITION
VIII 8.0 TO 13.0μ

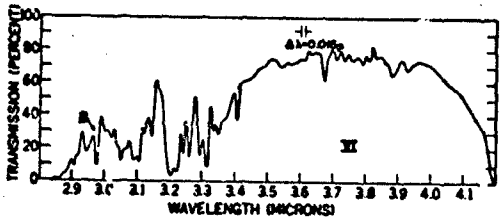

CURVE	PATH LENGTH	DATE	TIME	TEMP	R.H.	PRECIPITABLE WATER	VISUAL RANGE
B	34MI	3-20-56	10PM	34.5°F	47%	0.37MM	16 MI

WINDOW DEFINITION
VI 2.70 TO 4.30μ

(b) Experimental

FIGURE 79. COMPARISON BETWEEN TRANSMITTANCES CALCULATED BY THE AGGREGATE METHOD AND THE EXPERIMENTAL DATA OF TAYLOR AND YATES (1957 [249].) (Concluded)

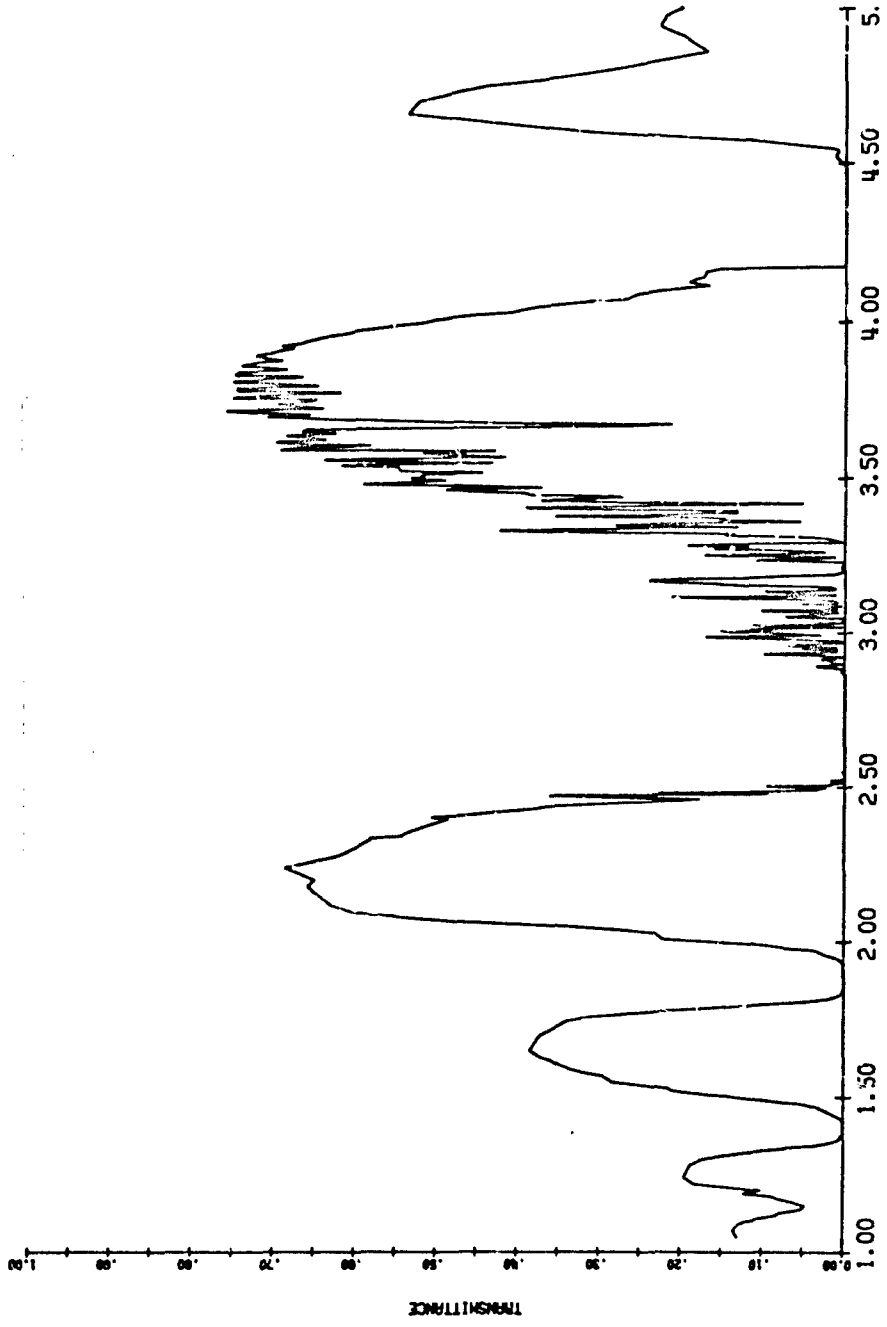

(a) Calculated

FIGURE 80. COMPARISON BETWEEN TRANSMITTANCES CALCULATED BY THE AGGREGATE METHOD AND THE EXPERIMENTAL DATA OF TAYLOR AND YATES (1957 [249]). H_2O = 52 pr mm.

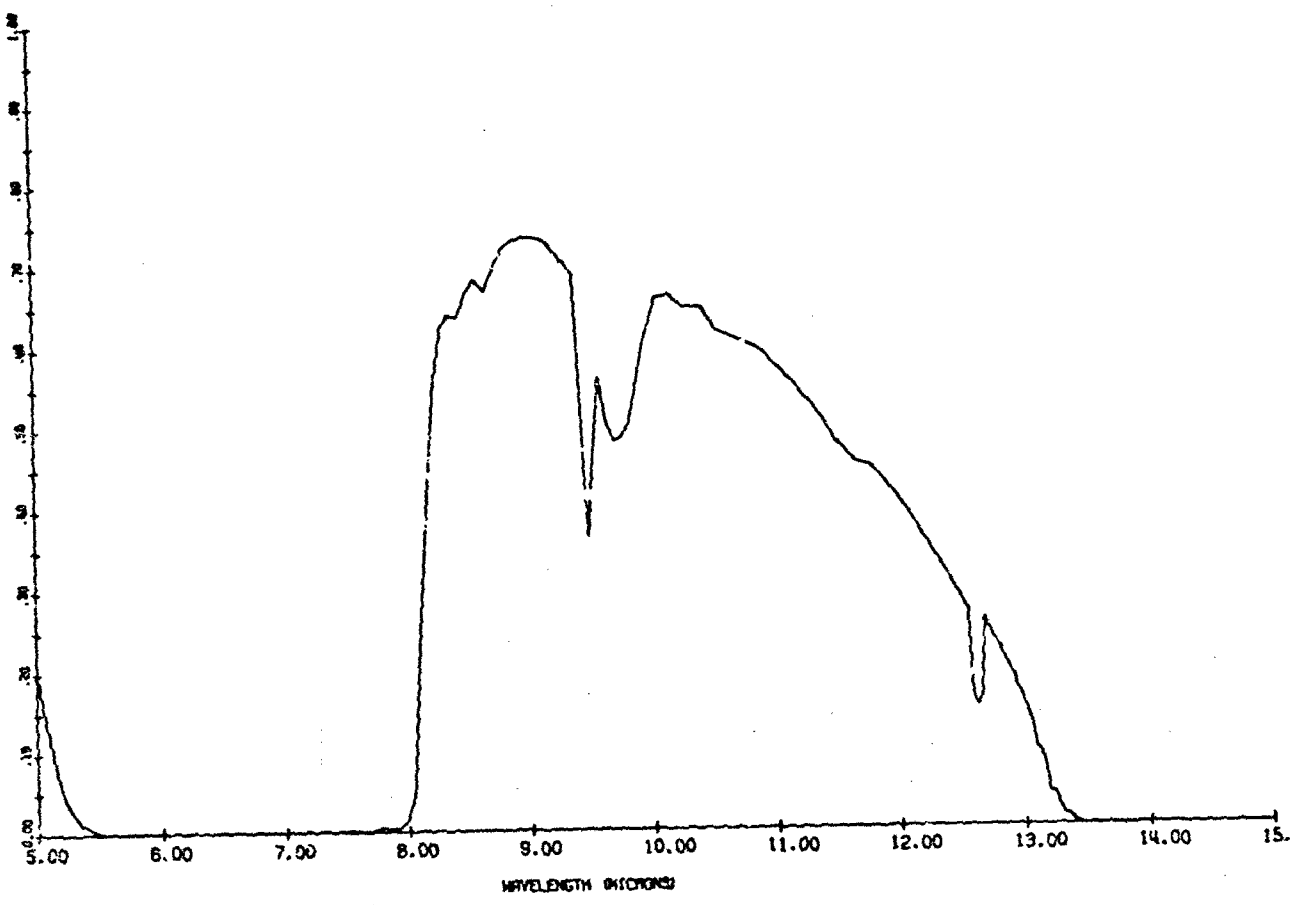

(a) Calculated (Concluded)

FIGURE 80. COMPARISON BETWEEN TRANSMITTANCES CALCULATED BY THE AGGREGATE METHOD AND THE EXPERIMENTAL DATA OF TAYLOR AND YATES (1957 [249]). H_2O = 52 pr mm.(Continued)

ERIM
FORMERLY WILLOW RUN LABORATORIES, THE UNIVERSITY OF MICHIGAN

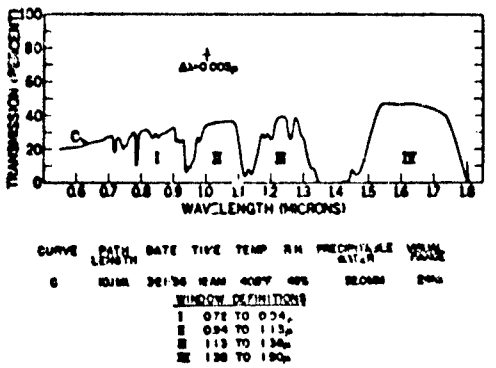

FIG. 4.

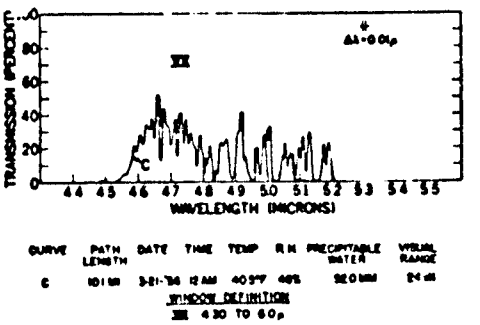

FIG. 7.

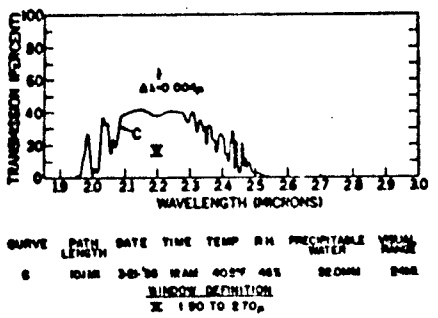

FIG. 5

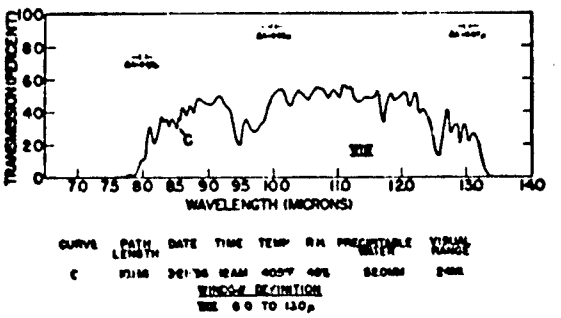

FIG. 8.

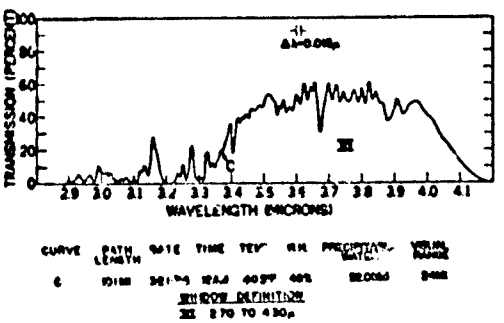

FIG. 6.

(b) Experimental

FIGURE 80. COMPARISON BETWEEN TRANSMITTANCES CALCULATED BY THE AGGREGATE METHOD AND THE EXPERIMENTAL DATA OF TAYLOR AND YATES (1957 [249].) (Concluded)

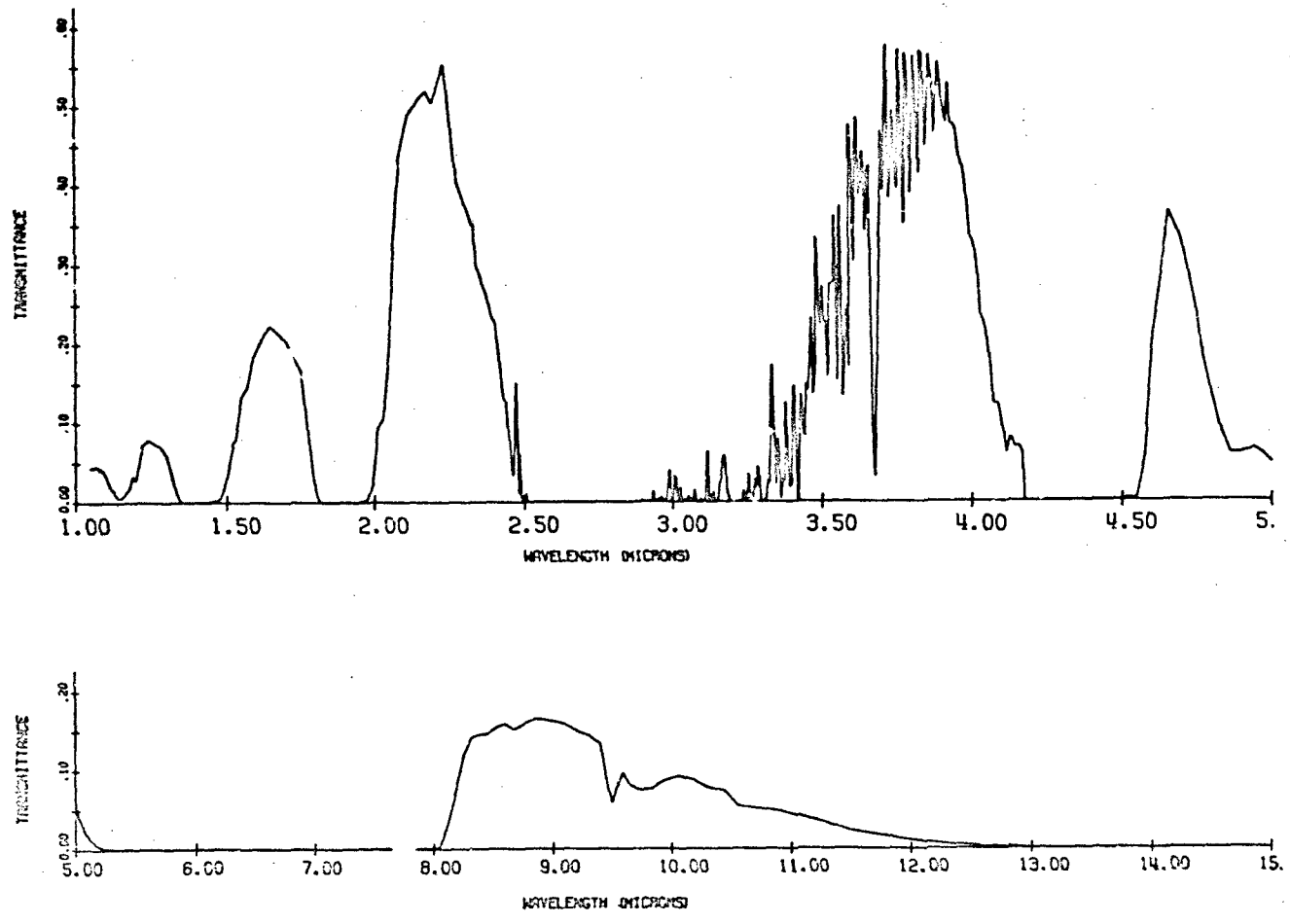

(a) Calculated

FIGURE 81. COMPARISON BETWEEN TRANSMITTANCES CALCULATED BY THE AGGREGATE METHOD AND THE EXPERIMENTAL DATA OF STREETE (1968 [250]). Path length = 25 km, amount of H_2O = 21.5 pr cm.

ERIM
FORMERLY WILLOW RUN LABORATORIES, THE UNIVERSITY OF MICHIGAN

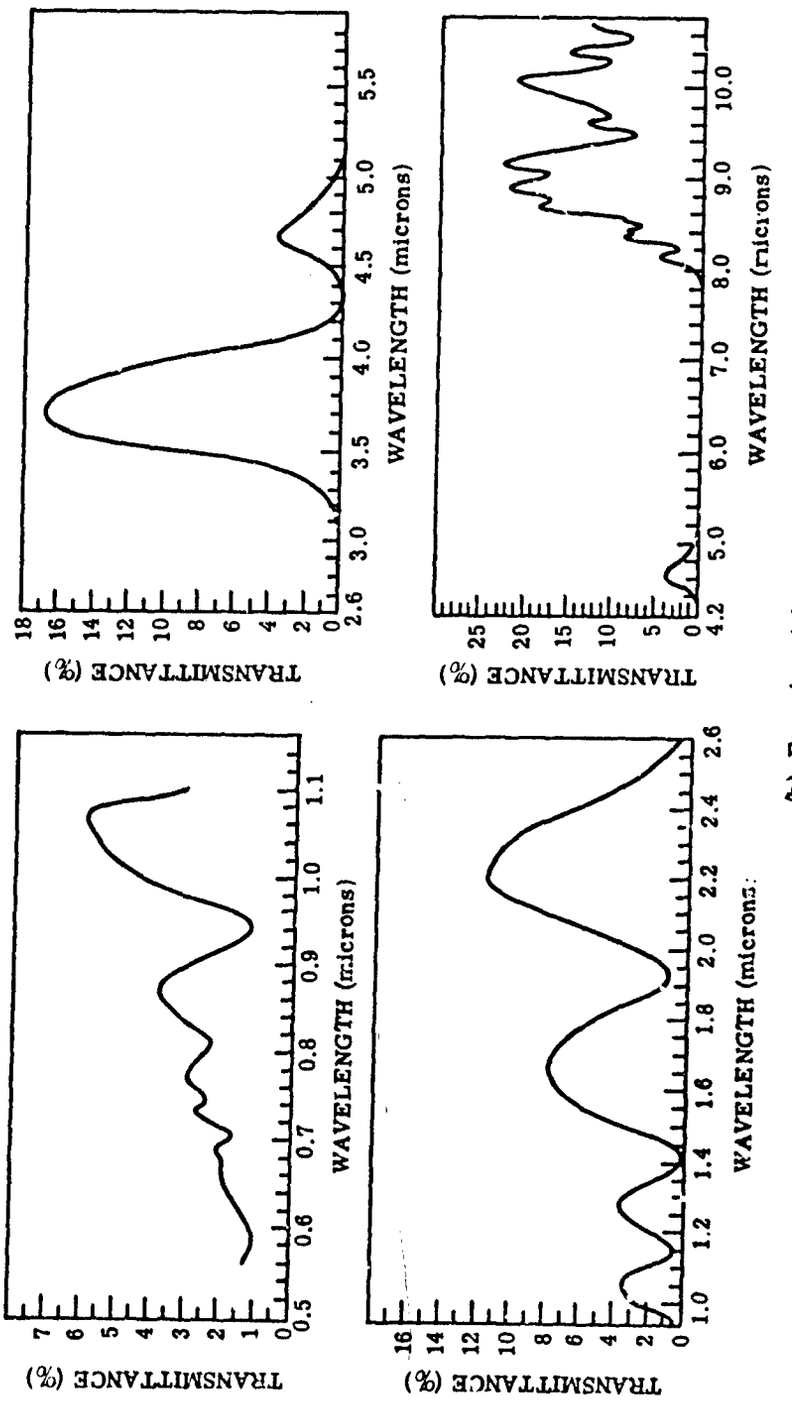

(b) Experimental

FIGURE 81. COMPARISON BETWEEN TRANSMITTANCES CALCULATED BY THE AGGREGATE METHOD AND THE EXPERIMENTAL DATA OF STREETE (1968 [250]). Path length = 25 km, amount of H_2O = 21.5 pr cm. (Concluded)

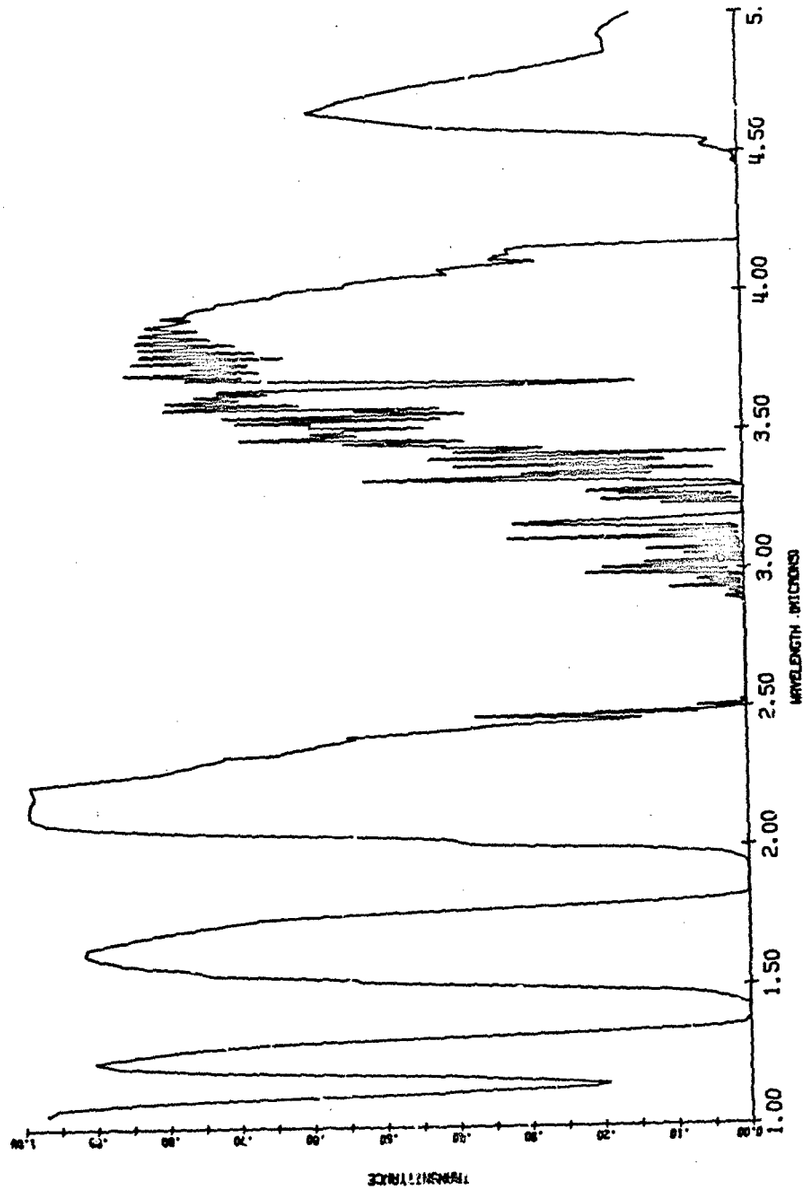

(a) Calculated (no scattering)

FIGURE 82. COMPARISON BETWEEN TRANSMITTANCE CALCULATED BY THE AGGREGATE METHOD AND THE EXPERIMENTAL DATA OF ASHLEY (PRIVATE COMMUNICATION). Path length = 39 Kft, amount of H_2O = 10 pr cm.

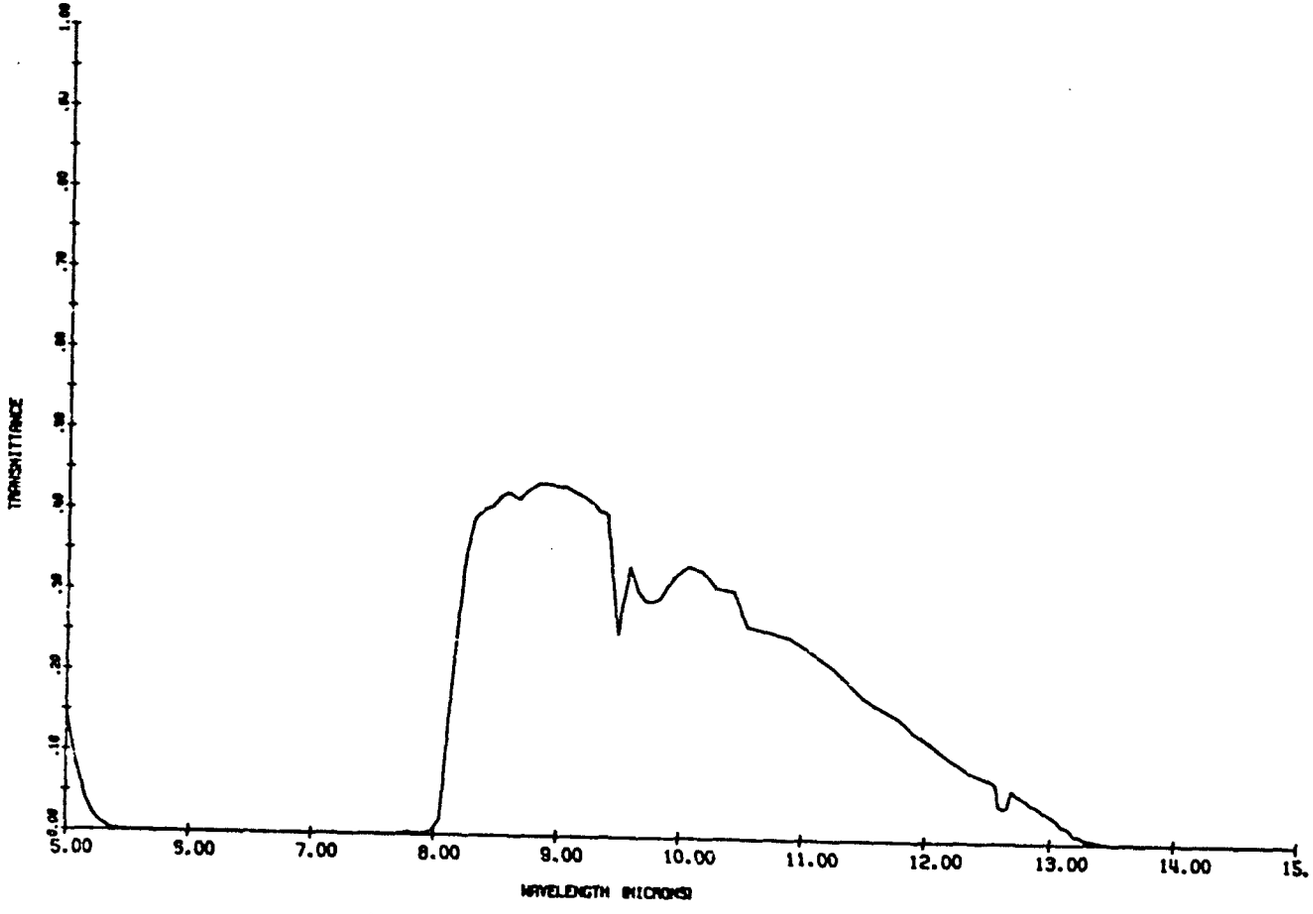

(a) Calculated (no scattering) (Concluded)

FIGURE 82. COMPARISON BETWEEN TRANSMITTANCE CALCULATED BY THE AGGREGATE METHOD AND THE EXPERIMENTAL DATA OF ASHLEY (PRIVATE COMMUNICATION). Path length = 39 Kft, amount of H_2O = 10 pr cm. (Continued)

ERIM
FORMERLY WILLOW RUN LABORATORIES, THE UNIVERSITY OF MICHIGAN

PATH LENGTH – 39,000 FEET
SPECTRAL RESOLUTION – 2 cm^{-1}
TEMPERATURE – 55°F
TOTAL H_2O – 10 cm
DATE – NOV 13, 1972
TIME – 20:39 PST
SOURCE ALT. – 3778 FT MSL
RECEIVER ALT. – 790 FT MSL

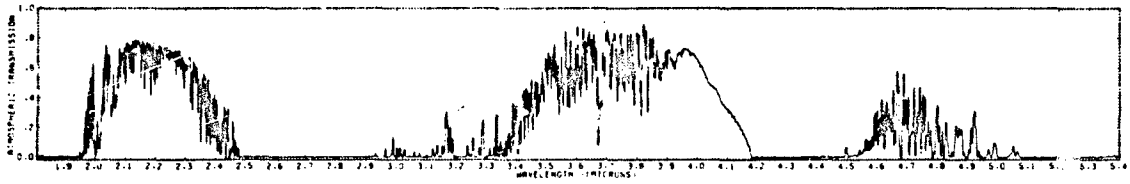

(b) Experimental

FIGURE 82. COMPARISON BETWEEN TRANSMITTANCES CALCULATED BY THE AGGREGATE METHOD AND THE EXPERIMENTAL DATA OF ASHLEY (PRIVATE COMMUNICATION). Path length = 39 Kft, amount of H_2O = 10 pr cm. (Concluded)

temperatures, etc. (see Section 10), derived from the 1962 U. S. Standard Atmosphere and its Supplements. The path of the transmitted beam is considered to be refracted (see Appendix) by changes in atmospheric density, and this fact is taken into account in the program in a subroutine which is optional.

7.5.1 METHOD OF DEVELOPMENT

The LOWTRAN 2 model (Selby and McClatchey, 1972) is the most clearly empirical of the so-called band models in that it takes on no analytically recognizable functional structure. In this way, it resembles the technique by Altshuler (1961) in the development of the empirical-functional form of the transmittance by CO_2 in the spectral regions for which the Elsasser model is deficient. The procedure used for presenting the data is also reminiscent of the Altshuler report, wherein a series of nomographs are included from which it is possible to determine all of the quantities needed for determining transmittance once the atmospheric conditions have been established.

The functional form of the average transmittance over the 20 cm^{-1} spectral interval obtained as a result of molecular absorption is given in terms of w^*, the equivalent amount of absorber as:

$$\tau = f(C_\nu, w^*) \tag{355}$$

$$\text{where } w^* = w\left\{\frac{P(z)}{P_0}\sqrt{\frac{T_0}{T(z)}}\right\}^n \tag{356}$$

with w = amount of absorber

n = empirically determined coefficient from laboratory experimental data and from calculations using the AFCRL line parameter compilation.

One may note the similarity between this expression and the expression used by Altshuler, which was:

$$\tau(\lambda) = f\left[\left(\frac{Sw}{d}\right)\left(\frac{\alpha_L}{d}\right)^n\right] \tag{357}$$

where $\tau(\lambda)$ reduces to the weak- and strong-line limits respectively, i.e.,

$$\tau(\lambda) = 1 - \frac{Sw}{d} \text{ and } \tau(\lambda) = e^{-\left(\frac{Sw\alpha_L}{d^2}\right)}$$

when $n = 0$ and $n = 1$. The values of n in the intermediate case of the LOWTRAN method have been calculated as follows:

n = 0.9 for H_2O

n = 0.4 for O_3

n = 0.75 for the so-called uniformly mixed gases (i.e., CO_2, N_2O, CO, CH_4 and O_2).

A comparison of Eqs. (355) with (357) shows an implicit neglect of the temperature dependence of S.

Writing Eq. (355) in a more general form expressing n explicitly:

$$\bar{\tau}_{\Delta\nu}(\nu) = f\,(C(\nu)wP^n) \tag{358}$$

shows the functional relationship of the parameters, with the temperature dependence of the half-width apparently being either ignored or assumed in the value of $C(\nu)$. Inverting Eq. (358) yields:

$$C(\nu)wP^n = f^{-1}\{\bar{\tau}(\nu)\} \tag{359}$$

and, taking logarithms:

$$n \log P + \log w = \log f^{-1}(\bar{\tau}) - \log C(\nu) \tag{360}$$

Selby [252] has provided the format for performing the data fit to Eq. (360) which requires a large quantity of data plotted in the form shown in Figure 83. $\bar{\tau}_{\Delta\nu}(\nu)$ vs log w is plotted in groups or families of curves corresponding to fixed pressures, P_1, P_2, P_3, etc. The $\bar{\tau}_{\Delta\nu}(\nu)$ are the transmittance values obtained from laboratory experimental data or calculated from the line parameters in the AFCRL compilation, and averaged over 20 cm^{-1} to represent the final resolution of the LOWTRAN results. The value of ν, the central frequency in the 20 cm^{-1} interval, is also fixed in each set of curves represented by Figure 83. Thus, for a fixed value of $\bar{\tau}_{\Delta\nu}(\nu)$ as shown, several values of w corresponding to the various curves, represented by the different pressures, are obtained. Since the right side of Eq. (360) is constant, the simultaneous solutions of two linear equations provide a value of n.

Thus, for each curve in Figure 83, Eq. (360) can be written:

$$n \log P_i + \log w_i = \text{const.}$$

in which the i designates the i-th curve (i = 1, 2, 3, . . .) and the constant involves the constant values of $\bar{\tau}$ and ν. A value of n can then be obtained for any pair of curves. Selby carries out this procedure for a large number of frequencies covering the important absorption bands

252. J. Selby, Atmospheric Transmittance, I., Advanced IR Conference Notes, University of Michigan Summer Conference, Ann Arbor, 1974.

for each molecule. In this way, a mean value of n is calculated for each molecule. These values are reproduced as follows:

Absorber	n	Spectral Regions
H_2O	0.9	2.7, 6.3, 20-30 μm
O_3	0.4	4.7, 9.6, 14 μm
Uniform Mixed (CO_2 + N_2O + . . .)	0.75	3-5, 7-10, 14-17 μm

The next step in the procedure is to plot the curve $\bar{\tau}_{\Delta\nu}(\nu)$ as a function of log wP^n for each frequency, using the previously calculated mean value for n, yielding a plot demonstrated schematically in Figure 84. The curve most representative of the scattered points in Figure 84 (the solid curve) is digitized for the LOWTRAN computer code, and is displayed also as the one-dimensional non-linear transmittance scale and associated scaling factor in the curves shown in Figure 85. The final step is to determine the value of $C(\nu)$ for each frequency, which produces the curve in each of the graphs of these figures. Resorting again to Eq. (36C), the value log $C(\nu)$ is solved from:

$$\log C(\nu) = \log \left\{ f^{-1}(\bar{\tau}_{\Delta\nu}(\nu)) \right\} - \log wP^n$$

and the curve in Figure 84. Thus, the intercept on the abscissa corresponding, via the curve, to the value of $\bar{\tau}$ is, in reality, log $\{f^{-1}(\bar{\tau})\}$ = log wP^n + log $C(\nu)$. The value of the abscissa corresponding to log wP^n is also calculated. The difference between these two points, is, therefore, the value of $C(\nu)$. By repeating this procedure for a large number and variety of w and P, i.e., absorber concentrations and pressures, an average $C(\nu)$ can be obtained for each ν. As the procedure is repeated for a large number of ν-values, the input to the production of curves represented by Figure 85 is provided.

The curves of Figure 86 show the plot of actual data from which the analytical curves are constructed. One is for ozone at ν = 1060 cm^{-1} for the family of pressures shown; and the other is for the uniformly mixed gases at ν = 2200 cm^{-1}. Note that the final curve is used to represent the desired function in each case, and that the points are packed reasonably close, showing that a single function approximates transmittance through the gas. Note also that the first and second curves in each set represent, respectively, the plot of the same data in terms of the weak- and strong-line functions. The disparity is obvious, as it should be in these cases in which the optical depths are intermediate to those which would produce the limiting effects.

Once the function, f, is plotted against a standardized amount of absorber for a given frequency, a scale is established between the two so that a transmittance curve common to all

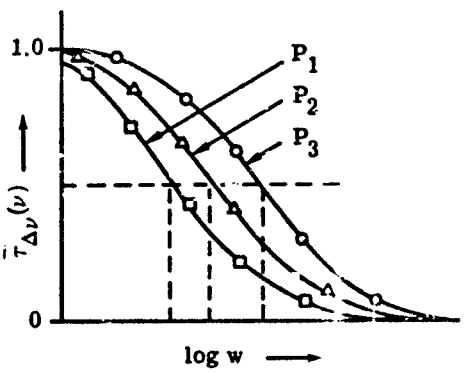

FIGURE 83. SCHEMATIC OF THE PLOT OF DATA FOR CALCULATING LOWTRAN PARAMETERS, $\bar{\tau}_{\Delta\nu}(\nu)$ VERSUS LOG w

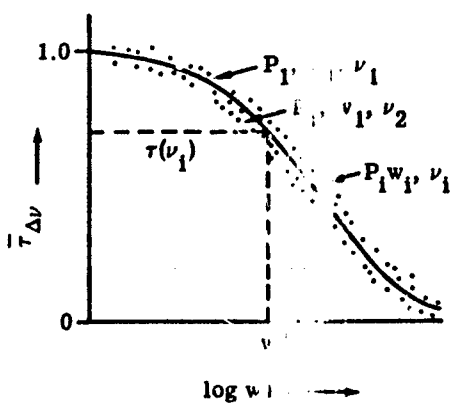

FIGURE 84. SCHEMATIC COMPOSITE OF ADJUSTED DATA, $\bar{\tau}_{\Delta\nu}$ VERSUS LOG w P^n

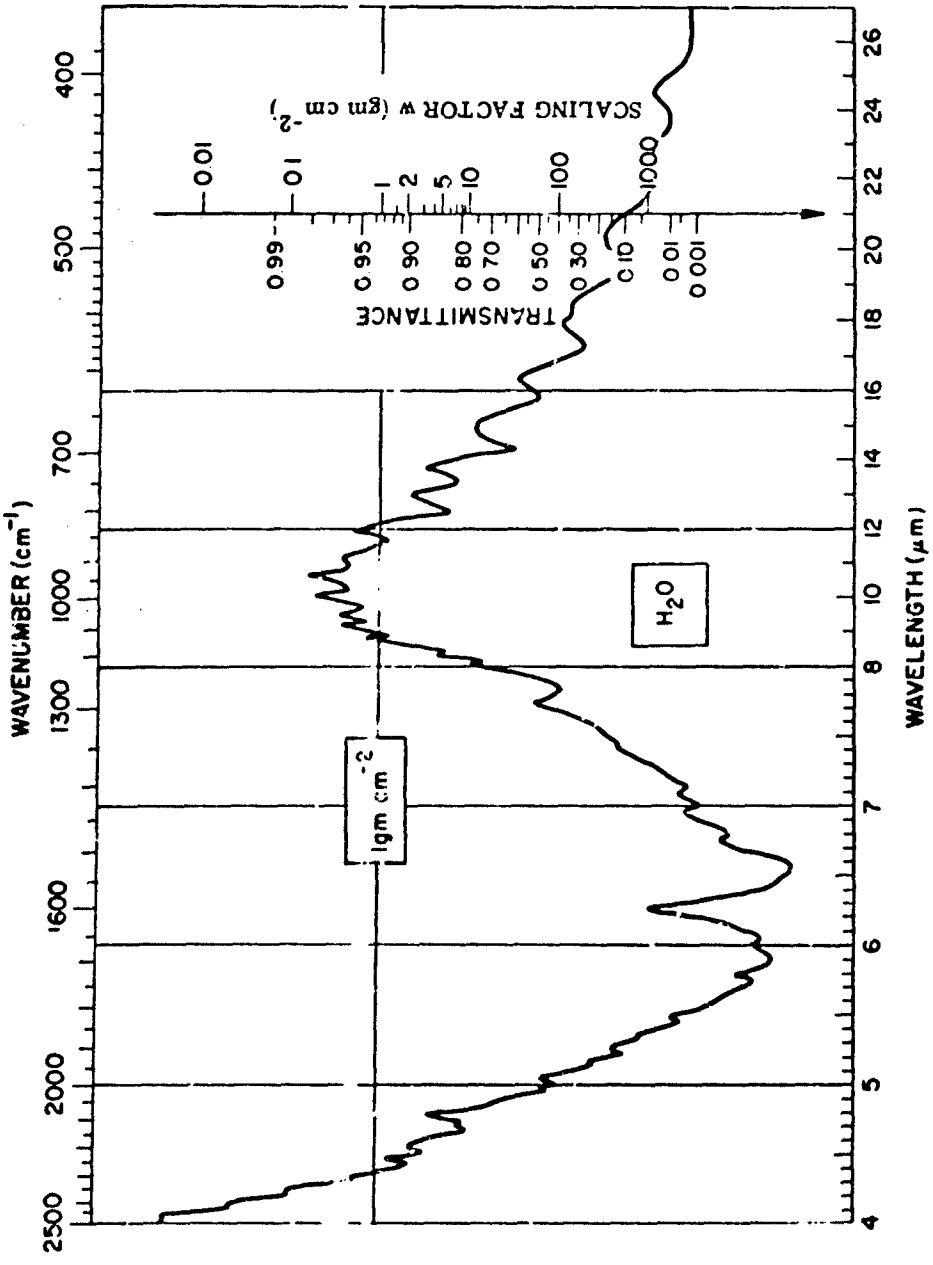

FIGURE 85. PREDICTION CHART FOR WATER VAPOR TRANSMITTANCE (4-26 μm)
(Reproduced from McClatchey, et al., 1972 [21].)

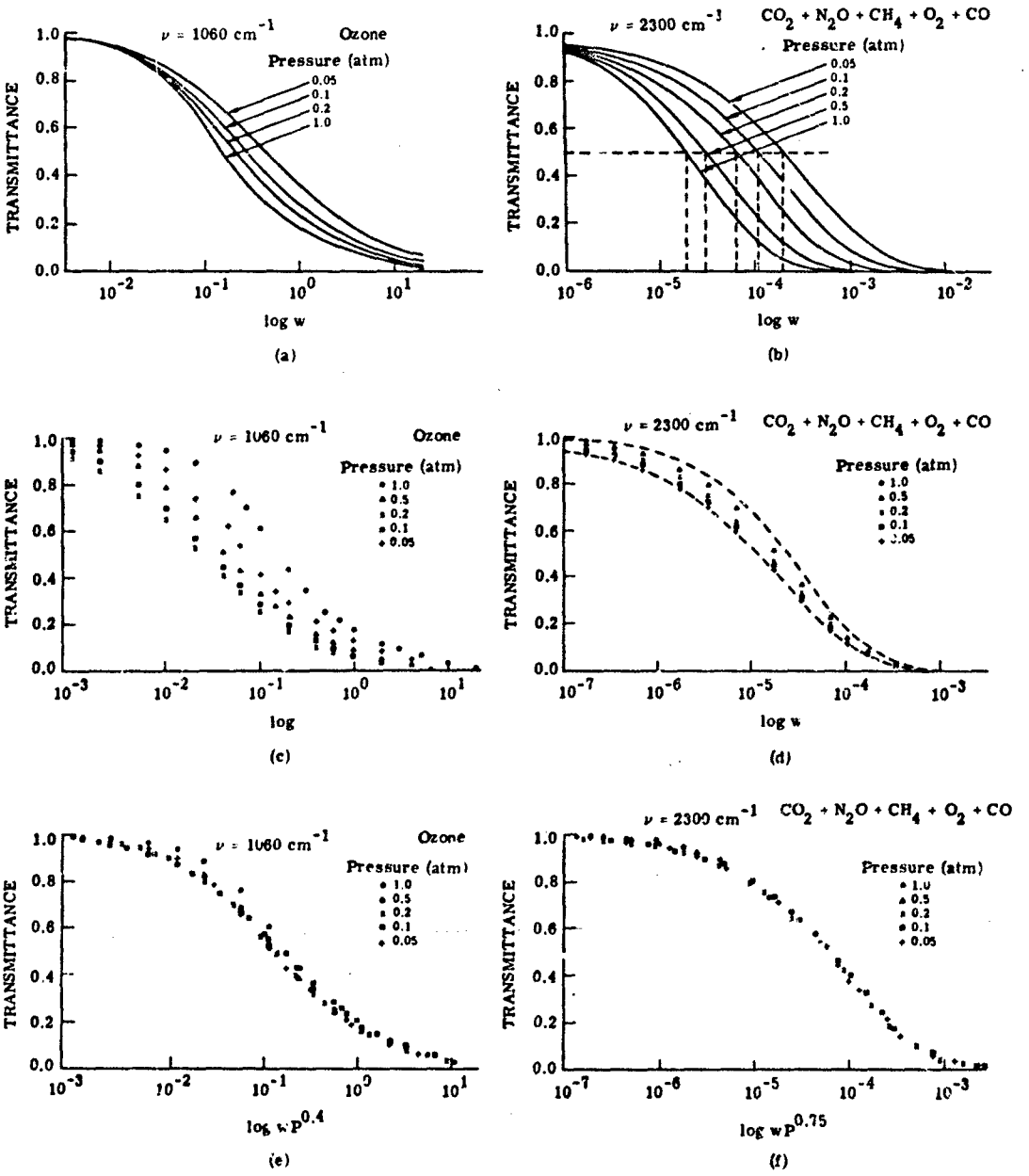

FIGURE 86. EXAMPLE SHOWING THE DEVELOPMENT OF TRANSMITTANCE FUNCTIONS FOR OZONE AND THE UNIFORMLY MIXED GASES. (From Selby, 1974[252].)

values of the absorber can be plotted as in Figure 85, with only a vertical movement of the scale shown at the right of the figure causing the curve to represent a new absorber configuration. Selby and McClatchey (1972) describe a computer code from which calculations of atmospheric transmittance can be made with a given set of inputs. Using the LOWTRAN model, McClatchey, et al. (1972) have published a set of curves from which rudimentary determinations can be made quickly and with reasonable accuracy, without resorting to the computer. Figure 85 is an example of the set.

These curves, which will be described subsequently, are useable for any kind of path, i.e., constant at various altitudes, or for slant paths. Since the curves are plotted for standard conditions, the equivalent path conditions must be determined before the curves can be used. The determination of these equivalent path conditions is made on the basis of a set of graphs (see next section), similar to those by Altshuler (1961). One notes, in reference to Section 7.4 on the Aggregate method, that part of the Aggregate code uses the results of Altshuler's investigation as input parameters.

The LOWTRAN 2 model calculates transmittance as affected by H_2O vapor, O_3 and the so-called uniformly mixed gases, i.e., CO_2, N_2O, CO, CH_4, and O_2. It includes also the effect of N_2 in a continuum in the 4.3 μm region, and H_2O in a continuum in the 10 μm region. In addition, it includes the effect on transmittance due to scattering by molecules and aerosols, from the point of view only of single scattering.

7.5.2 DETERMINATION OF ABSORBER AMOUNT

In using the curve of transmittance vs frequency shown in Figure 85, it is necessary first, by using curves similar to those in Figure 87, to determine the equivalent quantity of absorber in a slant path to apply to the transmittance curves. The set of curves depicting the absorber amount have been obtained from the following.

7.5.2.1 Water Vapor (H_2O)

If the path is horizontal then, at the altitude for which pressure is P:

$$w^* = w(z)\left(\frac{P}{P_0}\right)^{0.9} \tag{361}$$

is used to calculate the equivalent amount of absorber. The H_2O vapor concentration is given by w(z) gm/cm^2/km. The range, R, in km is multiplied by the appropriate value, which is plotted in the report by McClatchey, et al. (1972). For determining the equivalent absorber amount in a slant path, one uses the curve in Figure 87 obtained from:

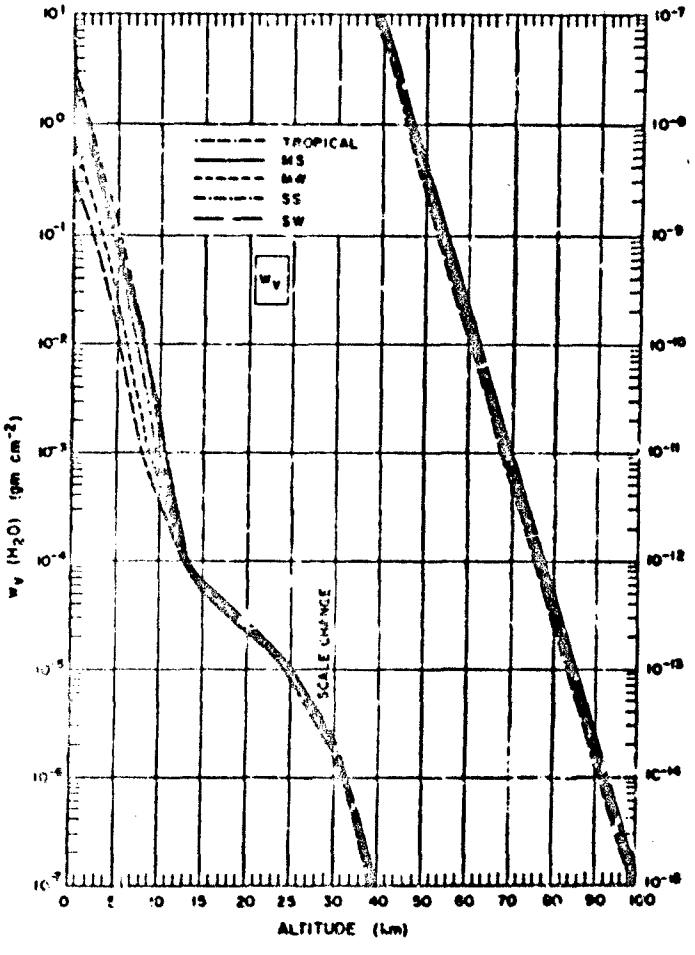

FIGURE 87. EQUIVALENT SEA LEVEL PATH LENGTH OF WATER VAPOR AS A FUNCTION OF ALTITUDE FOR VERTICAL ATMOSPHERIC PATHS. (Reproduced from McClatchey, et al., 1972 [21].)

$$w^* = \int_z^\infty w(z)\left(\frac{P}{P_0}\right)^{0.9} dz \qquad (362)$$

From this curve is obtained the value in a vertical path between the altitude shown on the abscissa and infinity. The amount in a slant path between two altitudes is determined by the difference in the values obtained at the two altitudes multiplied by the secant of the angle between the upward vertical and the slant path. Corrections for refraction and earth curvature are given by McClatchey, et al. (1972) for angles greater than 80°. Each curve in the family of curves in this figure represents a model atmosphere as described in Section 10. Similar curves are to be found in McClatchey, et al. (1972).

7.5.2.2 Ozone (O_3)

For ozone, the equations are similar with:

$$w^* = w(z)\left(\frac{P}{P_0}\right)^{0.4} \qquad (363)$$

for the horizontal path, with w(z) in (atm-cm)/km. For the slant path, the vertical component is calculated from:

$$w^* = \int_z^\infty w(z)\left(\frac{P}{P_0}\right)^{0.4} dz \qquad (364)$$

The curves representing the quantities $w(z)\left(\frac{P}{P_0}\right)^{0.4}$ and $\int_z^\infty w(z)\left(\frac{P}{P_0}\right)^{0.4} dz$, respectively, are to be found in McClatchey, et al. (1972).

For the spectral region between 0.25 and 0.75 μm, the absorption coefficient is independent of pressure, and the absorber curves take on a slightly different character. See McClatchey, et al. (1972).

7.5.2.3 Uniformly Mixed Gases (CO_2, N_2O, CO, CH_4, O_2)

For the uniformly mixed gases, with c the fractional concentration by volume, the amount of absorber, reduced to standard conditions, is:

$$w = cR\left(\frac{P}{P_0}\right)\left(\frac{T_0}{T}\right)$$

The value of n used for determining the equivalent amount is 0.75 for the uniformly mixed gases so that in the horizontal path, for which the calculation is made for the equivalent sea-level path length,

$$\frac{w^*}{c} = \left(\frac{P}{P_0}\right)^{1.75}\left(\frac{T_0}{T}\right) \tag{365}$$

For vertical (and thus, slant) paths the formula is given by:

$$\frac{w^*}{c} = \int_z^\infty \left(\frac{P}{P_0}\right)^{1.75}\left(\frac{T_0}{T}\right) dz \tag{366}$$

In the horizontal path case, the equivalent path length is obtained, as for the other constituents, by multiplying the value from the appropriate curve, for a chosen point on the abscissa, by the actual number of kilometers in the path. For the vertical case, the number of equivalent kilometers upward from the chosen altitude is obtained from the ordinate corresponding to a prescribed value on the abscissa. The slant path is obtained as before. The curve for the vertical case is reproduced from McClatchey, et al. (1972) in Figure 88.

7.5.2.4 N_2 Continuum

Absorption by the nitrogen collision induced band is taken proportional to P^2. Thus, for a concentration c, analogous to the case of the uniformly mixed gases:

$$\frac{w^*}{c} = \left(\frac{P}{P_0}\right)^{2}\left(\frac{T_0}{T}\right) \tag{367}$$

for the horizontal case; and

$$\frac{w^*}{c} = \int_z^\infty \left(\frac{P}{P_0}\right)^{2}\left(\frac{T_0}{T}\right) dz \tag{368}$$

for the vertical case. The figures representing these cases are to be found in McClatchey, et al. (1972).

7.5.2.5 H_2O Continuum

For the equivalent amount of H_2O vapor contributing to absorption in the 10 μm continuum region, the expression is given as:

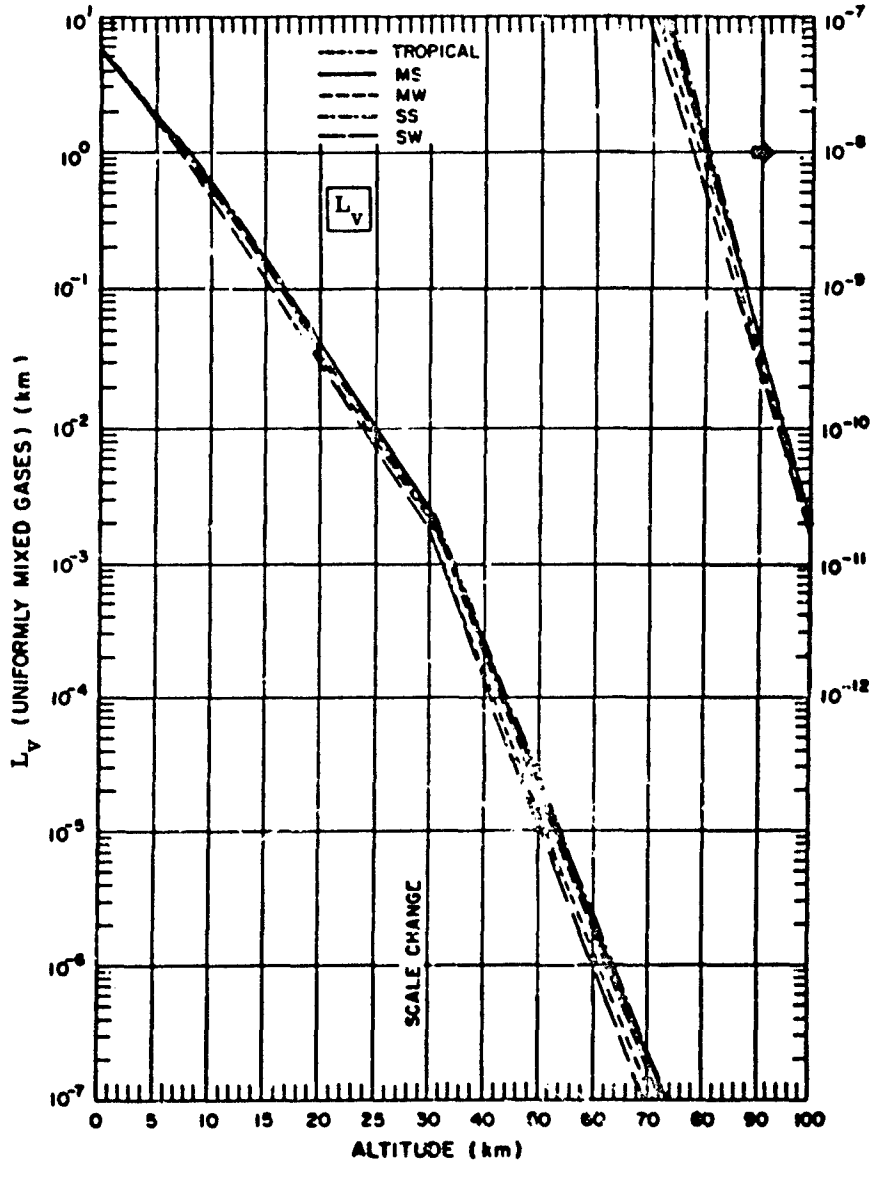

FIGURE 88. EQUIVALENT SEA LEVEL PATH LENGTH OF UNIFORMLY MIXED GASES AS A FUNCTION OF ALTITUDE FOR VERTICAL ATMOSPHERIC PATHS. (Reproduced from McClatchey, et al., 1972 [21].)

$$b_n = \frac{1}{P_0}\left[p_{H_2O} + 0.005\left(P - p_{H_2O}\right)\right] w'(z) \tag{369}$$

where w'(z) is the number of precipitable cm/km of H_2O vapor at altitude z, for which the total pressure is P and the partial pressure of H_2O vapor is p_{H_2O}. For vertical (and thus slant) paths the sea-level equivalent of the H_2O vapor is:

$$b_v(z) = \int_z^\infty \frac{1}{P_0}\left[p_{H_2O} + 0.005\left(P - p_{H_2O}\right)\right] w'(z)\,dz \tag{370}$$

Curves depicting these values for different model atmospheres are given in McClatchey, et al. (1972). Justification for the expressions used in Eqs. (369) and (370) is derived from the work of Burch (1970).

7.5.2.6 Molecular Scattering

Since molecular scattering is a function of atmospheric density, the scatterer concentration is normalized to sea-level concentration given by the dimensionless quantity (for the horizontal case):

$$m_h = \rho(z)/\rho_0 \tag{371}$$

where $\rho(z)$ is the atmospheric density obtained, usually from published tables (see Section 10). The equation in which this value is used in LOWTRAN 2 involves the function $9.307E - 20 \times \nu^{4.0117}$ included in the LOWTRAN 2 code to be consistent with the calculations for the absorbing components. For the vertical path (from which the slant path concentration can be calculated) the quantity is:

$$m_v = \int_z^\infty \rho(z)/\rho_0\,dz \tag{372}$$

which gives the effective length of the slant path.

7.5.2.7 Aerosol Extinction

The determination of aerosol extinction is made on the basis of the particle size distribution, which for LOWTRAN 2 is given in Section 10, and is considered to be constant with altitude. The number density, D(z), is also given in Section 10 and the dimensionless quantity:

$$a_h = \frac{D(z)}{D_0} \tag{373}$$

is plotted in McClatchey, et al. (1972) as a function of altitude for use with the function $3.745E - 5 \times \nu^{0.8543}$ in the case of a horizontal path. For the vertical path (and thus for use with the slant path) the quantity calculated for use in the transmittance equation is:

$$a_v = \int_z^\infty \frac{D(z)}{D_0} dz \qquad (374)$$

where D(z) is the number density at altitude, z, and D_0 is the value at sea-level.

7.5.3 USE OF THE LOWTRAN METHOD

The values of equivalent absorber amount are computed in the LOWTRAN 2 program. They can be used also with the scaling factors provided by referring to the charts provided in the report by McClatchey, et al. (1972), as a very convenient tool for determining rapidly and accurately the value of transmittance at any frequency (wavelength) and for any path conditions, provided one is willing to accept one of the standard model atmospheres as representative of the conditions pertinent to the prescribed situation. The charts are simple to use in conjunction with the charts from which the equivalent absorber amounts are determined and they are compatible with the latter so that the scale need only be moved to the properly determined absorber amount in the appropriate dimensions, and the transmittance is read on the accompanying transmittance scale from the curve.

It is interesting to compare the charts of McClatchey, et al. (1972) with the ones generated earlier by Altshuler (1961) and reproduced in abbreviated form from the report by Anding (1967). These are shown in Figures 89 through 91. The accuracy claimed by McClatchey, et al. in using the LOWTRAN 2 technique is decreasing as the transmittance approaches unity, which is apparent from the fact that the curves (see, for example, Fig. 83) in the development of the model change very slowly in the region of unity transmittance. The value of 10 percent is evidently an estimate based on an assumption that most conditions under which atmospheric transmittance calculations will be made will be consistent with the effective absorber amount calculated using P^n, with the n-values given above. Nothing in the literature has been found to check this allegation. Obviously, when conditions are more closely consistent with the weak- and strong-line representations of the model, then the LOWTRAN model will tend, respectively, to underestimate and overestimate the actual value of transmittance. On the other hand, one should refrain from using the model for the calculation of path radiance under conditions of high transmittance, since the uncertainty in atmospheric emissivity increases greatly.

McClatchey, et al. (1972) also caution that there may be an error introduced resulting from the neglect of a temperature dependence in the model. The temperature used for the determination of the curve representing the model was 273 K. No suggestion is given to the user regarding the confidence he can place in results calculated for cases in which the temperature differs greatly from those used in construction of the model, except a qualitative assessment of the effect of changes in energy state populations. However, Selby (1974a) has

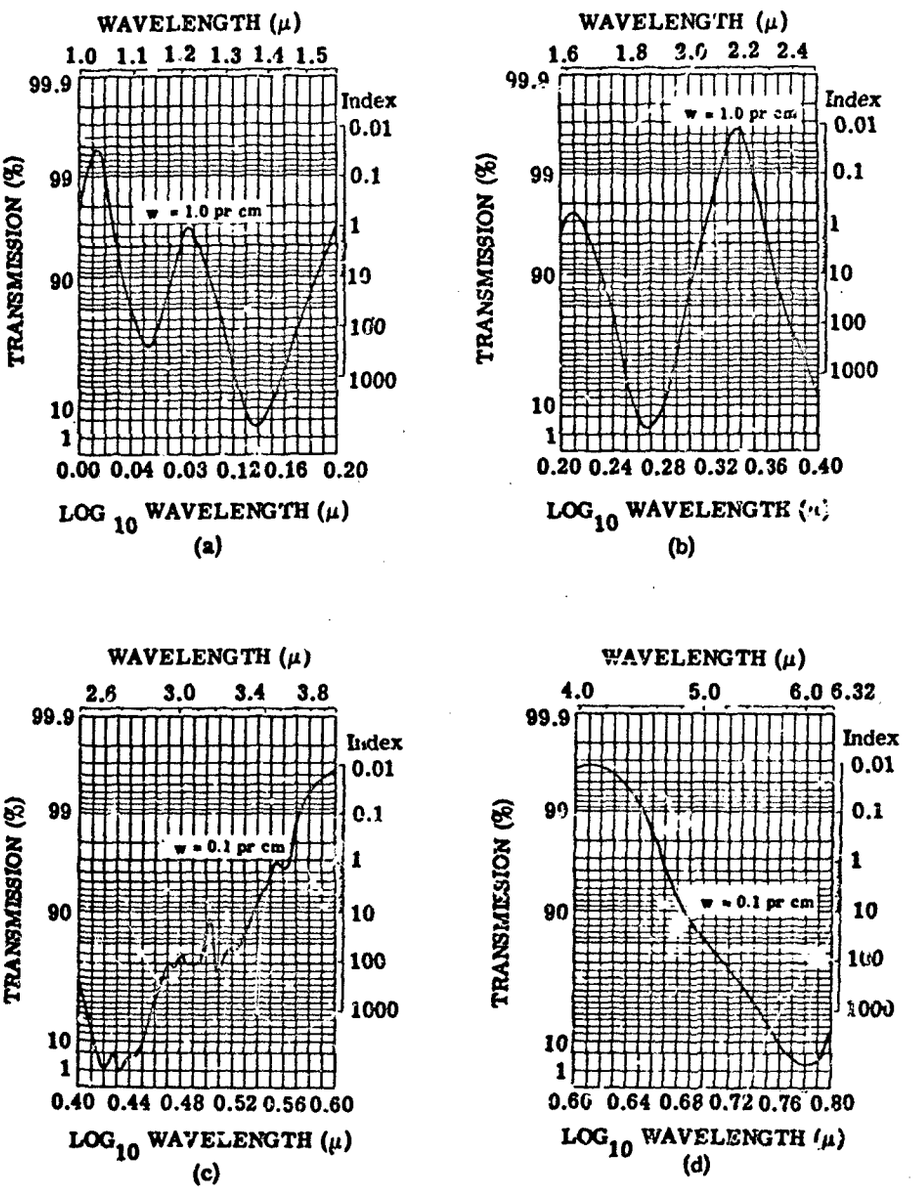

FIGURE 89. TRANSMISSION VS WAVELENGTH FOR WATER VAPOR

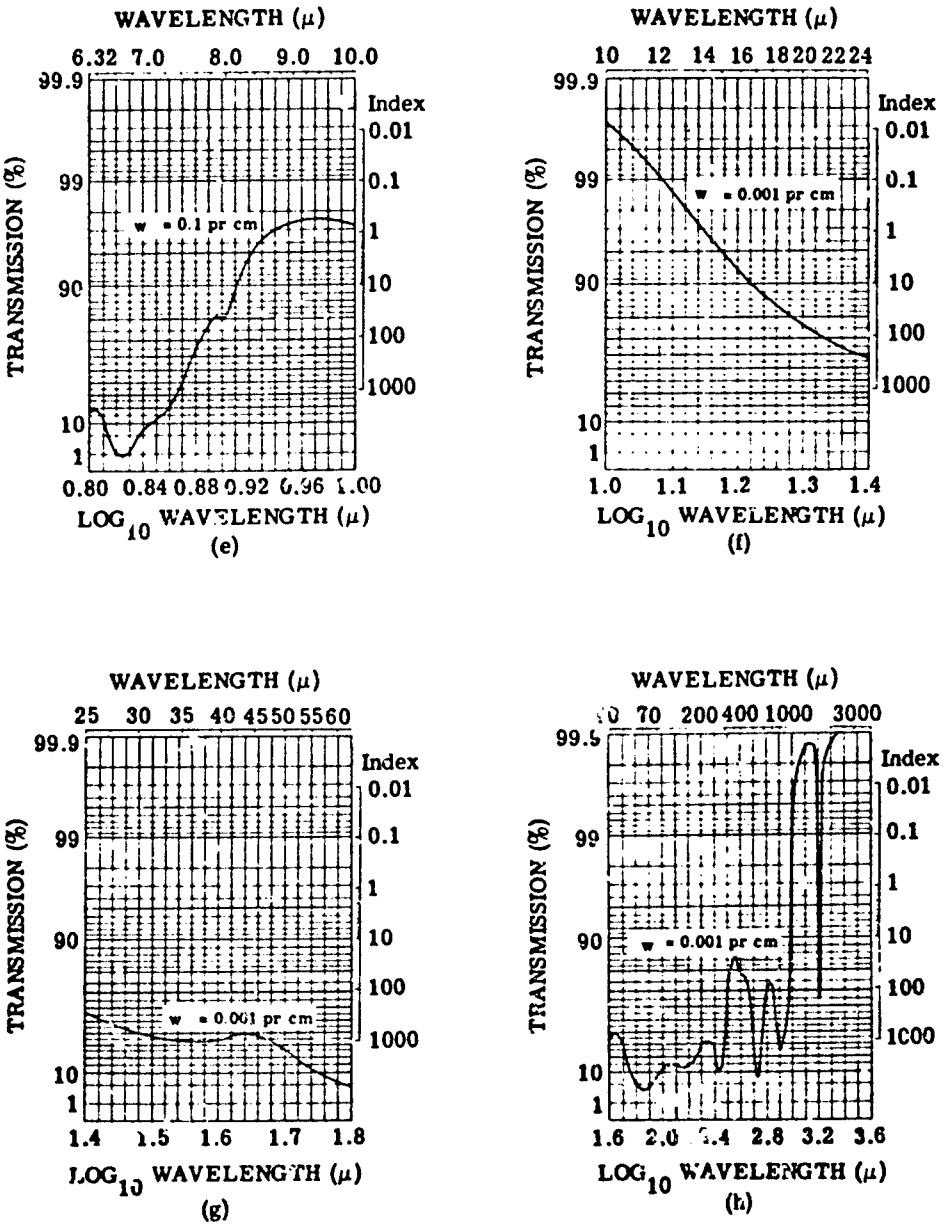

FIGURE 89. TRANSMISSION VS WAVELENGTH FOR WATER VAPOR
(Concluded)

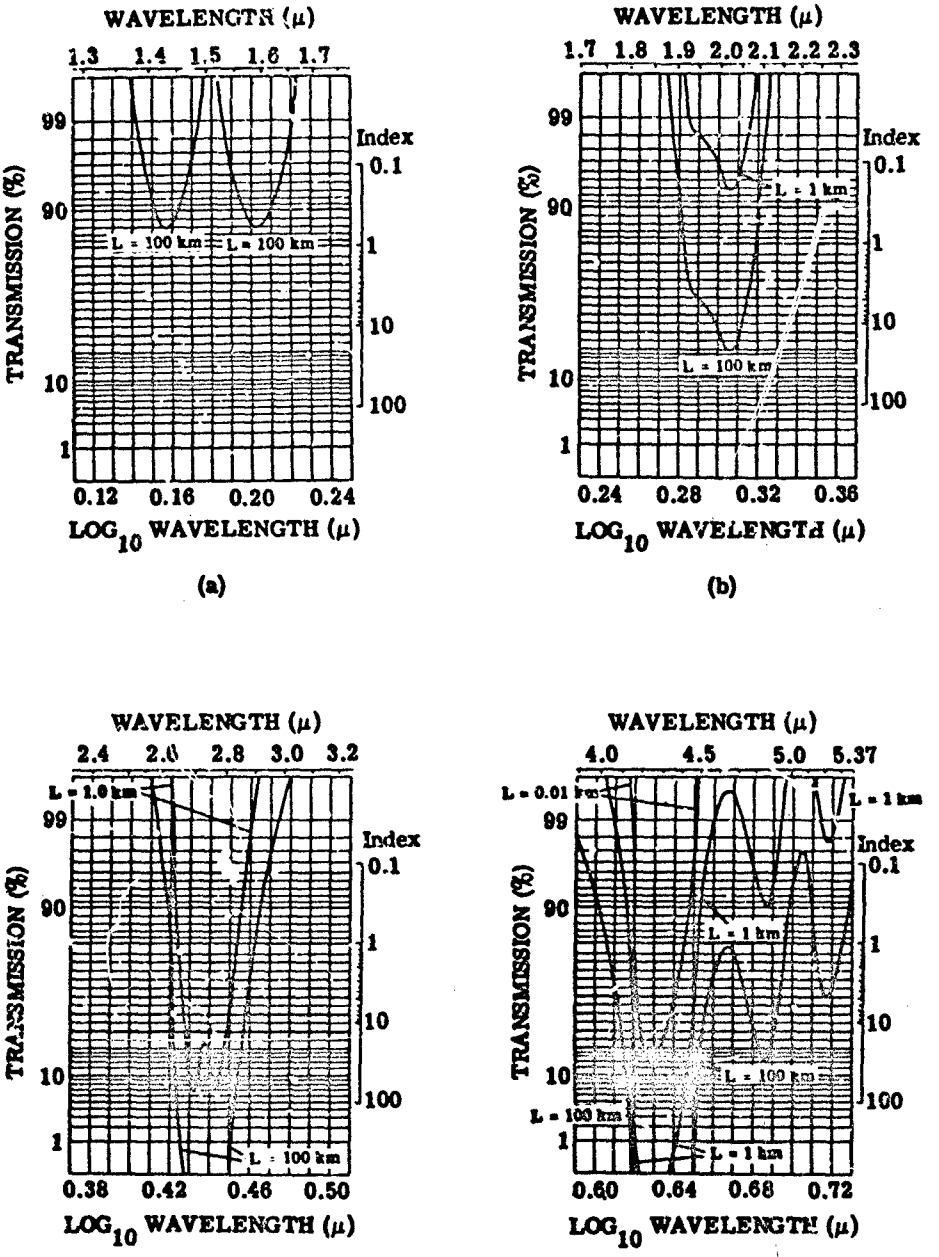

FIGURE 90. TRANSMISSION VS WAVELENGTH FOR CARBON DIOXIDE

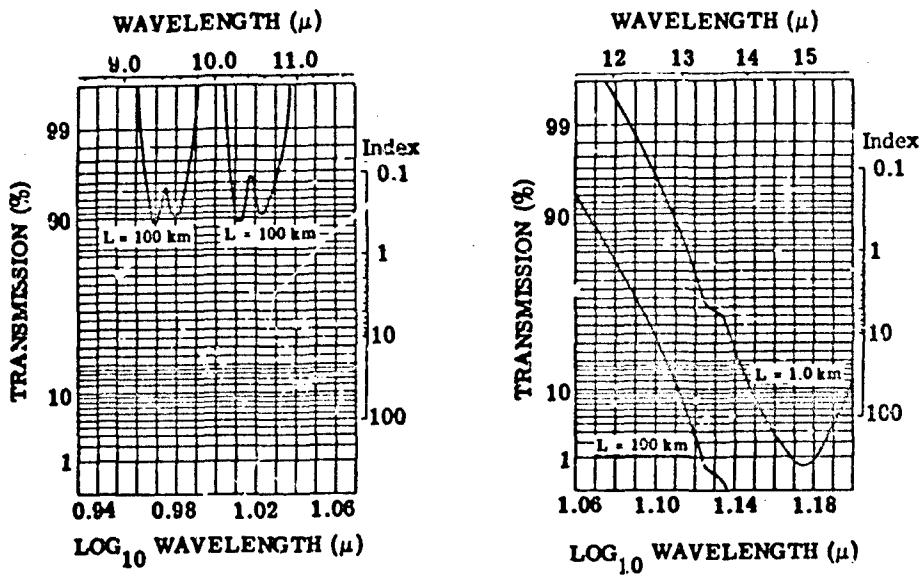

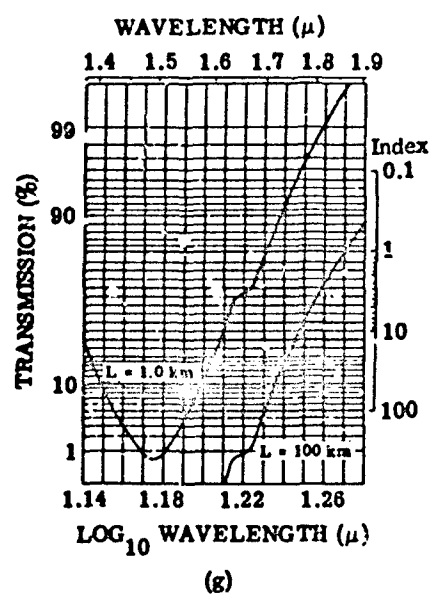

FIGURE 90. TRANSMISSION VS WAVELENGTH FOR CARBON DIOXIDE
(Concluded)

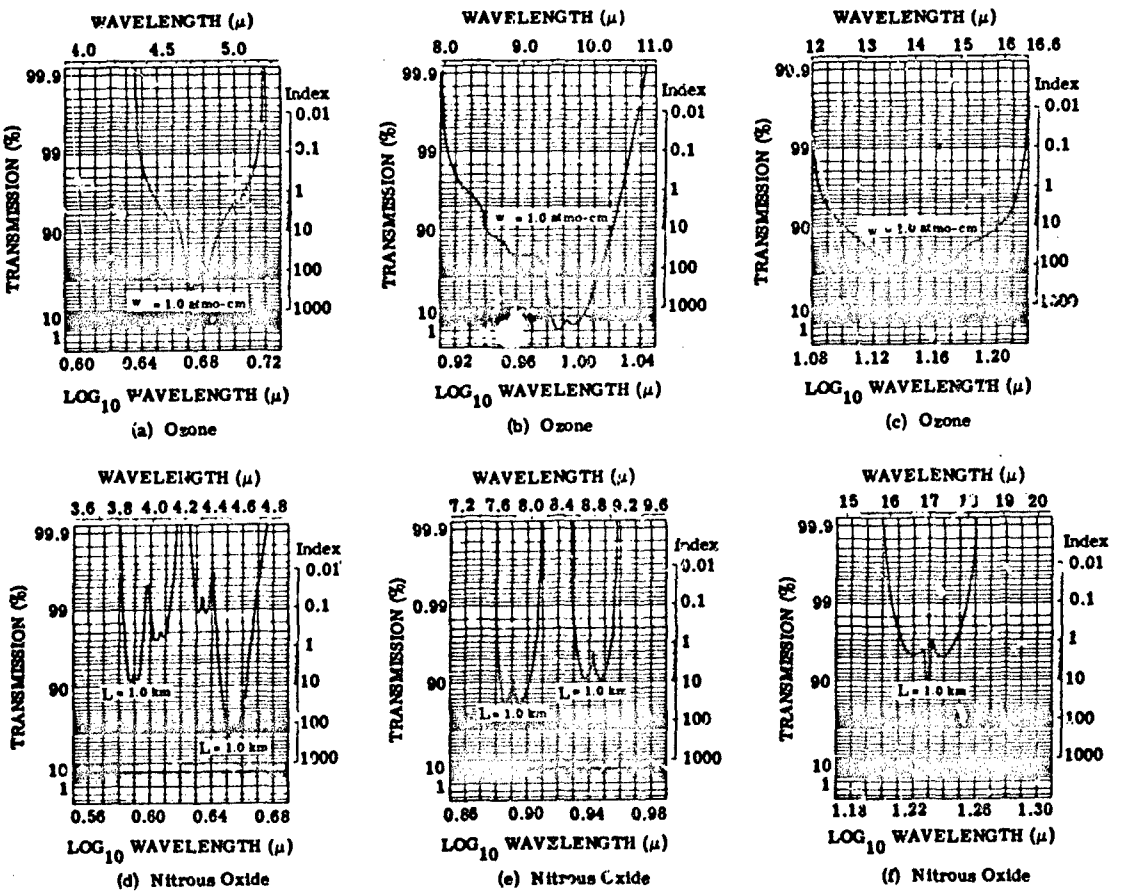

FIGURE 91. TRANSMISSION VERSUS WAVELENGTH FOR OZONE AND NITROUS OXIDE

performed a calculation of the radiance in a path downward looking toward the earth, and compared them with data taken from satellites. The comparison, as shown in Figure 92, is favorable, although one must always be careful in the interpretation of data for which meteorological parameters are not well known. See the additional discussion in Section 9.

In their report on the Optical Properties of the Atmosphere, McClatchey, et al. (1972) provide many of the user benefits not found in the operation of their LOWTRAN computer code, among which are certain scattering phenomena —although a simple function for extinction due to single scattering is used in LOWTRAN —and infrared emission by the earth and atmosphere. By the application of special formulas given in the above-mentioned report, limited generalized curves of solar radiation scattered from aerosols and clouds are furnished, as well as atmospheric radiance observed by a downward- or upward-looking sensor. The interested reader is referred to the report for these data, which are considered of secondary importance to this report and, therefore, are not reproduced here. Based on discussions with one of the authors of the LOWTRAN code (Selby, 1974a), it has been learned that a code to be used in conjunction with LOWTRAN will soon be available for calculating radiance from the earth and atmosphere.

7.5.4 COMPARISONS OF CALCULATED VALUES AND THE VALUES FROM FIELD EXPERIMENTAL DATA

The following figures portray comparisons between spectra calculated by the LOWTRAN 2 method and others obtained experimentally in field measurements.

Figure 93 is reproduced from Selby and McClatchey (1972) showing a comparison between the calculated values and the experimental values of Gebbie, et al. [253] in the upper set of curves. The quantity of absorber is small and good agreement is expected. The rest of the curves in the figure show a comparison of computed values with the experimental data of Yates and Taylor (1960), again for a small quantity of absorber.

Figure 94 was provided by J. E. A. Selby (1974a) to show a comparison between the transmittance values calculated with the LOWTRAN 2 method and experimental data from EMI* over a relatively short path with relatively small absorber amounts.

Figure 95 was provided by J. E. A. Selby (1974a) to show a comparison between values calculated with LOWTRAN 2 and experimental data of Ashley (General Dynamics, Pomona, 1974) over a path of moderate length.

*EMI Electronics, Ltd., Hayes, Middlesex, England.

253. H. A. Gebbie, W. Harding, C. Hilsum, A. Pryce and V. Roberts, "Atmospheric Transmission in the 1-14μ Region," Proc. of the Roy. Soc., Vol. 206A, 1951, p. 87.

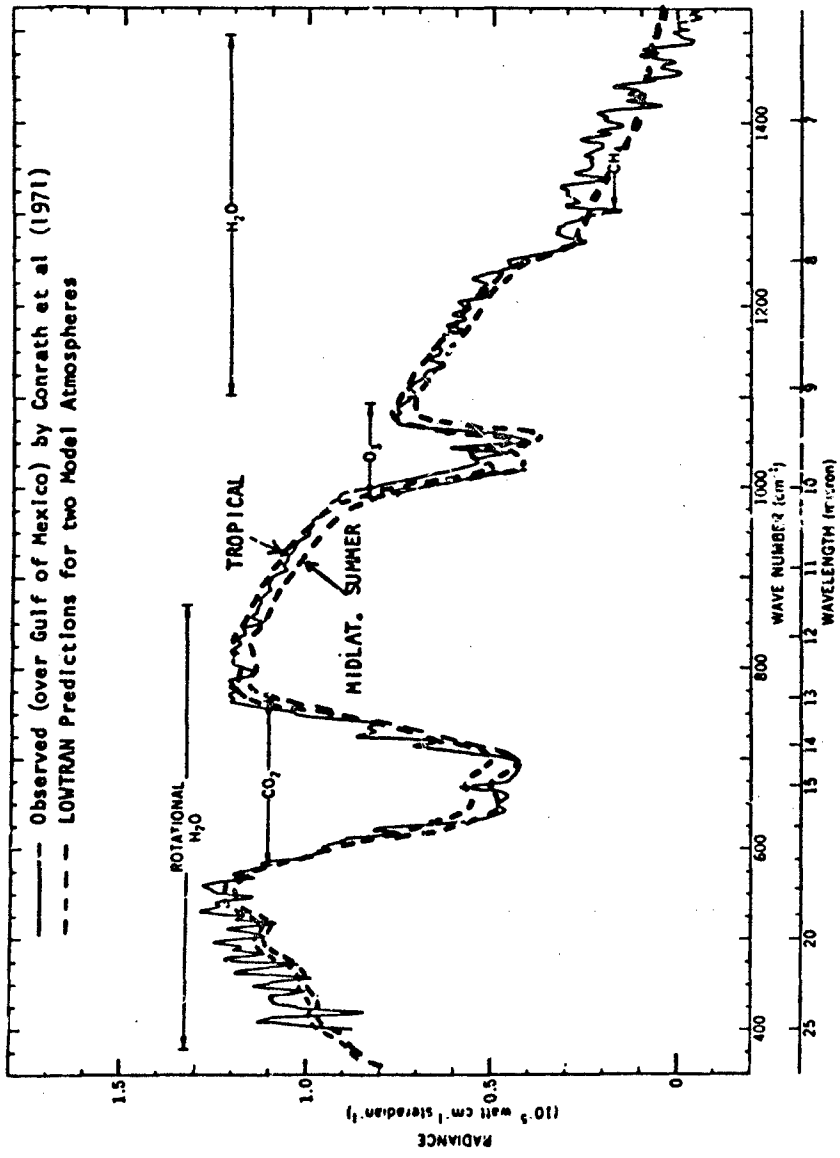

FIGURE 32. COMPARISON OF LOWTRAN 2 RADIANCE CALCULATION WITH NIMBUS DATA. (From Selby, 1974 [252].)

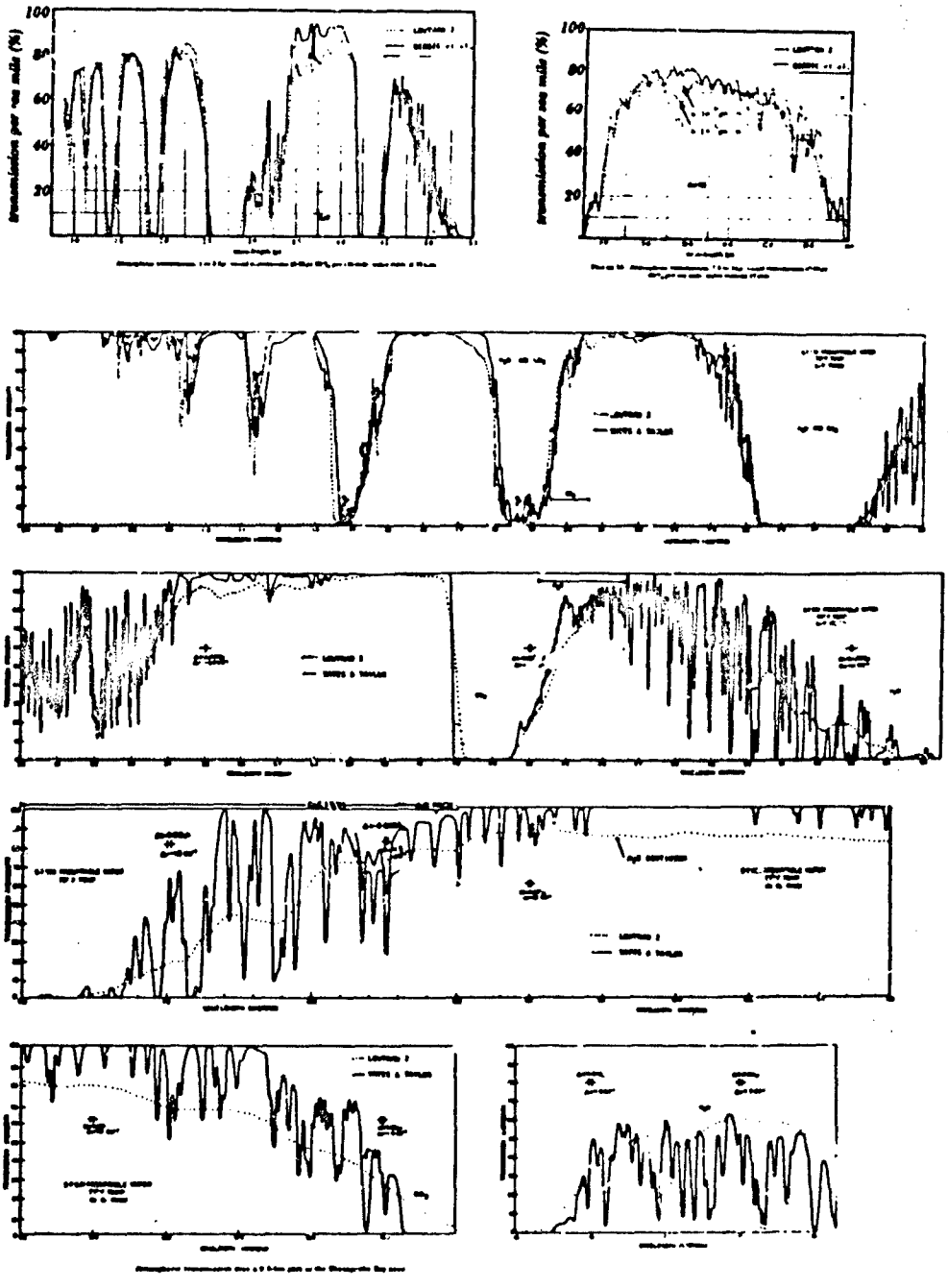

FIGURE 93. COMPARISON OF LOWTRAN 2 PREDICTIONS WITH MEASUREMENTS.
(Reproduced from Selby and McClatchey, 1972 [21].)

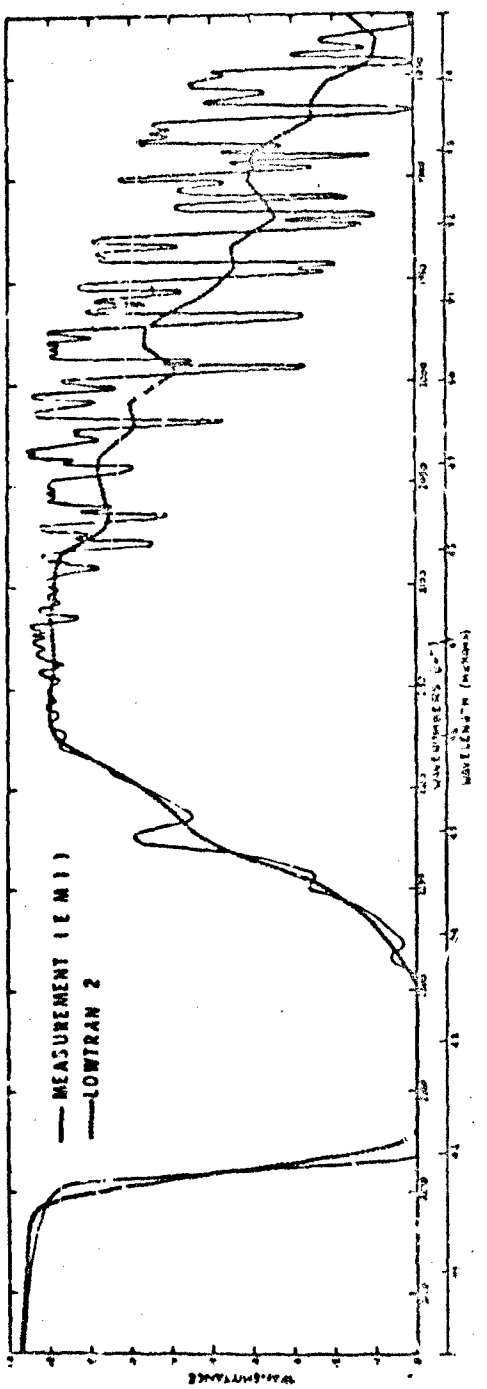

FIGURE 94 ATMOSPHERIC TRANSMITTANCE FOR A 1.9 km PATH AT 5.2 km ALTITUDE. 0.32 pr cms H_2O. (From Selby, 1974 [252].)

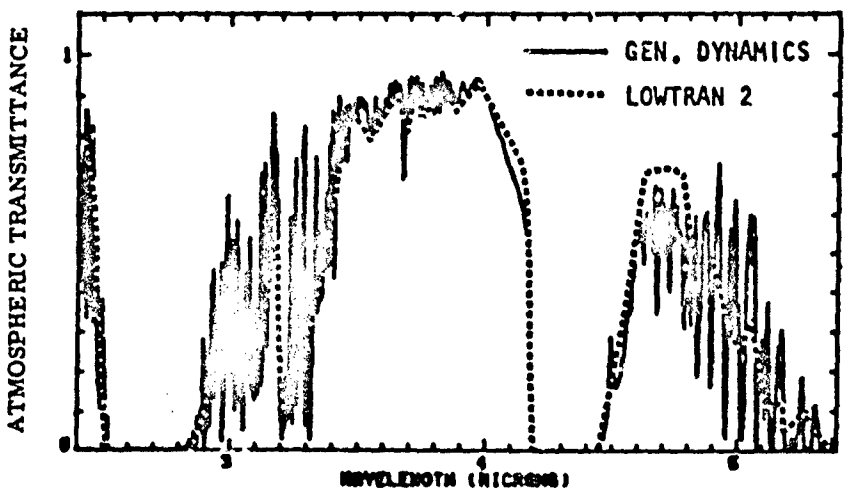

FIGURE 95. ATMOSPHERIC TRANSMITTANCE, 10679 ft (3.25 km) PATH AT SEA LEVEL. H_2O = 3.5 pr cm/km. (From Selby, 1974 [252].)

Figure 96 was provided by J. E. A. Selby (1974a) to show a comparison between values calculated with LOWTRAN 2 and experimental data of Ashley over a longer path with larger quantities of absorber.

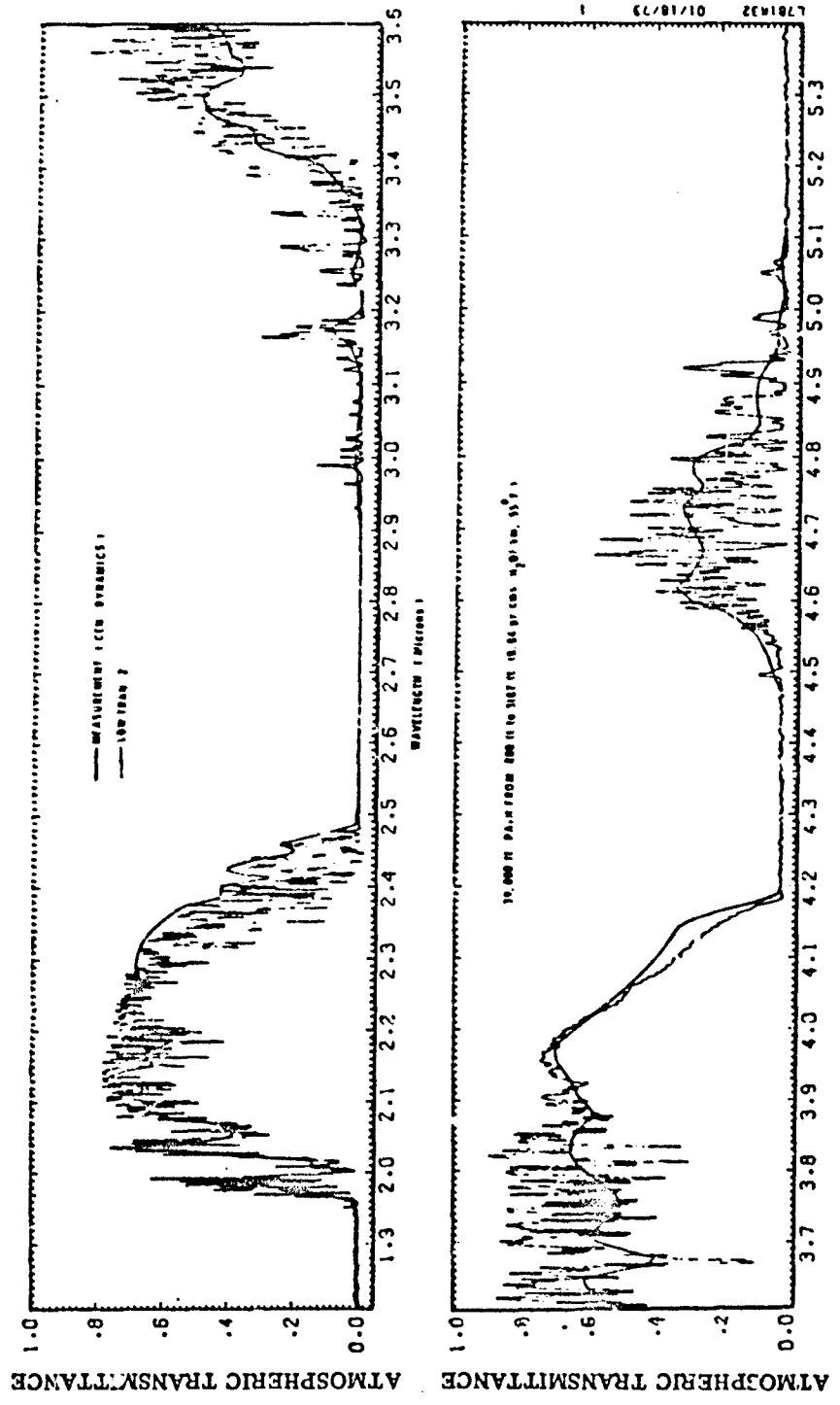

FIGURE 96. ATMOSPHERIC TRANSMITTANCE, CALCULATED AND MEASURED. (From Selby, 1974 [252].)

8
MULTI-PARAMETER ANALYTICAL PROCEDURES

The methods presented in the previous chapter, with the exception of LOWTRAN 2, are for the most part either ordinary models covering limited spectral ranges, or collections of models and approximations used to cover a broad spectral range. The LOWTRAN function is purely empirically derived. The procedures developed in this section are derived on the basis of analytical functions which suit the whole spectral range as long as special parameters are changed to suit each spectral interval.

8.1 ZACHOR'S FORMULATION

The starting-point for this section is the procedure originated by Zachor (1968a) in a manipulation of the mathematical expression of the statistical Goody band model (Mayer, 1947; Goody, 1952), i.e., an expression of the transmittance due to a infinite array of Lorentz lines which are Poisson-distributed in frequency, and distributed exponentially in strength. (See Eq. 184; Table 20.) This model has the form (See e.g., Eq. (325)).

$$\tau(\lambda) = \exp\left\{-wK_1(\lambda)/[1 + 2wK_2(\lambda)/P]^{1/2}\right\} \tag{375}$$

which is redefined here partly in terms of Zachor's nomenclature as:

$$\tau = \exp\left[-\gamma/(1 + 2\gamma/\beta)^{1/2}\right] = \exp\left\{-\left(\frac{1}{\gamma^2} + \frac{2}{\gamma\beta}\right)^{-1/2}\right\} \tag{376}$$

where $\gamma = \frac{Sw}{d}$, $\beta = \frac{2\pi\alpha_L}{d} = \beta_0 P$

w = absorber amount (e.g., pr cm)

S = mean line strength

d = mean line separation

α_L = Lorentz line half-width, proportional to broadening pressure, P

$\beta_o = \frac{2\pi\alpha^o_{L0}}{d}$

In the first form of Eq. (376), it is observed that for $\gamma/\beta >> 1$ there emerges the expression for the strong-line transmittance form of the Goody model (compare Expression #10, Table 20), namely:

$$\tau_s = \exp\left[-(\gamma\beta/2)^{1/2}\right] \tag{377}$$

whereas for $\gamma/\beta << 1$, the Beer's law expression results:

$$\tau_B = \exp(-\gamma) \tag{378}$$

which results in any band-model prediction of transmittance for overlapping lines. Zachor alleges that the curve rrepresented schematically in Figure 97 is typical of the plot of laboratory data in that format, and that the envelope of the curve represents the strong-line representation of different models given as $\tau_s = f(wP)$ where, for wP small, the straight-line portion corresponding to const·$(wP)^{1/2}$ is evident.

Since every model for overlapping lines results in the Beer's law expression in the limit, each horizontal line corresponds to an asymptote determined by a given quantity of absorber, $w = w_1, w_2, w_3, \ldots$ The generalization of these facts is that every model is represented by one of the numerous curves which can make up Figure 97 with "the essential dissimilarities between observations at different wavelengths in the same or in different bands (being) the mathematical form of f(wP) and 'rate of transition' between this function and Beer's law. These considerations suggest that all laboratory data of moderate resolution might be represented by an equation of general form:

$$\tau = g(\tau_s, \tau_B, M) \tag{379}$$

which depends explicitly on the Beer's law transmittance τ_B and an empirically determined function τ_s for the strong-line region. The function g should be asymptotic to τ_s and τ_B, with a transition rate governed by some adjustable parameter, M."

Zachor's derivation of a general function starts with a rearrangement of Eq. (376) in the form:

$$(-\ell n\, \tau)^{-2} = (\ell n\, \tau_B)^{-2} + (\ell n\, \tau_s)^{-2} = \gamma^{-2} + (\ell n\, \tau_s)^{-2} \tag{380}$$

which easily follows with the help of Eqs. (377) and (378) after the natural logarithm of each is taken and substituted into Eq. (376). In the form of Eq. (380), we observe that the Goody model, with no approximations, results from the sum of two vectors, perpendicular to each other, whose lengths are given by $(-\ell n\, \tau_B)^{-1} = \gamma^{-1}$ and $(-\ell n\, \tau_s)^{-1}$. It follows directly that as either vector vanishes the other is represented by one of the asymptotes to the curve of Figure 97. This vectorial approach to the formulation of a model then suggests that the generalization of the two-dimensional scheme is the introduction of a to-be-specified angle between the vectors, of any value whatever, dependent on the form of the model which describes the transmittance at a given frequency. The most general form of Eq. (380) would be, then:

$$(-\ell n\, \tau^*)^{-2} = \gamma^{-2} + (\ell n\, \tau_s)^{-2} + 2 \cos \xi (-\gamma \ell n\, \tau_s)^{-1} \tag{381}$$

in which τ^* is the model's approximation to the actual transmittance τ. By solving for τ^* and writing $M = 2 \cos \xi$, one finds

$$\tau^* = \exp\left\{-\left[\gamma^{-2} + (\ell n\, \tau_s)^{-2} - M(\gamma\, \ell n\, \tau_s)^{-1}\right]^{-1/2}\right\} \tag{382}$$

The similarity between this form and that for the Goody model is apparent, and indeed distinct, in light of the fact that Eq. (382) is the Goody model for M = 0.

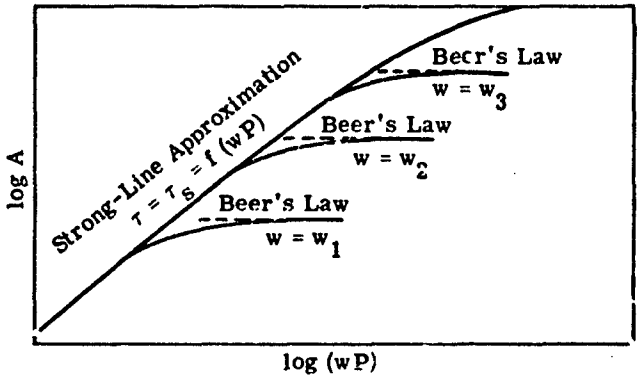

FIGURE 97. A PLOT OF LOG(A) AGAINST LOG(wP) FOR A TYPICAL LABORATORY RUN OR ABSORPTION BAND MODEL. The ordinate scale is greater than the scale of the abscissa to emphasize the strong-line and Beer's law regions. The straight portion of the strong-line envelope represents the "square-root approximation," A = const. $(wP)^{1/2}$.

8.1.1 DERIVATIONS OF KNOWN MODELS

In his paper, Zachor (1968a) makes a comparison between the model of Eq. (382) and three other well-known models (see Section 5, or Goody, 1964): the so-called random model, with randomly distributed lines of equal intensity (Elsasser, 1938); the Elsasser model; and the Curtis model, with equally spaced lines, but exponentially distributed in intensity (Goody, 1964). Figure 98 demonstrates the comparisons of τ vs β for the random model, the Elsasser model and the Curtis model. The equations approximating these models are as follows:

8.1.1.1 Random Model

$$\tau^* = \exp\left[-\left(\frac{1}{\gamma^2} + \frac{\pi}{2\gamma\beta} + \frac{\pi^{1/2}M}{\gamma(2\gamma\beta)^{1/2}}\right)^{-1/2}\right] \tag{383}$$

where: M = -0.2739059, by calculation.

8.1.1.2 Elsasser Model

$$\tau^* = \exp\left\{-\left[\gamma^{-2} + \left(\ln\left\{1 - \operatorname{erf}\left[\gamma\beta/2\right)^{1/2}\right]\right\}\right)^{-2} - M\left(\gamma \ln\left\{1 - \operatorname{erf}\left[\gamma\beta/2\right)^{1/2}\right]\right\}\right)^{-1}\right]^{-1/2}\right\} \tag{384}$$

where: M = -0.2739059, by comparison with the structure for the random model.

8.1.1.3 Curtis Model

$$\tau^* = \exp\left\{-\left[\gamma^{-2} + \left(\ln\left\{1 - \tanh\left[(\gamma\beta/2)^{1/2}\right]\right\}\right)^{-2}\right]^{-1/2}\right\} \tag{385}$$

where: M = 0, considering that the line intensity distribution is the same as for the Goody model.

8.1.2 GENERALIZATION OF ZACHOR'S FORMULATION

The importance of Zachor's model is not in the agreeable match it enjoys with the standard models of, e.g., Elsasser and Goody, but in the generalization it provides for calculations outside the limit of the models. The conventional model limits are small as is evident in the Aggregate method which must incorporate a large number of them, modified to some extent, to cover the whole infrared spectral range. It will be seen subsequently, that the Zachor method incorporates four adjustable parameters as opposed to the two parameters in the Aggregate method and one in the LOWTRAN method. It is this larger number of adjustable parameters which, one would infer, gives the Zachor method its flexibility, and naturally, adds to its complexity.

The generalized Zachor formulation is derived from a comparison with laboratory experimental data. In a paper which accompanied the publication of the formulation, Zachor (1968b) reported a table of the four generalized parameters for the CO_2 spectral region in 5 cm^{-1}

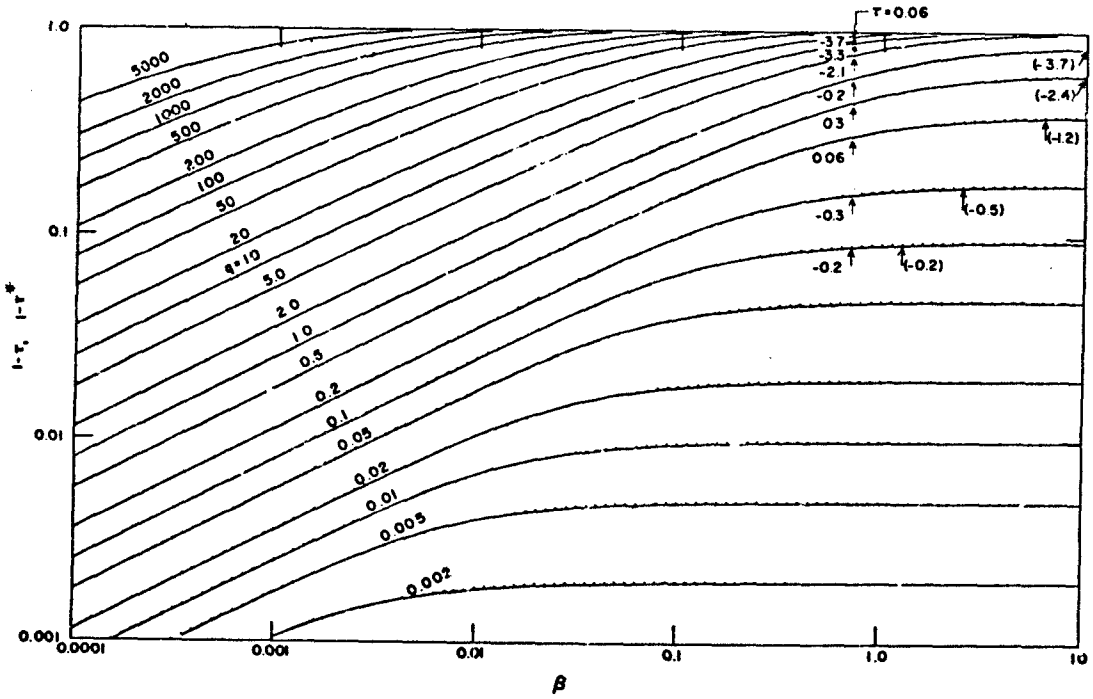

(a) Random Model

FIGURE 98. A COMPARISON OF τ (SOLID CURVES) AND τ^* (DOTS). Values of the percent error $\epsilon = 100\,(\tau^* - \tau)/\tau$ are shown for $\beta = 0.7$. The absolutely largest ϵ for several values of γ and for $\beta \leq 10$ are given in parentheses. (Reproduced from Zachor, 1938a [22].)

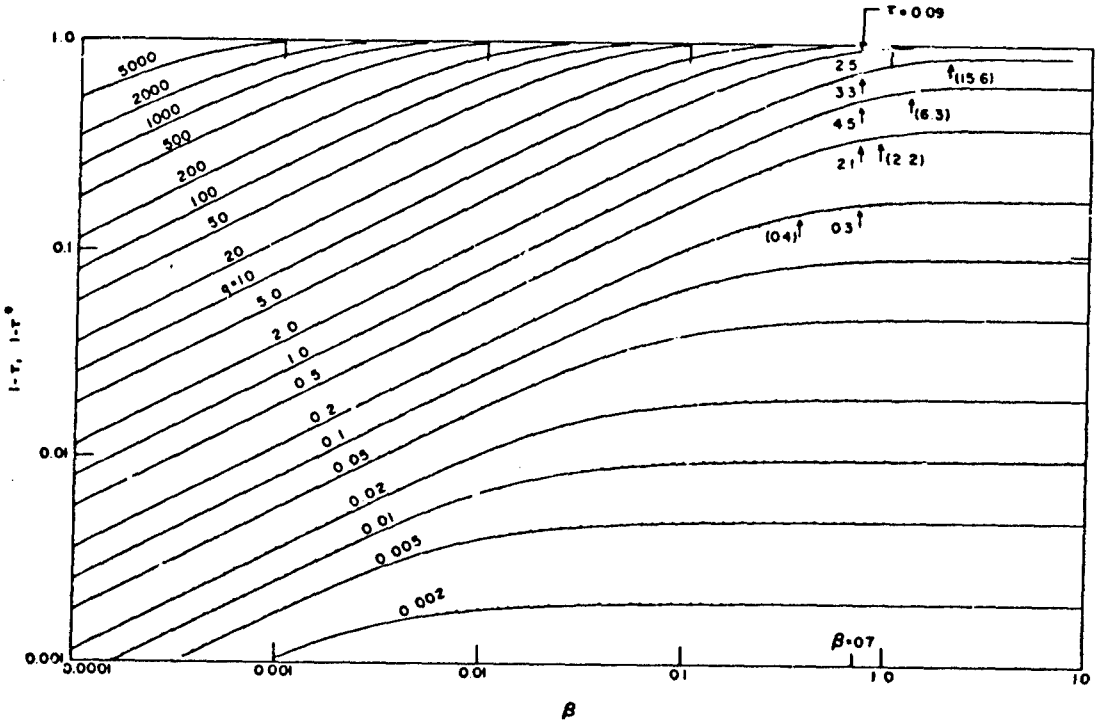

(b) Regular Model

FIGURE 98. A COMPARISON OF τ (SOLID CURVES) AND τ^* (DOTS). Values of the percent error $\epsilon = 10^2 (\tau^* - \tau)/\tau$ are shown for $\beta = 0.7$. The absolutely largest ϵ for several values of γ and for $\beta \leq 10$ are given in parentheses. (Reproduced from Zachor, 1968a [22].) (Continued)

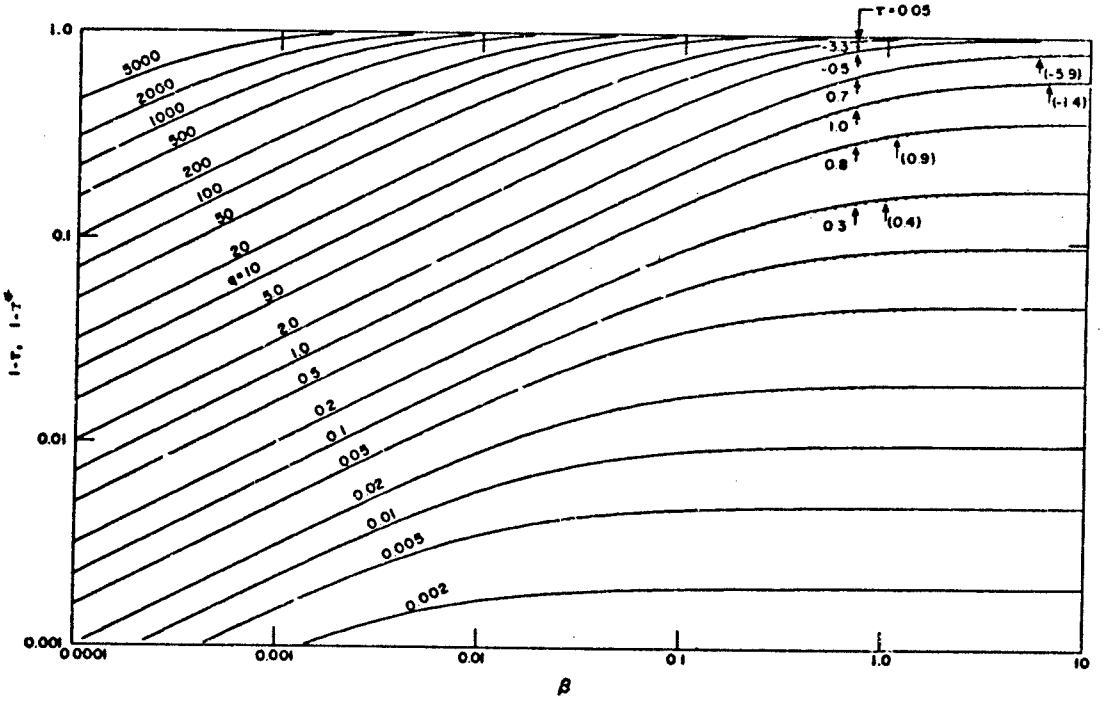

(c) Curtis Model

FIGURE 98. A COMPARISON OF τ (SOLID CURVES) AND τ^* (DOTS). Values of the percent error $\epsilon = 100\ (\tau^* - \tau/\tau$ are shown for $\beta = 0.7$. The absolutely largest ϵ for several values of γ and for $\beta \leq 10$ are given in parentheses. (Reproduced from Zachor, 1968a [22].) (Concluded)

intervals between 4590 and 5346 cm^{-1}, derived from the experimental data of Burch, Gryvnak and Patty [254]. The parametric form of Eq. (382) is more evident when written in terms of experimental parameters; thus:

$$\tau^* = \exp\left\{-\left[(Kw)^{-2} + (\ell n\, \tau_s)^{-2} - M(Kw\, \ell n\, \tau_s)^{-1}\right]^{-1/2}\right\} \tag{386}$$

where K = S/d, the weak-line parameter. The parameters, then, are K, M and $\ell n\, \tau_s$, the strong-line function, which itself is representable by two parameters. In fact, following the proposal of King (1964), the strong-line function can be written as the following two-parameter function:

$$\tau_s = 1 - \mathcal{P}\{n, [n\Gamma(n)(2CwP/\pi)^{1/2}]^{1/n}\} \tag{387}$$

where the parameters are n and C, and $\mathcal{P}(a, x)$ is the incomplete Gamma function:

$$\mathcal{P}(a, x) = [\Gamma(a)]^{-1}\int_0^x t^{a-1}e^{-t}dt \tag{388}$$

$\Gamma(a)$ is the Gamma function. King's formula, Eq. (387), derived from an analysis of the variance in the structure of different models, gives the correct strong-line equations for the regular (Elsasser) and random models for n = 1/2 and n = 1, respectively. In fact, the value 1/2, for equal distribution of line strengths, specifies randomness, while the value 1 specifies regularity. Equation (387) can be written in series form as:

$$\tau_s = 1 - n(CwP)^{1/2}\sum_{j=0}^{\infty}\{(-1)[n\Gamma(n)(2CwP/n)^{1/2}]^{1/n}\}^j/(a+j)!$$

The procedure that Zachor uses to fit experimental data is to plot log $(1 - \tau_s)$ from Eq. (387) as a function log (CwP) (which equals $\gamma\beta$) for several values of n, and match one of the resulting curves to the envelope of experimental data log $(1 - \tau)$ vs. log (wP). Figure 99, reproduced from the paper by Zachor (1968a), demonstrates a plot of log $(1 - \tau_s)$ vs. log $(\gamma\beta)$. Thus, from the curve match the value of n is deduced. Since the proper curve had to be displaced by the amount log C to effect the match, the amount of displacement on the abscissa between the calculated and experimental curve is the value of log C, from which the parameter C is obtained.

After the parameters n and C are found, the parameters M and K are determined simultaneously by a least squares fit of Eq. (381) to experimental data. Rewritten in terms of the parameters K and M, Eq. (381) becomes:

254. D. E. Burch, D. A. Gryvnak and R. F. Patty, Absorption by CO_2 Between 4500 and 5400 cm^{-1}, Report No. U-2955, Philco-Ford Corporation, 1964.

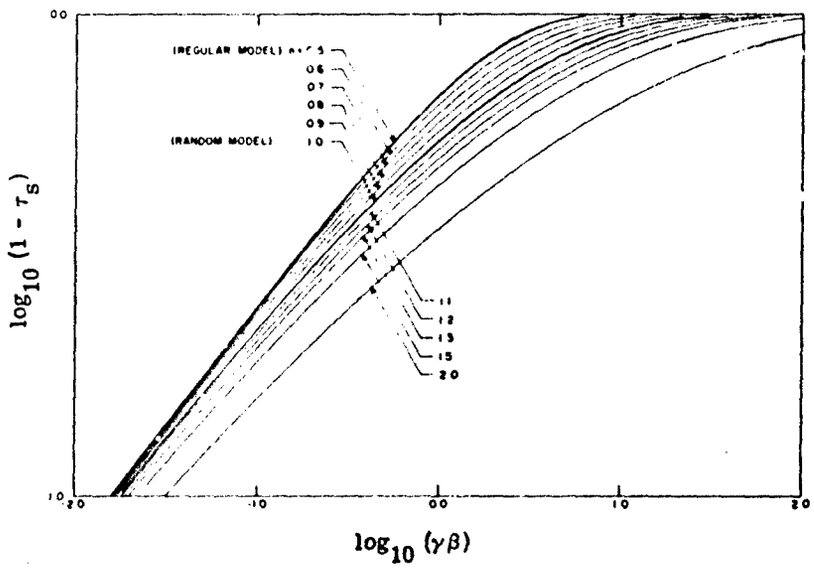

FIGURE 99. A PLOT OF THE STRONG-LINE TRANSMISSION FUNCTION PROPOSED BY KING (1964). (Reproduced from Zachor, 1968a [22].)

$$(-\ln\tau^*)^{-2} = (Kw)^{-2} + (\ln\tau_s)^{-2} - M(Kw\ln\tau_s)^{-1}$$

$$= K^{-2}w^{-2} + (\ln\tau_s)^{-2} - MK^{-1}(w\ln\tau_s)^{-1} \quad (390)$$

and Zachor minimizes the expression:

$$\Delta = \sum_I W_i\left[\left(\ln\tau_i^*\right)^{-2} - \left(\ln\tau_i\right)^{-2}\right]^2 \quad (391)$$

with respect to K^{-2} and M/K. The weighting function is taken as $W_i = \left(\ln\tau_i\right)^4$. Thus, taking $\frac{\partial\Delta}{\partial(K^{-2})} = 0$ and $\frac{\partial\Delta}{\partial(MK^{-1})} = 0$, the following solutions are obtained for experimental data for which the strong-line values yield accurate values of n and C:

$$K = (a_1)^{-1/2} \quad (392)$$

and

$$M = -Ka_2 \quad (393)$$

where: $a_1 = (c_1/q_{12} - c_2/q_{22})/(q_{11}/q_{12} - q_{12}/q_{22})$

$a_2 = (c_1/q_{11} - c_2/q_{12})/(q_{12}/q_{11} - q_{22}/q_{12})$

$$c_1 = \sum_i\left[(\ln\tau_i/w_i)^2\left[1 - (\ln\tau_i/\ln\tau_{si})^2\right]\right]$$

$$c_2 = \sum_i\left[(\ln\tau_i)^2/w_i\ln\tau_{si}\right]\left[1 - (\ln\tau_i/\ln\tau_{si})^2\right]$$

$$q_{11} = \sum_i\left[(\ln\tau_i)/w_i\right]^4$$

$$q_{12} = \sum_i\left[(\ln\tau_i)^4/w_i^3\ln\tau_{si}\right]$$

$$q_{22} = \sum_i\left[(\ln\tau_i)^4/(w_i\ln\tau_{si})^2\right]$$

and where τ_{si} is the strong-line transmittance calculated using experimental data in Eq. (387).

The accuracy of this method is dependent to a large extent on the quantity of data available in the strong-line region. Zachor observes parenthetically that, whereas M and K were determined using a digital computer, the use of a computer to determine n and C for all possible cases would require an elaborate code. The graphical technique can be checked by the success in using the graphically determined values of n and C. In the 2 μm region for which he determined these parameters, he found that at the parts of the spectrum where the absorption was relatively weak, the arbitrary choice of n = 1.00 gave reliable results. In these cases for which the determination

of C by the displacement between the data and the computed curve was compromised by a paucity of data, it was found that either errors tended to compensate each other, making the final result only mildly dependent on a very accurate choice of C; or the physical significance of C was open to question, in the case of the weaker regions of the 2 μm CO_2 bands.

8.1.3 RESULTS USING ZACHOR'S METHOD

Zachor used the data of Burch, Gryvnak and Patty (1964) in the region bounded by the following conditions to obtain model parameters: (1) $w/P < 10^5/1.5$ atm^{-1} cm, (2) Pw > 100 atm cm, (3) P ≤ 10 atm; and by the conditions 5 < w < 100 cm, 1 ≤ P ≤ 10 atm. He claims that the results "should be accurate for all w and P for which Pw > 100 atm cm, except perhaps in the spectral regions of relatively weak absorption when w and P represent strong-line conditions; that is, when n = 1.00 and the resulting values for τ and τ_s are approximately equal." The results are given in Table 49 which is reproduced from Zachor's (1968b) report, and shows the parameters used to calculate the transmittance for CO_2 in the region between 459.2 and 5346.0 cm^{-1} (1.87 and 2.18 μm). The first column, giving the interval over which the calculation was made, represents the resolution, which is approximately 5 cm^{-1} or less. The other four columns list the values of n, C, M and K, respectively. A comparison is made (Zachor, 1968b) between values of transmittance for various values of atmospheric parameters calculated from the mathematical formulation, and the values plotted from the Burch, Gryvnak and Patty data for the same conditions. This comparison is shown in Figure 100 in which the solid curve represents the experimental data and the discrete points the calculated data.

8.2 THE FIVE-PARAMETER FORMULATION OF GIBSON AND PIERLUISSI

Pierluissi (1973) has correctly pointed out that although there have been innumerable models derived for the calculation of atmospheric transmission, their developments can be traced either directly or indirectly back to two origins, the Elsasser (regular) and Goody (random) models. Except for excursions into the physical structure of molecules and in the absorptive mechanisms, these models should be eminently successful in predicting atmospheric transmittance. One obvious dificiency, however, is that the pattern of absorption by molecules is seldom either perfectly regular or random. Hence the need for modifications which account for the expected departures. As mentioned above, however, one feels that the ultimate preferable model would be of a more unified complexion. Zachor has attempted to develop this model on the foundation laid by King who recognized the apparent interdependence of various models through parameters which described the physical appearance of their absorption spectra in terms of their regularity, or their tendency to cluster.

TABLE 49. TRANSMITTANCE PARAMETERS FOR CO_2 BETWEEN 4590.2 AND 5346.0 cm^{-1}.* (From Zachor, 1968 [23].)

Interval (cm^{-1})	n	C (atm $^{-1}$ cm^{-1})	M	K (cm^{-1})
4590.2-4595.4	1.00	0.402E-06	-1.02	0.181E-05
4595.4-4600.3	1.00	0.518E-06	-0.94	0.218E-05
4600.3-4605.0	1.00	0.118E-05	-1.04	0.310E-05
4605.0-4609.7	1.00	0.234E-05	-1.07	0.407E-05
4609.7-4614.0	1.00	0.350E-05	-0.98	0.520E-05
4614.0-4619.1	1.00	0.486E-05	-0.90	0.635E-05
4619.1-4624.0	1.00	0.749E-05	-0.94	0.742E-05
4624.0-4628.5	1.00	0.901E-05	-0.96	0.807E-05
4628.5-4633.6	1.00	0.758E-05	-0.87	0.756E-05
4633.6-4638.3	1.00	0.252E-05	-0.98	0.440E-05
4638.3-4643.4	1.00	0.105E-05	-0.97	0.285E-05
4643.4-4648.4	1.00	0.917E-05	-0.96	0.828E-05
4648.4-4652.0	1.00	0.199E-04	-0.84	0.126E-04
4652.0-4656.0	1.00	0.208E-04	-0.90	0.124E-04
4656.0-4660.0	1.00	0.101E-04	-0.99	0.845E-05
4660.0-4664.1	1.00	0.134E-05	-0.99	0.319E-05
4664.1-4669.2	1.00	0.375E-06	-1.26	0.139E-05
4669.2-4674.3	1.00	0.402E-06	-1.07	0.160E-05
4674.3-4678.0	1.00	0.354E-06	-1.42	0.125E-05
4678.0-4681.6	1.00	0.369E-06	-1.01	0.161E-05

*The units given for C and K are consistent with the units cm S.T.P. for w and atmospheres for P in equations (386) and (387).

TABLE 49. TRANSMITTANCE PARAMETERS FOR CO_2 BETWEEN 4590.2 AND 5346.0 cm^{-1}.* (From Zachor, 1968 [23].) (Continued)

Interval (cm^{-1})	n	C ($atm^{-1} cm^{-1}$)	M	K (cm^{-1})
4681.6-4685.2	1.00	0.479E-0[illegible]	-1.12	0.170E-05
4685.2-4690.2	1.00	0.634E-06	-1.00	0.208E-05
4690.2-4695.0	1.00	0.977E-06	-1.07	0.252E-05
4695.0-4700.0	1.00	0.120E-05	-1.11	0.279E-05
4700.0-4704.0	1.00	0.122E-05	-1.12	0.287E-05
4704.0-4708.1	1.00	0.102E-05	-1.17	0.251E-05
4708.1-4711.8	1.00	0.167E-05	-1.17	0.326E-05
4711.8-4715.4	1.00	0.398E-05	-1.02	0.547E-05
4715.4-4719.0	1.00	0.749E-05	-1.04	0.753E-05
4719.0-4722.5	1.00	0.149E-04	-0.79	0.104E-04
4722.5-4726.0	1.00	0.188E-0[illegible]	-0.83	0.132E-04
4726.0-4731.1	1.00	0.277E-04	-0.73	0.166E-04
4731.1-4736.0	1.00	0.363E-04	-0.56	0.211E-04
4736.0-4740.9	1.00	0.457E-04	-0.39	0.226E-04
4740.9-4745.0	1.00	0.421E-04	-0.59	0.212E-04
4745.0-4750.0	1.00	0.451E-04	-0.57	0.206E-04
4750.0-4755.0	1.00	0.128E-03	-0.26	0.374E-04
4755.0-4760.0	1.00	0.172E-03	-0.28	0.502E-04
4760.0-4765.0	1.00	0.281E-03	0.20	0.672E-04
4765.0-4770.0	1.00	0.316E-03	-0.34	0.833E-04
4770.0-4775.0	1.00	0.340E-03	-0.23	0.107E-03
4775.0-4780.0	1.00	0.585E-03	0.54	0.192E-03
4780.0-4785.0	1.00	0.668E-03	0.25	0.259E-03
4785.0-4790.0	1.00	0.875E-03	0.86	0.337E-03
4790.0-4795.0	1.00	0.789E-03	0.23	0.385E-03
4795.0-4800.0	0.95	0.906E-03	-0.09	0.4[illegible]9E-03
4800.0-4805.0	0.95	0.767E-03	-0.27	0.324E-03
4805.0-4810.0	1.00	0.724E-03	0.34	0.28[illegible]E-03
4810.0-4815.0	1.00	0.109E-02	0.10	0.55[illegible] 03
4815.0-4820.0	0.90	0.142E-02	-0.05	0.104E-02
4820.0-4825.0	0.90	0.189E-02	0.01	0.171E-02
4825.0-4830.0	0.70	0.121E-02	-0.13	0.222E-02
4830.0-4834.6	0.75	0.298E-02	0.51	0.337E-02
4834.6-4838.1	0.60	0.185E-02	0.56	0.417E-02
4838.1-4843.1	0.55	0.169E-02	0.19	0.435E-02
4843.1-4848.0	0.55	0.159E-02	0.13	0.361E-02
4848.0-4851.2	0.60	0.109E-02	0.06	0.211E-02
4851.2-4855.2	0.65	0.504E-03	1.32	0.984E-03
4855.2-4859.7	0.60	0.134E-02	0.34	0.243E-02
4859.7-4864.1	0.60	0.237E-02	-0.00	0.455E-02
4864.1-4868.3	0.65	0.281E-02	-0.25	0.537E-02
4868.3-4872.4	0.60	0.264E-02	0.30	0.531E-02
4872.4-4876.4	0.65	0.212E-02	-0.00	0.386E-02
4876.4-4881.3	0.70	0.177E-02	0.34	0.239E-02
4881.3-4886.0	0.85	0.109E-02	0.08	0.975E-03
4886.0-4890.4	0.90	0.726E-03	0.13	0.388E-03
4890.4-4894.8	0.95	0.683E-03	-0.31	0.250E-03
4894.8-4898.9	0.85	0.436E-03	-0.20	0.258E-03
4898.9-4904.0	0.95	0.424E-03	-0.11	0.245E-03
4904.0-4908.6	0.95	0.434E-03	-0.14	0.218E-03

TABLE 49. TRANSMITTANCE PARAMETERS FOR CO_2 BETWEEN 4590.2 AND 5346.0 cm^{-1}.* (From Zachor, 1968 [23].) (Continued)

Interval (cm^{-1})	n	C ($atm^{-1}cm^{-1}$)	M	K (cm^{-1})
4908.6-4912.3	1.00	0.891E-03	-0.36	0.233E-03
4912.3-4916.3	1.00	0.107E-02	-0.35	0.269E-03
4916.3-4919.2	1.00	0.116E-02	-0.13	0.295E-03
4919.2-4924.0	0.85	0.132E-02	0.29	0.431E-03
4924.0-4928.7	1.00	0.144E-02	1.16	0.730E-03
4928.7-4933.2	0.90	0.206E-02	0.49	0.116E-02
4933.2-4937.6	0.65	0.213E-02	0.60	0.212E-02
4937.6-4942.0	0.70	0.266E-02	0.72	0.377E-02
4942.0-4946.1	0.70	0.378E-02	2.11	0.959E-02
4946.1-4950.2	0.70	0.555E-02	0.88	0.856E-02
4950.2-4954.2	0.70	0.789E-02	0.78	0.131E-01
4954.2-4958.0	0.70	0.982E-02	0.80	0.173E-01
4958.0-4961.7	0.65	0.105E-01	0.96	0.210E-01
4961.7-4965.4	0.70	0.125E-01	1.03	0.227E-01
4965.4-4970.5	0.65	0.118E-01	0.58	0.212E-01
4970.5-4975.4	0.70	0.129E-01	0.34	0.142E-01
4975.4-4979.4	0.70	0.672E-02	0.51	0.672E-02
4979.4-4983.8	0.70	0.108E-01	0.23	0.144E-01
4983.8-4988.0	0.65	0.167E-01	0.14	0.258E-01
4988.0-4993.1	0.60	0.150E-01	0.00	0.306E-01
4993.1-4997.8	0.60	0.127E-01	-0.03	0.247E-01
4997.8-5002.9	0.60	0.737E-02	0.03	0.140E-01
5002.9-5007.3	0.50	0.244E-02	-0.03	0.528E-02
5007.3-5011.4	0.70	0.917E-03	1.23	0.132E-02
5011.4-5015.8	0.75	0.211E-03	1.54	0.282E-03
5015.8-5020.8	0.80	0.118E-03	0.10	0.481E-04
5020.8-5025.5	1.00	0.140E-03	-0.60	0.233E-04
5025.5-5030.4	1.00	0.123E-03	-0.46	0.347E-04
5030.4-5034.4	1.00	0.110E-03	-0.57	0.336E-04
5034.4-5038.4	1.00	0.994E-04	-0.82	0.310E-04
5038.4-5042.7	0.80	0.407E-04	-0.93	0.342E-04
5042.7-5047.0	1.00	0.906E-04	-0.12	0.540E-04
5047.0-5051.2	0.80	0.194E-03	0.21	0.109E-03
5051.2-5055.3	0.80	0.196E-03	1.87	0.270E-03
5055.3-5059.3	0.80	0.246E-03	1.16	0.451E-03
5059.3-5063.3	0.60	0.218E-03	0.24	0.718E-03
5063.3-5067.2	0.60	0.973E-03	0.22	0.123E-02
5067.2-5071.1	0.60	0.683E-03	0.33	0.204E-02
5071.1-5074.8	0.60	0.101E-02	0.10	0.299E-02
5074.8-5078.5	0.55	0.132E-02	0.03	0.423E-02
5078.5-5082.1	0.55	0.192E-02	0.29	0.560E-02
5082.1-5085.7	0.55	0.237E-02	0.28	0.665E-02
5085.7-5090.8	0.60	0.263E-02	0.01	0.663E-02
5090.8-5095.7	0.55	0.244E-02	0.06	0.508E-02
5095.7-5099.6	0.70	0.166E-02	0.59	0.241E-02
5099.6-5104.2	0.60	0.179E-02	0.17	0.293E-02
5104.2-5108.6	0.60	0.434E-02	0.10	0.709E-02
5108.6-5112.6	0.65	0.572E-02	-0.03	0.919E-02
5112.6-5116.8	0.60	0.486E-02	0.05	0.907E-02
5116.8-5121.7	0.65	0.431E-02	0.39	0.684E-02

TABLE 49. TRANSMITTANCE PARAMETERS FOR CO_2 BETWEEN 4590.2 AND 5346.0 cm^{-1}.* (From Zachor, 1968 [23].) (Concluded)

Interval (cm^{-1})	n	C ($atm^{-1}\,cm^{-1}$)	M	K (cm^{-1})
5121.7-5126.5	0.75	0.296E-02	0.27	0.350E-02
5126.5-5130.8	0.60	0.177E-02	0.00	0.177E-02
5130.8-5135.1	0.70	0.140E-02	-0.22	0.119E-02
5135.1-5139.0	0.80	0.124E-02	-0.22	0.891E-03
5139.0-5143.0	1.00	0.103E-02	0.27	0.723E-03
5143.0-5147.7	1.00	0.988E-03	0.07	0.444E-03
5147.7-5152.6	0.85	0.342E-03	-0.06	0.235E-03
5152.6-5157.0	0.70	0.204E-03	-0.04	0.867E-04
5157.0-5162.0	1.20	0.124E-03	-0.62	0.327E-04
5162.0-5167.0	1.00	0.248E-04	-0.93	0.129E-04
5167.0-5172.0	1.00	0.989E-05	-1.23	0.482E-05
5172.0-5177.0	1.00	0.641E-06	-1.27	0.189E-05
5177.0-5181.5	1.00	0.203E-06	-1.22	0.109E-05
5239.0-5244.0	1.00	0.903E-06	-0.98	0.182E-05
5244.0-5248.0	1.00	0.102E-05	-1.18	0.317E-05
5248.0-5252.0	1.00	0.402E-06	-0.58	0.223E-05
5260.0-5264.0	1.00	0.465E-06	-1.49	0.198E-05
5264.0-5268.0	1.00	0.573E-06	-1.42	0.223E-05
5268.0-5272.0	1.00	0.402E-06	-1.02	0.216E-05
5272.0-5276.9	1.00	0.508E-06	-1.32	0.219E-05
5276.9-5281.7	1.00	0.102E-05	-1.35	0.269E-05
5281.7-5286.3	1.00	0.252E-05	-1.10	0.407E-05
5286.3-5290.7	1.00	0.104E-04	-0.81	0.109E-04
5290.7-5294.9	1.00	0.362E-05	-1.07	0.695E-05
5294.9-5298.9	1.00	0.575E-05	-0.85	0.842E-05
5298.9-5302.8	1.00	0.116E-04	-0.76	0.107E-04
5302.8-5306.6	1.00	0.180E-04	-0.91	0.191E-04
5306.6-5311.0	1.00	0.409E-04	-0.55	0.289E-04
5311.0-5316.0	0.90	0.197E-03	-0.37	0.100E-03
5316.0-5320.1	1.00	0.123E-04	-0.96	0.955E-05
5320.1-5324.2	1.00	0.180E-04	-0.69	0.130E-04
5324.2-5329.0	1.00	0.321E-04	-0.96	0.212E-04
5329.0-5334.0	1.00	0.998E-03	0.22	0.226E-04
5334.0-5338.0	1.00	0.162E-04	-0.80	0.108E-04
5338.0-5342.0	1.00	0.159E-05	-1.63	0.243E-05
5342.0-5346.0	1.00	0.230E-06	-3.42	0.433E-06

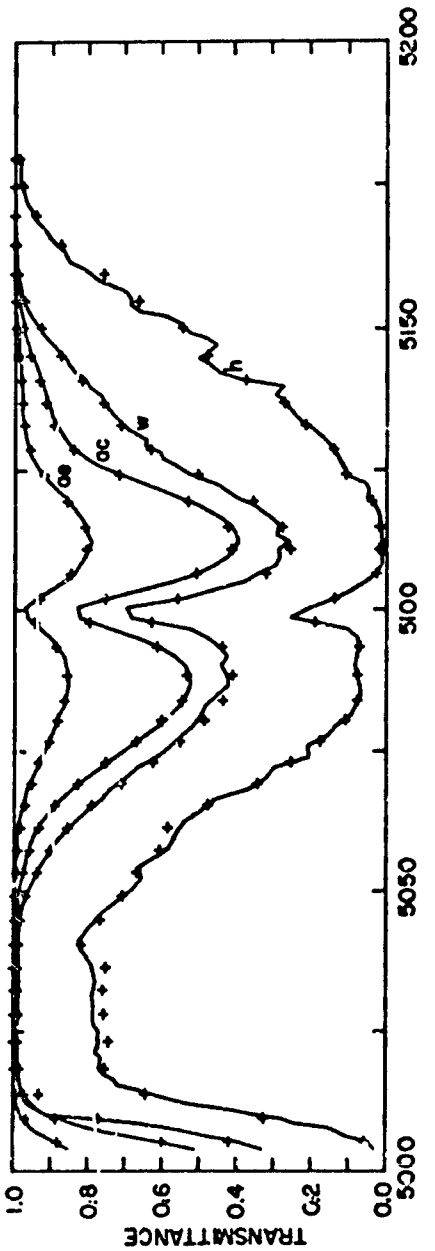

FIGURE 100. TRANSMITTANCE SPECTRA COMPUTED FROM TABLE 49 (CROSSES) AND FROM BURCH, GRYVNAK AND PATTY (1964) (SOLID CURVES). w and P are 3940 cm and 0.15 atm for sample h: 330 cm and 1.0 atm for sample w; 99.6 cm and 10 atm for sample ac; and 25.0 cm and 3.02 atm for sample ae. (Reproduced from Zachor, 1968b [23].)

Another attempt, by Gibson and Pierluissi (1971) to develop the generalized model leaves the user with an even higher degree of parameterization than does Zachor's model, which uses four parameters, n, C, M and K. It seems, then, that given a polynomial with high enough degree, the ultimate model might be achieved as closely as desired. But obviously there is a practical limit, and there should be no attempt here to establish how closely one ought to approach that limit except, perhaps, to remind the reader that every technique is an approximation, and that the closest approach to reality is the line-by-line calculation.

It is interesting, however, to take Zachor's approach one step further. Gibson and Pierluissi (1971) have taken this step in a paper in which they adjust the weight of the strong-line parameter in (Zachor's) Eq. (381), thereby adding a fifth parameter to the set constructed by Zachor. Thus, in Eq. (381), letting:

$$x = 1/w,\ y = 1/\ell n\ \tau_s,\ \text{and}\ z = -1/\ell n\ \tau^* \tag{394}$$

there results for Zachor's model:

$$z^2 = (1/K^2)x^2 + y^2 - (M/K)xy \tag{395}$$

in which the parameters n and C are implicit in y^2. This second-degree polynomial is made more general by incorporating an adjustable parameter for the coefficient of the y^2 term. Thus:

$$z^2 = B_w x^2 + B_s y^2 + B_{ws} xy \tag{396}$$

where B_w and B_s (weak- and strong-line parameters) are positive and $B_{ws}^2 < B_w B_s$. The reader is referred to the paper by Gibson and Pierluissi (1971) for the details in the determination of n, C, B_w, B_s and B_{ws}. In their paper are listed these parameters for CO_2 for frequencies from 550 to 9950 cm^{-1} derived from the transmittance tables of Stull, Wyatt and Plass [255] and Wyatt, Stull and Plass [256], in spectral intervals averaged over 50 cm^{-1}.

In a later paper Pierluissi (1973) published a partial list of the same parameters for CO_2 at 296 K averaged over 5 cm^{-1} intervals, derived in this case from the experimental data of Burch, Gryvnak and Patty (1964). The partial listing of parameters covering the CO_2 spectral region from 4795.0 to 4905.2 cm^{-1} is reproduced in Table 50. Comparisons are made in Table 50 between the 5-parameter model by Gibson and Pierluissi and those of Zachor and Mayer-Goody. Included also are results using modified versions of the Mayer-Goody and Elsasser models. Figure 101 is a plot of the spectrum calculated from the 5-parameter model, compared with the results of experimental data.

255. V. R. Stull, P. J. Wyatt and G. N. Plass, "The Infrared Transmittance of CO_2," Appl. Opt., Vol. 3, No. 2, February 1964, pp. 243-254.

256. P. J. Wyatt, V. R. Stull and G. N. Plass, App. Opt., No. 3, 1964, p. 229.

TABLE 50. TRANSMITTANCE PARAMETERS AND STATISTICS FOR CO_2 DATA AT 298 K AVERAGED OVER 5 cm^{-1} INTERVALS. (From Pierluissi, 1973 [26].)

Wavenumber Interval (cm^{-1})	Coefficients of Five-Parameter Formula					Mean Absolute Deviation of Models ($\times 10^3$)				
	n	C	B_w	B_s	B_{ws}	Five parameter	Zachor	Modified Mayer-Goody	Modified Elsasser	Mayer-Goody
4795.0–4800.0	0.784	6.216E-04	4.476E+06	0.792	−4.826E+02	8.32	9.37	12.37	12.86	17.95
4800.0–4805.0	0.835	5.854E-04	7.750E+06	0.820	7.069E+01	6.60	7.49	13.26	12.12	16.85
4805.0–4810.0	1.137	5.710E-04	1.135E+07	0.641	−1.510E+03	6.32	8.71	14.36	18.10	11.79
4810.0–4815.0	0.917	8.985E-04	3.029E+06	0.808	−6.022E+02	4.15	6.82	7.49	15.15	9.00
4815.0–4820.0	0.881	1.115E-03	7.802E+05	0.800	−1.203E+02	6.55	11.00	14.13	16.02	18.42
4820.0–4825.0	0.855	1.508E-03	2.871E+05	0.823	−2.053E+02	4.82	9.90	10.40	16.86	13.85
4825.0–4830.0	0.785	1.285E-03	1.397E+05	0.863	−1.955E+02	7.30	10.23	10.17	15.65	15.59
4830.0–4836.4	0.681	1.766E-03	6.153E+04	0.840	−1.887E+02	9.83	12.19	12.45	15.74	18.45
4836.4–4841.5	0.559	1.581E-03	4.661E+04	0.901	−6.524E+01	10.88	11.41	11.42	12.18	24.50
4841.5–4846.4	0.554	1.484E-03	5.784E+04	0.941	−4.680E+00	9.50	9.86	9.93	10.57	25.10
4846.4–4851.2	0.668	1.206E-03	1.477E+05	0.937	−3.079E+01	7.56	7.94	8.69	10.01	18.29
4851.2–4856.7	0.611	4.708E-04	5.969E+05	0.710	−9.982E+02	5.82	12.17	11.58	11.87	24.93
4856.7–4861.2	0.603	1.582E-03	8.154E+04	0.935	−3.813E+01	8.78	9.17	9.32	11.10	23.79
4861.2–4866.2	0.562	2.234E-03	3.509E+04	0.944	7.873E+00	8.06	8.38	8.88	10.44	22.82
4866.2–4871.1	0.626	2.473E-03	3.395E+04	0.982	2.580E+01	8.06	7.96	8.51	9.29	24.79
4871.1–4876.4	0.803	2.661E-03	5.886E+04	0.992	2.755E+01	10.11	9.96	10.06	12.89	17.44
4876.4–4881.3	0.798	1.700E-03	1.531E+05	0.874	−1.637E+02	7.52	8.25	8.42	12.72	13.71
4881.3–4886.0	0.828	8.603E-04	8.103E+05	0.729	−4.673E+02	6.49	13.24	14.83	15.41	19.87
4886.0–4890.4	0.834	5.691E-04	5.535E+06	0.825	−7.841E+02	5.94	6.54	8.11	13.95	10.81
4890.4–4894.8	0.845	4.907E-04	1.260E+07	0.804	3.407E+02	4.79	5.07	13.59	12.36	17.28
4894.8–4900.3	0.862	3.681E-04	1.235E+07	0.786	−8.474E+02	5.85	6.51	9.80	11.46	13.09
4900.3–4905.2	0.869	3.280E-04	1.306E+07	0.642	−2.519E+02	5.94	7.91	10.23	12.05	13.13
					Mean	7.24	9.09	10.82	13.13	17.79

ERIM
FORMERLY WILLOW RUN LABORATORIES, THE UNIVERSITY OF MICHIGAN

SYMBOL	P_e (ATM)	w (ATM.CM)
AF	10.0100	25.0
W	1.0000	330.0
L	0.1001	3320.0
H	0.1500	9940.0
I	0.3000	9950.0
G	1.3100	21900.0

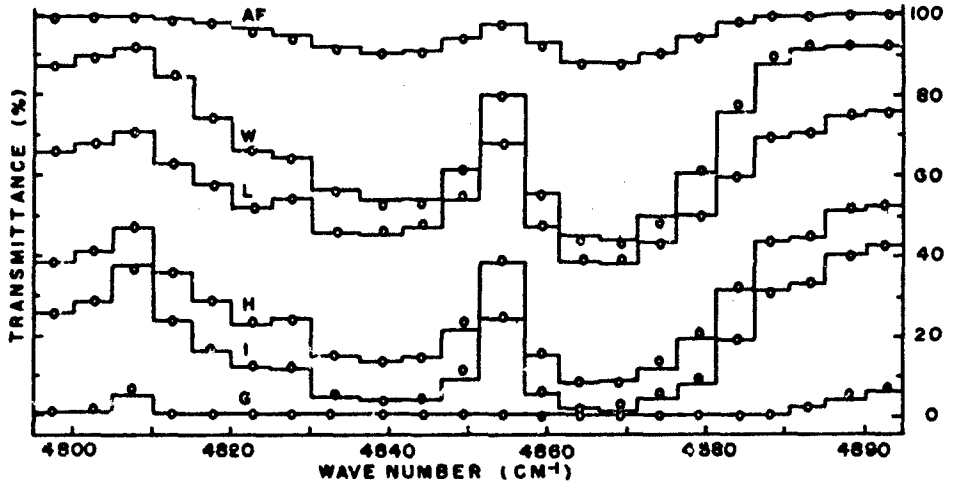

FIGURE 101. MEASURED (—) AND CALCULATED (–0–) TRANSMITTANCE FOR CO_2 BAND (Reproduced from Pierluissi, 1973 [26].)

8.3 POLYNOMIAL REPRESENTATION OF SMITH

Smith (1969) introduced a polynomial representation of carbon dioxide and water vapor transmission starting with the basic concepts of absorption, unembellished by conventional model techniques. Starting with the basic expression for the Lorentz line, he invoked Goody's (1964) approximation calling for a pressure-temperature-independent value of $\tilde{\alpha}$, giving.

$$\tau_\nu = \exp\left\{-\frac{w}{\pi}\sum_i \frac{\alpha_{L_i} S_i}{\left[(\nu - \nu_i)^2 + \tilde{\alpha}_i^2\right]}\right\} \tag{397}$$

which, upon substituting:

$$\alpha_{L_i} = \alpha_{L0_i}\left(\frac{P}{P_0}\right)\left(\frac{T_0}{T}\right)^{1/2}$$

gives:

$$\tau_\nu = \exp\left\{-\frac{w}{\pi}\left(\frac{P}{P_0}\right)\sqrt{\frac{T_0}{T}}\sum_i X_i S_i\right\} \tag{398}$$

where:

$$X_i = \alpha_{L0_i}\left[(\nu - \nu_i)^2 + \tilde{\alpha}_i^2\right]^{-1}$$

If the assumption is made that S_i and X_i are uncorrelated, true for the random models but also validated for a regular model for which S_i = const, then:

$$\tau_\nu = \exp - \frac{w}{\pi N_\nu}\left(\frac{P}{P_0}\right)\sqrt{\frac{T_0}{T}}\beta_\nu \sum_i S_i \tag{399}$$

where: $\beta_\nu = \sum_i X_i$, and N_ν is the number of lines counted at ν. Justifying other assumptions on the basis of earlier work [257], Smith obtains:

$$\sum_i S_i = \left(\frac{T}{T_0}\right)^{m_\nu} N_\nu \bar{S}_{0\nu} \tag{400}$$

257. K. Ya. Kondratyev and Yu. M. Timofeev, "The Applicability of Approximation Methods for Introducing Inhomogeneities into Calculations of the Transmission Functions of the Rotational Band of Water Vapor," Atmospheric and Oceanic Physics, Vol. 3, No. 3, 1967, pp. 236-244.

where: m_ν is a constant and $\bar{S}_{0\nu}$ is the mean line intensity under standardized conditions. The result is:

$$\tau_\nu = \exp\left[-\xi_\nu w P T^{n+m_\nu}\right] \tag{401}$$

with: $\xi_\nu = \beta_\nu \bar{S}_{0\nu}/\pi P_0 T_0^{n+m_\nu}$. The next step in generalization is to generalize the exponents of w and P as well as T to obtain:

$$\tau_\nu = \exp\left[-a_\nu w^{b_\nu} P^{c_\nu} T^{d_\nu}\right] \tag{402}$$

which, in the taking of logarithms, yields:

$$-\ell n\, \tau_\nu = a w^{b_\nu} P^{c_\nu} T^{d_\nu}$$

and taking a second logarithm yields:

$$\ell n\left(-\ell n \tau_\nu^*\right) = \ell n\, a_\nu + b_\nu\, \ell n\, w + c_\nu\, \ell n\, P + d_\nu\, \ell n\, T \tag{403}$$

where, as above, τ_ν^* is an approximation to the actual (measured) value of τ_ν. The difference between the value of Eq. (403) for τ^* and the actual value (using τ_ν) is:

$$\ell n\left(-\ell n\, \tau_\nu^*\right) = \ell n\, (-\ell n\, \tau_\nu) + R_\nu \tag{404}$$

the residual term R_ν being extended as far as necessary to make the two values as close as desired. Smith's expansion, applied in 5 cm^{-1} intervals to the 15 μm CO_2 data of Stull, Wyatt and Plass (1963) and the rotational H_2O data of H. J. Bolle of the Meteorological Institute of the University of Munich (by personal communication to Smith), yields the expression:

$$W(\Delta\nu) = C_0(\Delta\nu) + C_1(\Delta\nu)X + C_2(\Delta\nu)Y + C_3(\Delta\nu)Z + \ldots .$$

$$+ C_n(\Delta\nu)X^m Y^m Z^m \tag{405}$$

where:

$$W(\Delta\nu) = \ell n\, (-\ell n\, \tau_{\Delta\nu});$$

$$X = \ell n\left[w\frac{(273\ K)}{T}\right]$$

$$Y = \ell n\left(\frac{P}{1000\ mb}\right)$$

$$Z = \ell n\left(\frac{T}{273\ K}\right)$$

Smith has found that a nine-term expansion (C_i = 1, 2, ... , 8) produced the most significant parameters needed from the residual term to produce reasonable agreement with experimental (or theoretically produced) data. Two tables of data were derived, one for H_2O and one for CO_2, based on the atmospheric parameters in Table 51 pertinent to the fitted data. The lists of coefficients for the nine terms used in the expansion are shown in Table 52 for rotational H_2O vapor and in Table 53 for 15 μm CO_2. Unfortunately the data of Stull, Wyatt and Plass exhibit certain discrepancies, claimed by Smith, and apparently found also by Young [258]. A comparison of the calculated and experimental absorptance data, shown in Figure 102, points out the fact that discrepancies do exist. Similar discrepancies show up in otherwise well-fitting data in comparison between calculated and experimentally obtained upwelling radiance, as demonstrated in Figure 103. Comparison between transmittance spectra for H_2O calculated by Bo"e and those calculated by Smith from the polynomial model is shown in Figure 104, while a con parison with the experimental data of Palmer [259] is given in Table 54.

Calculation of $\tau_{\Delta\nu}$ is obtained from:

$$\tau_{\Delta\nu} = \exp\left[-\exp\left(W\right)\right] \tag{406}$$

where

$$W = \sum_{i=0}^{8} C_i A_i$$

in which the C_i's are given in Tables 52 and 53 and (see Eq. 405):

$$A_0 = 1.0;\ A_1 = X;\ A_2 = Y;\ A_3 = Z$$
$$A_4 = XY;\ A_5 = XZ;\ \text{and}\ A_6 = X^2$$

for both CO_2 and H_2O. Then, for CO_2:

$$A_7 = X^2Y;\ \text{and}\ A_8 = XZ^2$$

and for H_2O:

$$A_7 = X^2Z;\ \text{and}\ A_8 = YZ^2$$

258. L. G. Young, "Comments on Accurate Formula for Gaseous Transmittance in the Infrared," Appl. Opt., Vol. 11, No. 1, 1972, pp. 202-203.

259. C. H. Palmer, "Long Path Water Vapor Spectra With Pressure Broadening, I: 20 - 21.7," J. Opt. Soc. Am., Vol. 47, 1957, p. 1024.

TABLE 51 PRESSURES, TEMPERATURES AND PATH LENGTHS OF TABULATED TRANSMITTANCE DATA. (From Smith, 1969 [24].)

Pressure		Temperature		Path length	
CO_2	H_2O	CO_2	H_2O	CO_2	H_2O
Atm.	Atm.	°K.	°K.	Atm. cm.	Precipitable cm.
1.00	1.0	300	300	500.0	5.0
0.50	0.5	250	260	200.0	2.0
0.20	0.2	200	220	100.0	1.0
0.10	0.1	-	-	50.0	0.5
0.05	-	-	-	20.0	0.2
0.02	-	-	-	10.0	0.1
0.01	-	-	-	5.0	0.05
--	-	-	-	2.0	0.02
--	-	-	-	1.0	0.01
--	-	-	-	0.5	0.005
--	-	-	-	0.2	0.002
--	-	-	-		0.001

TABLE 52. EMPIRICAL ABSORPTION COEFFICIENTS FOR WATER VAPOR.
(From Smith, 1969 [24].)

Frequency (cm-1)	C_0	C_1	C_2	C_3	$C_4 \times 10$	C_5	$C_6 \times 10$	$C_7 \times 10$	$C_8 \times 10$	RMS error
202.5	6.1218	.9142	.9011	-.4375	.4956	0	.1814	0	0	0.3
207.5	6.1750	1.0287	.9764	0	.5409	.0989	.2440	0	0	0.6
212.5	5.6094	.9578	.9160	0	.5039	-.0841	.2266	0	0	0.5
217.5	4.8955	.9880	.9591	0	.4072	0	.1177	0	0	0.8
222.5	5.3723	.8413	.8257	-1.2625	.3251	-.2771	.1391	-.1445	0	0.5
227.5	4.8715	.6848	.6620	0	.2161	.0097	.0952	-.0131	1.0950	0.3
232.5	3.8296	.6492	.6619	0	.1255	-.2476	.0096	0	6.9852	0.7
237.5	4.0639	.9648	.9847	0	.1809	0	0	.2738	0	0.6
242.5	3.8635	.8289	.7743	0	.3037	0	.1542	.1957	5.0334	0.9
247.5	5.4739	.7970	.7156	2.1261	.2349	.4997	.1109	.3768	0	0.4
252.5	5.5674	1.0058	.9283	0	.6286	-.0611	.3032	0	0	0.6
257.5	3.5271	.5908	.6273	0	-.1128	-.1407	-.1135	0	0	0.8
262.5	4.2338	1.0235	1.0361	.5353	.5418	-.0352	.0699	0	0	0.7
267.5	3.0032	.6309	.6164	.4302	.2136	-.1506	.0892	0	0	1.0
272.5	3.9064	.8762	.8960	.3708	.2857	-.2616	0	0	11.7741	0.7
277.5	4.0603	.4581	.5423	0	-.0430	-.2114	-.1271	-.1834	0	0.7
282.5	3.9660	.6008	.5625	1.3724	.1139	.0731	.0522	0	0	0.5
287.5	4.5389	.9895	.8969	.9405	.6686	0	.3052	0	0	0.7
292.5	3.4817	.8052	.7685	1.0741	.2127	0	.1061	0	0	0.9
297.5	3.7495	.8629	.8675	1.1067	.4929	-.1472	.1056	0	0	0.7
302.5	4.4469	.7224	.6912	1.3678	.3165	0	.1193	0	0	0.5
307.5	3.8072	.8714	.8022	1.4930	.3570	0	0	0	0	0.7
312.5	3.4957	.9707	.8940	1.6149	.3745	0	.2854	-.1295	0	0.6
317.5	3.5555	1.0590	.9694	1.3177	.7048	.0567	.3522	0	0	0.5
322.5	3.4924	.7124	.6683	1.0064	.3905	0	.1392	0	0	0.5
327.5	4.1125	.7887	.7497	1.8533	.3729	.0722	.1516	0	0	0.7
332.5	3.6888	.9455	.8726	1.4606	.5094	0	.2220	-.2487	0	0.8
337.5	3.5936	.9852	.8872	1.0675	.7393	0	.3348	-.1585	0	0.6
342.5	3.1583	.7363	.7083	1.6959	.3384	.0346	.1185	0	0	0.6
347.5	3.2042	.8207	.7648	1.5694	.5751	0	.1980	0	0	0.6
352.5	4.7227	.8590	.7921	2.5143	.4153	0	.1961	-.1034	0	0.7
357.5	3.1130	.5768	.5826	1.6107	0	.0556	-.0328	0	0	0.7
362.5	2.5079	.9242	.9058	1.6898	.5049	0	0	.2292	0	0.8
367.5	2.2004	.8052	.7417	1.3649	.5537	0	.1964	0	0	1.3
372.5	2.9026	.7342	.6751	1.7771	.3578	0	.1517	0	0	0.8
377.5	2.3168	.5871	.5786	1.7172	.2019	-.1343	.0600	0	0	1.2
382.5	2.2132	.7155	.6467	1.5840	.4174	0	.1497	0	0	1.1
387.5	1.9742	.7330	.6939	1.1260	.3095	.2008	.1552	.0321	-6.3470	1.6
392.5	2.1226	.7255	.6879	2.1168	.3257	-.1092	.1478	0	0	0.9
397.5	3.5291	.6982	.6678	2.4057	.2918	.0462	.0977	0	0	0.7
402.5	1.8393	.7860	.7293	2.2630	.5824	.1450	.2125	.4745	0	1.4
407.5	1.4888	.9428	.9105	2.0498	.6569	-.1445	.0218	0	0	1.0
412.5	1.5987	.9750	.9429	1.4218	.6512	-.1439	.0204	0	0	1.1
417.5	2.1667	.4856	.4527	1.1492	.1137	-.0894	.0441	0	0	2.0
422.5	2.5673	.6986	.6758	2.7325	.1866	.1562	.0325	.3342	0	0.7
427.5	1.6873	.7293	.6967	1.2854	.5759	0	.0607	.4438	0	1.3

TABLE 52. EMPIRICAL ABSORPTION COEFFICIENTS FOR WATER VAPOR.
(From Smith, 1969 [24].) (Continued)

Frequency (cm-1)	C_0	C_1	C_2	C_3	$C_4 \times 10$	C_5	$C_6 \times 10$	$C_7 \times 10$	$C_8 \times 10$	RMS error
432.5	1.6176	.7252	.6952	1.3610	.5026	0	-.0711	0	0	1.0
437.5	1.6237	.7975	.7471	2.4456	.4392	-.3088	.1379	0	0	0.6
442.5	1.9632	.6293	.6136	1.2863	.3189	0	.0558	0	0	0.9
447.5	1.4718	.7564	.7010	2.8388	.6191	-.2990	.0544	.2790	5.2110	1.1
452.5	1.7591	.7715	.7163	2.7152	.5552	-.1637	.0638	.1725	3.0805	0.7
457.5	2.2759	.6790	.6232	1.6932	.3735	.0797	.1304	0	0	0.8
462.5	1.3413	.8111	.7501	2.3745	.5334	-.3210	.0833	.2130	6.8252	0.7
467.5	1.4035	.7618	.6937	2.4610	.6784	-.3545	.0104	.3859	2.6021	0.9
472.5	1.9396	.6500	.6059	1.4577	.3822	.0231	.1124	0	0	1.3
477.5	.9939	.8646	.8111	1.8684	.5137	-.3699	.1051	.5305	16.0593	0.9
482.5	1.4496	.6708	.6215	1.1994	.3321	.0669	.0691	0	0	0.7
487.5	1.0059	.8310	.7510	1.9138	.6045	-.3055	.0469	.5665	14.7211	1.1
492.5	1.1967	.6830	.6690	2.2477	.5734	-.1047	.0257	.2090	0	1.4
497.5	.4625	1.0025	.9270	1.9155	.5779	-.0633	0	0	0	0.7
502.5	1.7019	.7317	.6852	3.4872	.4462	0	.1091	0	.3921	0.8
507.5	1.3500	.7110	.6813	2.0314	.4018	0	.1015	0	0	0.8
512.5	1.0144	.7584	.6897	3.6419	.7208	-.4356	-.1145	.3452	4.3500	1.2
517.5	1.9939	.6404	.6237	3.4130	.3857	0	0	0	-.9615	0.9
522.5	.9659	.8832	.8170	3.4262	.5265	0	-.1085	0	0	0.9
527.5	.9526	.6237	.5793	2.4008	.2823	0	.0692	0	0	0.8
532.5	.1357	.8832	.7762	2.7012	.4390	-.5505	-.0961	0	17.4780	0.8
537.5	.6216	.7386	.6645	2.0522	.6975	0	0	0	0	1.2
542.5	.5969	.8461	.7347	3.7532	.6477	0	0	0	0	0.9
547.5	1.4393	.6638	.6326	2.6433	.5921	0	0	0	0	1.5
552.5	.6297	.7306	.6532	2.1938	.6557	0	0	.4194	0	1.3
557.5	.0977	.8421	.7290	2.3145	.5239	-.3976	-.1518	0	13.2521	0.8
562.5	.3250	.7953	.6907	1.3819	.7604	0	0	0	0	1.1
567.5	1.0674	.6348	.6022	1.3958	.4387	0	0	.2679	0	1.1
572.5	.4668	.8550	.7523	3.2109	.5747	-.5758	0	0	20.4500	0.9
577.5	.7381	.7151	.6861	2.9358	.4528	0	.1002	0	0	0.8
582.5	.8434	.6420	.5703	2.7075	.5805	0	0	.6374	0	1.9
587.5	.0030	.9233	.8748	3.4166	0	-.1839	-.0702	0	0	0.7
592.5	1.1164	.6576	.6491	2.4402	.6297	.1755	.0241	.5418	-4.5706	2.0
597.5	.2369	.7363	.7274	2.8881	0	-.2370	-.1633	0	0	1.2
602.5	.1762	.6831	.6424	2.8055	.6562	-.1720	0	.5876	0	1.3
607.5	-.6216	.9947	.8932	2.0704	.3317	-.1440	0	0	0	0.5
612.5	-.0405	.8616	.7103	1.4924	.8775	0	0	0	0	0.9
617.5	.3722	.6929	.6368	1.8036	.6057	0	0	.2005	0	1.1
622.5	.1257	.7646	.7079	2.9373	.5923	-.5088	-.1067	.2441	20.1896	1.1
627.5	.0336	.6296	.5867	2.0144	.5046	0	0	.5117	2.8412	1.5
632.5	.0114	.7898	.7005	3.0840	.8279	-.3355	0	0	2.0618	0.9
637.5	.6751	.6999	.6284	2.5580	.6208	0	0	.6243	-.9255	1.2
642.5	.1658	.7703	.6617	3.1227	.8209	0	0	.6665	0	1.3
647.5	-.6688	.8729	.7498	1.3178	.6925	0	-.1530	0	0	0.7
652.5	-.6415	.8613	.7676	1.5691	1.0389	-.5763	0	0	12.1192	1.1

TABLE 52. EMPIRICAL ABSORPTION COEFFICIENTS FOR WATER VAPOR. (From Smith, 1969 [24].) (Concluded)

Frequency (cm^{-1})	C_0	C_1	C_2	C_3	$C_4 \times 10$	C_5	$C_6 \times 10$	$C_7 \times 10$	$C_8 \times 10$	RMS error
657.5	-.1863	.5866	.5879	.9089	.7812	-.2625	-.1946	.2767	3.2135	2.0
662.5	-.3255	.8684	.7576	1.3227	.7789	0	0	.3708	0	1.0
667.5	-.1770	.7475	.6674	.9509	.7456	0	0	0	0	1.2
672.5	-.2946	.7933	.6489	2.0613	.9300	-.1035	-.1658	0	2.3320	1.0
677.5	-.6008	.8069	.7206	1.2687	.9204	-.2858	-.1060	0	0	1.1
682.5	-1.2156	1.0442	.9708	.2732	.2229	-.0567	.1363	0	0	0.7
687.5	.0344	.7086	.6034	1.8627	.5647	0	0	.8283	9.4146	1.5
692.5	-.1431	.6964	.6444	2.1392	.8160	-.4796	-.1772	0	6.5367	1.4
697.5	.0802	.6968	.6318	2.3108	.8782	-.2794	-.1659	.3327	0	1.4
702.5	-.5850	.8702	.7589	2.3139	.8826	-.5944	0	0	18.8005	1.1
707.5	-.0010	.6293	.5967	1.3822	.7426	-.2653	-.1974	.1468	0	1.6
712.5	-.5983	.7250	.6020	1.8982	.7491	-.6156	-.2065	0	19.1300	1.1
717.5	-1.2443	.9860	.8534	.6712	.3676	-.1938	0	0	0	0.6
722.5	-1.2809	.9800	.8618	1.0699	.6606	-.3200	0	0	0	0.8
727.5	-.9128	.7659	.6462	.7983	.6223	-.5689	-.1932	-.3856	15.2976	0.8
732.5	-.8131	.7871	.6877	2.1119	.9877	-.4306	-.1490	-.5300	0	0.9
737.5	-1.4145	1.0079	1.0109	0	0	0	0	0	0	0.3
742.5	-.2006	.7076	.6073	3.2032	.8244	-.5402	-.1924	0	0	1.2
747.5	-.8597	.8564	.7451	1.1123	1.0400	-.2107	-.0685	0	0	0.7
752.5	-.6852	.7274	.6021	2.0420	.7252	-.8034	-.2399	-.6718	13.6298	1.0
757.5	-1.2460	.9611	.8279	1.7905	.5220	-.6282	-.0120	-.7092	9.8989	0.9
762.5	-1.5561	1.0101	.8169	0	.6095	-.0926	0	0	14.0942	0.4
767.5	-1.2170	.9208	.7144	.6104	.9037	-.1291	-.0574	0	0	0.6
772.5	-1.3441	.9220	.7982	1.1841	.7038	-.6788	-.0429	-.5950	10.3903	0.5
777.5	-.6800	.7769	.5818	2.2546	.7059	-.4801	-.2203	0	24.2264	0.9
782.5	-1.0037	.7783	.6493	.9905	.9013	-.5305	-.1597	-.2272	12.1459	0.7
787.5	-1.5633	1.0068	.9896	0	0	0	0	0	0	0.3
792.5	-1.2125	.8780	.7274	1.7113	.6813	-.7937	-.0675	-.5651	18.8107	0.7
797.5	-.2592	.6565	.5666	2.2743	.6738	-.3331	-.2699	0	0	1.2

TABLE 53. EMPIRICAL ABSORPTION COEFFICIENTS FOR CARBON DIOXIDE.
(From Smith, 1969 [24].)

Frequency (cm-1)	C_0	C_1	C_2	C_3	C_4x10	C_5	C_6x10	C_7x10^6	C_8x10	RMS error
507.5	-12.5563	1.2519	0	0	-1.7329	0	0	3.9227	.4650	0.2
512.5	-9.0648	0	0	0	-1.3531	.4108	1.2205	3.4860	0	0.2
517.5	-9.1621	0	0	3.0247	-1.3506	0	1.3428	3.6523	0	0.3
522.5	-7.5255	-.5054	-.2076	3.1339	0	0	1.8291	1.8728	0	0.3
527.5	-7.8368	0	0	0	0	.7787	1.1912	1.2167	0	0.4
532.5	-11.4741	1.3374	-.1906	3.5957	0	0	0	1.9534	0	0.4
537.5	-7.9647	0	0	3.5359	0	0	1.2409	1.3978	0	0.5
542.5	-8.7190	.7699	0	.4472	-.4690	2.7900	.4769	1.9071	3.3903	0.6
547.5	-9.1824	1.1398	0	1.7502	0	2.3209	0	1.0606	-2.8910	0.6
552.5	-10.2269	1.2544	0	4.8560	0	0	0	1.4981	0	0.8
557.5	-8.1479	.5104	0	0	0	2.1621	.7902	1.4411	2.0992	1.2
562.5	-8.2175	.7508	0	8.0119	0	-.5037	.5557	1.5920	0	1.6
567.5	-8.0988	1.1254	-.0707	7.8956	.4621	0	0	.6407	-.5619	1.1
572.5	-6.9298	.8914	0	6.6812	0	.4478	.2279	1.2015	-1.1620	0.9
577.5	-6.2296	.9875	0	6.9821	.3299	0	0	.6158	-.6665	0.6
582.5	-5.6500	1.0686	.0281	6.2319	.3985	0	-.1791	.5240	-.6194	0.6
587.5	-4.8285	.9965	.0969	5.1455	.6422	-.0355	-.2150	0	-.5157	0.7
592.5	-4.0110	.9665	.1516	4.2198	.6243	-.0579	-.2806	-.1882	-.3566	0.7
597.5	-3.4122	.9520	.1649	4.3297	.5547	-.3231	-.2286	-.1121	.2233	0.8
602.5	-3.2484	.8980	.2463	3.0533	.7241	-.2081	-.2458	-.4735	.2096	0.8
607.5	-3.2611	.8686	.2645	2.5396	.6400	-.1455	-.1883	-.3600	.1449	0.8
612.5	-3.3509	.9495	.2150	2.7733	.7470	-.1834	-.2394	-.3601	.1682	0.6
617.5	-1.5126	.8122	.2711	2.7253	.6160	-.3039	-.4478	-.7887	.1[illegible]3	1.4
622.5	-1.9530	.8463	.2533	2.8342	.6691	-.2870	-.3243	-.5338	.1959	1.0
627.5	-2.1364	.9037	.2648	2.5698	.8027	-.2002	-.3121	-.6357	.1305	0.7
632.5	-1.5385	.8461	.3189	2.1161	.7001	-.1432	-.2476	-.5504	.1059	0.7
637.5	-1.0136	.7563	.3827	1.4426	.4969	-.0675	-.1575	-.3489	.0540	0.4
642.5	-.5586	.6964	.4134	1.0127	.3247	0	-.1025	-.1676	-.0434	0.3
647.5	-.0136	.7252	.4053	.6414	.3872	.0339	-.1753	-.3050	-.0781	0.5
652.5	.0036	.6937	.4501	.0877	.3590	.0180	-.0761	-.1986	-.0745	0.6
657.5	-.1140	.6918	.4622	-.2066	.3664	0	0	-.0950	0	0.6
662.5	.2529	.6475	.4216	-.3615	.2348	.0506	-.0542	0	-.0645	0.6
667.5	1.3638	.5246	.4340	.0297	.0662	-.0893	-.0503	-.0057	.0695	0.9
672.5	.3700	.5234	.3970	.1252	.2322	-.0779	.1301	.1827	0	1.4
677.5	.0693	.6726	.4955	-.1532	.3386	.0544	.0078	-.1429	-.0238	0.7
682.5	.0160	.6533	.4873	.0948	.2865	.0179	.0028	-.1026	-.0338	0.5
687.5	-.2339	.6633	.4764	.5516	.2986	.0232	.0071	-.0737	-.0520	0.5
692.5	-.5269	.6672	.4586	1.0241	.3113	0	-.0153	-.1029	0	0.5
697.5	-.9326	.6943	.4371	1.5664	.3741	-.0096	-.0634	-.2023	-.0233	0.7
702.5	-1.4106	.7520	.3814	2.2672	.4940	-.0849	-.1173	-.3104	.0301	0.7
707.5	-1.9623	.8219	.3270	2.8036	.6731	-.2118	-.1992	-.4881	.1569	0.9
712.5	-2.5460	.8790	.2863	2.9180	.7776	-.2568	-.2124	-.5446	.2821	0.9
717.5	-1.0850	.8043	.2803	2.9613	.6098	-.2636	-.3415	-.5813	.1779	1.0
722.5	-1.4270	.7581	.3052	2.4273	.5335	-.3081	-.4472	-.8055	.2170	1.5
727.5	-3.3026	.8857	.2736	2.4157	.7142	-.1082	-.1824	-.3395	.1325	0.8

TABLE 53. EMPIRICAL ABSORPTION COEFFICIENTS FOR CARBON DIOXIDE.
(From Smith, 1969 [24].) (Concluded)

Frequency (cm^{-1})	C_0	C_1	C_2	C_3	$C_4 \times 10$	C_5	$C_6 \times 10$	$C_7 \times 10^2$	$C_8 \times 10$	RMS error
732.5	-2.9767	.8424	.2938	2.4131	.6911	-.1974	-.1977	-.4364	.2716	0.9
737.5	-3.0163	.8741	.2597	3.1387	.6681	-.1210	-.2305	-.4251	.1214	1.0
742.5	-3.1692	.9078	.2253	3.9284	.6231	-.1710	-.2981	-.3541	0	0.7
747.5	-4.0990	.9514	.1827	4.3132	.8807	-.2173	-.2716	-.4737	0	0.7
752.5	-4.6736	.9831	.1180	5.3603	.6576	-.0190	-.2236	0	-.4328	0.7
757.5	-5.7219	.9980	.0484	7.2490	.3511	0	-.0874	.6046	-.6890	0.6
762.5	-6.6114	.9978	0	8.0478	.4330	0	0	.5637	-.7565	0.7
767.5	-7.4221	1.0581	0	9.1331	.4566	0	0	.4869	-.8853	0.8
772.5	-7.8763	.8391	-.0351	6.5719	.1215	.6383	.4162	1.2539	-1.1983	1.5
777.5	-8.3537	.8692	-.0411	7.3879	0	0	.3817	1.4924	-.5194	1.1
782.5	-9.0114	.9830	-.0311	2.0357	.1224	1.8100	.2775	1.4138	-2.2558	0.8
787.5	-7.4446	.9695	0	4.9493	.2164	1.0906	0	.5778	-1.8784	0.3
792.5	-7.1057	.9791	0	6.0877	0	.6197	0	.9747	-1.4249	0.5
797.5	-7.1605	.5334	.2257	10.4273	0	6.8167	.1921	0	-7.4102	1.1
802.5	-8.8450	1.0065	-.4454	3.2588	1.5741	-.8311	.0973	-.0534	0	0.4
807.5	-7.7652	.5169	0	0	0	2.5100	.5956	1.1644	-2.8153	0.3
812.5	-8.3196	.6049	0	-.8062	-.3048	3.0995	.5332	1.6666	-3.4150	0.3
817.5	-9.4568	1.0304	0	6.3498	0	0	0	1.0164	0	0.3

TABLE 54. COMPARISON OF EXPERIMENTAL AND EMPIRICAL TRANSMITTANCES. (From Smith, 1969 [24].)

Spectral interval (cm^{-1})	H_2O	Pressure	Transmittance	
			Exp.	Emp.
	G/cm^2	Atm.		
200 - 250	0.0030	0.0273	0.781	0.803
200 - 250	0.0140	0.2690	0.213	0.215
200 - 250	0.0350	0.2760	0.075	0.103
250 - 300	0.0025	0.0280	0.869	0.882
250 - 300	0.0071	0.2530	0.477	0.521
250 - 300	0.0270	0.2690	0.217	0.261
250 - 300	0.1320	0.3270	0.003	0.022
290 - 340	0.0025	0.0280	0.914	0.913
290 - 340	0.0071	0.2530	0.608	0.635
290 - 340	0.0270	0.2690	0.339	0.373
290 - 340	0.1320	0.3270	0.024	0.050
320 - 370	0.0041	0.0300	0.872	0.886
320 - 370	0.0077	0.2670	0.590	0.612
320 - 370	0.0330	0.2750	0.323	0.352
320 - 370	0.1340	0.3170	0.075	0.110
360 - 410	0.0041	0.0300	0.928	0.936
360 - 410	0.0077	0.2670	0.769	0.782
360 - 410	0.0330	0.2750	0.576	0.576
360 - 410	0.1340	0.3170	0.255	0.320
410 - 460	0.0041	0.0300	0.939	0.947
410 - 460	0.0077	0.2670	0.830	0.831
410 - 460	0.0330	0.2750	0.666	0.672
410 - 460	0.1340	0.3170	0.361	0.405
450 - 500	0.0041	0.0300	0.968	0.968
450 - 500	0.0077	0.2670	0.903	0.899
450 - 500	0.0330	0.2750	0.765	0.787
450 - 500	0.1340	0.3170	0.489	0.570

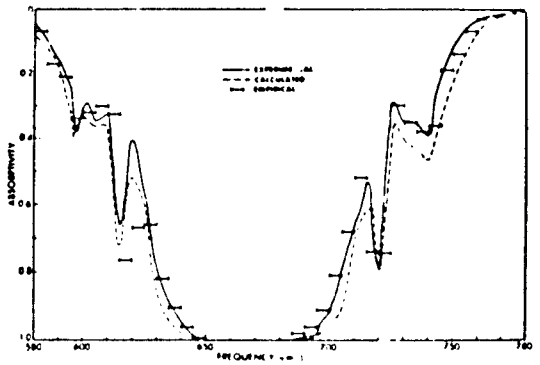

(a) Equivalent pressure - 768 mm Hg; Optical mass - 12.6 atm cm

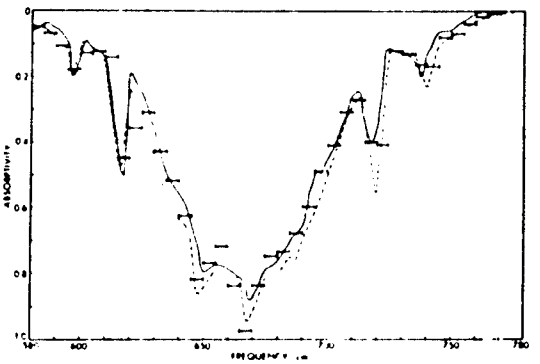

(b) Equivalent pressure - 67.2 mm Hg; Optical mass - 1264 atm cm

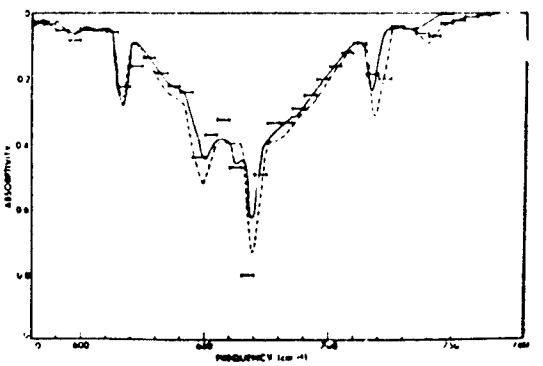

(c) Equivalent pressure - 15.6 mm Hg; Optical mass - 6.3 atm cm

FIGURE 102. COMPARISON BETWEEN EXPERIMENTAL (BURCH ET AL.) AND CALCULATED (DRAYSON AND YOUNG) TRANSMITTANCE SPECTRA FOR CO_2 AND TRANSMITTANCE SPECTRA DERIVED FROM THE EMPIRICAL TRANSMITTANCE COEFFICIENTS GIVEN IN TABLE 53. (Reproduced from Smith, 1969 [24].)

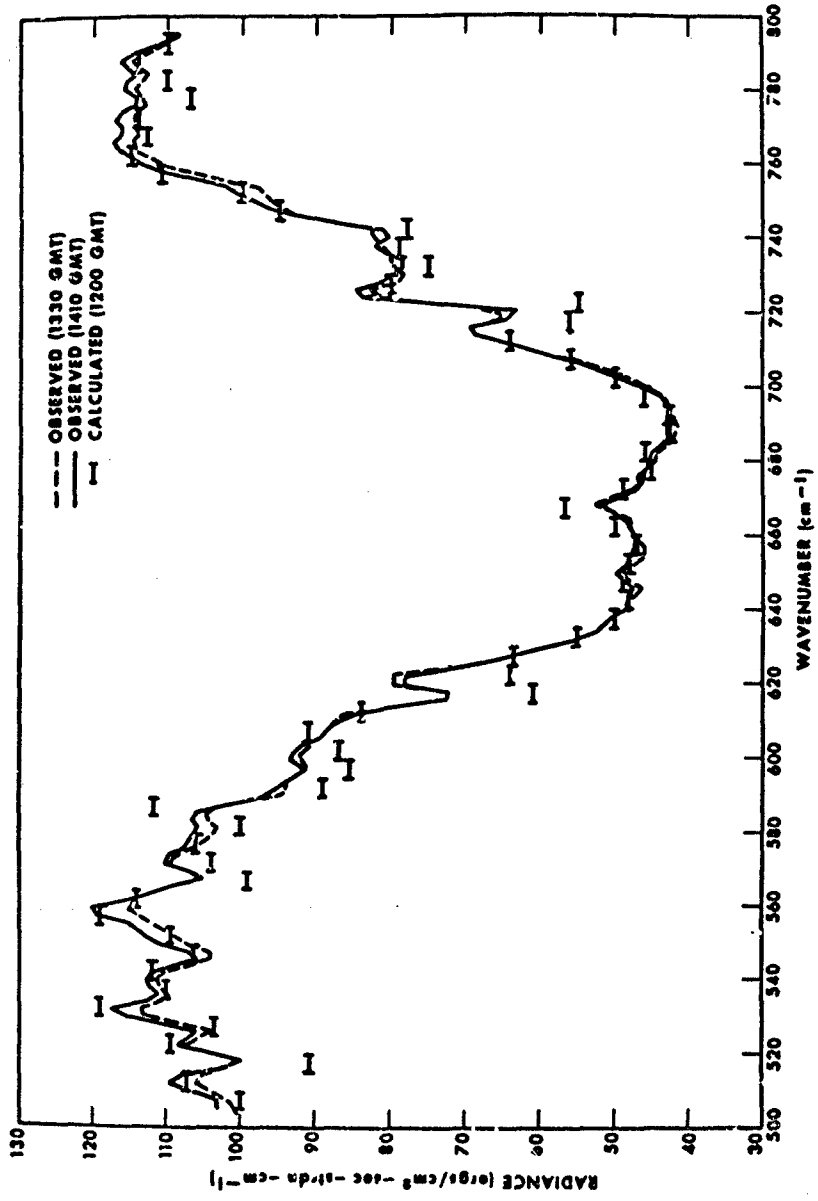

FIGURE 103. COMPARISON BETWEEN OBSERVED (VIA BALLOON-BORNE INTERFEROMETER) AND CALCULATED (VIA EMPIRICAL TRANSMITTANCE COEFFICIENTS) UPWARD RADIANCE SPECTRA NEAR PALESTINE, TEXAS.(Reproduced from Smith, 1969 [24].)

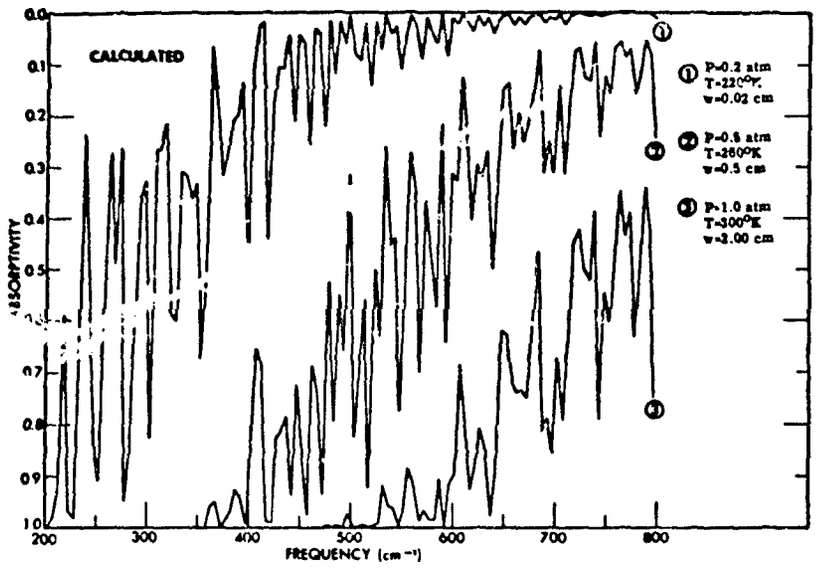

(a)

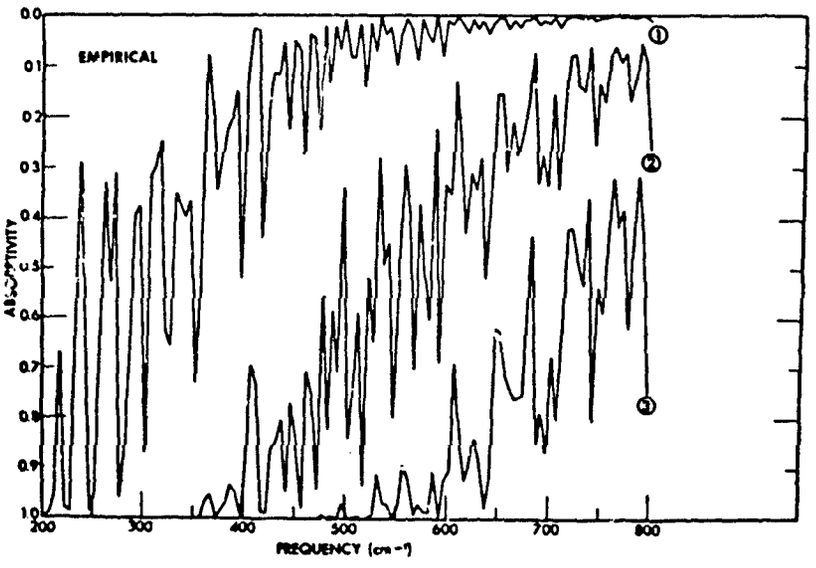

(b)

FIGURE 104. COMPARISON BETWEEN TRANSMITTANCE SPECTRA FOR H_2O CALCULATED BY BOLLE AND TRANSMITTANCE SPECTRA CALCULATED FROM THE EMPIRICAL TRANSMITTANCE COEFFICIENTS GIVEN IN TABLE 52. (Reproduced from Smith, 1939 [24].)

It is interesting to compare qualitatively the models given by Smith and for LOWTRAN 2. Prior to the logarithmic extraction of Eq. (402), the comparisons would show for a given center frequency, ν:

Smith: $\tau = \exp\left[-aw^{b}P^{c}T^{d}\right]$ which, for T = const,

becomes $\tau = \exp\left[-aw^{b}P^{c}\right]$; and

LOWTRAN: $\tau = f[CwP^{n}]$.

The similarities are striking, although actually the comparison is not complete, because Smith takes the next step and produces a polynomial to which he adds a residual term to account for differences between the model and the real world. In this case, it would be more appropriate to compare his model with the (less parameter-studded) models of Zachor and Gibson and Pierluissi, although a direct comparison is not possible without the resources needed to compile band-model parameters for each model in common spectral regions, especially where the model is put to the severest test.

9
LABORATORY MEASUREMENTS, FIELD MEASUREMENTS AND THE RESULTS OF CALCULATION FOR ABSORPTION

9.1 LABORATORY MEASUREMENTS

In the original state-of-the-art report (Anding, 1967) on atmospheric transmittance, a group of laboratory measurements were cited for the purpose of referring the user to original laboratory data which could be used for developing band-model parameters. It would be impossible, or at least impractical, to attempt to cite the innumerable measurements that were made up to the time of Anding's report (1967), or have been made since then. For this report, laboratory measurements are regarded as providing: (1) experimental data on line and band parameters which can be used in a compilation of line-parameter data; and (2) a variety of experimental conditions under which measurements are made, to produce a reliable data base for empirically fitting data to band-model functions and ultimately determining the reliability of band-model parameters.

The reference list of investigations cited in the Bibliography, and used for the compilation of line parameters, represents an excellent cross-section of important laboratory data. As appropriately indicated by Anding (1967), the range of values of experimental parameters should be commensurate with the range expected in actual calculations. Table 55, reproduced from Anding (1967) indicates the values used in some laboratory data on which he compiled information. Selby (1974a) has summarized another significant number of measurements in a table which is reproduced here in Table 56. These are cited by Selby as the important laboratory transmittance measurements which have been used as a basis for the majority of atmospheric transmittance prediction schemes. As would be expected, there is a slight overlap in Tables 55 and 56, with the first leaning toward earlier measurements and the second leaning toward later measurements. Neither is complete, and the reader should consult the literature for a fuller representation of laboratory measurements.

Missing from both tables is a set of data accumulated by Goldman, Bonomo, Williams and Murcray [274] and Goldman, Kyle and Bonomo (1971) on HNO_3. The first reference gives a set of data on the 21.8 μm bands at 7 cm^{-1} resolution on pure HNO_3 vapor at 40°C. The cell length ranged from 0.5 to 9.94 cm. Pressures varied from a few mm Hg to near saturation. The second reference gives data on the 5.9, 7.5 and 11.3 μm bands of pure HNO_3 at a resolution of approximately 0.5 cm^{-1}. The cell length was 9.94 cm and the pressure was 4.6 mm Hg. In this reference, tables of band-model parameters are also reported.

274. A. Goldman, Bonomo, Williams and Murcray, Private communication, 1974.

TABLE 55. SUMMARY OF LABORATORY MEASUREMENTS OF HOMOGENEOUS-PATH ABSORPTION SPECTRA

Gas	Band (μ)	Observed Interval	Range of Pressures* (mm Hg)	Range of Absorber, w**	No. of Curves	Resolution† (approx.)	Researchers
CO_2	1.6 & 1.4	6000-7200	75-760	540-8100	13	0.12	Howard et al. (1955)
	2.0	4800-5400	10-760	108-8630	22	0.9 μ	Howard et al. (1955)
	2.7	3300-4100	1-755	11-1619	67	0.07 μ	Howard et al. (1955)
	2.7	3450-3850	14.2-2063	0.164-24.4	32	10-15 cm^{-1}	Burch et al. (1962)
	4.3	2200-2450	3.8-2115	0.0108-22.8	53	5-10 cm^{-1}	Burch et al. (1962)
	4.3 & 4.8	2000-2500	1-735	9-1570	43	0.1 μ	Howard et al. (1955)
	4.3	2250-2450	38-760	1.0-200	10	10 cm^{-1}	Bradford (1963)
	5.2	1800-2000	10-735	104-1570	9	0.1 μ	Howard et al. (1955)
	9.398 & 10.41	900-1100	103-3800	48-11,200	25	5-10 cm^{-1}	Burch et al. (1962)
		720-875	103-3800	305-11,200	14	5-10 cm^{-1}	Burch et al. (1962)
	15	500-900	20-745	1-863	37	0.5 μ	Howard et al. (1955)
		495-975	0.26-3190	0.0118-2470	30	5-10 cm^{-1}	Burch et al. (1962)
H_2O	1.1	8250-9500	9.8-740	0.03-1.93	41	0.13 μ	Howard et al. (1955)
	1.38	6500-8000	3-740	0.026-3.85	62	0.12 μ	Howard et al. (1955)
	1.875	4000-6000	3-740	0.026-3.85	62	0.1 μ	Howard et al. (1955)
	1.875	4950-5800	27.5-862	0.0033-0.101	14	20 cm^{-1}	Burch et al. (1962)
	2.7 & 3.2	2800-4400	2-750	0.017-2.1	114	0.07 μ	Howard et al. (1955)
	2.7	3000-4300	27.5-862	0.0033-0.101	5	20 cm^{-1}	Burch et al. (1962)
	6.3	1000-2200	2.5-742	0.021-1.49	69	0.4 μ	Howard et al. (1955)
	6.3	1200-2200	14.0-805	0.0041	15	6 cm^{-1}	Burch et al. (1962)
H_2O		200-500	0.76-600	0.0041-0.143		5-10 cm^{-1}	Palmer (1957)
O_3	9.6	1000-2560	11.2-744	0.00278-1.968		7 cm^{-1}	Walshaw (1957)
CO	4.686	2000-2250	1-3210	0.00096-22.2	147	25 cm^{-1}	Burch et al. (1962)
	2.347	4100-4400	54-756	38.6-1140	26	15-20 cm^{-1}	Burch et al. (1962)
CH_4	3.311	2700-3200	2-3085	0.015-188	88	25 cm^{-1}	Burch et al. (1962)
	6.452 & 7.657	1100-1800	3.8-3050	0.026-188	86	10 cm^{-1}	Burch et al. (1962)
N_2O	4.0	2400-2650	22.4-746	0.38-12.6	8	20 cm^{-1}	Burch et al. (1962)
	4.5	2100-2300	1.0-3120	0.00016 76.1	177	25 cm^{-1}	Burch et al. (1962)
	4.5	2100-2300	99.8-849	0.01-2.3	65		Abels [260] (1962)
	7.78 & 8.57	1100-1400	3.2-3035	1.37-46.7	11	10 cm^{-1}	Burch et al. (1962)
	14.45 & 16.98	500-800	4.5-851	1.89-359	7	6 cm^{-1}	Burch et al. (1962)

*Pressure designated is generally the equivalent pressure.
**w is expressed in precipitable centimeters for H_2O and in atmospheric centimeters for the other gases.
†Resolution specified is ordinarily center-band resolution and is used only to give an approximate designation.

ERIM
FORMERLY WILLOW RUN LABORATORIES, THE UNIVERSITY OF MICHIGAN

TABLE 56. SUMMARY OF LABORATORY TRANSMITTANCE MEASUREMENTS. (From Selby, 1974 [252].)

Originator	Ref.	Absorber	Wavelength microns	Resolution cm^{-1}	Absorber Concentration	Path Length m	Pressure		Broadening Gas
							Partial mm Hg	Total mm Hg	
Howard, et al., (1955)	[240]	CO_2	1.4, 1.6, 2.0, 2.7, 4.3, 5.2, 15	50-200	1-1000 atm cm	88-1400	1-50	1-740	N_2
Kostkowski (1955)	[261]	CO_2	9.4, 10.4, 12.64	2-5	3-320 atm cm	3.28	7-740	370-740	N_2
Edwards (1960)	[262]	CO_2	1.4, 1.6, 2.7, 4.3, 4.8, 5.2, 9.4, 10.4, 15	20-250	0.5-1225 atm cm	0.388, 1.29	38-760	380-7600	N_2
Burch, et al., (1962)	[234]	CO_2	2.7, 4.3, 10, 15	~5	0.01-11,200 atm cm	0.0155-32	0.26-2920	0.26-3800	N_2
Burch, Gryvnak, and Patty (1964-68)	[263]	CO_2	1-1.4, 1.6, 2, 2.7, 4.3	0.3-2.5	$0.08-8.4\times10^{4}$ atm cm	4-933	0.005-1920	0.005-11,000	N_2
Howard, et al., (1955)	[240]	H_2O	0.94, 1.1, 1.38, 1.87	~100	0.001-3.8 pr cm	88-1936	2-28	2-740	N_2
Daw (1956)	[264]	H_2O	4.2-23						
Bell (1956)	[265]	H_2O	22-200	2.5	4×10^{-5} - 8×10^{-3}	0.125-9.06	3.8-10	760	Air
Yaroslavskii (1959)	[266]	H_2O	20-2500	10-3	0.007-0.0079 pr cm	7.5	10	760	Air
Izatt (1960)	[267]	H_2O	14.5-21.05						
Palmer (1960)	[268]	H_2O	20-40	3-8	0.0041-0.143 pr cm	196	0.015-0.7	0.015-61	N_2
Burch, et al., (1962)	[234]	H_2O	1.87, 2.7, 6.3	6-20	0.0017-0.109 pr cm	0.0155-48.75	2.8-22.5	2.8-775	N_2
Burch, Gryvnak and Patty (1965-73)	[269]	H_2O	0.69-1.98, 2.7, 4.4-6.3	0.4-1.75	0.0017-3.1 pr cm	4-933	4.16-1467	134-7530	N_2
Burch, et al., (1962)	[234]	N_2O	3.9, 4.06, 4.5, 7.8, 8.6, 7.8, 14.5, 17	6-20	1.6×10^{-4} - 359 atm cm	0.0155-16	0.09-760	1-3035	N_2
Burch, et al., (1971)	[270]	N_2O	1.5-1.5, 4.2-13.2	0.2-2.2	0.04-605 atm cm	0.091-900	0.07-10,000	47-10,000	N_2
Burch, et al., (1962)	[234]	CO	4.7, 2.35	15-20	9.6×10^{-4} - 1140 atm cm	0.0155-48.75	3-3000	3-3000	N_2
Burch, et al., (1962)	[234]	CH_4	3.3, 6.45, 7.7	10-25	0.015-188 atm cm	0.0635-16	1.52-100	3-3000	N_2
Summerfield (1941)	[271]	O_3	9.6	~25	0.02-0.5 atm cm	0.90	0.15-4.2	6-760	O_2
Gutowsky and Peterson (1950)	[272]	O_3	4.5 and 9.6	~10	2.7 atm cm	0-1, 0.4	100-200	100-760	O_2
Wilson and Ogg (1950)	[273]	O_3	9.6	~10	0.27 atm cm	0.04	50-760	50-760	O_2
Walshaw (1957)	[133]	O_3	9.6	6.5	0.03-1.5 atm cm	0.065, 0.35	0.5-33	10-760	Dry Air
McCaa and Shaw (1968)	[134]	O_3	3-15	5-40	0.009-36.7 atm cm	0.4, 32	0.002-800	15-1600	O_2
Burch (1970)	[189]	H_2O cont. (T=296K)	8.5-12		5.48×10^{22} mol/cm^2	1185	14.2	14.2	

References to Tables 55 and 56

260. L. A. Abels, A Study of Total Absorption near 4.5 by Two Samples of N_2O, As Their Total Pressure and N_2O Concentrations were Independently Varied, Scientific Report No. 3, AFCRL-62-236, Ohio State University, Columbus, January 1962.

261. E. J. Kostkowski, Half Widths and Intensities from the Infrared Transmission of Thermally Excited CO_2, Progress Report, Office of Naval Research Contract 248(01), Johns Hopkins University, Baltimore, Md., October 1955.

262. D. K. Edwards, et al., J. Opt. Soc. Am., Vol. 50, 1960, pp. 130, 617.

263. D. E. Burch, D. A. Gryvnak and R. R. Patty, Absorption by CO_2 Between 4500 and 5400 cm^{-1} (2 μm Region), Aeronutronic Report U-2955, (1964): 6600 and 7125 cm^{-1} (1.4 μm Region), Aeronutronic Report U-3127 (1965); 8000 and 10,000 cm^{-1} (1 to 1.25 μm Region), Aeronutronic Report U-3200 (1965); 5400 and 6600 cm^{-1} (1.6 μm Region), Aeronutronic Report U-3201 (1965); 1800 and 2850 cm^{-1} (3.5 - 5.6 μm Region), Aeronutronic Report U-3857 (1966); 7125 and 8000 cm^{-1} (1.25 to 1.4 μm Region), Aeronutronic Report U-3930 (1967); 3100 and 4100 cm^{-1} (2.44 to 3.22 μm Region), Aeronutronic Report U-4132 (1968); Philco-Ford Corporation.

264. H. A. Daw, Transmission of Radiation through Water Vapor Subject to Pressure Broadening in the Region 4.2 Microns to 23 Microns, Technical Report No. 10, University of Utah, Salt Lake City, 1956.

265. E. E. Bell, Infrared Techniques and Measurements (Interim Engineering Report for Period July-September 1956 on Contract AF 33(616)-3312), Ohio State University, Columbus, 1956.

266. N. G. Yaroslavskii and A. E. Stanevish, Opt. Spect., Vol. 7, 1959, p. 380, also Optika Spektrosk., Vol. 5, 1958, p. 382.

267. J. R. Izatt, Office of Naval Research Progress Report, Contract No. 248(01), Johns Hopkins University, Baltimore, Maryland, 1960.

268. C. H. Palmer, 1960: see Palmer (1957). Cited incorrectly by Selby (1974).

269. D. E. Burch, D. A. Gryvnak and R. R. Patty, Absorption by H_2O Between 2800 and 4500 cm^{-1} (2.7 μm Region), Aeronutronic Report U-3202 (1965); 5045 and 14,485 cm^{-1} (0.69 to 1.98 μm Region), Aeronutronic Report U-3704 (1966): 1630 and 2245 cm^{-1} (6.13 to 4.44 μm Region), Aeronutronic Report U-5090 (1973); Philco-Ford Corporation.

270. D. E. Burch, D. A. Gryvnak and J. D. Pembrook, Investigation of Infrared Absorption by Nitrous Oxide from 4000 to 6700 cm^{-1} (2.5 to 1.5 μm), Aeronutronic Report U-4943 (1971); 760 to 2380 cm^{-1} (13.2 to 4.2 μm), Aeronutronic Report U-4995 (1971); Philco-Ford Corporation.

271. M. Summerfield, "Pressure Dependence of the Absorption in the 9.6 Micron Band of Ozone," thesis, California Institute of Technology, Pasadena, 1941.

272. H. S. Gutowsky and E. M. Petersen, "The Infrared Spectrum and Structure of Ozone," J. Chem. Phys., Vol. 18, 1950, p. 564.

273. M. K. Wilson and R. A. Ogg, J. Chem. Phys., Vol. 18, 1950, p. 766.

Many measurements have been made by Burch and his coworkers, supported under contract by the Air Force Cambridge Research Laboratories. To cite them would overburden this report. The user who wants access to these reports is best advised to consult either the authors (Burch, et al.); the Defense Documentation Center, whose list is probably incomplete; or the Infrared Information and Analysis (IRIA) Center at the Environmental Research Institute of Michigan, where these documents and other literature can be consulted.

The urgency for the use of laboratory data for formulation of band model parameters has been allayed with the appearance of the AFCRL line-parameter compilation. The methods cited in Section 5 are easily adapted to the use of this compilation for calculating band-model parameters. Laboratory data, naturally, will always be needed as a check for validity, inasmuch as the line-parameters are less than perfect. The compilers of these parameters readily acknowledge that they are neither perfectly accurate nor complete. In addition, certain assumptions must be made about line shapes and strengths and their dependencies on physical conditions. Thus, the need for laboratory data will always exist for band-model predictions, although the emphasis on them may have shifted to the delineation of more fundamental parameters associated with the very basic nature of the individual lines.

9.2 FIELD MEASUREMENTS

The most direct, and probably the surest, way of checking the fidelity of a method of calculation atmospheric transmittance or radiance is to compare results obtained from the method with the results of experimental measurements. One technique involves laboratory measurements, of which a few were cited in Section 9.1. But the scope of laboratory experiments is narrow, and some of the limiting conditions are often difficult to achieve, making it necessary to resort to field measurements. This is especially so since, without laboratory results to achieve limiting parameters, extrapolations must be made to accommodate limiting conditions.

Selby ('974a) has compiled a summary of atmospheric transmission field measurements. The list, reproduced in this report in Table 57, is neither appropriately selective nor complete. But it is representative of certain types of measurements which have been performed in the past. Many of these results have been around for a very long time, and have been used by investigators in the past for making comparisons between experimental and calculated results.

Comparisons of results requires a very accurate description of the conditions under which the experiment has been performed. Most of the experiments listed in Table 57 have well documented conditions reported along with the results. It is not always possible,

TABLE 57. SUMMARY OF ATMOSPHERIC TRANSMISSION FIELD MEASUREMENTS.
(From Selby, 1974 [252].)

Originator	Ref.	Wavelength Range (Microns)	Resolution cm^{-1}	Path Length km	Water Vapor Content (pr cms)	Altitude km	Notes
Gebbie, et al., (1951)	[253]	1-14	5	2.26, 4.4	1.7	0.03	Visual Range 14.5 km
Arnulf, et al., (1957)	[275]	0.35-10	30	0.05-1.2		0	Fog, Haze Transmittance
Taylor and Yates (1957)	[249]	0.5-15	3-60	0.3, 5.5, 16.25	11-38	0	Over Water
Yates (1956)	[276]	0.5-15	3-60	27.7	8-20	0.3	Horizontal Paths
Yates and Taylor (1960)	[248]	0.5-26	1-50	0.3	0.22-0.57	0 and 3	Horizontal Paths
Farmer, et al., (1962)	[277]	3.7-5.5	5	0.77, 1.9, 8.4	0.24-1.9	5.2	Horizontal Paths
Curcio, et al., (1964)	[281]	0.54-0.85	0.4	16.25	22	0	Relative Transmittance
Street (1968)	[250]	0.56-10.7	50	25	21.5-43.3	0	----
Filippov, et al., (1969)	[278]	0.59-12	2.6-6	1.3, 2.6	0.047-3.5	0	Visual Range 1.5-20 km
Ashley, et al., (1971-72)	[279]	1.9-5.4 4-14	2.5-6	0.057-11	0.01-10	0 and 0.1	No Visual Range Data

275. A. Armulf, J. Bricard, E. Cure and C. Veret, J. Opt. Soc. Am., Vol. 47, 1957, p. 491.

276. H. W. Yates, The Absorption Spectrum from 0.5 to 25 microns of a 1000 ft. Atmospheric Path at Sea Level, NRL Report 5033, Naval Research Laboratory, Washington, D. C., September 1957.

277. C. B. Farmer, P. J. Berry and D. B. Lloyd, Atmospheric Transmission Measurements in the 3.5 - 5.5 micron band at 5,200 m. Altitude, EMI Electronics Report DMP 1578, Hayes, Middlesex, England, 1963.

278. V. L. Filippov, L. M. Artem'yeva, S. O. Mirumyants, Bull. Izv. Acad. Sci. USSR. Atmos. and Oceanic Physics, Vol. 5, 1969, pp. 521, 742.

279. G. Ashley, L. Gastineau and D. Blay, Unpublished data, 1971-1972.

FORMERLY WILLOW RUN LABORATORIES, THE UNIVERSITY OF MICHIGAN

however, to determine the conditions as accurately as one requires to check the accuracy of a calculation method; nor is it always necessary for the purpose of the measurement. The field experiment, nevertheless, can serve to indicate trends which might be used to check the consistency of a method which is designed to perform calculations in wide spectral regions.

9.2.1 SOME EXAMPLES OF FIELD MEASUREMENTS

Some examples of field measurements are given in this section, starting with one of the older set, that of Gebbie, et al. (1951), used for many years as a means for determination of atmospheric transmittance by extrapolation from experimental results. Figure 105, reproduced from Gebbie, et al. (1951), shows the transmittance per sea mile in the spectral region from 1 to 14 μm for which the visual transmission (at 0.61 μm) was 60% and the water vapor content was 17 mm. The almost classical curves of Taylor and Yates (1957) are reproduced in Figure 106 from an article reported in the journal literature. A broader coverage of the Taylor and Yates experiment can be found in the Handbook of Military Infrared Technology [280], and more still, if available, in the NRL report of the experiment (Yates and Taylor, 1960).

Another set of data on horizontal-path atmospheric transmittance measurements, not reproduced here, is that of Curcio, et al. [281] and Curcio, et al. [282] providing an atmospheric atlas in the spectrum from 5400 to 11,600 A (0.54 to 1.16 μm). Still another set of sea level measurements by Streete, et al. [283] and Streete (1968) provides further basis for comparing computed and measured results, and also for comparing different measured values. The original data (Streete, et al., 1967) are not absolute, and of only limited use. The latter report (Streete, 1968) shows data which are more poorly resolved. These data are not reproduced here.

One of the latest sets of horizontal-, or nearly-horizontal path data to be compiled is that of Ashley (1974). They are the highest-resolution transmittance data available for the long wavelength spectrum out to 14 μm. They are, unfortunately, unavailable in the open literature, being collected as auxiliary data in a continuously-generated set of the measurements of various sources. Samples of these measurements, taken with a Fourier Transform Spectrometer,

280. W. L. Wolfe (ed.), Handbook of Military Infrared Technology, Office of Naval Research, U. S. Government Printing Office, Washington, D. C., 1965.

281. J. Curcio, L. Drummeter and G. Knestrick, Appl. Opt., Vol. 3, No. 12, 1964. p. 1401.

282. J. Curcio, R. Eckardt, C. Acton and T. Cosden, An Atlas of the Absorption of the Atmosphere from 8512 to 11,500 A, Report No. 6352, U. S. Naval Research Laboratory, Washington, D. C., 1965.

283. J. L. Streete, et al., "Near Infrared Atmospheric Absorption over a 25 km Horizontal Path at Sea Level," Appl. Opt., Vol. 6, No. 3, 1967, pp. 489-496.

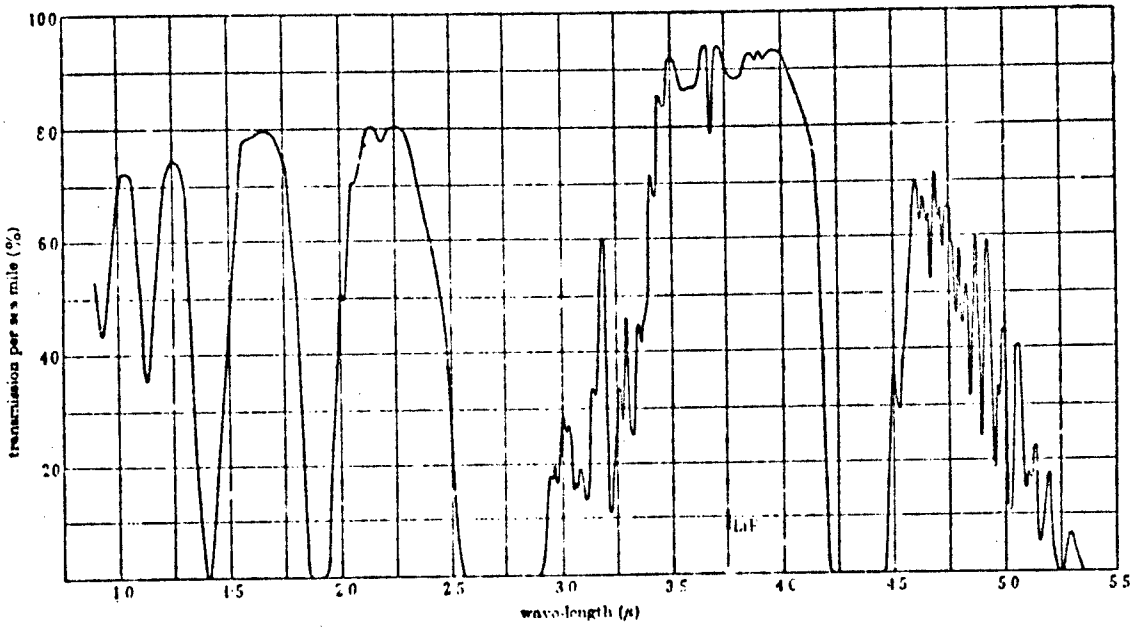

(a) 1 to 5.5 μm

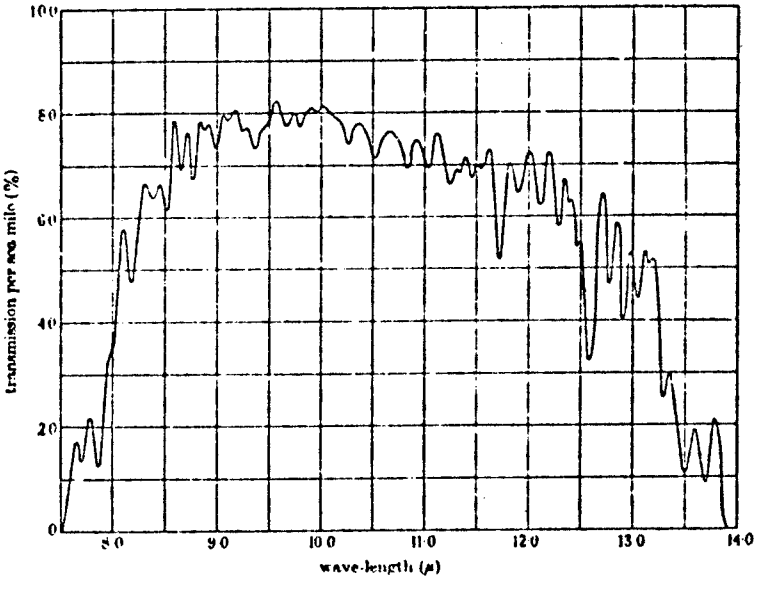

(b) 7.5 to 14 μm

FIGURE 105. ATMOSPHERIC TRANSMISSION. (Visual transmission (0.61 μ) 60% per sea mile; water-content 17 mm.) (Reproduced from Gebbie, et al., 1951 [253].)

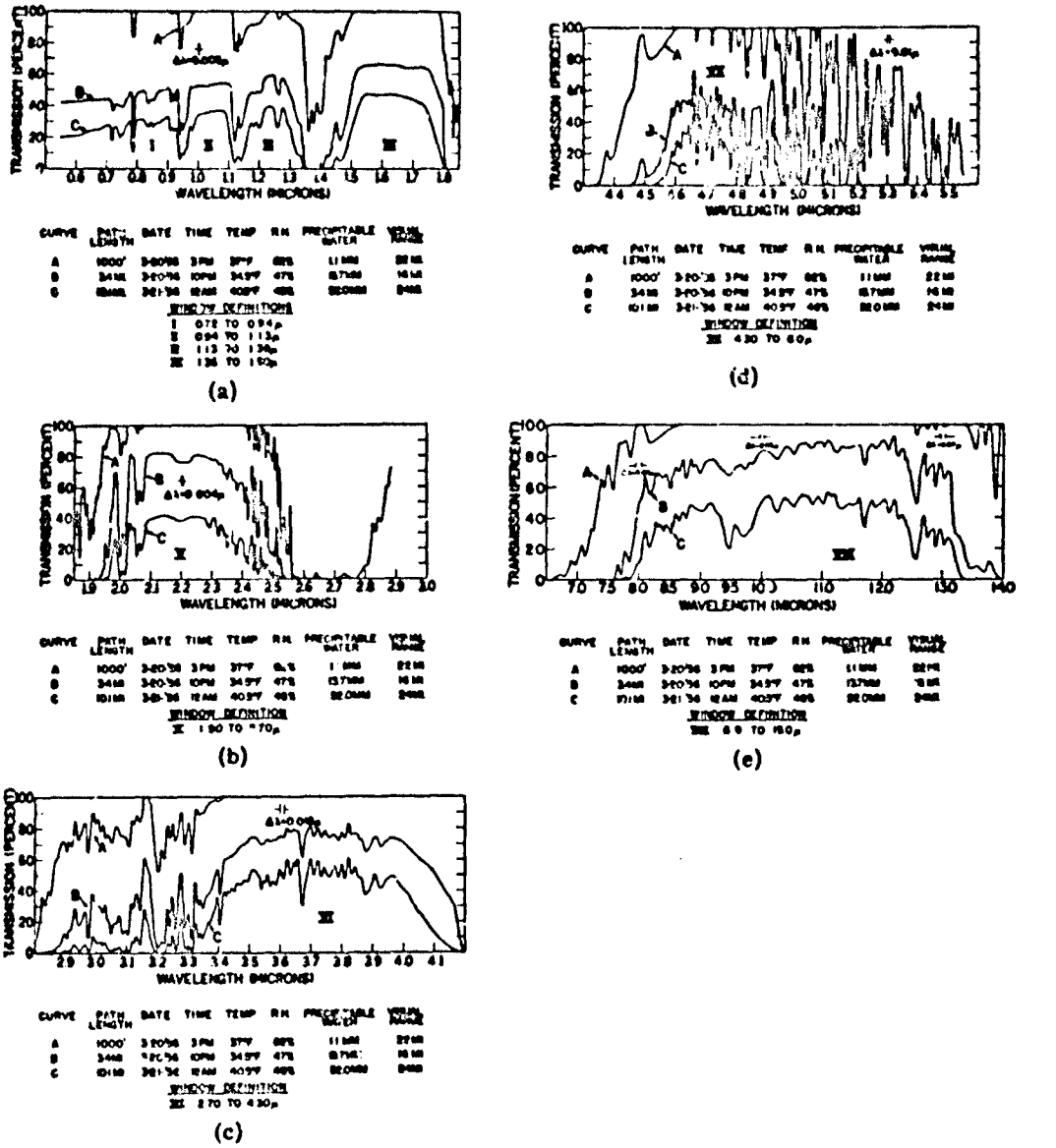

FIGURE 106. ATMOSPHERIC TRANSMISSION SPECTRA. (Reproduced from Taylor and Yates, 1957 [249].)

are shown in Figures 107, 108, 109 and 110. Information on the figures explains the physical conditions. Figure 111 shows a comparison of transmittances for various path lengths. Again, physical conditions are given on the figure.

Horizontal-path measurements are limited in that they do not emphasize atmospheric inhomogeneities. Thus, there is no way to check for variations of factors like line shapes and strengths. On the other hand, measurements through a slant atmospheric path are usually devoid of the necessary auxiliary information to make a valid check with calculation on an absolute basis. Nevertheless, measurements of solar radiation are quite useful, and a great deal can be learned in making comparisons with calculated results. To be sure, solar measurements are useful in and of themselves for determining line positions, atmospheric constituent identifications and concentrations, etc. We shall not dwell here, however, on these types of measurements. The reader is referred to the Bibliography by Laulainen (1972) in which a number of references to solar spectra literature are listed.

9.3 COMPARISONS OF THE CALCULATIONS (See also Sections 6.3, 7.1, 7.2, 7.4, 7.5, 8.1, 8.2 and 8.3.)

Except in the sections describing the various calculation techniques, intercomparisons of results are impossible because the computer programs for performing the calculations either are not available, or are too complex to use without the help of the programmer, through personal interview or documentation. Three exceptions to this fact make it possible to review some of the results discussed in the earlier sections. That is, we have available the programs associated with the Aggregate and LOWTRAN 2 methods, and with Drayson's method. In addition, we have available a model for the atmospheric constituents which is useable in each method, so the differences that arise in the results should be associated only with the specific performance of the calculation method.

To show how atmospheric transmittance in the long wavelength IR region varies with changes in the set of atmospheric parameters used, Figure 112 presents spectra pertaining to the five atmosphere models, described in Section 10, calculated by the Aggregate method. The data of Figure 112 are plotted as a function of wavelength, λ. Figures 113 through 117 show comparisons of the transmittances as functions of wave number, ν, obtained by the Aggregate and the LOWTRAN 2 methods. On the whole, one might comment that the agreement is fair; quite good in certain spectral regions and relatively poor in others. One might also speculate, because of the region in which the greatest disparity exists as a rule (i.e., in the 8 - 14 μm region where the H_2O vapor continuum is important), that the comparative stress on the H_2O vapor continuum between the two models is significant. We note here, by way of explanation, that the differences should reflect only the differences in the techniques used in calculation, since the atmospheric models used in both cases were identical.

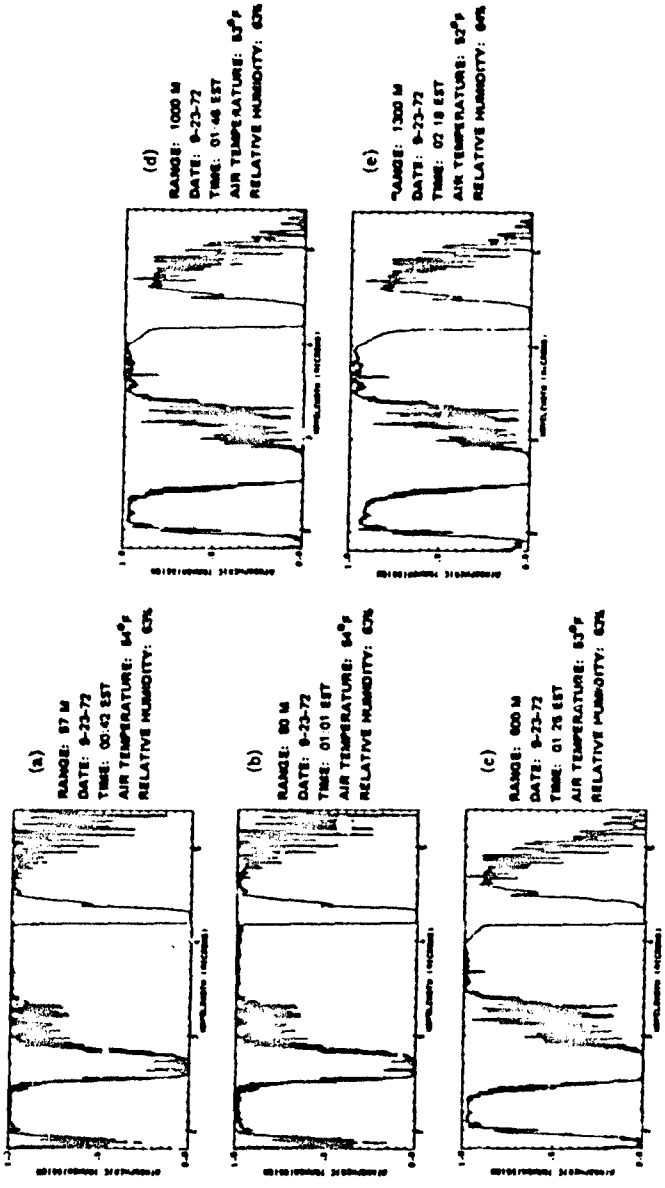

FIGURE 137. ATMOSPHERIC TRANSMISSION MEASUREMENTS FROM 57 TO 1300 METERS IN THE 2-5 μm REGION. (Reproduced from Ashley, private communication.)

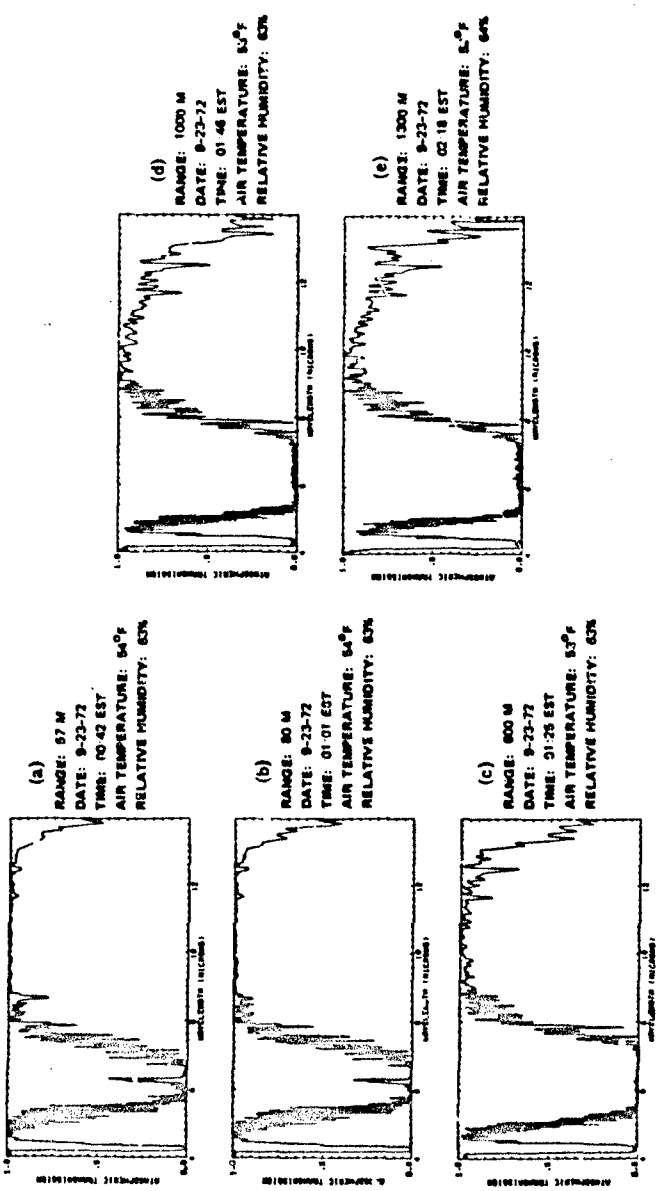

FIGURE 108. ATMOSPHERIC TRANSMISSION MEASUREMENTS FROM 57 TO 1300 METERS IN THE 4-14 μm REGION. (Reproduced from Ashley, private communication.)

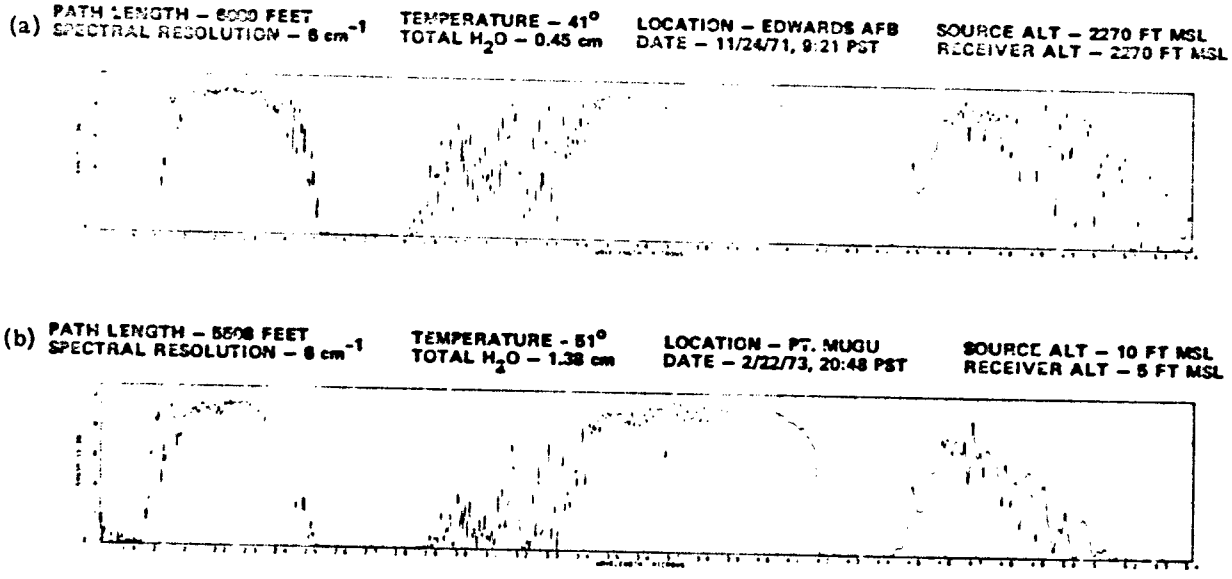

FIGURE 109. TRANSMISSION MEASUREMENTS OF THE ATMOSPHERE AT DESERT AND SEA COAST LOCATIONS. (Reproduced from Ashley, private communication.)

Reproduced from best available copy.

FORMERLY WILLOW RUN LABORATORIES, THE UNIVERSITY OF MICHIGAN

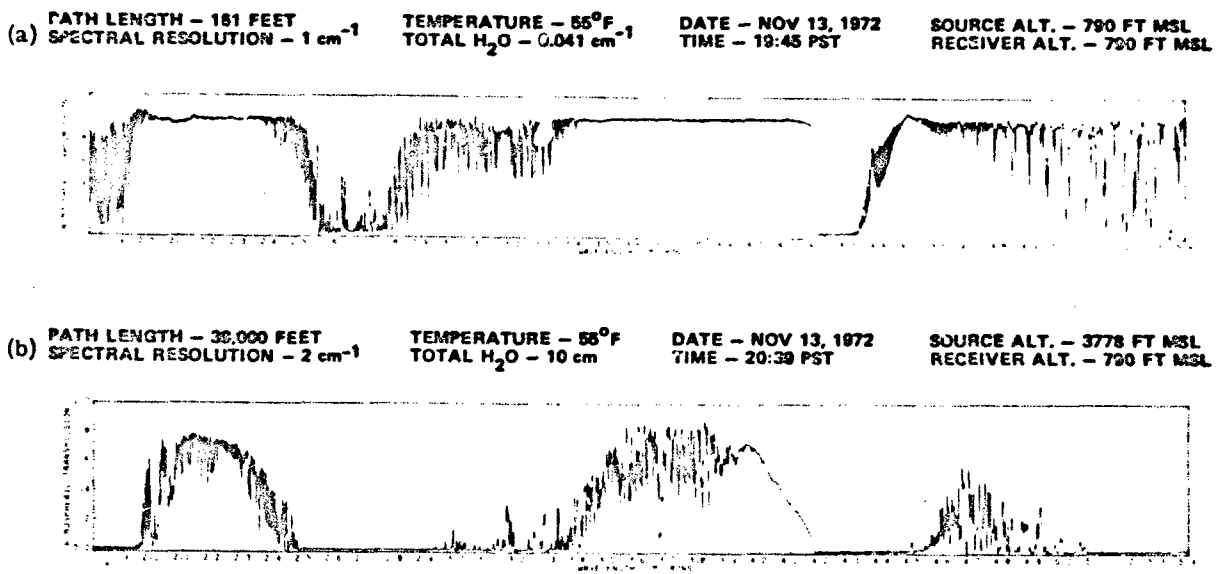

FIGURE 110. HIGH RESOLUTION TRANSMISSION MEASUREMENT OF THE ATMOSPHERE FOR PATH LENGTHS OF 161 FEET AND 39,000 FEET. (Reprcduced from Ashley, private communication.)

ERIM
FORMERLY WILLOW RUN LABORATORIES, THE UNIVERSITY OF MICHIGAN

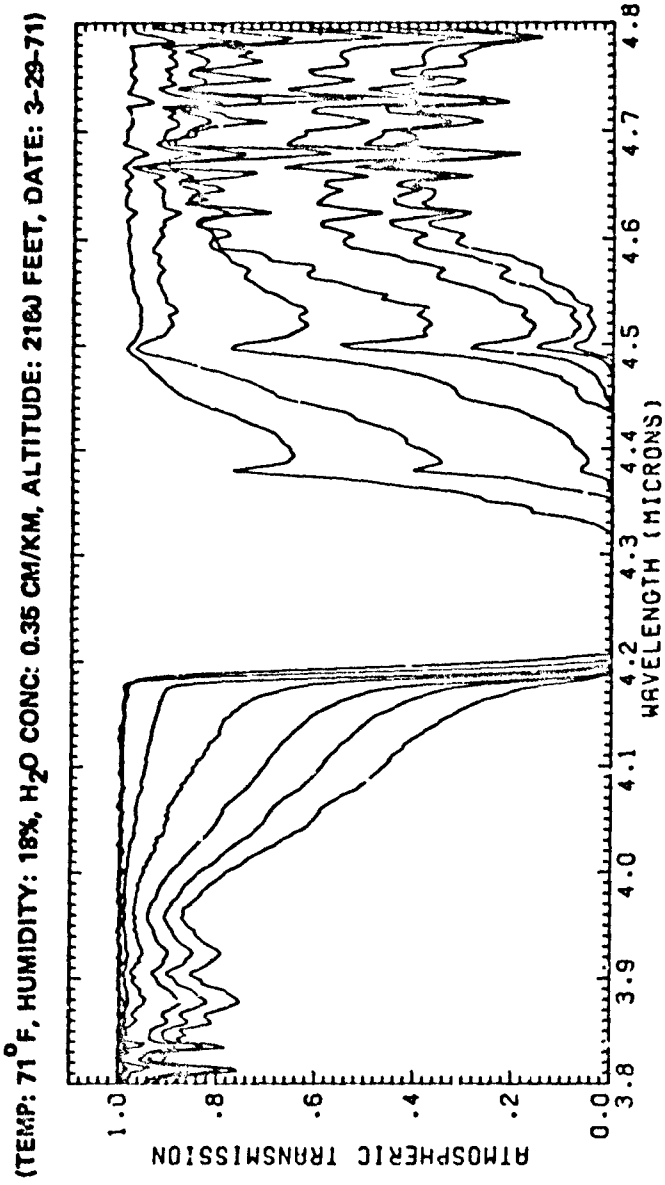

FIGURE 111. ATMOSPHERIC TRANSMISSION. Pathlengths of 150, 559, 1971, 5982, 10,679, 17,906 and 25,896 feet. (Reproduced from Ashley, private communication.)

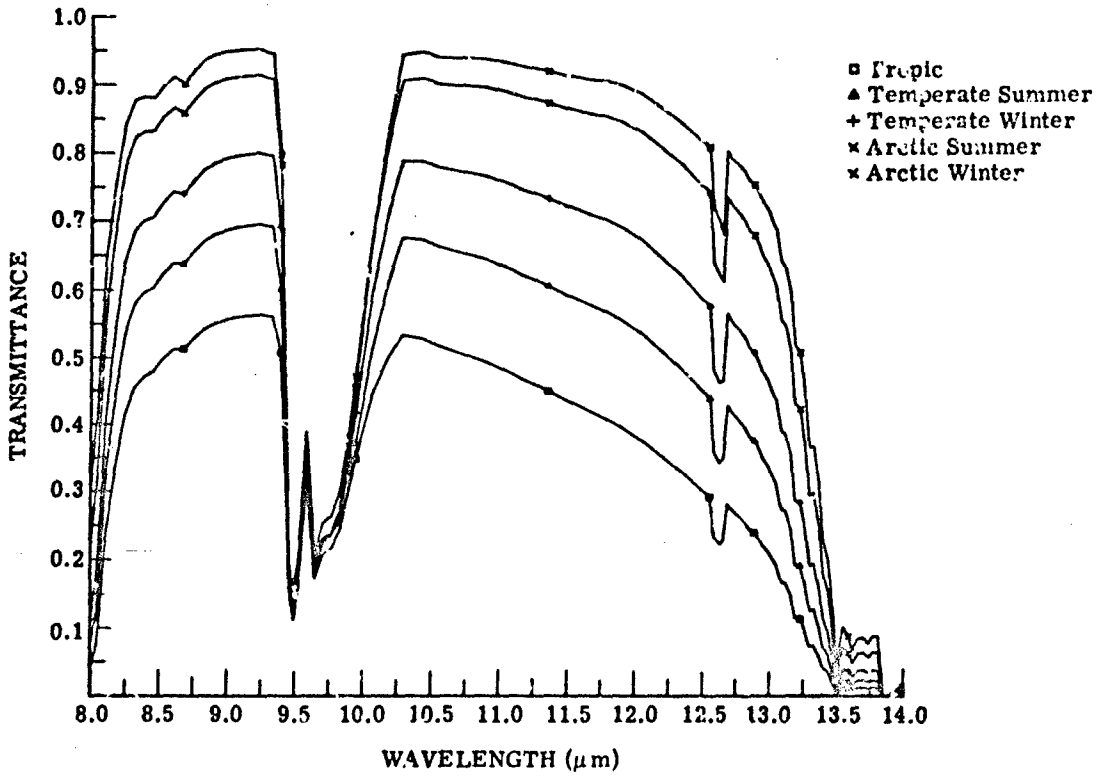

FIGURE 112. TRANSMITTANCE FOR AGGREGATE MODEL ATMOSPHERE IN THE 8-14 μm REGION FOR A VERTICAL PATH LOOKING DOWN FROM 100 km

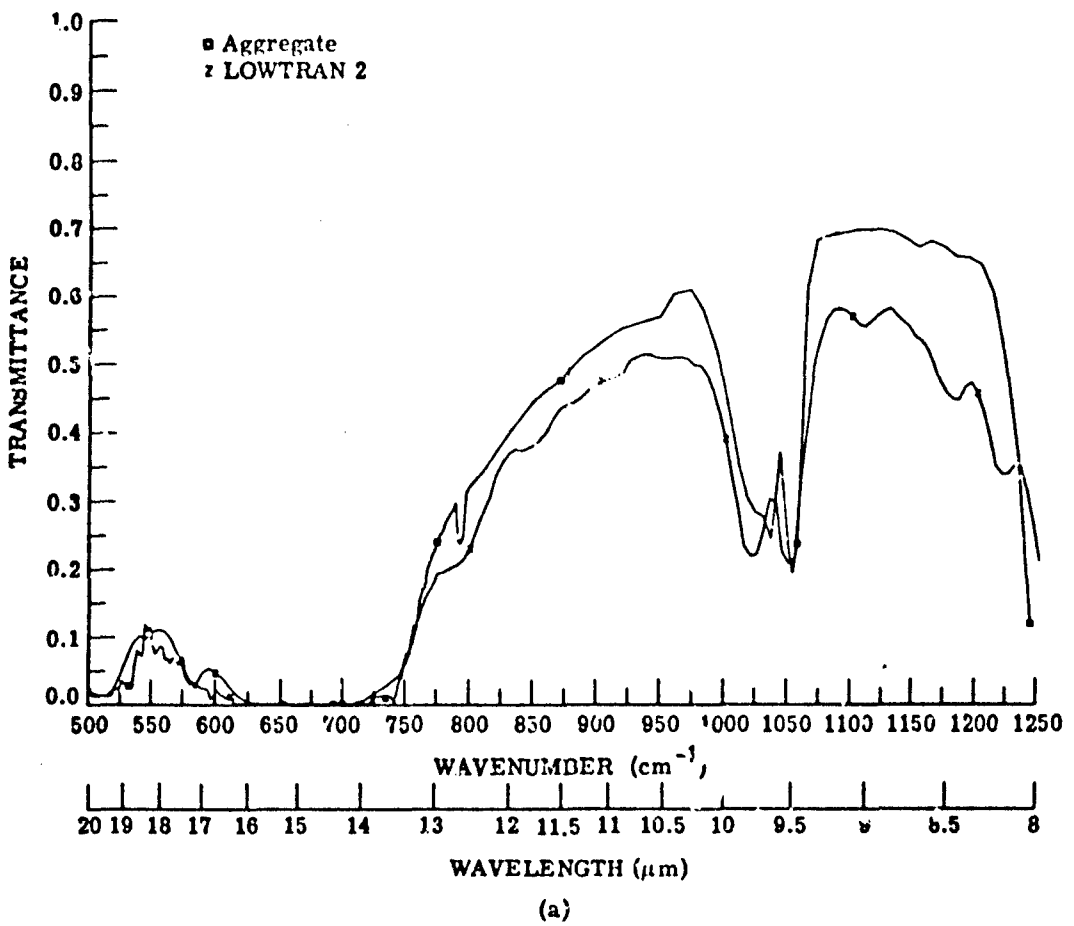

(a)

FIGURE 113. TRANSMITTANCE FOR A VERTICAL PATH LOOKING DOWN FROM 100 km. Tropic model atmosphere.

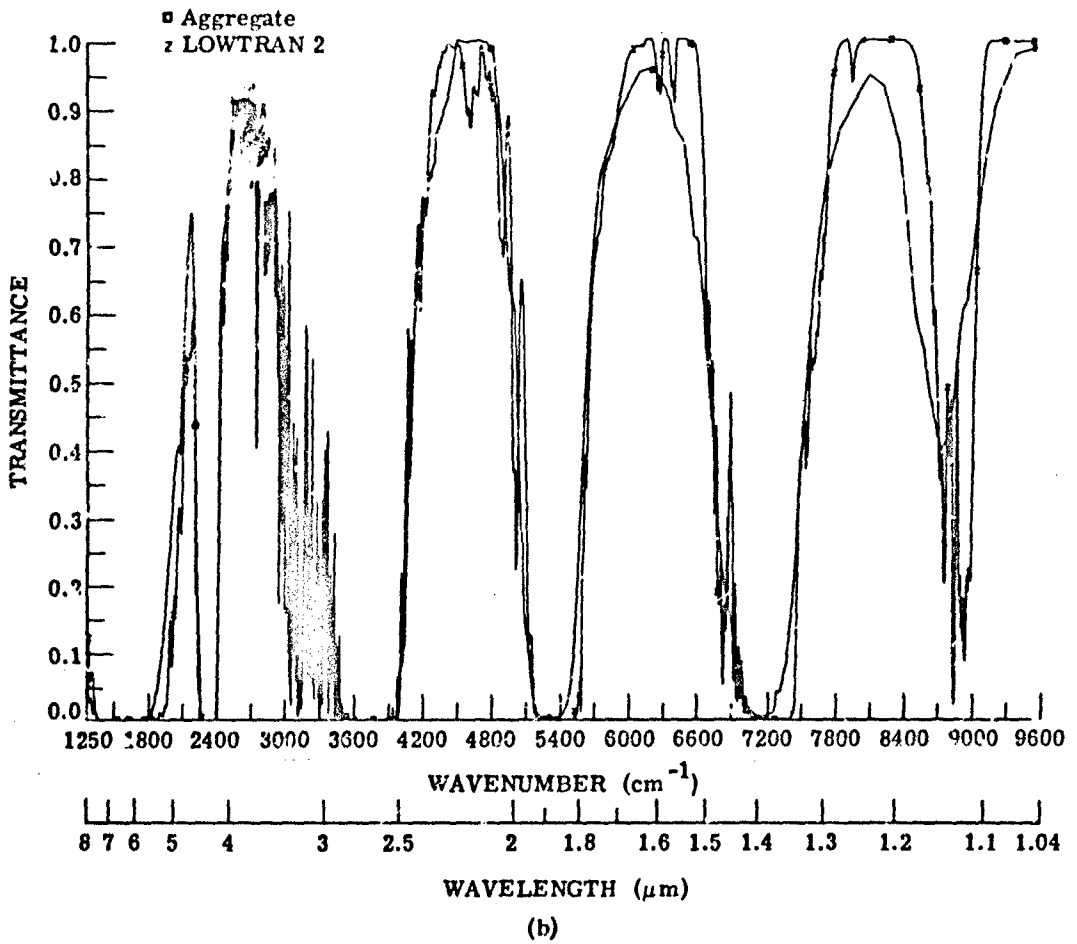

(b)

FIGURE 113. TRANSMITTANCE FOR A VERTICAL PATH LOOKING DOWN FROM 100 km. Tropic model atmosphere. (Concluded)

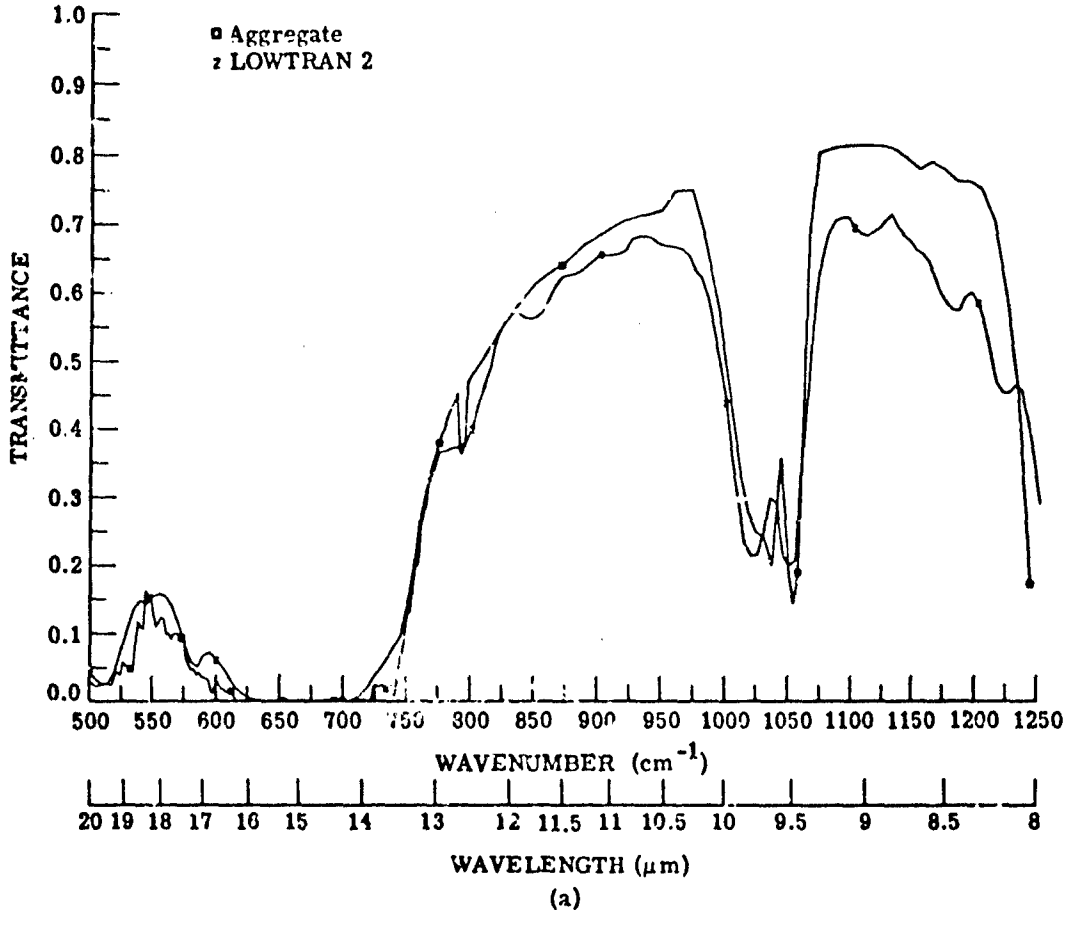

FIGURE 114. TRANSMITTANCE FOR A VERTICAL PATH LOOKING DOWN FROM 100 km. Temperate Summer atmosphere.

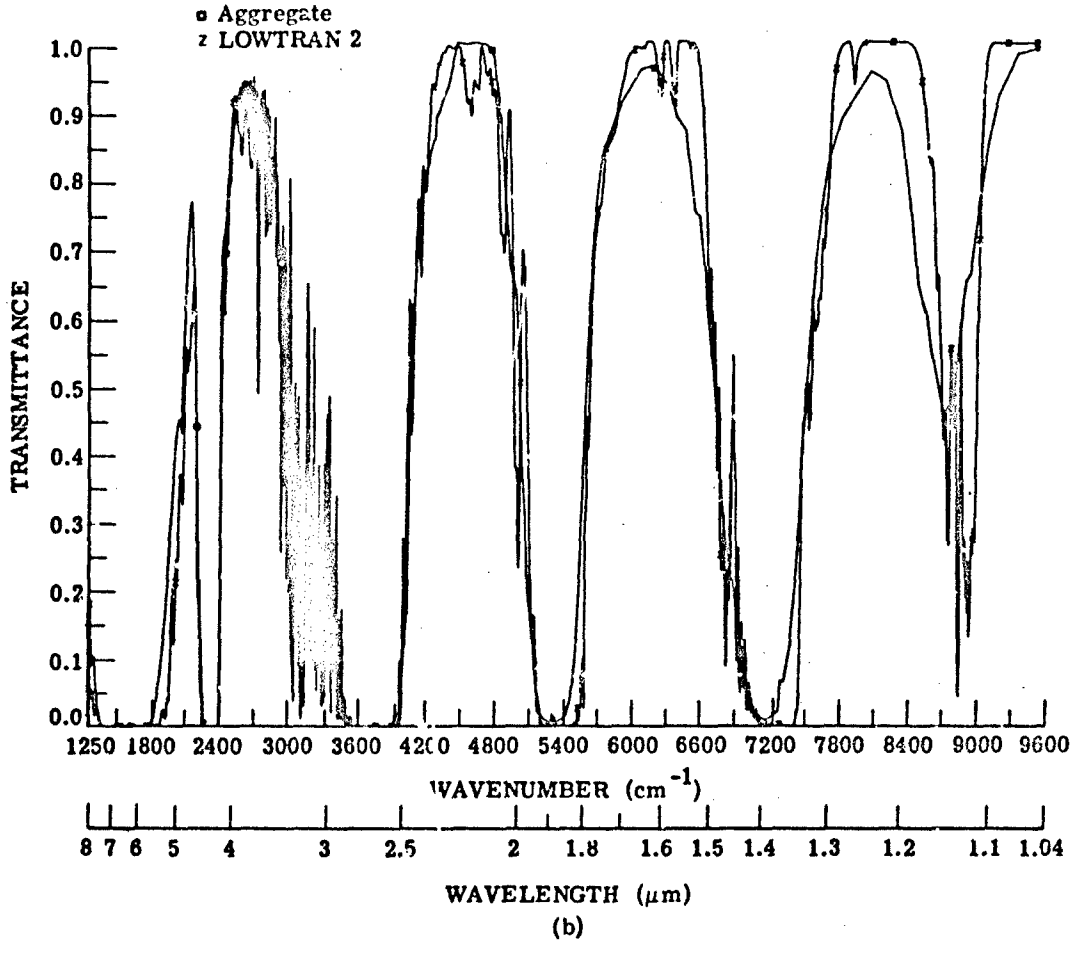

(b)

FIGURE 114. TRANSMITTANCE FOR A VERTICAL PATH LOOKING DOWN FROM 100 km. Temperate Summer atmosphere. (Concluded)

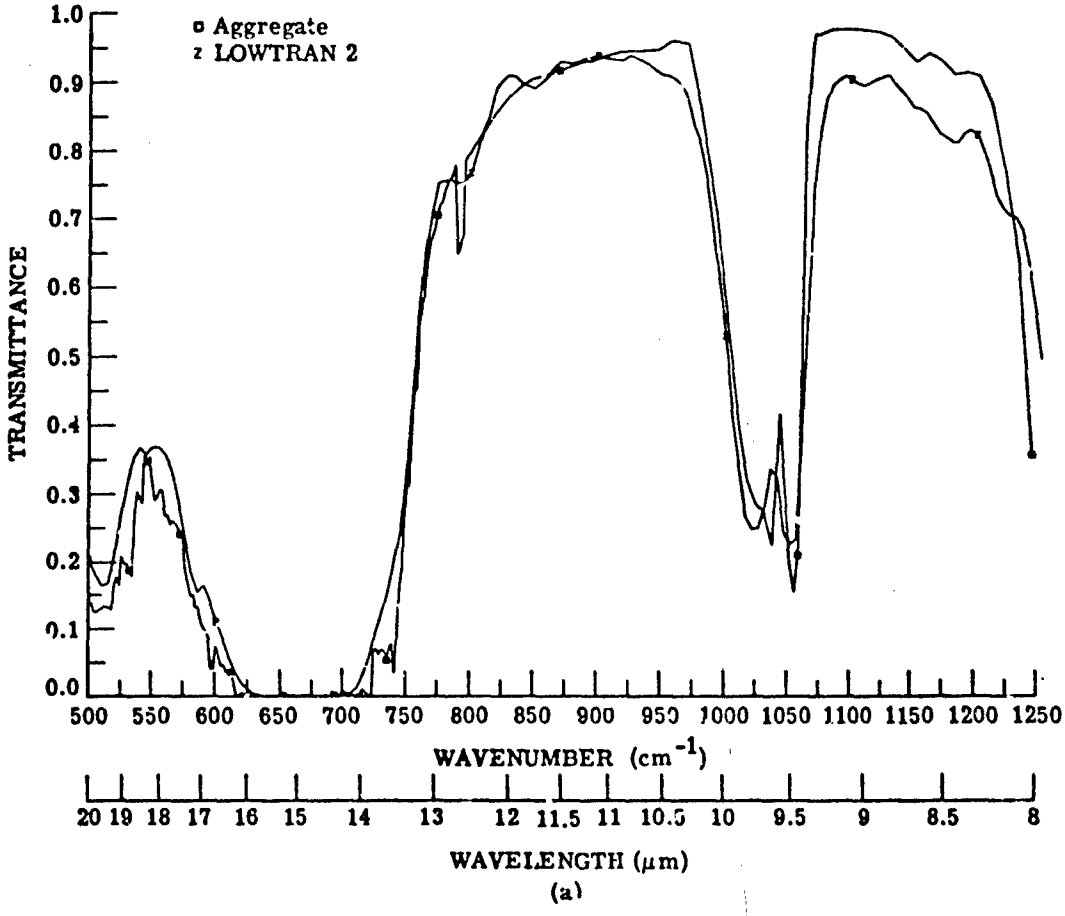

FIGURE 115. TRANSMITTANCE FOR A VERTICAL PATH LOOKING DOWN FROM 100 km. Temperate Winter atmosphere.

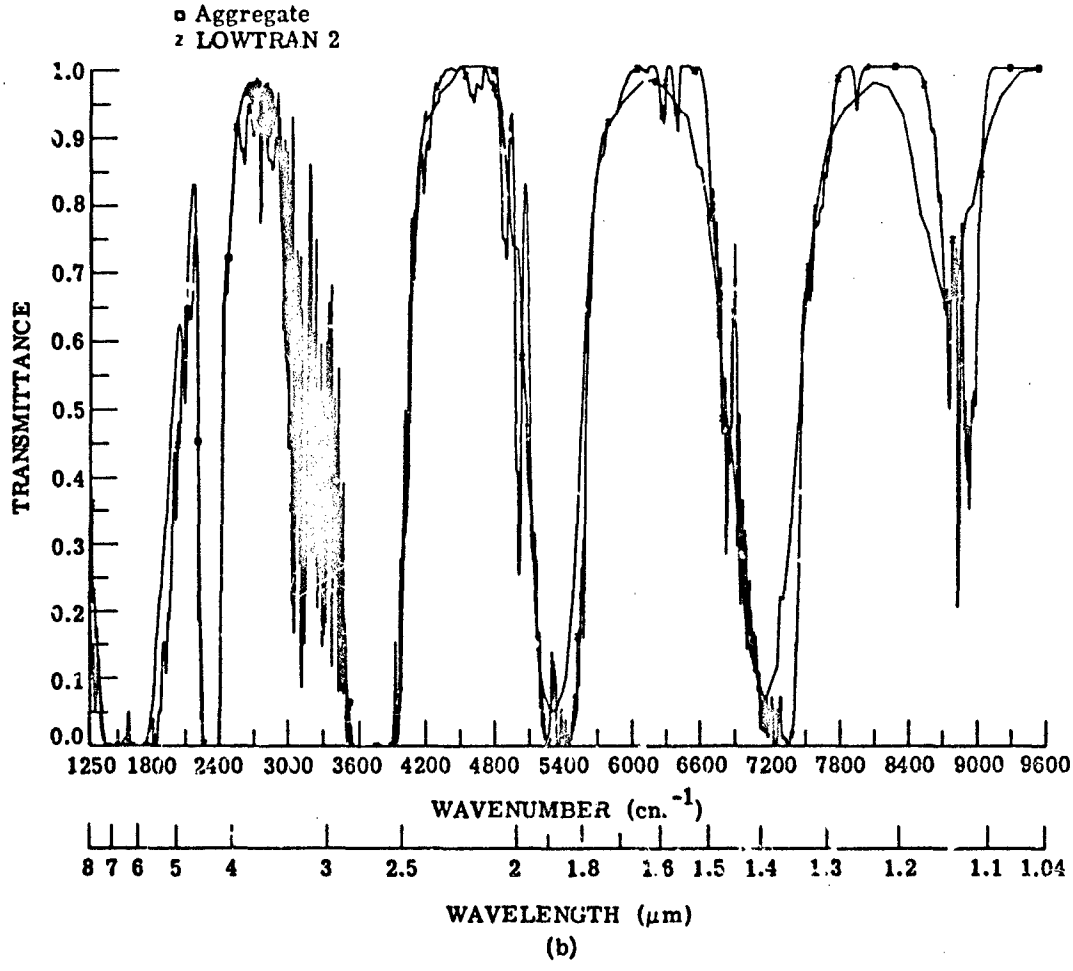

FIGURE 115. TRANSMITTANCE FOR A VERTICAL PATH LOOKING DOWN FROM 100 km. Temperate Winter atmosphere. (Concluded)

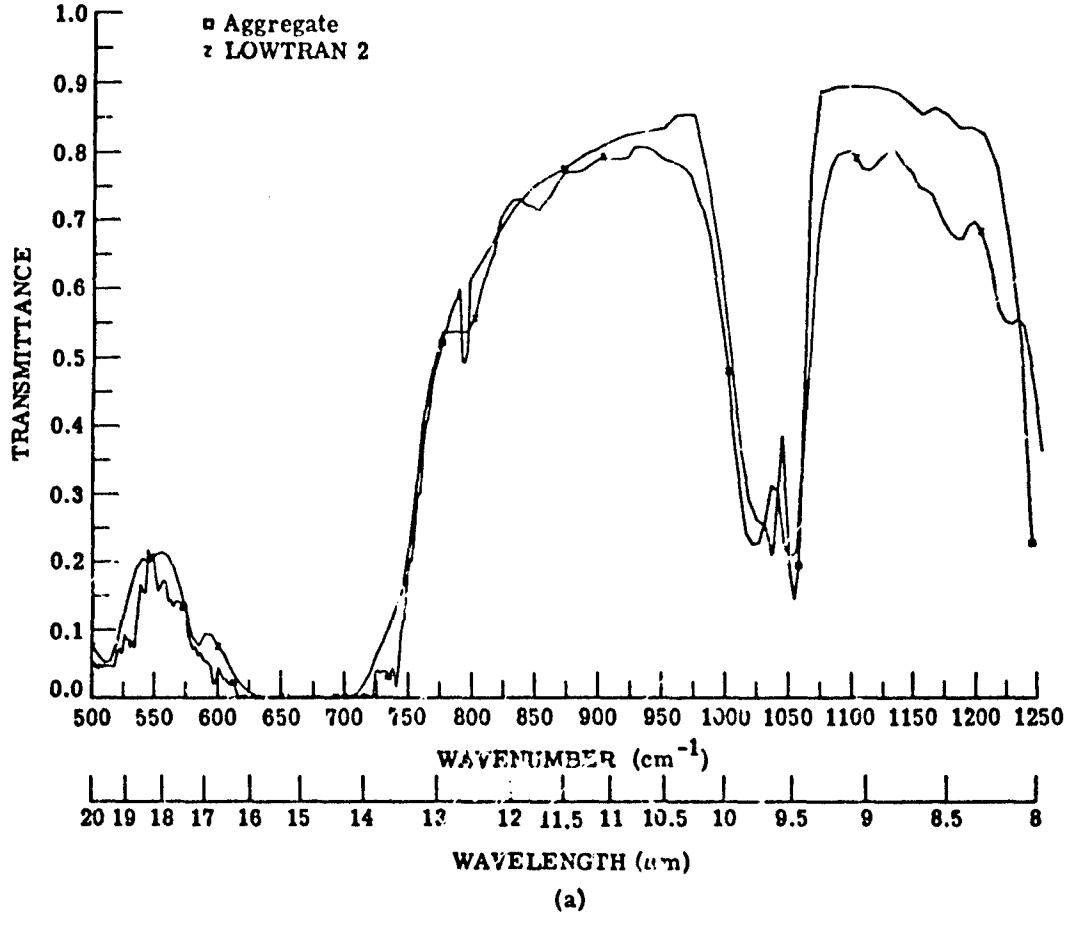

(a)

FIGURE 116. TRANSMITTANCE FOR A VERTICAL PATH LOOKING DOWN FROM 100 km. Arctic Summer atmosphere.

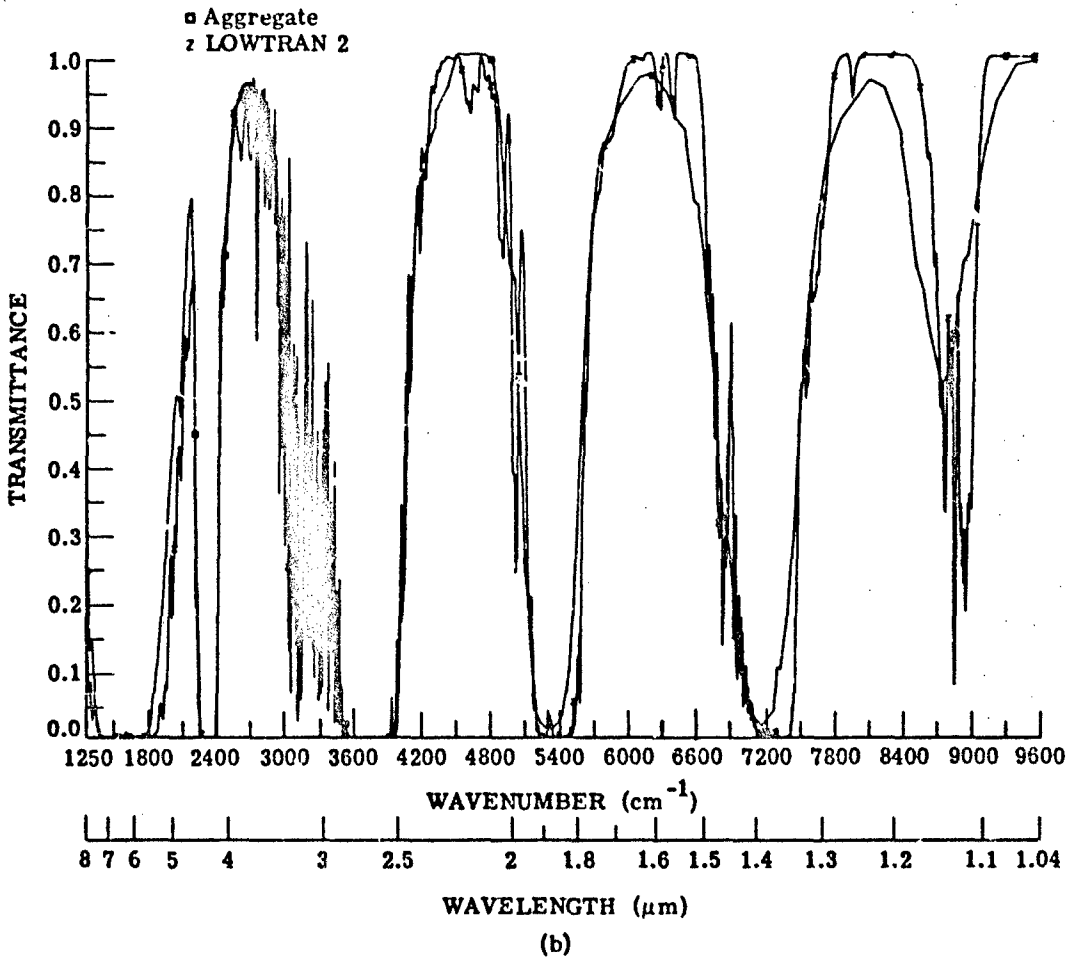

(b)

FIGURE 116. TRANSMITTANCE FOR A VERTICAL PATH LOOKING DOWN FROM 100 km. Arctic Summer atmosphere. (Concluded)

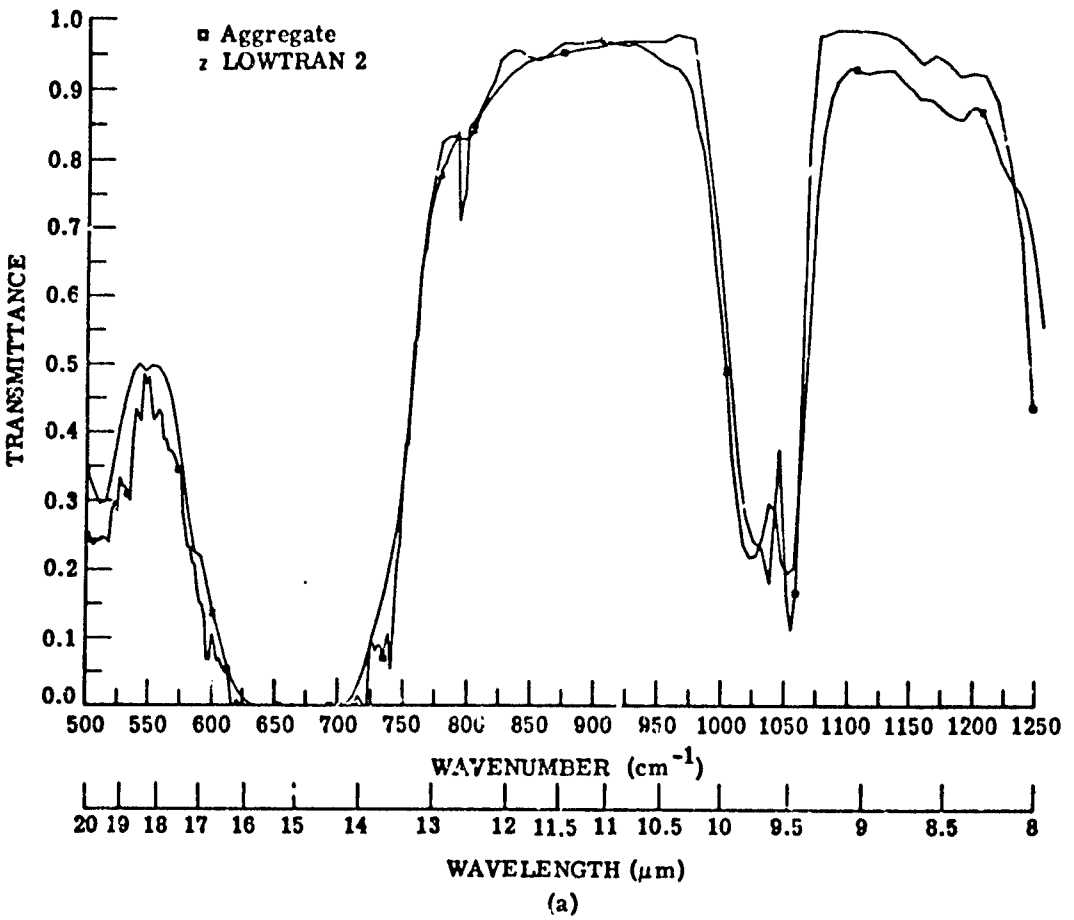

FIGURE 117. TRANSMITTANCE FOR A VERTICAL PATH LOOKING DOWN FROM 100 km. Arctic Winter atmosphere.

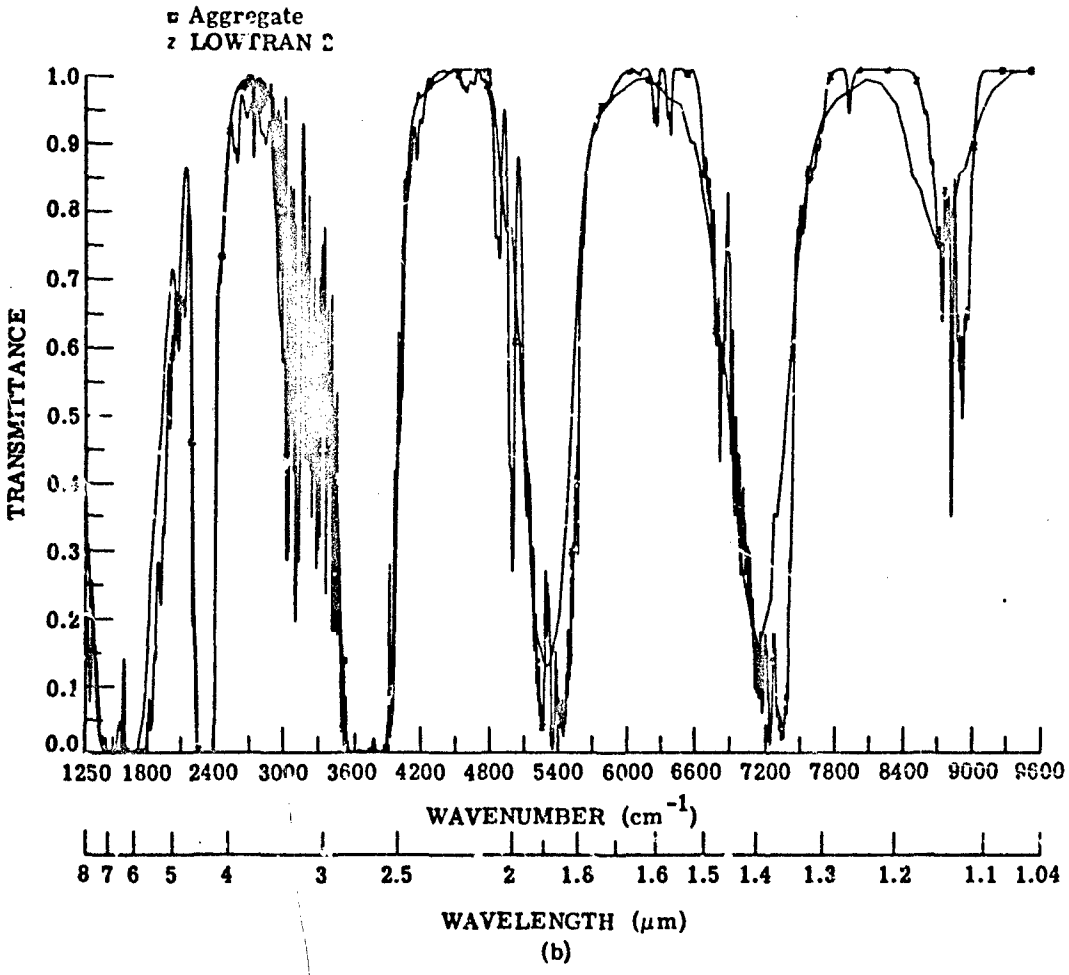

(b)

FIGURE 117. TRANSMITTANCE FOR A VERTICAL PATH LOOKING DOWN FROM 100 km. Arctic Winter atmosphere. (Concluded)

We do not have a program to calculate path radiance using the LOWTRAN 2 method, although to produce one would be no difficult task. Selby (1974a) has provided curves showing the variation of spectral radiance (looking down from space) for six model atmospheres, the five described in Section 10, plus the 1962 U.S. Standard Atmosphere. These curves are compiled in Figure 118. Selby has provided also another set of curves, given in Figure 92, allegedly comparing the radiance calculated using the LOWTRAN 2 transmittance with values presumably observed in a Nimbus experiment. The reference cited is Conrath, et al. (1971), although no reference information is provided. Thus, there is no way to check this result. The figure shows a rather good agreement between the observed and calculated values which were obtained using actual sounding data for the atmospheric parameters. Comparisons with Nimbus data, however, would usually be expected to have limited meaning without specific atmospheric data, because for any set of conditions which could purportedly fit the model atmosphere data, the Nimbus spectral radiance can vary considerably.

This latter fact points out the need for simultaneous measurement of environmental conditions if valid comparisons are to be made. Figure 119 gives evidence of the wide range of spectra one can accumulate from Nimbus measurements, all fitting the standardized atmospheric category of Midlatitude-Winter. The differences are obviously dependent on the particular atmospheric conditions which prevailed at the time of the measurement, including, presumably, actual temperature differences, amounts of ozone and water vapor, presence of clouds, etc. We can choose, incidentally, one spectrum out of another group of Nimbus data which would come close to a spectral radiance curve by the Aggregate method although not the nearly perfect fit shown in Figure 92. (Selby had access to actual sounding data in choosing the fit to Fig. 92.) Figure 120a is a result of the Aggregate calculation using the Midlatitude-Summer atmospheric model (see Section 10). Other curves of spectral radiance calculated using the Aggregate method for various model atmospheres are shown in Figures 121 through 124.

Comparing the spectral radiances of Figure 120 with their counterparts in Figure 92, we find that the values calculated with LOWTRAN are remarkably similar to those using the Aggregate method. Without more information on the manner in which Figure 92 was obtained it is not possible to say anything further about the comparison, especially since the LOWTRAN 2 method predicts generally lower transmittances in this spectral region.

On the other hand, we have made calculations of spectral radiance at two points, 650 and 850 cm^{-1}, using the Drayson program for calculating transmittance. Since the output of the program is an "infinitely" resolved spectrum, we smoothed the data to yield the equivalent of the result which would be obtained by an instrument with a triangular slit function of width 20 cm^{-1}. The 20 cm^{-1} width was used to coincide with that corresponding to the results of the LOWTRAN 2 method. The two values obtained are shown plotted as two points on Figure 120a,

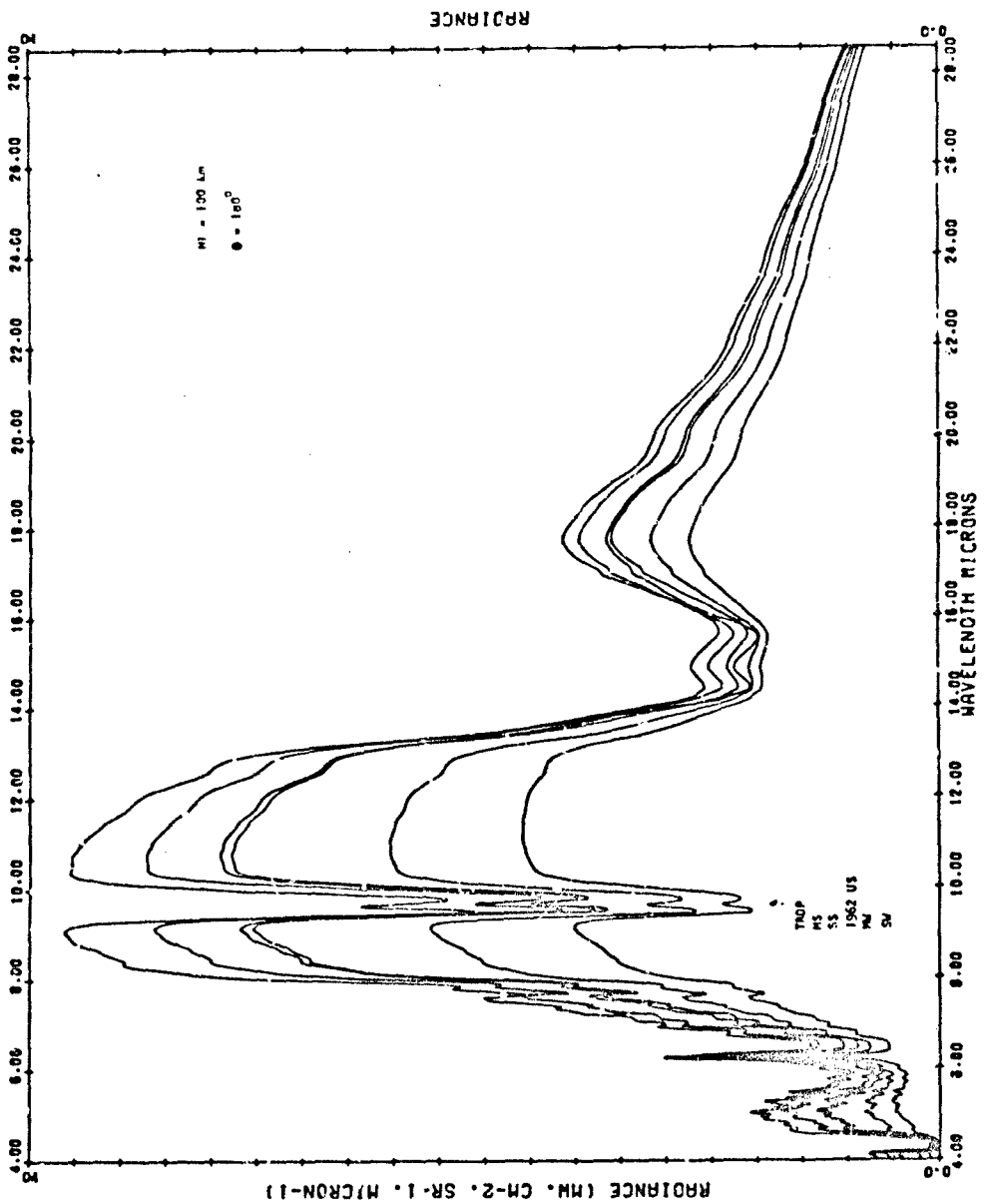

FIGURE 118. LOWTRAN 2 SPECTRAL RADIANCE FOR SIX MODEL ATMOSPHERES

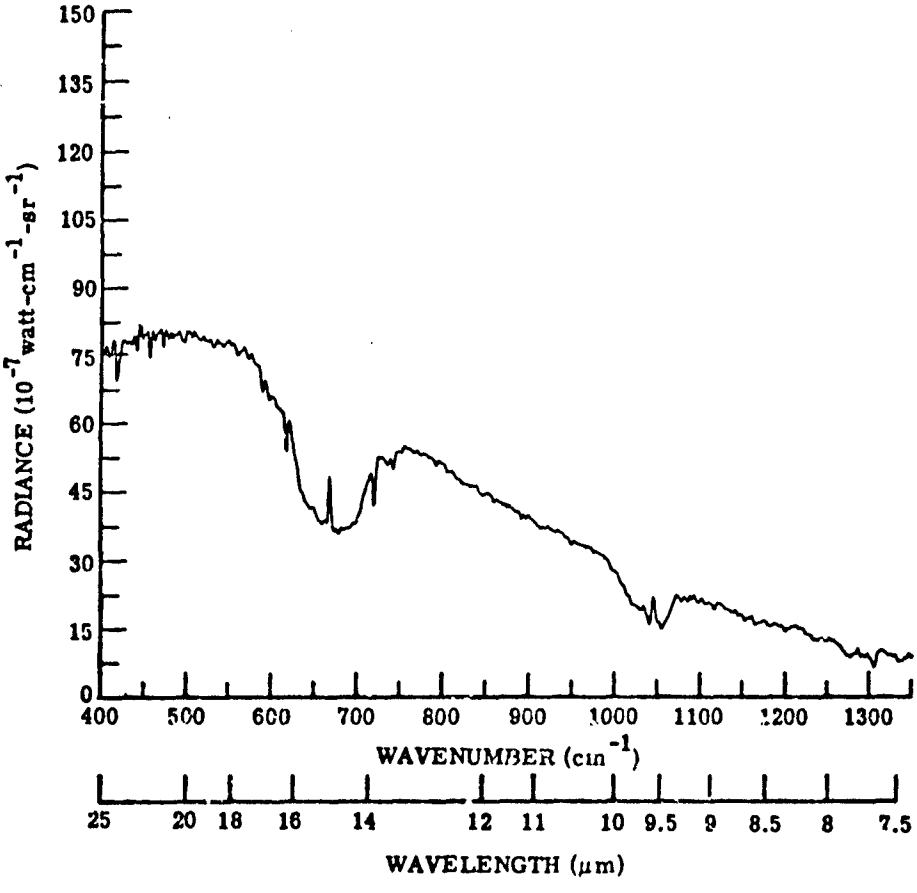

(a) 20 December 1970 at 48.374° latitude and 97.333° longitude

FIGURE 119. NIMBUS IV (IRIS) SATELLITE DATA

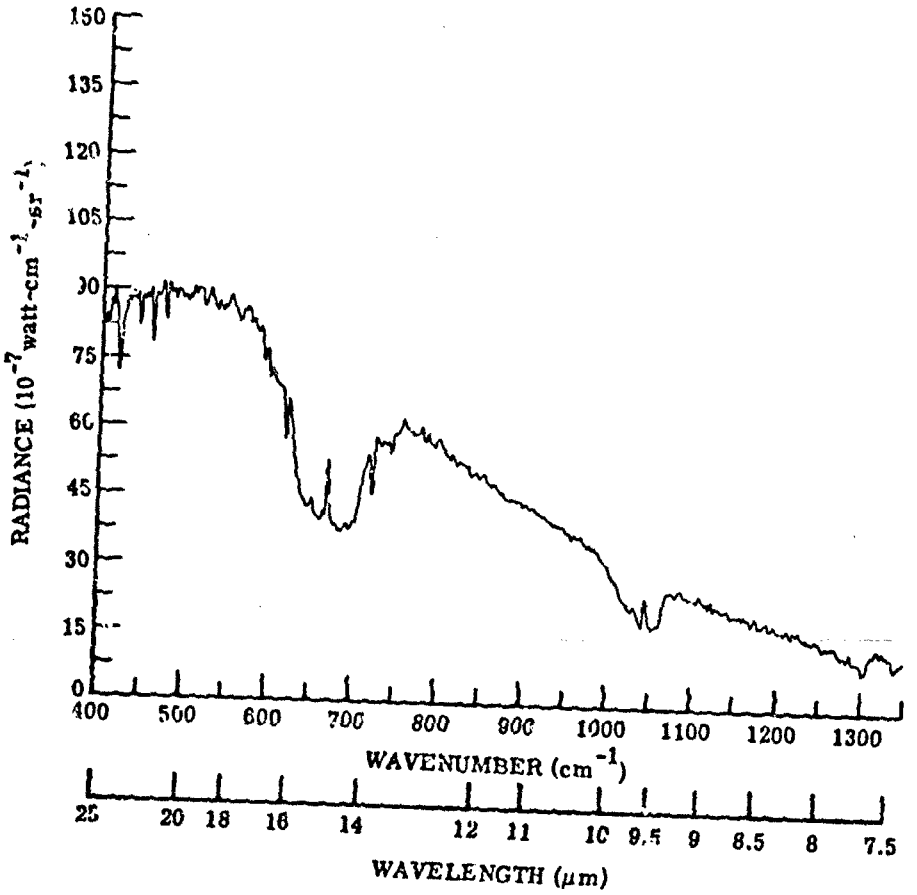

(b) 20 December 1970 at 44.028° latitude and 99.282° longitude

FIGURE 119. NIMBUS IV (IRIS) SATELLITE DATA (Continued)

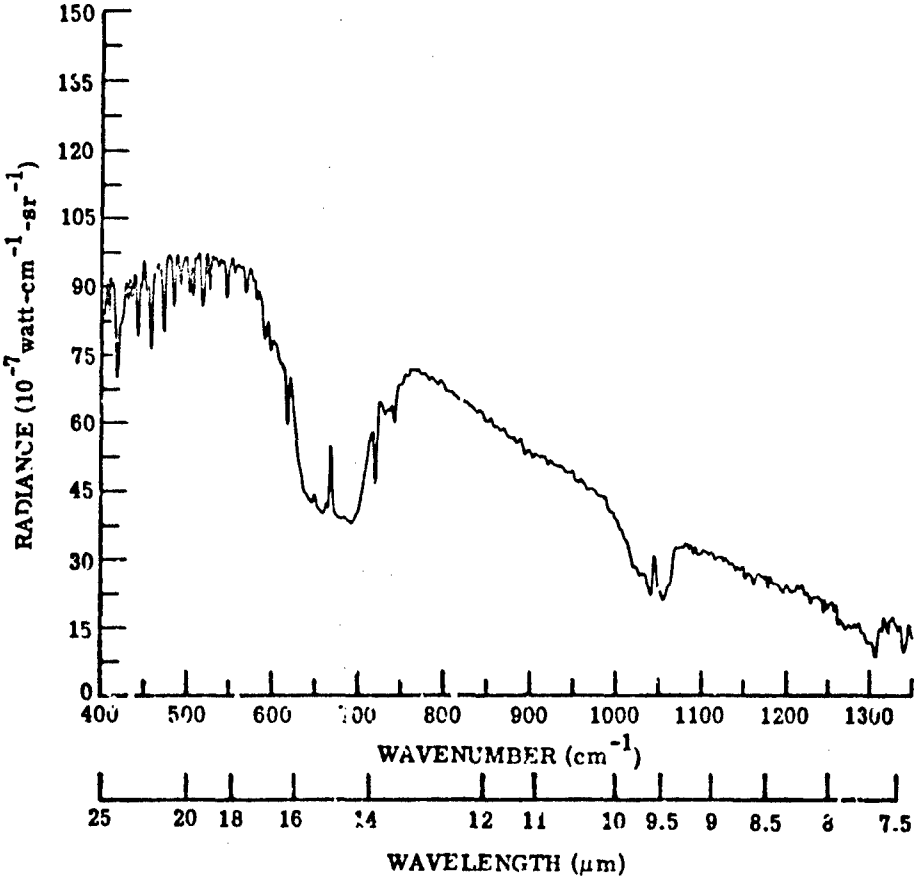

(c) 20 December 1970 at 41.410° latitude and 100.34° longitude

FIGURE 119. NIMBUS IV (IRIS) SATELLITE DATA (Continued)

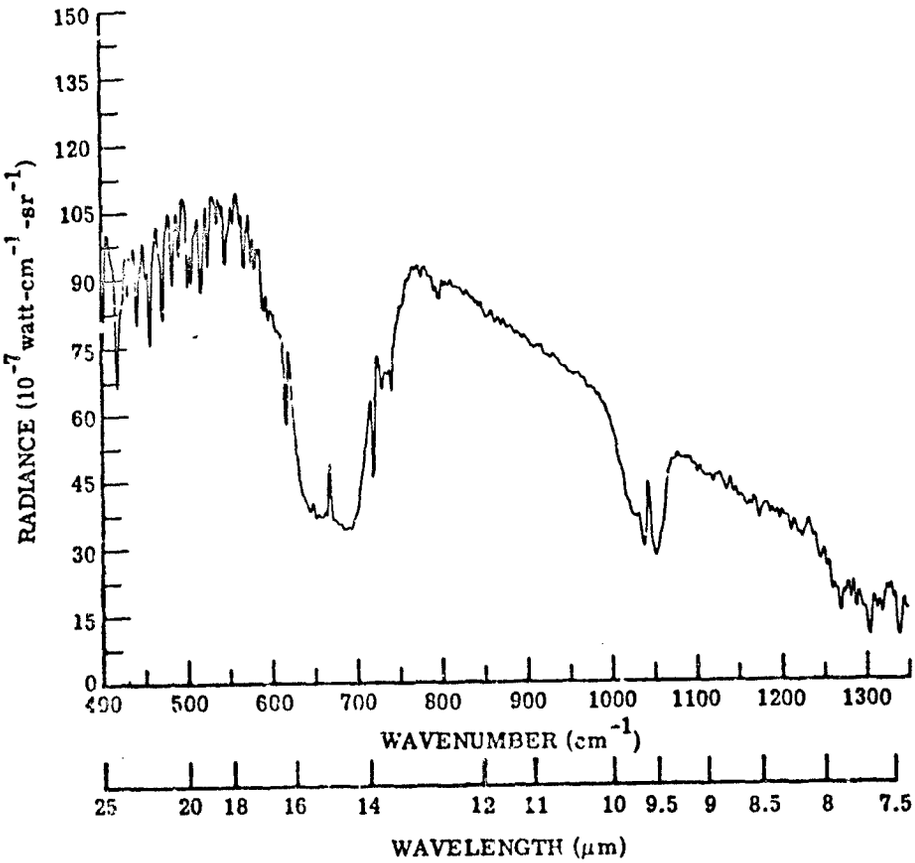

(d) 1 December 1970 at 47.291° latitude and 21.161° longitude (Atlantic Ocean)

FIGURE 119. NIMBUS IV (IRIS) SATELLITE DATA (Continued)

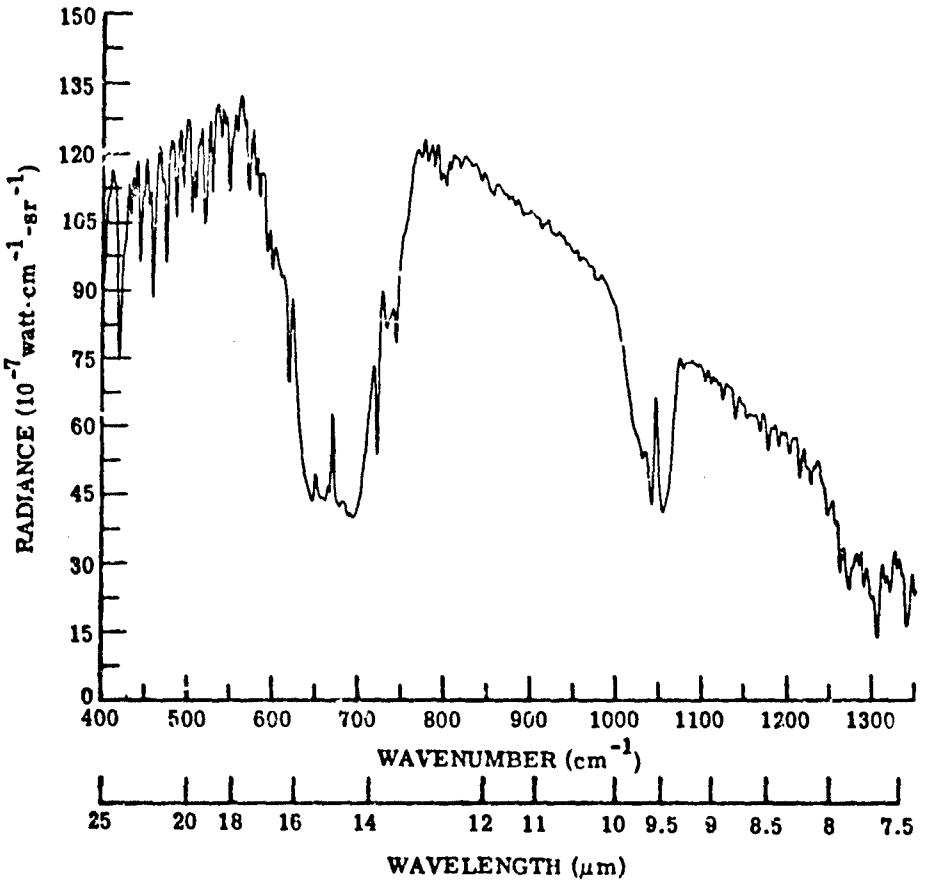

(e) 3 January 1971 at 41.271° latitude and 306.39° longitude

FIGURE 119. NIMBUS IV (IRIS) SATELLITE DATA (Continued)

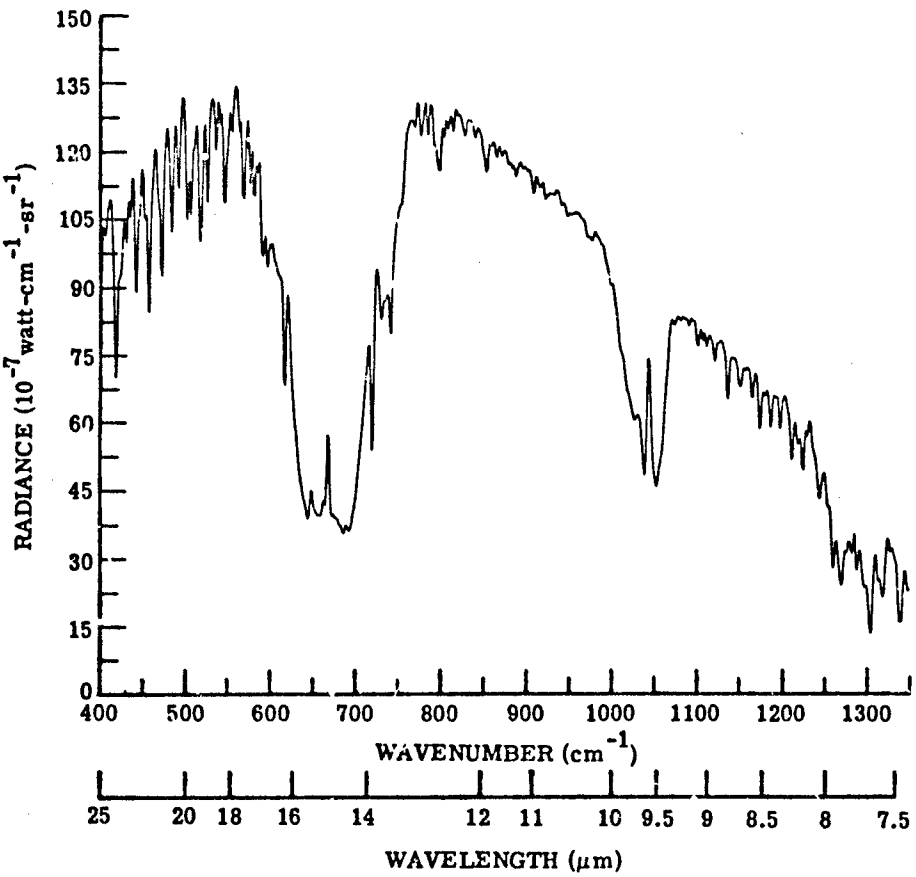

(f) 3 January 1971 at 44.474° latitude and 308.91° longitude

FIGURE 119. NIMBUS IV (IRIS) SATELLITE DATA (Concluded)

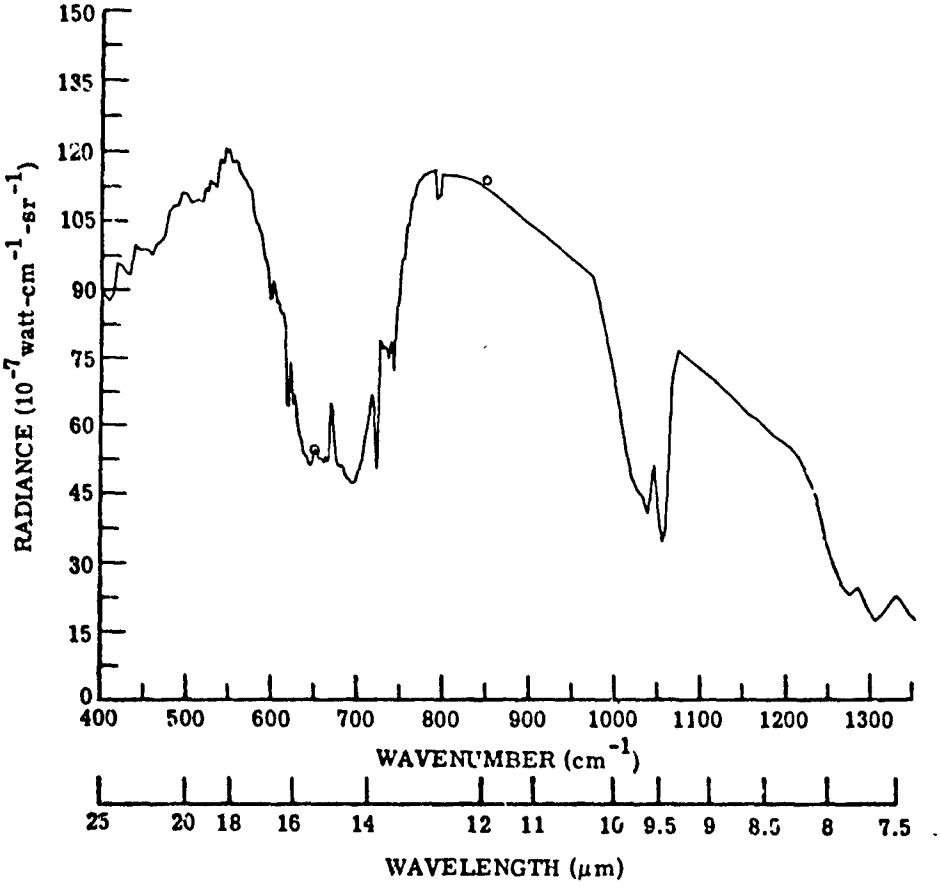

(a) Aggregate Method: Drayson data points shown at 650 cm^{-1} and 850 cm^{-1} for a vertical path looking down from 100 km. Temperate Summer model atmosphere.

FIGURE 120. COMPARISON BETWEEN RADIANCE FOR CALCULATION BY THE AGGREGATE METHOD AND OBSERVED NIMBUS IV SATELLITE DATA

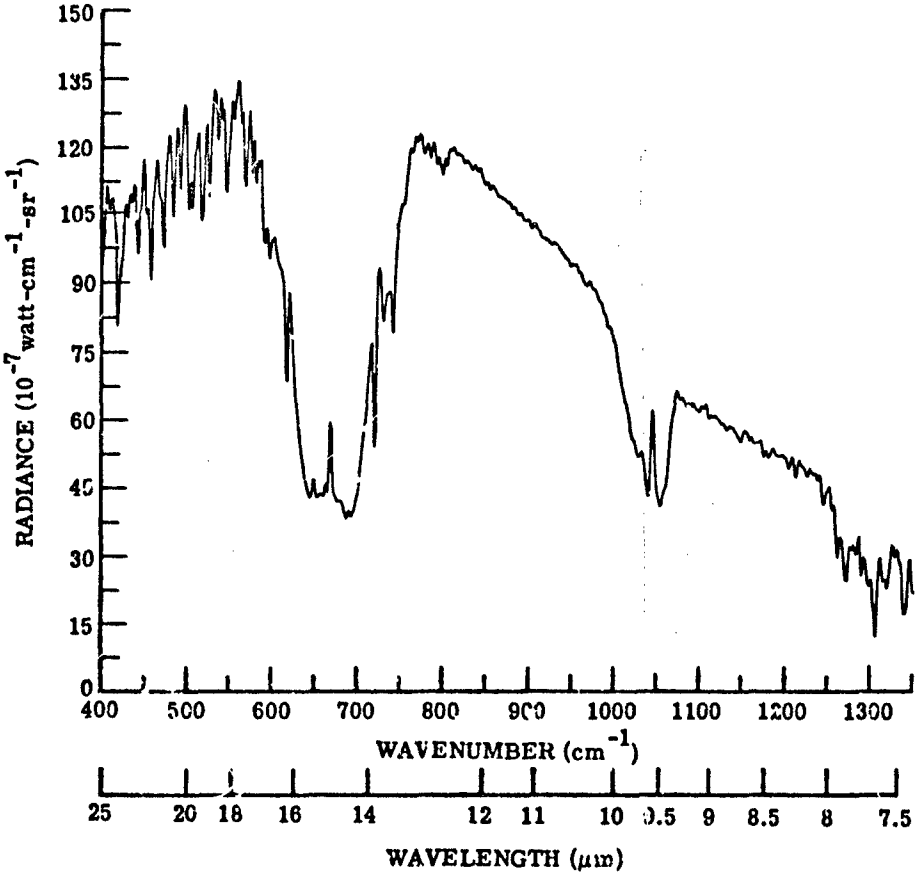

(b) Nimbus IV (IRIS) satellite data taken on 13 July 1970 at 25.537° latitude and 12.183° longitude at a height of 1095.0 km.

FIGURE 120. COMPARISON BETWEEN RADIANCE FOR CALCULATION BY THE AGGREGATE METHOD AND OBSERVED NIMBUS IV SATELLITE DATA (Concluded)

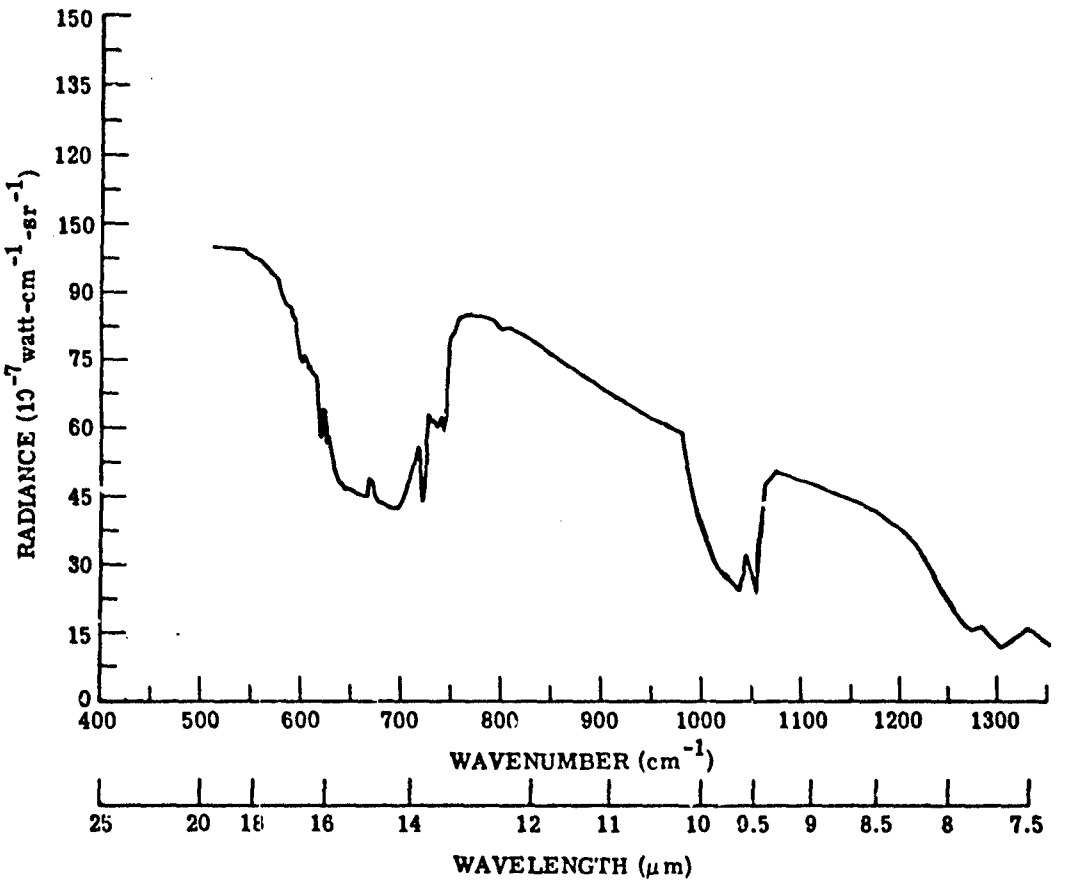

FIGURE 121. AGGREGATE MODEL ATMOSPHERE (TEMPERATE WINTER) FOR A VERTICAL PATH LOOKING DOWN FROM 100 km

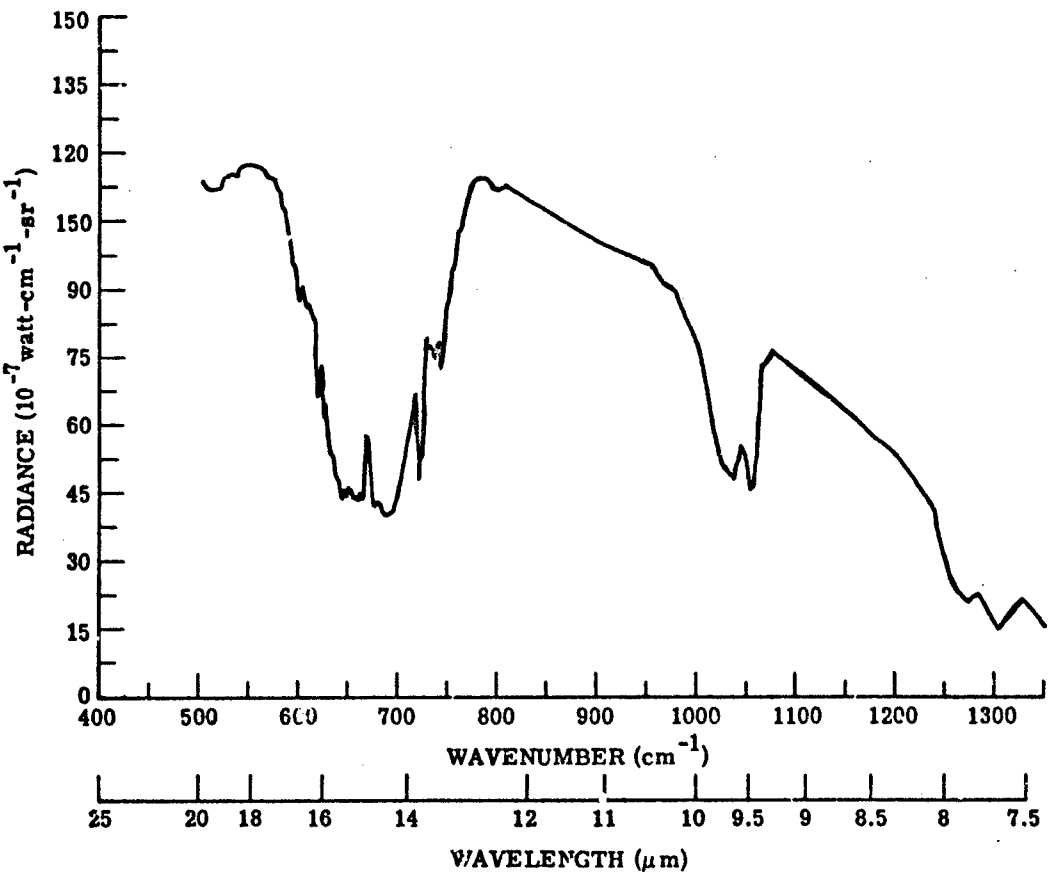

FIGURE 122. AGGREGATE MODEL ATMOSPHERE (TROPIC) FOR A VERTICAL PATH LOOKING DOWN FROM 100 km

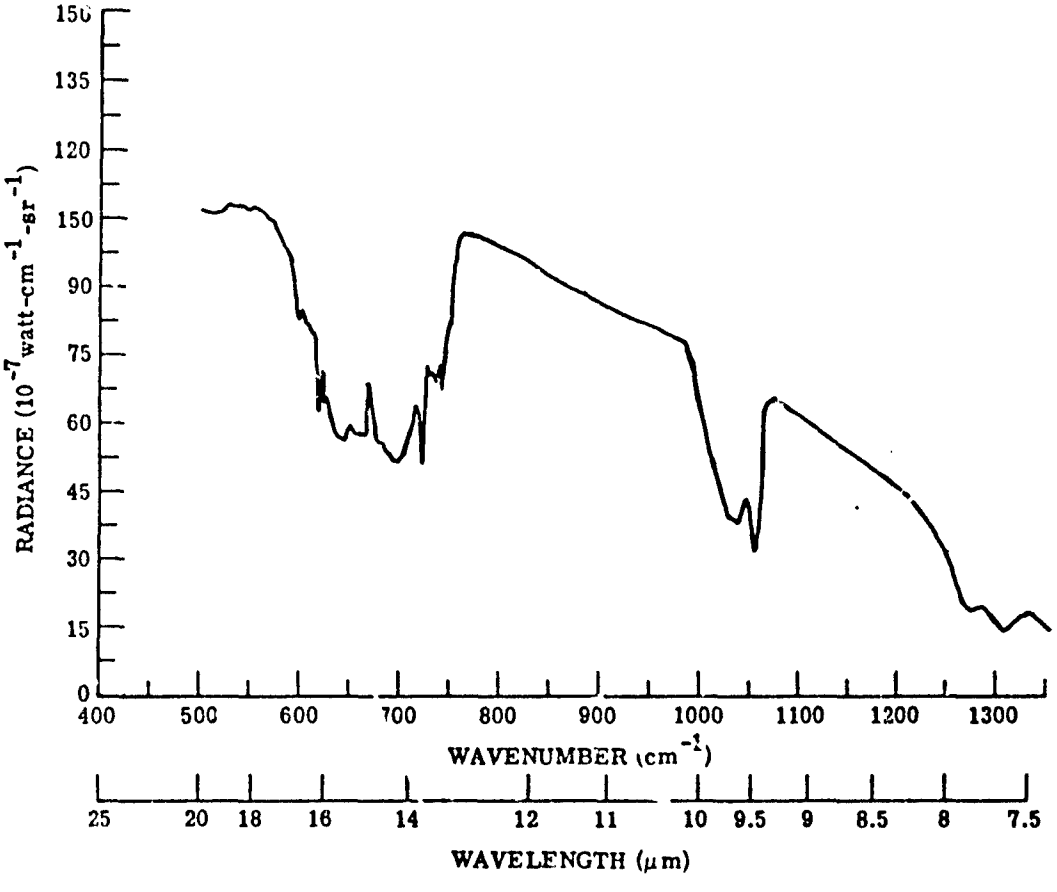

FIGURE 123. AGGREGATE MODEL ATMOSPHERE (ARCTIC SUMMER) FOR A VERTICAL PATH LOOKING DOWN FROM 100 km

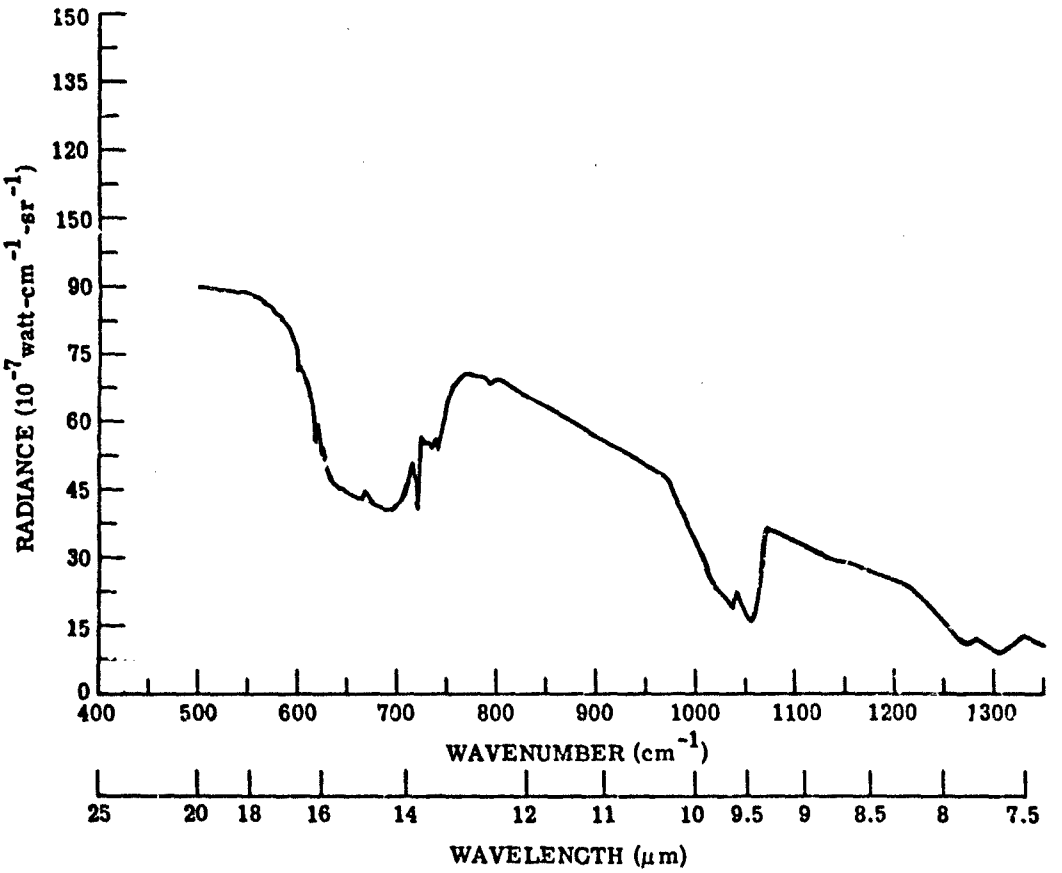

FIGURE 124. AGGREGATE MODEL ATMOSPHERE (ARCTIC WINTER) FOR A VERTICAL PATH LOOKING DOWN FROM 100 km

an Aggregate method spectrum computed for a Midlatitude-Summer atmospheric model. The spectral resolution corresponding to this region for the Aggregate model, as shown in Table 57, is about 5 cm^{-1}. Because this is somewhat smaller than the 20 cm^{-1} used in the line-by-line calculation, the agreement is perhaps less than the excellent agreement shown on the figure.

The difference between the spectrum and the point computed at 850 cm^{-1} with the line-by-line method seems to tend in the expected direction. Drayson's program does not account for absorption by the H_2O continuum, making transmittance by this method at 850 cm^{-1} a few percent higher than by the Aggregate method. The calculated radiance would ordinarily be higher by Drayson's technique, because the earth radiance in the Aggregate method would be attenuated, replaced by the lower radiance of the cooler H_2O vapor at higher altitude.

To show comparison of Nimbus data with the results of a line-by-line method (that of Kunde) of calculation we have reproduced a curve by Conrath, et al (1970) which seems to agree with the conditions given for the curves of Figure 92 and Figure 120a. This curve is shown in Figure 125. We have retained the scales in the original calculations, but note that they are all consistent.

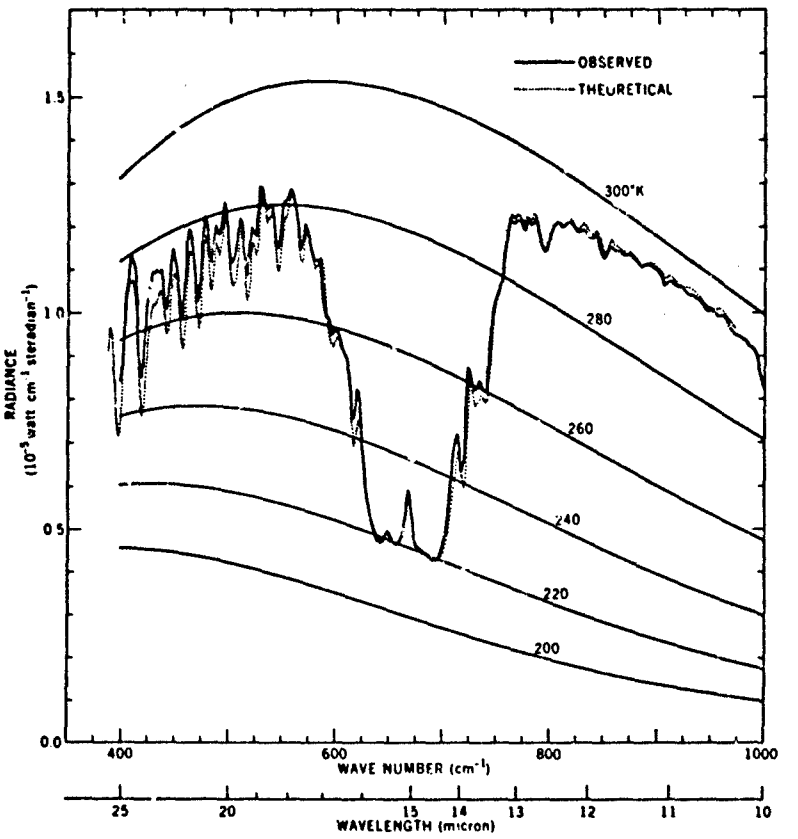

FIGURE 125. THE 400 TO 1000 cm^{-1} PORTION OF THE NIMBUS SPECTRUM. The dashed curve is calculated with Kunde's line-by-line method. (Reproduced from Conrath, et al., 1970 [224].)

10
ATMOSPHERIC CONSTITUENTS

10.1 INTRODUCTORY REMARKS

The accumulation of data that has been gathered by various investigations provides no basis upon which it would be practical to create a formal model for the various constituents in the atmosphere. Therefore, any models which appear in this report must be simply reproductions of those which have already been compiled in other reports for the calculation of atmospheric transmittance. A cursory search of the contents of the Journal of the Atmospheric Sciences revealed no important new models which should necessarily succeed the ones in current use. However, there is much work being done, for example, in studying the sizes and concentration of scattering constituents, and perhaps in the very near future some significant data will be forthcoming to provide more reliable inputs for model calculations. It is felt that the current inputs are reliable, but perhaps limited in that they do not account for the huge variations which are known to occur on a yearly and even daily basis, or between proximate geographical locations. It will be noticed, however, that the atmospheric models for, say, the Aggregate and LOWTRAN methods do not necessarily coincide.

The U.S. Standard Atmosphere, divided into regional and temporal groups, is the one most feasible for presentation of the more-or-less common, or basic, properties of the atmosphere, temperature, pressure and density of the stable components of air. All absorption models of which we are aware consider the fractional composition of certain of the chief absorbers, i.e., CO_2, CO, CH_4, N_2O, as constant with altitude in the troposphere. Obviously, this must be untrue under circumstances for which it is known that certain gases, for special reasons, appear in more than their normal concentrations. Even where extraordinary conditions do not exist, there can be temporal and geographical variations in the "fixed-concentration" gases. It is evident, then, that model atmospheres are just models, and are to be used to predict transmittance in those cases for which an average value, related to average conditions, can be accepted. When more precise information is required, the profiles of all important physical parameters must be known and used in the models for calculating atmospheric transmittance.

For the investigator who wishes to probe more deeply into the variability one might expect in the model atmospheres that are used for generalized transmittance calculations, there exist reports and articles covering many phases of investigations on the properties of the atmosphere which influence transmittance. Particular attention is given to aerosols, because their variability is so great, and the interest in this variability is keen because scattering phenomena are so sensitive to it. One issue of the Journal of Geophysical Research was devoted to the topic of sea-air chemistry, with the publication of many papers from a Working Symposium on Sea-Air Chemistry. Of particular interest to the person making atmospheric

transmittance calculations is a paper by Junge [284] on the physics-chemistry of aerosols in m -ine environments. In this paper, he discusses five different particle types: those with radii larger than 20 μm, sea spray particles, tropospheric background particles, mineral dust particles, and particles with radii smaller than 0.03 μm. In the same issue, Moyers and Duce [285], [286] discuss gaseous and particulate iodine and bromine in the marine atmosphere.

10.2 PRINCIPAL GASES FOR ABSORPTION

Since the absorptive properties of the gases are given in detail in Section 4, we present only the meteorologically related parameters in this section.

10.2.1 CARBON DIOXIDE (CO_2)

Carbon dioxide is chief among the fixed gases in absorption and emission of atmospheric radiation. In the predecessor to this report (Anding, 1967), a large section is devoted to a discussion of the accumulation of data on CO_2 and other atmospheric gases of importance to this study. No attempt will be made to reproduce that discussion here. Taken from that report, Table 58 depicts the values of the concentrations of CO_2 obtained by various investigators. The concentration chosen for the Aggregate method is 320 ppm. The value quoted by Laulainen (1972) is about 325 ppm, uniformly mixed up to the stratopause, "where it is presumably destroyed by photochemical decomposition." The yearly increase in CO_2 is considered to be about 1 ppm. The value used in the LOWTRAN 2 model is shown in Table 59, along with the values for other fixed gases used in that model.

10.2.2 NITROUS OXIDE (N_2O)

Considered in the early part of the century as a fixed constituent of the atmosphere, (which dissociates in the stratosphere), and later confirmed by Adel [287], [288], N_2O is considered, as quoted by Laulainen, to have a fractional volume abundance of 2.5×10^{-7}. Table 60 (see Anding, 1967) shows the values obtained by different investigators. The value

284. C. E. Junge, "Our Knowledge of the Physics-Chemistry of Aerosols in the Undisturbed Marine Environment," J. Geophys. Res., Vol. 77, No. 27, 1972, pp. 5183-5200.

285. J. L. Moyers and R. A. Duce, "Gaseous and Particulate Iodine in the Marine Atmosphere," J. Geophys. Res., Vol. 77, No. 27, pp. 5229-5238.

286. J. L. Moyers and R. A. Duce, Gaseous and Particulate Bromine in the Marine Atmosphere, J. Geophys. Res., Vol. 77, No. 27, 1972(b), pp. 5330-5338.

287. A. Adel and C. O. Lampland, "A New Band of the Absorption Spectrum of the Earth's Atmosphere," Astrophys. J., Vol. 87, 1938, p. 198.

288. A. Adel, "Note on the Atmospheric Oxides of Nitrogen," Astrophys. J., Vol. 90, 1939, p. 627.

TABLE 58. CONCENTRATION OF CARBON DIOXIDE

Source	CO_2 Content (ppm)
Valley [290]	31[illegible]
Keeling [291]	314
Callendar [292]	320
Glueckauff [293]	320
Fonselious [294]	321-329
Bray [295]	320
Average	321 ± 5

290. S. L. Valley, Handbook of Geophysics and Space Environments, Air Force Cambridge Research Laboratories, 1965.

291. C. D. Keeling, "The Concentration and Isotopic Abundance of Carbon Dioxide in the Atmosphere," Tellus, Vol. 12, 1960.

292. G. S. Callendar, "On the Amount of Carbon Dioxide in the Atmosphere," Tellus, Vol. 10, 1958, pp. 243-248.

293. E. G. Glueckauff, "CO_2 Content of the Atmosphere," Nature, Vol. 153, 1944, pp. 620-621.

294. S. Fonselious, F. Koroleff and K. Burch, "Microdetermination of CO_2 in the Air with Current Data for Scandinavia," Tellus, Vol. 7, 1955, pp. 258-265.

295. J. R. Bray, "An Analysis of the Possible Recent Change in Atmospheric Carbon Dioxide," Tellus, Vol. 11, 1959, pp. 220-230.

TABLE 59. CONCENTRATIONS OF UNIFORMLY MIXED GASES. (From McClatchey, et al., 1972 [21].)

Constituent	Molecular wt.	ppm by vol.	$(cm\text{-}atm)_{STP}$ in vertical path from sea level	$(cm\text{-}atm)_{STP}/km$ in horizontal path at sea level	gm cm^{-2}/mb	Ref.
Air	28.97	10^6	8×10^5	10^5	1.02	[290]
CO_2	44	330	264	33	5.11×10^{-4}	[296]
N_2O	44	0.28	0.22	0.028	4.34×10^{-7}	[297]
CO	28	0.075	0.06	0.0075	7.39×10^{-8}	[298]
CH_4	16	1.6	1.28	0.16	9.01×10^{-7}	[299]
O_2	32	2.095×10^5	1.68×10^5	2.095×10^4	0.236	[290]

296. U. Fink, D. H. Rank and T. A. Wiggins, J. Opt. Soc. Am., Vol. 54, 1964, p. 472.

297. J. W. Birkeland and J. H. Shaw, J. Opt. Soc. Am., Vol. 49, 1959, p. 637.

298. J. H. Shaw, Monthly Report on Infrared Temperature Sounding, RF Project 2469, Report No. 16, Ohio State University, Columbus, October 1968.

299. J. H. Shaw, A Determination of the Abundance of N_2O, CO, and CH_4 in Ground Level Air at Several Locations Near Columbus, Ohio, Sci. Report No. 1, Contract AF 19(604)-2256, AFCRL.

TABLE 60. CONCENTRATION OF NITROUS OXIDE

Author	Date	Location	Content (ppm)
Adel [300]	1941	Arizona	0.38
Shaw, Sutherland, and Wormell [301]	1943	England	1.25
McMath and Goldberg [302]	1948	Michigan	0.5
Slobod and Krogh [303]	1950	Texas	0.5
Birkeland, Burch, and Shaw [304]	1957	Chesapeake Bay	0.43
Birkeland [305]	1957	Ohio	0.28
Bowman [306]	1959	Ohio	0.28
U.S. Standard Atmosphere	1962		0.5

300. A. Adel, "Equivalent Thickness of the Atmospheric Nitrous Oxide Layer," Phys. Rev., Vol. 59, 1941, p. 944.

301. J. H. Shaw, G. B. B. M. Sutherland and T. W. Wormell, "Nitrous Oxide in the Earth's Atmosphere," Phys. Rev., Vol. 74, 1948, p. 978.

302. R. McMath and L. Goldberg, "The Abundance and Temperature of Methane in the Earth's Atmosphere," Proc. Am. Phys. Soc., Vol. 74, 1948, p. 623.

303. R. L. Slobod and M. E. Krogh, "Nitrous Oxide as a Constituent of the Atmosphere," J. Am. Chem. Soc., Vol. 72, 1950, pp. 1175-1177.

304. J. W. Birkeland, D. E. Burch and J. H. Shaw, "Some Comments on Two Articles by Taylor and Yates," J. Opt. Soc. Am., Vol. 47, 1957, p. 441.

305. J. W. Birkeland, "Determination of Ground Level N_2O," M.S. thesis, Ohio State University, Columbus, 1957.

306. A. L. Bowman, A Determination of the Abundance of Nitrous Oxide, Carbon Monoxide and Methane in Ground Level Air at Several Locations near Columbus, Ohio (Scientific Report No. 1 on Contract AF 19(604)-2259), Ohio State University, Columbus, 1959.

chosen for the Aggregate method is 0.28 ppm, as it is for the LOWTRAN 2 method (as shown in Table 59). Goldman, et al. [289] indicate that the measurements giving these results were made at ground level. From the measurement of emission spectra from balloons, they have determined that the mean value for a range of altitudes from 5 to 13 km is 0.14 ± 0.04 ppm.

10.2.3 CARBON MONOXIDE (CO)

As with the other fixed gases, CO is considered to be uniformly mixed vertically, at least up to the tropopause, above which it is oxidized to CO_2. The concentration then increases higher in the stratosphere and in the mesosphere. There is no strong indication that there are significant long-term increases in CO, partially because short-term temporal and spatial variations tend to conceal whatever small long-term increases might occur. Laulainen suggests that natural production and destruction of CO are sufficient to override man-produced causes. The variability from different regions causes a range of concentrations from 0.01 to 0.20 ppm in remote locations and from 0.4 to 2.2 ppm in urban areas. The fixed value used in the Aggregate method is 0.12 ppm, whereas as shown in Table 59, LOWTRAN 2 uses 0.075. Table 61 shows the ranges of CO concentrations obtained by various investigators.

10.2.4 METHANE (CH_4)

Laulainen (1972) reports a volume mixing ratio of almost 1.6 ppm, which is approximately constant with altitude up to the tropopause, then decreases rapidly in the lower stratosphere. The value used in the Aggregate method is 1.1 ppm and in the LOWTRAN method is 1.6 ppm as seen in Table 59.

10.2.5 NITRIC ACID (HNO_3)

Nitric acid, discovered recently in the stratosphere by Murcray, et al. [307], is considered as an absorber only in the Aggregate method. The values used for all atmospheric models (described in the next section under water vapor) are shown as a curve of mixing ratio vs altitude in Figure 126. More recent balloon-flight measurements by Murcray, et al. [308] show distributions with altitude produced as in Figure 127, where the absorber amounts corresponding to the measured data are shown on the curves.

---

289. A. Goldman, D. G. Murcray and F. H. Murcray, et al., "Abundance of N_2O in the Atmosphere between 4.5 and 13.5 km," J. Opt. Soc. Am., Vol. 60, No. 11, 1970, pp. 1466-1468.

307. L. G. Murcray, T. G. Kyle, F. H. Murcray and W. I. Williams, "Nitric Acid and Nitric Oxide in the Lower Stratosphere," Nature, Vol. 218, 1968, p. 78.

308. D. G. Murcray, A. Goldman and A. Csoeke-Poeckh, et al., "Nitric Acid Distribution in the Stratosphere," J. Geophys. Res., Vol. 78, No. 30, 1973, pp. 7033-7038.

TABLE 61. CONCENTRATION OF CARBON MONOXIDE

Location	Observers	Mean Concentration (ppm)	Range (ppm)
Columbus, Ohio	Migeotte [309]	0.125*	---
Columbus, Ohio	Bowman [306]	1.1	0.4-2.2
Columbus, Ohio	Shaw and Howard [310] [311], Shaw and Neilson [312]	0.125**	0.075-0.25
Columbus, Ohio	Shaw [313]	0.075**	0.05-0.125
Ottawa, Canada	Locke and Herzberg [314]	0.1625	0.09-0.18
Jungfraujoch, Switzerland	Benesch, Migeotte, and Neven [315]	0.075**	0.025-0.11
Flagstaff, Arizona	Adel [316]	0.125*	---

* Concentration determined from published spectra.

** Concentration reduced to sea level assuming uniform vertical distribution.

309. M. V. Migeotte, "The Fundamental Band of Carbon Monoxide at 4.7 μ in the Solar Spectrum," Phys. Rev., Vol. 75, 1949, p. 1108.

310. J. H. Shaw and J. N. Howard, "A Quantitative Determination of the Abundance of Telluric CO Above Columbus, Ohio," Phys. Rev., Vol. 87, 1952, p. 380.

311. J. H. Shaw and N. Howard, "Absorption of Telluric CO in the 23 μ Region," Phys. Rev., Vol. 87, 1952, p. 679.

312. J. H. Shaw and H. H. Nielson, Infrared Studies of the Atmosphere (Final Report on Contract AF 19(122)-65), Ohio State University Research Foundation, Columbus, 1954.

313. J. H. Shaw, The Abundance of Atmospheric CO above Columbus, Ohio (Contract AF 19(604)1003), Report No. AFCRC TN 57-212, Ohio State University Research Foundation, Columbus, 1957.

314. J. L. Locke and L. Herzberg, "The Absorption due to Carbon Monoxide in the Infrared Solar Spectrum," Can. J. Phys., Vol. 31, 1953, p. 504.

315. W. Benesch, M. V. Migeotte and L. Neven, "Investigations of Atmospheric CO at the Jungfraujoch," J. Opt. Soc. Am., Vol. 43, 1953, p. 1119.

316. A. Adel, "Identification of Carbon Monoxide in the Atmosphere above Flagstaff, Arizona," Astrophys. J., Vol. 116, 1952, p. 442.

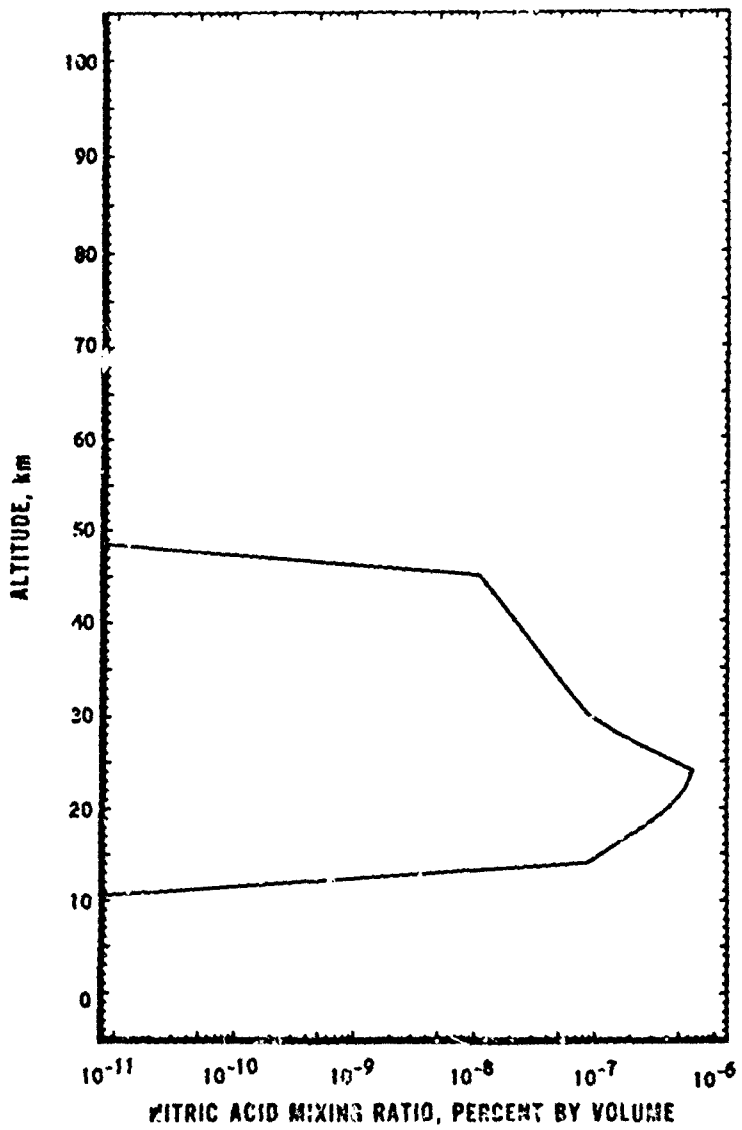

FIGURE 126. MODEL ATMOSPHERES - NITRIC ACID MIXING RATIO. (Reproduced from Hamilton, et al., 1973 [19].)

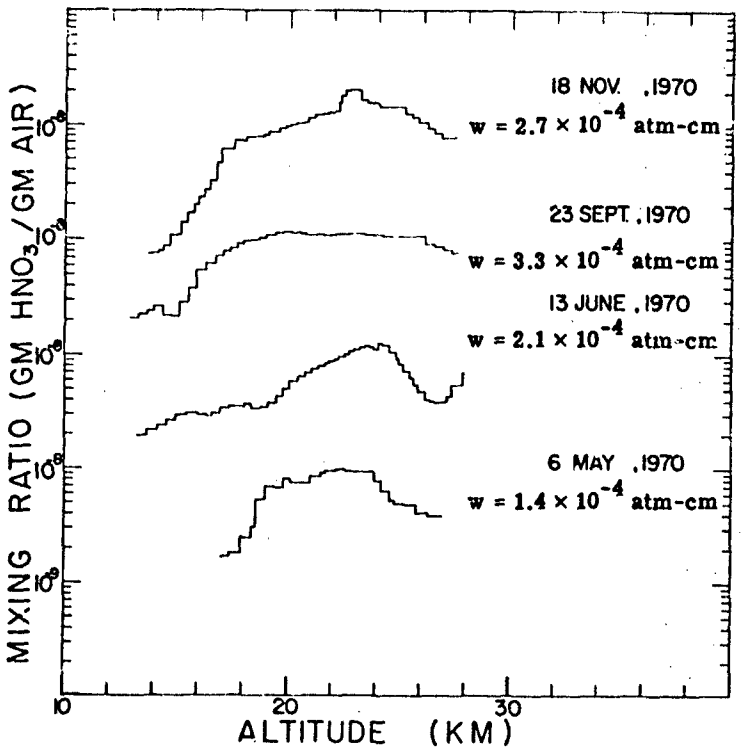

FIGURE 127. DISTRIBUTION OF HNO_3 WITH ALTITUDE AS DETERMINED FROM ATMOSPHERIC EMISSION DATA. (Reproduced from Brooks, et al., 1973 [319].)

10.2.6 WATER VAPOR (H_2O)

Water vapor is the atmosphere's most variable gaseous constituent from the standpoint of atmospheric transmittance. Anding (1967) has a lengthy discussion on the variability of water vapor and the numerous measurements made on it. Laulainen quotes the variability as 10^{-2} to 10^{-5} in the mixing ratio, with a diminution as a result of condensation and precipitation of about 1/3 for every 2 km, reaching the value of roughly 3×10^{-6} in the stratosphere. The profiles of water vapor are given in conjunction with the regional-temporal profile of pressure, temperature, and air density, corresponding to the following climates: tropical; midlatitude summer; midlatitude winter; subarctic summer; and subarctic winter. Tables of pressure, temperature and density as functions of altitude for these regions and climates are shown in Table 62. Values for the water vapor profile (Valley, 1965 and Sissenwine, et al. [317]) used in the LOWTRAN method (McClatchey, et al., 1972) and the ERIM version of the Aggregate method, are shown in the fifth column of each of these tables. The Aerospace version of the Aggregate method uses a somewhat different set of profiles (Hamilton, et al., 1973) shown in Figure 126 (Valley, 1965 and Goldman, et al. [318]). Recent results of measurements with balloon-borne instrumentation (Brooks, et al. [319]) are shown in Figure 129. A recent summary article [320] compares the values of various measurements. From a search of 37 winter months of synoptic charts, the author concludes that the 30-mbar H_2O vapor mixing ratio is approximately 6-8 ppm in the high latitudes of the Northern Hemisphere over populated areas.

10.2.7 OZONE (O_3)

Ozone is another highly variable atmospheric constituent, regarding both the time of year and geographical location. The concentration peaks at about 30 km, where Laulainen quotes a mixing ratio of better than 10 ppm. Anding has an extensive discussion of the variability of ozone and the measurements made on it. The Aerospace version of the Aggregate method

317. N. Sissenwine, D. Grantham and N. S. Salmela, Humidity Up to the Mesopause, Report No. AFCRL-68-0550, Air Force Cambridge Research Labs., Bedford, Mass., 1968.

318. A. Goldman, Distribution of Water Vapor in the Stratosphere as Determined from Balloon Measurements of Atmospheric Emission Spectra in the 24 to 29 m Region, Report No. AFCRL 72-0077, University of Denver, 1972.

319. J. N. Brooks, A. Goldman, J. J. Kosters, D. G. Murcray, F. H. Murcray and W. J. Williams, "Balloon-Borne Infrared Measurements," in Physics and Chemistry of Upper Atmospheres, B. N. McCormac (ed.), Proceedings of a Symposium organized by the Summer Advanced Study Institute, held at the University of Orleans, France, July 31-August 11, 1972, D. Reidel Publishing Co., Dordrecht, Holland, 1973, pp. 278-285.

320. J. L. Stanford, "Stratospheric Water-Vapor Upper Limits Inferred from Upper-Air Observations, Part I: Northern Hemisphere," Bull. Am. Met. Soc., Vol. 55, No. 3, 1974, p. 194.

TABLE 62. MODEL ATMOSPHERES USED AS A BASIS OF THE COMPUTATION OF ATMOSPHERIC OPTICAL PROPERTIES. (From McClatchey, et al., 1972 [21].)

(a) Tropical

Ht. (km)	Pressure (mb)	Temp. (°K)	Density (g/m^3)	Water Vapor (g/m^3)	Ozone (g/m^3)
0	1.013E+03	300.0	1.167E+03	1.9E+01	5.6E-05
1	9.040E+02	294.0	1.064E+03	1.3E+01	5.6E-05
2	8.050E+02	288.0	9.689E+02	9.3E+00	5.4E-05
3	7.150E+02	284.0	8.756E+02	4.7E+00	5.1E-05
4	6.330E+02	277.0	7.951E+02	2.2E+00	4.7E-05
5	5.590E+02	270.0	7.199E+02	1.5E+00	4.5E-05
6	4.920E+02	264.0	6.501E+02	8.5E-01	4.3E-05
7	4.320E+02	257.0	5.855E+02	4.7E-01	4.1E-05
8	3.780E+02	250.0	5.258E+02	2.5E-01	3.9E-05
9	3.290E+02	244.0	4.708E+02	1.2E-01	3.9E-05
10	2.860E+02	237.0	4.202E+02	5.0E-02	3.9E-05
11	2.470E+02	230.0	3.740E+02	1.7E-02	4.1E-05
12	2.130E+02	224.0	3.316E+02	6.0E-03	4.3E-05
13	1.820E+02	217.0	2.929E+02	1.8E-03	4.5E-05
14	1.560E+02	210.0	2.578E+02	1.0E-03	4.5E-05
15	1.320E+02	204.0	2.260E+02	7.6E-04	4.7E-05
16	1.110E+02	197.0	1.972E+02	6.4E-04	4.7E-05
17	9.370E+01	195.0	1.676E+02	5.6E-04	6.9E-05
18	7.890E+01	199.0	1.382E+02	5.0E-04	9.0E-05
19	6.660E+01	203.0	1.145E+02	4.9E-04	1.4E-04
20	5.650E+01	207.0	9.515E+01	4.5E-04	1.9E-04
21	4.800E+01	211.0	7.938E+01	5.1E-04	2.4E-04
22	4.090E+01	215.0	6.645E+01	5.1E-04	2.8E-04
23	3.500E+01	217.0	5.618E+01	5.4E-04	3.2E-04
24	3.000E+01	219.0	4.763E+01	6.0E-04	3.4E-04
25	2.570E+01	221.0	4.045E+01	6.7E-04	3.4E-04
30	1.220E+01	232.0	1.831E+01	3.6E-04	2.4E-04
35	6.000E+00	243.0	8.600E+00	1.1E-04	9.2E-05
40	3.050E+00	254.0	4.181E+00	4.3E-05	4.1E-05
45	1.590E+00	265.0	2.097E+00	1.9E-05	1.3E-05
50	8.540E-01	270.0	1.101E+00	6.3E-06	4.3E-06
70	5.780E-02	219.0	9.210E-02	1.4E-07	8.6E-08
100	3.000E-04	210.0	5.000E-04	1.0E-09	4.3E-11

TABLE 62. MODEL ATMOSPHERES USED AS A BASIS OF THE COMPUTATION OF ATMOSPHERIC OPTICAL PROPERTIES. (From McClatchey, et al., 1972[21].) (Continued)

(b) Midlatitude Summer					
Ht. (km)	Pressure (mb)	Temp. (°K)	Density (g/m^3)	Water Vapor (g/m^3),	Ozone (g/m^3)
0	1.013E+03	294.0	1.191E+03	1.4E+01	6.0E-05
1	9.020E+02	290.0	1.080E+03	9.3E+00	6.0E-05
2	8.020E+02	285.0	9.757E+02	5.9E+00	6.0E-05
3	7.100E+02	279.0	8.846E+02	3.3E+00	6.2E-05
4	6.280E+02	273.0	7.998E+02	1.9E+00	6.4E-05
5	5.540E+02	267.0	7.211E+02	1.0E+00	6.6E-05
6	4.870E+02	261.0	6.487E+02	6.1E-01	6.9E-05
7	4.260E+02	255.0	5.830E+02	3.7E-01	7.5E-05
8	3.720E+02	248.0	5.225E+02	2.1E-01	7.9E-05
9	3.240E+02	242.0	4.669E+02	1.2E-01	8.6E-05
10	2.810E+02	235.0	4.159E+02	6.4E-02	9.0E-05
11	2.430E+02	229.0	3.693E+02	2.2E-02	1.1E-04
12	2.090E+02	222.0	3.269E+02	6.0E-03	1.2E-04
13	1.790E+02	216.0	2.882E+02	1.8E-03	1.5E-04
14	1.530E+02	216.0	2.464E+02	1.0E-03	1.8E-04
15	1.300E+02	216.0	2.104E+02	7.6E-04	1.9E-04
16	1.110E+02	216.0	1.797E+02	6.4E-04	2.1E-04
17	9.500E+01	216.0	1.535E+02	5.6E-04	2.4E-04
18	8.120E+01	216.0	1.305E+02	5.0E-04	2.8E-04
19	6.950E+01	217.0	1.110E+02	4.9E-04	3.2E-04
20	5.950E+01	218.0	9.453E+01	4.5E-04	3.4E-04
21	5.100E+01	219.0	8.056E+01	5.1E-04	3.6E-04
22	4.370E+01	220.0	6.872E+01	5.1E-04	3.6E-04
23	3.760E+01	222.0	5.867E+01	5.4E-04	3.4E-04
24	3.220E+01	223.0	5.014E+01	6.0E-04	3.2E-04
25	2.770E+01	224.0	4.288E+01	6.7E-04	3.0E-04
30	1.320E+01	234.0	1.971E+01	3.6E-04	2.0E-04
35	6.520E+00	245.0	9.204E+00	1.1E-04	9.2E-05
40	3.330E+00	258.0	4.505E+00	4.3E-05	4.1E-05
45	1.760E+00	270.0	2.238E+00	1.9E-05	1.3E-05
50	9.510E-01	276.0	1.202E+00	6.3E-06	4.3E-06
70	6.710E-02	218.0	1.071E-01	1.4E-07	8.6E-08
100	3.000E-04	210.0	5.000E-04	1.0E-09	4.3E-11

*Original numbers have been corrected.

TABLE 62. MODEL ATMOSPHERES USED AS A BASIS OF THE COMPUTATION OF ATMOSPHERIC OPTICAL PROPERTIES. (From McClatchey, et al., 1972 [21].) (Continued)

(c) Midlatitude Winter					
Ht (km)	Pressure (mb)	Temp. (°K)	Density (g/m^3)	Water Vapor (g/m^3)	Ozone (g/m^3)
0	1.018E+03	272.2	1.301E+03	3.5E+00	6.0E-05
1	8.973E+02	268.7	1.162E+03	2.5E+00	5.4E-05
2	7.897E+02	265.2	1.037E+03	1.8E+00	4.9E-05
3	6.938E+02	261.7	9.230E+02	1.2E+00	4.9E-05
4	6.081E+02	255.7	8.282E+02	6.6E-01	4.9E-05
5	5.313E+02	249.7	7.411E+02	3.8E-01	5.8E-05
6	4.627E+02	243.7	6.614E+02	2.1E-01	6.4E-05
7	4.016E+02	237.7	5.886E+02	8.5E-02	7.7E-05
8	3.473E+02	231.7	5.222E+02	3.5E-02	9.0E-05
9	2.992E+02	225.7	4.619E+02	1.6E-02	1.2E-04
10	2.568E+02	219.7	4.072E+02	7.5E-03	1.6E-04
11	2.199E+02	219.2	3.496E+02	6.3E-03	2.1E-04
12	1.882E+02	218.7	2.999E+02	6.0E-03	2.6E-04
13	1.610E+02	218.2	2.572E+02	1.8E-03	3.0E-04
14	1.378E+02	217.7	2.206E+02	1.0E-03	3.2E-04
15	1.178E+02	217.2	1.890E+02	7.6E-04	3.4E-04
16	1.007E+02	216.7	1.620E+02	6.4E-04	3.6E-04
17	8.610E+01	216.2	1.388E+02	5.6E-04	3.9E-04
18	7.350E+01	215.7	1.188E+02	5.0E-04	4.1E-04
19	6.280E+01	215.2	1.017E+02	4.9E-04	4.3E-04
20	5.370E+01	215.2	8.690E+01	4.5E-04	4.5E-04
21	4.580E+01	215.2	7.421E+01	5.1E-04	4.3E-04
22	3.910E+01	215.2	6.338E+01	5.1E-04	4.3E-04
23	3.340E+01	215.2	5.415E+01	5.4E-04	3.9E-04
24	2.860E+01	215.2	4.624E+01	6.0E-04	3.6E-04
25	2.430E+01	215.2	3.950E+01	6.7E-04	3.4E-04
30	1.110E+01	217.4	1.783E+01	3.6E-04	1.9E-04
35	5.180E+00	227.8	7.924E+00	1.1E-04	9.2E-05
40	2.530E+00	243.2	3.625E+00	4.3E-05	4.1E-05
45	1.290E+00	258.5	1.741E+00	1.9E-05	1.3E-05
50	6.820E-01	265.7	8.954E-01	6.3E-06	4.3E-06
70	4.670E-02	230.7	7.051E-02	1.4E-07	3.6E-08
100	3.000E-04	210.2	5.000E-04	1.0E-09	4.3E-11

TABLE 62. MODEL ATMOSPHERES USED AS A BASIS OF THE COMPUTATION OF ATMOSPHERIC OPTICAL PROPERTIES. (From McClatchey, et al., 1972 [21].) (Continued)

(d) Subarctic Summer					
Ht. (km)	Pressure (mb)	Temp. (°K)	Density (g/m^3)	Water Vapor (g/m^3)	Ozone (g/m^3)
0	1.010E+03	237.0	1.220E+03	9.1E+00	4.9E-05
1	8.960E+02	282.0	1.110E+03	6.0E+00	5.4E-05
2	7.929E+02	276.0	9.971E+02	4.2E+00	5.6E-05
3	7.000E+02	271.0	8.985E+02	2.7E+00	5.8E-05
4	6.160E+02	266.0	8.077E+02	1.7E+00	6.0E-05
5	5.410E+02	260.0	7.214E+02	1.0E+00	6.4E-05
6	4.730E+02	253.0	6.519E+02	5.4E-01	7.1E-05
7	4.130E+02	246.0	5.849E+02	2.9E-01	7.5E-05
8	3.590E+02	239.0	5.231E+02	1.3E-02	7.9E-05
9	3.107E+02	232.0	4.663E+02	4.2E-02	1.1E-04
10	2.677E+02	225.0	4.142E+02	1.5E-02	1.3E-04
11	2.300E+02	225.0	3.559E+02	9.4E-03	1.8E-04
12	1.977E+02	225.0	3.059E+02	6.0E-03	2.1E-04
13	1.700E+02	225.0	2.630E+02	1.8E-03	2.6E-04
14	1.460E+02	225.0	2.260E+02	1.0E-03	2.8E-04
15	1.250E+02	225.0	1.943E+02	7.6E-04	3.2E-04
16	1.080E+02	225.0	1.671E+02	6.4E-04	3.4E-04
17	9.280E+01	225.0	1.436E+02	5.6E-04	3.9E-04
18	7.980E+01	225.0	1.235E+02	5.0E-04	4.1E-04
19	6.860E+01	225.0	1.062E+02	4.9E-04	4.1E-04
20	5.890E+01	225.0	9.128E+01	4.5E-04	3.9E-04
21	5.070E+01	225.0	7.849E+01	5.1E-04	3.6E-04
22	4.360E+01	225.0	6.750E+01	5.1E-04	3.2E-04
23	3.750E+01	225.0	5.805E+01	5.4E-04	3.0E-04
24	3.227E+01	226.0	4.963E+01	6.0E-04	2.8E-04
25	2.780E+01	228.0	4.247E+01	6.7E-04	2.6E-04
30	1.340E+01	235.0	1.978E+01	3.6E-04	1.4E-04
35	6.610E+00	247.0	9.320E+00	1.1E-04	9.2E-05
40	3.400E+00	262.0	4.526E+00	4.3E-05	4.1E-05
45	1.810E+00	274.0	2.314E+00 *	1.9E-05	1.3E-05
50	9.870E-01	277.0	1.240E+00	6.3E-06	4.3E-06
70	7.070E-02	216.0	1.137E-01	1.4E-07	8.6E-08
100	3.000E-04	210.0	5.000E-04	1.0E-09	4.3E-11

*Original numbers have been corrected.

TABLE 62. MODEL ATMOSPHERES USED AS A BASIS OF THE COMPUTATION OF ATMOSPHERIC OPTICAL PROPERTIES. (From McClatchey, et al., 1972 [21].) (Concluded)

(e) Subarctic Winter					
Ht. (km)	Pressure (mb)	Temp. (°K)	Density (g/m^3)	Water Vapor (g/m^3)	Ozone (g/m^3)
0	1.013E+03	257.1	1.372E+03	1.2E+00	4.1E-05
1	8.878E+02	259.1	1.193E+03	1.2E+00	4.1E-05
2	7.775E+02	255.9	1.058E+03	9.4E-01	4.1E-05
3	6.798E+02	252.7	9.366E+02	6.8E-01	4.3E-05
4	5.932E+02	247.7	8.339E+02	4.1E-01	4.5E-05
5	5.158E+02	240.9	7.457E+02	2.0E-01	4.7E-05
6	4.467E+02	234.1	6.646E+02	9.8E-02	4.9E-05
7	3.853E+02	227.3	5.904E+02	5.4E-02	7.1E-05
8	3.308E+02	220.6	5.226E+02	1.1E-02	9.0E-05
9	2.829E+02	217.2	4.538E+02	8.4E-03	1.6E-04
10	2.418E+02	217.2	3.879E+02	5.5E-03	2.4E-04
11	2.067E+02	217.2	3.315E+02	3.8E-03	3.2E-04
12	1.766E+02	217.2	2.834E+02	2.6E-03	4.3E-04
13	1.510E+02	217.2	2.422E+02	1.8E-03	4.7E-04
14	1.291E+02	217.2	2.071E+02	1.0E-03	4.9E-04
15	1.103E+02	217.2	1.770E+02	7.6E-04	5.6E-04
16	9.431E+01	216.6	1.517E+02	6.4E-04	6.2E-04
17	8.058E+01	216.0	1.300E+02	5.6E-04	6.2E-04
18	6.882E+01	215.4	1.113E+02	5.0E-04	6.2E-04
19	5.875E+01	214.8	9.529E+01	4.9E-04	6.0E-04
20	5.014E+01	214.1	8.155E+01	4.5E-04	5.6E-04
21	4.277E+01	213.6	6.976E+01	5.1E-04	5.1E-04
22	3.647E+01	213.0	5.966E+01	5.1E-04	4.7E-04
23	3.109E+01	212.4	5.100E+01	5.4E-04	4.3E-04
24	2.649E+01	211.8	4.358E+01	6.0E-04	3.6E-04
25	2.250E+01	211.2	3.722E+01	6.7E-04	3.2E-04
30	1.020E+01	216.0	1.645E+01	3.6E-04	1.5E-04
35	4.701E+00	222.2	7.368E+00	1.1E-04	9.2E-05
40	2.243E+00	234.7	3.330E+00	4.3E-05	4.1E-05
45	1.113E+00	247.0	1.569E+00	1.9E-05	1.3E-05
50	5.719E-01	259.3	7.682E-01	6.3E-06	4.3E-06
70	4.016E-02	245.7	5.695E-02	1.4E-07	3.6E-08
100	3.000E-04	210.0	5.000E-04	1.0E-09	4.3E-11

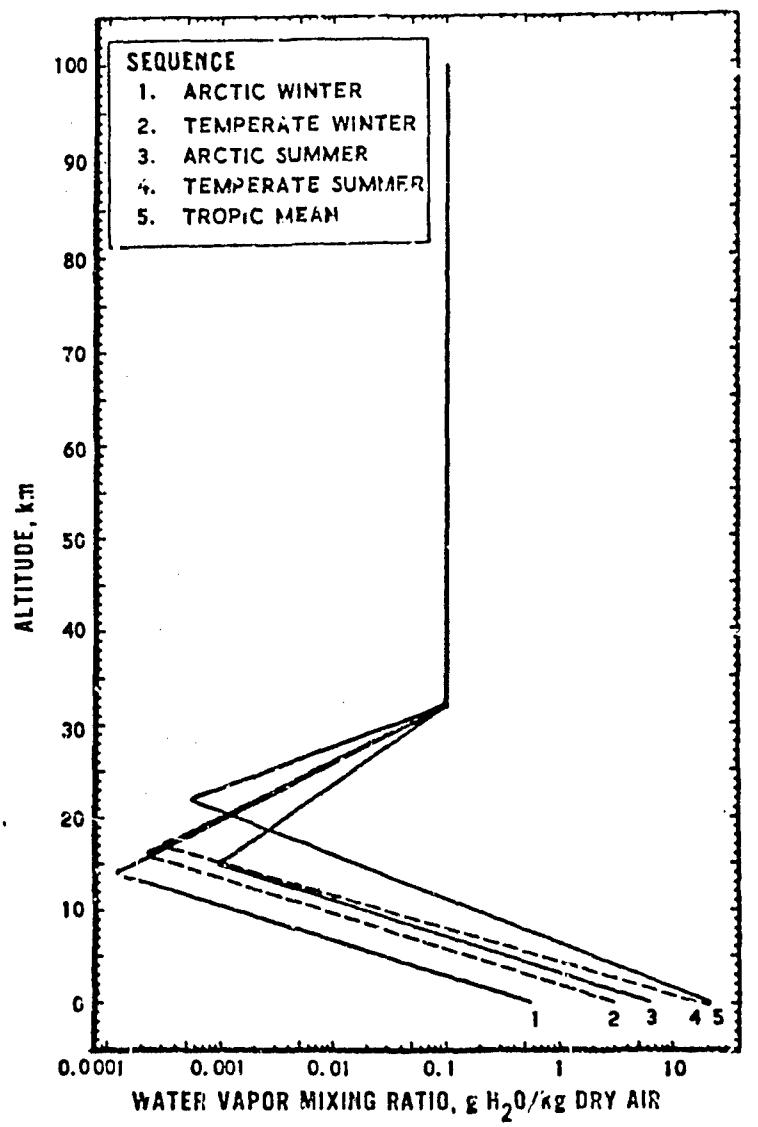

FIGURE 128. MODEL ATMOSPHERES - WATER VAPOR MIXING RATIO. (Reproduced from Hamilton, et al., 1973 [19].)

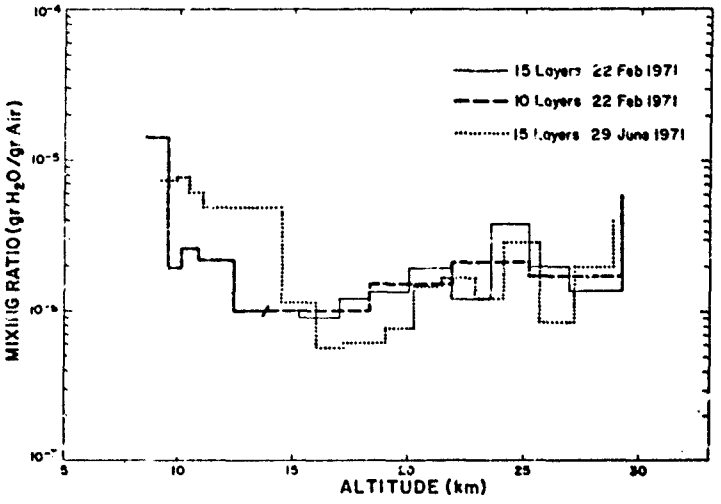

FIGURE 129. MIXING RATIO OF WATER VAPOR AS DERIVED FROM A 15-LAYER AND A 10-LAYER CALCULATION USING THE 25 μm LINE GROUP FOR THE 22 FEBRUARY 1971 BALLOON FLIGHT. The slash near 14 km indicates the boundary between two layers with similar mixing ratio. The mixing ratio derived from a 15-layer calculation using the 25 μm line group for the 29 June 1971 balloon flight is shown by the dotted line. (Reproduced from Brooks, et al., 1973 [319].)

uses only one (temperate-summer) profile (obtained from Hering, [321]) to fit all regional-temporal conditions. This is shown in Figure 130. The ERIM version of the Aggregate method and the LOWTRAN method use the tabulated values of the separate regional climates from Valley (1965). These are shown as the sixth column in Table 62. Krueger [322] reports the results of rocket soundings made from latitudes 58°S to 64°N. These results are reproduced in Figure 131, showing variabilities in the measurements.

10.3 SCATTERING CONSTITUENTS

10.3.1 EXTRATERRESTRIAL RADIATION

The major portion of the electromagnetic energy which arrives at the surface of Earth originates from the sun; and, to a great extent the solar radiation is responsible for atmospheric weather conditions. According to Drummond [323], more than 99% of the solar radiation is contained within the spectral band, 0.2 - 4.0 μm. Current values of the solar constant range from 1.365×10^6 mW/m^2 to 1.394×10^6 mW/m^2. Early work was done at the surface of Earth, and the results were extrapolated to the top of the atmosphere, whereas current investigations make use of high-altitude rockets and satellites.

For our present work we are interested, not in the total irradiance at the top of the atmosphere, but rather in the extraterrestrial solar spectral irradiance. Figure 132 shows this spectral irradiance as interpreted by Pettit [324]. For more accurate spectral values, one should consult Gates [325], Gast, et al. [326] and Thekaekara [327]. The units of solar irradiance are mW/cm^2-μm.

For particles with sizes much smaller than the size of the wavelergth of the radiation impinging upon them, the incident field is nearly uniform and, as a result, a dipole radiation field is produced. The scattering of this radiation is called Rayleigh scattering and was

321. W. S. Hering and T. R. Borden, Ozone Observations Over North America, OAR Research Report No. AFCRL-64-30, Vol. 2, 1964.

322. A. J. Krueger, The Mean Ozone Distribution from Several Series of Rocket Soundings to 52 km Latitudes from 54°S to 64°N, NASA Report No. X-651-73-67, Goddard Space Flight Center, Greenbelt, Md., 1973.

323. A. J. Drummond, Advances in Geophysics, H. E. Landsberg and J. Van Mieghem (eds.), Vol. 14, Academic Press, N. Y., 1970, p. 25.

324. E. Pettit, Astrophysics, J. A. Hynek (ed.), McGraw-Hill, N. Y., 1951, p. 259.

325. D. M. Gates, Science, Vol. 151, No. 3710, 1966, pp. 525-529.

326. P. R. Gast, A. Jursa, J. Castelli, S. Basu and J. Aarons, Handbook of Geophysics and Space Environments, S.L. Valley, ed., McGraw-Hill, New York, 1965, p. 16-1.

327. M. P. Thekaekara and A. J. Drummond, "Standard Values for the Solar Constant and Its Spectral Components," Nature Physical Science, Vol. 229, 1971.

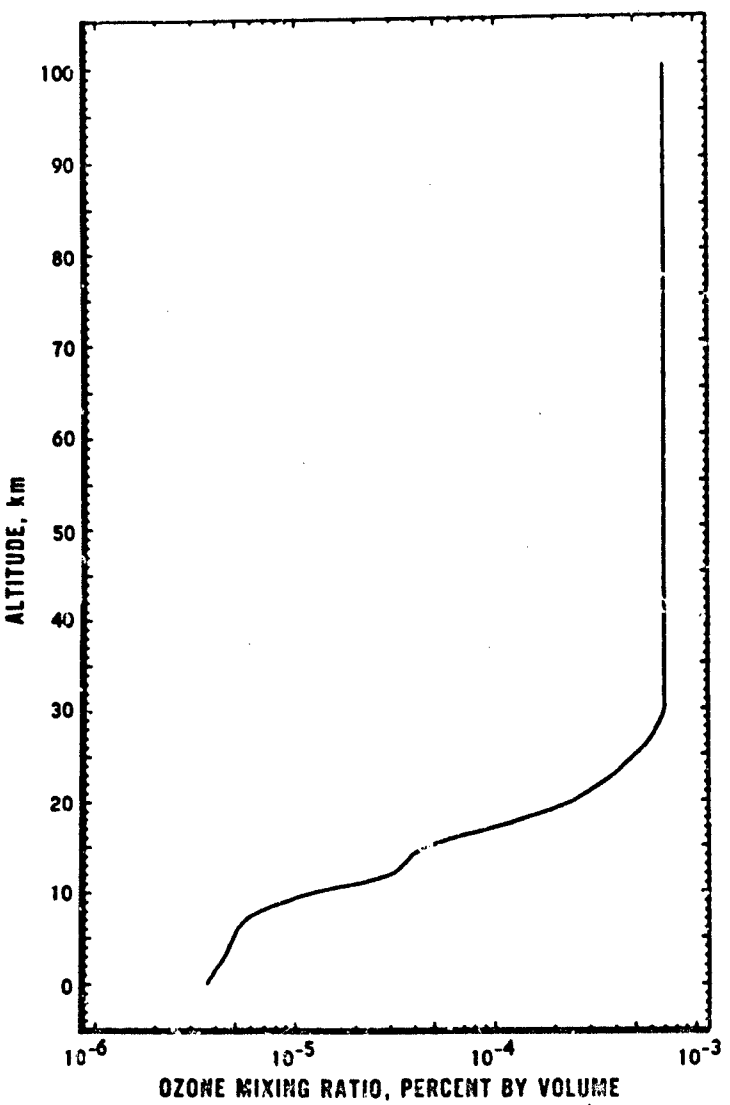

FIGURE 130. MODEL ATMOSPHERES - OZONE MIXING RATIO. (Reproduced from Hamilton, et al., 1973 [19].)

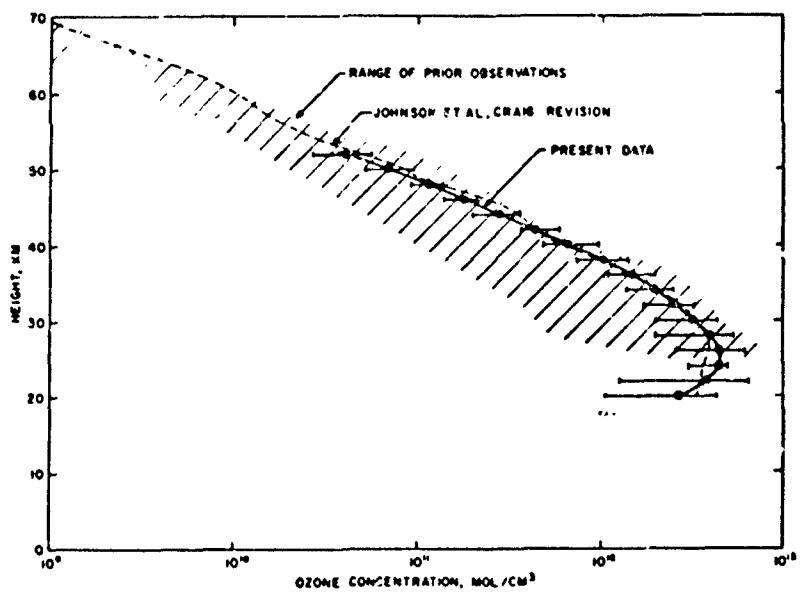

FIGURE 131. AVERAGE AND EXTREME RANGE OF VERTICAL OZONE DISTRIBUTION DATA. (Reproduced from Krueger, 1973 [322].)

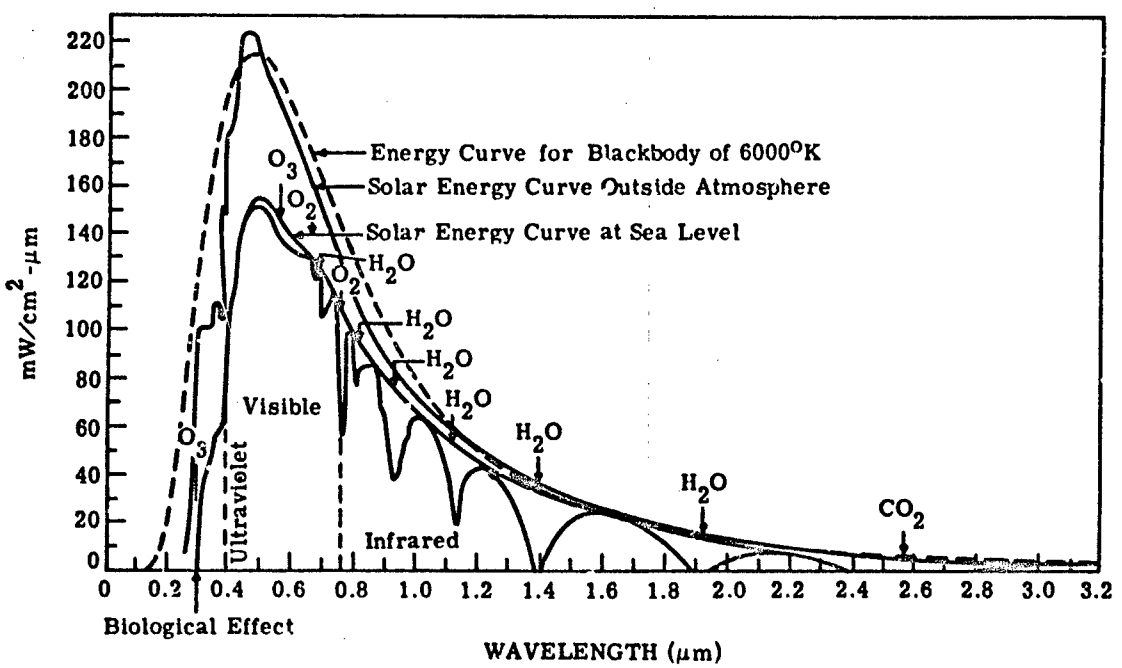

FIGURE 132. SPECTRAL SOLAR IRRADIANCE

attributed, by Lord Rayleigh, to the effect of molecules. We now know that this scattering process is caused by density fluctuations in the atmosphere. For Rayleigh scattering, the intensity of scattered radiation varies as $\lambda^{-4}(1 + \cos^2 \theta)$, where θ is the angle of scattering. Almost ten times as much radiation is scattered at the short visible wavelengths than is scattered at the long visible wavelengths. This accounts for the blue sky.

Besides Rayleigh scattering, we can consider two other processes. One is Thomson scattering, which is the scattering of radiation from unbound particles like free electrons. This type of scattering is independent of wavelength. Another important photon-scattering process is the strong resonance scattering which occurs because certain resonant frequencies of an atom or molecule are excited. Refer also to the absorptive properties of atmospheric constituents discussed in Section 4.

In all these scattering processes, the scattered radiation and the incident radiation have the same wavelength; therefore, in the context of this report these processes are said to be coherent. There are also incoherent processes, such as Raman scattering and Compton scattering, in which the scattered photon has an energy different from that of the incident photon. Compton scattering is important only at high photon energies, and Raman scattering is usually so weak that special techniques must be used to investigate it. (Luminescence can also be considered an incoherent scattering process, depending upon the lifetime of an excited state.) However, we shall not consider incoherent scattering processes in this report.

10.3.2 AEROSOLS

Generally, we can define an aerosol as a dispersed solid or liquid particle suspended in a gaseous medium, such as air. This definition includes hazes, clouds, mists, fogs, smokes, smogs, and dusts. For haze, clouds, and fogs, one usually assumes that the particles are composed of water in either the liquid or solid (ice) phase. Smokes, smogs, and dusts can consist of a variety of particulate matter, including metallic substances.

The study of aerosols is complicated by the dynamics of the atmosphere. A variety of sources exist; the particles are carried by the wind, coagulate, evaporate, condense, precipitate and are dispersed world-wide. The primary natural sources are: (1) dust rise by wind; (2) sea spray; (3) extraterrestrial material; and (4) dust from volcanoes and fires. In addition, there are secondary sources such as the emission of hydrocarbon vapors from conifers which react photochemically to produce the blue hazes seen over forests. Anthropogenic sources include smoke from stationary sources and motor vehicles. Table 63 from Hidy and Brock [328] illustrates the major sources of aerosols. It is interesting to note that the anthropogenic

TABLE 63. SOME IMPORTANT SOURCES OF ATMOSPHERIC AEROSOLS. Production Rate in Tons Day^{-1} on a Worldwide Basis. (From Hidy and Brock, 1971 [328].)

(a) Natural

Source	Estimated production rate	Max. % by wt. of total	Source	Estimated production rate	Max. % by wt. of total
1. Primary			2. Secondary		
Dust Rise by Wind	2×10^1-10^5	9.3	Vegetation (hydrocarbons-terpenes)	5×10^5-3×10^6	28.
Sea Spray	3×10^6	28.			
Extraterrestrial (meteoritic dust)	50-550		Sulfur Cycle (oxidation of H_2S—SO_4^{2-})	10^5-10^6	9.3
Volcanic Dust (intermittent)	10^4	0.09			
Forest Fires (intermittent)	4×10^5	3.8	Nitrogen Cycle		
			Ammonia	7×10^5	6.5
			NO_X—NO_3^-	10^6	8.3
			Volcanoes (volatiles, SO_2 and H_2S) — intermittent	~10^3	0.009
			Sub-total	10.1×10^6	94.

(b) Anthropogenic

Source	Estimated Production rate	Max. % by wt. of total
1. Primary		
Combustion and industrial	$1\text{-}3 \times 10^5$	2.8
Dust rise by cultivation (intermittent) (U.S. only)	10^2-10^3	0.009
2. Secondary		
Hydrocarbon vapors (incomplete combustion, etc.	7×10^3	0.065
Sulfates (oxidation of SO_2 and H_2S)	3×10^5	2.8
Nitrates (oxidation of NO_X)	6×10^4	0.56
Ammonia	3×10^3	0.028
Sub-total anthropogenic	6.7×10^5	7.1 -6%
Total: All sources	10.7×10^6 tons day^{-1}	

328. G. M. Hidy and J. R. Brock, An Assessment of the Global Sources of Tropospheric Aerosols, Proceedings of the 2nd International Clean Air Congress, H. M. England and W. T. Beerg (eds), 1971, pp. 1088-1097.

contribution is about 6 or 7% of the total. Nevertheless, there could be an amplification effect; i.e., a small aerosol input to the atmosphere could result in a large change in the climate. Man's impact on the global climate is a problem which has not yet been resolved.

Rozenburg [329] considers the optical weather of the atmosphere to be divided into five classes: (1) haze, resulting from dust clouds, smoke from forest fires and commercial objects, and products of volcanic activity; (2) mist, which results from the growth of very small particles called Aitken nuclei; (3) misty fog, a product of the condensation of moisture on larger particles; (4) fogs and clouds, produced in the condensation state in the atmosphere; and (5) mist with drizzle, a heterogeneous formation, resulting from mist penetrated by drizzle.

The composition of particles can range from pure water to strongly absorbing soot-like particles composed of phosphates, sulfates, iron, and other compounds. Most important from an optical point of view, however, is the refractive index of the particles. Deirmendjian [330], Lukes [331], and Kondratyev, et al. [332] have compiled data on water, soot, and ammonium sulfate, with the index of refraction represented by:

$$m(\lambda) = n(\lambda) - ik(\lambda) \tag{407}$$

where $n(\lambda)$ is the real part and $k(\lambda)$ is the imaginary part. These are presented in Figure 123. As one can see from the data there is a wide range of values which in turn can lead to large differences in the optics of the atmosphere.

If one considers condensation processes, the variability in the optical properties of the atmosphere is extreme. As an example, the scattering coefficient of air in the visible region of the spectrum varies from $10^{-2}km^{-1}$ for very light haze conditions to $10^{4}km^{-1}$ for extremely dense fogs. Because the optical properties of an aerosol particle depend on the size of that particle, it is important to consider the range in particle sizes. Junge [333] separates the particles into three regions as given in Table 64. The Aitken nuclei are believed to originate

329. G. V. Rozenburg, Optical Investigations of Atmospheric Aerosol, Soviet Physics Uspekhi, Vol. 11, No. 3, 1968, pp. 353-380.

330. D. Deirmendjian, Electromagnetic Scattering on Spherical Polydispersions, American Elsevier Publishing Company, New York, 1969.

331. G. D. Lukes, Optical Constants of Water Particulates for Wavelengths in the Visible and Infrared, Particulate Models: Their Validity and Applications, I. H. Blifford, Jr. (ed.), Report No. NCAR-TN/PROG-68, Boulder, Colo., 1971.

332. K. Ya. Kondratyev, O. B. Vasilyev, L. S. Iviev, G. A. Nikolsky and O. I. Smoktz, Influence of Aerosol on Radiative Transfer; Possible Climatic Consequences, University of Leningrad, 1973.

333. C. E. Junge, Air Chemistry and Radioactivity, Academic Press, N. Y., 1963.

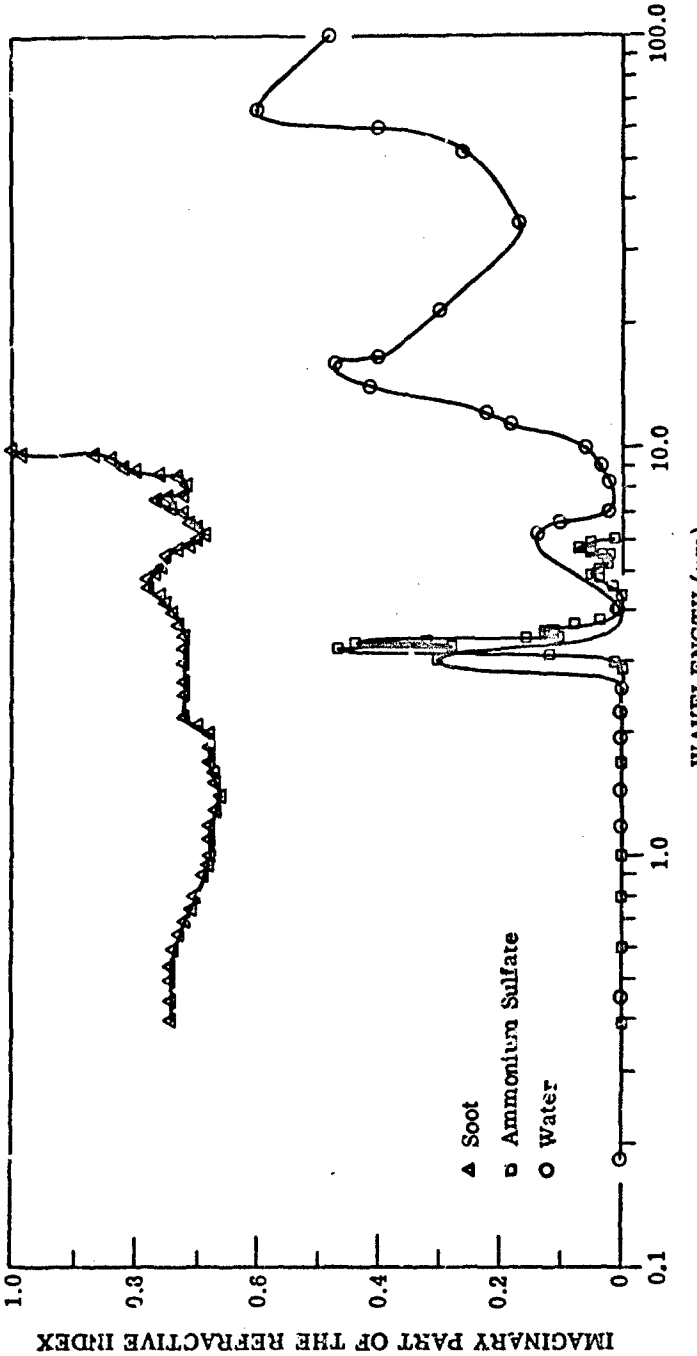

(a) Imaginary Part

FIGURE 133. THE REFRACTIVE INDEX OF VARIOUS AEROSOLS AS A FUNCTION OF WAVELENGTH

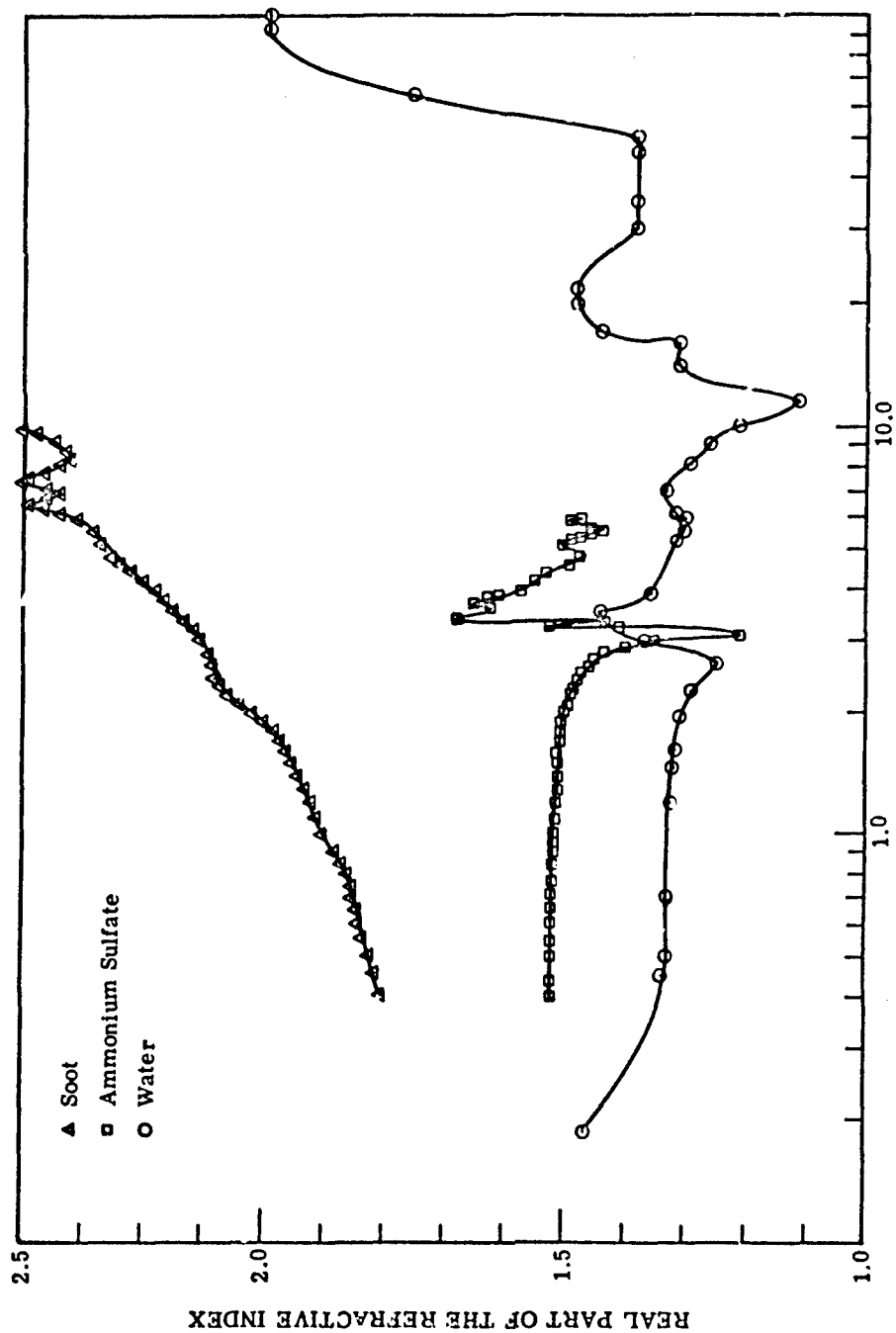

FIGURE 133. THE REFRACTIVE INDEX OF VARIOUS AEROSOLS AS A FUNCTION OF WAVELENGTH
(Concluded)

(b) Real Part

TABLE 64. SIZE DISTRIBUTION OF AEROSOL PARTICLES. (From Junge, 1963 [333].)

Range	Particle Radius (cm)
Aitken Nuclei	10^{-7} - 10^{-5}
Large Particles	10^{-5} - 10^{-4}
Giant Particles	$>10^{-4}$

from forest fires, volcanoes, and man-made sources. The concentration of these particles is about 10 to 100 times greater over the continents than over the oceans. Since their radii are much less than the wavelengths in the visible region of the spectrum, these particles do not seriously affect atmospheric visibility.

Condensation nuclei fall in the large-particle region and, since they are the nuclei activated during the formation of water droplets or fogs, they are important for visibility considerations. These nuclei, which constitute the bulk of the large continental aerosols, contain a wide range of chemical compounds, such as NH_4^+, Na^+, Mg^{++}, SO_4^{--}, NO_3^-, and NO_2^-. Aerosols near coastal regions or over the ocean have a different distribution of particle sizes, having more giant particles than the continental aerosols have. Moyers and Duce (1972a) collected air samples in a marine atmosphere showing a concentration of gaseous iodine from 5 to 20 mg/m^3. Particulate samples were collected in the ratio of 1:(2 to 4) compared with gaseous iodine. Gaseous bromine concentrations (Moyers and Duce, 1972b) covered about 50 ng/m^3. Particulate concentrations of bromine were in the ratio 1:(4 to 10) with respect to gaseous bromine.

For the purposes of dealing with the optical properties of hazes, Deirmendjian (1969) has represented hazes, fogs, clouds, rain, and hail by simple distribution functions. He considers a modified gamma distribution given by

$$N(r) = ar^{\delta} \exp(-br^{\gamma}) \qquad 0 \leq r < \infty \tag{406}$$

The four constants, a, δ, b, and γ, are positive and real but are not independent of each other. For example, by integrating Eq. (408) over r, the radius of the particles, we get the total particle number density D.

$$D = a\int_0^{\infty} r^{\delta} \exp(-br^{\gamma})\, dr = a\gamma^{-1}b^{-(\delta+1)/\gamma}\,\Gamma\left(\frac{\delta+1}{\gamma}\right) \tag{409}$$

Hence, the constant, a, can be given in terms of D. Also, by differentiating Eq. (408) with respect to r, one can find the maximum of the distribution. Thus

$$b = \frac{\delta}{\gamma r_c^{\gamma}} \tag{410}$$

where r_c is the mode radius of the distribution function.

Deirmendjian (1969) has considered essentially three haze models, each of which is described by the function (408) with different values of the constants in each case. Haze M is used to describe marine or coastal hazes; haze L is used to represent a continental-type aerosol; and, haze H is used to represent a high-level or stratospheric aerosol. These three distributions are illustrated in Figure 134. Junge's (1972) survey presents evidence "that the troposphere over the oceans is filled with a fairly uniform background aerosol on which the sea spray aerosol is superimposed only within the lowest kilometers above the sea surface." Figure 135, reproduced from Junge's article shows a summary of size distribution measurements over the North Atlantic. Figure 136, also reproduced from Junge (1972) includes data similar to that in Figure 135, but showing a differentiation between conditions with and without Sahara dust. Figure 137, reproduced from the same article shows a compilation of the undisturbed marine aerosols. The various features of the curves are explained in the caption as described by Junge.

10.3.3 SCATTERING PARAMETERS

The determination of the absorbing and scattering properties of even simple aerosol particles, such as spherical water droplets, is a rather involved procedure. Considering standard electromagnetic theory, one can find the scattering, absorption, and total extinction cross sections in terms of the wavelength of the radiation and the size and index of refraction of the particle. These are given by

$$\sigma_s(r) = \pi r^2 Q_s = \frac{2\pi r^2}{x^2} \sum_{\ell=1}^{\infty} (2\ell + 1)\left(|a_\ell|^2 + |b_\ell|^2\right) \tag{411}$$

$$\sigma_a(r) = \sigma_t(r) - \sigma_s(r) \tag{412}$$

$$\sigma_t(r) = \pi r^2 Q_t = \frac{2\pi r^2}{x^2} \sum_{\ell=1}^{\infty} (2\ell + 1)\,\mathrm{Re}\,(a_\ell + b_\ell) \tag{413}$$

where the parameters a_ℓ and b_ℓ are given in terms of Ricatti-Bessel functions, and the parameter $x = 2\pi r/\lambda$. The details of the dependence of these cross sections on the index of refraction, particle size, and structure is beyond the scope of this report. Excellent treatments of this

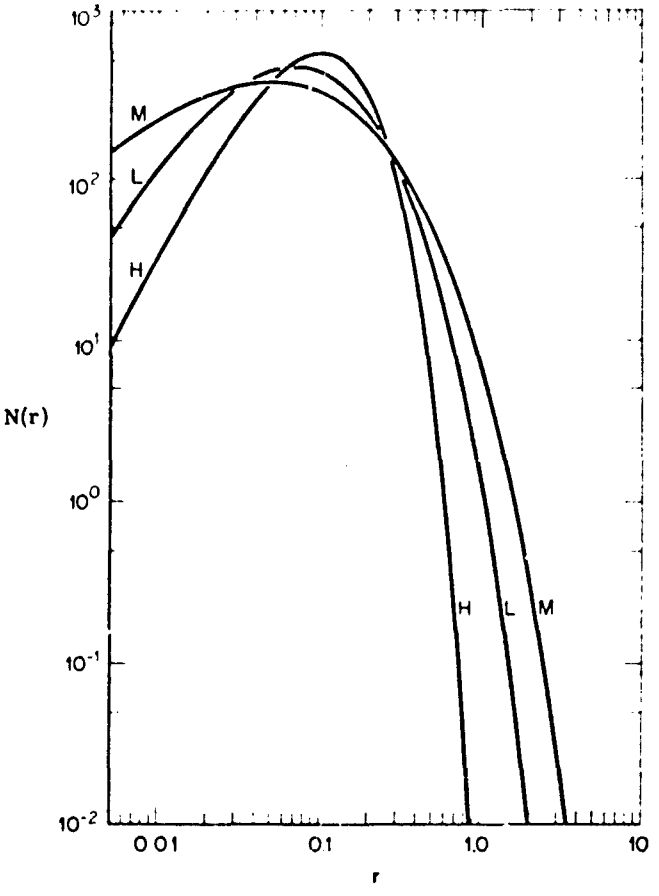

FIGURE 134. HAZE-TYPE DISTRIBUTION FUNCTIONS. The units for the radius r and for the unit volume in N(r) depend on the particular model. (Reproduced from Deirmendjian, 1969 [330].)

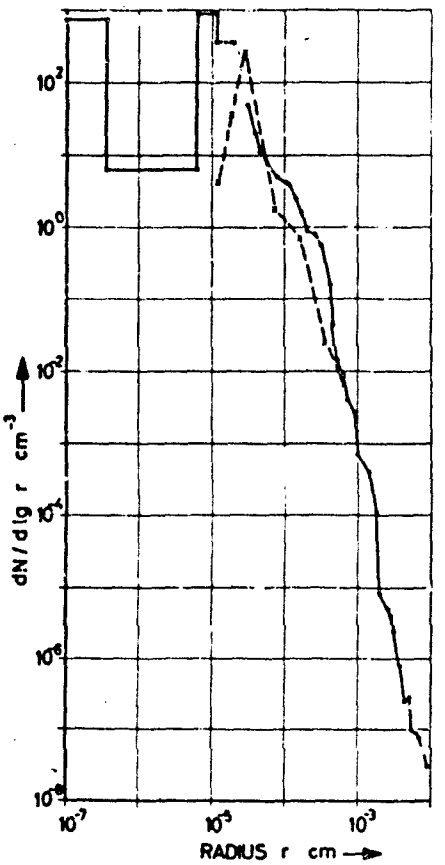

FIGURE 135. SUMMARY OF SIZE DISTRIBUTION MEASUREMENTS OVER THE NORTH ATLANTIC. The full curve for radii smaller than 2×10^{-5} cm was obtained by a combination of a photographic nuclei counter, diffusion boxes, and electrical denuders. The dashed line is obtained by a five-component, double stage impactor. The line above 5×10^{-5} cm is a combination of measurements by an optical counter (Royco) and by microscopic evaluation from a nozzle and a free wing impactor. Radii are given in centimeters ($1\ \mu = 10^{-4}$ cm), and the concentration density is given in particles per cubic centimeter and per unit log radius. (Reproduced from Junge, 1972 [284].)

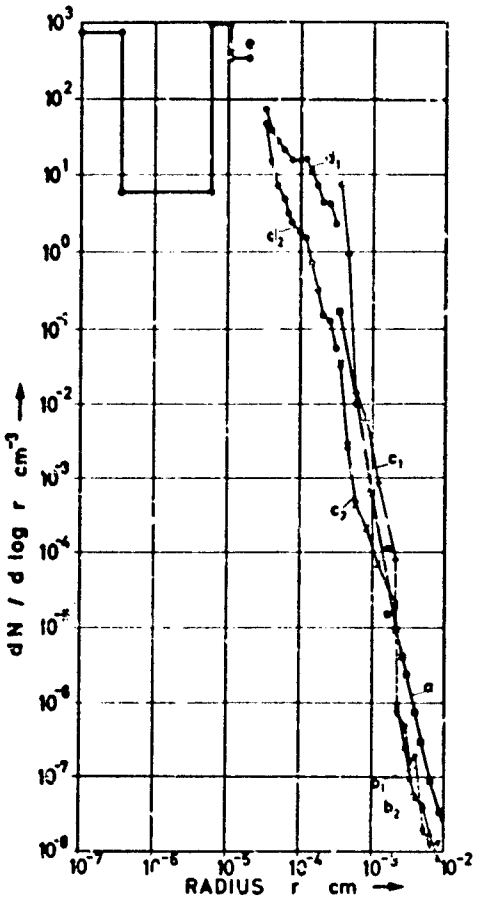

FIGURE 136. SOME OF THE DATA FROM FIGURE 135, BUT SEPARATED INTO DAYS WITH AND WITHOUT SAHARA DUST TO DEMONSTRATE THE DISTRIBUTION OF THE MINERAL DUST COMPONENT. Curve (a) is the average distribution for all data of the soluble fraction (sea salt,. Curves (b_1), (c_1) and (b_2), (c_2) represent the insoluble particles for days with and without Sahara dust. Curves (d_1) and (d_2) are distributions from the Royco counter and are also for days with and without Sahara dust. The Sahara dust has a range in radius size from about 3×10^{-5} to 2×10^{-3} cm. Curve (e) is the same as that in Figure 135 for comparison. (Reproduced from Junge, 1972 [284].)

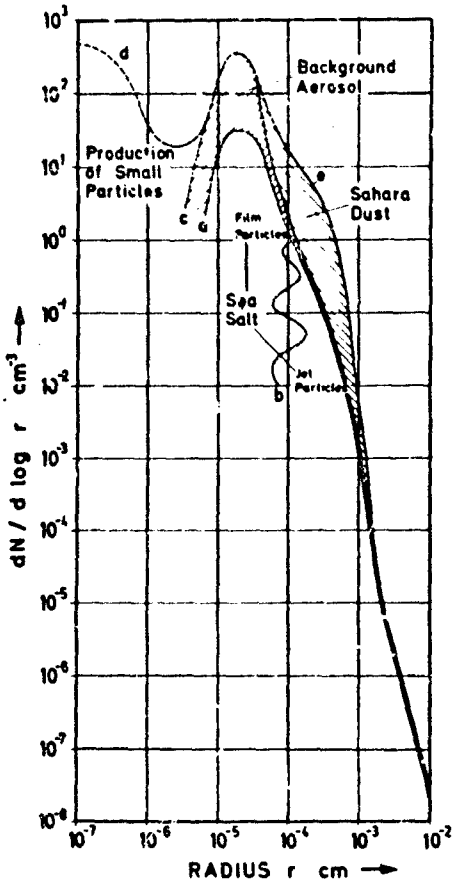

FIGURE 137. IDEALIZED DIAGRAM OF THE VARIOUS COMPONENTS OF THE UNDISTURBED MARINE AEROSOL. The diagram combines the information from several sources and tries to represent the present status of our knowledge. Below line (a) is the sea spray component separated by line (b) into film and jet particles. Line (b) is very uncertain and tries to demonstrate the fact that there is considerable overlapping of the two production mechanisms. Between line (c) and line (a) is the background aerosol, some part of which at least is of continental origin. Above about 10^{-4} cm the aerosol consists of about 15% of insoluble particles (at least over the Atlantic). Below 10^{-4} cm it consists most likely of sulfate, perhaps $(NH_4)_2SO_4$. Between lines (c) and (d) there is some indication of a component, which if confirmed may represent a steady-state distribution due to continuous production of very small particles. In air masses originating in Sahara dust storms the additional dust component is represented by line (e). All curves below about 10^{-4} cm are broken because they are rather uncertain. (Reproduced from Junge, 1972 [284].)

work are given by Stratton [334], van de Hulst [335], and Kerker [336].

One can find the angular properties of the scattering cross section by utilizing the dimensionless single-scattering phase function:

$$p(\theta, \phi) = i_2(\theta)\cos^2\phi + i_1(\theta)\sin^2\phi \tag{414}$$

where $i_1(\theta)$ and $i_2(\theta)$ are given in terms of Bessel functions. The integral of the phase function (414) over all space is related to the scattering cross section by:

$$\sigma_s(r) = \left(\frac{\lambda}{2\pi}\right)^2 \int_{4\pi} p(\theta, \phi)\sin\theta\, d\theta\, d\phi \tag{415}$$

The angular properties of the scattering functions involve lengthy calculations, but they have been carried out for a great variety of cases. A considerable amount of work has been done by Gumprecht and Sliepcevich [337] and by Denman, et al. [338].

For hazes, clouds, and fogs, we have a polydispersion of water droplets. Therefore, in order to find the scattering, absorption, and extinction coefficients, it is necessary to integrate over the particle size distribution; that is,

$$k'_a = \int_0^\infty \sigma_a(r)N(r)dr \tag{416}$$

$$k'_s = \int_0^\infty \sigma_s(r)N(r)dr \tag{417}$$

$$k' = \int_0^\infty \sigma_t(r)N(r)dr \tag{418}$$

334. J. A. Stratton, Electromagnetic Theory, McGraw-Hill, N. Y., 1941.

335. H. C. Van de Hulst, Light Scattering by Small Particles, John Wiley and Sons, N. Y., 1957.

336. M. Kerker, The Scattering of Light and Other Electromagnetic Radiation, Academic Press, N. Y., 1969.

337. R. O. Gumprecht and C. M. Sliepcevich, Tables of Light-Scattering Functions for Spherical Particles, University of Michigan, Ann Arbor, 1951.

338. H. H. Denman, W. Heller and W. J. Pangonis, Angular Scattering Functions for Spheres, Wayne State University Press, Detroit, 1966.

where k'_a, k'_s and k' are the volume absorption, scattering, and extinction coefficients, respectively.* The dimensions of k'_a, k'_s and k' are reciprocal lengths. Absorption in the visible region of the spectrum is generally small, and k'_a is only significant in the ultraviolet and infrared. The spectral dependence of the scattering cross-section $\sigma_s(r)$ is not as great as that for Rayleigh scattering. Thus

$$\sigma_s \text{ (Rayleigh)} \sim \lambda^{-4} \tag{419}$$

$$\sigma_s \text{ (Aerosols)} \sim \lambda^{-1.3} \tag{420}$$

From Eq.(420), it is clear that a thin haze will appear only slightly blue.

Knowing the number density of molecules in the atmosphere or the number density of statistical fluctuations, one can find the corresponding absorption, scattering, and extinction coefficients for Rayleigh scattering from Eqs. (416), (417) and (418). Likewise, one can also find the coefficients k'_a, k'_s, and k' for aerosol scattering. Therefore

$$k'_a = k'_{a_{\text{Rayleigh}}} + k'_{a_{\text{Aerosol}}} \tag{421}$$

$$k'_s = k'_{s_{\text{Rayleigh}}} + k'_{s_{\text{Aerosol}}} \tag{422}$$

$$k' = k'_{\text{Rayleigh}} + k'_{\text{Aerosol}} \tag{423}$$

For an atmosphere, the number density of particles decreases with increasing altitude, and it is convenient to define a quantity which is a measure of the amount of extinction. This quantity is the optical depth and is defined as (see Section 2.3):

$$q = \int_h^\infty -k'(z)dz \tag{424}$$

where h is some specific altitude and z is a variable altitude. The optical depth of the entire atmosphere for a given atmospheric density profile is then

$$q_0 = \int_0^\infty -k'(z)dz \tag{425}$$

*All quantities are spectral, unless otherwise stated.

If the particle size distribution function is independent of height, then

$$k'(z) = \sigma_t N(z) \tag{426}$$

and

$$q = \sigma_t \int_h^\infty N(z)dz \tag{427}$$

Thus, we see that $q = 0$ at the top of the atmosphere, and $q = q_0$ at the bottom surface.

As illustrated in Figure 138, the scattering of radiation from aerosols is quite different from that caused by density fluctuations (Rayleigh scattering) in the atmosphere. For comparison, the angular distributions resulting from Rayleigh, aerosol, and isotropic scattering are shown. Figure 139 shows the angular distribution of radiation scattered by a haze for different wavelengths and, for comparison, the Rayleigh function at 0.45 μm. The aerosol and Rayleigh curves in Figure 139 are normalized to different values and are not directly comparable.

For radiative-transfer calculations, it would be convenient to have a simple analytical expression describing the phase function. One such function is the Henyey-Greenstein phase function, defined as

$$p(\cos\theta) = \frac{1 - g^2}{(1 + g^2 - 2g\cos\theta)^{3/2}} \tag{428}$$

where g is the average value of the cosine of the scattering angle θ. Perhaps a more descriptive parameter is the anisotropy parameter η, the fraction of radiation scattered into a forward hemisphere. Thus

$$\eta = \frac{1}{4\pi}\int_0^{2\pi}\int_0^1 \frac{1 - g^2}{(1 + g^2 - 2g\cos\theta)^{3/2}}\, d(\cos\theta)d\phi \tag{429}$$

Figure 140 shows the Henyey-Greenstein phase function for various values of η, and Figure 141 shows a comparison between the Henyey-Greenstein phase function and a more realistic one by Deirmendjian. For typical haze-type aerosols in the visible region, the value of η is approximately 0.95 (i.e., 95% of the radiation is scattered into the forward hemisphere.)

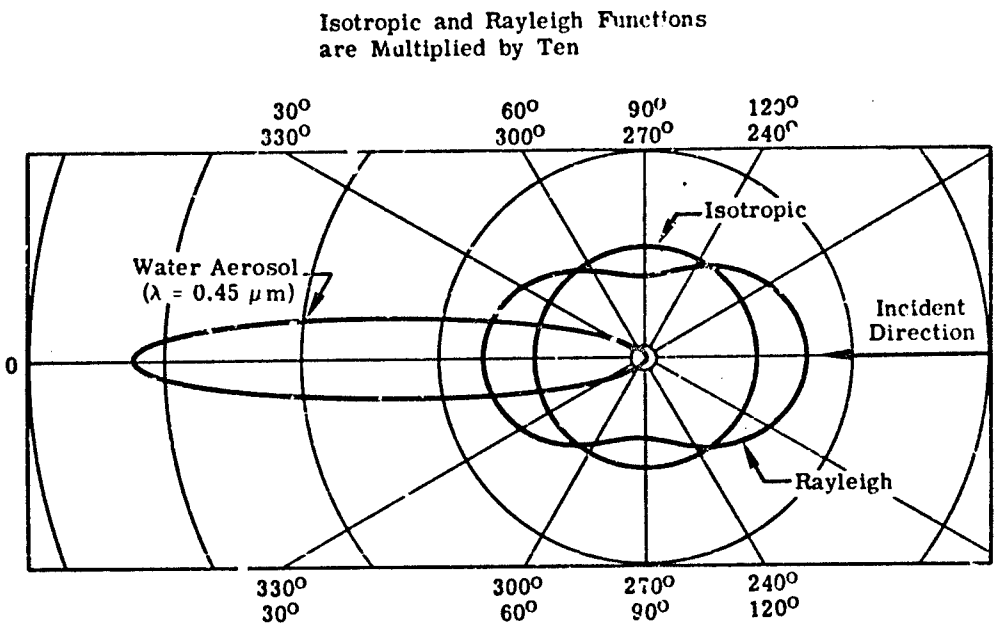

FIGURE 138. ANGULAR DEPENDENCE OF SINGLE-SCATTERING PHASE FUNCTIONS IN ANY AZIMUTHAL PLANE

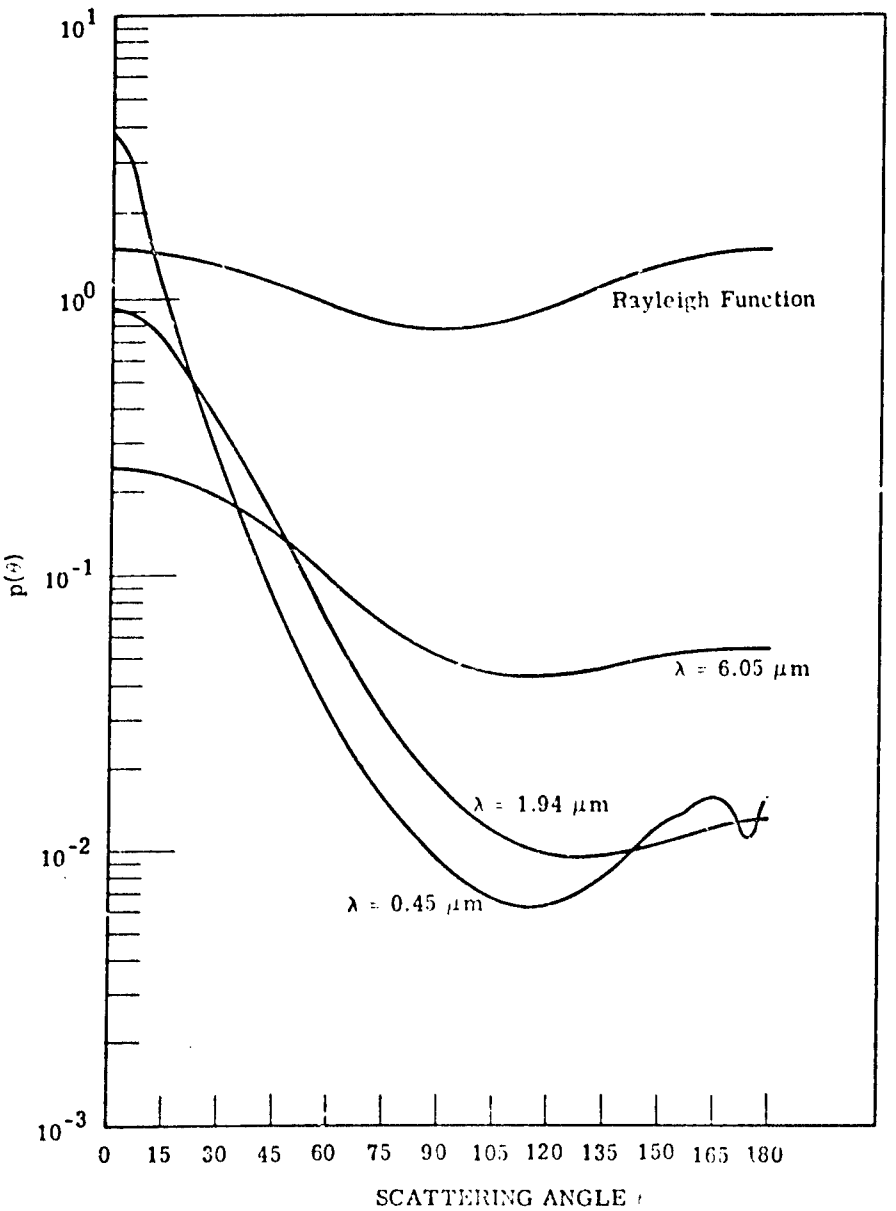

FIGURE 139. COMPARISON OF DEIRMENDJIAN'S PHASE FUNCTIONS AT DIFFERENT WAVELENGTHS FOR WATER HAZE L

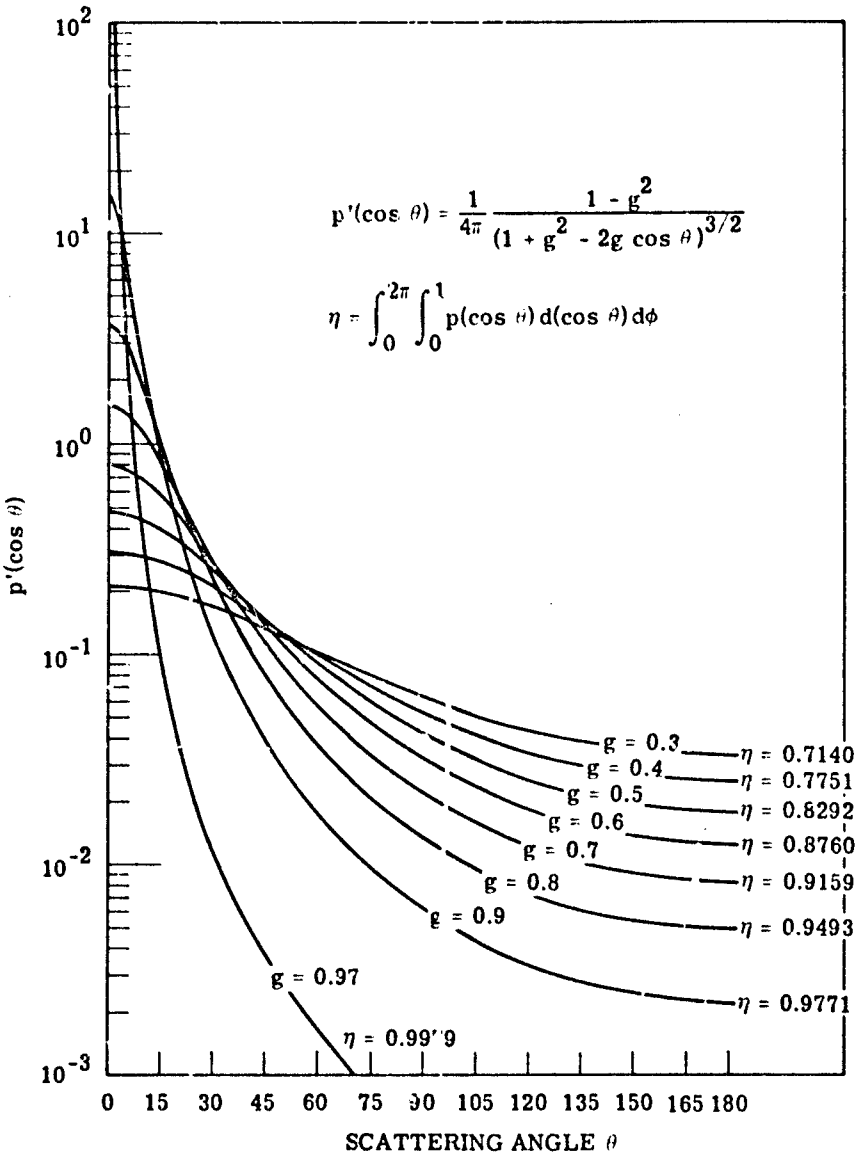

FIGURE 140. HENYEY-GREENSTEIN PHASE FUNCTION FOR DIFFERENT VALUES OF THE ANISOTROPY PARAMETER η

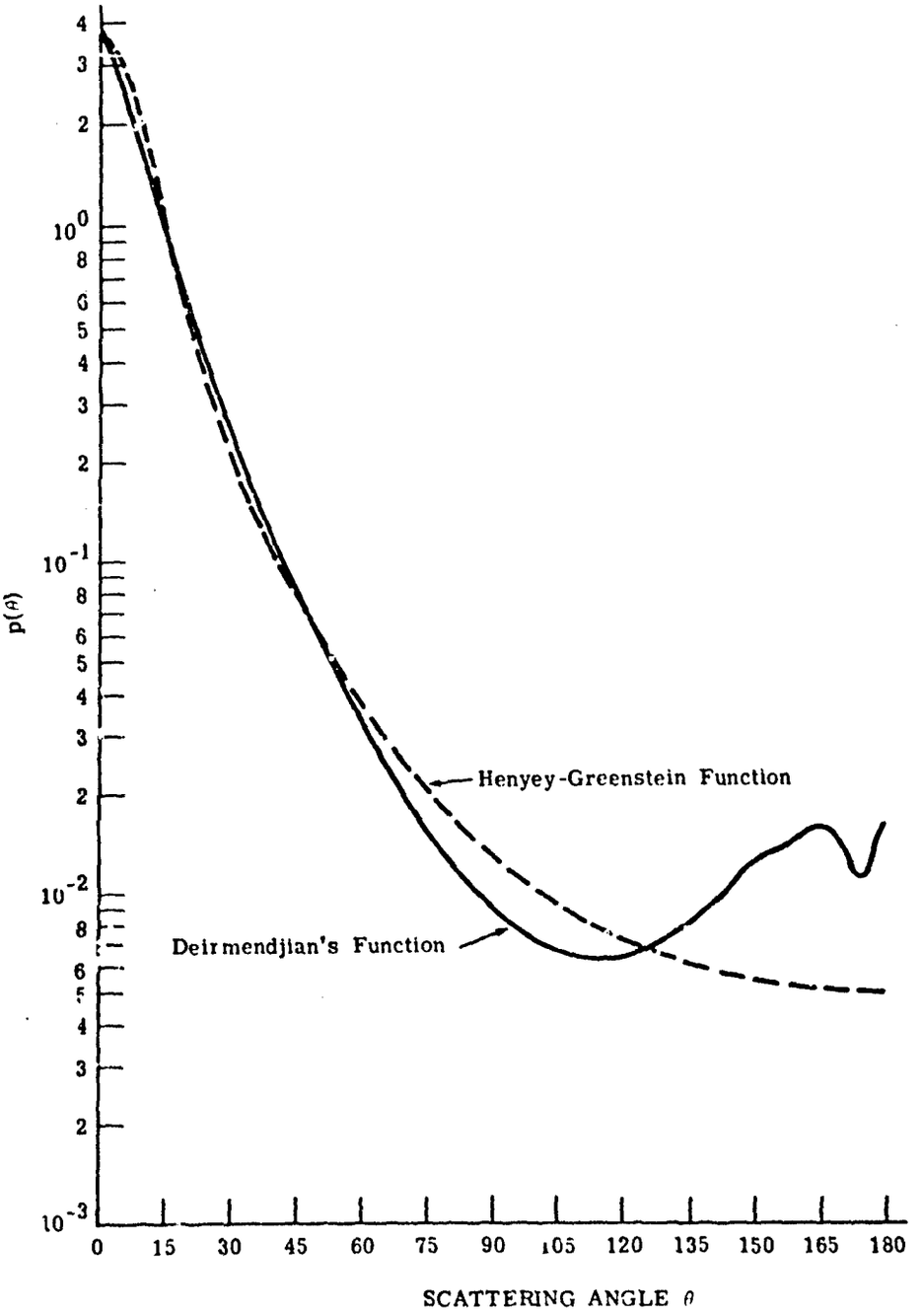

FIGURE 141. COMPARISON OF DEIRMENDJIAN'S PHASE FUNCTION FOR WATER HAZE L AT $\lambda = 0.45\ \mu m$ AND THE HENYEY-GREENSTEIN PHASE FUNCTION WITH ANISOTROPY PARAMETER $\eta = 0.9493$

10.3.4 VISIBILITY

In a parametric study of remote sensing techniques in the Earth's atmosphere, we should include effects of atmospheric variability. We are primarily interested in the variations of scattering properties in terms of short-term atmospheric conditions. The long-term, i.e., seasonal, variation is summarized quite well by Robinson [339].

One parameter which can be used for the description of the state of the atmosphere is the visual range, or visibility. In 1924, Koschmieder [340] assumed that the limiting contrast between objects in daylight was 0.02 in order for the objects to be just barely visible. Nevertheless, today it is quite conventional to use his value, and we refer to his limiting contrast as transmittance. Using this value, we find that a unique relationship exists between the extinction coefficient κ and visibility, V. According to Koschmieder's definition, we have

$$V = \frac{3.91}{\kappa} \tag{430}$$

which is shown in Figure 142.

It has been thought that dust particles emanating from volcanic eruptions significantly affect the transmission of solar radiation. New aerosol-density profile data from the well documented eruption of Agung, on Bali, have been analyzed and are used by Elterman [341] to determine a current, universal, optical depth-altitude relationship for wavelengths in the range of 0.27 μm to 4.0 μm. We use this relationship in our computations. Based on measurements by Curcio, Knestrick, and Cosden [342], Elterman [343] has developed formulas for the extinction coefficient as a function of visual range and wavelength. Using aerosol-density scale heights, he further determined an optical depth-altitude relationship for wavelengths in the range 0.27 μm to 2.17 μm, with wavelengths selected in the infrared region to correspond to windows, or regions where the transmission is large. This was done for a family of visual ranges from 2 km to 13 km. A three-dimensional plot of this relationship is shown, for a wavelength of 0.55 μm in Figure 143. We make use of these parameters in a detailed

339. N. Robinson, Solar Radiation, American Elsevier Publishing Company, N. Y., 1966.

340. H. Koschmieder, Beitr. Phys. freien Atm., Vol. 12, 1924, pp. 33-53; 171-181.

341. L. Elterman, UV, Visible, and IR Attenuation for Altitudes to 50 km, Report No. AFCRL-68-0153, Air Force Cambridge Research Laboratories, Bedford, Mass., 1968.

342. J. S. Curcio, G. L. Knestrick and T. H. Cosden, Atmospheric Scattering in the Visible and Infrared, Report No. 5567, U. S. Naval Research Laboratory, Washington, D. C., 1961.

343. L. Elterman, Vertical Attenuation Model with Eight Surface Meteorological Ranges 2 to 13 Kilometers, Report No. AFCRL-70-0200, Air Force Cambridge Research Laboratories, Bedford, Mass., 1970.

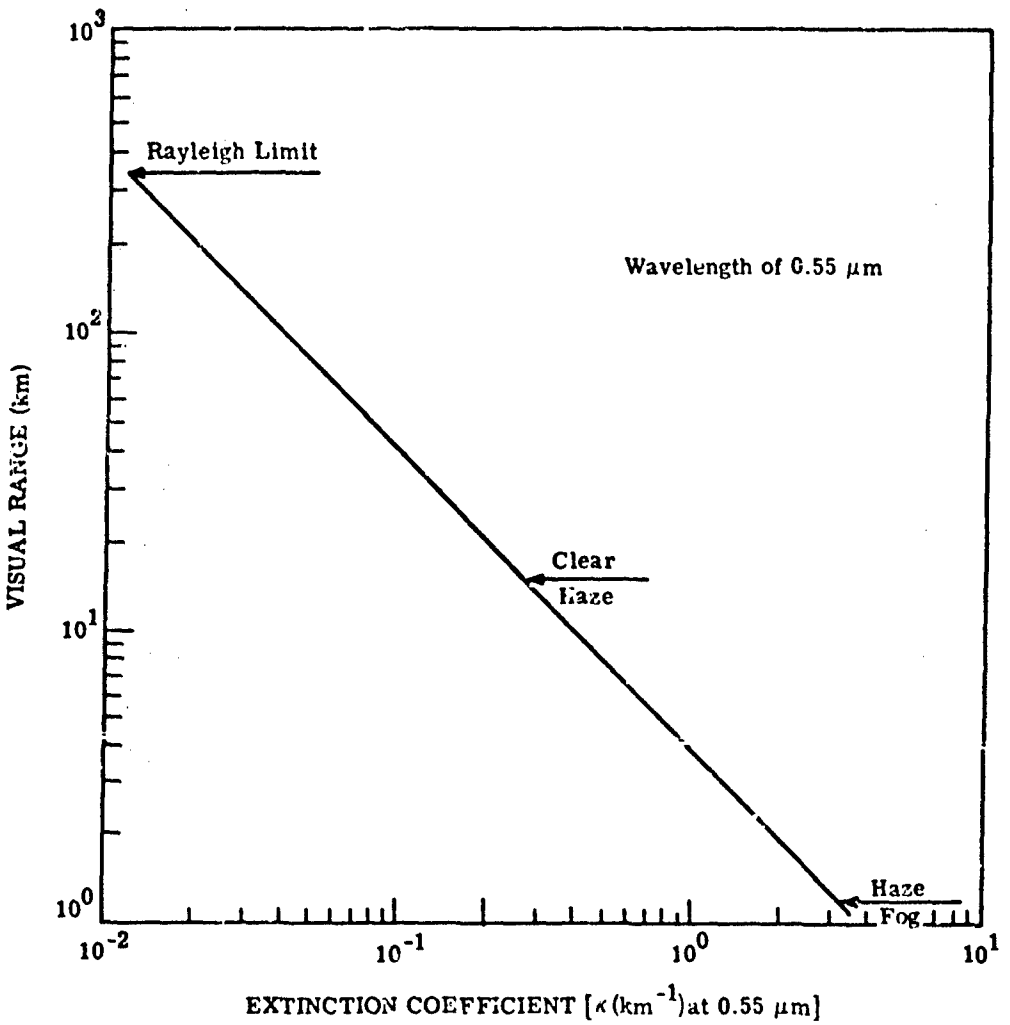

FIGURE 142. VARIATION OF VISUAL RANGE WITH EXTINCTION COEFFICIENT

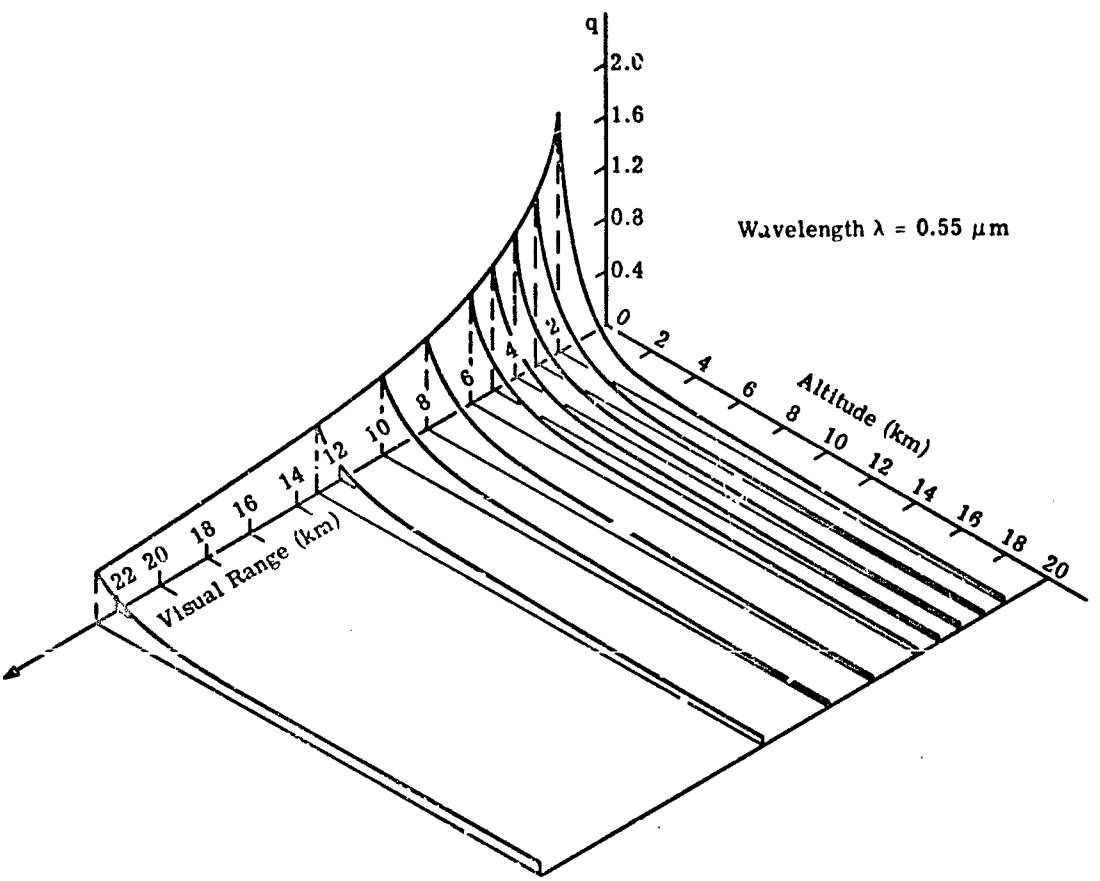

FIGURE 143. OPTICAL DEPTH VERSUS VISUAL RANGE AND ALTITUDE

analysis of radiative transfer in the atmosphere. We use a horizontal, sea-level, visual range. This range may also be the same for a different atmospheric aerosol-density profile. The profile used by Elterman is an exponential one; that is, the aerosol number density decreases exponentially with increases in altitudes. For additional information concerning the optical properties of the atmosphere, consult Rozenburg (1968), Kondratyev (1969), Robinson (1966), and Middleton [344].

10.3.5 PARTICLE DISTRIBUTION TO SUPPLEMENT ABSORPTION BAND MODEL CALCULATIONS IN THE IR SPECTRUM

Both of the generally available methods, Aggregate and LOWTRAN, use a simple extinction term to account for the usually small effect of scattering in the infrared spectral region. Each calls for particle densities and size distributions which have been adopted from some of the extensive, basic work that has been done in scattering phenomena. The Aggregate method uses a maritime haze model for water droplets (see Hamilton, 1973) with a size distribution shown in Figure 144 (see also Ref.[345] and a particulate density distribution shown in Figure 145).

The LOWTRAN model considers two aerosol models describing a "clear" and "hazy" atmosphere corresponding to visibilities of 23 and 5 km respectively at ground level. The size distribution considered, as in the Aggregate method, to be the same for all altitudes, is that suggested by Deirmendjian [346] for continental haze and shown in Figure 146 with the regions given by:

$$\begin{aligned} N_r(r) &= C_1 \cdot r^{-4} \text{ for } 0.1\ \mu m \le r < 10\ \mu m \\ N_r(r) &= C_1 \cdot 10^4 \text{ for } 0.02\ \mu m < r < 0.1\ \mu m \\ N_r(r) &= 0 \text{ for } r < 0.02 \text{ and } r > 10.0 \end{aligned} \qquad (431)$$

where $C_1 = 8.83 \times 10^{-4}$. The vertical distribution of particle densities for the "clear" and "hazy" atmospheres are given in Table 65. The imaginary part of the refractive index of the aerosols is considered to be zero below $\lambda = 0.6\ \mu m$, and to increase linearly from 0.6 to 2.0 μm.

344. W. E. K. Middleton, Vision Through the Atmosphere, University of Toronto Press, Toronto, 1952.

345. L. Elterman, "Parameters for Attenuation in the Atmosphere Windows for Fifteen Wavelengths," Appl. Opt., Vol. 3, No. 6, 1964, p. 745.

346. D. Deirmendjian, "Scattering and Polarization Properties of Polydispersed Suspensions with Partial Absorption," Proc. Interdisciplinary Conf. on Electromagnetic Scattering, Potsdam, Pergamon Press, New York, 1963.

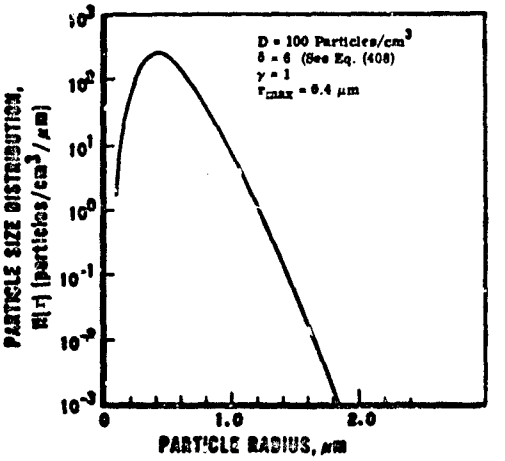

FIGURE 144. MARITIME HAZE WATER DROPLET DISTRIBUTION. (Reproduced from Hamilton, et al., 1973 [19].)

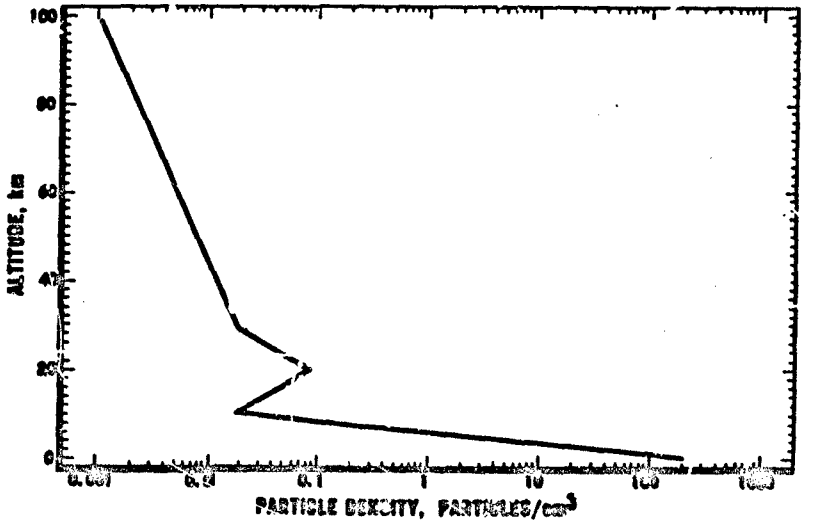

FIGURE 145. AEROSOL NUMBER DENSITY VERSUS ALTITUDE (Reproduced from Hamilton, et al., 1973 [19].)

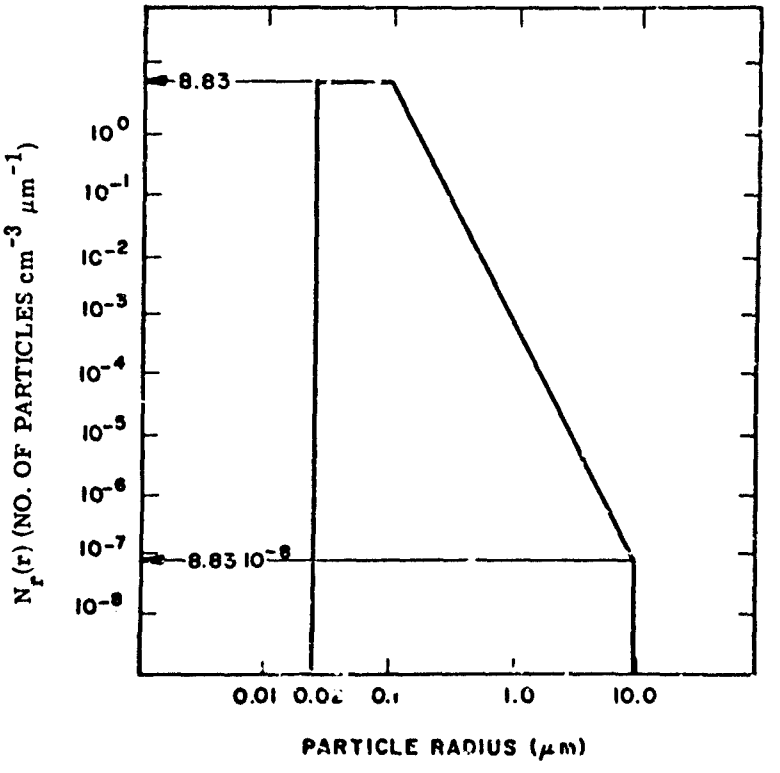

FIGURE 146. NORMALIZED PARTICLE SIZE DISTRIBUTION FOR AEROSOL MODELS. (Reproduced from McClatchey, et al., 1972 [21].)

TABLE 65. AEROSOL MODELS: VERTICAL DISTRIBUTIONS FOR A "CLEAR" AND "HAZY" ATMOSPHERE. (From McClatchey, et al., 1972 [21].)

	PARTICLE DENSITY D (PARTICLES PER cm^3)	
Altitude (km)	23 km Visibility Clear	5 km Visibility Hazy
0	2.828E+03	1.378E+04
1	1.244E+03	5.030E+03
2	5.371E+02	1.844E+03
3	2.256E+02	6.731E+02
4	1.192E+02	2.453E+02
5	8.987E+01	8.987E+01
6	6.337E+01	6.337E+01
7	5.890E+01	5.890E+01
8	6.069E+01	6.069E+01
9	5.818E+01	5.818E+01
10	5.675E+01	5.675E+01
11	5.317E+01	5.317E+01
12	5.585E+01	5.585E+01
13	5.156E+01	5.156E+01
14	5.048E+01	5.048E+01
15	4.744E+01	4.744E+01
16	4.511E+01	4.511E+01
17	4.458E+01	4.458E+01
18	4.314E+01	4.314E+01
19	3.634E+01	3.634E+01
20	2.667E+01	2.667E+01
21	1.933E+01	1.933E+01
22	1.455E+01	1.455E+01
23	1.113E+01	1.113E+01
24	8.826E+00	8.826E+00
25	7.429E+00	7.429E+00
30	2.238E+00	2.238E+00
35	5.890E-01	5.890E-01
40	1.550E-01	1.550E-01
45	4.082E-02	4.082E-02
50	1.078E-02	1.078E-02
70	5.550E-05	5.550E-05
100	1.969E-08	1.969E-08

The values in Table 65 are adjusted to match the Elterman (1968, 1970) coefficients at 0.55 μm wavelength. The effective ground-level visible range is 23 km. The "hazy" model is the same as the "clear" model above 5 km, but increased exponentially below 5 km to yield an effective visible range at ground level to 5 km.

There is always an aerosol component in the atmosphere, even on very clear days, but the Rayleigh limit, with $\kappa = 1.162 \times 10^{-2} km^{-1}$, corresponds to a horizontal visual range of 336 km. On the other hand, for large extinction coefficients such as those for a fog, the visual range is only about 1.2 km. This haze-fog transition is shown in Figure 142.

REFERENCES

To facilitate the use of this reference list, entries have been arranged in alphabetical order. Numbers in brackets after each entry indicate the reference number assigned in the text.

L. A. Abels, A Study of Total Absorption near 4.5 by Two Samples of N_2C, As Their Total Pressure and N_2O Concentrations were Independently Varied, Scientific Report No. 3, AFCRL-62-236, Ohio State University, Columbus, January 1962. [260]

M. Abramowitz and I. A. Stegun, Handbook of Mathematical Functions, National Bureau of Stardards, Applied Math. Series No. 55, Washington, D. C., 1964. [215]

A. Adel and C. C. Lampland, "A New Band of the Absorption Spectrum of the Earth's Atmosphere," Astrophys. J., Vol. 87, 1938, p. 198. [287]

A. Adel, "Note on the Atmospheric Oxides of Nitrogen," Astrophys. J., Vol. 90, 1939, p. 627. [288]

A. Adel, "Equivalent Thickness of the Atmospheric Nitrous Oxide Layer," Phys. Rev., Vol. 59, 1941, p. 944. [300]

A. Adel, "Identification of Carbon Monoxide in the Atmosphere above Flagstaff, Arizona," Astrophys. J., Vol. 116, 1952, p. 442. [316]

T. L. Altshuler, Infrared Transmission and Background Radiation by Clear Atmospheres, No. 61SD199, General Electric Co., 1961, 140 pp. [245]

V. A. Ambartsumian, "Diffuse Reflection of Light by a Foggy Medium," Compt. rend. (Doklady) Acad. Sci., USSR, Vol. 38, 1943, p. 229. [43]

D. Anding, Band Model Methods for Computing Atmospheric Slant-Path Molecular Absorption, Rept. No. 7142-21-T, Willow Run Laboratories of the Institute of Science and Technology, University of Michigan, Ann Arbor, 1967. [1]

D. Anding, Private Communication, New Technique in Parameter Calculation, 1974. [247]

A. Arking and K. Grossman, "The Influence of Line Shape and Band Structure on Temperatures in Planetary Atmosphere," J. Atmos. Sci., Vol. 29, 1972, pp. 937-949. [10]

B. H. Armstrong, "Spectrum Line Profiles: The Voigt Function," J. Quant. Spect. Rad. Trans., Vol. 7, 1967, pp. 61-88. [122]

B. H. Armstrong, "Analysis of the Curtis-Godson Approximation and Radiation Transmission Through Inhomogeneous Atmospheres," J. Atmos. Sci., Vol. 25, 1968, pp. 312-322. [212]

B. H. Armstrong, "Exponential Integral Approximations," J. Quant. Spect. Rad. Trans., Vol. 9, 1969, pp. 1039-1040. [217]

B. H. Armstrong and J. Dave, Gaussian Quadratures of the Exponential Integral, Rept. No. 320-3250, IBM Palo Alto Sci. Center, Palo Alto, Calif., 1969. [220]

R. L. Armstrong and H. L. Walsh, Spectrochim Acta, Vol. 16, 1960, p. 840. [186]

A. Arnulf, J. Bricard, E. Cure and C. Veret, J. Opt. Soc. Am., Vol. 47, 1957, p. 491. [275]

J. C. Arvesen, R. N. Griffin, Jr. and B. D. Pearson, Jr., "Determination of Extraterrestrial Solar Spectral Irradiance from a Research Aircraft," Appl. Optics, Vol. 8, No. 11, 1969. [34]

C. Ashley, L. Gastineau and D. Blay, Unpublished data, 1971-1972. [279]

G. Ashley, Private communication, 1974. [251]

Baumeister and Marquardt, Least-Squares Estimation of Non-Linear Parameters, SHARE Program No. 1423, FORTRAN Program, IBM. [201]

R. Beer, Private communication (1970) to McClatchey, et al., 1973. [169]

E. E. Bell, Infrared Techniques and Measurements (Interim Engineering Report for Period July-September 1956 on Contract AF 33(616)-3312), Ohio State University, Columbus, 1956. [265]

R. E. Bellman, H. H. Kagiwada and R. E. Kaloba, Time-Dependent Diffuse Reflection From Slabs with Multiple Scattering, Memo RM-5070-PR, The RAND Corporation, July 1966. [93]

R. Bellman, H. Kagiwada, R. Kaloba and M. Prestrud, Invariant Imbedding and Time Dependent Processes, American Elsevier Publishing Company, New York, 1964. [90]

R. Bellman and R. Kalaba, "On the Principle of Invariant Imbedding and Propagation Through Inhomogeneous Media," Proc. Nat. Acad. Sci., USA, Vol. 42, 1956, pp. 629-632. [68]

R. Bellman, R. Kalaba and M. Prestrud, Invariant Imbedding and Radiative Transfer in Slabs of Finite Thickness, American Elsevier Publishing Company, New York, 1963. [89]

Y. Ben-Aryeh, J. Quant. Spec. Rad. Trans., Vol. 7, 1970, p. 211. [163]

W. S. Benedict, Private communication (1973) to McClatchey, et al., 1973. [185]

W. S. Benedict and R. F. Calfee, Line Parameters for the 1.9 and 6.3 micron Water Vapor Bands, ESSA Professional Paper 2, (June 1967) U. S. Government Printing Office, June 1967. [141]

W. S. Benedict and R. Sams, Twenty-Sixth Symposium on Molecular Spectroscopy, Ohio State University, Columbus, 1971. [170]

W. S. Benedict, R. Herman, S. Moore and S. Silverman, "The Strengths, Widths and Shapes of Infrared Lines, I. General Considerations," Canadian J. of Physics, Vol. 34, 1956(a), pp. 830-849. [127]

W. S. Benedict, R. Herman, S. Moore and S. Silverman, "The Strengths, Widths and Shapes of Infrared Lines, II. The HCl Fundamental," Canadian J. of Physics, Vol. 34, 1956(b), pp. 850-875. [128]

W. S. Benedict, et al., "The Strengths, Widths, and Shapes of Lines in the Vibration-Rotation Bands of CO," Astrophys. J., Vol. 135, No. 1, pp. 277-297. [233]

W. S. Benedict, S. A. Clough, W. J. Lafferty, L. Frenkel, T. E. Sullivan, J. Bellet and G. Steenbeckeliers, (1973), to be published. [155]

W. S. Benedict, H. Chang, S. A. Clough and W. J. Lafferty, (1973), to be published. [168]

W. Benesch, M. V. Migeotte and L. Neven, "Investigations of Atmospheric CO at the Jungfraujoch," J. Opt. Soc. Am., Vol. 43, 1953, p. 1119. [315]

K. Bignell, F. Saiedy and P. A. Sheppard, "On the Atmospheric Infrared Continuum," J. Opt. Soc. Am., Vol. 53, No. 4, 1963, pp. 466-479. [187]

K. Bignell, "The Water Vapor Infrared Continuum," Quart. J. Roy. Met. Soc., Vol. 96, 1970, pp. 390-403. [241]

J. W. Birkeland, "Determination of Ground Level N_2O," M.S. thesis, Ohio State University, Columbus, 1957. [305]

J. W. Birkeland and J. H. Shaw, J Opt. Soc. Am., Vol. 49, 1959, p. 637. [297]

J. W. Birkeland, D. E. Burch and J. H. Shaw, "Some Comments on Two Articles by Taylor and Yates," J. Opt. Soc. Am., Vol. 47, 1957, p. 441. [304]

B. Bobin and K. Fox, J. Chem. Phys. and J. Phys. (Paris), 1973. [183]

A. L. Bowman, A Determination of the Abundance of Nitrous Oxide, Carbon Monoxide and Methane in Ground Level Air at Several Locations near Columbus, Ohio (Scientific Report No. 1 on Contract AF 19(604)-2259), Ohio State University, Columbus, 1959. [306]

W. R. Bradford, T. M. McCormick and J. A. Selby, Laboratory Representation of Atmospheric Paths for Infrared Absorption, Report No. DMP 1431, EMI Electronics, Hayes, Middlesex, England, 1963. [242]

J. R. Bray, "An Analysis of the Possible Recent Change in Atmospheric Carbon Dioxide," Tellus, Vol. 11, 1959, pp. 220-230. [295]

J. R. Breckenridge and D. N. B. Hall, Solar Physics, to be published, (1973). [178]

J. N. Brooks, A. Goldman, J. J. Kosters, D. G. Murcray, F. H. Murcray and W. J. Williams, "Balloon-Borne Infrared Measurements," in Physics and Chemistry of Upper Atmospheres, B. N. McCormac (ed.), Proceedings of a Symposium organized by the Summer Advanced Study Institute, held at the University of Orleans, France, July 31-August 11, 1972, D. Reidel Publishing Co., Dordrecht, Holland, 1973, pp. 278-285. [319]

D. E. Burch, Investigation of the Absorption of Infrared Radiation by Atmospheric Gases, Air Force Cambridge Research Labs., Philco Report No. U-4784, Philco-Ford Corporation, 1970. [189]

D. E. Burch and D. A. Gryvnak, Infrared Radiation Emitted by Hot Gases and Its Transmission Through Synthetic Atmospheres, Report No. U-1929, Philco-Ford Corporation, 1962. [227]

D. E. Burch and D. A. Gryvnak, Strengths, Widths and Shapes of the Lines of the 3ν CO Band, Report No. U-3972, Philco-Ford Corporation, 1967. [131]

D. E. Burch and D. Gryvnak, Unpublished data, (1971). [160]

D. E. Burch and D. Gryvnak, Unpublished data, (1973). [166]

D. E. Burch, D. A. Gryvnak and R. R. Patty, Absorption by CO_2 Between 4500 and 5400 cm^{-1}, Report No. U-2955, Philco-Ford Corporation, 1964. [254]

D. E. Burch, D. A. Gryvnak and R. R. Patty, Absorption by H_2O Between 2800 and 4500 cm^{-1} (2.7 Micron Region), Report No. U-3202, Philco-Ford Corporation, 1965. [228]

D. E. Burch, D. A. Gryvnak and R. R. Patty, Absorption by CO_2 Between 4500 and 5400 cm^{-1} (2 μm Region), Aeronutronic Report U-2955, (1964); 6600 and 7125 cm^{-1} (1.4 μm Region), Aeronutronic Report U-3127 (1965); 8000 and 10,000 cm^{-1} (1 to 1.25 μm Region), Aeronutronic Report U-3200 (1965); 5400 and 6600 cm^{-1} (1.6 μm Region), Aeronutronic Report U-3201 (1965); 1800 and 2850 cm^{-1} (3.5 - 5.6 μm Region), Aeronutronic Report U-3857 (1966); 7125 and 8000 cm^{-1} (1.25 to 1.4 μm Region), Aeronutronic Report U-3930 (1967); 3100 and 4100 cm^{-1} (2.44 to 3.22 μm Region), Aeronutronic Report U-4132 (1968); Philco-Ford Corporation. [263]

D. E. Burch, D. A. Gryvnak and R. R. Patty, Absorption by H_2O Between 2800 and 4500 cm^{-1} (2.7 μm Region), Aeronutronic Report U-3202 (1965); 5045 and 14,485 cm^{-1} (0.69 to 1.98 μm Region), Aeronutronic Report U-3704 (1966); 1630 and 2245 cm^{-1} (6.13 to 4.44 μm Region), Aeronutronic Report U-5090 (1973); Philco-Ford Corporation. [269]

D. E. Burch, D. A. Gryvnak and J. D. Pembrook, Investigation of the Absorption of Infrared Radiation by Atmospheric Gases, Report No. U-4829, Philco-Ford Corporation, 1970. [188]

D. E. Burch, D. A. Gryvnak and J. D. Pembrook, Investigation of Infrared Absorption by Nitrous Oxide from 4000 to 6700 cm^{-1} (2.5 to 1.5 μm), Aeronutronic Report U-4943 (1971); 760 to 2380 cm^{-1} (13.2 to 4.2 μm), Aeronutronic Report U-4995 (1971); Philco-Ford Corporation. [270]

D. E. Burch, D. A. Gryvnak and E. B. Singleton, et al., Absorption by Carbon Dioxide, Water Vapor, and Minor Atmospheric Constituents, Report No. AFCRL 62-298, Ohio State University, Columbus, 1962. [234]

D. E. Burch, D. A. Gryvnak and D. Williams, Science Report No. 2, AF 19(604)-2633, Ohio State University, Columbus, January 1961. [235]

I. W. Busbridge, Astrophys. J., Vol. 122, 1955, p. 327. [45]

I. W. Busbridge, The Mathematics of Radiative Transfer, Cambridge University Press, 1960. [46]

R. F. Calfee and W. S. Benedict, Carbon Dioxide Spectral Line Positions and Intensities Calculated for the 2.05 and 2.7 Micron Regions, Technical Note 332, National Bureau of Standards, 1966. [140]

G. S. Callendar, "On the Amount of Carbon Dioxide in the Atmosphere," Tellus, Vol. 10, 1958, pp. 243-248. [292]

J. Canosa and H. R. Penafiel, "A Direct Solution of the Radiation Transfer Equation: Application to Rayleigh and Mie Atmospheres," J. Quant. Spect. Rad. Trans., Vol. 13, 1973, pp. 21-39. [78]

B. G. Carlson and K. D. Lathrop, "Transport Theory, The Method of Discrete Ordinates," Computing Methods in Reactor Physics, H. Greenspan, C. N. Kelber and D. Okrent, (eds.), Gordon and Breach, New York, 1968. [82]

D. Carmer, Target Signature Analysis Center: Data Compilation, 7th Supplement, Infrared & Optical Sensor Laboratory, Willow Run Laboratories of the Institute of Science and Technology, University of Michigan, Ann Arbor, 1969. [38]

K. M. Case, "Elementary Solutions of the Transport Equation and Their Applications," Ann. Phys. (N.Y.), Vol. 9, 1960, pp. 1-23. [55]

K. M. Case, Recent Developments in Neutron Transport Theory, Michigan Memorial Phoenix Project, Lectures Presented at the Neutron Physics Conference, University of Michigan, Ann Arbor, 1961. [56]

K. M. Case, On the Boundary Value Problems of Linear Transport Theory, Transport Theory, Vol. I, R. Bellman, G. Birkhoff and I. Abu-Shumays (eds.), Proceedings of a Symposium in Applied Mathematics of the American Mathematical Society and the Society for Industrial and Applied Mathematics, Providence, R.I., 1969. [60]

K. M. Case and P. F. Zweifel, Linear Transport Theory, Addison-Wesley Publishing Company, Reading, Mass., 1967. [57]

J. W. Chamberlain and M. B. McElroy, Astrophys. J., Vol. 144, 1966, p. 1148. [53]

S. Chandrasekhar, Radiative Transfer, Oxford University Press, 1950. [42]

L. W. Chaney, High Resolution Spectroscopic Measurements of Carbon Dioxide and Carbon Monoxide, Rept. No. 036350-3-T, University of Michigan, Ann Arbor, 1972. [148]

S. A. Clough and F. X. Kneizys, Ozone Absorption in the 9.0 Micron Region, Report No. AFCRL-65-862, Air Force Cambridge Research Laboratories, Bedford, Mass., 1965. [143]

W. Cody and H. Thatcher, Jr., Math. Comp., Vol. 22, 1968, p. 641. [218]

D. G. Collins, Atmospheric Path Radiance Calculations for a Model Atmosphere, Report No. AFCRL-68-0124, Air Force Cambridge Research Laboratories, Bedford, Mass., 1968. [101]

D. G. Collins and M. B. Wells, Monte Carlo Codes for Study of Light Transport in the Atmosphere, Vol. I. Description of Codes, Vol. II, Utilization, ECOM-00240-F I, ECOM-00240-F II, 1965. [100]

J. Connes, P. Connes and J. P. Maillard, Near Infrared Spectra of Venus, Mars, Jupiter and Saturn and Atlas of Near Infrared Spectra of Venus, Mars, Jupiter and Saturn, Centre National de la Recherche Scientifique, Paris, 1969. [174]

B. J. Conrath, R. Hanel, V. Kunde and C. Prabhahara, "The Infrared Interferometer Experiment on Nimbus 3," J. Geophys. Res., Vol. 75, No. 30, 1970, pp. 5831-5857. [224]

K. L. Coulson, J. V. Dave and Z. Sekera, Tables Related to Radiation Emerging from a Planetary Atmosphere with Rayleigh Scattering, University of California Press, Berkeley, 1960. [44]

J. S. Curcio, G. L. Knestrick and T. H. Cosden, Atmospheric Scattering in the Visible and Infrared, Report No. 5567, U. S. Naval Research Laboratory, Washington, D. C., 1961. [342]

J. Curcio, L. Drummeter and G. Knestrick, Appl. Opt., Vol. 3, No. 12, 1964. p. 1401. [261]

J. Curcio, R. Eckardt, C. Acton and T. Cosden, An Atlas of the Absorption of the Atmosphere from 8512 to 11,600 A, Report No. 6352, U. S. Naval Research Laboratory, Washington, D. C., 1965. [282]

A. R. Curtis, "Discussion of Goody's 'A Statistical Model for Water-Vapour Absorption'," Quart. J. Roy. Met. Soc., Vol. 58, 1952, p. 638. [205]

M. Dang-Nhu, Thesis, Université de Paris, 1968. [181]

G. Daniels, AVCO Everett Research Laboratory, private communication 1973.

G. Daniels, "A Computer Program for Atmospheric Infrared Transmission and Background Calculations," Optical Engr., Vol. 13, No. 2, 1974, pp. 92-97. [18]

J. Dave, A Subroutine for Evaluation of the Exponential Integral with Fifteen Significant Figure Accuracy, Rept. No. 320-3251, IBM Palo Alto Science Center, Palo Alto, Calif., 1968. [219]

B. Davison, Neutron Transport Theory, Oxford University Press, 1957. [70]

H. A. Daw, Transmission of Radiation through Water Vapor Subject to Pressure Broadening in the Region 4.2 Microns to 23 Microns, Technical Report No. 10, University of Utah, Salt Lake City, 1956. [264]

D. Deirmendjian, "Scattering and Polarization Properties of Polydispersed Suspensions with Partial Absorption," Proc. Interdisciplinary Conf. on Electromagnetic Scattering, Potsdam, Pergamon Press, New York, 1963. [346]

D. Deirmendjian, Electromagnetic Scattering on Spherical Polydispersions, American Elsevier Publishing Company, New York, 1969. [330]

F. C. De Lucia, P. Helminger, R. L. Cook and W. Gordy, J. Chem. Phys., Vol. 55, 1971, p. 5334. [154]

F. C. De Lucia, P. Helminger, R. L. Cook and W. Gordy, Phys. Rev. A 3, Vol. 5, 1972, p. 487. [152]

H. H. Denman, W. Heller and W. J. Pangonis, Angular Scattering Functions for Spheres, Wayne State University Press, Detroit, 1966. [538]

J. Dionne, Atmospheric Spectra from 9.1 to 11.6μ, Thesis, Université de Paris, 1972. [161]

S. R. Drayson, Atmospheric Slant-Path Transmission in the 15μ CO_2 Band, Report No. 05863-6-T, University of Michigan, Ann Arbor, 1964. [120]

S. R. Drayson, The Calculation of Long-Wave Radiative Transfer in Planetary Atmospheres, Report No. 07584-1-T, University of Michigan, Ann Arbor, 1967. [8]

S. R. Drayson, "Polynomial Approximations of Exponential Integrals," J. Quant. Spect. Rad. Trans., Vol. 8, 1968, pp. 1733-1738. [216]

S. R. Drayson, "Transmittances for Use in Remote Soundings of the Atmosphere," Space Research XI, Akademie-Verlag, Berlin, 1971, p. 585. [135]

S. R. Drayson, A Listing of Wave Numbers and Intensities of Carbon Dioxide Absorption Lines Between 12 and 20μm, Report No. 036350-4-T, University of Michigan, Ann. Arbor, 1973. [147]

S. R. Drayson, Private communication, 1974. [222]

S. R. Drayson and C. Young, Theoretical Investigations of Carbon Dioxide Radiative Transfer, Report No. 07349-1-F, University of Michigan, Ann Arbor, 1966. [221]

S. R. Drayson and C. Young, The Frequencies and Intensities of Carbon Dioxide Absorption Lines Between 12 to 18 Microns, Report No. 08183-1-T, University of Michigan, Ann Arbor, 1967. [142]

A. J. Drummond, Advances in Geophysics, H. E. Landsberg and J. Van Miegham (eds.), Vol. 14, Academic Press, N. Y., 1970, p. 25. [323]

R. V. Dunkle, Spectral Reflectance Measurements, Surface Effects on Spacecraft Materials, J. Clauss (ed.), John Wiley & Sons, N. Y., 1960. [40]

A. S. Eddington, The Interval Constitution of the Stars, Cambridge University Press, 1926. [106]

B. Edlen, "The Refractive Index of Air," Metrologia, Vol. 2, No. 2, 1966, p. 71. [347]

D. K. Edwards, et al., J. Opt. Soc. Am., Vol. 50, 1960, pp. 130, 617. [262]

R. G. Ellingson, A New Long-Wave Radiative Transfer Model: Calibration and Application to the Tropical Atmosphere, Report No. 72-4, Florida State University, Tallahassee, 1972. [11]

W. M. Elsasser, Phys. Rev., Vol. 54, 1938, p. 126. [191]

W. M. Elsasser, Heat Transfer by Infrared Radiation in the Atmosphere, Report No. 6, Harvard University, Cambridge, 1942. [231]

L. Elterman, "Parameters for Attenuation in the Atmosphere Windows for Fifteen Wavelengths," Appl. Opt., Vol. 3, No. 6, 1964, p. 745.

L. Elterman, UV, Visible, and IR Attenuation for Altitudes to 50 km, Report No. AFCRL-68-0153, Air Force Cambridge Research Laboratories, Bedford, Mass., 1968. [341]

L. Elterman, Vertical Attenuation Model with Eight Surface Meteorological Ranges 2 to 13 Kilometers, Report No. AFCRL-70-0200, Air Force Cambridge Research Laboratories, Bedford, Mass., 1970. [343]

R. Ely and T. McCubbin, "The Temperature Dependence of the Self-Broadened Half Width of the P-20 Line in the 001-100 Band of CO_2," Appl. Opt., Vol. 9, No. 5, May 1970, p. 1230. [136]

A. Erdelyi, et al., Higher Transcendental Functions, Vol. 2, McGraw-Hill, N. Y., 1953, p. 147. [123]

C. B. Farmer, P. J. Berry and D. B. Lloyd, Atmospheric Transmission Measurements in the 3.5 - 5.5 micron band at 5.200 m. Altitude, EMI Electronics Report DMP 1578, Hayes, Middlesex, England, 1963. [277]

V. Feddeyeva and N. Tarentev, Tables of the Probability Integral for Complex Argument, Pergamon Press, N. Y., 1961. [125]

E. M. Feigelson, M. S. Malkevich, S. Ya. Kogan, T. D. Koronatova, K. S. Glazova and M. A. Kuznetsova, Calculation of the Brightness of Light in the Case of Anisotropic Scattering, Consultants Bureau Inc., N. Y., 1960. [75]

V. L. Filippov, L. M. Artem'yeva, S. O. Mirumyants, Bull. Izv. Acad. Sci. USSR. Atmos. and Oceanic Physics, Vol. 5, 1969, pp. 521, 742. [278]

U. Fink, D. H. Rank and T. A. Wiggins, J. Opt. Soc. Am., Vol. 54,1964, p. 472. [296]

J. M. Flaud, C. Camy-Peyret and A. Valentin, J. Phys., 8-9: 741, 1972. [175]

S. Fonselius, F. Koroleff and K. Burch, "Microdetermination of CO_2 in the Air with Current Data for Scandinavia," Tellus, Vol. 7, 1955, pp. 258-265. [294]

K. Fox, Bull. Am. Phys. Soc., Vol. 18, 1973, p. 232. [184]

P. E. Fraley, K. N. Rao and L. H. Jones, J. Mol. Spect., Vol. 29, 1969, pp. 312, 348. [172]

B. Fried and S. Conte, The Plasma Dispersion Function, Academic Press, N. Y., 1961. [126]

A. L. Fymet and K. D. Abhyankar, "Theory of Radiative Transfer in Inhomogeneous Atmospheres, I. Perturbation Method," Astrophys. J., No. 158, 1969. [54]

N. M. Gailar and F. P. Dickey, J. Mole. Spect., Vol. 4, 1960, p. 1. [165]

P. R. Gast, A. Jursa, J. Castelli, S. Basu and J. Aarons, Handbook of Geophysics and Space Environments, S.L. Valley, ed., McGraw-Hill, New York, 1965, p. 16-1. [326]

D. M. Gates, R. F. Calfee and D. W. Hansen, et al., Line Parameters and Computed Spectra for Water Vapor Bands at 2.7μ, National Bureau of Standards, Monograph No. 71, 1964. [139]

D. M. Gates, Science, Vol. 151, No. 3710, 1966, pp. 525-529. [325]

H. A. Gebbie, W. Harding, C. Hilsum, A. Pryce and V. Roberts, "Atmospheric Transmission in the 1-14μ Region," Proc. of the Roy. Soc., Vol. 206A, 1951, p. 87. [253]

E. M. Gelbard, Spherical Harmonics Methods: P_ℓ and Double-P_ℓ Approximations, in Computing Methods in Reactor Physics, H. Greenspan, C. N. Kelber and D. Okrent (eds.), Gordon and Breach, N. Y., 1968. [72]

G. A. Gibson and J. H. Pierluissi, "Accurate Formula for Gaseous Transmittance in the Infrared," Appl. Opt., Vol. 10, No. 7, 1971, pp. 1509-1518. [25]

J. C. Gille, "Methods of Calculating Infrared Transfer - A Review," The UCLA International Conference on Radiation and Remote Probing of the Atmosphere, (see Kuriyan, 1973).

J. C. Gille and R. G. Ellingson, "Correction of Random Exponential Band Transmissions for Doppler Effects," Appl. Opt., Vol. 7, No. 3, 1968, pp. 471-474. [230]

E. G. Glueckauff, "CO_2 Content of the Atmosphere," Nature, Vol. 153, 1944, pp. 620-621. [293]

W. L. Godson, "Spectral Models and the Properties of Transmission Functions," Proc. Toronto Meteor. Conf., 1953, pp. 35-42. [206]

S. A. Golden, "The Doppler Analog of the Elsasser Band Model," J. Quant. Spect. Rad. Trans., Vol. 7, 1967, pp. 483-494. [197]

A. Goldman, Distribution of Water Vapor in the Stratosphere as Determined from Balloon Measurements of Atmospheric Emission Spectra in the 24 to 29 m Region, Report No. AFCRL 72-0077, University of Denver, 1972. [318]

A. Goldman and T. G. Kyle, "A Comparison Between Statistical Model and Line-by-Line Calculation with Application to the 9.6μ Ozone and the 2.7μ Water Vapor Bands," Appl. Opt., Vol. 7, No. 6, 1968, pp. 1167-1177. [202]

A. Goldman, D. G. Murcray and F. H. Murcray, et al., "Abundance of N_2O in the Atmosphere between 4.5 and 13.5 km," J. Opt. Soc. Am., Vol. 60, No. 11, 1970, pp. 1466-1468. [289]

A. Goldman, T. G. Kyle and F. S. Bonomo, "Statistical Band Model Parameters and Integrated Intensities for the 5.9μ, 7.5μ, and 11.3μ Bands of HNO_3 Vapor," Appl. Opt., Vol. 10, No. 1, 1971, pp. 65-73. [244]

A. Goldman, Bonomo, Williams and Murcray, Private communication, 1974. [274]

R. M. Goody, "A Statistical Model for Water-Vapour Absorption," Royal Meteor. Soc., Vol. 78, 1952, pp. 165-169. [193]

R. M. Goody, Atmospheric Radiation, Oxford University Press, 1964(a). [28]

R. M. Goody, "The Transmission of Radiation Through an Inhomogeneous Atmosphere," J. Atmos. Sci., Vol. 21, No. 6, 1964(b), pp. 575-581. [210]

I. P. Grant and G. E. Hunt, "Discrete Space Theory of Radiative Transfer, I: Fundamentals," Proc. Roy. Soc. Lond. A., Vol. 313, 1969(a), pp. 183-197. [85]

I. P. Grant and G. E. Hunt, "Discrete Space Theory of Radiative Transfer, II: Stability and Non-Negativity," Proc. Roy. Soc. Lond. A., Vol. 313, 1969(b), pp. 199-216. [86]

A. E. S. Green, C. Lindenmeyer and M. Griggs, "Molecular Absorption in Planetary Atmosphere," J. Geophys. Res., Vol. 69, No. 3, 1964, pp. 493-504. [229]

J. C. Guillemot, "Contribution a L' Etude du Transfert de Rayonnement dans les Nuages par la Methods des Harmoniques Spheriques," Revue d'Optique, Vol. 46, No. 6, 1967, pp. 281-308. [77]

R. O. Gumprecht and C. M. Sliepcevich, Tables of Light-Scattering Functions for Spherical Particles, University of Michigan, Ann Arbor, 1951. [337]

M. Gutnick, "How Dry is the Sky?," J. Geophys. Res., Vol. 66, 1961, pp. 286-287. [237]

M. Gutnick, "Mean Atmospheric Moisture Profiles to 31 km for Middle Latitudes," Appl. Opt., Vol. 1, 1932, p. 670. [238]

H. S. Gutowsky and E. M. Petersen, "The Infrared Spectrum and Structure of Ozone," J. Chem. Phys., Vol. 18, 1950, p. 564. [272]

D. N. B. Hall, Observations of the Infrared Sunspot Spectrum Between 11340 A and 24778 A, Thesis, Harvard University, Cambridge, 1970. [173]

D. N. B. Hall, Unpublished data, 1972. [167]

R. T. Hall and J. M. Dowling, J. Chem. Phys., Vol. 47, 1967, p. 2454. [156]

J. N. Hamilton, J. A. Rowe and D. Anding, Atmospheric Transmission and Emission Program, Report No. TOR-0073(3050-02)-3, Aerospace Corporation, 1973. [19]

J. E. Hansen, "Exact and Approximate Solutions for Multiple Scattering by Cloudy and Hazy Planetary Atmospheres," J. Atmos. Sci., Vol. 29, No. 3, May 1969(a), pp. 478-487. [95]

J. E. Hansen, "Radiative Transfer by Doubling Very Thin Layers," Astrophys. J., Vol. 155, February 1969(b). [96]

F. D. Haurwitz, The Distribution of Tropospheric Infrared Radiative Fluxes and Associated Radiative Fluxes and Associated Heating and Cooling Rates in the Southern Hemisphere, University of Michigan, Ann Arbor, 1972. [14]

H. L. Helmholtz, Physiological Optics, 3rd Ed., 1909. [36]

S. T. Henderson, Daylight and Its Spectrum, American Elsevier Publishing Company, New York, 1970, pp. 72-73. [33]

W. S. Hering and T. R. Borden, Ozone Observations Over North America, OAR Research Report No. AFCRL-64-30, Vol. 2, 1964. [321]

B. M. Herman and S. R. Browning, "A Numerical Solution to the Equation of Radiative Transfer," J. Atmos. Sci., Vol. 22, No. 5, 1965, pp. 559-566. [67]

B. M. Herman, S. R. Browning and R. J. Curran, "The Effect of Atmospheric Aerosols on Scattered Sunlight," J. Atmos. Sci., Vol. 28, No. 3, 1971, pp. 419-428. [69]

G. Herzberg, Infrared and Raman Spectra of Polyatomic Molecules, Van Nostrand, N. Y., 1945. [149]

G. Herzberg, Spectra of Diatomic Molecules, Van Nostrand, N. Y., 1950. [151]

G. M. Hidy and J. R. Brock, An Assessment of the Global Sources of Tropospheric Aerosols, Proceedings of the 2nd International Clean Air Congress, H. M. England and W. T. Beerg (eds.), 1971, pp. 1088-1097. [328]

F. B. Hildebrand, Methods of Applied Mathematics, Prentice-Hall, N. Y., 1952. [66]

F. B. Hildebrand, Introduction to Numerical Analysis, McGraw-Hill, N. Y., 1956. [68]

E. D. Hinkley, K. Nill and S. Blum, "Laser Spectroscopy of Atoms and Molecules," Topics in Applied Physics, Vol. 2, H. Walther (ed.), Springer-Verlag, Berlin, 1974. [137]

W. Hitschfield and J. T. Houghton, "Radiation-Transfer in the Lower Stratosphere Due to the 9.6 Micron Band of Ozone," Quart. J. Roy. Meteor. Soc., Vol. 87, 1961, pp. 562-577. [214]

J. N. Howard, D. Burch and D. Williams, Near-Infrared Transmission Through Synthetic Atmospheres, Geophysics Research Paper No. 40, Report No. AFCRL-TR-55-213, Ohio State University, Columbus, 1955. [240]

J. N. Howard and J. Garing, "Atmospheric Optics and Radiative Transfer," EOS, Vol. 52, No. 6, IUGG 371, June 1971. [3]

D. Hummer, Maths. Comput., Vol. 18, 1964, p. 317. [124]

C. E. Hunt and I. P. Grant, "Discrete Space Theory of Radiative Transfer and Its Application to Problems in Planetary Atmospheres," J. the Atmos Sci., Vol. 26, September 1969, pp. 963-972. [87]

E. Inonu and P. F. Zweifel (eds.), Developments in Transport Theory, Academic Press, N. Y., 1967. [50]

W. M. Irvine, Astrophys. J., Vol. 152, 1968, p. 823. [63]

W. M. Irvine, "Multiple Scattering by Large Particles, II: Optically Thick Layers," Astrophys. J., Vol. 152, June 1968. [64]

W. M. Irvine, An Evaluation of Romanova's Method in the Theory of Radiative Transfer, in The Atmospheres of Venus and Mars, J. C. Brandt and M. B. McElroy (eds.), Gordon and Breach, N. Y., 1968. [65]

J. R. Izatt, Office of Naval Research Progress Report, Contract No. 248(01), Johns Hopkins University, Baltimore, Maryland, 1960. [267]

J. R. Izatt, H. Sakai and W. S. Benedict, J. Opt. Soc. Am., Vol. 59, 1969, p. 19. [158]

H. T. Jackson Jr., A Model for the Spectral Emissivity of Carbon Dioxide in the 4.3-Micron Band, Rept. No. RE-TR-69-6, U.S. Army Missile Command, 1969. [239]

C. E. Junge, Air Chemistry and Radioactivity, Academic Press, N. Y., 1963. [333]

C. E. Junge, "Our Knowledge of the Physics-Chemistry of Aerosols in the Undisturbed Marine Environment," J. Geophys. Res., Vol. 77, No. 27, 1972, pp. 5183-5200. [284]

H. H. Kagiwada and R. E. Kalaba, "Estimation of Local Anisotropic Scattering Properties Using Measurements of Muliply Scattered Radiation," J. Quant. Spect. Rad. Trans., Vol. 7, 1967, pp. 295-303. [91]

A. B. Kahle, "Global Radiation Emerging from a Rayleigh-Scattering Atmosphere of Large Optical Thickness," Astrophys. J., Vol. 151, February 1968. [115]

L. D. Kaplan, "Regions of Validity of Various Absorption-Coefficient Approximations," J. Meteorol., Vol. 10, 1953(a). [196]

L. D. Kaplan, "A Quasi-Statistical Approach to the Calculation of Atmospheric Transmission," Proc. Toronto Meteor. Conf., 1953(b), pp. 43-48. [213]

L. D. Kaplan, "A Method for Calculation of Infrared Flux for Use in Numerical Models of Atmospheric Motion," The Atmosphere and the Sea in Motion, The Rockefeller Institute Press, N. Y., 1959, pp. 170-177. [208]

C. D. Keeling, "The Concentration and Isotopic Abundance of Carbon Dioxide in the Atmosphere," Tellus, Vol. 12, 1960. [291]

M. Kerker, The Scattering of Light and Other Electromagnetic Radiation, Academic Press, N. Y., 1969. [336]

G. V. Kattawar and G. N. Plass, "Infrared Cloud Radiance," Appl. Optics, Vol. 8, No. 6, June 1969, pp. 1169-1178. [104]

J. I. F. King, "Band Absorption Model for Arbitrary Line Variance," J. Quant. Spect. Rad. Trans., Vol 4, 1964, pp. 705-711. [199]

W. Kofink, Recent Developments in the Spherical Harmonics Method and New Integral Solutions of the Boltzmann Equation in Spherical Geometry, in Developments in Transport Theory, E. Inonu and P. F. Zweifel (eds.), Academic Press, N. Y., 1967. [73]

K. Ya. Kondratyev, Radiation in the Atmosphere, Academic Press, N. Y., 1969. [228]

K. Ya. Kondratyev and Yu. M. Tumofeev, "The Applicability of Approximation Methods for Introducing Inhomogeneities into Calculations of the Transmission Functions of the Rotational Band of Water Vapor," Atmospheric and Oceanic Physics, Vol. 3, No. 3, 1967, pp. 236-244. [257]

K. Ya. Kondratyev, O. B. Vasilyev, L. S. Ivlev, G. A. Nikolsky and O. I. Smoktz, Influence of Aerosol on Radiative Transfer; Possible Climatic Consequences, University of Leningrad, 1973. [332]

C. L. Korb, R. Hunt and E. Plyler, "Measurement of Line Strengths at Low Pressures: Application to the 2-0 Band of CO," J. Chem. Phys., Vol. 48, No. 9, May 1968, p. 1452. [130]

G. A. Korn and T. Korn, Mathematical Handbook for Scientists and Engineers, McGraw-Hill, N. Y., 1961. [225]

H. Koschmieder, Beitr. Phys. freien Atm., Vol. 12, 1924, pp. 33-53; 171-181. [340]

H. J. Kostkowski, Half Widths and Intensities from the Infrared Transmission of Thermally Excited CO_2, Progress Report, Office of Naval Research Contract 248(01), Johns Hopkins University, Baltimore, Md., October 1955. [261]

V. Kourganoff, Introduction to the General Theory of Particle Transfer, Gordon and Breach, N. Y., 1969. [30]

M. Krook, Astrophys. J., Vol. 122, 1955, p. 488. [97]

A. J. Krueger, The Mean Ozone Distribution from Several Series of Rocket Soundings to 52 km Latitudes from 54°S to 64°N, NASA Report No. X-651-73-67, Goddard Space Flight Center, Greenbelt, Md., 1973. [322]

V. G. Kunde, Tables of Theoretical Line Positions and Intensities for the $\Delta V = 1$, $\Delta V = 2$, and $\Delta V = 3$ Vibration-Rotation Bands of $C^{12}O^{16}$ and $C^{13}O^{16}$, NASA Report No. TMX-63183, Goddard Space Flight Center, Greenbelt, Md., 1967(a). [144]

V. G. Kunde, Theoretical Computations of the Outgoing Infrared Radiance from a Planetary Atmosphere, NASA Report No. TN-D-4045, Goddard Space Flight Center, Greenbelt, Md., 1967(b). [13]

V. G. Kunde and W. C. McGuire, Direct Integration Transmittance Model, NASA Report No. X-622-73-258, Goddard Space Flight Center, Greenbelt, Md., 1973. [223]

V. G. Kunde and W. C. McGuire, "Direct Integration Transmittance Model," J. Quant. Spect. Rad. Trans., Vol. 14, 1974, p. 303. [9]

J. G. Kuriyan (ed.), The UCLA International Conference on Radiation and Remote Probing of the Atmosphere, UCLA, Los Angeles, August 1973. [2]

T. G. Kyle, "Absorption by Doppler-Lorentz Atmospheric Lines," J. Quant. Spect. Rad. Trans., Vol. 8, 1968(a), pp. 1455-1462. [145]

T. G. Kyle, Line Parameters of the Infrared Methane Bands, Report No. AFCRL-68-0521, Air Force Cambridge Research Laboratories, Bedford, Mass., 1968(b). [146]

T. G. Kyle, "Net Interval for Calculating Absorption Spectra," J. Opt. Soc. Am., Vol. 58, No. 2, 1968(c), pp. 192-195. [6]

T. G. Kyle, R. D. Blatherwick and F. S. Bonomo, J. Chem. Phys., Vol. 53, 1970, p. 2800. [179]

R. Ladenburg and F. Reiche, "Uber Selektive Absorption," Ann. Phys., Vol. 42, 1913, p. 181. [132]

K. D. Lathrop, "Discrete Ordinates Methods for the Numerical Solution of the Transport Equation," Reactor Technology, Vol. 15, No. 2, 1972, pp. 107-135. [81]

N. Laulainen, Project ASTRA, Astronomical and Space Techniques for Research on the Atmosphere, ASTRA Publication No. 18, University of Washington, Seattle, 1972. [4]

N. Laulainen, "Bibliography of the Spectra of Atmospheric Minor Gases," Appl. Opt., Vol. 12, No. 3, 1973, p. 617. [5]

C. E. Lee, The Discrete S_N Approximation for Transport Theory, Report No. LA-2595, Los Alamos Scientific Laboratory of the University of Calif., Los Alamos, N. M., 1962. [83]

R. T. Liner, Jr., Moment and Discrete Ordinate Methods in Radiative Transfer Problems, Vol. 9, 1969, pp. 721-732. [99]

J. L. Locke and L. Herzberg, "The Absorption due to Carbon Monoxide in the Infrared Solar Spectrum," Can. J. Phys., Vol. 31, 1953, p. 504. [314]

C. B. Ludwig, W. Malkmus, J. E. Reardon and J. A. L. Thomson, Handbook of Infrared Radiation from Combustion Gases, NASA Report No. SP-3080, Marshall Space Flight Center, 1973. [207]

G. D. Lukes, Optical Constants of Water Particulates for Wavelengths in the Visible and Infrared, Particulate Models: Their Validity and Applications, I. H. Blifford, Jr. (ed.), Report No. NCAR-TN/PROG-68, Boulder, Colo., 1971. [331]

R. P. Madden and W. S. Benedict, J. Chem. Phys., Vol. 25, 1956, p. 294 and unpublished data, 1956. [159]

W. A. Malila, R. B. Crane, A. Omarzu and R. E. Turner, Studies of Spectral Discrimination, Report No. 31650-22-T, Willow Run Laboratories of the Institute of Science and Technology, University of Michigan, Ann Arbor, 1971. [117]

W. A. Malila, R. B. Crane and R. E. Turner, Information Extraction Techniques for Multispectral Scanner Data, Report No. 31650-74-I, Willow Run Laboratories of the Institute of Science and Technology, University of Michigan, Ann Arbor, 1972. [118]

W. Malkmus, "Random Lorentz Band Model with Exponential-Tailed S^{-1} Line-Intensity Distribution Function," J. Opt. Soc. Am., Vol. 57, No. 3, 1967, pp. 323-329. [198]

J. Marengo, "Application Numerique de la Methode des Harmoniques Spheriques," Nouv. Rev. d'Optique Appliquie, Vol. 1, No. 3, 1970, pp. 181-190. [76]

H. Mayer, Methods of Opacity Calculations, V. Effect of Lines on Opacity, Methods for Treating Line Contribution, Report No. AECD-1870, Los Alamos Scientific Laboratory, Los Alamos, Calif., 1947. [192]

D. J. McCaa and J. H. Shaw, "The Infrared Spectrum of Ozone," J. Mol. Spec., Vol. 25, pp. 374-397. [134]

R. A. McClatchey and J. E. A. Selby, Atmospheric Attenuation of Laser Radiation from 0.76 to 31.25 μm, Report No. TR-74-0003, Air Force Cambridge Research Laboratories, Bedford, Mass., January 1974. [190]

R. A. McClatchey, et al., Optical Properties of the Atmosphere, Third Edition, Report No. AFCRL-72-0497, Air Force Cambridge Research Laboratories, Bedford, Mass., 1972. [21]

R. A. McClatchey, et al., AFCRL Atmospheric Absorption Line Parameters Compilation, Report No. AFCRL-TR-73-0096, Air Force Systems Command, 1973. [138]

N. J. McCormick and I. Kuscer, "Half-Space Neutron Transport with Linearly Anisotropic Scattering," J. Math. Phys., Vol. 6, 1965, pp. 1939-1945. [59]

R. S. McDowell, J. Mol. Spec., Vol. 21, 1966, p. 280. [182]

R. McMath and L. Goldberg, "The Abundance and Temperature of Methane in the Earth's Atmosphere," Proc. Am. Phys. Soc., Vol. 74, 1948, p. 623. [302]

H. J. McNicholas, "Absolute Methods of Reflectometry," J. Res. Natl. Bur. Std., Vol. 1, 1928, pp. 29-72. [39]

F. Michelot and K. Fox, (1973), to be published. [180]

W. E. K. Middleton, Vision Through the Atmosphere, University of Toronto Press, Toronto, 1952. [344]

M. V. Migeotte, "The Fundamental Band of Carbon Monoxide at 4.7 μ in the Solar Spectrum," Phys. Rev., Vol. 75, 1949, p. 1108. [309]

M. Migeotte, L. Neven and J. Swensson, The Solar Spectrum from 2.8 to 23.7 Microns, Measures and Identifications, Mem. Soc. Roy. Sci. Liege, Special Volume 2, 1957. [162]

J. L. Moyers and R. A. Duce, "Gaseous and Particulate Iodine in the Marine Atmosphere," J. Geophys. Res., Vol. 77, No. 27, pp. 5229-5238. [285]

J. L. Moyers and R. A. Duce, Gaseous and Particulate Bromine in the Marine Atmosphere, J. Geophys. Res., Vol. 77, No. 27, 1972(b), pp. 5330-5338. [286]

T. W. Mullikin, "Radiative Transfer in Finite Homogeneous Atmospheres with Anisotropic Scattering, II: The Uniqueness Problem for Chandrasekhar's ψ_ℓ and ϕ_ℓ Equations," Astrophys. J., Vol. 139, No. 4, 1964(a). [47]

T. W. Mullikin, "Radiative Transfer in Finite Homogeneous Atmospheres with Anisotropic Scattering, I: Linear Singular Equations," Astrophys. J., Vol. 139, No. 1, 1964(b). [48]

T. W. Mullikin, "Chandrasekhar's X and Y Equations," Trans. of the Amer. Math. Soc., Vol. 113, No. 2, 1964(c). [49]

T. W. Mullikin, "The Complete Rayleigh-Scattered Field Within a Homogeneous Plane Parallel Atmosphere," Astrophys. J., Vol. 145, No. 3, 1966. [50]

D. G. Murcray, T. G. Kyle, F. H. Murcray and W. I. Williams, "Nitric Acid and Nitric Oxide in the Lower Stratosphere," Nature, Vol. 218, 1968, p. 78. [307]

D. G. Murcray, A. Goldman and A. Csoeke-Poeckh, et al., "Nitric Acid Distribution in the Stratosphere," J. Geophys. Res., Vol. 78, No. 30, 1973, pp. 7033-7038. [308]

R. C. Nelson, Atlas and Wavelength Tables, Summary Report IV, Northwestern University, Evanston, Ill., 1949. [176]

M. N. Ozisik, Radiative Transfer and Interactions with Conduction and Convection, John Wiley & Sons, N. Y., 1973. [61]

C. H. Palmer, "Long Path Water Vapor Spectra With Pressure Broadening, I: 20 - 21.7," J. Opt. Soc. Am., Vol. 47, 1957, p. 1024. [259]

C. H. Palmer, 1960: see Palmer (1957). Cited incorrectly by Selby (1974). [268]

S. Penner, Quantitative Molecular Spectroscopy and Gas Emissivities, Addison-Wesley, Reading, Mass., 1959. [129]

E. Pettit, Astrophysics, J. A. Hynck (ed.), McGraw-Hill, N. Y., 1951, p. 259. [324]

J. H. Pierluissi, "Polynomial Representation of Transmittance Models," Appl. Opt., Vol. 12, No. 4, 1973, pp. 776-778. [26]

G. N. Plass, "Models for Spectral Band Absorption," J. Opt. Soc. Am., Vol. 48, 1958, p. 690. [194]

G. N. Plass, "Useful Representations for Measurements of Spectral Band Absorption," J. Opt. Soc. Am., Vol. 50, 1960, pp. 868-875. [200]

G. N. Plass, Infrared Transmission Studies, Vol. V - Transmittance Tables for Slant Path in the Stratosphere, Report No. SSD-TDR-62-127, Ford Motor Company, 1963. [236]

G. N. Plass and G. W. Kattawar, "Influence of Single Scattering Albedo on Reflected and Transmitted Light from Clouds," Appl. Optics, Vol. 7, No. 2, February 1968, pp. 361-367. [103]

E. Plyler and E. Barker, "Infrared Spectrum and Molecular Configuration of N_2O," Phys. Rev., Vol. 38, 1931, p. 1827. [243]

R. Preisendorfer, Radiative Transfer on Discrete Spaces, Pergamon Press, Oxford, 1965. [84]

L. A. Pugh, A Detailed Study of the Near Infrared Spectrum of Water Vapor, Thesis, Ohio State University, Columbus, 1972. [171]

K. N. Rao, W. W. Brim, J. L. Sinnett and R. M. Wilson, J. Opt. Soc. Am., Vol. 52, 1962. [157]

N. Robinson, Solar Radiation, American Elsevier Publishing Company, N. Y., 1966. [339]

C. D. Rodgers and C. D. Walshaw, "The Computation of Infrared Cooling Rate in Planetary Atmospheres," Qrtly. J. Royal Meteor. Soc., Vol. 89, 1966, pp. 67-92. [12]

L. M. Romanova, "The Solution of the Radiative-Transfer Equation for the Case When the Indicatrix of Scattering Greatly Differs from the Spherical One, I," Opt. Spek., Vol. 13, 1962(a), p. 429. [107]

L. M. Romanova, "Solution of the Radiative-Transfer Equation for the Case of a Highly Nonspherical Scattering Index, II," Opt. Spek., Vol. 13, 1962(b), p. 819. [108]

L. M. Romanova, "Radiation Field in Plane Layers of a Turbid Medium with Highly Anisotropic Scattering," Opt. Spek., Vol. 14, 1963, p. 262. [109]

B. W. Roos, Analytic Functions and Distributions in Physics and Engineering, John Wiley & Sons, N. Y., 1969. [62]

H. Rose, Private communication - Line Parameter Determination of Band Model Parameters, 1974. [243]

G. V. Rozenburg, Optical Investigations of Atmospheric Aerosol, Soviet Physics Uspekhi, Vol. 11, No. 3, 1968, pp. 353-330. [329]

R. E. Samuelson, Radiative Transfer in a Cloudy Atmosphere, NASA Report No. TR-R-215, Goddard Space Flight Center, Greenbelt, Md., Office of Technical Services, Dept. of Commerce, Washington, D. C., 1965. [31]

A. Schuster, "Radiation Through a Foggy Atmosphere," Astrophys. J., Vol. 21, 1905, p. 1. [27]

K. Schwarzschild, "Uber das Gleichgewicht der Sonnenatmosphere," Gottinger Nachrichten, Vol. 41, 1906. [105]

N. A. Scott, "A Direct Method of Computation of the Transmission Function of an Inhomogeneous Gaseous Medium. I: Description of the Method," J. Quant. Spec. Rad. Trans., Vol. 14, 1974, pp. 691-704. [7]

Z. Sekera, RAND Publication R-413-PR, RAND Corporation, Santa Monica, Calif., 1963. [52]

Z. Sekera, Reduction of Equations of Radiative Transfer in a Planetary Plane-Parallel Atmosphere, RM-4951-PR and RM-5056-PR, The RAND Corporation, Santa Monica, Calif., 1966. [51]

Z. Sekera and A. B. Kahle, Scattering Functions of Rayleigh Atmospheres of Arbitrary Thickness, R-4520PR, The RAND Corporation, Santa Monica, Calif., 1966. [116]

J. Selby, Atmospheric Transmittance, I., Advanced IR Conference Notes, University of Michigan Summer Conference, Ann Arbor, 1974. [252]

J. Selby and R. M. McClatchey, Atmospheric Transmittance from 0.25 to 2.85μm: Computer Code LOWTRAN 2, Report No. AFCRL-72-0745, Air Force Cambridge Research Laboratories, Bedford, Mass., 1972. [20]

J. H. Shaw, The Abundance of Atmospheric CO above Columbus, Ohio (Contract AF 19(604)1003), Report No. AFCRC TN 57-212, Ohio State University Research Foundation, Columbus, 1957. [313]

J. H. Shaw, A Determination of the Abundance of N_2O, CO, and CH_4 in Ground Level Air at Several Locations Near Columbus, Ohio, Sci. Report No. 1, Contract AF 19(604)-2259, AFCRL. [299]

J. H. Shaw, Monthly Report on Infrared Temperature Sounding, RF Project 2469, Report No. 16, Ohio State University, Columbus, October 1968. [298]

J. H. Shaw and J. N. Howard, "A Quantitative Determination of the Abundance of Telluric CO Above Columbus, Ohio," Phys. Rev., Vol. 87, 1952, p. 380. [310]

J. H. Shaw and N. Howard, "Absorption of Telluric CO in the 23 μ Region," Phys. Rev., Vol. 87, 1952, p. 679. [311]

J. H. Shaw and H. H. Nielson, Infrared Studies of the Atmosphere (Final Report on Contract AF 19(122)-65), Ohio State University Research Foundation, Columbus, 1954. [312]

J. H. Shaw, G. B. B. M. Sutherland and T. W. Wormell, "Nitrous Oxide in the Earth's Atmosphere," Phys. Rev., Vol. 74, 1948, p. 978. [301]

M. P. Sherman, "Moment Methods in Radiative Transfer Problems," J. Quant. Spect. Rad. Trans., Vol. 7, 1967, pp. 29-109. [96]

R. Siegel and J. R. Howell, Thermal Radiation Heat Transfer, New York, McGraw-Hill, N. Y., 1972. [41]

N. Sissenwine, D. Grantham and N. S. Salmela, Humidity Up to the Mesopause, Report No. AFCRL-68-0550, Air Force Cambridge Research Labs., Bedford, Mass., 1968. [317

R. L. Slobod and M. E. Krogh, "Nitrous Oxide as a Constituent of the Atmosphere," J. Am. Chem. Soc., Vol. 72, 1950, pp. 1175-1177. [303]

W. L. Smith, A Polynomial Representation of Carbon Dioxide and Water Vapor Transmission, Report No. NESC 47, National Environmental Satellite Center, Washington, D. C., 1969. [24]

J. L. Stanford, "Stratospheric Water-Vapor Upper Limits Inferred from Upper-Air Observations, Part I: Northern Hemisphere," Bull. Am. Met. Soc., Vol. 55, No. 3, 1974, p. 194. [320]

G. Steenbeckeliers and J. Bellet, Comptes Rendus Acad. Sci., B273·288, Paris, 1971. [1

J. C. Stewart, Some Topics in Radiative Transfer in Developments in Transport Theory, E. Inonu and P. F. Zweifel (eds.), Academic Press, N. Y., 1967. [29]

J. A. Stratton, Electromagnetic Theory, McGraw-Hill, N. Y., 1941. [334]

J. L. Streete, et al., "Near Infrared Atmospheric Absorption over a 25 km Horizontal Path at Sea Level," Appl. Opt., Vol. 6, No. 3, 1967, pp. 489-496. [283]

J. L. Streete, "Infrared Measurements of Atmospheric Transmission at Sea Level," Appl. Opt., Vol. 7, No. 8, 1968, pp. 1545-1549. [250]

V. R. Stull, P. J. Wyatt and G. N. Plass, Infrared Transmission Studies, Vol. 3: The Infrared Absorption of Carbon Dioxide, Report No. SSD-TDR-62-127-Vol. 3, Ford Motor Company, 1963. [16]

V. R. Stull, P. J. Wyatt and G. N. Plass, "The Infrared Transmittance of CO_2," Appl. Opt., Vol. 3, No. 2, February 1964, pp. 243-254. [255]

M. Summerfield, "Pressure Dependence of the Absorption in the 9.6 Micron Band of Ozone," thesis, California Institute of Technology, Pasadena, 1941. [271]

J. Swensson, W. S. Benedict, L. Delbouille and G. Roland, The Solar Spectrum from λ 7498 to λ 12016. A Table of Measures and Identifications, Mem. Soc. Roy. Sci. Liege, Special Volume 5, 1970. [177]

Target Signature Analysis Center, Data Compilation, Eleventh Supplement: Vol. I, Bidirectional Reflectances; Definition, Discussion and Utilization, and Vol. II: Bidirectional Reflectance; Graphic Data, Report No. AFAL-TR-72-266, TSAC, Willow Run Laboratories of the Institute of Science and Technology, University of Michigan, Ann Arbor, 1972. [37]

J. H. Taylor and H. W. Yates, "Atmospheric Transmission in Infrared," J. Opt. Soc. Am., Vol. 47, No. 3, 1957, pp. 223-226. [249]

M. P. Thekaekara, Proposed Standard Values of the Solar Constant and the Solar Spectrum, J. Environ. Sci., Vol. 13, No. 4, September-October 1970, pp. 6-9. [35]

M. P. Thekaekara and A. J. Drummond, "Standard Values for the Solar Constant and Its Spectral Components," Nature Physical Science, Vol. 229, 1971. [327]

R. E. Turner, Transport of High-Energy Cosmic Rays in the Interstellar Medium, Ph.D Thesis, Washington University, St. Louis, Mo., 1970. [32]

R. E. Turner, Remote Sensing in Hazy Atmospheres, Proceedings of ACSM/ASP, Meeting in Washington, D. C., March 1972. [111]

R. E. Turner, "Atmospheric Effects in Remote Sensing," Remote Sensing of Earth Resources, Vol. II, F. Shahrokhi (ed.), University of Tennessee, 1973. [112]

R. E. Turner, "Contaminated Atmospheres and Remote Sensing," Remote Sensing of Earth Resources, Vol. III, F. Shahrokhi (ed.), University of Tennessee, 1974. [113]

R. E. Turner, Radiative Transfer on Real Atmospheres, Report No. 190100-24-T, Environmental Research Institute of Michigan, Ann Arbor, July 1974. [114]

S. Ueno, H. Kagiwada and R. Kalaba, "Radiative Transfer in Spherical Shell Atmospheres with Radial Symmetry," J. of Math. Physics, Vol. 12, No. 6, 1971, pp. 1279-1285. [92]

S. L. Valley, Handbook of Geophysics and Space Environments, Air Force Cambridge Research Laboratories, 1965. [290]

H. C. Van de Hulst, "Theory of Absorption Lines in the Atmosphere of the Earth," Annales d'Astrophys., Vol. 8, 1945, pp. 21-34. [211]

H. C. Van de Hulst, Light Scattering by Small Particles, John Wiley and Sons, N. Y., 1957. [335]

H. C. Van de Hulst and K. Grossman, "Multiple Light Scattering in Planetary Atmospheres," The Atmospheres of Venus and Mars, J. C. Brandt and M. B. McElroy (eds.), Gordon and Breach, N. Y., 1968. [94]

C. Walshaw, "Integrated Absorption by the 9.6 μm Band of Ozone," Quant. J. Roy. Meteorol. Soc., Vol. 83, 1957, pp. 315-321. [133]

M. C. Wang and E. Guth, Phys. Rev., Vol. 84, 1951, p. 1092. [110]

M. P. Weinreb and A. C. Neuendorffer, "Method to Apply Homogeneous-Path Transmittance Models to Inhomogeneous Atmospheres," J. Atmos. Sci., Vol. 30, 1973, pp. 662-666. [209]

M. B. Wells and J. D. Marshall, Monochromatic Light Intensities Above the Atmosphere Resulting from Atmospheric Scattering and Terrestrial Reflection, Radiative Research Assoc., Inc., Ft. Worth, Tex., 1968. [102]

C. Whitney, "Implications of a Quadratic Stream Definition in Radiative Transfer Theory," J. Atmos. Sci., Vol. 29, No. 8, November 1972, pp. 1520-1530. [80]

G. C. Wick, Z. Phys., Vol. 121, 1943, p. 702. [79]

M. M. R. Williams, Mathematical Methods in Particle Transport Theory, Wiley-Interscience. N. Y., 1971. [74]

J. G. Williamson, K. N. Rao and L. H. Jones, J. Mol. Spect., Vol. 40, 1971. [164]

M. K. Wilson and R. A. Ogg, J. Chem. Phys., Vol. 18, 1950, p. 766. [273]

B. H. Winters, et al., "Line Shape in the Wing Beyond the Band Head of the 4.3μ Band of CO_2," J. Quant. Spec. Rad. Trans., Vol. 4, 1964, pp. 527-537. [119]

W. L. Wolfe (ed.), Handbook of Military Infrared Technology, Office of Naval Research, U. S. Government Printing Office, Washington, D. C., 1965. [280]

P. J. Wyatt, V. R. Stull and G. N. Plass, Infrared Transmission Studies, Vol. 2: The Infrared Absorption of Water Vapor, Report No. SSD-TDR-62-127-Vol. 2., Ford Motor Company, 1962(a). [15]

P. J. Wyatt, V. R. Stull and G. N. Plass, "Quasi-Random Model of Band Absorption," J. Opt. Soc. Am., Vol. 52, No. 11, 1962(b), p. 1209. [195]

P. J. Wyatt, V. R. Stull and G. N. Plass, App. Opt., No. 3, 1964, p. 229. [256]

G. Yamamoto and M. Aida, "Transmission in a Non-Homogeneous Atmosphere with an Absorbing Gas of Constant Mixing Ratio," J. Quant. Spec. Rad. Trans., Vol. 10, 1970, pp. 593-608. [203]

G. Yamamoto, et al., "Improved Curtis-Godson Approximation in a Non-Homogeneous Atmosphere," J. Atmos. Sci., Vol. 29, 1972, pp. 1150-1155. [204]

N. G. Yaroslavskii and A. E. Stanevish, Opt. Spect., Vol. 7, 1959, p. 380, also Optika Spektrosk., Vol. 5, 1958, p. 382. [266]

H. W. Yates, The Absorption Spectrum from 0.5 to 25 microns of a 1000 ft. Atmospheric Path at Sea Level, NRL Report 5033, Naval Research Laboratory, Washington, D. C., September 1957. [276]

H. W. Yates and J. H. Taylor, Infrared Transmission of the Atmosphere, NRL Report 5453. Naval Research Laboratory, Washington, D. C., 1960. [248]

C. Young, A Study of the Influence of Carbon Dioxide on Infrared Radiative Transfer in the Stratosphere and Mesosphere, Report No. 04682-1-T, University of Michigan, Ann Arbor, 1964. [232]

C. Young, "Calculation of the Absorption Coefficient for Lines with Combined Doppler-Lorentz Broadening," J. Quant. Spect. Rad. Trans., Vol. 5, 1965, pp. 549-552. [121]

L. A. Young, "CO Infrared Spectra," J. Quant. Spect. Rad. Trans., Vol. 8, 1968, pp. 693-716. [150]

L. G. Young, "Comments on Accurate Formula for Gaseous Transmittance in the Infrared," Appl. Opt., Vol. 11, No. 1, 1972, pp. 202-203. [258]

J. Yvon, "La Diffusion Macroscopique des Neutrons: Une Methode d' Approximation," J. Nucl. Energy I, Vol. 4, 1957, pp. 305-318. [71]

A. S. Zachor, "A General Approximation for Gaseous Absorption," J. Quant. Spect. Rad. Trans., Vol. 8, 1968(a), pp. 771-781. [22]

A. S. Zachor, "Equations for the Transmittance of the 2μ CO_2 Bands," J. Quant. Spect. Rad. Trans., Vol. 8, 1968(b), pp. 1341-1349. [23]

BIBLIOGRAPHY

This bibliography comes primarily from the AFCRL Atmospheric Absorption Line Parameters Compilation (McClatchey, et al., 1973), and is intended for use with Section 4.

H_2O Vapor

Beer, R., (1970), private communication to McClatchey, et al., (1973).

Ben-Aryeh, Y., (1970), Quant. Spec. Rad. Trans., Vol.7, p.211.

Benedict, W.S., H.H. Classen and J.H. Shaw, (1952), J. Res. of NBS, Vol.49, 2:2247.

Benedict, W.S. and L.D. Kaplan, (1959), J. Chem. Phys., Vol.30, No.2, p.388.

Benedict, W.S. and R.F. Calfee, (1967), Line Parameters for the 1.9 and 6.3 micron Water Vapor Bands, ESSA Professional Paper No.2, U.S. Government Printing Office, Washington, D.C., June 1967.

Benedict, W.S., S.A. Clough, W.J. Lafferty, L. Frenkel, T.E. Sullivan, J. Bellet and G. Steenbeckeliers, (1973), to be published.

Benedict, W.S., H. Chang, S.A. Clough and W.J. Lafferty, (1973), to be published.

Benedict, W.S. and R. Sams, (1971), Twenty-Sixth Symposium on Molecular Spectroscopy, Ohio State University, Columbus, Ohio, June 1971.

Blum, F.A., K.W. Nill, P.L. Kelley, A.P. Calawa and T.C. Harman, (1972), Science, Vol.177, p.694.

Brault, J., (1972), Kitt Peak National Observatory, private communication to McClatchey, et al., (1973).

Breckenridge, J.R. and D.N.B. Hall, (1973), Solar Physics, to be published.

Burch, D.E. and D. Gryvnak, (1971), unpublished data.

Burch, D.E. and D. Gryvnak, (1973), unpublished data.

Clough, S.A. (AFCRL) and Y. Beers (NBS-Boulder), (1973), to be published.

Connes, J., P. Connes and J.P. Maillard, (1969), Near Infrared Spectra of Venus, Mars, Jupiter, and Saturn, Centre National de la Recherche Scientifique, Paris.

Connes, J., P. Connes and J.P. Maillard, (1969), Atlas of Near Infrared Spectra of Venus, Mars, Jupiter and Saturn, Editions du C.N.R.S., Paris.

De Lucia, F.C., P. Helminger, R.L. Cook and W. Gordy, (1972), Phys. Rev. A3, Vol.5, p.487.

De Lucia, F.C., P. Helminger, R.L. Cook and W. Gordy, (1971), J. Chem. Phys., Vol.55, p.5334.

Dionne, J., (1972), Atmospheric Spectra from 9.1 to 11.6 μ, Thesis, Universite de Paris VI.

Dyke, T., and J. Muenter, (1972), Molecular Beam Studies of Water, Symposium on Molecular Structure and Spectroscopy, Ohio State University, Columbus, Ohio, June 1972.

Flaud, J.M., C. Camy-Peyret and A. Valentin, (1972), J. Phys., Vol.8, No.9, p.741.

Fraley, P.E., K.N. Rao and L.H. Jones, (1969), J. Mol. Spec., Vol.29, pp.312, 348.

Gailar, N.M. and F.P. Dickey, (1960), J. Mol. Spec., Vol.4, p.1.

Gates, D.M., R.F. Calfee, D.W. Hanson and W.S. Benedict, (1964), Line Parameters and Computer Spectra for Water Vapor Bands at 2.7 μm, NBS Monograph No.71, U.S. Government Printing Office, Washington, D.C., August 1964.

Hall, R.T. and J.M. Dowling, (1967), J. Chem. Phys., Vol.47, p.2454.

Hall, D.N.B., (1970), Observations of the Infrared Sunspot Spectrum Between 11340 A and 24778 A, Thesis, Harvard University, Cambridge, Mass.

Hall, D.N.B., (1972), unpublished data.

Izatt, J.R., H. Sakai and W.S. Benedict, (1969), J. Opt. Soc. Am., Vol.59, p.19.

Madden, R.P. and W.S. Benedict, (1956), J. Chem. Phys., Vol.25, p.594 and unpublished data.

Migeotte, M., L. Neven and J. Swensson, (1957), The Solar Spectrum from 2.8 to 23.7 Microns, Measures and Identifications, Mem. Soc. Roy. Sci. Liege, Special Volume 2, Liege, Belgium.

Nelson, R.C., (1949), Atlas and Wavelength Tables, Summary Report IV, Northwestern University, Evanston, Ill.

Pugh, L.A., (1972), A Detailed Study of the Near Infrared Spectrum of Water Vapor, Thesis, Ohio State University, Columbus, Ohio.

Rao, K.N., W.W. Brim, J.L. Sinnett and R.M. Wilson, (1962), J. Opt. Soc. Am., Vol.52, p.862.

Steenbeckeliers, G. and J. Bellet, (1971), Comptes Rendus Acad. Sci., Vol. B273, p.288, Paris, France.

Swensson, J., W.S. Benedict, L. Delbouille and G. Roland, (1970), The Solar Spectrum from λ 7498 to λ 12016: A Table of Measures and Identifications, Mem. Soc. Roy. Sci. Liege, Special Volume 5, Liege, Belgium.

Williamson, J.G., K.N. Rao and L.H. Jones, (1971), J. Mol. Spec., Vol.40, p.372.

CO_2

Amat, G. and M. Pinder, (1955), J. Mol. Spec., Vol.16, p.226.

Burch, D.E., D.A. Gryvnak, R.R. Patty and C. Bartky, (1968), The Shapes of Collision-Broadened CO_2 Absorption Lines, Aeronutronic Report No. U-3203, Philco-Ford Corporation, 31 August 1968.

Burch, D.E., (1970), Semi-Annual Technical Report: Investigation of the Absorption of Infrared Radiation by Atmospheric Gases, Aeronutronic Report No. U-4784, Philco-Ford Corporation, 31 January 1970.

Calfee, R.F. and W.S. Benedict, (1966), Carbon Dioxide Spectral Line Positions and Intensities Calculated for the 2.05 and 2.7 Micron Regions, NBS Technical Note No. 332, U.S. Government Printing Office, Washington, D.C., 15 March 1966.

Chaney, L.W., S. Drayson and C. Young, (1967), Fourier Transform Spectrometer - Radiative Measurements and Temperature Inversion. Appl. Opt., Vol.6, pp.347-349.

Cihla, A. and A. Chedin, (1972), J. Mol. Spec., Vol.40, p.337.

Connes, J., P. Connes and J.P. Maillard, (1969), Near Infrared Spectra of Venus, Mars, Jupiter, and Saturn, Centre National de la Recherche Scientifique, Paris.

Connes, J., P. Connes and J. P. Maillard, (1969), Atlas of Near Infrared Spectra of Venus, Mars, Jupiter and Saturn, Editions du C.N.R.S., Paris.

Drayson, S.R. and C. Young, (1967), The Frequencies and Intensities of Carbon Dioxide Absorption Lines Between 12 and 18 Microns, Technical Report No. 08183-1-T, University of Michigan, Ann Arbor, Michigan.

Drayson, S.R., S.Y. Li and C. Young, (1968), Atmospheric Absorption by Carbon Dioxide, Water Vapor and Oxygen, Report No. 08183-2-F, University of Michigan, Ann Arbor, Michigan.

Gordon, H.R. and T.K. McCubbin, (1965), J. Mol. Spec., Vol.18, p.73.

Gordon, H.R. and T.K. McCubbin, (1966), J. Mol. Spec., Vol.19, p.137.

Kaplan, L. and D. Eggars, (1956), Intensity and Line-Width of the 15 Micron CO_2 Band Determined by Curve-of-Growth Method, J. Chem. Phys., Vol.25, pp.876-883.

Oberly, R., K.N. Rao, Y.H. Hahn and T.K. McCubbin, (1962), J. Mol. Spec., Vol.25, p.138.

Yamamoto, G., M. Tanaka and T. Aoki, (1969), J. Quant. Spec. Rad. Trans., Vol.9, p.371.

O_3

Clough, S.A. and F.X. Kneizys, (1965), Ozone Absorption in the 9.0 Micron Region, AFCRL-65-89?

Clough, S.A. and F.X. Kneizy., (1966), J. Chem. Phys., Vol.44, p.1855.

Goldman, A., T.G. Kyle, D.G. Murcray, F.H. Murcray and W.J. Williams, (1970), Appl. Opt., Vol.9, p.565.

Lichtenstein, M., J.J. Gallagher and S.A. Clough, (1971), J. Mol. Spec., Vol.40, p.10.

McCaa, D.J. and J.H. Shaw, (1968), J. Mol. Spec., Vol.25, p.374.

McCaa, D.J., et al., (1967), The Infrared Absorption Bands of Ozone, Report No. AFCRL-67-0237, Ohio State University, Columbus, Ohio.

Snider, D.C. and J.H. Shaw, (1971), Twenty-Sixth Symposium on Molecular Structure and Spectroscopy, Ohio State University, Columbus, Ohio, June 14-16, 1971.

Tanaka, T. and Y. Morino, (1968), J. Chem. Phys., Vol.49, p.2877.

Tanaka, T. and Y. Morino, (1970a), J. Mol. Spec., Vol.33, p.538.

Tanaka, T. and Y. Morino, (1970b), J. Mol. Spec., Vol.33, p.552.

N_2O

Benedict, W.S., (1973), private communication to McClatchey, et al., (1973).

Burch, D.E., D.A. Gryvnak and J.D. Pembrook, (1971a), Report No. U-4897, Aeronutronic Division, Philco-Ford Corporation. (ASTIA No. AD 882 876)

Burch, D.E., D.A. Gryvnak and J.D. Pembrook, (1971b), Report No. U-4897, Aeronutronic Division, Philco-Ford Corporation. (ASTIA No. AD 733 839)

Burch, D.E., D.A. Gryvnak and J.D. Pembrook, (1972), Report No. U-5037, Aeronutronic Division, Philco-Ford Corporation. (ASTIA No. to be assigned)

Burch, D.E., D.A. Gryvnak and J.D. Pembrook, (1971c), Report No. U-4995, Aeronutronic Division, Philco-Ford Corporation. (ASTIA No. AD 733 839)

Fraley, P.E., W.W. Brim and K.N. Rao, (1962), J. Mol. Spec., Vol.9, p.487.

Lowder, J.E., (1972), J. Quant. Spec. Rad. Trans., Vol.12, p.873.

Margolis, J.S., (1972), J. Quant. Spec. Rad. Trans., Vol.12, p.751.

Oppenheim, U.P. and A. Goldman, (1966), J. Opt. Soc. Am., Vol.56, p.675.

Pliva, J., (1964), J. Mol. Spec., Vol.12, p.360.

Pliva, J., (1968a), J. Mol. Spec., Vol.25, p.62.

Pliva, J., (1968b), J. Mol. Spec., Vol.27, p.461.

Tidwell, E.D., E.K. Plyler and W.S. Benedict, (1960), J. Opt. Soc. Am., Vol.50, p.1243.

Toth, R.A., (1971a), J. Mol. Spec., Vol.40, p.588.

Toth, R.A., (1971b), J. Mol. Spec., Vol.40, p.605.

Young, L.D.G., (1972), J. Quant. Spec. Rad. Trans., Vol.12, p.3.

CO

Burch, D.E. and D.A. Gryvnak, (1967), J. Chem. Phys., Vol.47, No.12, p.4930.

Hunt, R.H., R.A. Toth and E.K. Plyler, (1968), J. Chem. Phys., Vol.49, p.9.

Kunde, V.G., (1967), Tables of Theoretical Line Positions and Intensities for the $\Delta V = 1$, $\Delta V = 2$, and $\Delta V = 3$ Vibration-Rotation Bands of $C^{12}O^{16}$ and $C^{13}O^{16}$, NASA TMX-63183.

Young, L.A. and W.J. Eachas, (1966), J. Chem. Phys., Vol.44, p.11.

Young, L.A., (1968), J. Quant. Spec. Rad. Trans., Vol.8.

CH_4

Armstrong, P.L. and H.L. Walsh, (1960), Spectrochim Acta, Vol.16, p.840.

Barnes, W.L., J. Suskind, R.H. Hunt and E.K. Plyler, (1972), J. Chem. Phys., Vol.56, p.5160.

Benedict, W.S., (1973), Private communication to McClatchey, et al., (1973).

Bobin, B. and K. Fox, (1973), J. Chem. Phys. and J. Phys., Paris.

Botineau, J., (1970), Rev. Phys. Appl., Vol.5, p.829, Paris; and (1972), J. Mol. Spec., Vol.41, p.186.

Bregier, R., (1970), J. Phys., Vol.31, p.301, Paris.

Dang Nhu, M., (1968), Thesis, Universite' de Paris.

Dang Nhu, M., (1969), Ann. Phys., Vol.4, p.273, Paris.

Fox, K., (1962), J. Mol. Spec., Vol.9, p.381.

Fox, K., (1973), Bull. Am. Phys. Soc., Vol.18, p.232.

Hall, D.N.B., (1973), To be published.

Hecht, K.T., (1960), J. Mol. Spec., Vol.5, pp.355, 390.

Henry, L., N. Husson, R. Andia and A. Valentin, (1970), J. Mol. Spec., Vol.36, p.511.

Herranz, J., (1961), J. Mol. Spec., Vol.6, p.343.

Hilico, J.C., (1970), J. Phys., Vol.31, p.289, Paris.

Hussan, N. and G. Poussigue, (1971), J. Phys., Vol.32, p.859, Paris.

Husson, H. and M. Dang Nhu, (1971), J. Phys., Vol.32, p.627, Paris.

Jahn, H.A., (1938), Proc. Roy. Soc., Vol.A168, pp.469, 495, London.

Kyle, T.G., (1968), Line Parameters of the Infrared Methane Bands, Report No. AFCRL-68-0521, October 1968.

Kyle, T.G., R.D. Blatherwick and F.S. Bonomo, (1970), J. Chem. Phys., Vol.53, p.2800.

McDowell, R.S., (1966), J. Mol. Spec., Vol.21, p.280.

Michelot, F. and K. Fox, (1973), To be published.

Moret-Bailly, J., (1961), Cah. Phys., Vol.15, p.237.

Ozier, I., P.N. Yi, A. Khosla and N.F. Ramsey, (1970), Phys. Rev. Letters, Vol.28, p.642.

Plyler, E.K., E.D. Tidwell and L.R. Blaine, (1960), J. Res. NBS, Vol.64A, p.201.

Susskind, J., (1972), J. Chem. Phys., Vol.56, p.5152.

Shaffer, W.H., H.H. Nielsen and L.H. Thomas, (1939), Phys. Rev., Vol.56, p.895.

Tejwani, G.O.T. and P. Varanasi, (1971), J. Chem. Phys., Vol.55, p.1075.

Varanasi, P., (1971), J. Quant. Spec. Rad. Trans., Vol.11, p.1711.

Varanasi, P. and G.O.T.Tejwani, (1972), J. Quant. Spec. Rad. Trans., Vol.12, p.849.

O_2

Babcock, H.D. and L. Herzberg, (1948), Astrophys. J., Vol.108, p.167.

Burch, D.E. and D.A. Gryvnak, (1969), Appl. Opt., Vol.8, p.1489.

Gordy, W., W.V. Smith and R.F. Trambarulo, (1953), Microwave Spectroscopy, J. Wiley and Sons, New York, p.207.

Herzberg, L. and G. Herzberg, (1947), Astrophys. J., Vol.105, p.353.

Jones, A.V. and A.W. Harrison, (1958), J. Atmos. and Terrest. Phys., Vol.13, p.45.

Krupenie, P.H., (1972), J. Phys. and Chem., p.423.

McKnight, J.S. and W. Gordy, (1968), Phys. Rev. Letters, Vol.21, p.1787.

Noxon, J.F., (1961), Can. J. Phys., Vol.39, p.1110.

Wark, D.Q. and D.M. Mercer, (1965), Appl. Opt., Vol.5, No.7, p.839.

West, B.G. and M. Mizushima, (1966), Phys. Rev., Vol.143, p.31.

Zimmerer, R.W. and M. Mizushima, (1961), Phys. Rev., Vol.121, p.152.

Appendix

EARTH CURVATURE AND REFRACTION

For the calculation of atmospheric absorption, the earth is sometimes considered as being constructed of plane-parallel layers, as it usually is for multiple scattering; or as is more often the case, it can be considered as made up of concentric layers, bounded by shells which form concentric spheres with the curved (assumed circular) surface of the earth. The first approximation in this model is to assume no refraction, as is done in the calculation with the Aggregate method described in Section 7.4. This is a reasonable approximation since refractive effects are of minor importance in most cases for which the accuracies are of the order usually expected from band-model calculations; and of less importance than the effect of curvature. A schematic of this type of model is shown in Figure 76 in Section 7.

In the LOWTRAN 2 model (see Section 7.5) refractive effects, which can be important for large zenith angles, are considered. Consideration of refraction is not difficult but it requires an addition to the numerical procedure in the computer program which should be explained. This description, which is slightly different from that given for LOWTRAN, has been given previously in the 1967 State-of-the-Art report (Anding, 1967). The procedure is straightforward and considers a spherical earth surrounded by a spherical atmosphere. It is assumed that the atmosphere exists in spherical shells, each shell being homogeneous. Under this assumption the refractive index will be constant throughout a given shell, changing abruptly as one passes from one shell to the next. The slant path is defined by the lowest point in the path Z_1, the highest point in the path Z_2, and the angle subtended by Z_1 and Z_2 at the earth's center (see Figure A-1).

The first approximation to the true path is the straight line joining Z_1 and Z_2 (see Figure A-2). The angle ϕ is divided into N equal angular increments $\Delta\phi_1, \Delta\phi_2, \ldots, \Delta\phi_N$, where N is determined from the equation

$$N = \max\left\{\frac{Z_2 - Z_1}{200}; \frac{\text{range}}{2000}\right\}$$

where Z_1, Z_2 and range are expressed in meters. This method of incrementing the path insures that a point be calculated at least every 200 m altitude. α_1 is defined as the angle between the line of sight and the radial line r_1. Point b is the point where the line of sight intersects the second radial line r_2. If a tangent line t_1 is drawn through b which is normal to r_2, it is obvious that the angle θ_2 will be given by

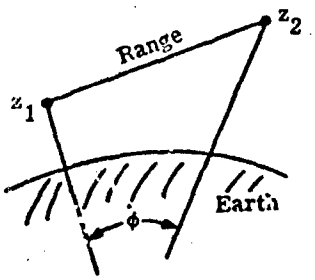

FIGURE A-1. PARAMETERS DEFINING GEOMETRY OF SLANT PATH

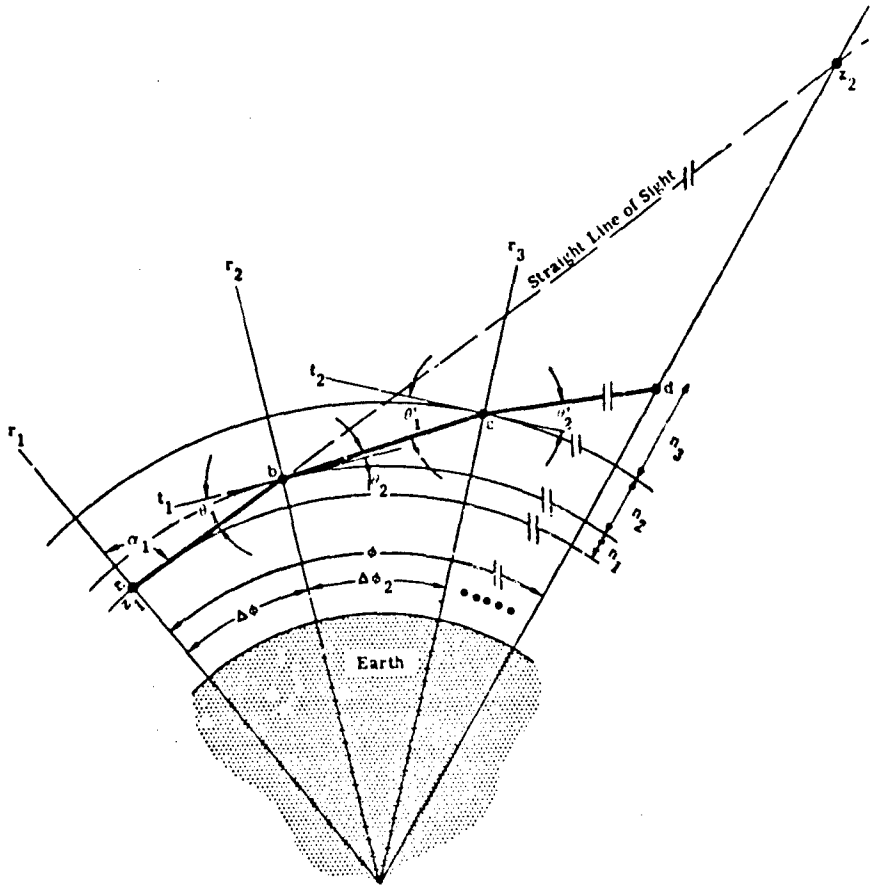

FIGURE A-2. SCHEMATIC DIAGRAM OF ATMOSPHERIC REFRACTED PATH

$$\theta_2 = \text{arc sin}\left[\frac{n_2}{n_1}\left(\frac{R_e + Z_2}{R_e + Z_1}\right)\sin\theta_1\right] \qquad (A$$

when n_1 and n_2 are the refractive indexes of the lower shell and upper shell, respectively and R_e is the radius of the earth.

To determine the refractive index of any given shell a simple version of the results of Edlen [347] is used. This is given by:

$$(n_a - 1)\times 10^6 = \left(77.46 + \frac{0.459}{\lambda^2}\right)\frac{P}{T} - p_{H_2O}\left(43.49 - \frac{0.347}{\lambda^2}\right)$$

where n_a = refractive index of air at temperature T and pressure P

λ = wavelength in microns

T is in Kelvin

P is atmospheric pressure

p_{H_2O} is the partial pressure of H_2O vapor in millibars

As was stated previously, the refractive index of a given shell is assumed to be constant throughout the shell. Also, for purposes of this calculation it is assumed that the value of for the i-th shell is the value calculated for the lowest altitude of the shell. LOWTRAN assumes an average value for the shell.

The angle θ_2 in Eq. (A-1) defines a new line of sight which intersects the radial line at point c. A tangent line t_2 is drawn normal to r_3. Then the refracted angle θ_2' is given by Snell's law as before. This procedure is continued until the path intersects the radial line passing through Z_2 at point d. The altitude difference between Z_2 and d is used to increase the angle α. The entire procedure is then repeated until the point d converges to Z_2 within than 10 m. When the final refracted path is calculated, a range-altitude table is compiled the range is measured from the lowest point in the path.

LOWTRAN 2 has a thorough description of the procedure used in its program for different types of trajectories. The user is referred to Selby and McClatchey, (1972) for the descr which covers the cases delineated in Figure A-3 and specified as:

Type 1: Horizontal path, for which earth curvature and refraction are neglected

Type 2: Slant path between points at two different altitudes

Type 3: Slant path between a point in the atmosphere and space.

347. B. Edlen, "The Refractive Index of Air," Metrologia, Vol. 2, No. 2, 1966, p. 71.

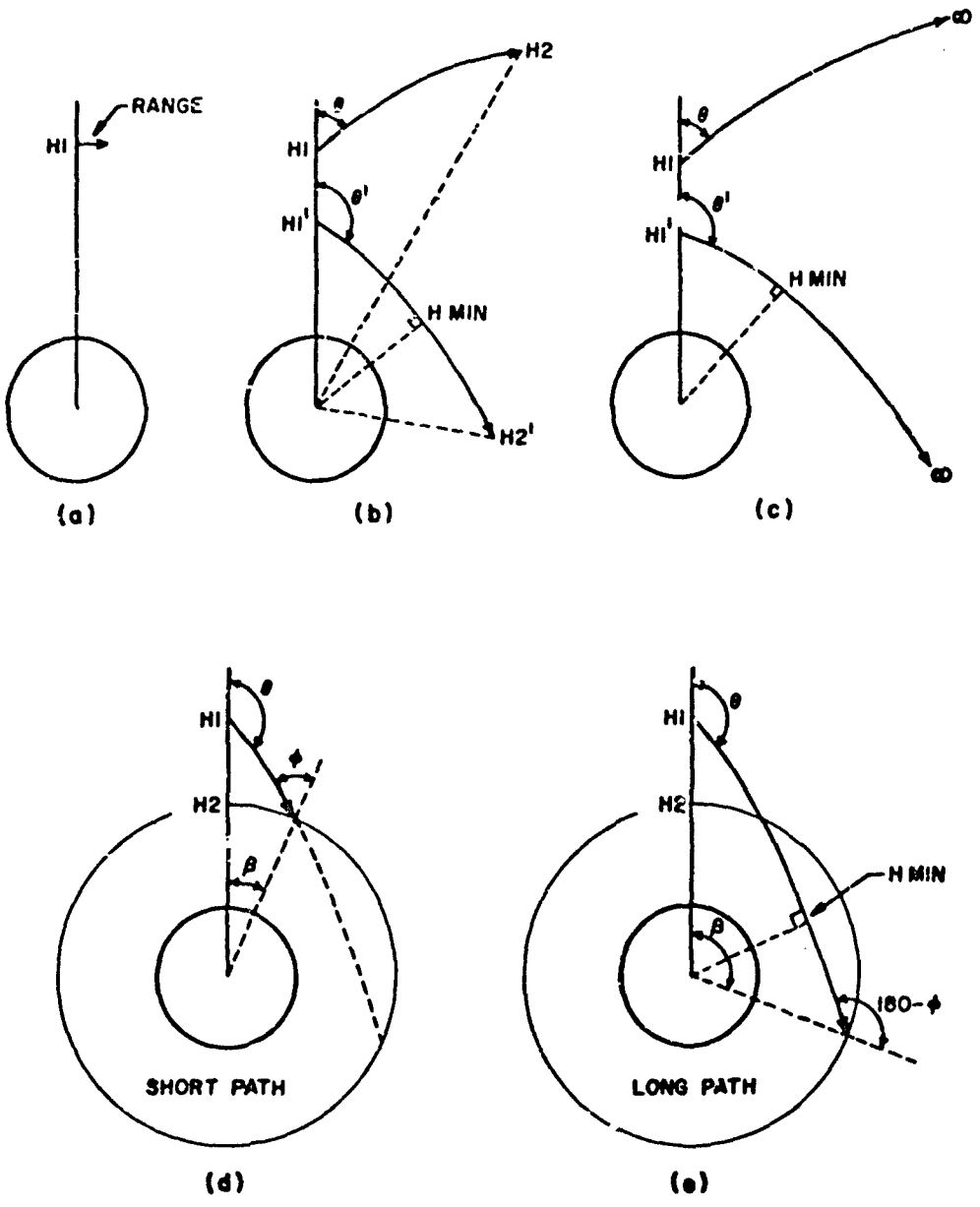

FIGURE A-3. GEOMETRICAL PATH CONFIGURATIONS. (a) Horizontal paths (Type 1); (b) slant paths between two altitudes H1 and H2 (Type 2); and (c) slant paths to space (Type 3). For downward looking paths where HMIN < H2 < H1, two trajectories are possible as indicated in (d) and (e). (Reproduced from Selby and McClatchey, 1972 [20].)

SYMBOLS

		Section*
A	Absorptance, Absorptivity	
A	Constant (Quasi-Random)	
A	Area (cm^2)	
A_n	Scattering parameters (Aggregate)	7
A_0	Variable (Smith)	8
A_1	Variable (Smith)	8
A_1	Spectral parameters (Aggregate)	7
A_2	Variable (Smith)	8
A_2	Spectral parameters (Aggregate)	7
A_3	Variable (Smith)	8
A_3	Spectral parameters (Aggregate)	7
A_4	Variable (Smith)	8
A_4	Spectral parameters (Aggregate)	7
A_5	Variable (Smith)	8
A_6	Variable (Smith)	8
$A(\lambda)$	Spectral absorptance (Absorptivity)	
$A(\nu)$	Spectral absorptance (Absorptivity)	
$A_{\Delta\lambda}$	Absorptance (Absorptivity) over a band	
$A_{\Delta\nu}$	Absorptance (Absorptivity) over a band	
$A_{\ell m}$	Legendre polynomial expansion coefficient	3
A_ℓ	Legendre polynomial expansion coefficient	3
$\tilde{\tilde{A}}$	Matrix	3
a	Constant (Quasi-Random)	7
$a(T - T_0)$	Variable (Ellingson)	7
a	Lorentz line modification constant	4
a	Argument for Gamma function	8
a	Rotational constant	4
a	Slit width at half intensity (cm^{-1})	
a_1	Least squares parameter (Zachor)	8
a_2	Least squares parameter (Zachor)	8
$a'(T - T_0)$	Variable (Ellingson)	7
a_h	Number density ratio (LOWTRAN)	7
a_v	Number density ratio (LOWTRAN)	7
a_ℓ	Scattering parameter	10

*Section numbers are omitted for symbols used throughout the report.

		Section
a_ν	Parameter (Smith)	8
B	Self-broadening coefficient	
B_n	Scattering parameter (Aggregate)	7
B_v	Rotational energy level parameter	4
B_w	Band-model parameter (Gibson-Pierluissi)	8
B_s	Band-model parameter (Gibson-Pierluissi)	8
B_{ws}	Band-model parameter (Gibson-Pierluissi)	8
b	Breadth of strong lines (Benedict, et al.)	4
b	Rotational constant	4
b	Lorentz line modification constant	4
b	Constant (Quasi-random)	7
b	Maximum of particle distribution	10
$b(T - T_o)^2$	Variable (Ellingson)	7
b(u, y)	Mixed Lorentz-Doppler shape = $\sqrt{\frac{\ell n\, 2}{\pi}} \frac{1}{\alpha_D} H(u, y)$	
$b(\nu, \nu_i)$	Line-shape factor	
$b'(T - T_0)^2$	Variable (Ellingson)	7
$b_a(\lambda)$	Absorption coefficient (Aggregate-scattering)	7
$b_s(\lambda)$	Scattering coefficient (Aggregate-scattering)	7
$b_{ext}(\lambda)$	Extinction coefficient (Aggregate-scattering)	7
b_h	Equivalent absorber amount for H_2O continuum (LOWTRAN)	7
$b_v(z)$	Equivalent absorber amount for H_2O continuum (LOWTRAN)	7
b_ℓ	Scattering parameter	10
$b_{\ell m}$	Coefficient in spherical harmonics method	3
b_ν	Parameter (Smith)	8
C	Exponent (Ellingson)	7
C	Parameter (Zachor)	8
$C(\nu)$	Spectral parameter (LOWTRAN)	7
$C_0(\Delta\nu)$	Expansion coefficient (Smith)	8
$C_1(\Delta\nu)$	Expansion coefficient (Smith)	8
$C_2(\Delta\nu)$	Expansion coefficient (Smith)	8
$C_n(\Delta\nu)$	Expansion coefficient (Smith)	8
C_1	Coefficient (Ellingson)	7
C_2	Coefficient (Ellingson)	7
$C_1(\lambda)$	Spectral coefficient (Aggregate)	7
$C_2(\lambda)$	Spectral coefficient (Aggregate)	7
$C_3(\lambda)$	Spectral coefficient (Aggregate)	7
$C_4(\lambda)$	Spectral coefficient (Aggregate)	7

		Section
c	Variable (Drayson (=dw/dP)	6
c	Fractional concentration of gases	7
c	Rotational constant	4
c	Velocity of light (2.99793×10^{10} cm-sec^{-1})	
$c(\lambda)$	Spectral parameter (Aggregate)	7
c_ν	Parameter (Smith)	3
c_1	Least squares parameter (Zachor)	8
c_2	Least squares parameter (Zachor)	8
D	Number density	
D	Step size (Kyle)	6
D_i	Particle density in i-th layer (Aggregate)	7
D_v	Rotational energy level parameter	4
d	Rotational constant	4
d	Lorentz line modification constant	4
d	Line spacing (cm^{-1})	
d_ν	Parameter (Smith)	8
E''	Energy of lower state	7
E_H	Irradiance (solar, attenuated)	
$\overline{E_{ij}(T_0)}$	Average ground state energy (Daniels)	7
$E_N(x)$	Exponential integral (Drayson)	6
E_+	Diffuse irradiance in upward direction (Turner)	3
E_-	Diffuse irradiance in downward direction (Turner)	3
$\tilde{E}_-$	Total downward irradiance (Turner)	3
$E_{v,j}$	Rotational energy level	4
E_0	Extra-terrestrial solar irradiance	
E_λ	Spectral irradiance (watt-cm^{-2}-μm^{-1})	
E_ν	Spectral irradiance [watt-cm^{-2}-(cm^{-1})$^{-1}$]	
e	Rotational constant	4
$\overline{F}$	Fourier transform of slit function (Kunde and Maguire) $[= f(\lvert\nu_i - \nu^*\rvert, a)]$	6
f	Rotational constant	4
f	Bi-directional reflectance function $\equiv \frac{dL(x, y, 0, \mu, \phi)}{L(x, y, 0, -\mu', \phi')\mu' d\Omega'}$	
G_v	Vibrational energy level	4
G_v^{unp}	Energy level, vibrational (unperturbed)	4
g	Acceleration of gravity	

		Section
g	Subscript for ground level (Drayson)	6
g	Average value cosine of the scattering angle θ	10
g_{22}	Coefficient in energy level calculation	4
g_{ri}	Polynomial coefficient (Ellingson)	7
H	Operator	3
H	Scale height (= ℓ n P)	7
H	Line-width factor (Ellingson)	7
H(u, y)	Line-shape function (Kunde and Maguire)	6
H_v	Rotational energy level parameter	4
h	Distance (vertical) (cm, km)	
h	Planck's constant (6.6252×10^{-34} watt sec^2)	
h	Half width ratio (Ellingson) [= $2(\alpha_L/\alpha_D)$]	7
h_i	Absorption-coefficient distribution function (Arking-Grossman)	6
I	Unit Operator	3
I(H, h)	Line-shape function (Ellingson)	7
$I(\theta_0, \theta, x)$	Specific intensity of reflected radiation (Invariant Bedding)	3
I_0	Bessel Function	
I_1	Bessel Function	
i	Index	
i	Exponent	
J	Rotational quantum number	
J	Source function	2
J''	Lower vibrational state	
j	Index	
K	Eddington field	3
K	H_2O continuum broadening absorption coefficient	6
K	Weak-line parameter (Zachor) (= S/d)	8
K(λ)	Spectral coefficient (Aggregate)	7
$K_f(\lambda)$	Spectral coefficient for foreign broadening (Aggregate)	7
K_j	Coefficient (Scott)	6
$K_s(\lambda)$	Spectral coefficient for self-broadening (Aggregate)	7
$K_1(\lambda)$	Spectral coefficient (Aggregate) (= S/d)	7
$K_1'(\lambda)$	Spectral coefficient (Aggregate) [= $(2\pi\alpha_{L0})/d$]	7
$K_2(\lambda)$	Spectral coefficient (Aggregate) [= $S/(2\pi\alpha_{L0})$]	7
k	Boltzmann's constant (1.38042×10^{-23} erg-K^{-1})	
k_c	Foreign broadening H_2O continuum coefficient (Ellingson)	7
k_e	Self-broadening H_2O continuum coefficient (Ellingson)	7
k	Index	

		Sectio
$k(\lambda)$	Extinction coefficient (mass) $(gm\text{-}cm^{-2})^{-1}$	
$k(\lambda)$	Index of refraction (imaginary part)	
$k'(\lambda)$	Extinction coefficient (volume) (cm^{-1})	
$k_1(\lambda)$	Spectral coefficient for H_2O continuum (Kunde and Maguire)	6
$k_2(\lambda)$	Spectral coefficient for H_2O continuum) (Kunde and Maguire)	6
$k_a(\lambda)$	Absorption coefficient (mass)(= k in pure absorption)	
$k'_a(\lambda)$	Absorption coefficient (volume)	
$k'_s(\lambda)$	Scattering coefficient (volume)	
$k_0(\lambda)$	Doppler line-broadening factor $(= (S/\alpha_D)(\ell n\, 2/\pi)^{1/2})$	
L	Path length (cm)	
L_e	Equivalent path length (cm)	5
$L(\psi)$	Ladenburg-Reiche function	
L_B	Radiance (beam)	2
L_D	Radiance (diffuse)	2
L_{DN}	Radiance (downwelling)	2
L_G	Radiance (surface, or ground) $(= L_{GE} + L_{GH} + L_{GS})$	2
L_{GE}	Radiance (surface, emitted)	2
L_{GS}	Radiance (surface, diffusely-scattered)	2
L_{GH}	Radiance (surface, solar-reflected)	2
L_H	Radiance (solar)	2
L_{HSS}	Radiance (solar, singly-scattered)	2
L_I	Radiance (intrinsic)	2
L_P	Radiance (path) $(= L_{PSS} + L_{PE} + L_{PMS})$	2
L_{PE}	Radiance (path, emitted)	2
L_{PMS}	Radiance (path, multiply-scattered)	2
L_{PSS}	Radiance (path, singly-scattered)	2
L_S	Sky radiance	3
L_T	Total radiance for downward looking observer (Turner)	3
L_{UP}	Radiance (upwelling)	2
L_+	Radiance in upward direction (Schuster-Schwarzschild)	3
L_-	Radiance in downward direction (Schuster-Schwarzschild)	3
L_λ	Spectral radiance $(watt\text{-}cm^{-2}\text{-}ster^{-1}\text{-}\mu m^{-1})$	
L_ν	Spectral radiance $(watt\text{-}cm^{-2}\text{-}ster^{-1} - [cm^{-1}]^{-1})$	
L^*_ν	Planck function $(= 2c^2h\nu^3(e^{hc\nu/kT} - 1)^{-1})$	
L^*_λ	Planck function $(= 2c^2h\lambda^{-5}(e^{hc/\lambda kT} - 1)^{-1})$	
$\bar{\bar{\mathscr{L}}}$	Fourier transform of radiance	6

		Section
$\bar{L}$	Average radiance over space (Ellingson)	3
ℓ	Angular momentum quantum number	4
ℓ	Number of lines in integration interval (Scott)	6
ℓ	Path length (cm)	
ℓ	Index	
ℓ	Index (Daniels)	7
M	Ratio of half-width to mesh size (Scott)	6
M	Transition rate (Zachor)	8
M	Radiant exitance (watt-cm^{-2})	
M	Kernel (maximum value)	3
M	Molecular weight (gm-mole^{-1})	
M	mixing ratio	
M'	Pressure ratio (Aggregate)	7
M'(s)	Ratio of partial pressure of absorber to total pressure (Aggregate)	7
M_N^+	Moment	3
M_N^-	Moment	
M_ρ	Radiant Exitance (caused by reflection)	2
M^*	Radiant Exitance (Planckian) (= πL^*) (w/cm^{-2})	
m	Exponent	
m	Index	
m	Number of lines (Kunde and Maguire)	6
m	P, Q or R branch index	4
m(λ)	Index of refraction (complex)	
m_h	Mass density ratio (LOWTRAN)	7
m_v	Effective slant path (LOWTRAN)	7
m_ν	Exponent (Smith)	8
N	Number of atmospheric layers (Drayson)	6
N	Number (of lines in a spectral interval)	5
N	Number of integration points (Scott)	6
N(r)	Particle size distribution	
N_ν	Number of lines (Smith)	8
n	Exponent	
n	Index	
n	Parameter (Zachor)	8
n(ζ_k)	Number of representation points (Scott)	6
n(λ)	Index of refraction (real part)	
n_r	Number of lines (Quasi-Random)	7
P	Pressure (atmospheres, mm Hg, mbar, etc.)	

		Section
$\bar{\bar{P}}$	Curtis-Godson equivalent broadening pressure (Aggregate)	7
$\bar{P}$	Mean pressure (Ellingson)	7
$\tilde{P}$	Curtis-Godson equivalent pressure	5
P(s)	Probability distribution function (line strength)	5
P_e	Effective (equivalent) broadening pressure	
P_N	Legendre polynomial	
P_M	Polynomial (Drayson)	6
P_f^*	Effective pressure for foreign gas broadening (N_2 continuum) (Aggregate)	7
P_s^*	Effective pressure for self-broadening (N_2 continuum) (Aggregate)	7
P_ℓ	Legendre polynomial	
P_ℓ^m	Associated Legendre polynomial	
$\bar{P}'$	Average pressure (Aggregate) [$= (P_0/w)w_1$] [$= (P_0/w)w_2$]	7
$\mathcal{P}(a, x)$	Incomplete gamma function	
ρ	Partial pressure of absorbing gas	
p	Phase function, single-scattering	
Q	Intrinsic emission	
Q_{ext}	Extinction efficiency factor	7
Q_s	Scattering efficiency factor	7
q	Intrinsic emission	
ϱ	Optical path (depth, thickness) $\left(= \int_h^\infty -k'(z)dz\right)$	2
q_{11}	Least squares parameter (Zachor)	8
q_{12}	Least squares parameter (Zachor)	8
q_{22}	Least squares parameter (Zachor)	8
R	Distance (total path) (cm)	7
R_ν	Residual term (Smith)	8
R_E	Earth radius	
r	Index	
r	Number of atmospheric layers (Scott)	6
r	Radius vector	
r	Particle radius	
r	Diffusivity factor (Elsasser) (= 1.667)	7
r_c	Mode radius of distribution function	10
S	Line strength (gm^{-1}-cm) [cm^{-1} $(atm\text{-}cm)^{-1}$] [cm^{-1} $(mol\ cm^{-2})^{-1}$]	
S^ω	Line strength per unit pressure	

		Section
S_0	Line strength under standard conditions	
S_E	Parameter, exponential tailed S^{-1} random model	5
$\overline{S_{ij}(T)}$	Average line strength (Daniels)	7
s	Distance (slant, variable)	
s	Parameter, Elsasser Model (= $2\pi\nu/d$)	
T	Temperature (Kelvins)	
T_0	Standard temperature (usually ~ 273.16 K)	
T_g	Ground temperature	6
$\tilde{T}_i$	Average temperature	5
T_h	Temperature for homogeneous path (Aggregate)	7
T'_0	Temperature at which band model parameters are defined	
t	Variable	5
t	Tangent vector	
u	Doppler-Lorentz (Voigt) line broadening factor $\left[= (\alpha_L/\alpha_D)\,(\ell n\, 2)^{1/2}\right]$	
V	Visibility (Koschmieder)	10
v_i	Vibrational quantum number	4
W	Equivalent width	
W^0	Equivalent width per unit pressure	
W	Variable (Smith)	8
W_i	Weights for integration (Scott)	6
$W_{ij}(CG)$	Curtis-Godson effective absorber amount (Daniels)	7
W_ℓ	Weights (Gaussian Quadrature)	6
w	Absorber amount	
w_1	Adjusted absorber amount (Aggregate)	7
w_2	Adjusted absorber amount (Aggregate)	7
w'	Absorber amount per km (LOWTRAN)	7
w^*	Equivalent amount of absorber (Aggregate)	7
w^*	Equivalent amount of absorber (LOWTRAN)	7
w_f	Effective absorber amount, foreign broadening N_2 continuum (Aggregate)	7
w_i	Christoffel Numbers	
w_f	Equivalent absorber amount (Aggregate)	7
w_k	Weights for integration (Scott)	6
w_s	Equivalent absorber amount (Aggregate)	7
$\tilde{w}$	Scaled absorber amount	5
X	Variable (Smith) $\{= \ell n\,[w(273\ K/T]\}$	8
x	Variable (general)	

		Section
x	Variable (Quasi-Random) (= ℓn P)	7
x	Variable (Gibson-Pierluissi)	8
x	Thickness of slab	3
x	Particle size parameter (= $2\pi r/\lambda$)	10
x	Distance (horizontal) (cm, km)	
x_{ij}	Coefficient in energy level calculation	4
x_ℓ	Abscissae (Gaussian quadrature)	6
Y	Parameter (Elsasser) (= $\beta\psi/\sinh\beta$)	5
Y	Variable (Smith) [ℓn (P/10^3 mb)]	8
y	Distance (horizontal) (cm, km)	
y	Variable (Quasi-Random) (= ℓn w)	7
y	Variable (Gibson-Pierluissi)	8
y	Doppler line broadening variable $\left[= (\nu - \nu_0/\alpha_D)(\ell n\ 2)^{1/2}\right]$	4
v	Variable (Quasi-Random [= $\nu_i - \nu_0 = (1/2\delta)$]	7
y_{ijk}	Coefficient in energy level calculation	4
z	Vertical distance	
Z	Variable (Smith) [ℓn (T/273 K)]	8
Z_i	Gaussian nodes (Ellingson)	7
z	Variable (Gibson-Pierluissi)	8
z	Distance (vertical) (cm, km)	2
z	Variable (Quasi-Random) (= $\nu - \nu_0 - 1/2\delta$)	7
z_i	Gaussian nodes (Ellingson)	7
z_T	Top of the atmosphere (Ellingson)	7
α	Angle	Appendix
α_D	Doppler line half width (cm^{-1})	
α'_D	Pseudo Doppler half-width (Daniels)	7
$\tilde{\alpha}_i$	Effective half width	5
α_{ij}(CG)	Curtis-Godson half width (Daniels)	7
α_L	Lorentz line half width (cm^{-1})	
α_{L0}	Lorentz half width under standard conditions	
α^o_{L0}	Lorentz half-width at standard pressure, per unit pressure (= α_{L0}/P_0)	
α_{LC}	Characteristic Lorentz half width (Arking&Grossman) (= α_L/d)	6

		Section
α_{m+1}	Matrix element	3
β	Band-model parameter ($= 2\pi\alpha_L/d$)	
β^o	Band-model parameter ($= 2\pi\alpha_{L0}^{\delta}/d$)	8
β_ν	Variable (Smith)	8
β'	Band-model parameter (Quasi-Random) $\left(= 2\alpha_D(\ell n\, 2)^{1/2}/\delta\right)$	7
β_{m+1}	Matrix element	3
ψ	Band-model parameter ($= Sw/2\pi\alpha_L$)	8
δ	Delta function	
δ	Exponent	
δ	Distance from line center (Kunde and Maguire)	6
δ_r	Subinterval (Quasi-Random)	7
δ_j^s	Shifted interval (Quasi-Random)	7
δ_j^u	Unshifted interval (Quasi-Random)	7
Δ	Layer thickness	3
Δ	Displacement from Line center (Kyle)	6
ϵ	Emissivity	
ϵ	Radiance, path rate of change	2
ϵ	Variable (Quasi-Random) ($= 2z/\delta$)	7
ϵ_M	Wing contribution calculation (Quasi-Random)	7
$\epsilon_c(\lambda)$	Emissivity of cloud (Aggregate)	7
$\epsilon_s(\lambda)$	Emissivity of source (Aggregate)	7
η	Radiation scattered into forward hemisphere (Turner)	3
η	Anisotropy parameter	10
η	Exponent	
η	Variable (Quasi-Random) ($= 2y/\delta$)	7
Φ	Flux	
$\Phi(T)$	Weighting function (Ellingson)	7
ϕ	Direction, azimuth angle	
$\Gamma(a)$	Gamma function	
γ	Variable (Zachor) ($= Sw/d$)	8
γ	Exponent	
$\gamma'(\lambda, s)$	Spontaneous-emission-coefficient	
$\gamma''(\lambda, s)$	Stimulated-emission-coefficient	
$\chi(T)$	Weighting function (Ellingson)	7
χ_i	Parameter (Smith)	8

		Section
λ	Wavelength (in micrometers) (= $1/\nu$)	
μ	Direction (= cos θ)	2
ν	Frequency (wavenumber) (reciprocal centimeters) (= $1/\lambda$)	
ν_F	Center of final interval (Quasi-Random)	7
ν_I	Center of starting interval (Quasi-Random)	7
ν_0	Center frequency (cm^{-1})	4
ν^*	Center of the slit width	6
$\Delta\nu(Z_k)$	Representation step (Scott)	6
Ω	Solid angle (steradians)	
ω_i	Coefficient in energy level calculation	
ω_0	Single scattering albedo	
ρ	Surface albedo	2
ρ	Target reflectance	
ρ	Density (mass) (gms/cm^3)	4
ρ	Variable (Quasi-Random) (= $2\alpha_L/\delta$)	7
$\bar{\rho}$	Background albedo	3
$\sigma_a(r)$	Absorption cross section	
$\sigma_s(r)$	Scattering cross section	
$\sigma_t(r)$	Total extinction cross section	
τ	Transmittance	
$\bar{\tau}$	Average transmittance	
$\bar{\tau}$	Fourier transform of transmittance function (Kunde and Maguire)	6
τ^*	Approximation to actual transmittance	
τ'	Transmittance with scattering (Aggregate)	7
τ_s	Strong-line transmittance (Zachor)	8
τ_w	Continuum Transmittance (Ellingson)	7
θ	Angle	Appendix
θ	Zenith angle	
θ	Angle of scattering	10
θ	Direction, elevation angle	2
$\vartheta_3(z, q)$	Theta function (Kyle)	6
ξ_ν	Variable (Smith)	8
ξ_i	Lorentz line parameter (Quasi-Random) (= $S_i w/\pi\alpha_L$)	7
ξ_i'	Doppler line parameter (Quasi-Random) $\left[= (S_i w/\alpha_D)(\ell n\, 2/\pi)^{1/2}\right]$	7

best sellers

NTIS

from NATIONAL TECHNICAL INFORMATION SERVICE

Product Liability: Industry Study. Volumes I and II
PB-265 542/PSK 986 p PC$21.25/MF$3.00

An Atlas of Radiation Histopathology
TID-26676/PSK 234 p PC$7.60/MF$3.00

The Medical School Admissions Process. A Review of the Literature, 1955-75
PB-263 962/PSK 193 p PC$7.50/MF$3.00

Integrated Energy Vocabulary
PB-259 000/PSK 459 p PC$22.50/MF$3.00

Nuclear Air Cleaning Handbook. Design, Construction, and Testing of High-Efficiency Air Cleaning Systems for Nuclear Application
ERDA-76/21/PSK 300 p PC$9.75/MF$3.00

Evaluation of the Air-To-Air Heat Pump for Residential Space Conditioning
PB-255 652/PSK 293 p PC$9.25/MF$3.00

Federal Information Processing Standards Register: Guidelines for Documentation of Computer Programs and Automated Data Systems. Category: Software. Subcategory: Documentation
FIPS-PUB38/PSK 55 p PC$4.50/MF$3.00

Life Cycle Costing Emphasizing Energy Conservation: Guidelines for Investment Analysis
ERDA-76/130/PSK 117 p PC$5.50/MF$3.00

Analysis of Projected Vs. Actual Costs for Nuclear and Coal-Fired Power Plants
FE-2453-2/PSK 38 p PC$4.00/MF$3.00

Quality Criteria for Water
PB-263 943/PSK 537 p PC$13.00/MF$3.00

Passive Solar Heating and Cooling Conference and Workshop Proceedings May 18-19, 1976, University of New Mexico, Albuquerque, New Mexico
LA-6637-C/PSK 352 p PC$10.50/MF$3.00

Predicting the Performance of Solar Energy Systen
AD-A035 608/PSK 45 p PC$4.00/MF$3.00

NIOSH Analysis Methods for Set J
PB-263 959/PSK 128 p PC$6.00/MF$3.00

Flat-Plate Solar Collector Handbook: A Survey of Principles, Technical Data and Evaluation Result
UCID-17086/PSK 96 p PC$5.00/MF$3.00

How to Order

When you indicate this method of payment, please note if a purchase order is not accompanied by payment, you will be billed an additional $5.00 *ship and bill* charge. And please include the card expiration date when using American Express.

Normal delivery time takes three to five weeks. It is vital that you order by number or your order will be manually filled, insuring a delay. You can opt for *priority mail* for $3.00 outside North American continent charge per item. Just check the *priority mail* box. If you're really pressed for time, call the NTIS Rush Handling Service (703) 557-4700. For a $10.00 charge per item, your order will be sent *priority mail* within 48 hours. Or, you can pick up your order in the Washington Information Center & Bookstore or Springfield Operations Center within 24 h a $6.00 per item charge.

You may also place your order by telepl if you have an NTIS Deposit Account American Express card order through 1 The order desk number is (703) 557-46 the TELEX number is 89-9405.

Thank you for your interest in NTIS. preciate your order.

METHOD OF PAYMENT

- ☐ Charge my NTIS deposit account no. _____
- ☐ Purchase order no. _____
- ☐ Check enclosed for $ _____
- ☐ Bill me. Add $5.00 per order and sign below. (Not available outside North American continent.)
- ☐ Charge to my American Express Card account number

Card expiration date _____

Signature _____

☐ Priority mail requested

NAME _____

ADDRESS _____

CITY, STATE, ZIP _____

Item Number	Quantity		Unit price*	Total Price
	Paper Copy (PC)	Microfiche (MF)		

All prices subject to change. The prices above are accurate as of 3/31/78
Foreign Prices on Request.

Sub Total _____

Additional Charge _____

Enter Grand Total _____

Clip and mail to:

NTIS

National Technical Information Service
U.S. DEPARTMENT OF COMMERCE
Springfield, Va. 22161
(703) 557-4650 TELEX 89-9405